PB88-166830

Fundamental Combustion Research Applied to Pollution Formation. Volume 2C
Physics and Chemistry of Two-Phase Systems
Heterogeneous NO Reduction

Energy and Environmental Research Corp.
Irvine, CA

Prepared for

Environmental Protection Agency
Research Triangle Park, NC

Jan 88

U.S. Department of Commerce
National Technical Information Service
NTIS

PB88-166830

EPA/600/7-88/001c
January 1988

FUNDAMENTAL COMBUSTION RESEARCH APPLIED TO POLLUTION FORMATION

Volume IIc. Physics and Chemistry of Two-Phase Systems: Heterogeneous NO Reduction

by

W. R. Seeker, M. P. Heap, and T. J. Tyson

Energy and Environmental Research Corporation
18 Mason
Irvine, CA 92714

EPA Contract No. 68-02-2631
EPA Project Officer: W. Steven Lanier
Air and Energy Engineering Research Laboratory
Research Triangle Park, North Carolina 27711

AIR AND ENERGY ENGINEERING RESEARCH LABORATORY
OFFICE OF RESEARCH AND DEVELOPMENT
U.S. ENVIRONMENTAL PROTECTION AGENCY
RESEARCH TRIANGLE PARK, NC 27711

REPRODUCED BY
U.S. DEPARTMENT OF COMMERCE
NATIONAL TECHNICAL
INFORMATION SERVICE
SPRINGFIELD, VA. 22161

TECHNICAL REPORT DATA
(Please read Instructions on the reverse before completing)

1. REPORT NO. EPA/600/7-88/001c	2.	3. RECIPIENT'S ACCESSION NO. PB88 166830/AS
4. TITLE AND SUBTITLE Fundamental Combustion Research Applied to Pollution Formation; Volume IIc. Physics and Chemistry of Two-Phase Systems: Heterogeneous NO Reduction		5. REPORT DATE January 1988
		6. PERFORMING ORGANIZATION CODE
7. AUTHOR(S) W. R. Seeker, M. P. Heap, and T. J. Tyson		8. PERFORMING ORGANIZATION REPORT NO.
9. PERFORMING ORGANIZATION NAME AND ADDRESS Energy and Environmental Research Corporation 18 Mason Irvine, California 92714		10. PROGRAM ELEMENT NO.
		11. CONTRACT/GRANT NO. 68-02-2631
12. SPONSORING AGENCY NAME AND ADDRESS EPA, Office of Research and Development Air and Energy Engineering Research Laboratory Research Triangle Park, NC 27711		13. TYPE OF REPORT AND PERIOD COVERED
		14. SPONSORING AGENCY CODE EPA/600/13

15. SUPPLEMENTARY NOTES Project officer W. S. Lanier is no longer with the Agency. For details, contact William P. Linak, Mail Drop 65, 919/541-5792.

16. ABSTRACT The reports included in this three-part volume describe eight studies by various investigators, to better understand the physics and chemistry of two-phase combustion with respect to pollution formation. Volume IIc gives information on the kinetic rates and mechanisms of nitrogen oxide (NO) reduction on solid particles, in three parts: (1) trials on NO and NH3, alumina, quartz, graphite and soot; (2) comparative study of coal and char; and (3) trials on flyashes and study of reactions involving hydrogen cyanide.

17. KEY WORDS AND DOCUMENT ANALYSIS

a. DESCRIPTORS		b. IDENTIFIERS/OPEN ENDED TERMS	c. COSATI Field/Group	
Pollution	Nitrogen	Pollution Control	13B	07B
Combustion	Nitrogen Oxide (NO)	Stationary Sources	21B	
Research	Pulverized Fuels	Fundamental Research	14F	21D
Physics	Fuel Oil		20A	
Chemistry	Kinetics		07A	20K
Flames				

18. DISTRIBUTION STATEMENT Release to Public	19. SECURITY CLASS *(This Report)* Unclassified	21. NO. OF PAGES 462
	20. SECURITY CLASS *(This page)* Unclassified	22. PRICE

EPA Form 2220-1 (9-73)

NOTICE

This document has been reviewed in accordance with U.S. Environmental Protection Agency policy and approved for publication. Mention of trade names or commercial products does not constitute endorsement or recommendation for use.

ABSTRACT

This document is one of the series of reports describing work performed under the Fundamental Combustion Research (FCR) Applied to Pollution Formation Program (EPA Contract 68-02-2631). The FCR program was structured under a master contract concept with Energy and Environmental Research as the prime contractor and with individual studies generally performed under subcontract. Volume IIC of the final report series documents an extensive research effort performed by the Institut Francais du Petrol (French Petroleum Institute). The focus of the study was development of information on reaction pathways and associated reaction rates leading to the heterogeneous reduction of nitrogen oxides. Experiments were conducted in a fixed bed reactor using a wide range of reactant gases and solid-phase bed materials. The bed materials were examined in a systematic test matrix ranging from simple inorganics such as aluminia beads, through more complex solids and finishing with coal char and soot from oil flames. Reactant gases were also systematically varied as was the reaction temperature. Results are presented showing important reaction paths, partial order of those reactions as well as intrinsic reaction rates.

TABLE OF CONTENTS

Page

INTRODUCTION v

Part I. TRIALS ON NO AND NH_3, ALUMINA, QUARTZ, GRAPHITE, AND SOOT . . . . I-i

Part II. COMPARATIVE STUDY OF COAL AND CHAR . . . . II-i

Part III. TRIALS ON FLY ASHES AND STUDY OF REACTIONS INVOLVING HYDROGEN CYANIDE . . . . III-i

INTRODUCTION

The objective of the FCR program is to provide fundamental research support to the Combustion Research Branch (CRB) of the EPA in its efforts to develop and demonstrate low-NO_x combustion modification for stationary sources. In meeting this objective, the FCR program approach was to generate fundamental understanding of critical combustion phenomena controlling formation and destruction of combustion generated pollutants. Three major program areas, representing key elements in the pollutant formation process, were selected for in-depth investigation. These included:

- Transport Processes in Reacting Systems
- Physics and Chemistry of Two-Phase Systems
- Gas Phase Chemistry

Supporting studies were also pursued in the evaluation of analytical measurement systems and in the development of computer-based analytical tools.

Documentation of research performed under the major program area, Physics and Chemistry of Two-Phase Systems, is contained in three separately bound volumes (Volumes II-A, B, and C). This is the third of that three-volume set and specifically addresses heterogeneous reactions between NO or reduced nitrogen species and solid-phase material generally present in coal or heavy oil-fired flames.

The processes which take place in a large-scale utility flame burning either pulverized coal or heavy fuel oil, involve a complex series of physical and chemical transformations. In order to interpret data from pilot-scale studies, to extrapolate from pilot scale to full scale, and to develop new advanced NO_x control technologies, it is important to understand these transformations. The goal of any combustion modification applied to fuels containing significant amounts of bound nitrogen is to maximize the conversion of the nitrogen released from the fuel to molecular nitrogen and thereby minimize conversion to NO_x. One of the transformations that could be important is heterogeneous reduction of nitrogeneous species. Such a transformation would provide another reduction path which would be in addition to the gas-phase reduction paths discussed in Volume I of this final report series.

The fact that NO_x can be reduced to N_2 via reactions involving solid surfaces has been known for some time. The development of NO_x reducing catalysts for the external treatment of exhaust gases has been the direct result of the study of such processes. The question remains, however, as to the relative importance of heterogeneous processes which may occur in-flame or post-flame, and which occur via reaction with combustion-generated particulate. The key engineering issue which needs to be addressed is whether such processes, if they do exist, can be used to enhance combustion modification approaches to NO_x control.

The combustion of relatively dirty fuels such as coal and heavy fuel oils results in a wide variety of particulate which could potentially reduce nitrogeneous species. For example, the direct visualization of burning coal particles (Volume II, section A, of the FCR Final Report) indicates several types of particulate and several zones of interaction where nitrogen species and solid surfaces are in contact. Examples include:

- The parent coal particle can be in contact with recirculated combustion products.
- Reduced nitrogen species (e.g., HCN and NH_3) which are released internal to the coal particle matrix are in intimate contact with the partially devolatilized particle.
- The devolatilized coal particle can be surrounded by a volatile cloud which contains both reduced and oxidized nitrogen.
- The volatile cloud contains both large amounts of soot particles and nitrogen species from the devolatilization process.
- The char particles contain nitrogen and can be in contact with post-volatile-flame nitrogen species.
- Ash particles are released at various stages of the combustion sequence and are therefore in contact with nitrogen species in the flame zone, the postflame zone and in the flue gas.

To address whether or not significant reduction occurred during these interactions, requires knowledge of both the rates and mechanisms involved with heterogeneous reactions. As a first step toward development of such a mechanism, a cost-shared program was initiated at the Institut Francais du Petrole in France to study the global reactions of NO_x and reduced nitrogen species (HCN and NH_3) with solid materials typically found in flames.

The goals of this program were to provide information on the kinetic mechanisms of heterogeneous NO reduction for typical combustion-generated particulate and gas compositions and to determine the rates which govern disappearance of NO, formation of intermediates and formation of molecular nitrogen. The approach taken was to use a heated, packed-bed, quartz reactor containing different types of solids and to flow gases of different compositions throughout the bed. The gas composition could be controlled and thus the influence of species found in combustion gases such as H_2, CO, CO_2, and O_2 could be investigated. A methodology which incorporated trials of increasing complexity in both solid phase and gas phase speciation allowed the influence of each separate component to be determined. Simple Arrhenius rate expressions were obtained using the bed as a differential reactor along with independent measurements of the activation energy (temperature dependence) and the reaction order (gas component dependence).

The data generated in this program was not designed to be directly transferable to modeling activities of flame-zone reactions, but rather was intended to supply information suitable for assessments of the relative importance of heterogeneous reduction processes. For example, the processes that occur in flame are not equilibrium processes as are studied here. Flame-zone reactions would involve radicals, active sites, higher temperatures, dispersed-phase particulate, and nonequilibrium absorption/desorption. Such complexity requires additional studies which better simulate flame-zone conditions. Nonetheless, the global mechanisms do allow an assessment of the magnitude of the impact of the heterogeneous processes for contacting between the various types of nitrogen species and solid materials in flames. Detailed estimates, however, will certainly require further experimental work if, in fact, assessments based upon this early work indicate that such an effort is warranted.

The structure of the remainder of this volume includes the subcontract final report from IFP as edited and retyped by EER. It was not EER's intention to resolve all questions concerning the details of technical approach or data interpretation. On the contrary, such questions and differences in opinion generally result in exchanges of ideas (which can themselves yield unexpected results) and is advantageous to the overall FCR program. For this reason, no strict format was established but rather, the IFP report was kept in its general form with only slight modifications of style. The volume is in three parts which denote the various phases of the program:

I. Trials of NO and NH_3 on Alumina, Quartz, Graphite, and Soot

II. Trials With Coals and Chars

III. Trials on Fly Ashes and Study of Reactions Involving Hydrogen Cyanide.

I. TRIALS OF NO AND NH_3 ON ALUMINA, QUARTZ, GRAPHITE, AND SOOT

Prepared by:

Gerard G. DeSoete

Institute Francais du Petrole

Prepared for:

Energy and Environmental Research Corporation

TABLE OF CONTENTS

Section Page (I-)

INTRODUCTION 1

1.0 THE EXPERIMENTAL METHOD 3

2.0 GENERAL MECHANISMS OF HETEROGENEOUS NO REDUCTION 8

3.0 DISCUSSION OF THE EXPERIMENTAL RESULTS 21

3.1 Method Used for Determination of Reaction Rates. . . . 21

3.1.1 Homogeneous and Heterogeneous Reactions . . . 21
3.1.2 Determination of Reaction Rates 24

3.2 Identification of Reaction Paths and Determination of Reaction Rates 31

3.2.1 Trials on Alumina and Quartz (Family 1 Solids) 31

3.2.1.1 Gas Flows Without Nitrogen-Containing Species 31
3.2.1.2 Gas Flows Containing Nitrogen Species but no Oxygen 43
3.2.1.3 Effect of the Presence of Molecular Oxygen on the NO Reduction 81

3.2.2 Trials on Graphite (Case 2) 117

3.2.2.1 Argon + NO on Graphite (Case F.2) . . . 117
3.2.2.2 Argon + NO + CO on Graphite (Case K.2) . 120
3.2.2.3 Argon + NH_3 on Graphite (Case D.2) (Figure 63) 122
3.2.2.4 Argon + NO + NH_3 on Graphite (Case R.2). 122
3.2.2.5 Argon + NO + H_2 on Graphite (Case O.2) . 125

3.2.3 Trials on Soot From Ethylene (Case 4) 127

3.2.3.1 Gas Flows Without Nitrogen-Containing Species 127
3.2.3.2 Gas Flows Containing Nitrogen Species but no Oxygen 129
3.2.3.3 Effects of Molecular Oxygen on Selected Reactions 168

3.2.4 Trials on Soot From Heavy Fuel Oil (Porcheville Soot) (Case 5). 181

3.2.4.1 Gas Flows Without Nitrogen-Containing Species 181

TABLE OF CONTENTS (Concluded)

Section Page (I-)

3.2.4.2 Gas Flows Containing Nitrogen Species but no Oxygen 187
3.2.4.3 Effects of Molecular Oxygen on NO Reduction 210

4.0 GENERAL CONCLUSIONS 214

4.1 Direct Reduction of NO 214
4.2 Indirect Reduction With Hydrogen 221
4.3 Enhancement of Reduction With Gaseous Reducing Species 224
4.4 Effects of Molecular Oxygen 224

5.0 REFERENCES 226

LIST OF FIGURES

Figure Page (I-)

1 Schematic View of the Experimental Apparatus 4

2 Gas Composition: Ar + 29.17% H_2 + 0.1575% NO; D = 15.3 cm^3s^{-1} 22

3 Gas Composition: Ar + 2.10% CO + 0.0108% NO; D = 15 cm^3s^{-1} 23

4 Argon + CO on Alumina: D = 14.7 cm^3s^{-1}; $(CO)_i$ = 1.53% . . 32

5 Argon + CO on Alumina: D = 14.7 cm^3s^{-1}; $(CO)_i$ = 1.53% . . 34

6 Argon + H_2 + CO on Alumina: D = 14.3 cm^3s^{-1}; $(H_2)_i$ = 0.62%; $(CO)_i$ = 0.74% 36

7 Argon + CO + O_2 on Alumina: D = 13.6 cm_3s^{-1}; $(CO)_i$ = 0.81%; $(O_2)_i$ = 2.08% 38

8 Argon + CO + O_2 on Alumina: D = 13.6 cm^3s^{-1}; $(CO)_i$ = 0.85%; $(O_2)_i$ = 18.11% 39

9 Argon + CO + O_2 on Alumina: D = 13.8 cm^3s^{-1}; $(CO)_i$ = 4.0; $(O_2)_i$ = 0.67% 40

10 Argon + CO + O_2 on Alumina: D = 13.6 cm^3s^{-1}; $(CO)_i$ 4.00%; $(O_2)_i$ = 2.12% 41

11 Determination of Rate Constant k_{20} on Alumina; Different Initial Concentrations of CO and O_2 42

12 Argon + H_2 + O_2 on Alumina: Upper Curve: D = 13.7 cm^3s^{-1}; $(O_2)_i$ = 0.35%; $(O_2)_i$ = 0.33%. Lower Curve: D = 13.4 cm^3s^{-1}; $(H_2)_i$ = 1.56%; $(O_2)_i$ = 0.70% 44

13 Argon + Ammonia on Alumina. Lower Curve (A): D = 14.6 cm_3s^{-1}. $(NH_3)_i$ = 2030 ppm. Upper Curve (B): D = 15.0 cm^3s^{-1}; $(NH_3)_i$ = 715 ppm 46

14 Argon + NO + CO on Alumina: D = 14.8 cm^3s^{-1}; $(NO)_i$ = 9000 ppm; $(CO)_i$ = 2.44% 48

15 Argon + NO + CO on Alumina: D = 14.4 cm^3s^{-1}; $(NO)_i$ = 2200 ppm; $(CO)_i$ = 0.94% 49

16 Argon + NO + CO on Alumina: D = 14.0 cm^3s^{-1}; $(NO)_i$ = 1760 ppm; $(CO)_i$ = 5.16% 50

17 Argon + NO + CO on Alumina: Determination of the Rate Constant k_8 According to eq. (24), for Different Initial Concentrations of NO and CO 52

LIST OF FIGURES (Continued)

Figure Page (I-)

18 Argon + Ammonia + CO on Alumina: D = 13.9 cm^3s^{-1}; $(NH_3)_i$ = 475 ppm; $(CO)_i$ = 2.59% 53

19 Argon + Ammonia + CO on Alumina: D = 14.5 cm^3s^{-1}; $(CO)_i$ = 2.37%; $(NH_3)_i$ = 2700 ppm 54

20 Argon + Ammonia + CO on Alumina: D = 14.2 cm^3s^{-1}; $(NH_3)_i$ = 2400 ppm; $(CO)_i$ = 5.09% 55

21 Argon + Ammonia + CO on Alumina: D = 13.8 cm^3s^{-1}; $(NH_3)_i$ = 8200 ppm; $(CO)_i$ = 0.88% 56

22 Argon + Ammonia + CO on Alumina: Determination of the Rate Constant of the Overall Ammonia Disappearance According to eq. (35), for Different Initial Concentrations of Ammonia and CO 60

23 Argon + Ammonia + CO on Alumina: Determination of Rate Constant k_{15} According to eq. (39), for Different Initial Concentrations of Ammonia and CO. 61

24 Argon + Ammonia + CO on Alumina: Determination of Rate Constant k_9 According to eq. (39), for Different Initial Concentrations of Ammonia and CO 63

25 Argon + Ammonia + NO on Alumina: D = 14.3 cm^3s^{-1}; $(NH_3)_i$ = 400 ppm; $(NO)_i$ = 1730 ppm 64

26 Argon + Ammonia + NO on Alumina: D = 14.6 cm^3s^{-1}; $(NH_3)_i$ = 1800 ppm; $(NO)_i$ 8600 ppm 65

27 Argon + Ammonia + NO on Alumina: D = 14.6 cm^3s^{-1}; $(NH_3)_i$ = 1840 ppm; $(NO)_i$ = 1680 ppm 66

28 Argon + Ammonia + NO on Alumina: D = 14.6 cm^3s^{-1} $(NH_3)_i$ = 2040 ppm; $(NO)_i$ = 144 ppm 67

29 Argon + Hydrogen + NO on Alumina: D = 14.5 cm^3s^{-1}; $(NO)_i$ = 7000 ppm; $(H_2)_i$ = 5.52% 72

30 Argon + Hydrogen + NO on Alumina: D = 14.9 cm^3s^{-1}; $(NO)_i$ = 1330 ppm; $(H_2)_i$ = 5.52% 73

31 Argon + Hydrogen + NO on Alumina: D = 16.0 cm^3s^{-1}; $(NO)_i$ = 1270 ppm; $(H_2)_i$ = 13.10% 74

LIST OF FIGURES (Continued)

Figure Page (I-)

32 Argon + Hydrogen + NO on Alumina: Determination of the Rate Constant of the Overall NO Disappearance According to eq. (44), for Different Initial Concentrations of NO and Hydrogen 75

33 Argon + Hydrogen + NO on Alumina: Determination of the Rate Constant k_{14} According to eq. (47), for Different Initial Concentrations of NO and Hydrogen 77

34 Argon + Hydrogen + NO on Alumina: Determination of Rate Constant k_{11} According to eq. (48), for Different Initial Concentrations of NO and Hydrogen 78

35 Argon + NO + Methane on Alumina: $D = 12.6\ cm^3s^{-1}$; $(NO)_i = 900$ ppm; $(CH_4)_i = 0.29\%$ 79

36 Argon + NO + CO + O_2 on Alumina: $D = 17.0\ cm^3s^{-1}$; $(NO)_i = 1150$ ppm; $(CO)_i = 2.80\%$; $(O_2)_i = 0.17\%$ 83

37 Argon + NO + CO + O_2 on Alumina: $D = 15.3\ cm^3s^{-1}$; $(NO)_i = 1100$ ppm; $(CO)_i = 0.64\%$ $(O_2)_i = 0.13\%$ 84

38 Argon + NO + CO + O_2 on Alumina: $D = 17.1\ cm^3s^{-1}$; $(NO)_i = 1025$ ppm; $(CO)_i = 0.60\%$ $(O_2)_i = 0.17\%$ 85

39 Argon + NO + CO + O_2 on Alumina: $D = 15.3\ cm^3s^{-1}$; $(NO)_i = 5750$ ppm; $(CO)_i = 0.66\%$; $(O_2)_i = 0.13\%$ 86

40 Argon + NO + CO + O_2 on Alumina: $D = 14.5\ cm_3s_{-1}$; $(CO)_i = 1100$ ppm; $(CO)_i = 0.71\%$; (02)i = 8.76% 87

41 Argon + Ammonia + O^2 on Alumina: $D = 14.6\ cm^3s^-$ 1; $(NH3)_i = 2050$ ppm; $(O_2)_i = 0.15\%$ 90

42 Argon + Ammonia + O_2 on Alumina: $D = 14.3\ cm^3s^{-1}$; $(NH3)_i = 2350$ ppm; $(O_2)_i = 0.75\%$ 91

43 Argon + Ammonia + O_2 on Alumina: $D = 14.2\ cm^3s^{-1}$; $(NH_3)_i = 2310$ ppm; $(O_2)_i = 37.0\%$ 92

44 Argon + Ammonia + O_2 on Alumina: $D = 15.2\ cm^3s^{-1}$; $(NH_3)_i = 385$ ppm; $(O_2)_i = 0.71\%$ 93

45 Argon + Ammonia + O_2 on Alumina: $D = 14.3$ to $15.3\ cm^3s^{-1}$; Effect of Oxygen Concentration on NH_3 Removal . 94

LIST OF FIGURES (Continued)

Figure — Page (I-)

46 Argon + Ammonia + O_2 on Alumina: Determination of Rate Constant k_{17} According to eq. (67), for Different Initial Concentrations of Ammonia and Oxygen 97

47 Argon + Ammonia + O_2 on Alumina: Determination of Rate Constant k_{16} According to eq. (66), for Different Initial Concentrations of Ammonia and Oxygen 98

48 Argon + NO + Hydrogen + O_2 on Alumina: D = 15.1 cm^3s^{-1}; $(NO)_i$ = 1140 ppm; $(H_2)_i$ = 2.50%; $(O_2)_i$ = 0.28% . 101

49 Argon+ NO + Hydrogen + O_2 on Alumina: D = 16.2 cm^3s^{-1}, $(NO)_i$ = 1130ppm;$(H_2)_i$ = 7.40%; $O\ _2{}^i$ = 0.25% 102

50 Argon + NO + Hydrogen + O_2 on Alumina: D = 16.0 cm^3s^{-1}; (NO)i = 1170 ppm; (H_2)i = 18.80%; (O_2)i = 0.29% 103

51 Argon + NO + Hydrogen - O_2 on Alumina: D = 16.6 cm^3s^{-1}; (NO)i = 1250 ppm; (H_2,i = -.50%; (O_2,i = 0.13% 104

52 Argon + NO + Hydrogen + O_2 on Alumina: D = 16.1 cm^3s^{-1}; $(NO)_i$ = 1250 ppm; $(H2)_i$ = -.57%; $(O_2)_i$ = 2.3=% . 105

53 Argon + NO + Hydrogen + O_2 on Alumina: D = 15.1 cm^3s^{-1}; $(NO)_i$ = 6300 ppm; $(H_2)_i$ = -.50%; $(O_2)_i$ = 0.22% 106

54 Argon + NO + Hydrogen + O_2 on Alumina: D = 14.8 cm^3s^{-1}; Effect of Initial Oxygen concentration on NO Removal as a Function of Temperature 107

55 Argon + NO + Hydrogen + O_2 on Alumina: Effect of Initial Oxygen Concentration on Intermediate Ammonia Formation as a Function of Temperature. Same mixtures Compositions as for Figure 54. Key of Symbols: See Figure 54 108

56 Argon + NO + Hydrogen + O_2 on Alumina: Determination of the Rate Constant of KNOT.1 According to eq. (78), for Different Initial oxygen Concentrations. 111

57 Argon + NO + Hydrogen + O_2 on Alumina: Variation of $k_{NOT.1}$ and $E_{NOT.1}$ as a Function of Initial oxygen Concentration 112

LIST OF FIGURES (Continued)

Figure Page (I-)

58 Argon + NO + Hydrogen + O_2 on Alumina: Determination of Partial Reactor Order of VNOT.1 With Respect to Oxygen, According to eq. (79) 113

59 Argon + NO + Hydrogen + O_2 on Alumina: Dependence of the Ratio kNOT.1/kO.1 on Temperature, According to eq. (79) 114

60 Argon + NO on Graphite: $D = 14.5\ cm^3s^{-1}$; $(NO)_i = 1300$ ppm 118

61 Argon + NO on Graphite: $D - 14.5\ cm^3s^{-1}$; $(NO)_i =$ 6800 ppm 119

62 Argon + NO + CO on Graphite: $D = 14.5\ cm^3s^{-1}$; $(NO)_i = 7200$ ppm; $(CO)_i = 4.0\%$. 121

63 Argon + Ammonia on Graphite: $D = 13.3\ cm^3s^{-1}$; $(NH_3)_i =$ 2900 ppm 123

64 Argon + Ammonia + NO on Graphite: $D = 14.5\ cm^3s^{-1}$; $(NO)_i = 1560$ ppm; $(NH_3)_i = 2350$ ppm 124

65 Argon + NO + Hydrogen on Graphite: $D = 14.5\ cm^3s^{-1}$; $(NO)_i = 1325$ ppm; (H2)i = 1.60% 126

66 Argon (+CO) on Ethylene Soot: $D = 14.6\ cm^3s^{-1}$; Curve A: $(CO)_i = 0$; Curves B: $(CO)_i = 0.96\%$ 128

67 Argon + Oxygen on Ethylene Soot: $D = 12.3\ cm^3s^{-1}$; $(O_2)_i = 2.12\%$ 130

68 Argon + Ammonia on Ethylene Soot: $D = 12.4\ cm^3s^{-1}$; $(NH_3)_i = 3100$ ppm 131

69 Argon + Ammonia on Ethylene Soot: $D = 12.3\ cm^3s^{-1}$; T = 765°C 132

70 Argon + Ammonia on Ethylene Soot, Determination of Partial Order of V_{13} With Respect to Ammonia, According to eq. (107). 134

LIST OF FIGURES (Continued)

Figure Page (I-)

71 Argon + Ammonia on Ethylene Soot: Determination of Rate Constant k_3 According to eq. (107), for Different Initial Ammonia Concentrations. 134

72 Argon + Ammonia on Ethylene Soot: Determination of Partial Order of V_5 With Respect to Ammonia, According to eq. (105) 135

73 Argon + Ammonia on Ethylene Soot: Determination of Rate Constant k_5 According to eq. (105), for Different Initial Concentrations of Ammonia 135

74 Argon + NO on Ethylene Soot: $D = 14.0\ cm^3s^{-1}$; $(NO)^i = 130$ ppm 137

75 Argon + NO on Ethylene Soot: $D = 14.0\ cm^3s^{-1}$; $(NO)_i = 1360$ ppm 138

76 Argon + NO on Ethylene Soot: Determination of k_1 According to eq. (115), for Different Initial NO Concentrations 140

77 Argon + NO on Ethylene Soot: Determination of Rate Constant k_2 According to eq. (116), for Different Initial Concentrations of NO. 141

78 Argon + NO on Ethylene Soot: Determination of the Rate Constant k_{F4} According to eq. (111), for Different Initial NO Concentrations 142

79 Argon + NO + Ammonia on Ethylene Soot: $D = 12.0\ cm^3s^{-1}$; $(NO)_i$ = 1040 ppm; $(NH_3)_i$ = 4150 ppm 143

80 Argon + NO + Ammonia on Ethylene Soot: $D = 13.7\ cm^3s^{-1}$; $(NH_3)_i$ = 3440 ppm; T = 668°C 144

81 Argon + NO + Ammonia on Ethylene Soot: $D = 12.3\ cm^3s^{-1}$; $(NO)_i$ = 1045 ppm; T = 673°C 145

82 Argon + NO + Ammonia on Ethylene Soot: Determination of Partial Order of V_4 With Respect to Ammonia, According to eq. (124); $D = 12.3\ cm^3s^{-1}$.; $(NO)_i$ = 1045 ppm; T = 673°C 147

83 Argon + NO + Ammonia on Ethylene Soot: Determination of Partial Order of V4 With Respect to Nitric Oxide, According to eq. (124); $D = 13.7\ cm^3s^{-1}$; $(NH_3)_i$ = 3440 ppm; T = 668°C . . . 147

LIST OF FIGURES (Continued)

Figure Page (I-)

84 Argon + NO + Ammonia on Ethylene Soot: Determination of Rate Constant k_4 According to eq. (124); $(NO)_i = 1040$ ppm; $(NH_3)_i = 4150$ ppm; $D = 12.0\ cm^3s^{-1}$ 148

85 Argon + Ammonia + CO on Ethylene Soot: $D = 12.6\ cm^3s^{-1}$; $(NH_3)_i = 2420$ ppm; $(CO)_i = 1.26\%$ 150

86 Argon + Ammonia + CO on Ethylene Soot: $D = 13.3\ cm^3s^{-1}$; $(NH_3)_i = 2540$ ppm; $(CO)_i = 0.15\%$ 151

87 Argon + Ammonia + CO on Ethylene Soot: $D = 13.0\ cm^3s^{-1}$; $(NH_3)_i = 1925$ ppm; $(CO)_i = 4.15\%$ 152

88 Argon + Ammonia + CO on Ethylene Soot: $D = 11.8\ cm^3s^{-1}$; $(CO)_i = 0.91\%$; T = 766°C 153

89 Argon + Ammonia + CO on Ethylene Soot: $D = 13.8\ cm^3s^{-1}$; $(NH_3)_i = 2230$ ppm; T = 760°C 154

90 Argon + NO + CO on Ethylene Soot: $D = 13.1\ cm^3s^{-1}$; $(NO)_i = 1250$ ppm; $(CO)_i = 0.76\%$ 156

91 Argon + NO + CO on Ethylene Soot: $D = 12.1\ cm^3s^{-1}$; $(NO)_i = 1090$ ppm; T = 683°C 157

92 Argon + NO + CO on Ethylene Soot: $D = 12.1\ cm^3s^{-1}$; $(CO)_i = 0.90\%$; T = 683°C 158

93 Argon + NO + CO on Ethylene Soot: Determination of Rate Constant k_{K4} (Curve B) According to eq. (134), and Determination of Rate Constant k_8 (Curve A) According to eq. (138), for Different Initial Concentrations of CO and NO 161

94 Argon + NO + Hydrogen on Ethylene Soot: $D = 14.3\ cm^3s^{-1}$; $(NO)_i = 127$ ppm; $(H_2)_i = 5.52\%$ 162

95 Argon + NO + Hydrogen on Ethylene Soot: $D = 14.3\ cm^3s^{-1}$; $(NO)_i = 1280$ ppm; $(H_2)_i = 5.52\%$ 163

96 Argon + NO + Hydrogen on Ethylene Soot: $D = 14.3\ cm^3s^{-1}$; $(NO)_i = 1330$ ppm; $(H_2)_i = 1.63\%$ 164

97 Argon + NO + Hydrogen on Ethylene Soot: $D = 14.3\ cm^3s^{-1}$; $(NO)_i = 6800$; $(H_2)_i = 1.63\%$ 165

LIST OF FIGURES (Continued)

Figure Page (I-)

98 Argon + NO + Hydrogen on Ethylene Soot: Determination of Rate Constant k_{04} According to eq. (141), for Different Initial Concentrations of Hydrogen and Nitric Oxide 167
99 Argon + Ammonia + O_2 on Ethylene Soot: D = 13.4 cm^3s^{-1}; $(NH_3)_i$ = 3200 ppm; $(O_2)_i$ = 1.84% 169
100 Argon + Ammonia + O_2 on Ethylene Soot: D = 13.4 cm^3s^{-1}; $(NH_3)_i$ = 3200 ppm; $(O_2)_i$ = 0.55% 170
101 Argon + Ammonia + O_2 on Ethylene Soot: D = 12.3 cm^3s^{-1}; $(O_2)_i$ = 1.12%; T = 538°C 171
102 Argon + Ammonia + O_2 on Ethylene Soot: D = 13.4 cm^3s^{-1}; $(NH_3)_i$ = 3380 ppm; T = 537°C 172
103 Argon + Ammonia + O_2 on Ethylene Soot: D = 13.4 cm^3s^{-1}; $(NH_3)_i$ = 3200 ppm. curve A: $(O_2)_i$ = 0. Curve B: $(O_2$,i = 0.55%. Curve C: $(O_2)_i$ = 1.84% 173
104 Argon + Ammonia + O_2 on Ethylene Soot: Determination of Rate Constant k_{17} According to eq. (151), and Determination of Rate Constant k_{16} According to eq. (155), for Two Different Initial Oxygen Concentrations 175
105 Argon + Ammonia + O_2 on Ethylene Soot: Determination of Rate Constant According to eq. (153), for Two Different Initial Concentrations 176
106 Argon + NO + 02 on Ethylene Soot: D = 12.4 cm^3s^{-1}; $(NO)_i$ = 940 ppm, Curve A: = 0. Curve B: $(O_2)_i$ = 1.56%. Curve C: $(O_2)_i$ = 1.56% 178
107 Argon on Porcheville Soot: D = 15.0 cm^3s^{-1}; 182
108 Argon + CO on Porcheville Soot: D = 14.5 cm^3s^{-1}; $(CO)_i$ = 2.10% 184
109 Argon + O_2 on Porcheville Soot: D = 13.4 cm^3s^{-1}; $(O_2)_i$ = 2.19% 185
110 Argon + O_2 on Porcheville Soot: D = 13.3 cm^3s^{-1}; $(O_2)_i$ = 1.04%; M_i = 1.00 g; T = 588°C 186

LIST OF FIGURES (Continued)

Figure Page (I-)

111 Argon + Hydrogen on Porcheville Soot: D = 14.5 cm^{3}s^{-1}; $(H_2)_i$ = 1.60% 188

112 Argon + Ammonia on Porcheville Soot: D = 14.5 cm^{3}s^{-1}; $(NH_3)_i$ = 2560 ppm 189

113 Argon + NO on Porcheville Soot: D = 14.5 cm^{3}s^{-1}; $(NO)_i$ = 125 ppm 191

114 Argon + NO on Porcheville Soot: D = 14.5 cm^{3}s^{-1}; $(NO)_i$ = 7300 ppm 192

115 Argon + NO on Porcheville Soot: Determination of the Rate Constant k eq. (180), for Different Overall NO Removal, According to Initial Concentrations of NO . 194

116 Argon + NO + Ammonia on Porcheville Soot: D= 14.5 cm^{3}s^{-1}; $[NO)_i$ = 1700 ppm; $(NH_3)_i$ = 2690 ppm 195

117 Argon + Ammonia + CO on Porcheville Soot: D=12.6 cm^{3}s^{-1}; $(NH_3)_i$ = 2270 ppm; $(CO)_i$ = 4.15%. 197

118 Argon + Ammonia + CO on Porcheville Soot: Determination of the Overall NO Removal Rate Constant kI.5; D= 12.6 cm^{3}s^{-1}; $(NH_3)_i$ 2270 ppm; $(CO)_i$ = 4.15% 198

119 Argon + NO + VO on Porcheville Soot: D = 14.5 cm^{3}s^{-1}; $(NO)_i$ = 109 ppm; $(CO)_i$ = 2.10% 200

120 Argon + NO + CO on Porcheville Soot: D = 14.5 cm^{3}s^{-1}; $(NO)_i$ = 1325 ppm; $(CO)_i$ = 2.10% 201

121 Argon + NO + CO on Porcheville Soot: D = 14.5 cm^{3}s^{-1}; $(NO)_i$ = 7150 ppm; $[CO)_i$ = 2.10% 202

122 Argon + NO + CO on Porcheville Soot: D = 14.5 cm^{3}s^{-1}; $(NO)_i$ = 1350 ppm; $(CO)_i$ = 9.80% 203

123 Argon + NO + Hydrogen on Porcheville Soot: D=14.5 cm^{3}s^{-1};$(NO)^i$ = 1290 ppm $(H_2)_i$ = 1.60% 205

124 Argon + NO + Hydrogen on Porcheville Soot: D=14.5 cm^{3}s^{-1}; $(NO)_i$ = 7400 ppm; $(H_2)_i$ = 1.60% 206

125 Argon + NO + Hydrogen on Porcheville Soot: D=14.5 cm^{3}s^{-1}; $(NO)_i$ = 129 ppm; $(H_2)_i$ = 5.50% 207

LIST OF FIGURES (Concluded)

Figure Page (I-)

126 Argon + NO + Hydrogen on Porcheville Soot: $D = 14.5\ cm^3s^{-1}$; $(NO)_i = 1290$ ppm; $(H_2)_i = 5.50\%$ 208

127 Argon + NO + O_2 on Porcheville Soot: $D = 14.5\ cm^3s^{-1}$; $(NO)_i = 1310$ ppm. Curve A: = 0.06%. Curve B: $(O_2)_i = 0.82\%$.Curve C: $(O_2) - 5.08\%$ 211

128 Argon + NO + O_2 on Porcheville Soot: Variation of the Overall NO Removal Rate V_{T5}, Calculated From eq. (5), as a Function of Temperature, for Three Different Initial Oxygen Concentrations. Curve A: = 0.06%; Curve B: $(O_2)_i = 0.82\%$. Curve C: $(O_2)_i = 0.82\%$, $(NO)_i = 1310$ ppm . . 212

LIST OF TABLES

Table Page (I-)

1 Overall Heterogeneous Reactions as a Function of Gas Composition and Nature of Solid Particles 10

2 List of Heterogeneous Reactions Appearing in Table 1 . . . 27

3 Overall Rates of Heterogeneous NO Reduction ($cm^3\ g^{-1}\ s^{-1}$) . 215

4 Overall NO Disappearance Rates [$-d(NO)/dt$, $cm^3\ g^{-1}\ s^{-1}$] as a Function of Gas Composition and Nature of Solid Particles 219

INTRODUCTION

During the last decade substantial effort has been made by different laboratories to study the kinetics of catalytic NO reduction on solid particles (Ref. 1-6). The principal aim of those studies was to develop an understanding in order to optimize NO reducing catalysis for external treatment of exhaust gases from internal combustion engines as well as the external treatment of flue gases from stationary combustion sources. This effort has mainly focused on metals and metal oxide catalyst. A few studies have also been performed on carbonaceous materials (Ref. 7-13) with the same industrial motivation; however, only in the last few years has attention been explicitly focused on the role which may be played by solid particles, naturally present in the flue gases of stationary sources fired on heavy fuel oils or solid fossil fuels (e.g. gas-phase-generated soot, cenospheres, coal, char, fly ashes, etc.). Heterogeneous reduction of nitric oxides may occur "in situ" on these materials; i.e. in the flame itself or in the hot combustion products. For this application, three main problems have to be solved:

1. Elucidate the kinetic mechanisms of heterogeneous NO reduction under typical flame and flue gas conditions. Special attention should be paid to the nature of the reaction products of this reduction. From a pollution point of view, it is not sufficient to observe that the NO has disappeared from the combustion products; generally, it is required that nitric oxides be transformed directly into molecular nitrogen which is unlikely to reoxidize if the temperatures are sufficiently low. Whenever other intermediate, nitrogen-containing products are formed during NO reduction, it will be important to identify them and to check carefully the conditions of their further transformation into N_2. Indeed, the replacement of NO by other nitrogen pollutants (e.g. HCN, NH_3) may hardly be considered as progress from the pollution point of view.
2. Determine the reaction rates which govern the disappearance of NO, the formation of eventual intermediate nitrogen-containing species; and, finally, the transformation rates of NO and of the

eventual intermediate species into molecular nitrogen. The effect of typical combustion product components (e.g. H_2, CO, SO_2, O_2...) on these reduction rates should also be examined.

3. Check the importance of the heterogeneous reduction paths by comparing them with homogeneous NO reducing reactions, under real conditions in two-phase industrial flames.

The scope of the present study was to provide general information on the first two problems by performing trials in packed bed reactors. The study has been deliberately restricted to a general investigation of the heterogeneous NO reduction mechanisms; no attempt has been made to elucidate the detailed mechanisms of this phenomenon. Because of the complexity of these general mechanisms, many years of experimental study would be required to fully understand the mechanisms.

In what follows, we (1) describe the experimental method, (2) give a survey of the general mechanisms of heterogeneous NO reduction on solid particles, and (3) provide a detailed description of the findings with respect to obtaining overall reaction rates of heterogeneous nitric oxide reduction.

1.0 THE EXPERIMENTAL METHOD

A schematic of the experimental facility is given in Figure 1. The packed bed reactor (A) is made of quartz. The central bulb of the reactor has an inner diameter of 23 mm. The packed bed of solid particles has a height ranging from 10 to 24 mm (corresponding respectively to a volume of 4.2 to 10 cm^3). The solid particles are supported by a sintered quartz plate located at the bottom of the reactor bulb. The reactor is located at the inside of an electrically heated and regulated furnace (B); a shielded Alumel/Chromel thermocouple (C) is used for monitoring the temperature in the packed bed. The temperature of the latter has been varied between 100 and $1000^{o}C$. Different feedlines (D) are available for mixing the gas components with each feedline having its own flow metering system. Sonic orifices of very small diameter are utilized for the measurement of the flow rates. The general carrier gas is argon into which the different minor components are mixed. Every minor component is previously mixed with argon in a high-pressure cylinder on a separate mixing device, prior to being fed through one of the feedlines. The total flow rate through the reactor is set at between 10 and 15 cm^3s^{-1}, which, owing to the volume of the packed bed, results in a space velocity comprised between 1 and 3.6 s^{-1}. The lower limit of the total flow rate is imposed by the flow rate required for the analysers. In preliminary trials it has been determined that, for the given flow rates, diffusion control within the packed bed did not take place. On the gas mixture manifold (E) a drying column (F) is located in a bypass, which allows the gas mixture to be dried on either calcium chloride, phos pher pentoxide or water-free magnesium perchlorate when necessary. Another bypass (G) allows the analysis of the gas composition at the reactor inlet. This inlet composition will be designated by the subscript "i"; for example, $(Y)_i$ and $(X_Y)_i$ are the concentration (in ppm or volume percent) and the molar fraction of the component Y, respectively. The pressure within the reactor is adjusted by means of needle valve (H) and manometer (I). A constant pressure, slightly higher than the reactor pressure drop, has been selected for all runs (30 cm Hg). The reactor outlet flow can be entered either into a scrubber unit (J) for HCN and NH_3 absorption, or into a bloc of on-line analyzers; the latter consists of a nondispersive infrared

A	Packed Bed Reactor
B	Furnace
C	Thermocouple
D	Gaseous Reactant Feed Line
E	Gas Mixing Manifold
F	Drying Column
G	Reactant Bypass Line
H	Needle Valve
I	Manometer
J	Scrubber or Impinger Units
K-N	Continuous Monitors for CO, CO_2, O_2, NO/NO_x
O	Gas Chromatograph

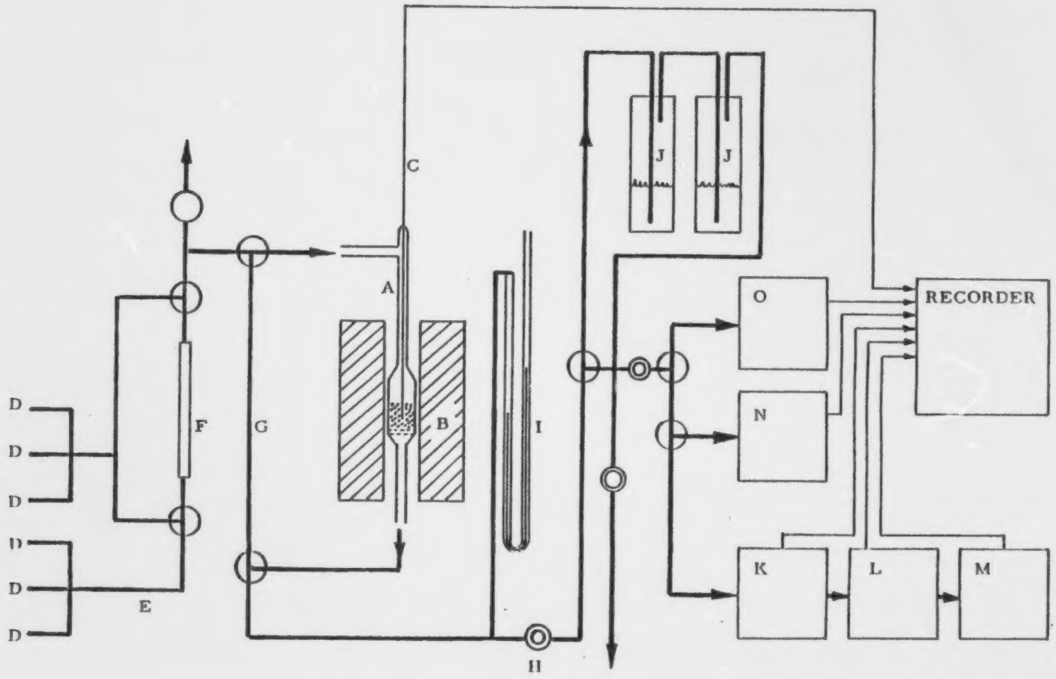
C
A
B
F
G
I
J
J
O
N
K
L
M
RECORDER
D
D
D
D
D
D
E
H

Figure 1. Schematic View of the Experimental Apparatus.

analyzer for carbon oxide (K) and carbon dioxide (L) analysis; a paramagnetic oxygen analyzer (M); a chemiluminescent nitric oxide/nitric dioxide analyzer (N); and a chromatograph (O) intended specially for N_2 analysis. The scrubbers contain a well-defined amount of 0.1 N aqueous KOH solution in which HCN and NH_3 are trapped as CN^- ions and a solution of NH_3 gas, respectively. An electrochemical method utilizing specific CN^- and NH_3 electrodes is used for determination of the content of HCN and NH_3 in the reactor inlet or outlet stream. A multichannel recorder stores the informations coming from the analyzers and from the thermocouple.

For every point of a given run, a complete analysis of the species NO, NO_2, HCN, NH_3, CO, CO_2, and O_2 is made (inasfar as their presence is possible owing to the reactor inlet composition). With no molecular nitrogen in the input stream, the concentration of molecular nitrogen is obtained by the following expression:

$$(N_2)_f = 0.5\left[(NO)_i + (NH_3)_i + (HCN)_i - (NO)_f - (NO_2)_f - (NH_3)_f - (HCN)_f\right] \qquad (1)$$

where the subscripts i and f indicate the reactor inlet and the reactor outlet concentrations, respectively. Only in a few recent cases has an attempt been made to check the N_2 concentration at the reactor outlet by gas chromatography. Owing to the relative imprecision of this method (in its actual state) this experimental check was only possible for N_2 concentrations larger than a few hundred ppm, and in these cases an acceptable agreement could be found with the concentrations calculated according to eq. (1).

In all cases treated in the present report, NO_2 has never been found in measurable concentrations, even in the presence of O_2 in the reactor inlet flow. This is due to the fact that, over the whole temperature range studies, the NO/NO_2 equilibrium is completely shifted towards NO.

For all input gas mixtures, high-purity gases have been used. The following five types of solid particles have been utilized throughout the trials described in the present report (motivation of their choice being given in the next section).

1. Alumina

Pure Al_2O_3, the characteristics of which are as follows:

Mean particle diameter: 60 to 150 microns

Specific surface area (BET method): 150 to 170 m^2/g

Apparent density: 1.00 ± 0.1g/cm

2. Quartz (So-Called "Electro Quartz") SiO_2

Mean particle size: 100 microns

Specific surface area: less than 1 m^2/g (BET method)

Apparent density: 1.38 g/cm^3

3. Graphite

Graphite carbon of 99.999 percent purity

Impurities: Aluminum (0.5 ppm); Boron (<0.01 ppm); Calcium (<0.2 ppm); Copper (0.5 ppm); Iron (0.8 ppm); Magnesium (0.2 ppm); Silicon (0.4 ppm); Sodium (0.2 ppm); Titanium (<0.1 ppm); Vanadium (<0.2 ppm).

Mean particle size: 25 $microns^3$

Specific surface area (BET method): $2m^2/g$

Apparent density: 0.37 g/cm

4. Gas-Phase-Generated Soot From Ethylene

Origin: Fuel-rich $C_2H_4/O_2/Ar$ premixed laminar flames (ϕ = 2.8)

Composition: atomic ratios: H/C = 0.29; small quantities of oxygen also present

Mean particle size: spherical particles of about 300 Å loosely granulated to particles of 250 to 500 microns

Specific surface area (BET method): 146 m^2/g

Apparent density: 0.032 to 0.036 g/cm^3

5. Industrial Cenospherical Soot From Heavy Fuel Oil

Origin: Power plant of Porcheville (France); sampled in the cyclones

Composition: (mass--percent): Carbon (78.2); H (0.4); S (3.5); N (0.8); Va (1.2); Ni (0.68); Na (0.6); Ca (0.33); Fe (1.2); also not specified quantities of oxygen, mostly as metal oxides.

Mean particle size: 50 microns

Specific surface area (BET method): 2.5 m^2/g

Apparent density: 1.38 g/cm^3

Principally, a new solid charge is used for each trial. In the rare cases where a charge from a foregoing trial has been utilized, it was pretreated at 1000°C under argon flow for at least one hour, in order to desorb all active molecules. The soot generated from ethylene flames was devolatilized at 900°C under argon flow for three hours.

For runs in which the solid charge is progressively consumed (e.g. runs with oxygen in the gas phase, on soot), the decrease in solid mass was taken into account for the determination of rate constants. From the values of $(CO)_f$ and $(CO_2)_f$ the decrease of the solid mass ΔM was calculated by the expression:

$$\Delta M = \left[(CO)_f + (CO_2)_f\right] \quad (M_C + q\, M_H)\, \frac{D}{v_M} \quad \Delta t$$

where M_C and M_H are the atomic mass of carbon and hydrogen atoms, respectively; q is the atomic ratio H/C characteristic for the soot and Δt is a time interval during which the concentrations CO_f and CO_2 are remaining constant (e.g. because the initial gas composition and the temperature remain constant). v_M is the molar volume at standard conditions, and D is the total volumetric flow rate.

2.0 GENERAL MECHANISMS OF HETEROGENEOUS NO REDUCTION

The gas-phase reduction of nitric oxides by gaseous reducing agents (like hydrogen, carbon monoxide, hydrocarbons...) is, even at flame temperatures, a rather slow process in the absence of hydrocarbon radicals (Ref. 14). Therefore, it is mostly restricted to the oxidation zone of the flame, where these radicals are present in nonnegligible concentrations.

In many cases the presence of solid particles in the oxidation zone, as well as in the hot flue gases, gives rise to the existence of heterogeneous nitric oxide reduction reactions on the solid/gas contact surface. The temperature dependence of heterogeneous reactions is generally much lower than that of the homogeneous gas-phase NO reduction reactions. Therefore, the relative effect of the former reaction on NO reduction, especially at lower temperatures, should be taken in consideration when dealing with the NO history in particle-laden industrial flames.

These heterogeneous NO reducing reactions may belong to two different types:

1. True catalytic reactions, in which the role of the solid phase is limited to a merely catalytic action. The solid then merely catalyzes phase contact reactions and does not participate in them as a reactant.
2. Reactions between solid and gas, in which the solid participates as a reactant for NO reduction. These solid + gas reactions may eventually also bear a catalytic character. In this second type of heterogeneous reaction, the solid must contain reducing agents, such as bound hydrogen or bound carbon atoms.

In both cases, the reactions take place, at least partly, at the gas/solid interface and may strongly depend on the adsorption/desorption rates and on the adsorption/desorption equilibria of one or more of the gaseous reactants and/or products.

From the point of view of possible reaction paths, these heterogeneous NO reduction reactions, considered as overall reactions, may be divided into two groups:

(a) DIRECT reduction reactions, in which molecular nitrogen is generated as the only nitrogen containing gaseous product.

(b) INDIRECT reduction reactions, in which the reduction of NO into N_2 passes through intermediate nitrogen-containing gaseous species, especially ammonia and hydrogen cyanide. The intermediate formation of ammonia requires the presence of a hydrogen source, whereas the intermediate formation of hydrogen cyanide requires the existence of both a carbon and a hydrogen source. Gaseous molecules (e.g. H_2, CO) as well as solid bound hydrogen and carbon atoms (-H, -C) may act as hydrogen and carbon sources for the formation of NH_3 and HCN.

It should also be emphasized that, in the case where the solid contains bound nitrogen atoms (as for coal or cenospherical soot) NH_3 and HCN formation may also occur. This could occur, for example, during thermal decomposition, during further oxidation or also upon reaction of the solid with a gaseous hydrogen carbon source.

From the foregoing it follows that the mechanism of heterogeneous NO reduction, even when limited to overall reaction paths, depends strongly on the chemical nature of the solid phase, and the composition of the gas phase (especially the presence of reducing and oxidizing components). In what follows heterogeneous reduction will be examined in more detail, by considering a sequence of cases of progressively increasing complexity in the chemical nature of the solid particles and the composition of the gas phase. The discussion will be focused on the NO-reducing effects of flue gases containing a dispersed solid phase. For this reason, the presence and the effects of hydrocarbons in the gas phase will normally be disregarded. The situation is illustrated in Table 1, showing overall heterogeneous reactions occurring when shifting from a rather simple to progressively more complex solids. The reaction paths are characterized exclusively by their overall mass balance (the choice of their stoichiometry being based on the experimentally observed mass balance, as will be shown in the next section of T1

Table 1. Overall Heterogeneous Reactions as a Function of Gas Composition and Nature of Solid Particles

ROW	GAS COMPOSITION	SOLID-BOUND ATOMS					
	(one component)	COLUMN 1: -O		COLUMN 2 : -C		COLUMN 3 : -C, -H	
		OVERALL REACTIONS	PRODUCTS	OVERALL REACTIONS	PRODUCTS	OVERALL REACTIONS	PRODUCTS
A	Thermal decomposition of solid						
B	CO	$CO + (-O) \xrightarrow{12} CO_2$					
C	H_2	$H_2 + (-O) \xrightarrow{19} H_2O$					
D	NH_3	$NH_3 \xrightarrow{13} 0.5\ N_2 + 1.5\ H_2$	H_2	$NH_3 \xrightarrow{13} 0.5\ N_2 + 1.5\ H_2$ $NH_3 + (-C) \xrightarrow{5} HCN + H_2$	H_2 HCN	$NH_3 \xrightarrow{13} 0.5\ N_2 + 1.5\ H_2$ $NH_3 + (-C) \xrightarrow{5} HCN + H_2$	H_2 HCN
E	O_2			$O_2 + (-C) \xrightarrow{24} CO, CO_2$	CO	$O_2 + (-C) \xrightarrow{24} CO, CO_2$ $O_2 + (-H) \xrightarrow{23} H_2O$	CO
F	NO			$NO + a\ (-C) \xrightarrow{1} 0.5\ N_2 + (2a - 1)\ CO + (1 - a)\ CO_2$	CO	$NO + a\ (-C) \xrightarrow{1} 0.5\ N_2 + (2a - 1)\ CO + (1 - a)\ CO_2$ $NO + a\ (-C) + b\ (-H) \xrightarrow{2} NH_3 + \frac{b-3}{2} H_2O + (\frac{b-5}{2} + 2a)\ CO + (\frac{5-b}{2} - a)\ CO_2$	CO NH_3
G	HCN	$HCN \xrightarrow{15} 0.5\ N_2 + 0.5\ H_2 + C$	H_2	$HCN \xrightarrow{15} 0.5\ N_2 + 0.5\ H_2 + C$	H_2	$HCN \xrightarrow{15} 0.5\ N_2 + 0.5\ H_2 + C$	H_2

Table 1. Overall Heterogeneous Reactions as a Function of Gas Composition and Nature of Solid Particles (Continued)

ROW	GAS COMPOSITION (one component)	SOLID-BOUND ATOMS			
		COLUMN 4: -C, -H, -O		COLUMN 5: -C, -H, -O, -N	
		OVERALL REACTIONS	PRODUCTS	OVERALL REACTIONS	PRODUCTS
A	Thermal decomposition of solid	$(-C) + (-O) \rightarrow CO, CO_2$	CO	$(-C) + (-O) \rightarrow CO, CO_2$ $(-C) + (-N) + (-H) \rightarrow HCN$	CO HCN
B	CO	$CO + (-O) \xrightarrow{12} CO_2$		$CO + (-O) \xrightarrow{12} CO_2$	
C	H_2	$H_2 + (-O) \xrightarrow{19} H_2O$		$H_2 + (-O) \xrightarrow{19} H_2O$ $H_2 + (-N) \xrightarrow{21} NH_3$ $H_2 + (-N) + (-C) \xrightarrow{22} HCN$	 NH_3 HCN
D	NH_3	$NH_3 \xrightarrow{13} 0.5\ N_2 + 1.5\ H_2$ $NH_3 + (-C) \xrightarrow{5} HCN + H_2$	H_2 HCN	$NH_3 \xrightarrow{13} 0.5\ N_2 + 1.5\ H_2$ $NH_3 + (-C) \xrightarrow{5} HCN + H_2$ $NH_3 + (-N) \xrightarrow{26} N_2 + 1.5\ H_2$	H_2 HCN
E	O_2	$O_2 + (-C) \xrightarrow{24} CO, CO_2$ $O_2 + (-H) \xrightarrow{23} H_2O$	CO	$O_2 + (-C) \xrightarrow{24} CO, CO_2$ $O_2 + (-H) \xrightarrow{23} H_2O$ $O_2 + (-N) \xrightarrow{25} NO$	CO NO
F	NO	$NO + a\ (-C) \xrightarrow{1} 0.5\ N_2 + (2a-1)\ CO + (1-a)\ CO_2$ $NO + a(-C) + b(-H) \xrightarrow{2} NH_3 + \frac{b-3}{2}\ H_2O + (\frac{b-5}{2} + 2a)\ CO + (\frac{5-b}{2} - a)\ CO_2$	CO NH_3	$NO + a(-C) \xrightarrow{1} 0.5\ N_2 + (2a-1)\ CO + (1-a)\ CO_2$ $NO + a(-C) + b(-H) \xrightarrow{2} NH_3 + \frac{b-3}{2}\ H_2O + (\frac{b-5}{2} + 2a)\ CO + (\frac{5-b}{2} - a)\ CO_2$	CO NH_3
G	HCN	$HCN \xrightarrow{15} 0.5\ N_2 + 0.5\ H_2 + C$	H_2	$HCN \xrightarrow{15} 0.5\ N_2 + 0.5\ H_2 + C$ $HCN + (-N) \xrightarrow{27} N_2 + \ldots$	H_2

Table 1. Overall Heterogeneous Reactions as a Function of Gas Composition and Nature of Solid Particles (Continued)

ROW	GAS COMPOSITION (two components)	SOLID-BOUND ATOMS					
		COLUMN 1 : -O		COLUMN 2 : -C		COLUMN 3 : -C, -H	
		OVERALL REACTIONS	PRODUCTS	OVERALL REACTIONS	PRODUCTS	OVERALL REACTIONS	PRODUCTS
H	$CO + H_2$	reaction (12)(19) of B1, C1 and: $CO + H_2 \xrightarrow{39} H_2O + C$		$CO + H_2 \xrightarrow{39} H_2O + C$		$CO + H_2 \xrightarrow{39} H_2O + C$	
I	$CO + NH_3$	reactions (12) and (13) of B1 and D1 and: $NH_3 + CO \xrightarrow{9} HCN + H_2O$	H_2 HCN	reactions (5) and (13) of D2 and: $NH_3 + CO \xrightarrow{9} HCN + H_2O$	H_2, HCN HCN	reactions (5) and (13) of D3 and: $NH_3 + CO \xrightarrow{9} HCN + H_2O$	H_2, HCN HCN
J	$CO + O_2$	reaction (12) of B1 and: $CO + 0.5\ O_2 \xrightarrow{20} CO_2$		reaction (24) of E2 and: $CO + 0.5\ O_2 \xrightarrow{20} CO_2$		reactions (24) and (23) of E3 and: $CO + 0.5\ O_2 \xrightarrow{20} CO_2$	
K	CO + NO	reaction (12) of B1 and: $CO + NO \xrightarrow{8} 0.5\ N_2 + CO_2$		reaction (1) of F2 and: $CO + NO \xrightarrow{8} 0.5\ N_2 + CO_2$		reactions (1) and (2) of F3 and: $CO + NO \xrightarrow{8} 0.5\ N_2 + CO_2$ $CO + NO + 3\ (-H) \xrightarrow{6} NH_3 + CO_2$	NH_3 NH_3
L	CO + HCN	reactions (12) and (15) of B1 and G1 (no supplementary inter-reaction between CO and HCN)	H_2	reaction (15) of G2	H_2	reaction (15) of G3	H_2

Table 1. Overall Heterogeneous Reactions as a Function of Gas Composition and Nature of Solid Particles (Continued)

ROW	GAZ COMPOSITION (two components)	SOLID-BOUND ATOMS			
		COLUMN 4: -C, -H, -O		COLUMN 5: -C, -H, -O, -N	
		OVERALL REACTIONS	PRODUCTS	OVERALL REACTIONS	PRODUCTS
H	$CO + H_2$	reactions (12) and (19) of B4 and C4 ; reactions of A4, and: $CO + H_2 \xrightarrow{39} H_2O + C$		reactions (12)(19)(21) and (22) from B5 and C5 ; reactions of A5 ; and: $CO + H_2 \xrightarrow{39} H_2O + C$	NH_3, HCN
I	$CO + NH_3$	reactions (5)(12) and (13) from B4 and D4 ; reactions of A4 and: $NH_3 + CO \xrightarrow{9} HCN + H_2O$	HCN	reactions (5)(12)(13) and (26) of B5 and D5 ; reactions of A5 and: $NH_3 + CO \xrightarrow{9} HCN + H_2O$	HCN
J	$CO + NH_3$	reactions (12)(23) and (24) of B4 and E4 ; reactions of A4, and: $CO + 0.5\ O_2 \xrightarrow{20} CO_2$		reactions (12)(23)(24) and (25) of B5 and E5 ; reactions of A5, and: $CO + 0.5\ O_2 \xrightarrow{20} CO_2$	NO, HCN
K	CO + NO	reactions (1)(2) and (12) of B4 and F4 ; reactions of A4, and: $CO + NO \xrightarrow{8} 0.5\ N_2 + CO_2$	NH_3	reactions (1)(2) and (12) of B5 and F5 ; reactions of A5, and: $CO + NO \xrightarrow{8} 0.5\ N_2 + CO_2$	NH_3 , HCN
L	CO + HCN	reactions (12) and (15) of B4 and G4 ; reactions of A4	H_2	reactions (12) and (15) of B5 and G5 ; reactions of A5	H_2

Table 1. Overall Heterogeneous Reactions as a Function of Gas Composition and Nature of Solid Particles (Continued)

NOW	GAS COMPOSITION (two components)	SOLID-BOUND ATOMS					
		COLUMN 1 : -0		COLUMN 2 : -C		COLUMN 3 : -C, -H	
		OVERALL REACTIONS	PRODUCTS	OVERALL REACTIONS	PRODUCTS	OVERALL REACTIONS	PRODUCTS
M	$H_2 + NH_3$	reactions (13) and (19) of C1 and D1		reactions (5) and (13) of D2	HCN	reactions (5) and (13) of D3	HCN
N	$H_2 + O_2$	reaction (19) of C1 and: $H_2 + 0.5\ O_2 \xrightarrow{18} H_2O$		reaction (24) of E2 and: $H_2 + 0.5\ O_2 \xrightarrow{18} H_2O$		reactions (23) and (24) of E3 and: $H_2 + 0.5\ O_2 \xrightarrow{18} H_2O$	
Ø	$H_2 + NO$	reaction (19) of C1 and: $NO + 2.5\ H_2 \xrightarrow{11} NH_3 + H_2O$ $NO + H_2 \xrightarrow{14} 0.5\ N_2 + H_2O$	NH_3	reaction (1) of F2 and: $NO + 2.5\ H_2 \xrightarrow{11} NH_3 + H_2O$ $NO + H_2 \xrightarrow{14} 0.5\ N_2 + H_2O$	CO NH_3	reactions (1) and (2) of F3 and: $NO + 2.5\ H_2 \xrightarrow{11} NH_3 + H_2O$ $NO + H_2 \xrightarrow{14} 0.5\ N_2 + H_2O$	CO, NH_3 NH_3
P	$H_2 + HCN$	reactions (15) and (19) of C1 and G1, and: $HCN + H_2 \xrightarrow{45} NH_3 + \ldots$	NH_3	reaction (15) of G2, and: $HCN + H_2 \xrightarrow{45} NH_3 + \ldots$	NH_3	reaction (15) of G3, and: $HCN + H_2 \xrightarrow{45} NH_3 + \ldots$	NH_3
Q	$NH_3 + O_2$	reaction (13) of D1, and: $NH_3 + 0.75\ O_2 \xrightarrow{16} 0.5\ N_2 + 1.5\ H_2O$ $NH_3 + 1.25\ O_2 \xrightarrow{17} NO + 1.5\ H_2O$	H_2 NO	reactions (5), (13) and (24) of D2 and E2, and: $NH_3 + 0.75\ O_2 \xrightarrow{16} 0.5\ N_2 + 1.5\ H_2O$ $NH_3 + 1.25\ O_2 \xrightarrow{17} NO + 1.5\ H_2O$	H_2, HCN, CO NO	reactions (5)(13)(23) and (24) of D3 and E3, and: $NH_3 + 0.75\ O_2 \xrightarrow{16} 0.5\ N_2 + 1.5\ H_2O$ $NH_3 + 1.25\ O_2 \xrightarrow{17} NO + 1.5\ H_2O$	H_2, HCN, CO NO

Table 1. Overall Heterogeneous Reactions as a Function of Gas Composition and Nature of Solid Particles (Continued)

ROW	GAZ COMPOSITION (two components)	SOLID-BOUND ATOMS			
		COLUMN 4: -C, -H, -O		COLUMN 5: -C, -H, -O, -N	
		OVERALL REACTIONS	PRODUCTS	OVERALL REACTIONS	PRODUCTS
M	$H_2 + NH_3$	reactions (5)(13) and (19) of C4 and D4 ; reactions of A4	CO, HCN	reactions (5)(13)(19)(21)(22) and (26) ; reactions of A5	CO, HCN
N	$H_2 + O_2$	reactions (19)(23) and (24) of C4 and E4 ; reactions of A4 and: $H_2 + 0.5\ O_2 \xrightarrow{18} H_2O$	CO	reactions (19)(21)(22)(23)(24) and (25) of C5 and E5 ; reactions of A5, and: $H_2 + 0.5\ O_2 \xrightarrow{18} H_2O$	CO, NH_3, HCN, NO
O	$H_2 + NO$	reactions (1)(2) and (19) of C4 and F4 ; reactions of A4, and: $NO + 2.5\ H_2 \xrightarrow{11} NH_3 + H_2O$ $NO + H_2 \xrightarrow{14} 0.5\ N_2 + H_2O$	CO, NH_3	reactions (1)(2)(19)(21) and (22) of C5 and F5 ; reactions of A5, and: $NO + 2.5\ H_2 \xrightarrow{11} NH_3 + H_2O$ $NO + H_2 \xrightarrow{14} 0.5\ N_2 + H_2O$	CO, HCN NH_3
P	$H_2 + HCN$	reactions (15) and (19) of C4 and G4 ; reactions of A4, and: $HCN + H_2 \xrightarrow{45} NH_3 + \ldots$	NO, CO NH_3	reactions (15)(19)(21)(22) and (27) ; reactions of A5, and: $HCN + H_2 \xrightarrow{45} NH_3 + \ldots$	CO, NH_3, NO
Q	$NH_3 + O_2$	reactions (5)(13)(23) and (24) of D4 and E4 ; reactions of A4, and: $NH_3 + 0.75\ O_2 \xrightarrow{16} 0.5\ N_2 + 1.5\ H_2O$ $NH_3 + 1.25\ O_2 \xrightarrow{17} NO + 1.5\ H_2O$	H_2, CO, HCN	reactions (5)(13)(23)(24)(25) and (26) of D5 and E5 ; reactions of A5, and: $NH_3 + 0.75\ O_2 \xrightarrow{16} 0.5\ N_2 + 1.5\ H_2O$ $NH_3 + 1.25\ O_2 \xrightarrow{17} NO + 1.5\ H_2O$	H_2, CO, NO, HCN

Table 1. Overall Heterogeneous Reactions as a Function of Gas Composition and Nature of Solid Particles (Continued)

ROW	GAS COMPOSITION	SOLID-BOUND ATOMS					
		COLUMN 1 : -O		COLUMN 2 : -C		COLUMN 3 : -C, -H	
		OVERALL REACTIONS	PRODUCTS	OVERALL REACTIONS	PRODUCTS	OVERALL REACTIONS	PRODUCTS
R	$NH_3 + NO$	reaction (13) of D1, and: $NO + n\ NH_3 \xrightarrow{4} (\frac{1+n}{2})\ N_2$ $+ H_2O + (\frac{3n-2}{2})\ H_2$	H_2	reactions (1)(5) and (13) of D2 and F2, and: $NO + n\ NH_3 \xrightarrow{4} (\frac{1+n}{2})\ N_2$ $+ H_2O + (\frac{3n-2}{2})\ H_2$	H_2, HCN, CO	reactions (1)(2)(5) and (13) of D3 and F3, and: $NO + n\ NH_3 \xrightarrow{4} (\frac{1+n}{2})\ N_2$ $+ H_2O + (\frac{3n-2}{2})\ H_2$	H_2, HCN, CO
S	$NH_3 + HCN$	reactions (13) and (15) of D1 and G1 and: $NH_3 + HCN \xrightarrow{10} N_2 + 2\ H_2 + C$	H_2	reactions (5)(13) and (15) of D2 and G2 and: $NH_3 + HCN \xrightarrow{10} N_2 + 2\ H_2 + C$	H_2	reactions (5)(13) and (15) of D3 and G3 and: $NH_3 + HCN \xrightarrow{10} N_2 + 2\ H_2 + C$	H_2
T	$O_2 + NO$			reactions (1) and (24) of E2 and F2	CO	reactions (1)(2)(23) and (24) of E3 and F3	
U	$O_2 + HCN$	reaction (15) of G1, and: $HCN + n\ O_2 \xrightarrow{38}$ N_2, NO, H_2O, CO, CO_2	H_2 NO, CO	reactions (15) and (24) of E2 and G2 and: $HCN + n\ O_2 \xrightarrow{38}$ N_2, NO, H_2O, CO, CO_2	CO, H_2 NO	reactions (15)(23) and (24) of E3 and G3 and: $HCN + n\ O_2 \xrightarrow{38}$ N_2, NO, H_2O, CO, CO_2	H_2, CO NO
V	NO + HCN	reaction (15) of G1, and: $HCN + NO \xrightarrow{40} N_2 + \ldots$	H_2	reactions (1) and (15) of F2 and G2, and: $HCN + NO \xrightarrow{40} N_2 + \ldots$	CO, H_2	reactions (1)(2) and (15) of F3 and G3, and: $HCN + NO \xrightarrow{40} N_2 + \ldots$	CO, H_2 NH_3

Table 1. Overall Heterogeneous Reactions as a Function of Gas Composition and Nature of Solid Particles (Concluded)

ROW	GAS COMPOSITION (two components)	SOLID-BOUND ATOMS			
		COLUMN 4: $-C, -H, -O$		COLUMN 5: $-C, -H, -O, -N$	
		OVERALL REACTIONS	PRODUCTS	OVERALL REACTIONS	PRODUCTS
R	$NH_3 + NO$	reactions (1)(2)(5) and (13) of D4 and F4 ; reactions of A4, and: $NO + n\ NH_3 \xrightarrow{4} (\frac{1+n}{2})\ N_2 + H_2O + (\frac{3n-2}{2})\ H_2$	CO, H_2 , HCN	reactions (1)(2)(5)(13) and (26) of D5 and F5 ; reactions of A5 and: $NO + n\ NH_3 \xrightarrow{4} (\frac{1+n}{2})\ N_2 + H_2O + (\frac{3n-2}{2})\ H_2$	CO, H_2 , HCN
S	$NH_3 + HCN$	reactions (5)(13) and (15) of D4 and G4 ; reactions of A4, and: $NH_3 + HCN \xrightarrow{10} N_2 + 2\ H_2 + C$	CO, H_2	reactions (5)(13)(15)(26) and (27) of D5 and G5 ; reactions of A5, and: $NH_3 + HCN \xrightarrow{10} N_2 + 2\ H_2 + C$	CO, H_2
T	$O_2 + NO$	reactions (1)(2)(23) and (24) of E4 and F4 ; reactions of A4	CO, NH_3	reactions (1)(2)(23)(24) and (25) of E5 and F5 ; reactions of A5	CO, HCN, NH_3
U	$O_2 + HCN$	reactions (15)(23) and (24) of E4 and G4 ; reactions of A4 and: $HCN + n\ O_2 \xrightarrow{38} N_2$, NO, H_2O, CO_2, CO	CO, H_2 NO	reactions (15)(23)(24)(25) and (27) of E5 and G5 ; reactions of A5, and: $HCN + n\ O_2 \xrightarrow{38} N_2$, NO, H_2O, CO, CO_2	CO, H_2 , NO
V	$NO + HCN$	reactions (15)(1) and (2) of F4 and G4 ; reactions of A4, and: $HCN + NO \xrightarrow{40} N_2 + \ldots$	CO, NH_3 , H_2	reactions (1)(2)(15)(27) of F5 and G5 ; reactions of A5, and: $HCN + NO \xrightarrow{40} N_2 + \ldots$	CO, NH_3 , H_2

the present report), without any reference to detailed mechanism, which is still largely unknown. Based upon relative chemical complexity of the solids, five families of solid particles are displayed in Table 1 as five successive columns, numbered 1 to 5. For each family of solid, different gas compositions are considered on Table 1 and are displayed in horizontal rows, numbered from A to V. Roughly, the different gas compositions given on Table 1 correspond to the compositions used in the experimental part of the work (see section 3). The following components are listed, either separately (rows B to G) or in their binary combinations (rows H to V): CO, H_2, NH_3, HCN, O_2, NO. Neither H_2O, CO_2 nor hydrocarbons have been considered, although it has become clear from very recent trials (performed since the end of the period under consideration here) that H_2O and hydrocarbons may have an important effect. Reactions involving HCN have not been studied up to now in a systematic manner (studied in Part III).

Column 1 represents refractory oxides (e.g. CaO, SiO_2, Al_2O_3...) having only bound oxygen atoms as potential reactants. In this rather simple case, nitrogen intermediates (HCN, NH_3) will only appear if a hydrogen and carbon source is supplied in the gas phase (e.g. H_2, CO, CH_4...).

Column 2 applies to particles having exclusively bound carbon atoms as potential reactants (e.g. graphite, carbides,...), which introduces into the mechanism a supplementary, solid bound carbon source.

Column 3 considers the case where there exist both a solid bound hydrogen and a solid bound carbon source. This would apply in the case of soot formed by thermal cracking of pure hydrocarbons in the absence of oxygen.

Column 4 applies to most soots formed in the gas phase during the combustion of fuel-rich, pure hydrocarbon/oxygen mixtures. These soots generally contain some oxygen in addition to bound carbon and hydrogen atoms.

Column 5 covers the most complex configuration, which generally applies to all kinds of coal and char particles, as well as industrial, cenospherical soot generated in the liquid phase from heavy fuel oils. Generally, this kind of particulate simultaneously contains bound oxygen, carbon, hydrogen, nitrogen, and sulphur. The presence of bound nitrogen atoms in non-negligible amounts, contributes significantly to the complexity of the nitric oxide reducing mechanisms. In the present phase of the experimental study, sulphur/nitrogen interactions have been disregarded.

In the cases where there is only one reactive component in the gas phase (rows B to G), a great number of the heterogeneous reactions are of the gas+solid type. When there are two reactive components in the gas phase (rows H to V), reactions between these two gas components may supplement the gas+solid bound atoms reactions. These gas+gas reactions are generally also of the heterogeneous type (i.e. are contact catalyzed by the solid surface). In some cases however, they may develop in a homogeneous way within the gas phase (e.g. the relatively fast $H_2 + 0.5\ O_2 \xrightarrow{18} H_2O$ reaction at elevated temperatures, which may even bear an explosive character). At the right hand side of every column are indicated those reaction products which are themselves reactive components with respect to nitrogen species. The formation of these reaction products thus automatically switches to the row (or rows) where these products appear as reactants.

From the foregoing it should be clear that, in order to understand, even qualitatively, the complex NO reducing mechanisms and to define the overall rates of the dominant reactions will require an experimental study under conditions of progressively increasing complexity in solid and gas phase composition:

1. Increasing complexity of the solid matter:

   The five different types of particles utilized in the experimental study are representative of four of the five families given on Table 1: Alumina and Quartz (Family 1); Graphite (Family 2); Gas-phase-generated soot from ethylene/oxygen flames (Family 4); Industrial cenospherical soot from heavy fuel oil combustion (Family 5).

2. Increasing complexity of the gas-phase composition:

For this distinction it is useful to distinguish between primary and secondary reactions:

Primary Reactions are reactions in which the reactants are components present in the reactor inlet flow.

Secondary Reactions are reactions in which at least one of the reactants was not present in the reactor inlet flow, but has been formed as a product of a primary reaction. When only one of the reactants is the product of a primary reaction, the coreactant being present in the reactor inlet flow, then the reaction will be called a secondary reaction of first order. When both reactant and coreactant are products of primary reactions, then the secondary reaction is of second order.

In analogy tertiary reactions will be referred to as reactions in which at least one of the reactants is the product of a secondary reaction.

The study of the overall reaction rates of secondary or tertiary reactions usually requires trials in which the products of primary (or secondary) reactions are added into the reactor inlet flow. For this reason, trials have been made in which ammonia and hydrogen cyanide are doped into the inlet gas flow.

3.0 DISCUSSION OF THE EXPERIMENTAL RESULTS

In this main section a twofold task is performed: (1) define the overall reaction paths from the mass balances experimentally obtained under different conditions of gas composition and nature of the solid; (2) determine the overall reaction rates of these reaction paths. Since a rather large number of experimental conditions is to be treated in this section, we preliminarily present a summary:

3.1 Description of the General Method Followed in Deriving the Reaction Rates

3.2 Reactions and Reaction Rates for Each Individual Type of Solid

3.2.1 Trials on Alumina and Quartz (Family 1 Solids)

3.2.2 Trials on Graphite (Family 2 Solids)

3.2.3 Trials on Soot From C_2H_4 (Family 4 Solids)

3.2.4 Trials on Soot From Heavy Fuel Oil (Family 5 Solids)

In each of these four subdivisions are successive discussions of:

(a) Preliminary trials utilizing gas flows without nitrogen containing species.

(b) Trials with gas flows containing nitrogeneous species but no oxygen.

(c) Effect of the presence of molecular oxygen on the nitric oxide reduction mechanisms.

3.1 Method Used for Determination of Reaction Rates

3.1.1 Homogeneous and Heterogeneous Reactions

The first question arising is how to recognize that a given reaction is heterogeneous and not a gas-phase reaction. This problem is not simple. At a first glance one might expect to obtain direct information by performing a trial in an empty reactor (i.e. without solid-packed charge). In most cases, however, the reactor walls are found to catalyze many of the heterogeneous reactions under study. Two typical examples are shown on Figures 2 and 3 where mixtures of NO/H_2 and NO/CO are flowed through both an empty reactor and a reactor charged with soot. In these cases, the

F 2
F 3

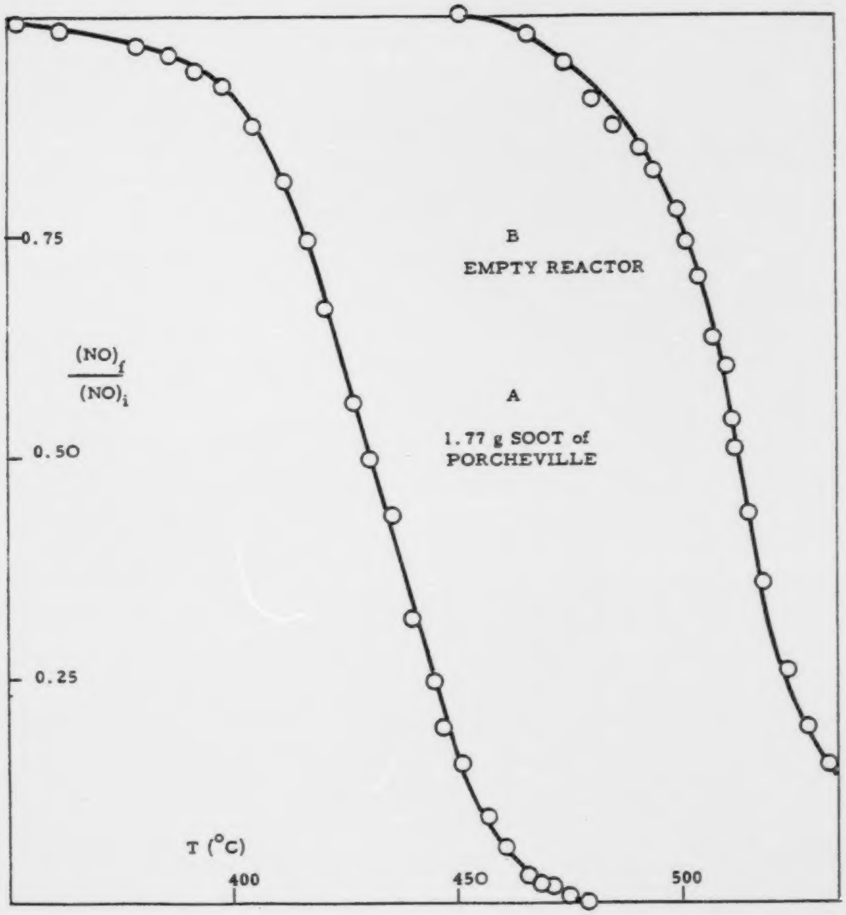

Figure 2. Gas Composition: Ar + 29.17% H_2 + 0.1575% NO; D = 15.3 cm^3s^{-1}.

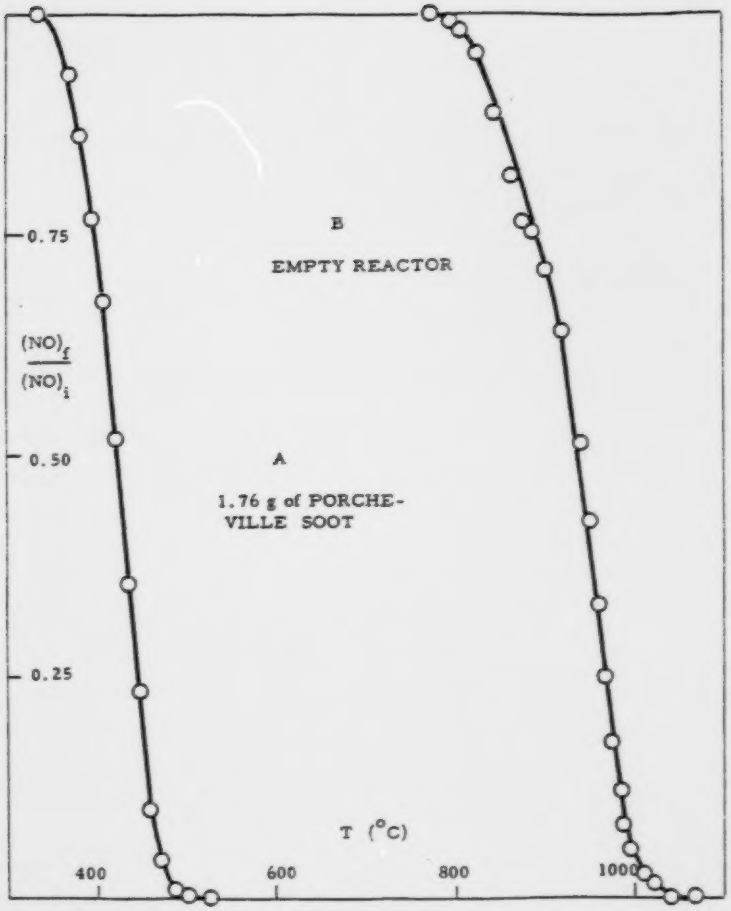

Figure 3. Gas Composition: Ar + 2.10% CO + 0.0108% NO; D = 15 $cm^3 s^{-1}$.

observed difference in NO reduction when the solid packing is removed from the reactor, clearly demonstrates that solid particles are the cause of NO disappearance. However, it is not clear from these experiments whether or not the NO disappearance reaction observed in the empty reactor is of the heterogeneous type. To answer this question, one should also vary the volume/surface ratio of the empty reactor. Fortunately, owing to the relatively high concentrations of the packed solid particles, the heterogeneous reactions taking place at the reactor walls do not interfere with those taking place on the packed solid, as may be seen in Figures 2 and 3, for example.

3.1.2 Determination of Reaction Rates

A. From a theoretical point of view, the most appropriate overall rate expressions should bear reference to the active site theories, utilizing expressions according to an adsorption isotherm, e.g. of Langmuir or Freundlich. Apart from the fact that the derivation of these active site expressions requires a large number of parametric experimental trials, it should be emphasized that, according to Levenspiel (Ref. 15), in most cases simple rate expressions may be as suitable for practical purposes under well-defined conditions. Therefore, owing to the large number of overall reaction rates which are to be determined, we opted to use simple rate expressions of the general form:

$$V = k\, X_n^a\, X_m^b = k_o \exp(-\,\theta/T)\, X_n^a\, X_m^b \qquad (2)$$

where θ is a mean activation temperature; X_n and X_m are the mole fractions of the gaseous reactants; a and b are partial reaction orders.

In only a few simple cases was the packed-bed reactor treated as an integral reactor. In most cases the packed bed was considered as a differential reactor, the reaction rate expressed with respect to the time variation of a species "n" then being given by:

$$V = d(n)/dt = \left[(X_n)_f - (X_n)_i\right] D/M \qquad (3)$$

D being the total flow rate through the reactor at normal temperature and pressure; M is the mass of packed solid. The reaction rates derived in this way have the dimensions of volume/mass/time, and, in the present report, are given in the units: $cm^3g^{-1}s^{-1}$. Actually, both the integral reactor and the differential reactor treatment yield rate constants which are in good agreement under two conditions: (1) the differential reactor treatment was to be limited to small variations of the reactant concentrations, and (2) mean values of the reactant concentrations used in expression (2) are defined as follows:

$$X_n = \left[(X_n)_i + (X_n)_f\right] /2 \qquad (4)$$

B. The general method for determination of primary reaction rates was as follows: (a) as a first step, the partial reaction orders are determined by means of a series of runs in which all parameters (temperature, concentration of gas components, bed packing) are kept constant except the concentration of that component for which the partial order is to be determined; (b) in the second step, the activation temperature (θ) and the preexponential constant, k_o, are determined from a series of runs where only the temperature is progressively increased (normally the temperature was increased stepwise and analysis of the reactor outlet flow was performed ten to fifteen minutes after the new temperature value was reached).

To determine reaction rates for secondary reactions (or for tertiary reactions), two different techniques have been used:

(1) It is preferable to study these secondary reactions under experimental conditions where they actually become primary reactions. This was accomplished by blending that reactant, which was a product from a primary reaction, directly into the initial reactor inlet flow. In this way, the rate constant and the partial orders can be determined in exactly the same manner as in the case of a true primary reaction.

(2) In exceptional cases, the rate constant determination was made from the results of trials where the reaction was a true secondary reaction. In that case, the method involved three steps: (a) From parametric trials where all but the temperature are kept constant, the reaction rate, V, is determined by eq. (3). This results in a number of ln (V) versus 1/T(K) curves, each of which corresponds to a given concentration of these primary reactants, the reaction of which leads to the formation of the reactant of the secondary reaction under consideration; (b) by successive converging trials, a best fit value of the partial orders of the secondary reaction is determined; (c) finally, in a last step utilizing the so-derived partial orders, the activation temperature (θ) and the preexponential rate constant (k_0) are obtained from an Arrhenius plot, using all the available experimental points.

Actually this latter, rather imprecise, method has only been utilized for the determination of one or two secondary reactions involving hydrogen cyanide as a reactant, since, in that phase of the program, no HCN was available. Since secondary reactions involving HCN will be studied later using the more precise first method, they will be included in the present report only in a few exceptional cases (e.g. determination of V_{15} and V_{10} on Alumina).

C. Table 2 summarizes the individual reaction paths treated separately in Table 1. In addition, it is of interest to determine overall NO formation and destruction rates.

(1) The overall NO disappearance rate (designated by the symbol $\overline{V}$) is obtained directly from the experimental values:

$$\overline{V} = \left[(X_{NO})_f - (X_{NO})_i\right] \; D/M \tag{5}$$

and is expressed as a function of the concentrations of reactants present in the reactor inlet flow (e.g. NO and CO):

$$\overline{V}_K = k \, X_{NO}^a \, X_{CO}^b$$

Table 2. List of Heterogeneous Reactions Appearing in Table 1

REACTION N°:	REMARKS
1. $NO + a\ (-C) \rightarrow 0.5\ N_2 + (2a-1)\ CO + (1-a)\ CO_2$ $(0.5 \leqslant a \leqslant 1)$	ratio $(CO)/(CO_2)$ in the reaction products depends on the temperature and on the nature of soot
2. $NO + a\ (-C) + b\ (-H) \rightarrow NH_3 + \left(\frac{b-5}{2} + 2a\right) CO + \left(\frac{5-b}{2} - a\right) CO_2 + \frac{b-3}{2}\ H_2O$ $(0 \leqslant a \leqslant 1\ ;\ 5 \geqslant b \geqslant 3)$	
4. $NO + nNH_3 \rightarrow \left(\frac{1+n}{2}\right) N_2 + H_2O + \left(\frac{3n-2}{2}\right) H_2$	the true stoichiometry of this reaction path seems to be situated between 4a and 4b
4a. $NO + 0.67\ NH_3 \rightarrow 0.83\ N_2 + H_2O$	
4b. $NO + NH_3 \rightarrow N_2 + H_2O + 0.5\ H_2$	
5. $NH_3 + (-C) \rightarrow HCN + H_2$	
6. $CO + NO + 3\ (-H) \rightarrow NH_3 + CO_2$	some indication seems to exist for this reaction path to be considered as distinct from reaction (2)
8. $CO + NO \rightarrow 0.5\ N_2 + CO_2$	
9. $NH_3 + CO \rightarrow HCN + H_2O$	
10. $NH_3 + HCN \rightarrow N_2 + \ldots$	(existence to be checked)
11. $NO + 2.5\ H_2 \rightarrow NH_3 + H_2O$	
12. $CO + (-O) \rightarrow CO_2$	
13. $NH_3 \rightarrow 0.5\ N_2 + 1.5\ H_2$	
14. $NO + H_2 \rightarrow 0.5\ N_2 + H_2O$	**See Part III**
15. $HCN \rightarrow 0.5\ N_2 + \ldots$	(not studied until now)
16. $NH_3 + 0.75\ O_2 \rightarrow 0.5\ N_2 + 1.5\ H_2O$	
17. $NH_3 + 1.25\ O_2 \rightarrow NO + 1.5\ H_2O$	
18. $H_2 + 0.5\ O_2 \rightarrow H_2O$	at temperatures beyond 500°C may become a gas phase reaction with explosive character
19. $H_2 + (-O) \rightarrow H_2O$	has not been checked, but is assumed in analogy with (12)

Table 2. List of Heterogeneous Reacrions Appearing in Table 1 (Continued)

REACTION PATH N°:	REMARKS
20. $CO + 0.5\ O_2 \rightarrow CO_2$	may become an explosive gas phase reaction
21. $0.5\ H_2 + (-N) \rightarrow NH_3$	
22. $H_2 + (-N) + (-C) \rightarrow HCN$	
23. $0.5\ O_2 + 2\ (-H) \rightarrow H_2O$	has not been checked, but assumed in analogy with (24)
24. $O_2 + (-C) \rightarrow CO,\ CO_2$	the ratio $(CO)/(CO_2)$ in the reaction products depends on temperature and nature of soot
25. $0.5\ O_2 + (-N) \rightarrow NO$	
26. $NH_3 + (-N) \rightarrow N_2 + 1.5\ H_2$	with the actual equipment, this reaction path cannot be distinguished from reaction path (13)
27. $HCN + (-N) \rightarrow N_2 + \ldots$	this reaction path cannot be distinguished from (15)
28. $NO + (-N) + (-C) \rightarrow N_2 + CO$	to check the existence of this reaction path, the N balance would be required; (28) has been disregarded
29. $CO + (-H) + (-N) \rightarrow HCN + \ldots$	has not been observed (below 1100°C)
30. $2\ CO \rightarrow CO_2 + C$	has not been observed
31. $NH_3 + (-O) \rightarrow NO + 1.5\ H_2$	has not been observed (below 1100°C)
32. $NO \rightarrow 0.5\ O_2 + 0.5\ N_2$	has not been observed (below 1100°C)
33. $2\ NO \rightarrow NO_2 + 0.5\ O_2$	has not been observed
34. $HCN + (-O) \rightarrow NO + \ldots$	has not been checked, but is not more probable than (31) in reducing medium
35. $NO + (-H) + (-C) \rightarrow HCN + \ldots$	has not been observed
36. $H_2 + HCN \rightarrow NH_3 + \ldots$	(still to be checked)
37. $NO + 0.5\ O_2 \rightarrow NO_2$	not observed at these elevated temperatures
38. $HCN + n\ O_2 \rightarrow N_2,\ NO,\ H_2O,\ CO,\ CO_2$	(still to be checked)
39. $CO + H_2 \rightarrow H_2O + C$	

Table 2. List of Heterogeneous Reactions Appearing in Table 1 (Continued)

REACTION PATH N°:	REMARKS
40. $HCN + NO \rightarrow N_2 + \ldots$	(still to be checked)
42. $CO_2 + H_2 \rightarrow CO + H_2O$	
44. $HCN + H_2O \rightarrow NH_3 + CO$	(reverse reaction of 9 ; still to be checked)
45. $HCN + H_2 \rightarrow NH_3 + \ldots$	(still to be checked)

Remark: 1) Reactants placed between brackets (e.g. (-C), (-H), (-N) etc.) are solid bound atoms

2) The numbering of the different reaction paths is the same as in the previous partial reports

The subscript "K" refers to the row on Table 1, and is generally accompanied by a number (1 to 5) indicating the column of Table 1.

The rate constant and partial orders of this overall NO disappearance reaction are obtained by the method described previously for primary reactions. Attention is focused once again on the fact that the overall NO disappearance rate, although interesting to characterize a given solid particle, is not a good criteria from the point of view of pollution control (see Introduction).

(2) The overall N_2 formation reaction designated by symbol $\overline{V}_n$, is an excellent antipollution criteria as explained in the Introduction; therefore, its knowledge is of some practical interest. This rate can be obtained in either of two ways:

(a) It may be obtained directly from the experimental value of the time variation of all the other present nitrogen-containing species, i.e. by time derivation of equation 1:

$$\overline{V_n} = d(N_2)/dt = \frac{D}{2\,M}\Big[(X_{NO})_i + (X_{NH_3})_i + (X_{HCN})_i - (X_{NO})_f - (X_{NH_3})_f - (X_{HCN})_f\Big] \quad (6)$$

This rate might also be expressed as a function of the active reactants concentrations present in the reactor inlet flow.

(b) A second approach is to take the algebraic sum of all the reaction rates which play a role in the formation of molecular nitrogen, as indicated in section 3.2 for each individual case.

D. Special attention should be focused on the fact that quantitative information on the different reaction rates derived in this work are obtained under conditions (especially: residence time of the solid particles at a given temperature and contact duration with a gas phase of given composition) for which the adsorption/desorption rates are almost equilibrated. Under practical conditions of a dispersed solid phase "in situ" in industrial flames or in their flue gases, these equilibria are seldom reached. The consequences of nonequilibrium conditions with respect to reaction rates of heterogeneous NO reduction should be carefully checked whenever modeling is performed on "in situ" behavior of the dispersed particles existing in flame products.

3.2 Identification of Reaction Paths and Determination of Reaction Rates

3.2.1 Trials on Alumina and Quartz (Family 1 Solids)

A thorough investigation has been made utilizing Alumina as a solid packing. In a few cases comparison has been made with Quartz particles.

3.2.1.1 Gas Flows Without Nitrogen-Containing Species

In this family of solids, special attention was paid to solid bound oxygen atoms, which may play a role in oxidizing gaseous reducing agents (e.g. hydrogen or carbon monoxide). Due to the relatively high bond energy of the oxygen atoms in refractory oxides, reactions of that type are expected to be rather slow compared to the oxidation by free oxygen molecules.

3.2.1.1.1 Argon + CO on Alumina (Case B.1)*

The oxidation of carbon monoxide by solid bound oxygen according to the expression:

$$CO + (-O) \xrightarrow{12} CO_2$$

or, more specifically in the case of alumina:

$$3\ CO + Al_2O_3 \longrightarrow 3\ CO_2 + 2\ Al$$

shows an appreciable rate at temperatures beyond 500°C, as may be seen for example from Figure 4. The experimental observed mass balance:

$$(CO)_i - (CO)_f = (CO_2)_f \tag{7}$$

---

*The different trials are characterized by a letter followed by a number, referring respectively to the ROW and the COLUMN of Table 1.

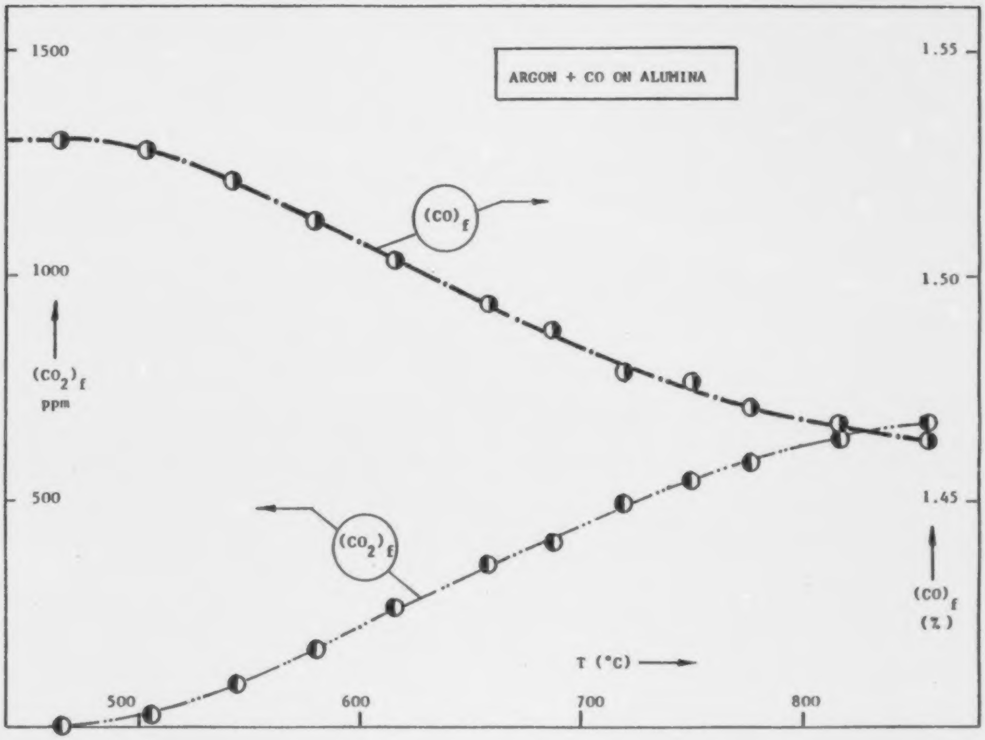

Figure 4. Argon + CO on Alumina: D = 14.7 cm^3s^{-1}; $(CO)_i$ = 1.53%.

proves that CO disappears effectively and exclusively be reaction (12) and not by the alternative one:

$$CO + CO \xrightarrow{30} CO_2 + C$$

Reaction (12) slows down with time, since the metal (aluminum) formed by reduction of the solid support progressively replaces the aluminum oxide at the surface of the particles. This is clearly seen from Figure 5, showing the evolution of $(CO)_f$ and $(CO_2)_f$ as a function of time at constant-bed temperature. No attempt has been made to determine the rate of reaction (12), since its interference with the NO reduction (resulting from the CO consumption) will be accounted for in every case by measuring the instantaneous value of $(CO)_f$. On the contrary, the effect of reaction (12) on the alteration of the chemical nature of the solid surface, could only be minimized by changing the bed after each trial.

3.2.1.1.2 Argon + H_2 on Alumina (Case C.1)

Oxidation of H_2 by solid bound oxygen according to reaction (19):

$$H_2 + (-O) \xrightarrow{19} H_2O$$

or, more specifically in the case of alumina:

$$3\ H_2 + Al_2O_3 \longrightarrow 3\ H_2O + 2\ Al$$

is assumed to take place in analogy with reaction (12). It was not possible to get sufficient quantitative information on the importance of this reaction, since the available H_2 analysis method (gas chromatography) did not allow sufficient precision. For this reason, a continuous, quantitative measure of the instantaneous value of $(H_2)_f$ was not attempted. However, the perturbing effect of this unknown decrease of $(H_2)_f$ due to reaction (19), has been minimized in two ways: (a) by using sufficiently large initial concentrations $(H_2)_i$ whenever it was used as a gas component, and (b) by waiting a sufficiently long time between the change of the bed temperature and the measurement. This insured that the measurement was taken under conditions where the rate of this H_2 decrease was beginning to level off (due to progressive coating of the surface by the aluminum metal formed (see Figure 5).

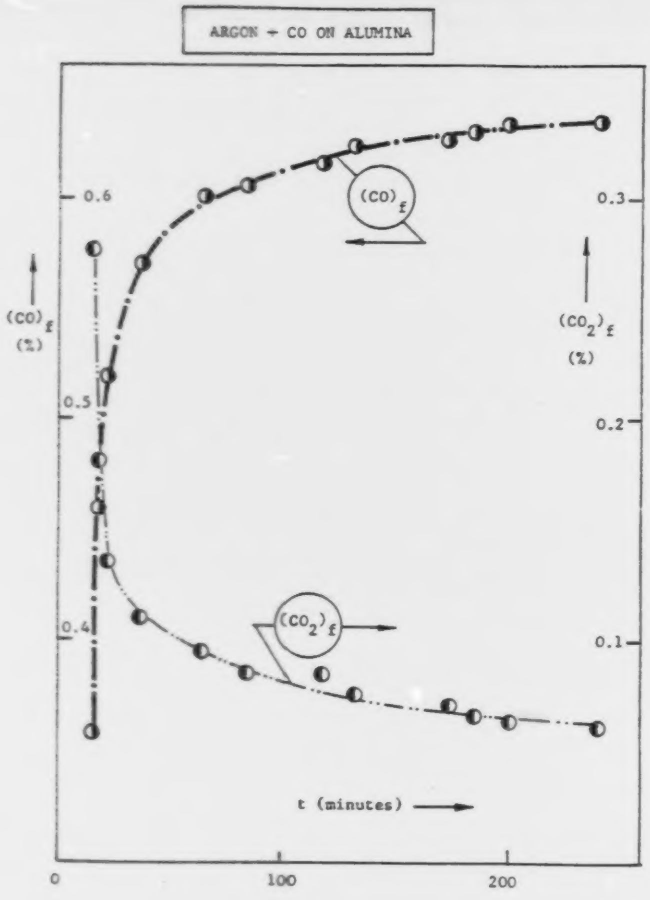

Figure 5. Argon + CO on Alumina: D = 14.7 cm^3s^{-1}; $(CO)_i$ = 1.53%.

3.2.1.1.3 Argon + CO + H_2 on Alumina (Case H.1)

In these trials, one observes a progressive decrease of CO as a function of temperature (see Figure 6) as in case B.1, but no CO_2 is formed at all. This can only be explained by the existence of an overall reaction between hydrogen and carbon monoxide, corresponding to the following mass balance (although other CHO compounds might eventually be formed):

F6

$$CO + H_2 \xrightarrow{39} H_2O + C$$

Since we also have to assume the existence of reactions (12) and (19), we have to postulate another reaction path which is responsible for the removal of CO_2 formed by reaction (12), e.g.:

$$CO_2 + H_2 \overset{42}{\text{------}} CO + H_2O$$

Taking into account reactions (12), (19), (39), and (42), the variation of CO and CO_2 concentrations may be written as follows:

$$d(CO)/dt = -V_{12} - V_{39} + V_{42} \qquad (8)$$

$$d(CO_2)/dt = V_{12} \qquad -V_{42} \qquad (9)$$

Since no CO_2 is formed at all, eq. (9) is equal to zero, and hence $V_{12} = V_{42}$. Substitution of the latter equality into eq. (2) yields:

$$d(CO)/dt = V_{39} \qquad (10)$$

If we assume that 39 is first order with respect to CO and H_2 concentration, we obtain the following value for the rate constant of V_{39}:

$$\boxed{k_{39} = 1.0 \text{ to } 3.5 \times 10^3 \exp\left[-5000(\pm 750)/T\right]} \qquad (11)$$

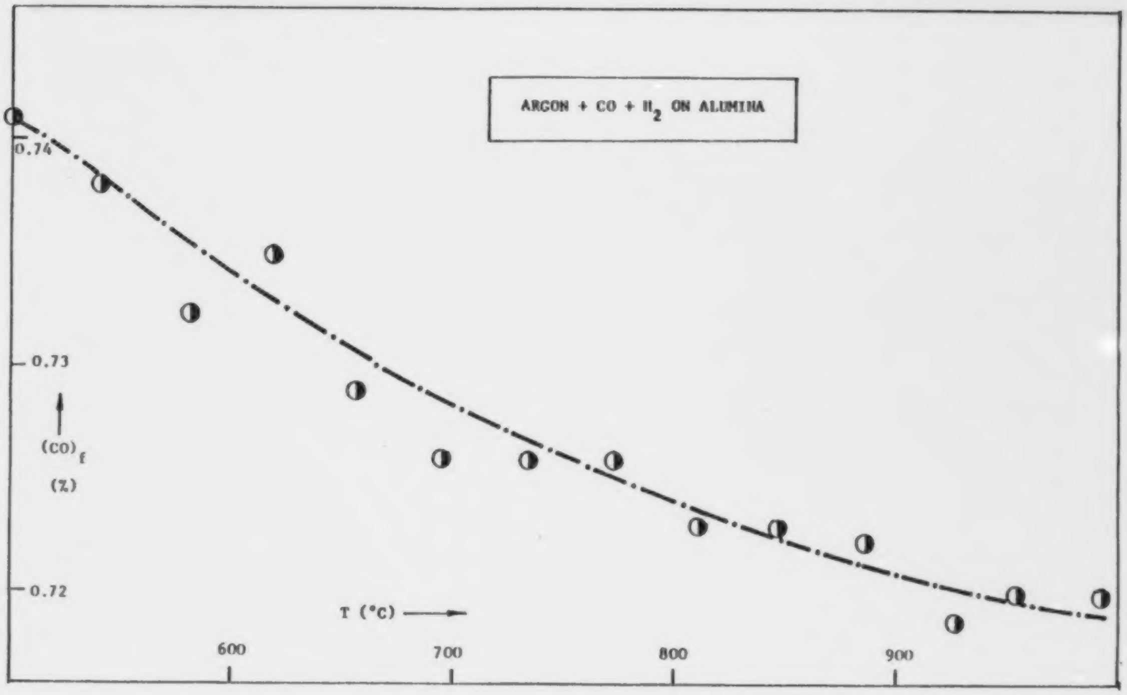

Figure 6. Argon + H_2 + CO on Alumina: D = 14.3 cm^3s^{-1}; $(H_2)_i$ = 0.62%; $(CO)_i$ = 0.74%.

3.2.1.1.4 Argon + CO + O_2 on Alumina (Case J.1)

With the addition of O_2 to the input gas stream with CO, reaction (12) competes with the other CO oxidizing reaction path:

$$CO + 0.5\ O_2 \xrightarrow{20} CO_2$$

However, from the mass balance it may be seen that reaction (12) becomes negligible compared with reaction (20); indeed, it is found experimentally that:

$$(CO)_i - (CO)_f = (CO_2)_f = \left[(O_2)_i - (O_2)_f\right] /2 \qquad (12)$$

Examples of these trials are shown on Figures 7 through 10. From Figures 9 and 10 it is seen that this reaction becomes very fast when oxygen and/or carbon monoxide are sufficiently large. This indicates that this is primarily a rapid oxidation or combustion taking place mainly in the gas phase.

F7 – F10

The following reaction rate has been derived for oxidation reaction (20) (see Figure 11):

F11

$$\boxed{V_{20} = -d(CO)/dt = 9.0\ 10^8 \exp\left[-20400(\pm 2000)/T\right] X_{O_2}^{0.5}\ X_{CO}^{0.25}} \qquad (13)$$

3.2.1.1.5 Argon + H_2 + O_2 on Alumina (Case N.1)

By analogy with the carbon monoxide oxidation, it is assumed that reaction path (19) is neglibible when compared with the oxidation by gaseous oxygen, given by:

$$H_2 + 0.5\ O_2 \xrightarrow{18} H_2O$$

As in the foregoing case, the oxidation according to reaction (18) demonstrates a twofold behavior:

A. At temperatures below 520°C, it behaves as a rather slow reaction, eventually of catalytic nature. Under these conditions an approximate overall reaction rate has been determined. The partial reaction orders are relatively imprecise:

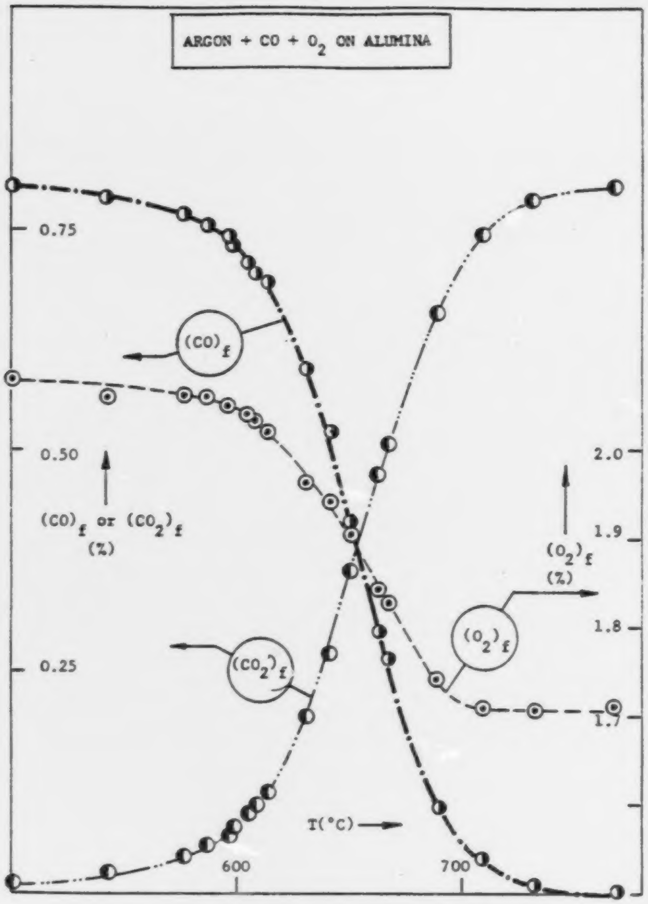

Figure 7. Argon + CO + O_2 on Alumina: D = 13.6 $cm^3 s^{-1}$; $(CO)_i$ = 0.81%; $(O_2)_i$ = 2.08%.

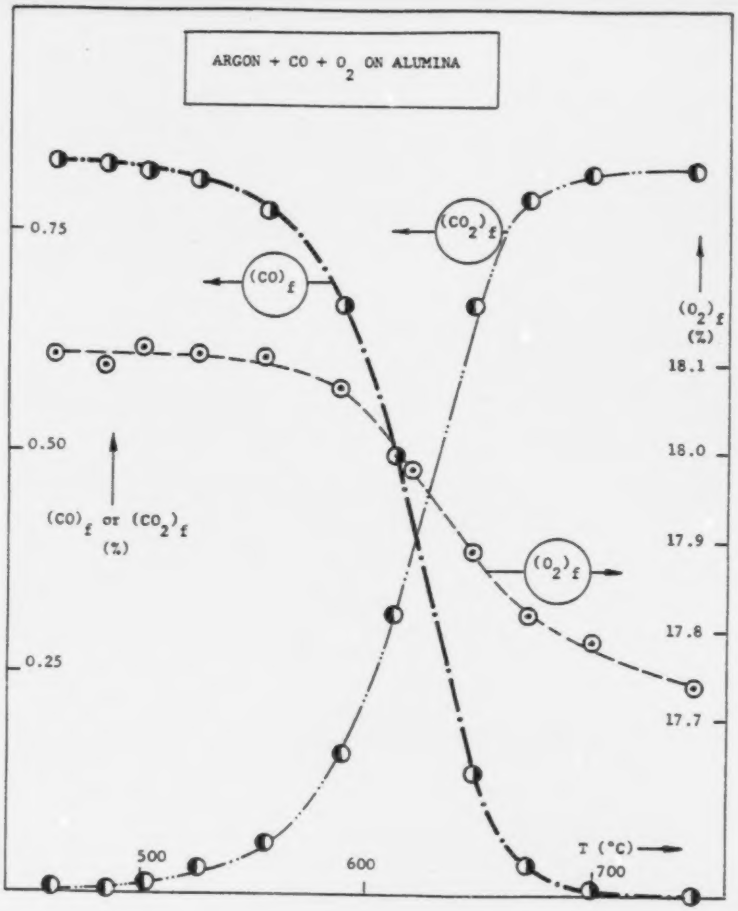

Figure 8. Argon + CO + O_2 on Alumina; D = 13.6 $cm^3 s^{-1}$; $(CO)_i$ = 0.85%; $(O_2)_i$ = 18.11%.

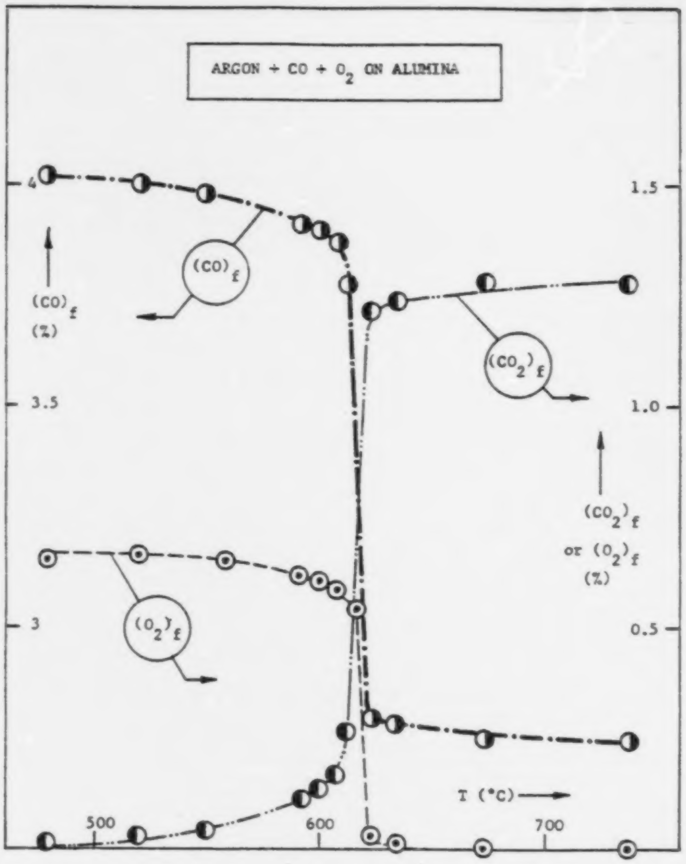

Figure 9. Argon + CO + O_2 on Alumina: D = 13.8 cm^3s^{-1}; $(CO)_i$ = 4.02%; $(O_2)_i$ = 0.67%.

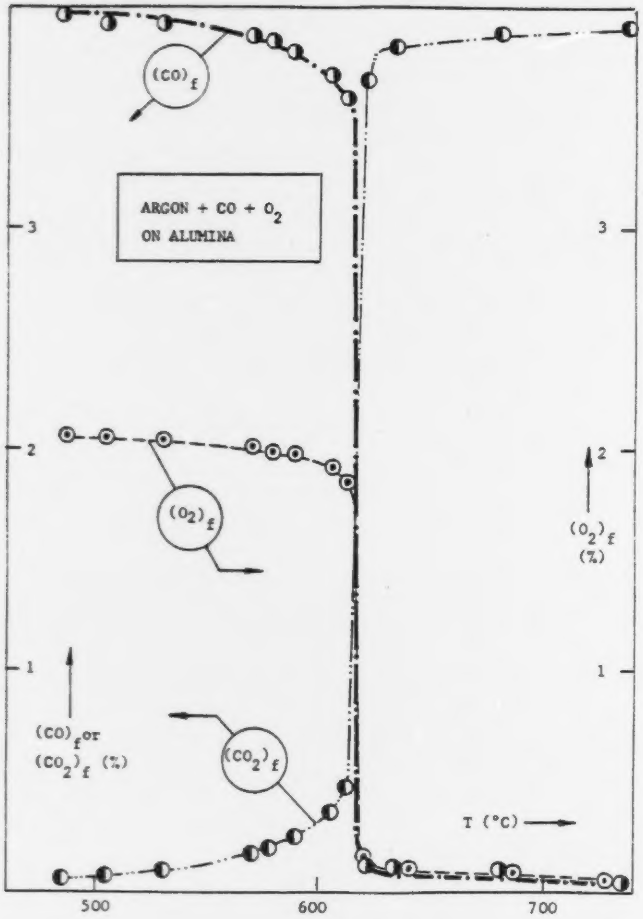

Figure 10. Argon + CO + O_2 on Alumina; D + 13.6 cm^3s^{-1}; $(CO)_i$ = 4.00%; $(O_2)_i$ = 2.12%.

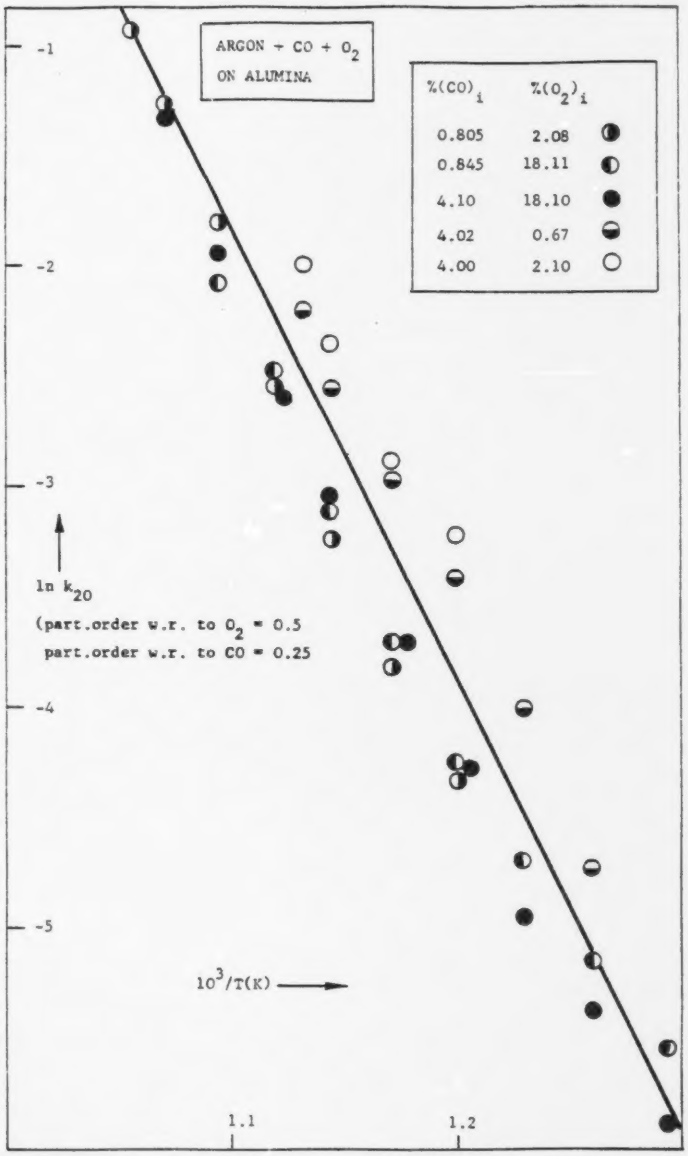

Figure 11. Determination of Rate Constant k_{20} on Alumina; Different Initial Concentrations of CO and O_2.

$$\boxed{V_{18} = -d(H_2)/dt = 1.7 \times 10^2 \text{ to } 1.6 \times 10^3 \exp[9000(\pm 500)/T]\, X_{O_2}^a\, X_{H_2}^b}$$

(14)

where: $-1 \leq a \leq -0.75$
$1 \leq b \leq 1.4$

The negative partial reaction order with respect to oxygen may be explained in different ways:

(1) By a gas-phase chain branching reaction, oxidations of that type often show negative partial reaction orders with respect to the initial reactants;*

(2) In case it is a heterogeneous reaction, by the assumption that the reaction takes place between an oxygen molecule and a hydrogen molecule, both absorbed on the solid surface, but O_2 being more strongly absorbed than H_2 and H_2O.

B. At temperatures beyond 520°C and significant concentrations of H_2 and/or O_2, the reaction becomes very fast (see e.g. Figure 12). Eventually this will be a rapid gas-phase oxidation of explosive character (or combustion), which may even develop in the freeboard at the top of the bed. At the end of this fast oxidation, an excess of O_2 or H_2 is left, the deficient reactant having disappeared almost completely, according to whether the ratio $(H_2)_i/(O_2)_i$ is smaller or larger than 2.

3.2.1.2 Gas Flows Containing Nitrogen Species but no Oxygen

3.2.1.2.1 Argon + NO on Alumina (Case F.1)

No nitric oxide reduction was observed whatsoever in these trials, at least at the utilized experimental conditions (especially T<1100°C); therefore, reaction (32)

$$NO \xrightarrow{32} 0.5\ O_2 + 0.5\ N_2$$

---

*See, e.g. Van Tiggelen, A. and Cow.- "Kinetical Parameters in Premixed Laminar Flames," Monitoring Agency Document: AFOSR-TN 59-1149, February 1960.

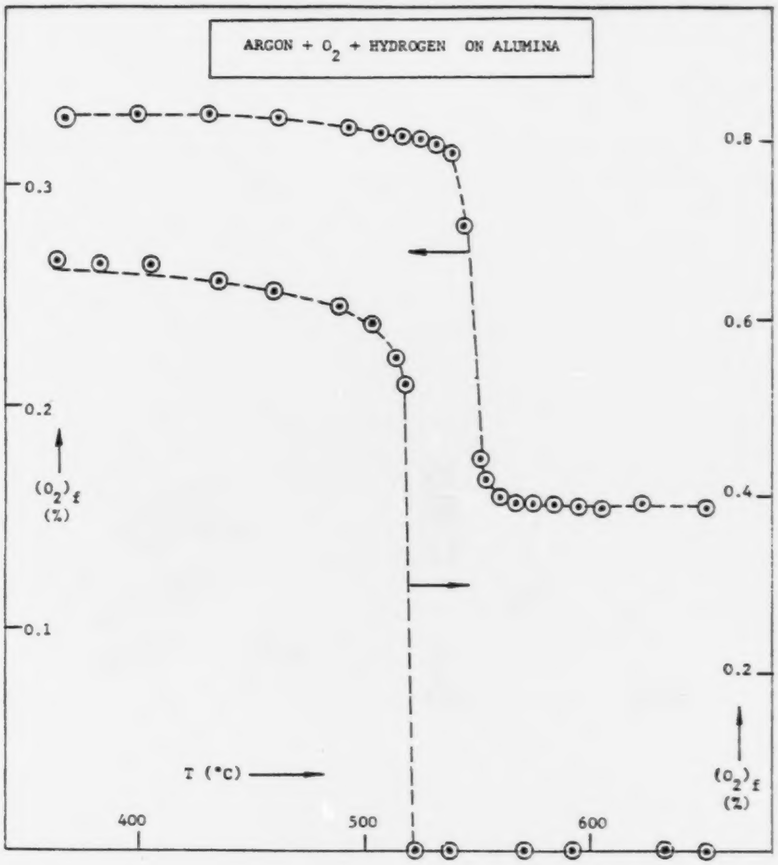

Figure 12. Argon + H_2 + O_2 on Alumina: Upper curve: D = 13.7 cm^3s^{-1}; $(H_2)_i$ = 0.35%; $(O_2)_i$ = 0.33%. Lower curve: D = 13.4 cm^3s^{-1}; $(H_2)_i$ = 1.56%; $(O_2)_i$ = 0.70%.

may be completely neglected in all trials performed on Alumina or Quartz. It will be hardly worthwhile to be mentioned, that reaction (33) was also nonexistent under the experimental conditions of these trials, since at these temperatures the equilibrium NO/NO_2 is completely shifted towards NO.

3.2.1.2.2 Argon + NH_3 on Alumina (Case D.1)

Some typical results of this trial series are shown on Figure 13 for two different initial ammonia concentrations. No nitric oxide has been observed in the reactor outlet flow over the whole temperature range (200 to 1100°C). Therefore it has been assumed that reaction

$$NH_3 + (-O) \xrightarrow{31} NO + 1.5\ H_2O$$

is nonexistent or at least negligible under these experimental conditions. We also provisionally disregard, for the same reason, the analogous reaction with hydrogen cyanide:

$$HCN + (-O) \xrightarrow{34} NO + \ldots$$

Of course, this reaction yields hydrogen as a reaction product and therefore also brings reaction (19) into the mechanism, but this reaction does not directly change the pool of nitrogen-containing species. Moreover, for relatively small advancements of reaction (13), the hydrogen concentrations are sufficiently small for reaction (19) to be disregarded.

Therefore, the time derivative of the ammonia concentration is given by the expression:

$$-d(NH_3)/dt = 2\ d(N_2)/dt = V_{13} \qquad (15)$$

The partial reaction order "a" with respect to ammonia was difficult to determine with precision. Values between 0.5 and 1.0 were determined. Determination of V_{13} has been made with both the differential reactor and with the integral reactor hypothesis. Both treatments yielded comparable rate expressions:

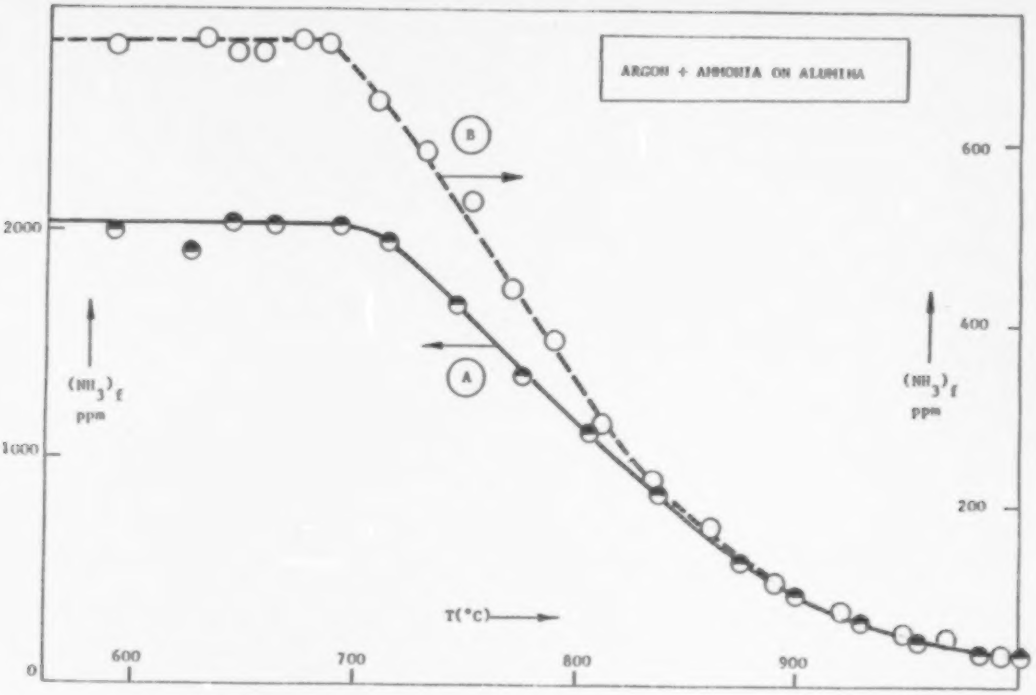

Figure 13. Argon + Ammonia on Alumina: Lower Curve (A): $D = 14.6\ cm^3 s^{-1}$; $(NH_3)_i = 2030$ ppm. Upper Curve (B): $D = 15.0\ cm^3 s{-1}$; $(NH_3)_i = 715$ ppm.

Differential reactor calculations indicated:

$$\boxed{\begin{array}{l} V_{13} = 1.6 \text{ to } 2.5\ 10^5 \exp[-16600(\pm 750)/T]\ X_{NH_3}^{0.5} \\ V_{13} = 4.8 \text{ to } 9.0\ 10^6 \exp[-16700(\pm 750)/T]\ X_{NH_3} \end{array}}$$

(16)

(17)

Integral reactor calculations indicated:

$$\boxed{\begin{array}{l} V_{13} = 4.8\ 10^6 \exp[-18000(\pm 750)/T]\ X_{NH_3}^{0.5} \\ V_{13} = 2.0 \text{ to } 4.0\ 10^8 \exp[-18600(\pm 750)/T]\ X_{NH_3} \end{array}}$$

(18)

(19)

Some comparative trials have been made on electroquartz. The rates determined on these solid particles show good agreement with respect to the temperature dependence of reaction (13). The preexponential part of the rate constant for quartz is about ten times smaller than that determined with alumina. For electroquartz one thus finds:

$$V_{13} = 2.8\ 10^4 \exp[-16600(\pm 800)/T]\ X_{NH_3}^{0.5} \quad \text{or} \tag{20}$$

$$V_{13} = 5.1\ 10^5 \exp[-16700(\pm 800)/T]\ X_{NH_3} \tag{21}$$

3.2.1.2.3 Argon + NO + CO on Alumina (Case K.1)

Trials of this series are illustrated in Figures 14, 15, and 16. As may be easily seen from these figures, the following mass balance is experimentally observed:

$$(CO)_i - (CO_f) = (CO_2)_f \tag{22}$$

$$(CO)_i - (CO)_f \leq (NO)_i - (NO)_f \tag{23}$$

These two experimental balances are exactly accounted for by the existence of both reactions (12) and (8). Since reaction (12) does not change the pool concentration of nitrogen species (NH_3 and N_2, in this case), we may write (taking the precautions indicated previously in section 3.2.1.1.1):

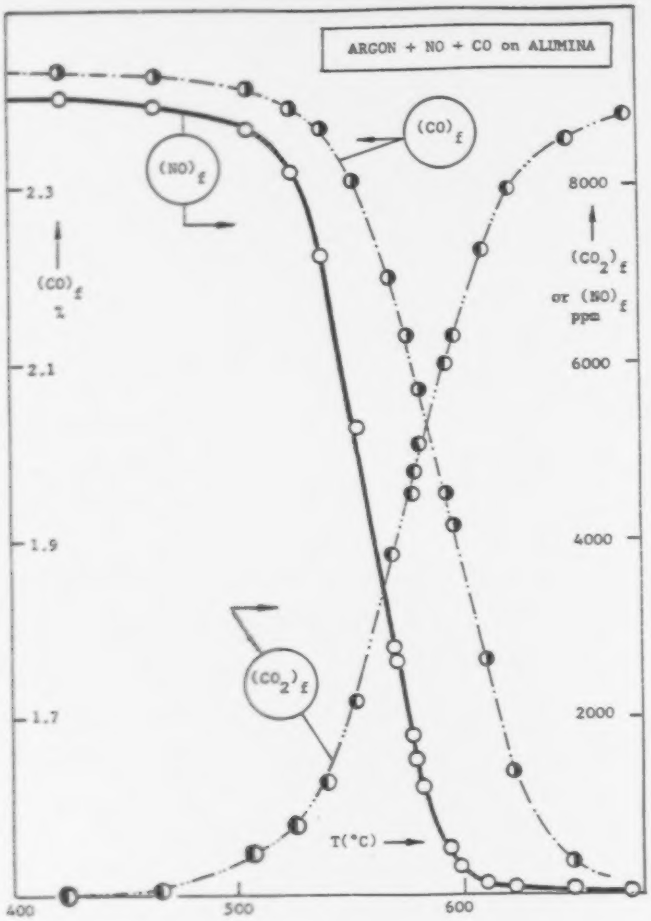

Figure 14. Argon + NO + CO on Alumina: $D = 14.8\ cm^3 s^{-1}$; $(NO)_i = 9000$ ppm; $(CO)_i = 2.44\%$.

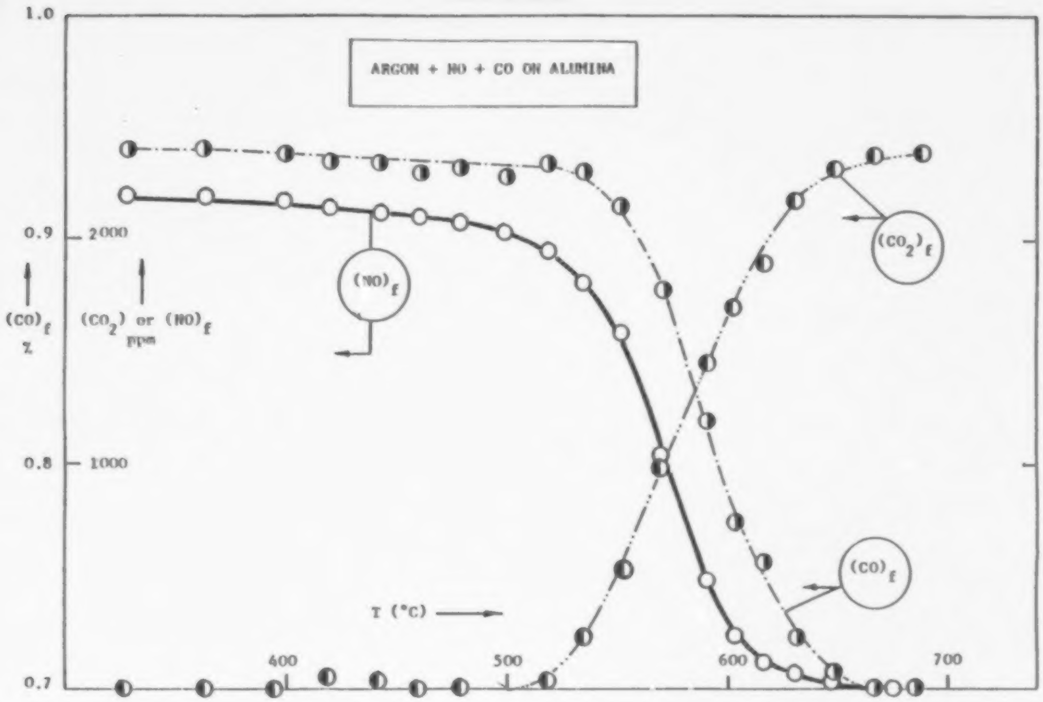

Figure 15. Argon + NO + CO on Alumina; D = 14.4 $cm^3 s^{-1}$; $(NO)_i$ = 2200 ppm; $(CO)_i$ = 0.94%.

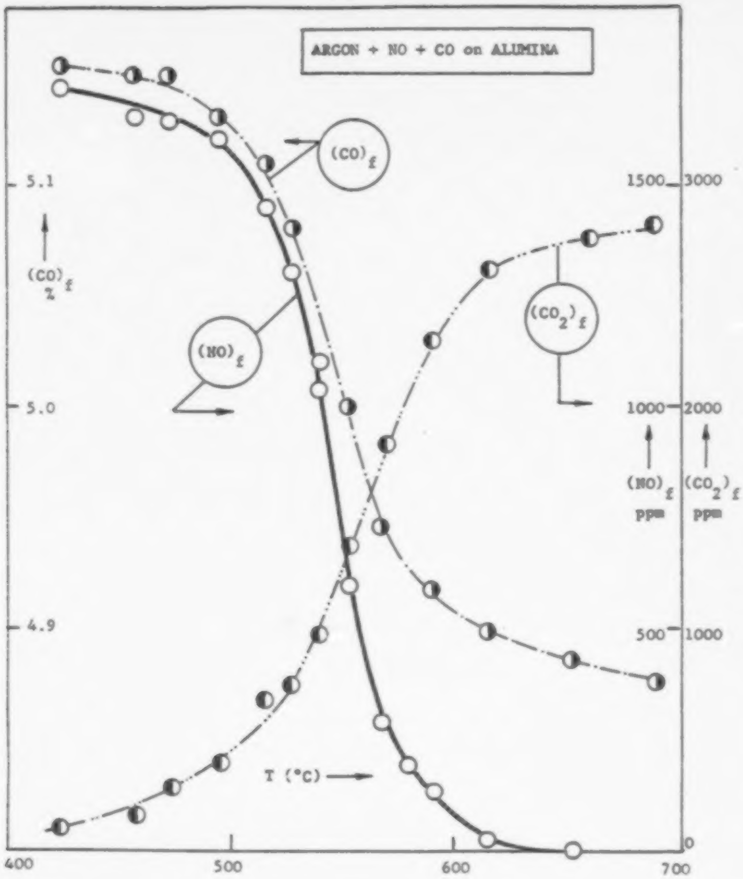

Figure 16. Argon + NO + CO on Alumina: D = 14.0 cm^{3}s^{-1}; (NO)$_i$ = 1760 ppm; (CO)$_i$ = 5.16%.

$$-d\,(NO)/dt = 2\,d\left(N_2\right)/dt = V_8 \qquad (24)$$

Application of the differential bed calculation yields the following overall rate expression (see Figure 17):

$$\boxed{V_8 = 5.1 \text{ to } 7.3\ 10^8 \exp\left[-15800(\pm 1000)/T\right] X_{NO}\, X_{CO}^{0.3}} \qquad (25)$$

3.2.1.2.4 Argon + NH_3 + CO on Alumina (Case 1.1)

Of all the trial series mentioned up to now, this is the first for which there is simultaneously a hydrogen source, a carbon source and a nitrogen source. It is therefore not surprising to find the formation of hydrogen cyanide as is illustrated in Figures 18 through 21. The following specific experimental observations have been made:

- NH_3 and CO decrease simultaneously, whereas HCN and CO_2 increase. Only at higher temperatures is molecular nitrogen $\left(N_2\right)$ formed in appreciable quantities. Variation of NH_3, HCN, CO and CO_2 begins at about 500°C, whereas hardly any N_2 is formed under 600°C.
- The formation of NO is not observed over the entire temperature range. This suggests that reaction 31 is negligible (see section 3.2.1.2.2) and also that the formation of NO by the reaction of CO with NH_3 or HCN is excluded.

The oxygen unbalance:

$$\left(CO\right)_i - \left(CO\right)_f > \left(CO_2\right)_f \qquad (26)$$

observed experimentally, together with the fact that reaction (30) does not exist under the given conditions (see section 3.2.1.1.1), indicates that part of the oxygen from the CO reactant goes into a reaction product other than CO_2 or NO, viz. into H_2O. Another possibility would be CH_2O, but we shall provisionally omit this hypothesis.

- Except for very small values of CO_i, there is also a carbon unbalance expressed by:

$$\left(CO\right)_i > \left(CO\right)_f + \left(CO_2\right)_f + \left(HCN\right)_f\ . \qquad (27)$$

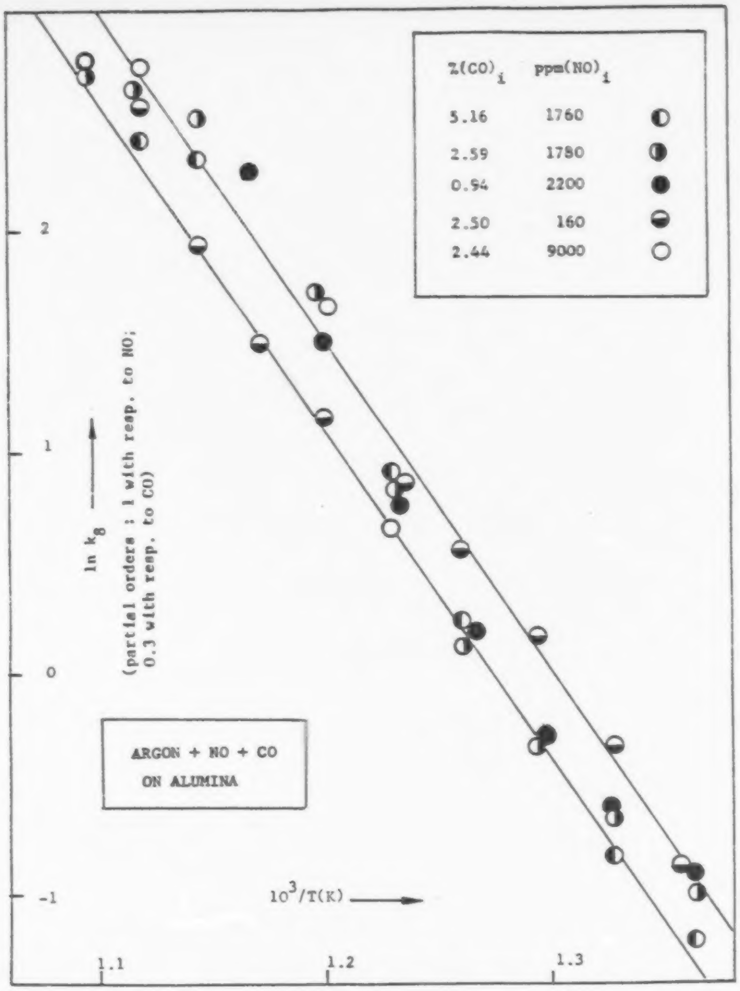

Figure 17. Argon + NO + CO on Alumina: Determination of the Rate Constant k_8 According to eq. (24), For Different Initial Concentrations of NO and CO.

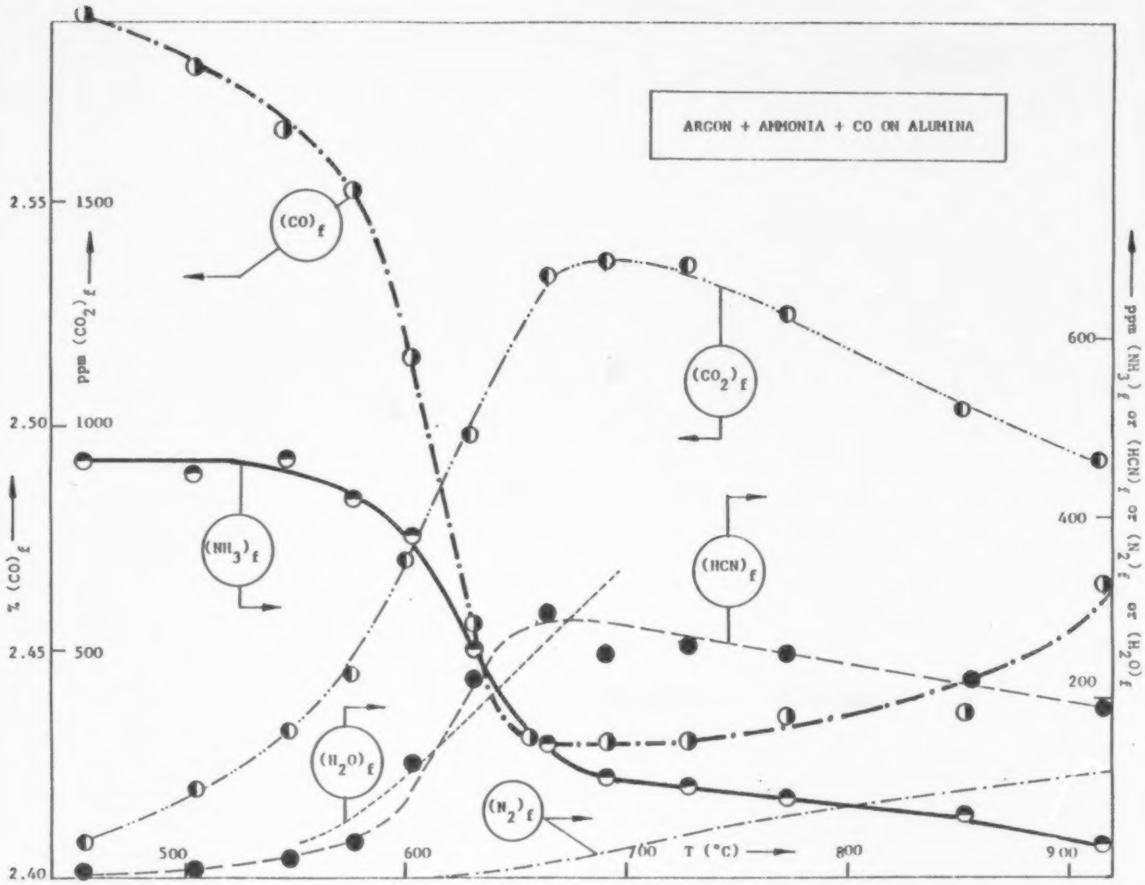

Figure 18. Argon + Ammonia + CO on Alumina: D = 13.9 cm^3s^{-1}; $(NH_3)_i$ = 475 ppm; $(CO)_i$ = 2.59%.

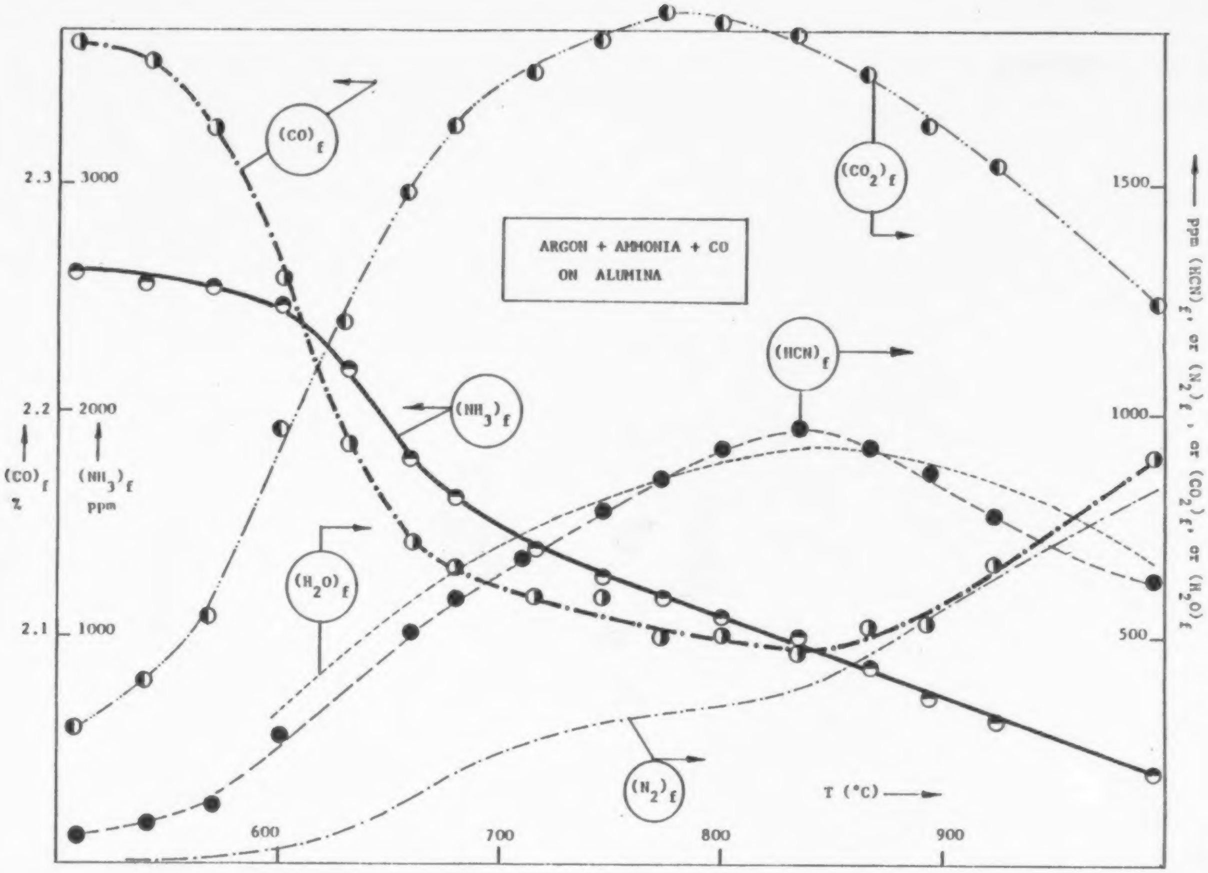

Figure 19. Argon + Ammonia + CO on Alumina: D = 14.5 $cm^3 s^{-1}$; $(CO)_i$ = 2.37%; $(NH_3)_i$ = 2700 ppm.

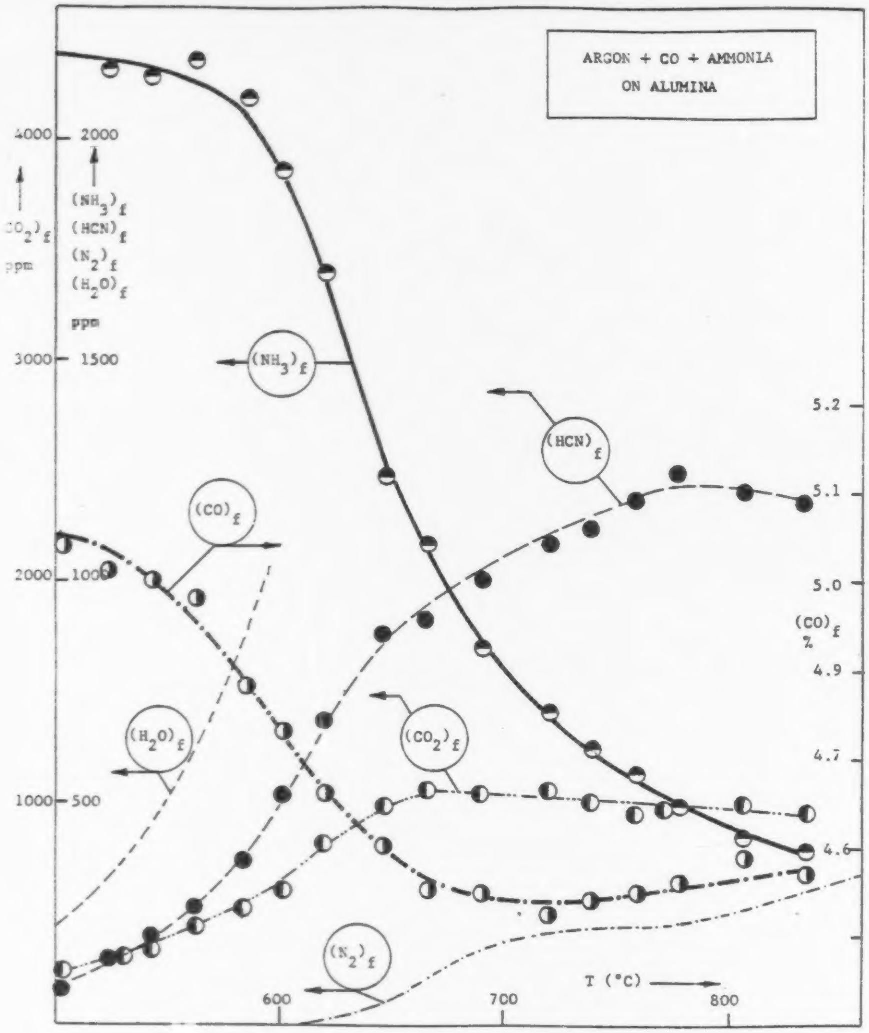

Figure 20. Argon + Ammonia + CO on Alumina: D = 14.2 cm^3s^{-1}; $(NH_3)_i$ = 2400 ppm; $(CO)_i$ = 5.09%.

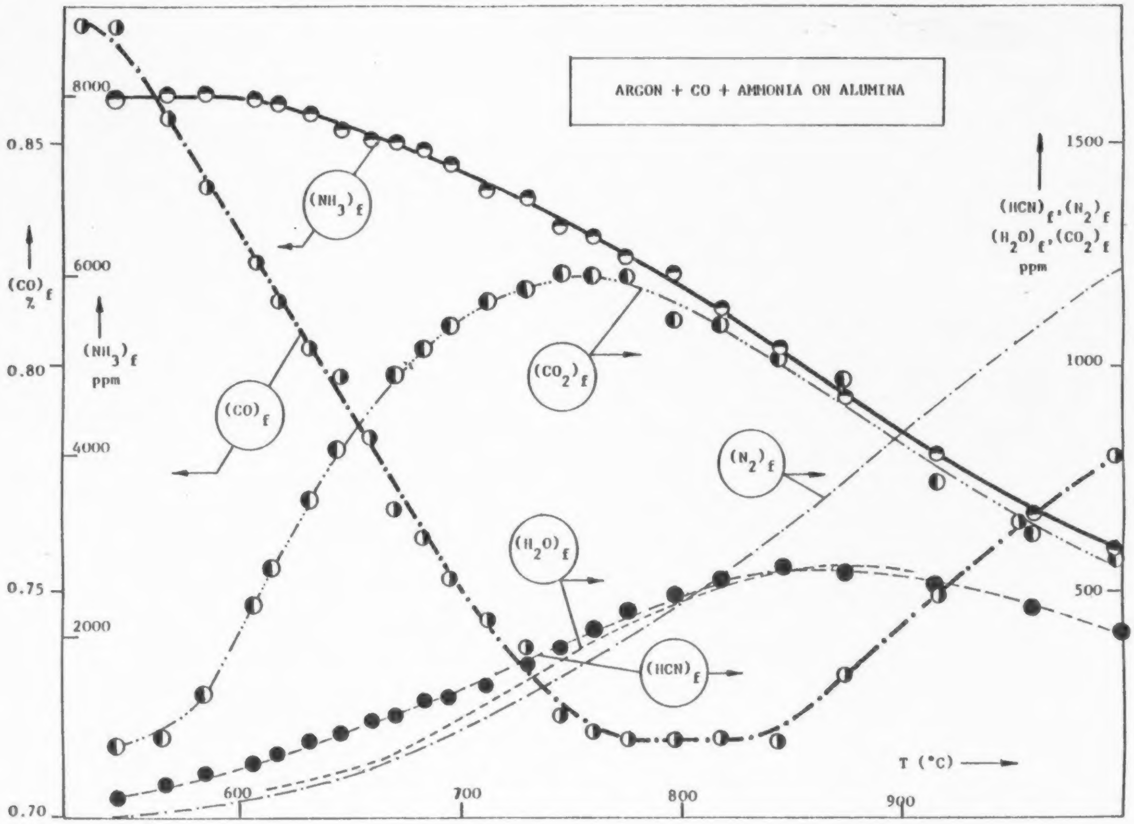

Figure 21. Argon + Ammonia + CO on Alumina: D = 13.8 $cm^3 s^{-1}$; $(NH_3)_i$ = 8200 ppm; $(CO)_i$ = 0.88%.

This suggests the formation of other carbon-containing species such as free carbon or CH_4, or (CH_2O).

Taking into account the existence of reaction (12) and of reaction (19), CO_2 and H_2O may also be formed by both reaction paths. Therefore, the mass balances must be:

O balance: $(CO)_i + (-O)_f = (CO)_f + 2(CO_2)_f + (H_2O)_f$ (28)

H balance: $3(NH_3)_i = 3(NH_3)_f + (HCN)_f + 2(H_2)_f + 2(H_2O)_f + 4(CH_4)_f$ (29)

C balance: $(CO)_i = (CO)_f + (CO_2)_f + (HCN)_f + (C)_f + (CH_4)_f$ (30)

N balance: $(NH_3)_i = (NH_3)_f + (HCN)_f + 2(N_2)_f$ (31)

where $(-O)_f$ represents oxygen atoms contributed by the solid matrix through reactions (12) and (19). The N-balance is independent of the other three balances and allows the calculation of $(N_2)_f$ under all circumstances. The system constituted by eqs. (28) through (31) can only be solved under some simplifying assumptions:

- A first assumption, which appears reasonable, is to admit that reaction (19) is negligible in comparison to reaction (12), since it is a secondary reaction and may therefore be disregarded.
- A second reasonable assumption is to assume that CO_2 behaves as an inert gas.
- A third assumption states that CO_2 is exclusively formed by reaction (12), since other possible reaction paths of CO_2 formation are highly unlikely. From this assumption it follows that:

  $(-O)_f = (CO_2)_f$ (32)
- Finally, there is the assumption that either CH_4 or C are formed, but not both together. The most convenient solution of equations (28) through (31) assumes that only free carbon, $(C)_f$, is formed and not methane.

Using these assumptions, it becomes possible to calculate $(H_2O)_f$ and $(H_2)_f$. As a general rule, it is found that for relatively small advancements of the ammonia decrease, i.e. for not too large values of the difference of $(NH_3)_i - (NH_3)_f$, the concentration of hydrogen in the reactor outlet gas is almost equal to the concentration of hydrogen cyanide:

$$(H_2O)_f \text{ (calculated)} = (HCN)_f \tag{33}$$

Moreover, for small reaction extents, at temperatures where no molecular nitrogen is observed in the reactor outlet gas ($T<600^{o}C$), one has:

$$(NH_3)_i - (NH_3)_f = (HCN)_f \tag{34}$$

Equations (33) and (34) suggest that the main reaction path which is responsible for the initial decrease of ammonia, is one where NH_3 is transformed into equimolar amounts of H_2O and HCN, utilizing the only oxygen source available in the present case, vis. CO:

$$NH_3 + CO \xrightarrow{9} HCN + H_2O$$

Reactions (12) and (13) will exist as well, and since HCN is the main reactive reaction product of reaction (9), one or more HCN involving reactions may also take place; in particular, a reaction which is analogous to reaction (13) may occur:

$$HCN \xrightarrow{15} 0.5\ N_2 + 0.5\ H_2 + C$$

as well as the reaction between HCN and NH_3:

$$HCN + NH_3 \xrightarrow{10} N_2 + 2\ H_2 + C.$$

Neither reaction (10) nor reaction (15) have been studied up to now utilizing respectively Argon+HCN+NH_3 mixtures (Case S.1) or Argon+HCN mixtures (Case G.1); but one of them, or both, should be postulated to explain the observed decrease of HCN at elevated temperatures (see e.g. Figures 18, 19, and 21).

From eqs. (33) and (34), which apply for small reaction extents, it follows that, at temperatures below 600 or $650^{o}C$, reactions 10, 15, and 13 should be vanishingly slow in comparison to reaction (9).

The time derivative of the nitrogen species may thus be written as:

$$d(NH_3)/dt = -V_9 - V_{10} - V_{13} \left(= - \overline{V_{I.1}}\right) \tag{35}$$

$$d(HCN)/dt = V_9 - V_{10} \qquad -V_{15} \tag{36}$$

$$d(N_2)/dt = V_{10} + \frac{1}{2} V_{13} + \frac{1}{2} V_{15} \tag{37}$$

The overall reaction rate of NH_3 disappearance $\overline{V_{I.1}}$ may be obtained from eq. (35) and is found to be given by (see Figure 22):

$$\boxed{\overline{V_{I.1}} = 0.3 \text{ to } 1.9\ 10^8 \exp[-13600(\pm 1000)/T]\ X_{NH_3}\ X_{CO}} \tag{38}$$

Subtraction of eq. (35) from eq. (36) yields:

$$0.5 \left[\frac{d(HCN)}{dt} - \frac{d(NH_3)}{dt}\right] = V_9 + 0.5\ V_{13} + 0.5\ V_{15} \tag{39}$$

Since, at lower temperatures, V_{13} and V_{15} are small compared to V_9, eq. (39) yields directly the value of V_9 for small reaction extents. Under these low temperature conditions, a value of the rate V_9 is found to be:

$$\boxed{V_9 = 1.3\ 10^7 \exp[-13800(\pm 500)/T]\ X_{NH_3}^{0.75}\ X_{CO}} \tag{40}$$

We now may utilize eq. (39) to determine the reaction rate of V_{15} at temperatures beyond 700°C (i.e. where V_{15} is no longer negligible with respect to V_9) upon substitution of the values of V_9 and V_{13}, given respectively by equations (40) and (19), into eq. (39) and solving for V_{15}. The concentrations X_{NH_3} and X_{CO} appearing in eqs. (40) and (19) are given by their experimental values at any given temperature. The resultant rate (see Figure 23) is found to be:

$$\boxed{V_{15} = 3.2\ 10^8 \exp[-18200(\pm 800)/T]\ X_{HCN}} \tag{41}$$

Finally, utilizing the expressions of V_{13} and V_{15}, respectively given by equations (19) and (41), substituting them into eq. (39), then solving this equation for V_9, the latter may now also be determined at temperatures beyond

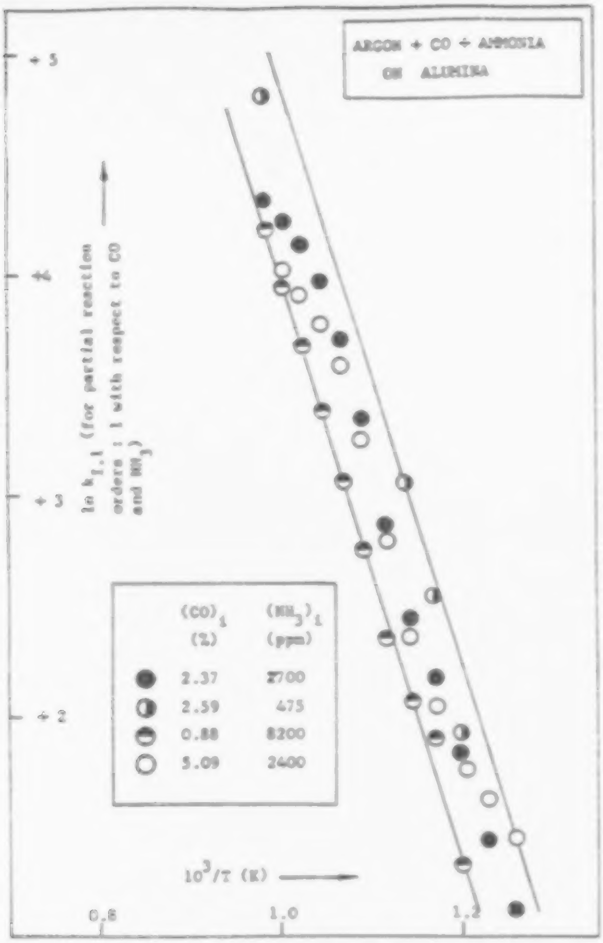

Figure 22. Argon + Ammonia + CO on Alumina: Determination of the Rate Constant of the Overall Ammonia Disappearance According to eq.(35), for Different Initial Concentrations of Ammonia and CO.

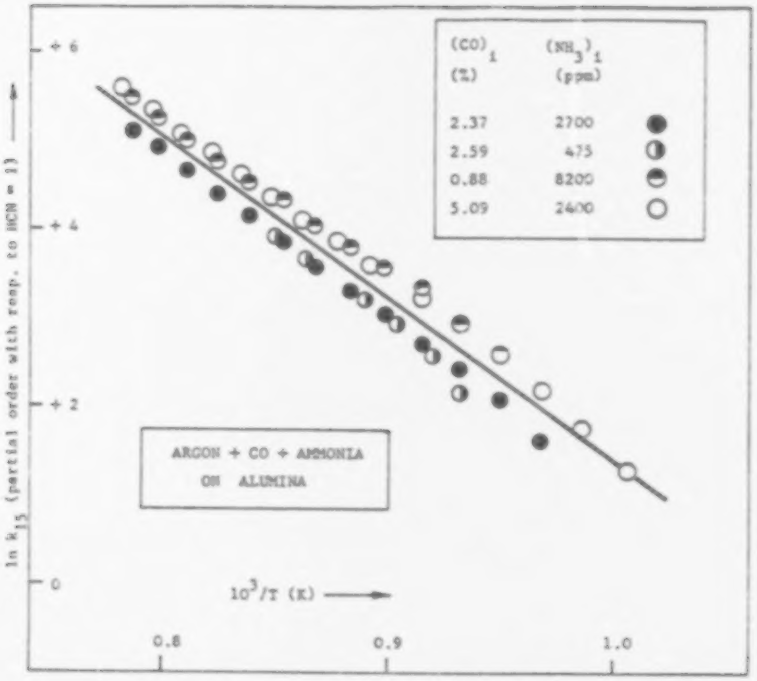

Figure 23. Argon + Ammonia + CO on Alumina: Determination of Rate Constant k_{15} According to eq.(39), For Different Initial Concentrations of Ammonia and CO.

650^{0}C. Comparing this high temperature rate with that determined at low temperatures--given by eq. (40) indicates a fairly good reaction rate, V_9, is obtained which is valid over the whole temperature range of the trials (see Figure 24).

The reaction rate V_{10} may be estimated from either eq. (35) or eq. (36) upon substitution of the rate expressions V_9 and V_{13} or V_{15}, respectively--given by eqs. (40), (19), and (41)--into one of these two equations and solving for V_{10}. When doing so, it is found that V_{10} is almost negligibly small over the whole temperature and concentration range studied. Determination of a more accurate value for V_{10} must await trials utilizing HCN in the inlet gas flow (see part III of this report). As previously mentioned in section 3.1.2.B., the rate of V_{15} and expecially the partial order with respect to the HCN concentration obtained here is only approximate.

3.2.1.2.5 Argon + NO + NH_3 on Alumina (Case R.1)

Results from these trials are shown in Figures 25 through 28. In the case of Figures 25 and 26, the initial NO concentration is larger than the initial ammonia concentration, whereas in Figures 27 and 28, the initial nitric oxide concentration is smaller than that of ammonia. The overall behavior of the ammonia and nitric oxide concentrations as a function of temperature suggest that there exists a reaction between nitric oxide and ammonia. Since no other nitrogen-containing species (other than molecular nitrogen) can be formed*; and since no oxygen molecules have been detected in the reactor outlet flow, the overall balance of this reaction path should be of the form:

$$NO + n\,NH_3 \xrightarrow{4} \left(\frac{1+n}{2}\right) N_2 + H_2O + \frac{3n-2}{2}\; H_2 \qquad (42)$$

Determination of the factor n for this reaction may in principle be made from the experimental ratio

$$n = \left[(NH_3)_i - (NH_3)_f\right] \;/\; \left[(NO)_i - (NO)_f\right] \qquad (43)$$

---

*Although in the simultaneous presence of NO and NH_3 small amounts of N_2O have been found on Pt, Pd, or Ru containing catalysts (Refs.16 and 17), this is not the case on pure alumina (Ref. 18).

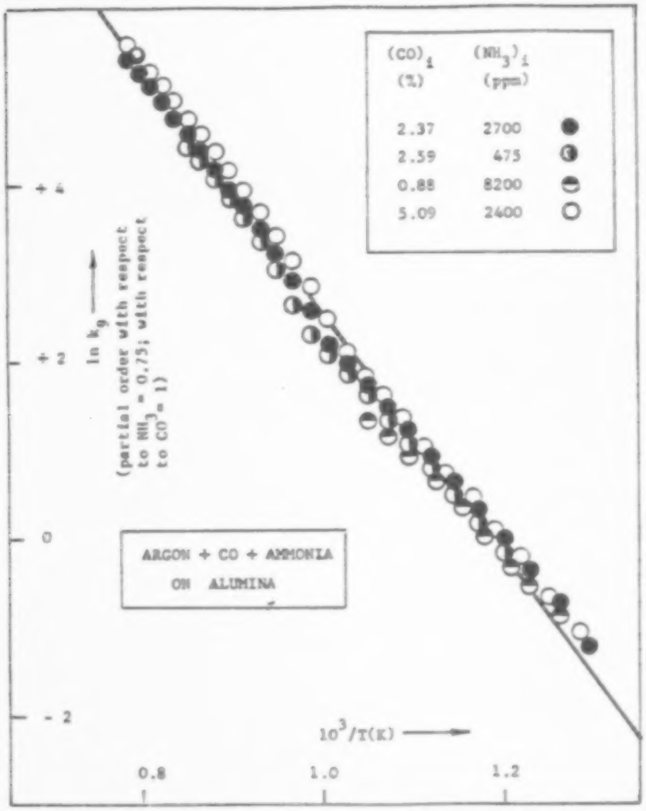

Figure 24. Argon + Ammonia + CO on Alumina: Determination of Rate Constant k_9 According to eq.(39), For Different Initial Concentrations of Ammonia and CO.

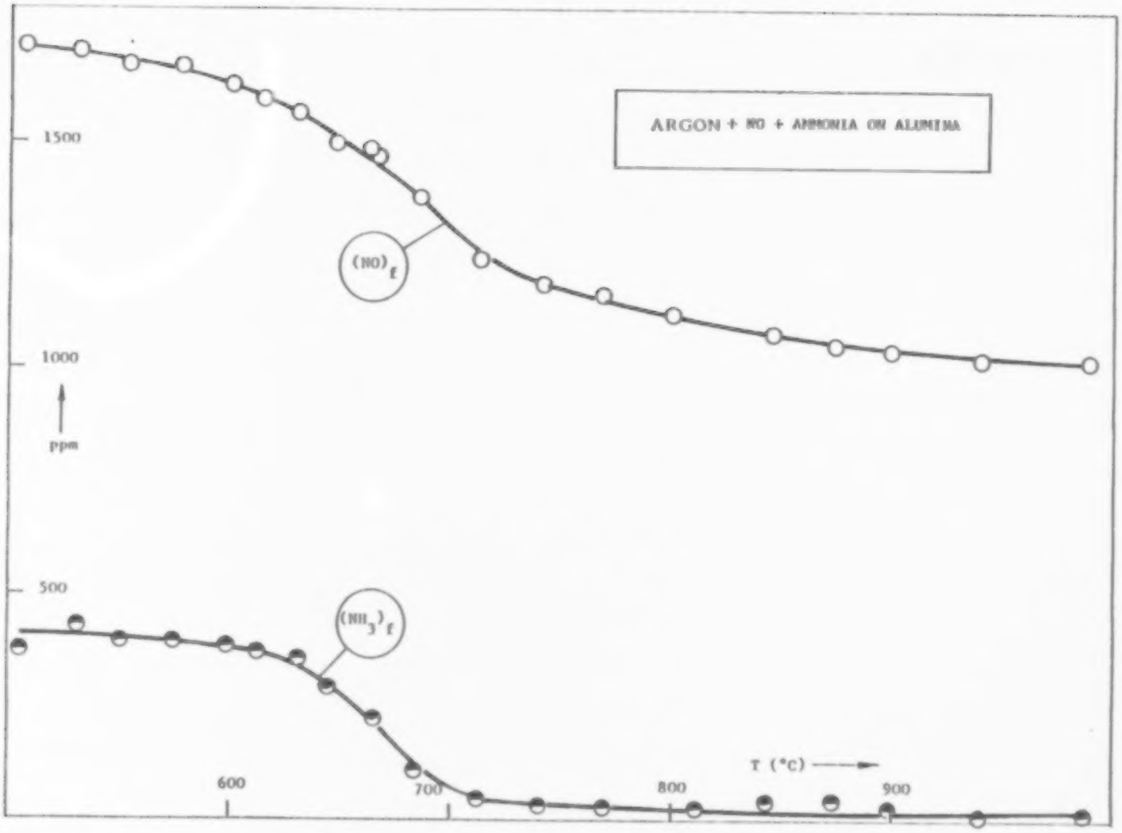

Figure 25. Argon + Ammonia + NO on Alumina: D = 14.3 cm^3s^{-1}; $(NH_3)_i$ = 400 ppm; $(NO)_i$ = 1730 ppm.

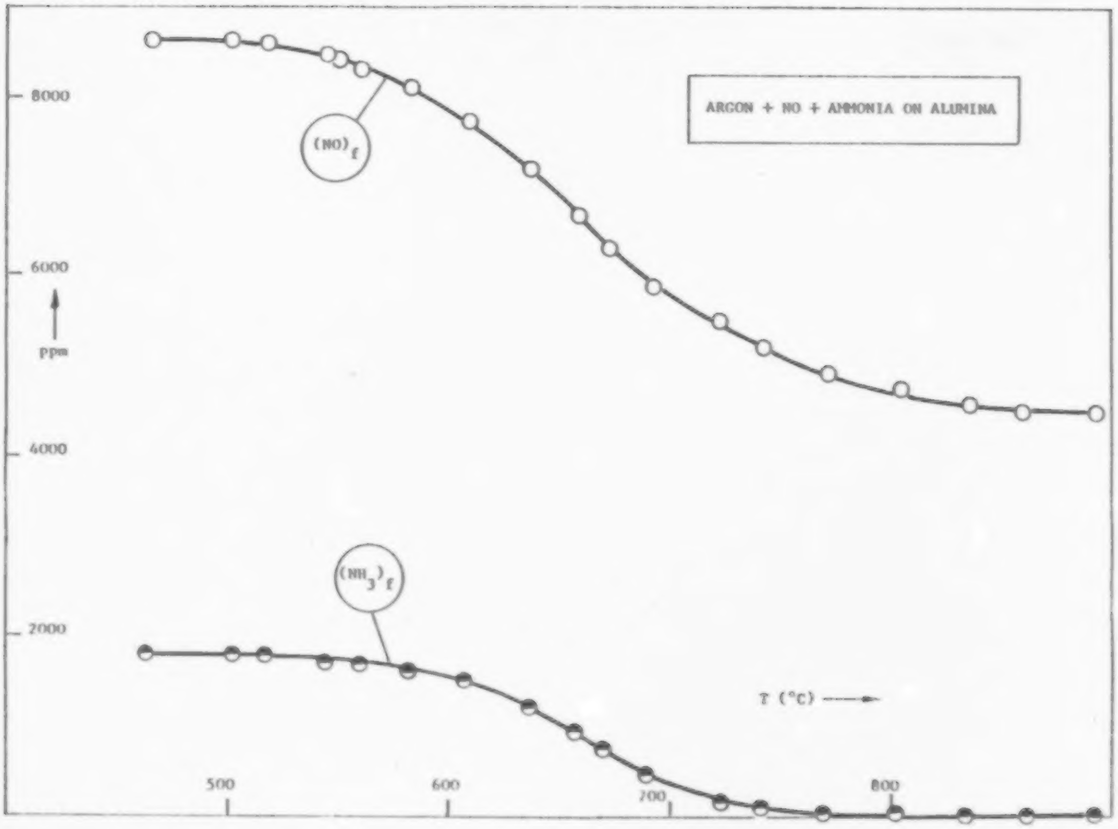

Figure 26. Argon + Ammonia + NO on Alumina: D = 14.6 cm^3s^{-1}; $(NH_3)_i$ = 1800 ppm; $(NO)_i$ = 8600 ppm.

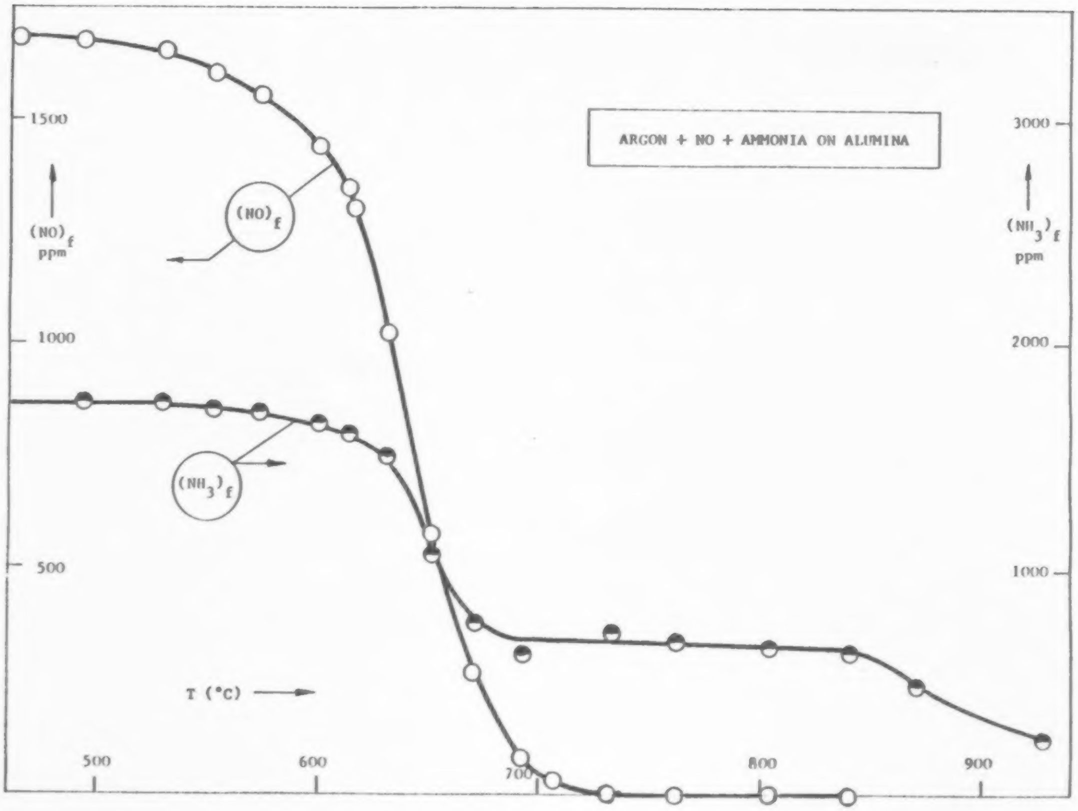

Figure 27. Argon + Ammonia + NO on Alumina: $D = 14.6\ cm^3s^{-1}$; $(NH_3)_i = 1840$ ppm; $(NO)_i = 1680$ ppm.

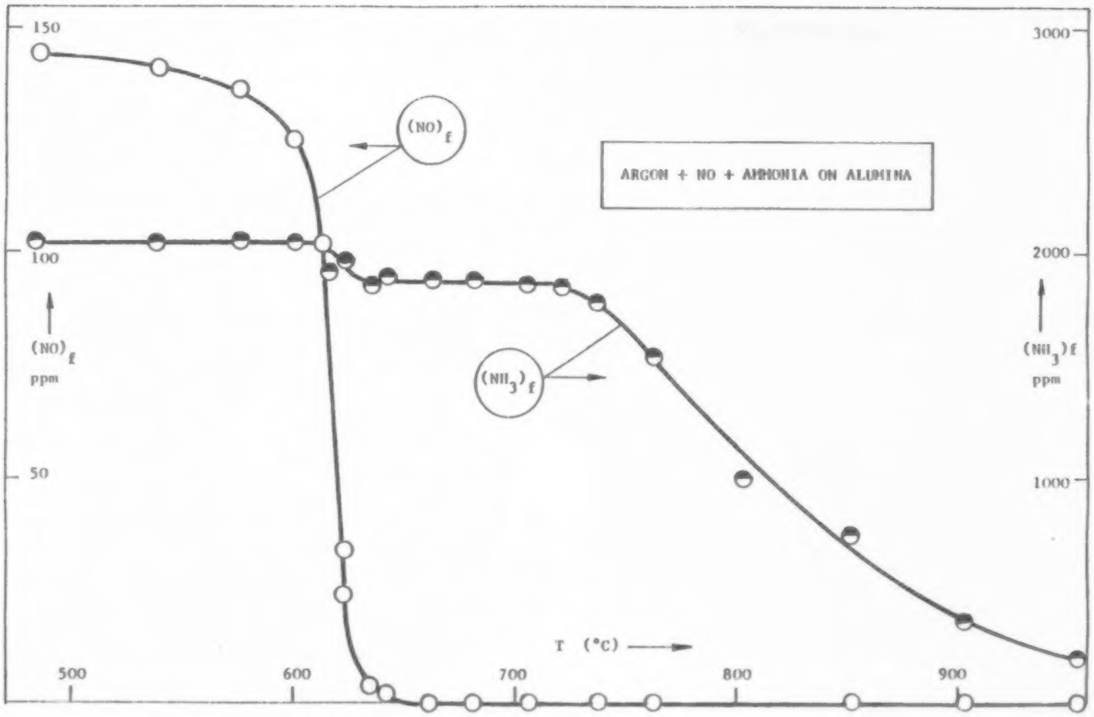

Figure 28. Argon + Ammonia + NO on Alumina: D = 14.6 cm^{3}s^{-1}; (NH$_3$)$_i$ = 2040 ppm; (NO)$_i$ = 144 ppm.

which is strictly correct under conditions where reaction (4) is the only reaction responsible for NO and NH_3 variations. From Table 1 it is seen that reaction (13) also takes place. Since both reactions (4) and (13) yield hydrogen as a product, the secondary reactions (11) and (14) are also expected to take place.

Reaction (13) is of little importance to the determination of the ratio n because reaction (4) is always completed at temperatures where reaction (13) has hardly started. This is illustrated by the comparison of Figure 13, curve A (this figure corresponding to case D.1) with either Figure 27 or Figure 28 (corresponding to the present case R.1). One may clearly see in Figure 28 the temperature value ($\sim 725^{0}C$) where the onset of reaction (13) initiates an additional new reduction in NH_3 after NO has already disappeared. Superpositioning Figures 13 and 28 indicates that this part of the $(NH_3)_f$ curves have very similar temperature dependencies.

On the contrary, as will be seen in the paragraph treating the case O.1, reactions (11) and (14) take place in the same temperature range as reaction (4) and are therefore corresponsible for the variation of ammonia and nitric oxide concentrations. The experimental ratio n, given by eq. (43), should therefore take into account reactions (4), (11) and (14). However, as a first order approximation, the two latter reaction paths (11 and 14) may be disregarded as secondary reactions, in comparison to the primary reaction (4). Further, since reaction (4) depends on NO as a reactant, and since reactions (11) and (14) depend on NO both as a reactant and as a source of their coreactant (H_2, formed by reaction 4), one expects the ratio V_{11}/V_4 as well as the ratio V_{14}/V_4 to decrease with decreasing $(NO)_i/(NH_3)_i$. Thus, for sufficiently small values of the latter ratio, the expression (43) becomes valid. This may be seen from the table presented below, where experimental values of the ratio n (as defined by eq. 43), measured at reaction completion (i.e. for temperatures corresponding to total disappearance of the deficient reactant), are tabulated against the ratio of initial concentrations of nitric oxide and ammonia. It is observed that the coefficient n approaches a value situated between 0.7 and 1, when the ratio $(NO)_i/(NH_3)_i$ is sufficiently small. In Table 1 and Table 2, two extreme values of the stoichiometric coefficient n are indicated (4a and 4b)

Argon + NH_3 + NO Mixtures on Alumina; ($T<700^{o}C$)

Figure	$\frac{(NO)_i}{(NH_3)_i}$	$n = \frac{(NH_3)_i - (NH_3)_f}{(NO)_i - (NO)_f}$
28	0.07	1.10
27	0.96	0.83
25	4.32	0.56
26	5.06	0.43 to 0.50

Corresponding to either only H_2O formation ($n = 0.67$) or to formation of both H_2O and H_2 ($n = 1$).

Without simplification, the variation of the nitrogen containing species* as a function of time are given by the following set of equations:

$$d(NO)/dt = -V_4 - V_{11} \quad - V_{14} = -\overline{V_{R.1}} \tag{44}$$

$$d(NH_3)/dt = -n\ V_4 + V_{11} - V_{13} \tag{45}$$

$$d(N_2)/dt = \frac{1 + n}{2}\ V_4 \quad + 0.5V_{13} + 0.5V_{14} \tag{46}$$

This set of differential equations is identical to the one we shall deal with in the case 0.1 (see below, paragraph 3.2.1.2.6). In the present case, however, reaction rate V_4 and, at higher temperatures, reaction rate V_{13}, are dominant as primary reactions over the secondary reactions V_{11} and V_{14}. In case 0.1 we have to deal with the reverse situation, V_{11} and V_{14} prevailing as the primary reactions over the secondary reactions V_4 and V_{13} (at least for small reaction extents).

---

*Although in the simultaneous presence of NO and NH_3 small amounts of N_2O have been found on Pt, Pd, or Ru containing catalysis (Refs. 16 and 17), this is not the case on pure alumina (Ref. 18).

Combining eqs. (44) and (45) yields:

$$-d(NO)/dt - d(NH_3)/dt = (1+n)V_4 + V_{13} + V_{14} = 2d(N_2)/dt \tag{47}$$

$$-d(NO)/dt + \frac{1}{n}\, d(NH_3)/dt = \left(\frac{1}{n} + 1\right)V_{11} - \frac{1}{n} V_{13} + V_{14} \tag{48}$$

The overall NO disappearance reaction rate $\overline{V_{R.1}}$ is obtained from eq. (44). This expression is relatively imprecise, and the partial order with respect to NO is between 0.75 and 1; and, with respect to NH_3, between 0.5 and 1. The following derived expressions are almost equivalent over the temperature range of 500 to 1000°C:

$$\overline{V_{R.1}} = 6.6 \times 10^7 \text{ to } 1 \times 10^9 \exp[-16400(\pm 1300)/T]\ X_{NO}^{0.75}\ X_{NH_3}^{0.5} \tag{49}$$

$$5.4 \times 10^8 \text{ to } 7 \times 10^9 \exp[-17000(\pm 1300)/T]\ X_{NO}\ X_{NH_3}^{0.5} \tag{50}$$

$$3.0 \times 10^{11} \exp[-18200(\pm 1300)/T]\ X_{NO}\ X_{NH_3} \tag{51}$$

For temperatures below 700°C, V_{13} can be neglected, and when (in that temperature range) we limit the calculation to small decreases of NH_3, we also may disregard the secondary reaction V_{14}. Under these limiting conditions, eq. (47) yields an expression suitable for evaluation of V_4. Again substantial doubt exists concerning the partial reaction orders. In the given range of temperatures and concentrations, the following two expressions are almost equivalent:

$$V_4 = \frac{1.1 \times 10^8}{1 + n} \exp[-15300(\pm 1000)/T]\ X_{NO}^{0.75}\ X_{NH_3}^{0.5} \tag{52}$$

$$= \frac{9.3 \times 10^9}{1 + n} \exp[-15000(\pm 1000)/T]\ X_{NO}\ X_{NH_3} \tag{53}$$

An analogous rate expression has been derived for electroquartz, which is characterized by a preexponential constant about 20 times smaller than that obtained with alumina:

$$V_4 = \frac{6.4 \times 10^6}{1 + n} \exp[-17600(\pm 1500)/T]\ X_{NO}^{0.75}\ X_{NH_3}^{0.50} \tag{54}$$

3.2.1.2.6 Argon + NO + H_2 on Alumina (Case 0.1)

Results obtained by this trial series are shown on Figures 29, 30, and 31. As may be observed from these examples, there is formation of ammonia as soon as nitric oxide begins to decrease. For very small values of extent of reaction, the quantity of ammonia in the reactor outlet flow equals the disappeared quantity of nitric oxide. This suggests there exists a reaction path corresponding to a mole-to-mole transformation of NO into NH_3, using hydrogen as a coreactant, viz.

$$NO + 2.5\ H_2 \xrightarrow{11} NH_3 + H_2O$$

However, shortly after the first decrease in NO, one finds that:

$$(NO)_i - (NO)_f > (NH_3)_f \qquad (55)$$

This inequality suggests that a direct reduction of NO by H_2 without the formation of NH_3 is taking place. This conclusion is based on the observation that reaction 13 is negligible in the temperature range where equation (55) holds ($T<700^{o}C$). Also, since reaction (4) has a stoichiometric coefficient, n, less than or equal to one, it cannot account for a preferential decrease of NH_3 compared to nitric oxide. Thus, the direct transformation of NO to molecular nitrogen is postulated:

$$NO + H_2 \xrightarrow{14} 0.5\ N_2 + H_2O$$

As stated in the previous section, the same set of differential equations as for case R.1 will describe the variation of the nitrogen-containing species. In the present case, V_4 and V_{13} are secondary reactions and may be disregarded for small percents of NO disappearance.

The variation d(NO)/dt, given by eq. (44), yields an expression for the overall NO disappearance rate $\overline{V_{01}}$. The partial reaction order with respect to NO is found to be between 0.2 and 0.5, and one finds (see Figure 32):

$$\boxed{\begin{aligned} V_{0.1} &= 8.6 \times 10^5 \exp[-11900(\pm 1000)/T]\ X_{NO}^{0.5}\ X_{H_2} \\ &= 2.3 \text{ to } 13 \times 10^5 \exp[-13000(\pm 1000)/T]\ X_{NO}^{0.2}\ X_{H_2} \end{aligned}} \qquad \begin{aligned} &(56) \\ &(57) \end{aligned}$$

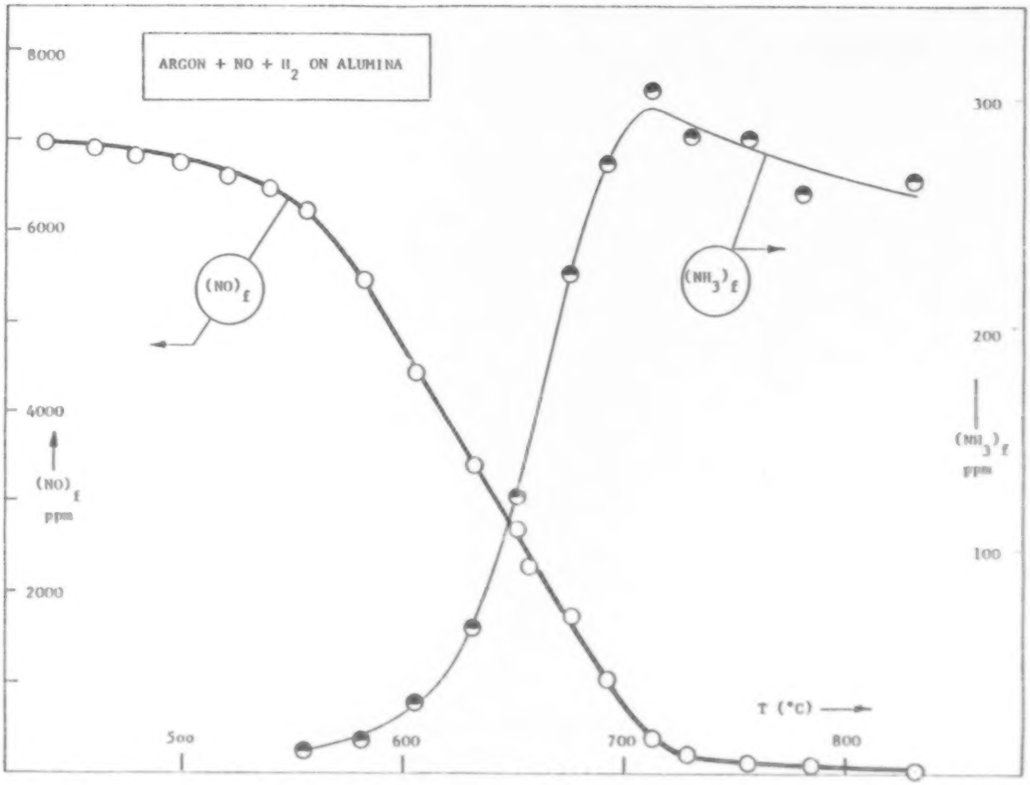

Figure 29. Argon + Hydrogen + NO on Alumina: $D = 14.5\ cm^3s^{-1}$; $(NO)_i = 7000$ ppm; $(H_2)_i = 5.52\%$.

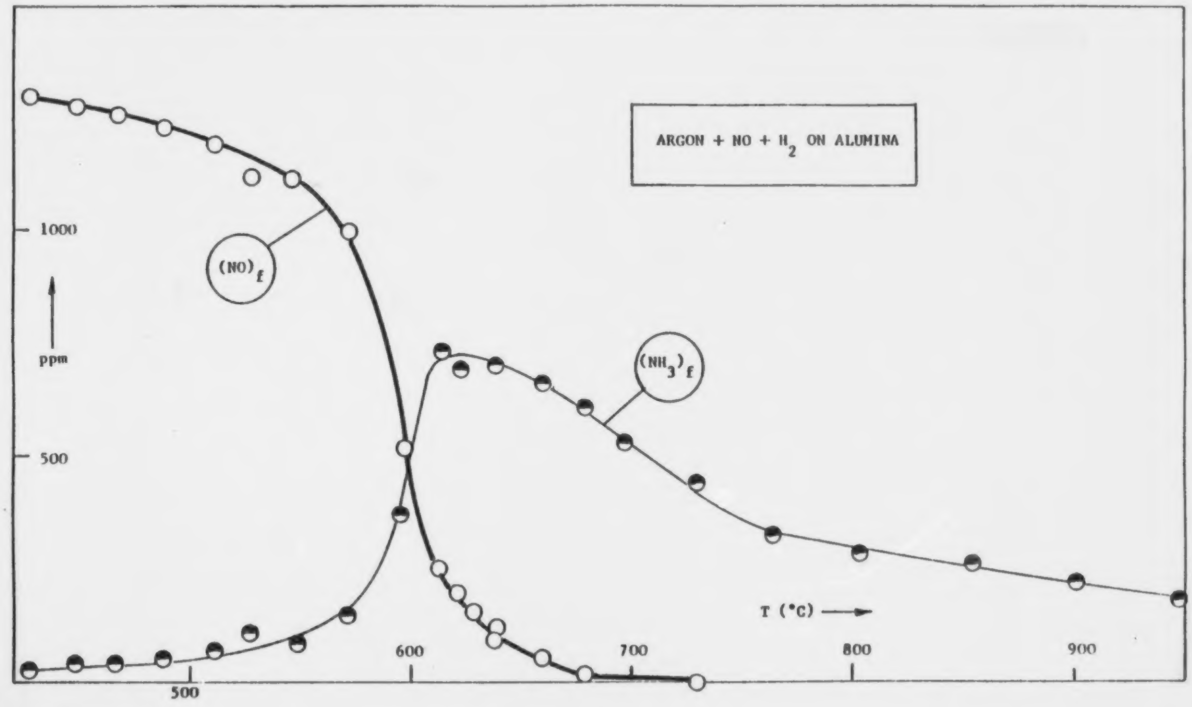

Figure 30. Argon + Hydrogen + NO on Alumina: D = 14.9 cm^3s^{-1}; $(NO)_i$ = 1330 ppm; $(H_2)_i$ = 5.52%.

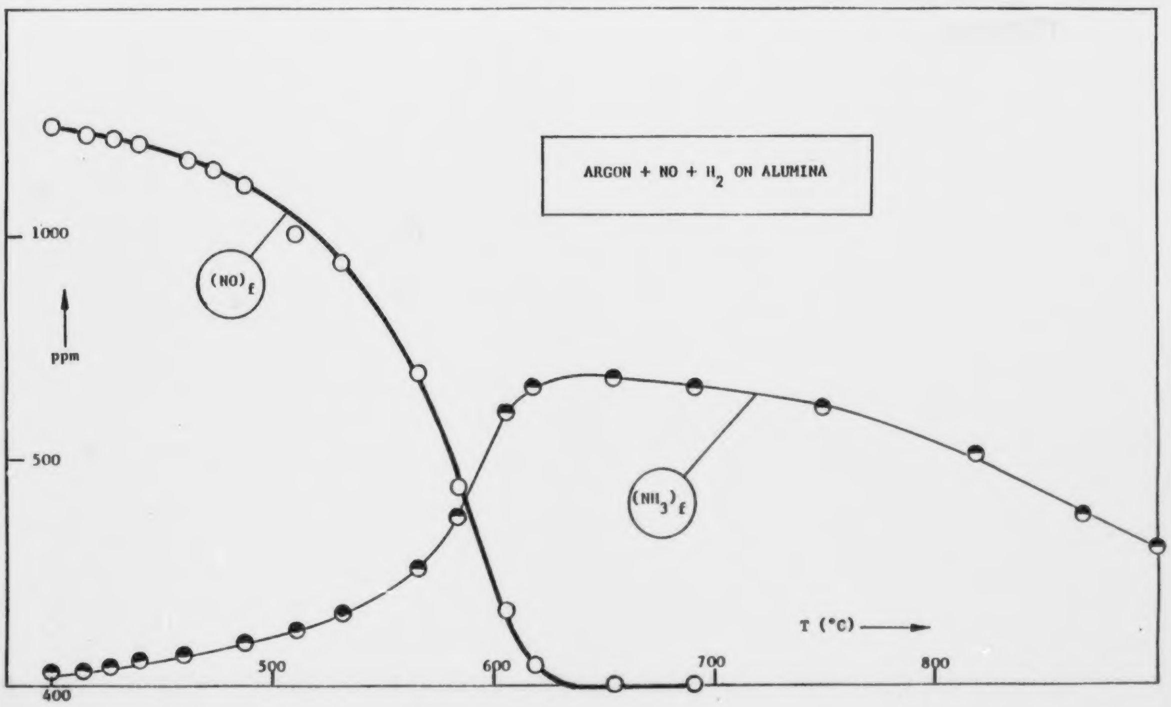

Figure 31. Argon + Hydrogen + NO on Alumina: D = 16.0 cm^3s^{-1}; $(NO)_i$ = 1270 ppm; $(H_2)_i$ = 13.10%.

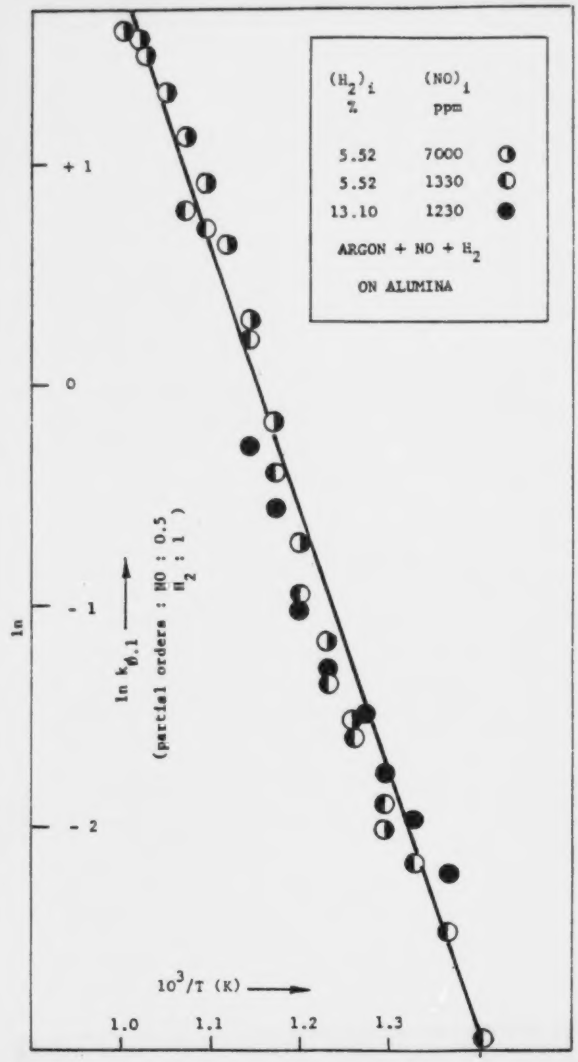

Figure 32. Argon + Hydrogen + NO on Alumina: Determination of the Rate Constant of the Overall NO Disappearance According to eq.(44), for Different Initial Concentrations of NO and Hydrogen.

Since reaction (13) may be neglected over the entire temperature range where NO disappears, the term V_{13} may be dropped from eq. (47). Equation (49) can then be utilized to calculate V_{14} after substitution of V_4 from its value calculated with eq. (52). As illustrated by Figure 33, one finds that:

$$\boxed{V_{14} = 6.4 \times 10^{7} \exp\left[-13500(\pm 800)/T\right] \; X_{NO} \, X_{H_2}} \tag{58}$$

Finally, upon substituting the values of V_{14} and even of V_{13} (although negligibly small) given by eqs. (58) and (16), into equation (48), one determines reaction rate V_{11}, as shown on Figure 34:

$$\boxed{V_{11} = 2.3 \text{ to } 4.7 \times 10^{3} \exp\left[-8200(\pm 1300)/T\right] \; X_{NO}^{0.5} \; X \; H_2} \tag{59}$$

3.2.1.2.7 Argon + NO + CH_4 on Alumina

It was not our intention to study the effect of methane or other hydrocarbons as reducing agents for heterogeneous NO reduction. A few runs have been made only to illustrate this reducing effect. An example is shown on Figure 35. Since under our experimental conditions NO was not reduced when passed alone over alumina (see section 3.2.1.2.1), it should be concluded from these runs that either the hydrocarbon molecules themselves or their pyrolysis products (H_2, C) will reduce NO. As may be observed, nonnegligible quantities of NH_3, CO, and CO_2 are also released during that NO reduction. The reaction is shifted towards relatively high temperature values.

3.2.1.2.8 Conclusion of Section 3.2.1.2

As a conclusion to the reactions treated up to now, a discussion is in order that addresses a question that touches the fundamentals of the heterogeneous mechanism of nitric oxide reduction on refractory oxides.

A question can be raised when considering three major experimental observations discussed previously:

1. The fact that NO, when alone, is not reduced when passed over a metal oxide (MeO);

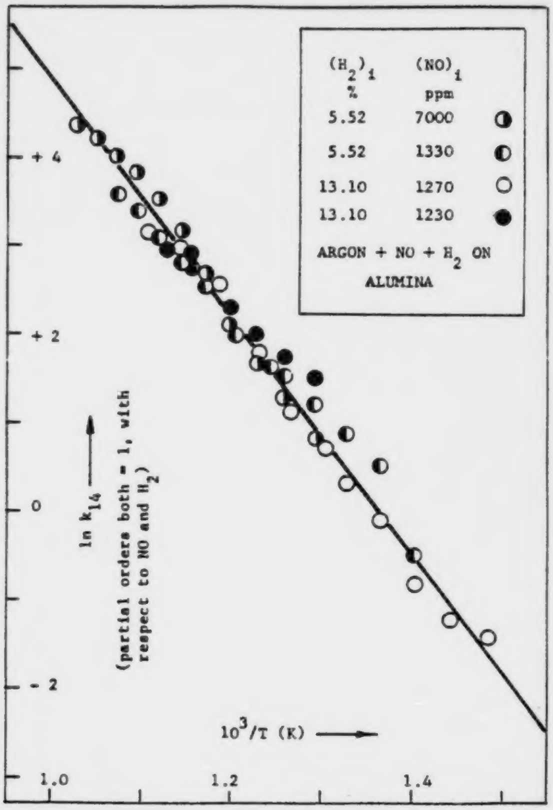

Figure 33. Argon + Hydrogen + NO on Alumina: Determination of the Rate Constant k_{14} According to eq.(47), for Different Initial Concentrations of NO and Hydrogen.

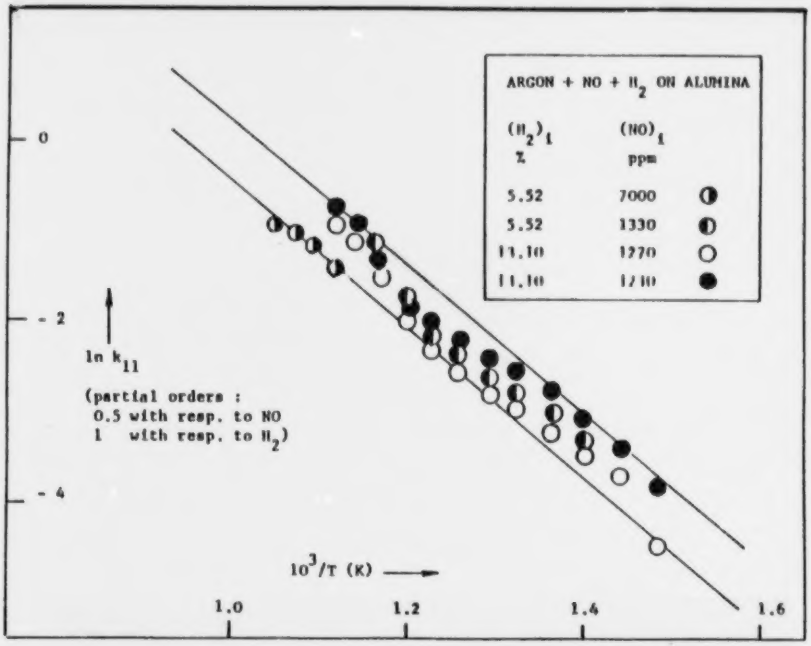

Figure 34. Argon + Hydrogen + NO on Alumina: Determination of Rate Constant k_{11} According to eq.(48), for Different Initial Concentrations of NO and Hydrogen.

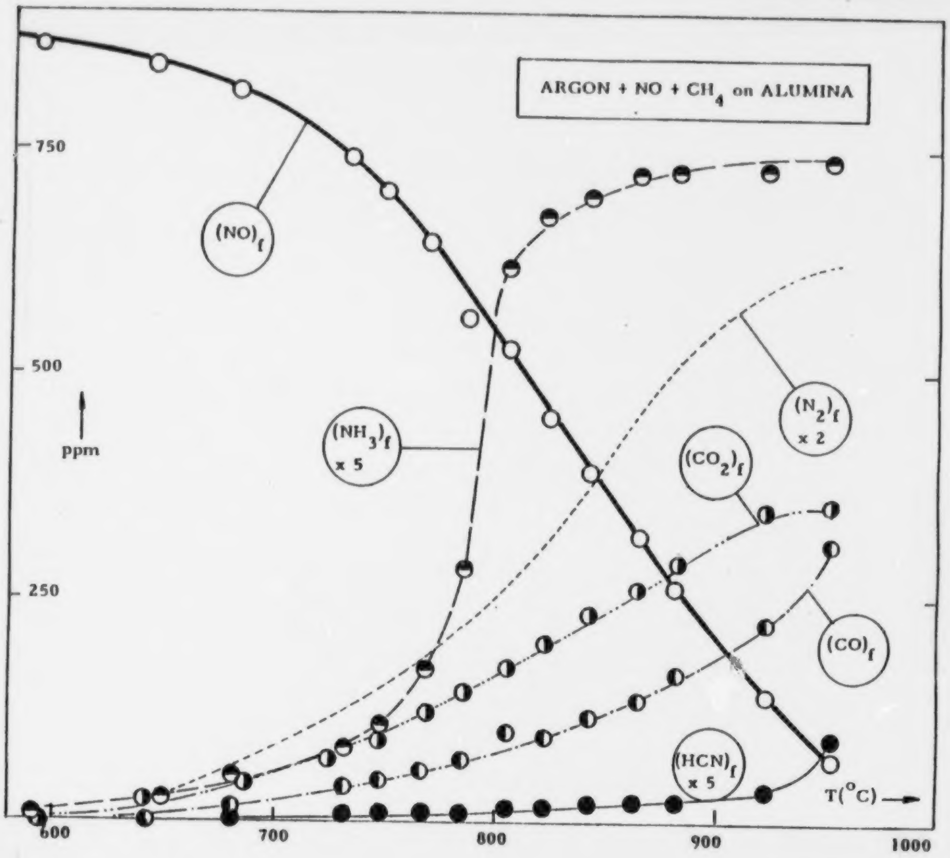

Figure 35. Argon + NO + Methane on Alumina: D = 12.6 cm^3s^{-1}; $(NO)_i$ = 900 ppm; $(CH_4)_i$ = 0.29%.

2. The fact that NO is reduced (directly to N_2, or through NH_3 or HCN as intermediates) on MeO as soon as a gaseous reducing agent is present (e.g. H_2 or CO).
3. Finally, the fact that these gaseous reducing agents also reduce the metal oxides into metal.

Thus, the following question arises: which one of the two possible reduction paths is followed whenever NO is reduced on MeO:

1. NO is reduced directly by the gaseous reducing agent, this reduction being contact-catalyzed by the solid surface of MeO. In this case, the reduction of MeO into Me by the gaseous reducing agent is merely a parallel reaction but not an intermediate reaction required for NO reduction.
2. NO is reduced indirectly by the gaseous reducing agent, but directly by the metal. The gaseous reducing agent acts only to reduce MeO into Me, the latter then reducing NO. In that case, the reduction of MeO into Me is an indispensable intermediate reaction required for the NO reduction.

The question is not a merely philosophical one. In the first assumption, the NO reduction mechanism depends primarily on the chemical properties of the gaseous reducing agents, whereas in the second hypothesis the bond energy of the oxygen atom in the MeO molecule will play an important role.

A few trials have been run in order to throw some light on this question. Argon containing exclusively NO was fed over very pure aluminum metal (small pellets, obtained by filing an aluminum rod, previously treated thermally under hydrogen flow). Over a temperature range extending up to the melting point of aluminum (659.7^{o}C) there was no indication of NO reduction at the reactor outlet. This might suggest that the first hypothesis is the right one; i.e., not only is the reduction of MeO not an indispensable intermediate reaction required for NO reduction, but the reduction of MeO into Me is not even sufficient in order to reduce nitric oxide.

3.2.1.3 Effect of the Presence of Molecular Oxygen on the NO Reduction

Oxidation reactions of CO and H_2 have been treated earlier in this report. In the present section, attention is focused on the influence of oxygen on the heterogeneous reduction of nitric oxide, which should at least partially be due to reactions between oxygen and nitrogen-containing species.

3.2.1.3.1 Argon + CO + NO + O_2 on Alumina (Combined Case JKT.1)

In this "combined" case, all reaction possibilities belonging to the cases J.1, K.1 and T.1 are expected. Cases J.1 and K.1 have been treated in previous sections. Case T.1 by itself does not add supplementary reaction paths, since the reaction

$$NO + 0.5\ O_2 \xrightarrow{37} NO_2$$

has never been observed over the temperature range up to 1100°C when feeding Argon + NO + O_2 over Alumina.

The only reactions of concern are (8), (20), and (12). As pointed out earlier, however, reaction (12) is negligible compared to (20) as long as there is sufficient molecular oxygen. We thus only have to deal with oxidation by two competing reaction paths:

1. The oxidation of the gaseous reducing agent (CO) by reaction (20).
2. The oxidation of the gaseous reducing agent (CO) by NO, via reaction (8).

Beyond this competition between reactions (8) and (20) there is no direct interaction between molecular oxygen and the nitrogen-containing species present (which, in this case, are NO and N_2 exclusively). Therefore, what one would expect as an effect of molecular oxygen in this case, is merely a decrease in the rate V_8 due to the decrease of (CO) caused by its oxidation via reactions (20) and (12). Whenever the ratio $(O_2)_i/(CO)_i$ is sufficiently high, and if reaction (20) has a rate at least comparable to the rate V_i, then CO may be consumed (by reaction 20) prior to total consumption of NO (by reaction 8). In this case nitric oxide would not be further reduced, since that reduction becomes impossible in the absence of a gaseous reducing agent.

Actually, the experimental observations only partly fit these á priori expectations. Some typical measurements are shown in Figures 36 through 40. The initial conditions for these trials correspond to decreasing values of the ratios $(CO)_i / \left[(NO)_i + 2(O_2)_i\right]$ and $(CO)_i/2(O_2)_i$, as indicated in the table below:

Argon + CO + NO + O_2 on Alumina		
Figure	$\frac{(CO)_i}{(NO)_i + 2(O_2)_i}$	$\frac{(CO)_i}{2(O_2)_i}$
36	6.15	8.23
37	1.73	2.46
38	1.36	1.76
39	0.80	2.54
40	0.04	0.04

These figures should be compared with the results obtained either with the Argon+CO+O_2 series (given in Figures 7 through 10), or with the Argon+CO+NO series (illustrated in Figures 14, 15, and 16). Although the initial concentrations of the reactants are not exactly comparable for these three series, qualitative interpolation quickly allows the following observations to be made:

1. The presence of O_2 enhances the NO reduction rate V_8: For the Ar+NO+CO series (Figures 14 through 16), the NO disappears mainly between 500 and 600°C; whereas for the Ar+NO+CO+O_2 trials (Figures 36 through 39) this mainly occurs between 400 and 550°C (at comparable CO and NO concentrations). In a more quantitative way, the effect of molecular oxygen on reaction rate V_8 may be described by the following expression, which should be compared with eq. (25).

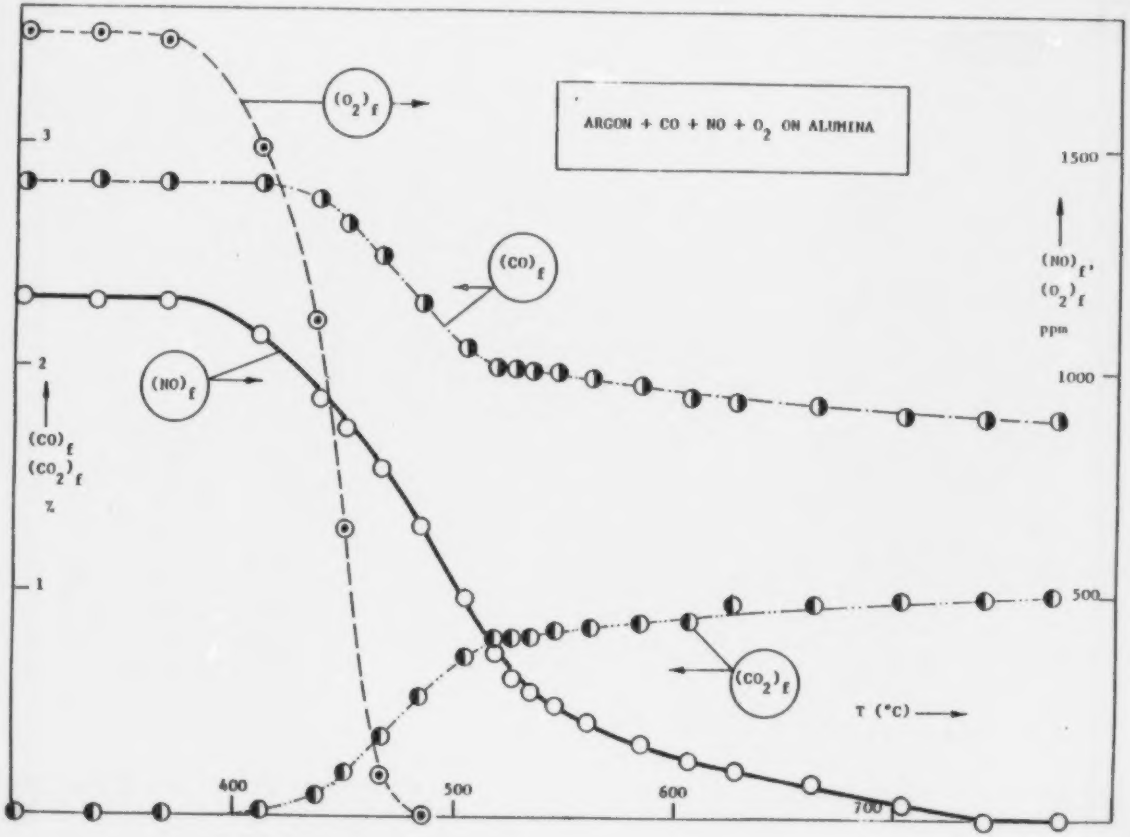

Figure 36. Argon + NO + CO + O_2 on Alumina: D = 17.0 cm^3s^{-1}; $(NO)_i$ = 1150 ppm; $(CO)_i$ = 2.80%; $(O_2)_i$ = 0.17%.

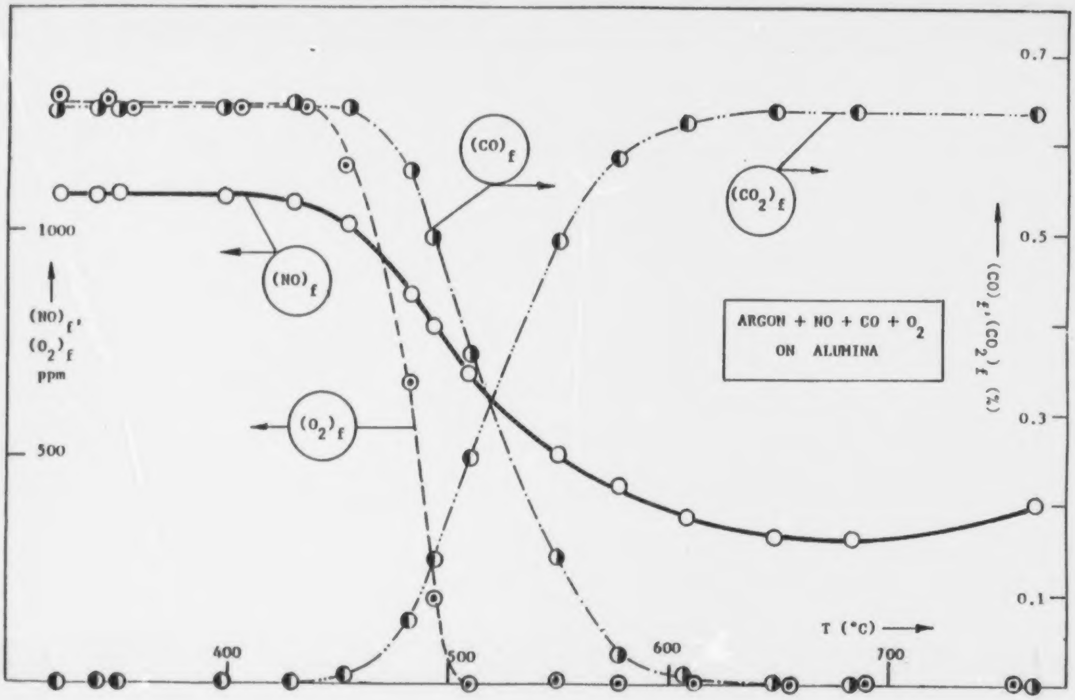

Figure 37. Argon + NO + CO + O_2 on Alumina: D = 15.3 cm^3s^{-1}; $(NO)_i$ = 1100 ppm; $(CO)_i$ = 0.64%; $(O_2)_i$ = 0.13%.

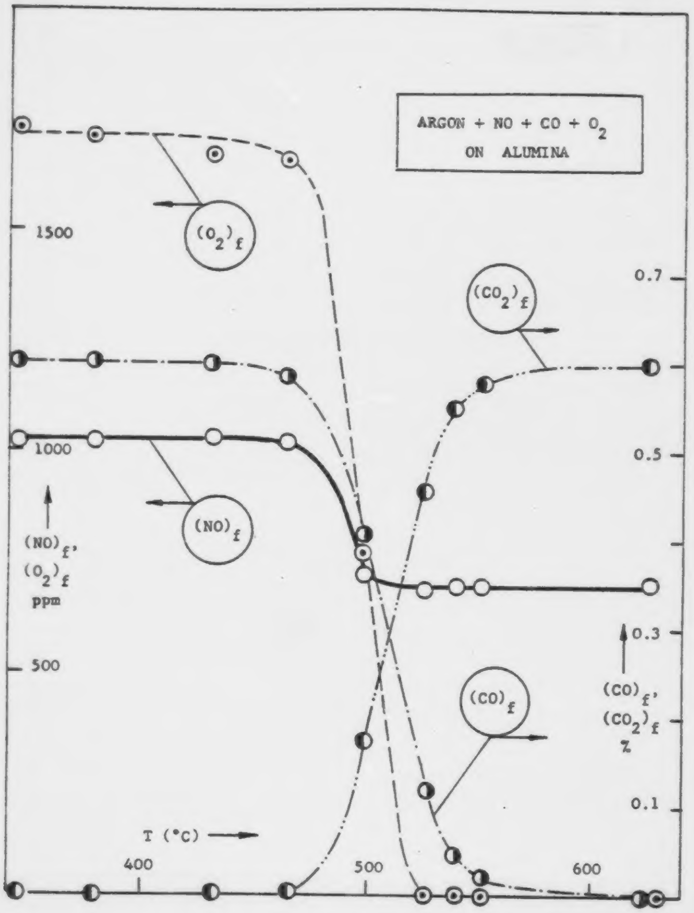

Figure 38. Argon + NO + CO + O_2 on Alumina: D = 17.1 cm^3s^{-1}; $(NO)_i$ = 1025 ppm; $(CO)_i$ = 0.60%; $(O_2)_i$ = 0.17%.

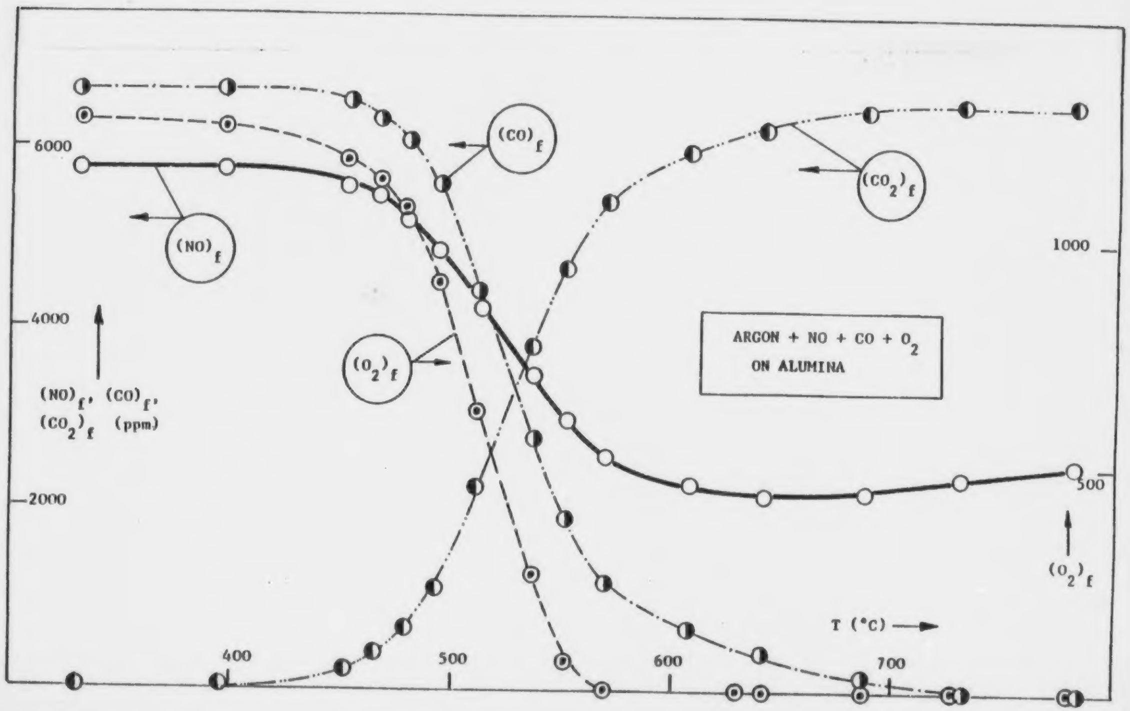

Figure 39. Argon + NO + CO + O_2 on Alumina: D = 15.3 cm^3s^{-1}; $(NO)_i$ = 5750 ppm; $(CO)_i$ = 0.66%; $(O_2)_i$ = 0.13%.

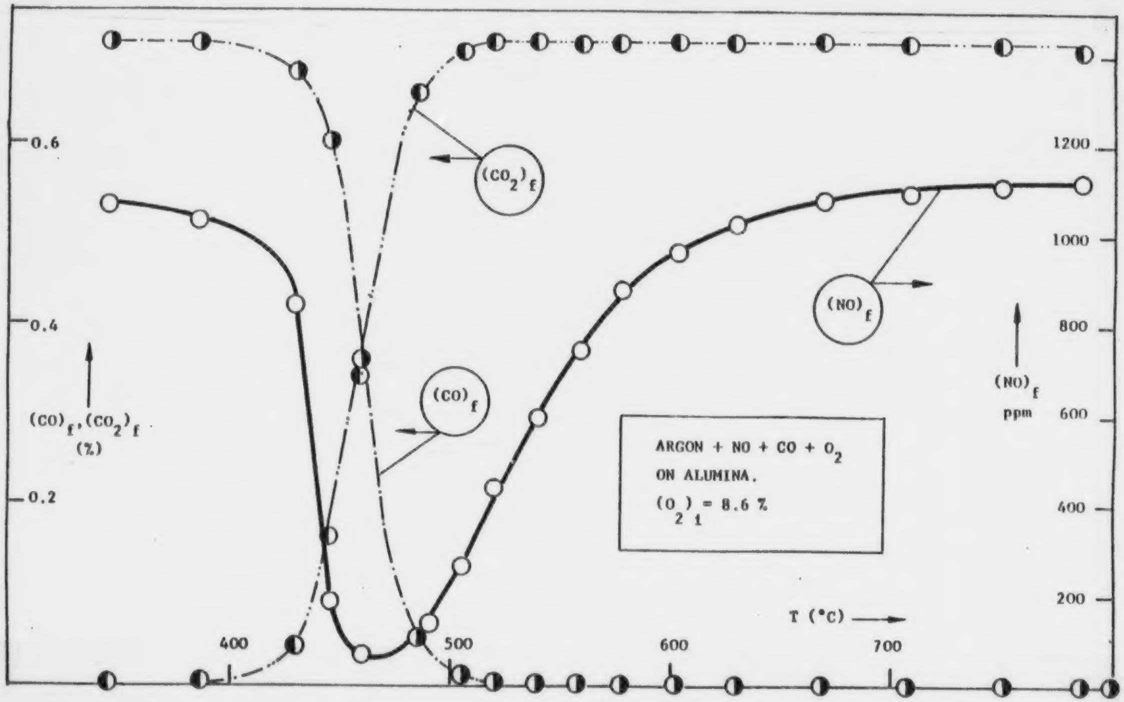

Figure 40. Argon + NO + CO + O_2 on Alumina: D = 14.5 cm^3s^{-1}; $(CO)_i$ = 1100 ppm; $(CO)_i$ = 0.71%; $(O_2)_i$ = 8.76%.

$$\overline{V_{JKT.1}} = -d(NO)/dt$$

$$= 6.2 \times 10^{8} \exp[-15600(\pm 2000)/T] \; X_{NO} X_{CO}^{0.3} \; (1+43) X_{O_2}^{0.36} \tag{60}$$

The precision is rather poor, but it is seen that for X_{O_2} dropping to zero, one finds rate expression V_8 given by eq. (25). The presence of O_2 seems to affect primarily the value of the preexponential constant, but not the temperature dependence of reaction (8).

2. The presence of NO, in turn, also enhances the rate of CO oxidation by molecular oxygen (reaction 20), which shifts to lower temperature ranges when nitric oxide is present in the gas. For example, compare Figures 7 through 9 with Figures 36 through 40.
3. Finally, the presence of O_2 and NO seems to enhance even CO oxidation by solid bound oxygen (reaction 12). The decrease of CO after total consumption of available gaseous oxygen (either in the form of O_2 or in the form of NO) is much faster than the rate of CO decrease in the absence of NO and O_2 (see Figure 4).

In summary, the presence of a supplementary oxidizer enhances the carbon monoxide oxidation rates. NO acts as a supplementary oxidizer for the CO + O_2 oxidation, O_2 acts as the supplementary oxidizer for the CO + NO oxidation, and both NO and O_2 enhance the CO + (-O) oxidation. If the latter case is readily understandable by the reoxidation of the reduced metal into metal oxide, the former two phenomena are more difficult to explain without a knowledge of the intimate heterogeneous mechanism of the oxidation reactions (8) and (20).

At a first flance, the presence of oxygen seems to promote NO reduction by CO rather than to inhibit it. This, of course, is only totally true if the reaction medium is globally reducing. Indeed, as was expected á priori, when the reaction medium becomes globally oxidizing, and at temperatures where the CO oxidation is fast enough to consume all the available CO, NO cannot be further reduced (see Figure 40). Notwithstanding that observation, even in strongly oxidizing conditions, NO may be reduced at lower temperatures, where V_8 is faster than V_{20} (the overall activation energy of the latter being higher than that of the former, compare eqs. 13 and 19). In determining whether the mixture is globally reducing or oxidizing, one should take into account the role played by solid bound oxygen. In fact, independent of the ratio $(CO)_i/2\left(O_2\right)_i$, as soon as CO has disappeared, the NO reduction stops and part of the initial nitric oxide will be found in the outlet gas (see Figures 37 through 39).

3.2.1.3.2 Argon + NH_3 + O_2 on Alumina (Case Q.1)

F 41-44

Trials of this series are illustrated in Figures 41 through 44. The following experimental observations have been made:

1. NO_2 is never found in the reactor outlet gas. Therefore, it may be assumed with reasonable probability that the only nitrogen-containing species are: NH_3, NO, and N_2.
2. NO is formed as soon as NH_3 begins to decrease. The amounts of NO formed are roughly proportional to the initial ammonia concentration (compare Figures 42 and 44), but depend only weakly on the initial O_2 concentration as long as it is sufficiently high (compare Figures 41, 42, and 43). Under all circumstances, only a relatively small fraction of ammonia is transformed into NO. Even with as much as 36 percent O_2 in the initial gas composition, the maximum value of $(NO)_f$ only corresponds to 22 percent of the initial amount of ammonia (see Figure 43). At higher temperatures, NO again decreases due to reaction (4).
3. The decrease of ammonia takes place at lower temperatures when oxygen is present than when oxygen is absent. This enhancement of the global NH_3 reduction rate becomes more important as $\left(O_2\right)_i$ is increased. This is clearly shown on Figure 45, giving the relative ammonia decrease $\left(NH_3\right)_f/\left(NH_3\right)_i$ as a function of temperature for different initial oxygen concentrations.
4. Calculation of the mass balances demonstrates that practically no free hydrogen molecules are present in the reactor outlet flow

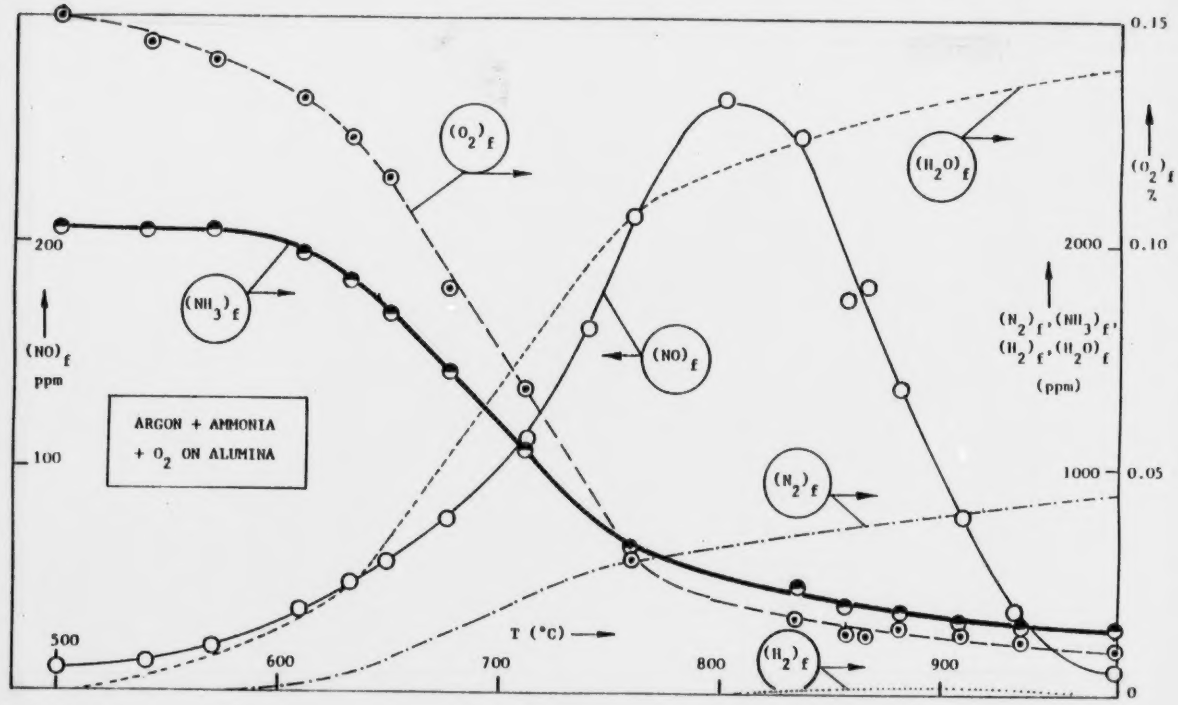

Figure 41. Argon + Ammonia + O_2 on Alumina: D = 14.6 cm^3s^{-1}; $(NH_3)_i$ = 2050 ppm; $(O_2)_i$ = 0.15%.

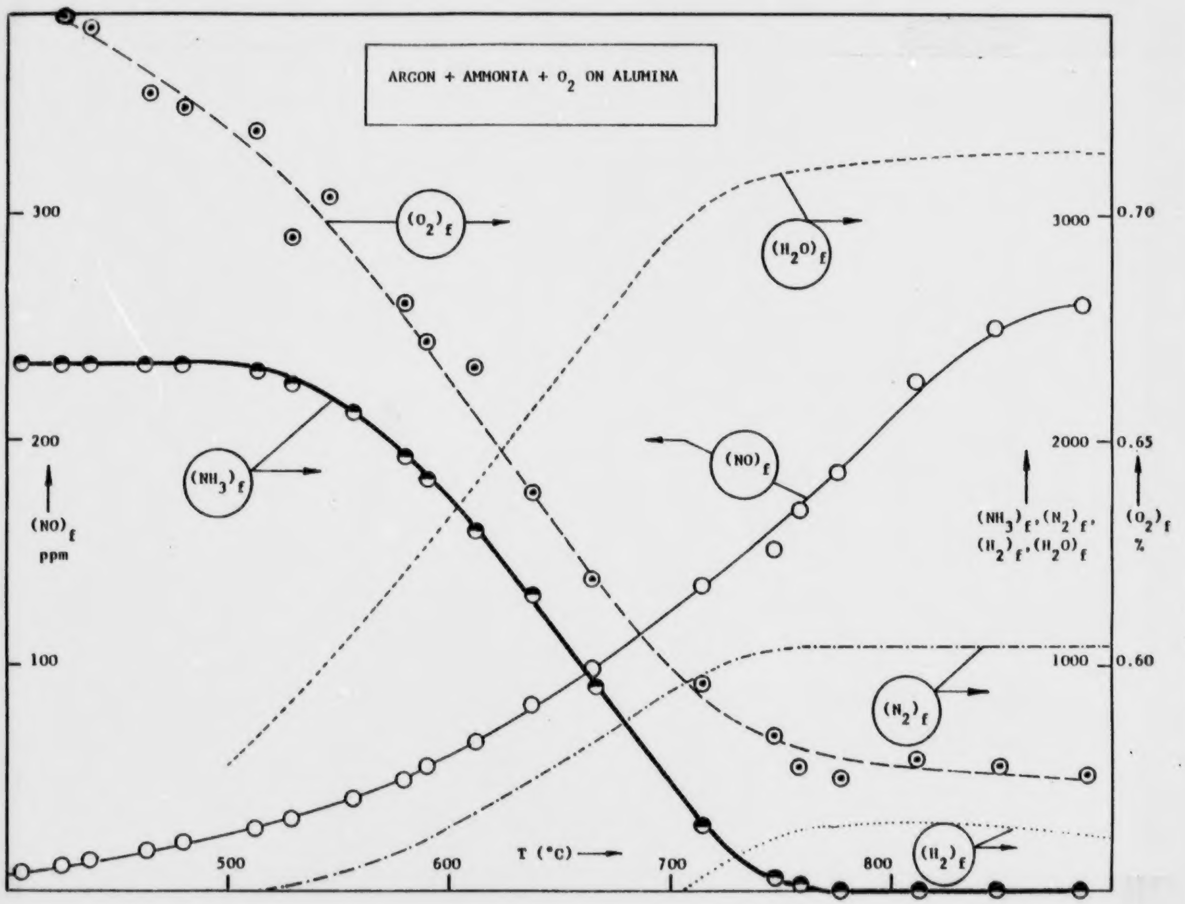

Figure 42. Argon + Ammonia + O_2 on Alumina; D = 14.3 cm^3s^{-1}; $(NH_3)_i$ = 2350 ppm; $(O_2)_i$ = 0.75%.

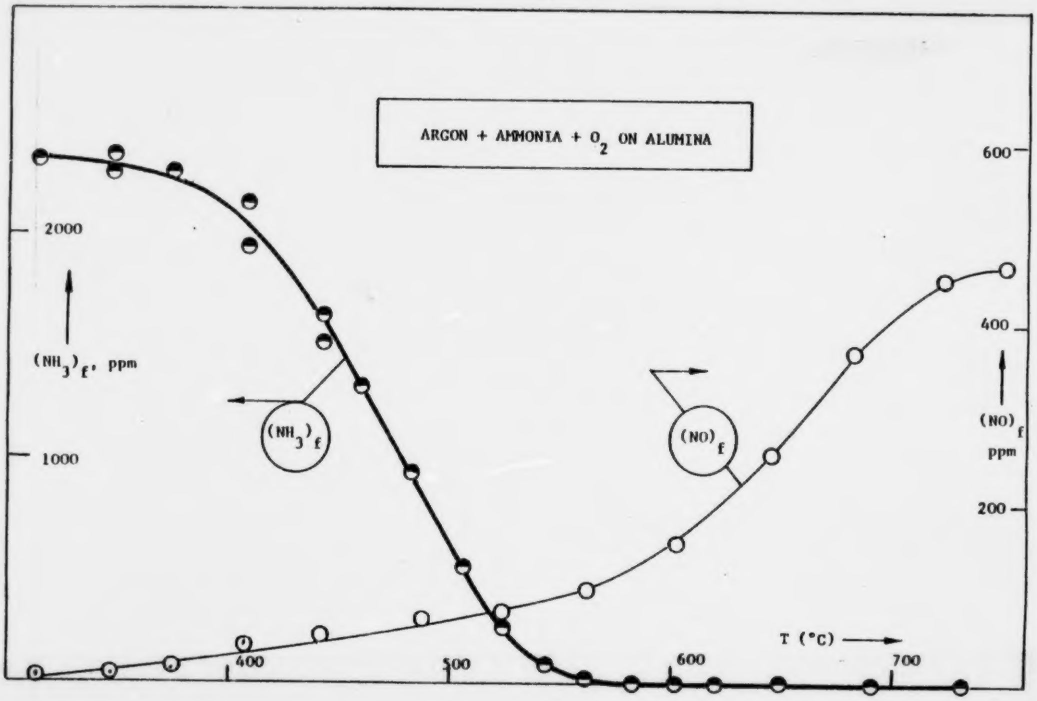

Figure 43. Argon + Ammonia + O_2 on Alumina; D = 14.2 cm^3s^{-1}; $(NH_3)_i$ = 2310 ppm; $(O_2)_i$ = 37.00%.

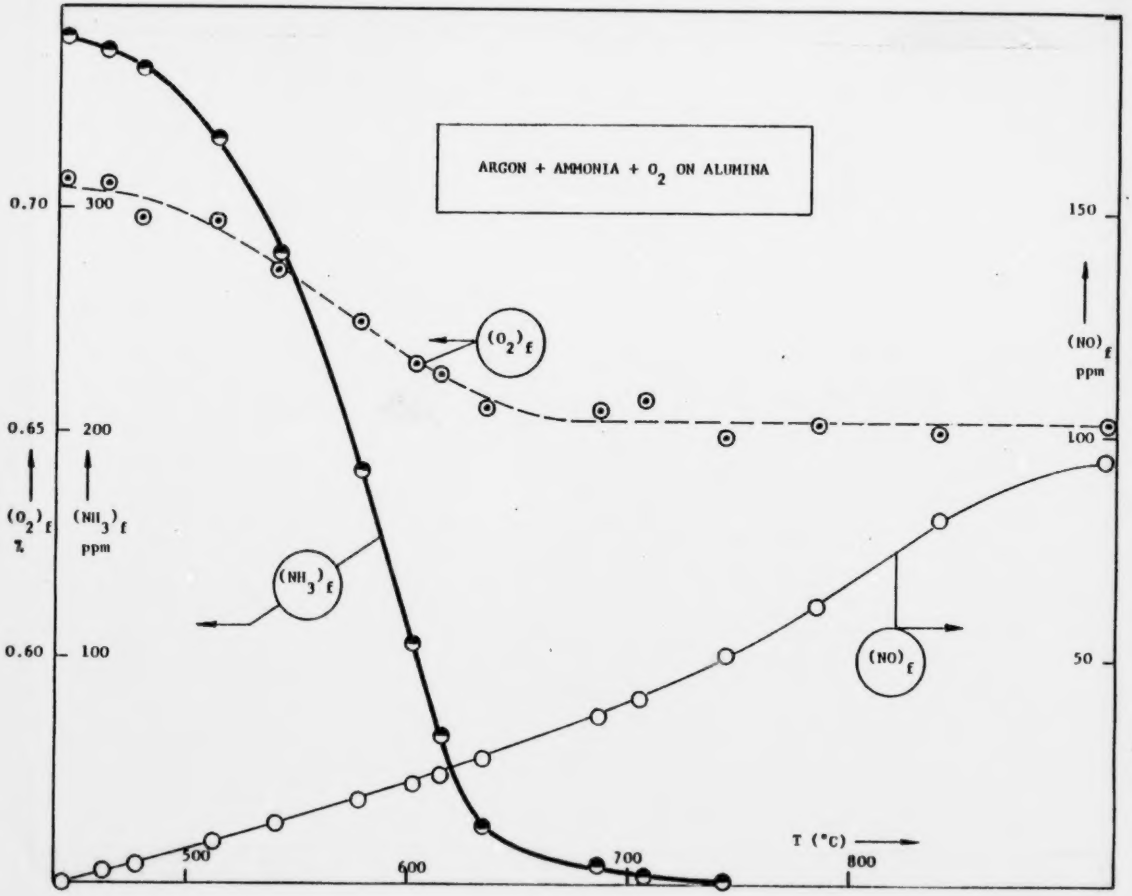

Figure 44. Argon + Ammonia + O_2 on Alumina; D = 15.2 $cm^3 s^{-1}$; $(NH_3)_i$ = 385 ppm; $(O_2)_i$ = 0.71%.

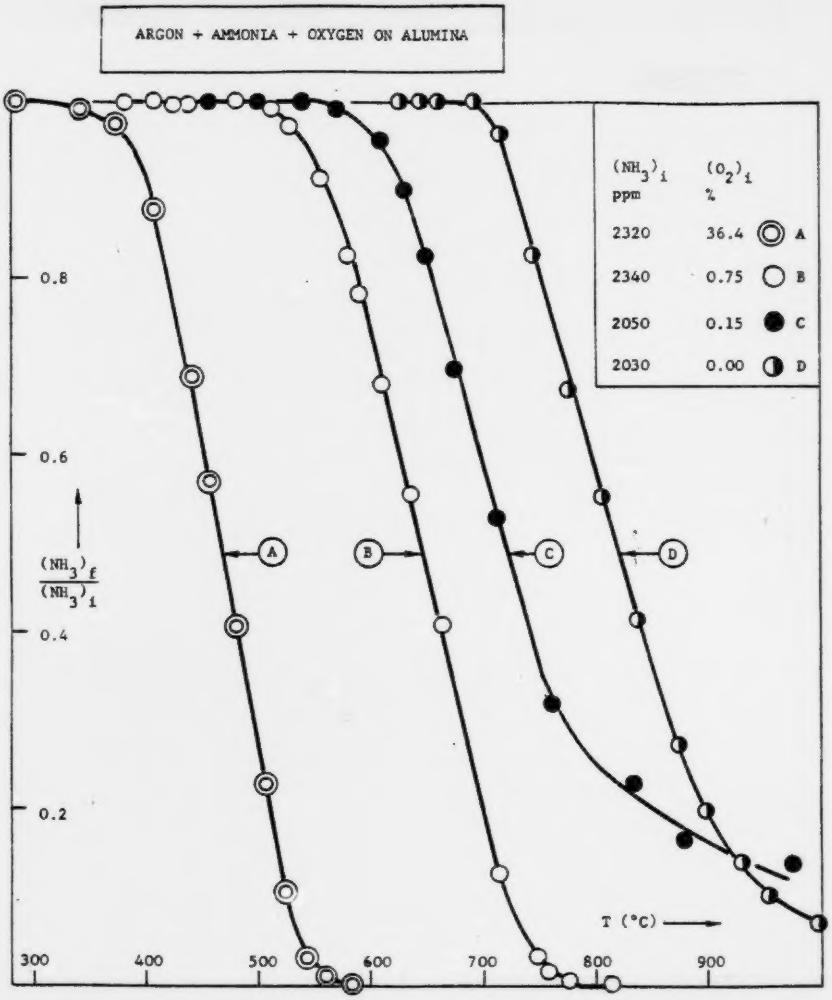

Figure 45. Argon + Ammonia + O_2 on Alumina; D = 14.3 to 15.3 $cm^3 s^{-1}$; Effect of Oxygen Concentration on NH_3 Removal.

since sufficient oxygen is present. The mass balance is given by the following equations:

O-balance: $2(O_2)_i = 2(O_2)_f + (NO)_f + (H_2O)_f$ (61)

N-balance: $(NH_3)_i = (NH_3)_f + (NO)_f + 2(N_2)_f$ (62)

H-balance: $3(NH_3)_i = 3(NH_3)_f + 2(H_2O)_f$ (63)

Calculated values of $(H_2O)_f$, $(H_2)_f$ and $(N_2)_f$ are also given on Figures 41 and 42.

Existence of the following reaction paths is concluded from the observations discussed above:

1. Since the presence of oxygen molecules enhances the decrease of ammonia (observation 3) and since the NO thus formed accounts for only a small fraction of the NH_3 which disappeared (observation 2); and, finally, since no free hydrogen is formed, we apparently have to look for a reaction path by which ammonia and oxygen yield NO and as well as N_2 as products. Even N_2 formation from NH_3 must go through a reaction with oxygen, since reaction (13) (i.e. $NH_3 \rightarrow 0.5\ N_2 + 1.5\ H_2$) has been observed to be too slow (observation 3). The absence of H_2 as a product suggests that the other reaction product is water vapor:

   $(2a + b)NH_3 + (1.5a + 0.75b)\ O_2 \rightarrow aN_2 + bNO + (3a + 1.5b)\ H_2O$ (64)

   We shall consider this global conversion of ammonia into NO and N_2 as the result of two different extreme reaction paths, one leading exclusively to NO, the other exclusively to N_2, both of which have H_2O as the other product:

   $N_3 + 0.75\ O_2 \xrightarrow{16} 0.5\ N_2 + 1.5\ H_2O$

   $NH_3 + 1.25\ O_2 \xrightarrow{17} NO + 1.5\ H_2O$

When only these two reactions are considered (the others being assumed negligibly slow), then their relative rates determine the ratio a/b of eq. (64), as well as the relative concentrations of products N_2 and NO:

$$0.5\ V_{16}/V_{17} = (N_2)_f/(NO)_f = a/b \tag{65}$$

This relation should be true only for small advancements of ammonia decrease, since only in that case may other reactions be neglected (in particular, reaction 13, which only becomes important at temperatures beyond 700°C).

2. The reaction typical of case D.1, [i.e. reaction (13)] also plays a role in the formation of N_2, but only at higher temperatures where its rate is comparable to that of (16), as follows from observation 3.

3. The formation of NO as a product from reaction (17), also brings reaction (4) into the present mechanism.

We thus have for the time variation of nitrogen-containing species, the following set of equations:

$$d(NH_3)/dt = -V_{16} - V_{17} - V_{13} - nV_4 \tag{66}$$

$$d(NO)/dt = V_{17} - V_4 \tag{67}$$

$$d(N_2)/dt = \frac{1}{2}V_{16} + \frac{1}{2}V_{13} + \frac{1+n}{2} V_4 \tag{68}$$

Substituting the value of V_4 calculated from eq. (52), into eq. (67), solving this equation for V_{17}, and employing the data of Figure 46, yields the following expression:

$$\boxed{V_{17} = 418 \text{ to } 15 \times 10^4 \exp[-12200(\pm 1000)/T]\ X_{NH_3}^{0.6}\ X_{O_2}^{0.3}} \tag{69}$$

Substituting values of V_4, V_{13}, and V_{17}, calculated according to eq. (52), (16), and (69), into eq. (66) and solving for V_{16} yields (see Figure 47):

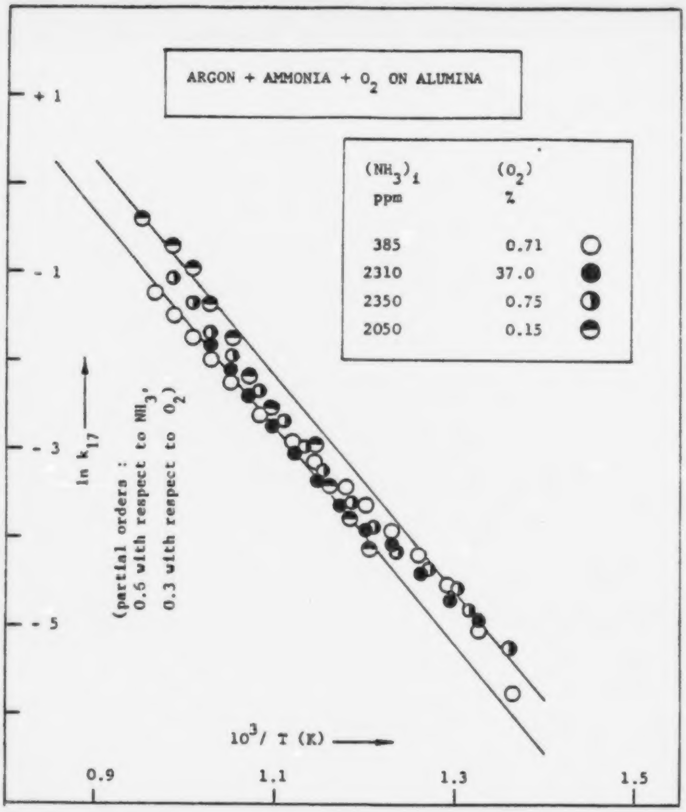

Figure 46. Argon + Ammonia + O_w on Alumina: Determination of Rate Constant k_{17} According to eq.(67), for Different Initial Concentrations of Ammonia and Oyxgen.

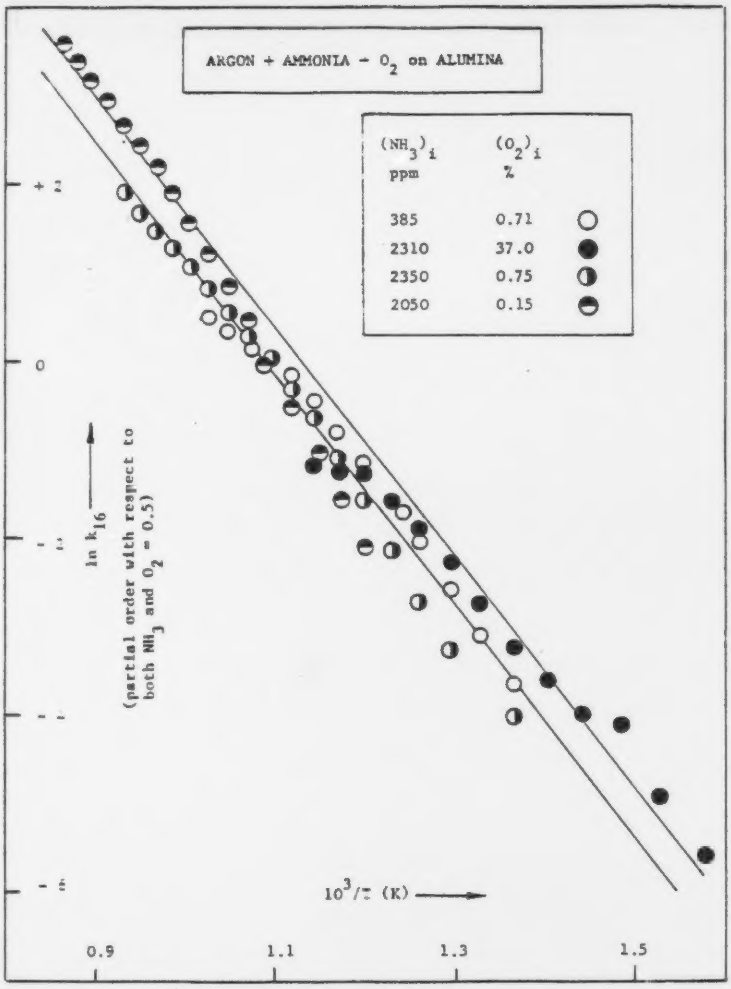

Figure 47. Argon + Ammonia + O_2 on Alumina: Determination of Rate Constant k_{16} According to eq. (66), for Different Initial Concentrations of Ammonia and Oxygen.

$$\boxed{V_{16} = 1.3 \text{ to } 3.1\ 10^{6} \exp[-13000(\pm 1000)/T]\ X_{NH_3}^{0.5}\ X_{O_2}^{0.5}} \qquad (70)$$

In the following table we compare the ratio V_{16}/V_{17} (obtained from eqs. 69 and 70), to the ratio $(N_2)_f/(NO)_f$ (calculated from the mass balance 62), under conditions of sufficiently small advancement of the ammonia decrease.

Argon + Ammonia + O_2 on Alumina				
$(NH_3)_i$	$(O_2)_i$	T(°C)	0.5 V_{16}/V_{17}	$(N_2)_f/(NO)_f$
2050	0.150	640	3.88	2.25
		700	4.08	3.85
2350	0.750	520	4.65	
		580	5.04	3.80
		640	5.47	6.07
		700	5.90	7.25
385	0.705	560	5.94	
		620	6.59	
2310	37.000	360	7.64	
		420	8.70	

From this table it may be shown that the stoichiometric ratio a/b (equation 64) of the combined reactions (16) and (17) is between 3 and 9.

The study of the case Q.1, (i.e. Argon + ammonia + oxygen mixtures fed over an alumina bed), has thus shown the existence of another possible effect of oxygen on NO reduction by solid particles. Unlike the former case (section 3.2.1.3.1) there does exist an interaction between oxygen and nitrogen containing species (NH_3). This reaction between oxygen and ammonia leads to the undesirable formation of nitric oxide (reaction 17), but also leads (and even much faster) to an important transformation of the ammonia molecules into molecular nitrogen at temperatures much lower than would be possible without oxygen. The final "yield" or ratio of N_2 and NO formed from ammonia, is always favorable towards preferential N_2

formation, even with significant excesses of oxygen. The destructive oxidation of NH_3 is preferentially directed towards molecular nitrogen formation. It is worthwhile to stress the difference between this particular type of heterogeneous ammonia destruction and the behavior of ammonia in the gas phase under oxidizing conditions. The behavior of gas-phase ammonia oxidation is well known due to extensive studies in nonsooting premixed flames. Under such conditions NO is the dominant nitrogeneous product when there is an excess of oxygen (Ref. 19).

The fact that oxygen can promote heterogeneous NO reduction in the presence of ammonia has been reported earlier for Pt catalysts (Ref. 18, 20).

3.2.1.3.3 Argon + NO + H_2 + O_2 on Alumina (Combined Case NOT.1)

F48 –
F53

Illustration of the results of these trials is given in Figures 48 through 53. The effect of initial hydrogen concentration can be implied by comparing Figures 48, 49, and 50. For the effect of the initial oxygen concentration, see Figures 48, 51, and 52; for the effect of the initial NO concentration, compare Figures 48 and 53. More specifically the effect of increasing amounts of molecular oxygen on the decrease of nitric oxide and the formation of ammonia, is illustrated in Figures 54 and 55.

F54 –
F55

Experimentally, the following observations can be made:

1. NO_2 has never been detected at the reactor outlet, and is therefore disregarded.
2. During the disappearance of NO and O_2, the formation of ammonia is observed. The gas-phase products are thus: H_2, O_2, H_2O, NO, NH_3, and N_2. The values of $(N_2)_f$ and $(H_2O)_f$ may thus be calculated from the following mass balances:

$$\text{O-balance:}\quad (NO)_i + 2(O_2)_i = (NO)_f + 2(O_2)_f + (H_2O)_f{}^* \qquad (71)$$

---

*As long as O_2 was present in the outlet gas flow, reaction (19) has been disregarded. Consequently, the concentration $(\text{-}O)_f$ does not appear in the oxygen balance.

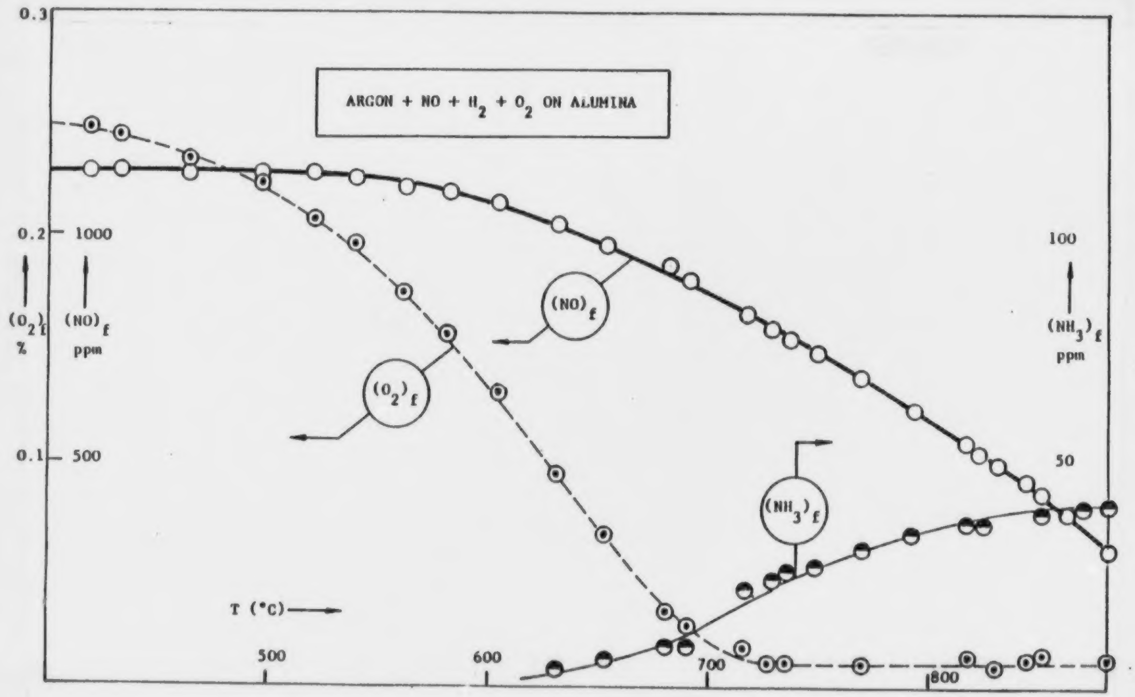

Figure 48. Argon + NO + Hydrogen + O_2 on Alumina: D = 15.1 cm^3s^{-1}; $(NO)_i$ = 1140 ppm; $(H_2)_i$ = 2.50%; $(O_2)_i$ = 0.28%.

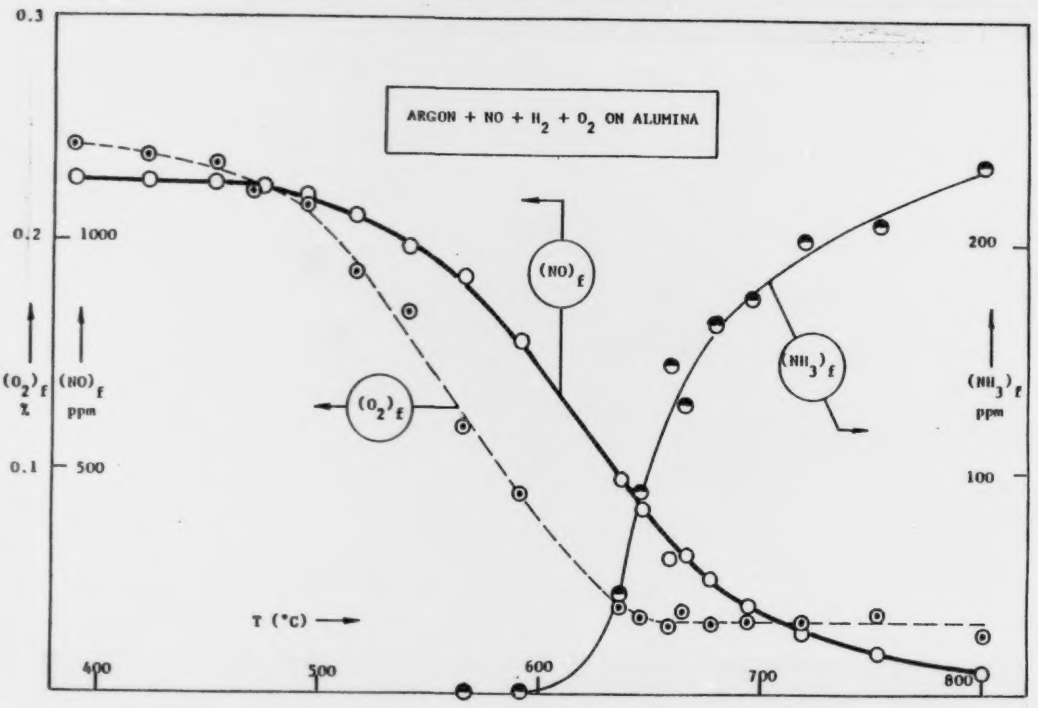

Figure 49. Argon + NO + Hydrogen + O_2 on Alumina: D = 16.2 cm^3s^{-1}; $(NO)_i$ = 1130 ppm; $(H_2)_i$ = 7.40%; $(O_2)_i$ = 0.25%.

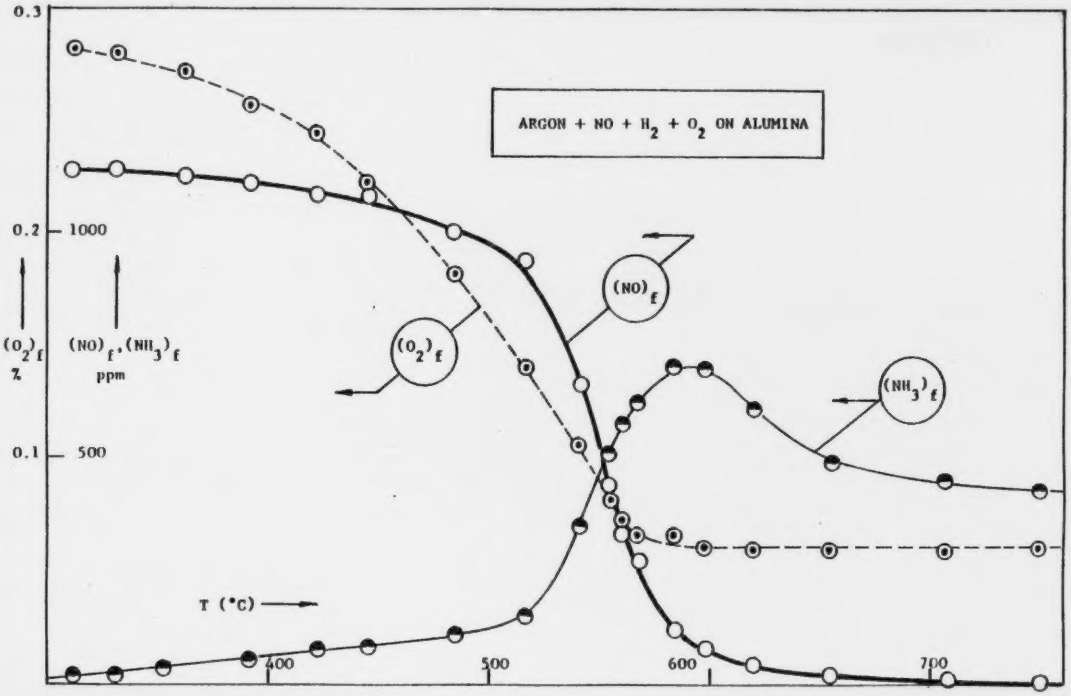

Figure 50. Argon + NO + Hydrogen + O_2 on Alumina: D = 16.0 cm^3s^{-1}; $(NO)_i$ = 1170 ppm; $(H_2)_i$ = 18.80%; $(O_2)_i$ = 0.29%.

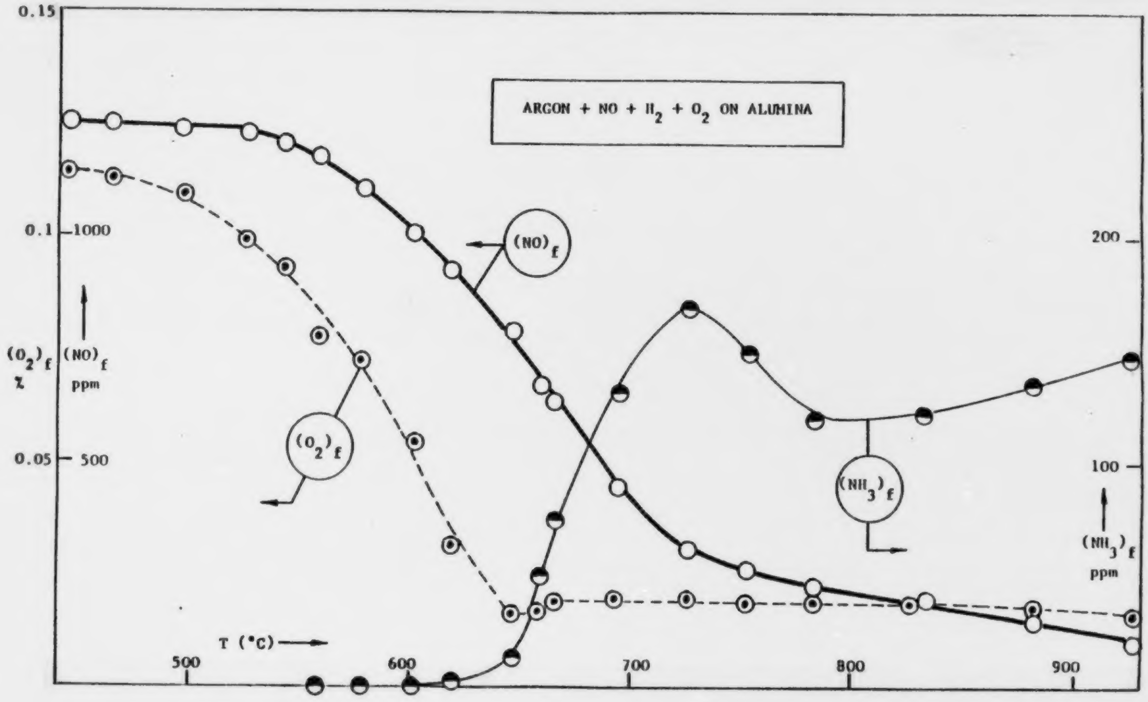

Figure 51. Argon + NO + Hydrogen + O_2 on Alumina: D = 16.6 cm^3s^{-1}; $(NO)_i$ = 1250 ppm; $(H_2)_i$ = 2.50%; $(O_2)_i$ = 0.13%.

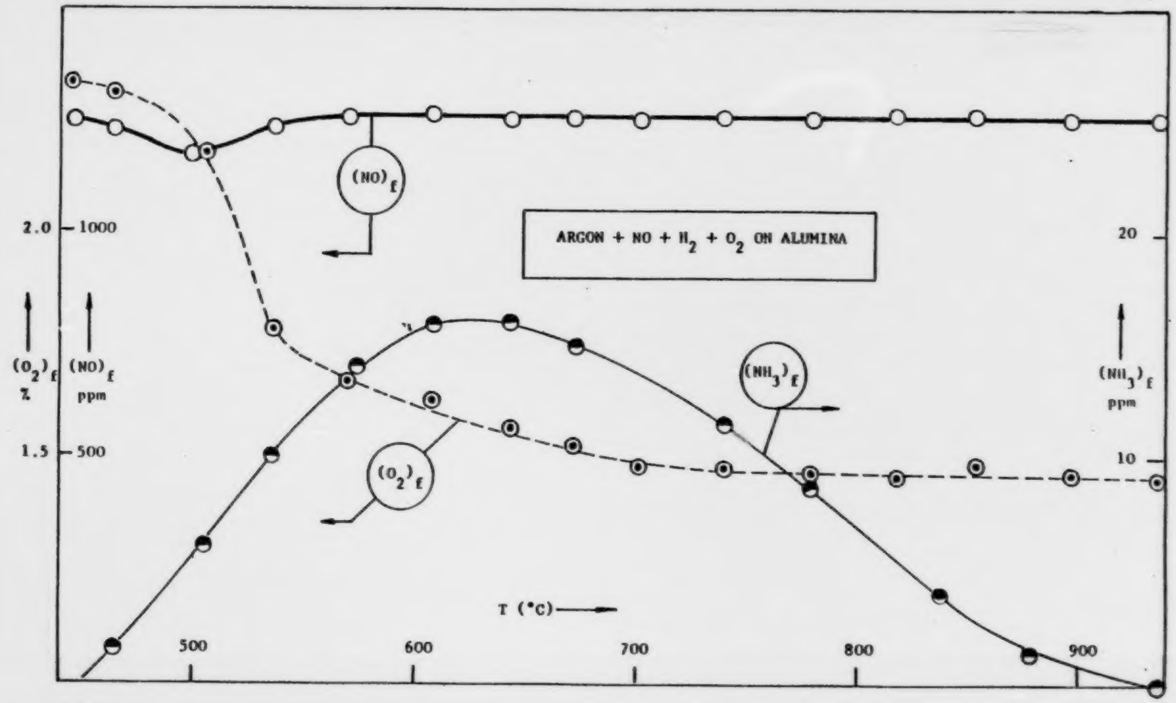

Figure 52. Argon + NO + Hydrogen + O_2 on Alumina: D = 16.1 cm^3s^{-1}; $(NO)_i$ = 1250 ppm; $(H_2)_i$ = 2.57%; $(O_2)_i$ = 2.37%.

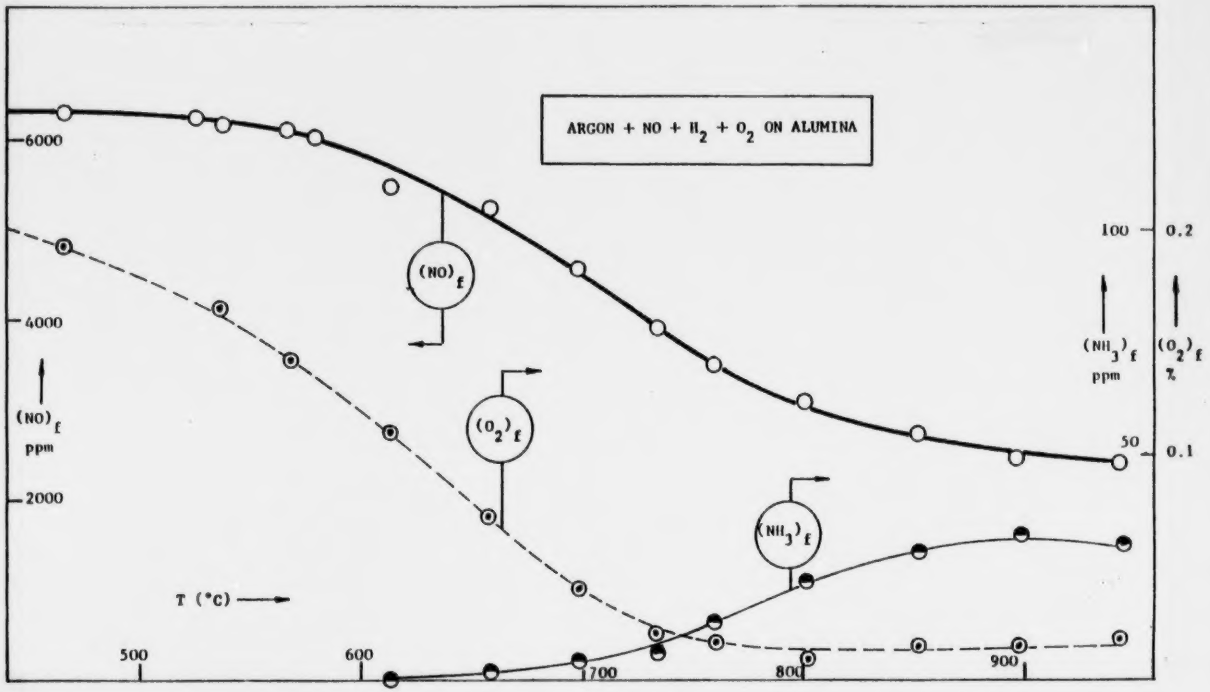

Figure 53. Argon + NO + Hydrogen + O_2 on Alumina: D = 15.1 cm^3s^{-1}; $(NO)_i$ = 6300 ppm; $(H_2)_i$ = 2.50%; $(O_2)_i$ = 0.22%.

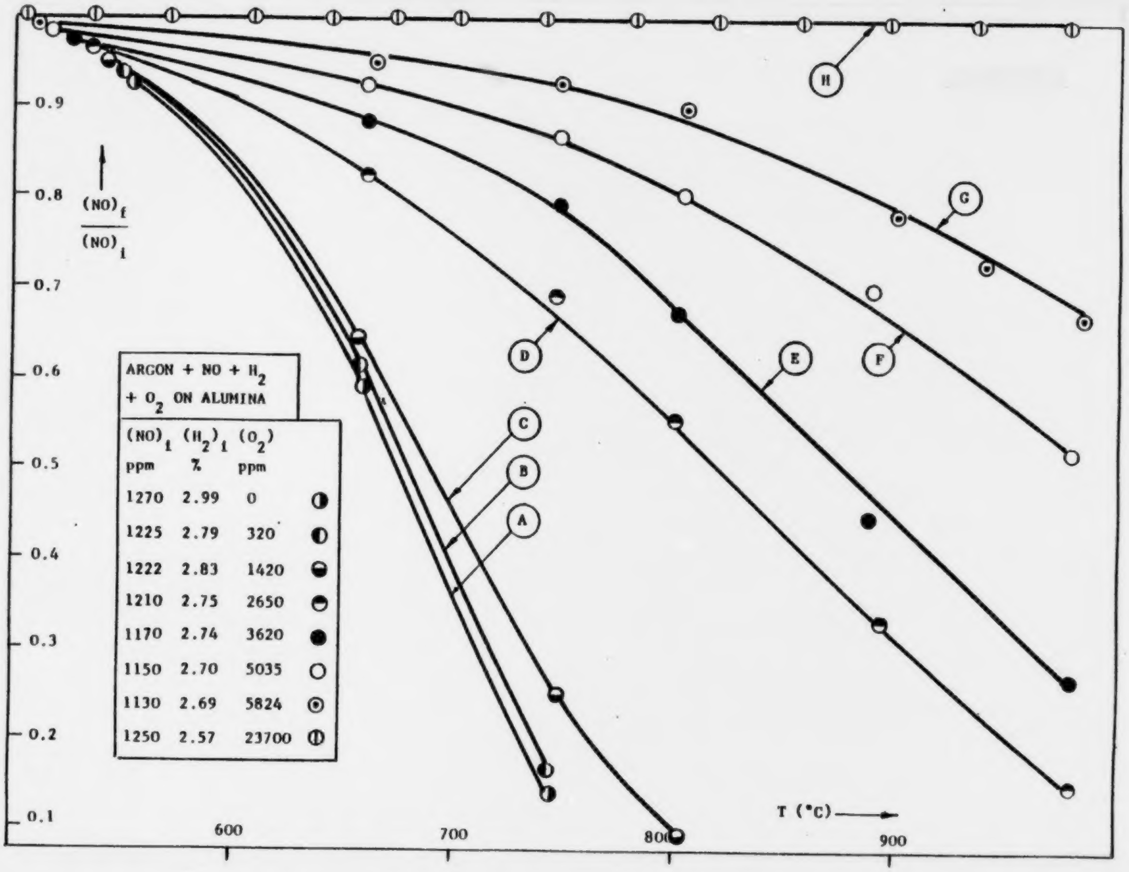

Figure 54. Argon + NO + Hydrogen + O_2 on Alumina: D = 14.8 cm^3s^{-1}; Effect of Initial Oxygen Concentration on NO Removal as a Function of Temperature.

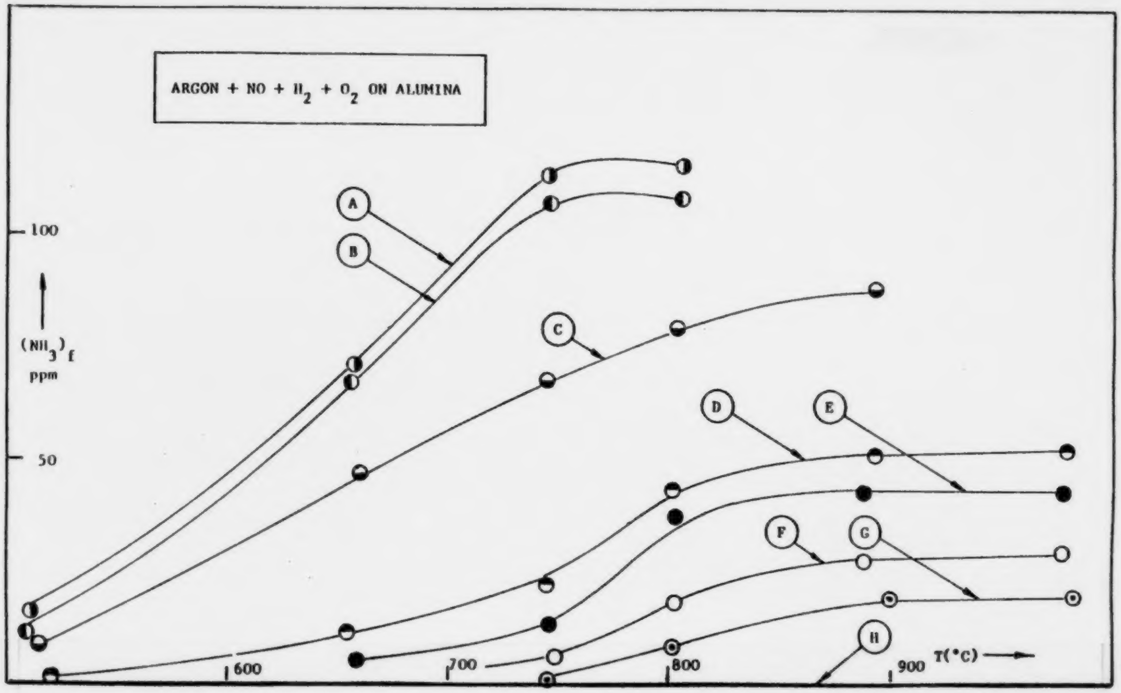

Figure 55. Argon + NO + Hydrogen + O_2 on Alumina: Effect of Initial Oxygen Concentration on Intermediate Ammonia Formation as a Function of Temperature. Same mixtures compositions as for Figure 54. Key of symbols: see Figure 54.

N-balance: $(NO)_i = (NO)_f + (NH_3)_f + 2(N_2)$ (72)

H-balance: $2(H_2)_i = 2(H_2)_f + 2(H_2O)_f + 3(NH_3)_f$ (73)

3. Contrary to the $NH_3 + O_2$ trials and to the $CO+O_2+NO$ trials, the presence of molecular oxygen in this case inhibits the heterogeneous NO reduction by hydrogen. This is clearly shown on Figure 54. For sufficiently high values of $(O_2)_i/(H_2)_i$, nitric oxide reduction is completely suppressed. This may also be seen in Figure 52.

The reactions playing a role in this combined case NOT.1, are reactions (11), (14, (4), (13), (16), (17), and (18). The variation of the nitrogen-containing species is described by the following set of differential equations:

$$d(NO)/dt = -V_4 - V_{11} - V_{14} + V_{17} = -\overline{V_{NOT.1}} \tag{74}$$

$$d(NH_3)/dt = -nV_4 + V_{11} - V_{17} - V_{16} - V_{13} \tag{75}$$

$$d(N_2)/dt = \frac{1+n}{2} V_4 + \frac{1}{2} V_{14} + \frac{1}{2} V_{16} + \frac{1}{2} V_{13} \tag{76}$$

The overall decreasing rate $\overline{V_{NOT.1}}$ differs from that which exists in the absence of oxygen (i.e. $\overline{V_{0.1}}$, given by equation 44) by the term V_{17}:

$$\overline{V_{NOT.1}} = \underbrace{-\ d(NO)/dt}_{I} = \underbrace{\overline{V_{0.1}} - V_{17}}_{II} \tag{77}$$

Equation (77) is based on the assumption that the total inhibiting effect of oxygen presence on nitric oxide reduction arises from the presence of reaction (17) in the mechanism. Only if this is true will the righthand side (II) and the lefthand side (I) of equation (77) be reasonably equal. To check this assumption, the global reaction $\overline{V_{NOT.1}}$ is determined by two approaches: (1) from the experimental decrease of nitric oxide (according to part I of equation 77), and (2) from part II of equation (77) by substituting the values of $\overline{V_{0.1}}$ and V_{17}, calculated respectively by equations (56) and (69). Comparison of these two sets of values should give information on whether or not the existence of V_{17} is the only factor of inhibition.

1. Calculation of $\overline{V_{NOT.1}}$ from the experimental values of d(NO)/dt.

The determination is made according to the expression:

$$\overline{V_{NOT.1}} = k_{NOT.1}\ X_{NO}^{m}\ X_{H_2}^{n} = -d(NO)/dt \tag{78}$$

The calculation has been made for trials where the initial H_2 and NO concentrations are kept constant, $O_{2\ i}$ being the only variable gas component. Therefore, the exact value of the partial order m and n should be of little importance; thus, they have been imposed to match the values defined earlier for equation (56) (m = .5, n = 1). Values of $k_{NOT.1}$ calculated according to eq. (78) are shown in Figure 56.

From this figure it is seen that the overall activation temperature $\left(E_{NOT.1}\right)$ and the preexponential part of the rate constant $k_{NOT.1\ o}$, vary with oxygen concentration. For very small oxygen concentrations or for zero oxygen concentration, these two parameters should respectively become equal to $E_{0.1}$ and $\left(k_{0.1}\right)_o$, which are the overall activation energy and the preexponential constant of rate $\overline{V_{0.1}}$. This dependence on the oxygen concentration, also shown in Figure 57, may be expressed as follows:

$$k_{NOT.1} = k_{0.1} / \left[1 + A\ (T)\ .X_{O_2}^{s}\right] \tag{79}$$

where A (T) indicates a function of temperature and s is a partial reaction order with respect to oxygen. The value of s was determined at constant temperature (see Figure 58) and found equal to 2. With s set equal to 2, the function A (T) is then determined, as shown in Figure 59. Finally, the following expression for $\overline{V_{NOT.1}}$ from eq. (78) is derived:

$$\begin{aligned}\overline{V_{NOT.1}} &= \frac{8.6 \times 10^{5} \exp -11900(+1000)/T}{1 + 1.1 \times 10^{8} \exp(-6000/T)\ .X_{O_2}^{2}}\ X_{O_2}^{0.5}\ X_{H_2} \\ &= \overline{V_{0.1}} \Big/ \left[1 + 1.1 \times 10^{8} \exp(-6000/T)\ .X_{O_2}^{2}\right]\end{aligned} \tag{80}$$

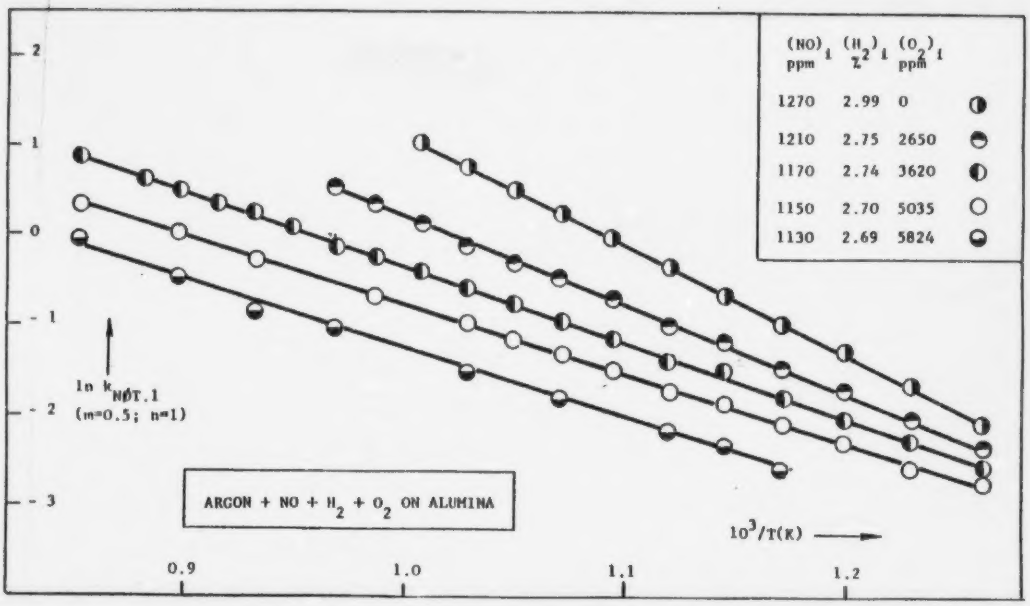

Figure 56. Argon + NO + Hydrogen $\pm$ O_2 on Alumina: Determination of the Rate Constant of $\overline{V_{NOT}}_{,1}$ According to eq.(78), for Different Initial Oxygen Concentrations.

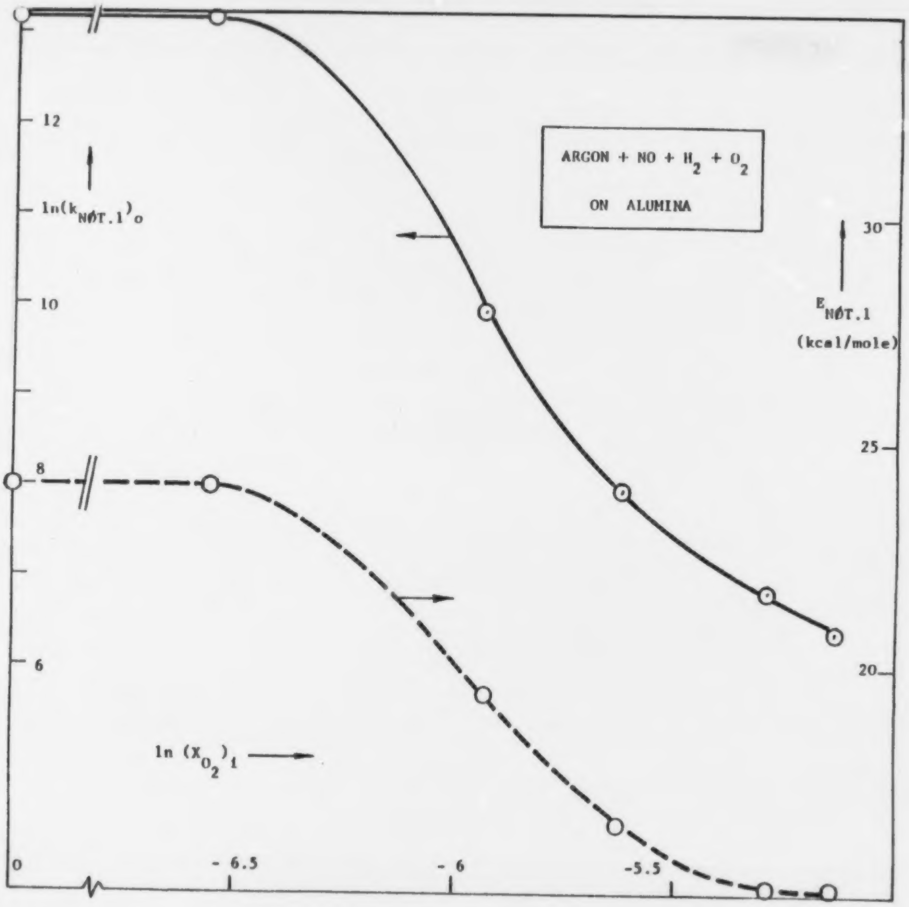

Figure 57. Argon + NO + Hydrogen + O_2 on Alumina: Variation of $k_{NØT.1}$ and $E_{NØT.1}$ as a Function of Initial Oxygen Concentration.

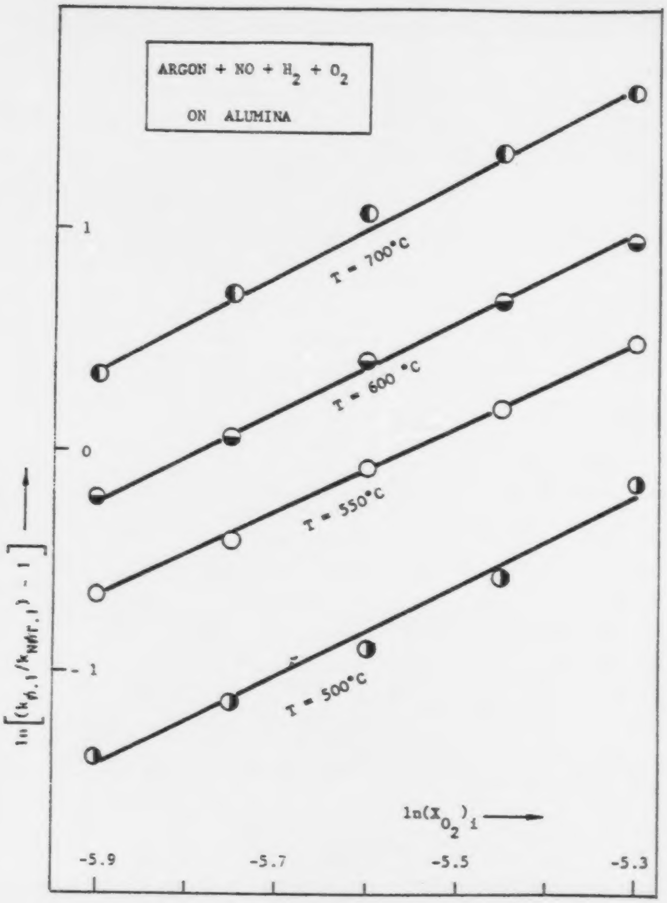

Figure 58. Argon + NO + Hydrogen + O_2 on Alumina: Determination of Partial Reaction Order of $V_{NØT,1}$ with Respect to Oxygen, According to eq.(79).

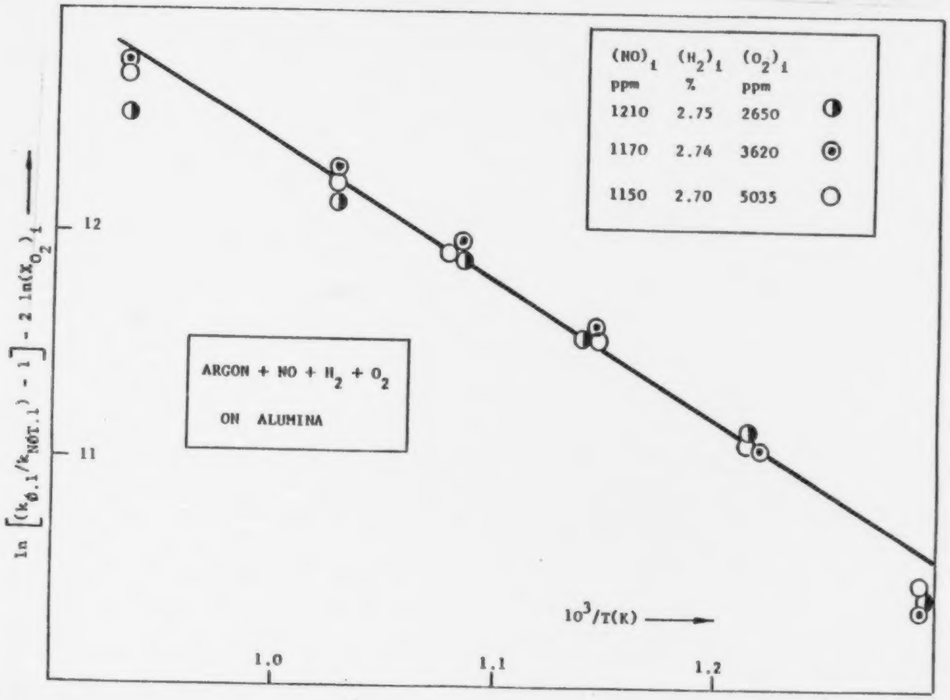

Figure 59. Argon + NO + Hydrogen + O_2 on Alumina: Dependence of the Ratio $k_{N\emptyset T.1}/k_{\emptyset.1}$ on Temperature, According to Equation (79).

2. Calculation of $\overline{V_{NOT.1}}$ from the righthand part of eq. (71).

Calculations according to eq. (77,II) are made and compared with the values computed according to equation (74) for different initial oxygen concentrations. The experimental values of $(NH_3)_f$ are utilized in the calculation of V_{17}. Results of this comparison are shown on the table below.

As may be seen from this table, the values of $\overline{V_{NOT.1}}$ calculated according to eq. (80), are systematically much smaller than the values calculated by eq. (77,II). From this observation, it may be concluded that the oxidation of the ammonia formed intermediately by reaction (17) is not sufficient to account for the experimentally observed inhibiting effect of O_2 on the

Effect of Oxygen on Nitric Oxide Reduction;
Argon + NO + H_2 + O_2 on Alumina. $(H_2)_i$ = 2.7%

NO_i ppm	$O_{2\,i}$ %	T °C	$\frac{\overline{V_{NOT.1}}\text{(eq. 77,II)}}{\overline{V_{0.1}}}$	$\frac{\overline{V_{NOT.1}}\text{ (eq. 80)}}{\overline{V_{0.1}}}$
1225	0.032	520	0.007	0.988
		560	0.995	0.987
		600	0.994	0.986
		640	0.993	0.984
		680	0.991	0.982
		720	0.989	0.980
		760	0.987	0.978
1170	0.362	520	0.999	0.635
		560	0.999	0.560
		600	0.998	0.507
		640	0.997	0.498
		680	0.996	0.515
		720	0.994	0.513
		660	0.992	0.477
		800	0.988	0.427
		840	0.986	0.378
		880	0.985	0.335
1130	0.582	520	0.999	0.389
		560	0.998	0.321
		600	0.998	0.284
		640	0.998	0.298
		680	0.998	0.308
		720	0.998	0.292
		760	0.996	0.263
		800	0.994	0.226
		840	0.991	0.192
		880	0.990	0.164
		920	0.988	0.141
		960	0.988	0.123
		1000	0.988	0.107

heterogeneous nitric oxide reduction by hydrogen. The general form of the empirically derived rate expression $\overline{V_{NOT.1}}$ (eq. 80) suggests the existence of a strong absorption of oxygen molecules on the active surface sites, probably stronger than the NO or H_2 molecules. The oxygen molecules must take the place of NO and/or H_2 on the active sites and cause the heterogeneous reduction of NO by H_2 to become strongly inhibited.

3.2.1.3.4 Conclusions of Section 3.2.1.3

In section 3.2.1.3, different ways for oxygen molecules to interfere with nitric oxide reduction have been observed. Results indicate that oxygen can serve either as an inhibitor or even as a promoter of that reduction:

- Inhibiting Effects of Oxygen
    1. The most trivial form of inhibition comes from the fact that, upon oxidizing the gaseous reducing agent (CO, H_2, NH_3), the oxygen decreases the concentration of one of the reactants of nitric reduction. In the case where the reducing agent is ammonia, this effect even results in supplementary NO formation (reaction 17). Whenever the experimental conditions (temperature, initial concentrations) are such that this oxidation reaction is faster than the NO reducing reaction, NO reduction may become impossible, viz. if the gaseous reducing agent is the deficient reactant in the oxidation reaction.
    2. The preferential absorption of oxygen molecules on the active surface sites may strongly inhibit heterogeneous NO reducing reactions as was found in the case of NO reduction by hydrogen.
- Promoting Effects of Oxygen
    1. As was found in the case of NO reduction by CO on alumina, there seems to exist a synergetic effect between the different oxidation reactions. The NO reduction by CO is an oxidation of CO by NO. This effect is found to be enhanced by additional oxygen molecules, which act as the co-oxidant for CO.

2. Another typical promoting effect is found with respect to ammonia, which, by virtue of reaction (4), acts as a gaseous reducing agent for nitric oxide reduction. It also plays the role of a NO reducing intermediate by the sequence of reactions (11) and (13), eventually being transformed into N_2. The transformation of ammonia into molecular nitrogen is strongly enhanced by the presence of oxygen, via the appearance of a new reaction path: the oxidation of NH_3 by oxygen into N_2 and NO, the ratio of these two products being always strongly in favor in N_2.

3.2.2 Trials on Graphite (Case 2)

In our investigation of overall NO reducing mechanisms on solid particles, graphite offers an interesting intermediate step, in that it has only bound carbon atoms and therefore allows the isolation of some typical reaction paths using bound carbon as a correactant, e.g. reactions (1) and (5) (see Table 2). Since this is the main area of interest for these series of trials, only cases D.1, F.2, K.2, O.2, and R.2 have been studied. In particular, no trials with oxygen addition have been made.

Because of the vastly different nature of graphite and alumina, it is not surprising that rates of reaction derived for graphite are different than those previously derived for alumina. The rates derived for graphite are numbered according to Table 2, but keep in mind that these now apply to graphite solid and not to alumina derived previously.

3.2.2.1 Argon + NO on Graphite (Case F.2)

Two examples of these trials are shown in Figures 60 and 61. It is observed that at relatively high temperatures (above 700°C) nitric oxide begins to decrease and at the same time CO and CO_2 are formed. Examination of these figures indicates that

$$(NO)_i = (NO)_f + (CO)_f + 0.5\left(CO_2\right)_f \qquad (81)$$

Since neither ammonia nor hydrogen cyanide can be formed under these conditions, the overall reaction responsible for NO decrease is the formation

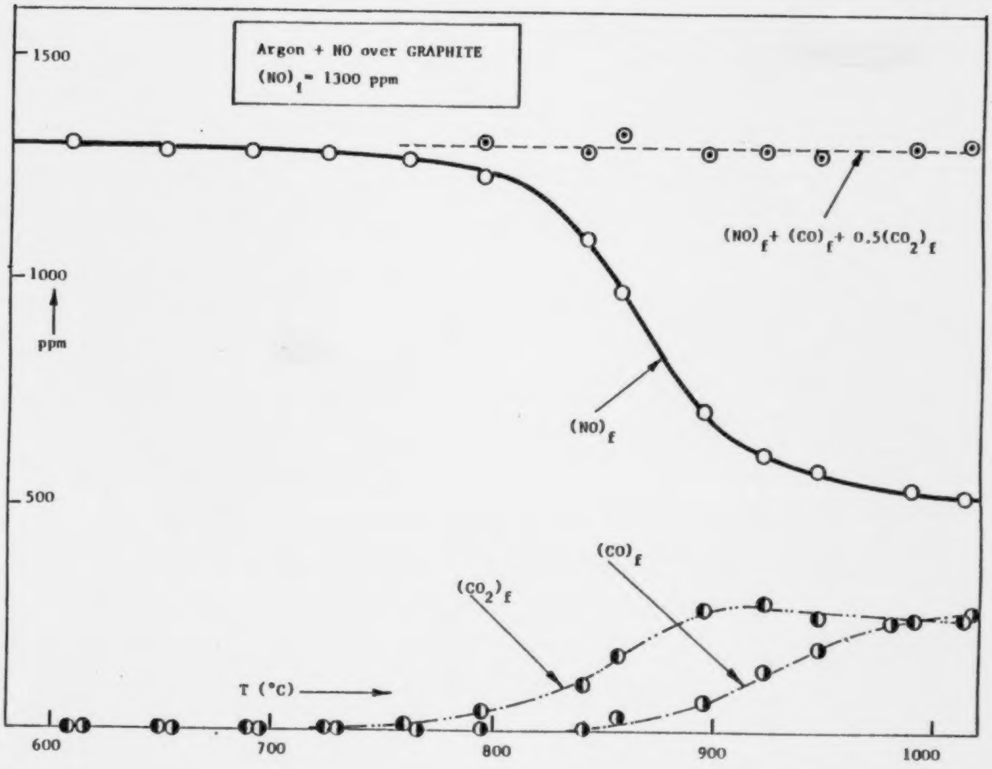

Figure 60. Argon + NO on Graphite: $D = 14.5\ cm^3s^{-1}$; $(NO)_i = 1300$ ppm.

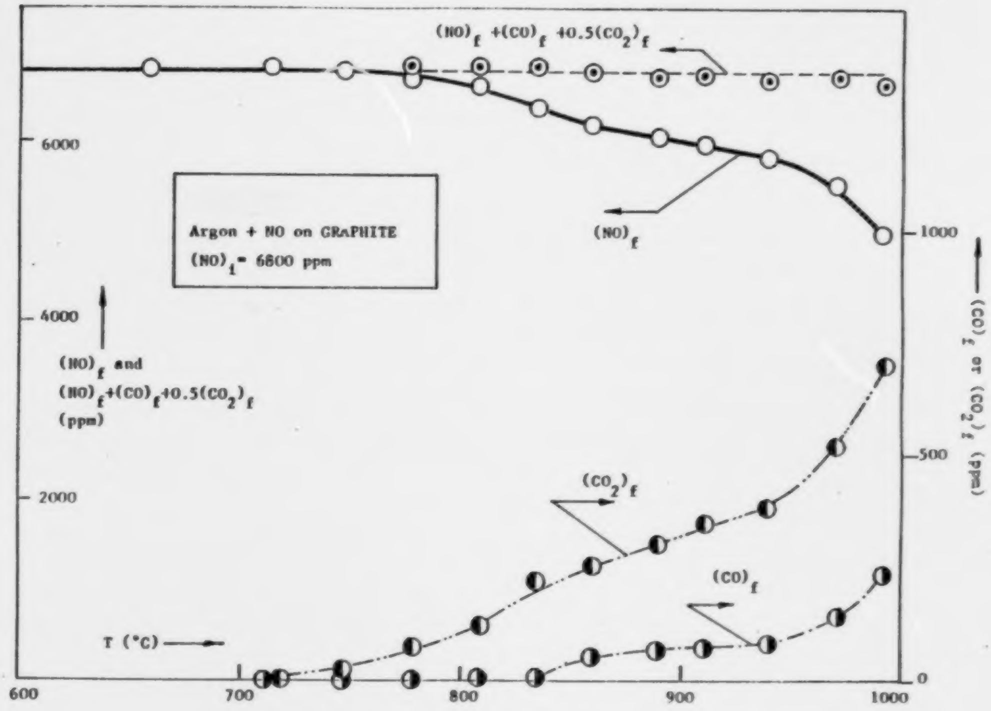

Figure 61. Argon + NO on Graphite: D - 14.5 cm^3s^{-1}; $(NO)_i$ = 6800 ppm.

of molecular nitrogen according to reaction:

$$NO + a(-C) \xrightarrow{1} 0.5\ N_2 + (2a-1)CO + (1-a)CO_2$$

with the coefficient "a" falling between 0.5 and 1, depending on temperature. Since CO is a reaction product, reaction (8) can become a possible secondary reaction. Therefore:

$$-d(NO)/dt = 2\ d\left(N_2\right)/dt = V_1 + V_8 = \overline{V_{F2}} \tag{82}$$

If V_8 is neglected as a secondary reaction for small NO decrease advancements, eq. (82) yields:

$$\boxed{V_1 = \overline{V_{F2}} = 1.9 \times 10^{11} \exp\left[-29000(\pm 1500)/T\right]\ X_{NO}} \tag{83}$$

As expected, the activation temperature is relatively high.

3.2.2.2 Argon + NO + CO on Graphite (Case K.2)

As indicated above, evidence of direct reduction of NO by graphite is observed for temperatures in excess of 700°C. The addition of CO to the inlet mixture results in complete NO disappearance before that temperature limit is reached. The data of Figure 62 indicates that an oxygen balance is closely represented by equation 84.

$$NO_i - NO_f \simeq CO_i - CO_f \simeq CO_{2_f} \tag{84}$$

This demonstrates that reaction 8 is responsible for the NO decrease in the temperature and concentration ranges examined. The total variation of NO and N_2 is given by eq. (82), but in this particular case, V_8 is the dominant primary reaction, and V_1 is of little importance.

Substitution of V_1 (calculated from eq. (83) into eq. (82), yields the value of V_8. As expected, the overall NO disappearance rate V_{K2}, calculated according to eq. (5), is found experimentally to be equal to V_8:

$$\boxed{V_8 = \overline{V_{K2}} = 10^5 \exp\left[-10100(\pm 1500)/T\right]\ X_{NO}\ X_{CO}} \tag{85}$$

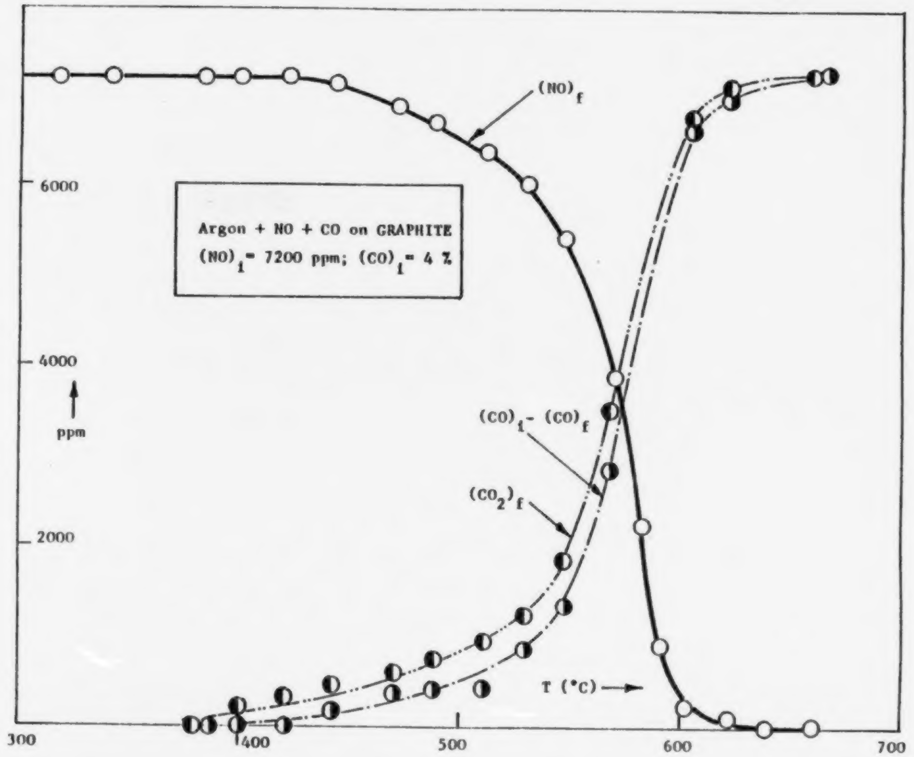

Figure 62. Argon + NO + CO on Graphite: D = 14.5 cm^3s^{-1}; $(NO)_i$ = 7200 ppm; $(CO)_i$ = 4.00%.

3.2.2.3 Argon + NH_3 on Graphite (Case D.2) (Figure 63)

As in the analogous case D.1 (Argon + NH_3 on Alumina), ammonia does not decrease at temperature below 700°C. Very small quantities of HCN (less than 3 ppm) are observed in the reactor outlet flow indicating that in the particular case of graphite, reaction (5) is almost negligible. The variation of HCN and NH_3 are determined by:

$$d(NH_3)/dt = -V_5 - V_{10} - V_{13} = -V_{D2} \tag{86}$$

$$d(HCN)/dt = V_5 - V_{10} - V_{15} \tag{87}$$

$$d(N_2)/dt = V_{10} + 0.5\, V_{13} + 0.5\, V_{15} \tag{88}$$

Combination of eqs. (86) and (87) yields:

$$-d(NH_3)/dt - d(HCN)/dt = V_{13} + 2\, V_{10} + V_{15} \tag{89}$$

Neglecting reactions V_{10} and V_{15} because they are secondary, this expression yields the value of V_{13}. Due to the very slow rate for the primary reaction V_5, determination of the value for $\overline{V}_{D2}$ by equation (5) yields a result which is identical to V_{13}. The derived rate expression is:

$$\boxed{V_{13} = \overline{V_{D2}} = 1 \times 10^8 \exp\left[-18800(\pm 1300)/T\right] X_{NH_3}} \tag{90}$$

3.2.2.4 Argon + NO + NH_3 on Graphite (Case R.2)

This case is illustrated by Figure 64. It is found experimentally that the decrease of NO is paralleled by an equal decrease of ammonia:

$$(NO)_i - (NO)_f = (NH_3)_i - (NH_3)_f \tag{91}$$

During the disappearance of nitric oxide, neither CO, CO_2 nor HCN is formed, suggesting that over this range reaction 4 is the only important reaction path. HCN begins to appear only after NO has already disappeared, and is probably formed by reaction 5:

$$NH_3 + (-C) \xrightarrow{5} HCN + H_2$$

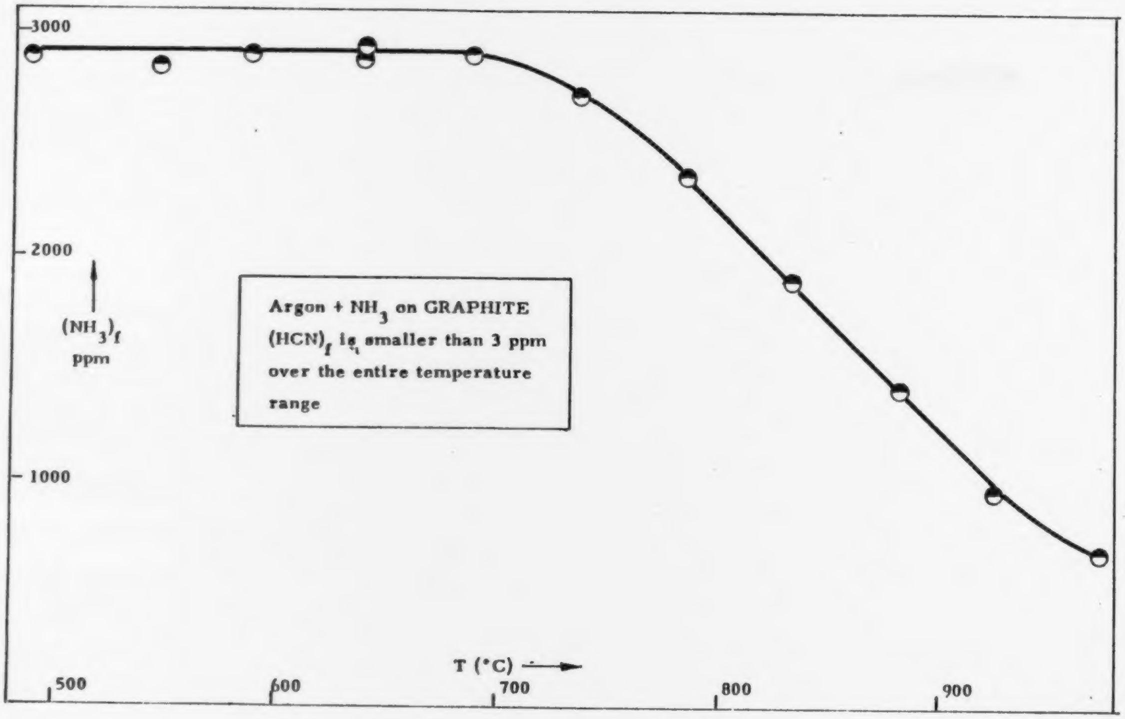

Figure 63. Argon + Ammonia on Graphite: D = 13.3 cm^3s^{-1}; $(NH_3)_i$ = 2900 ppm.

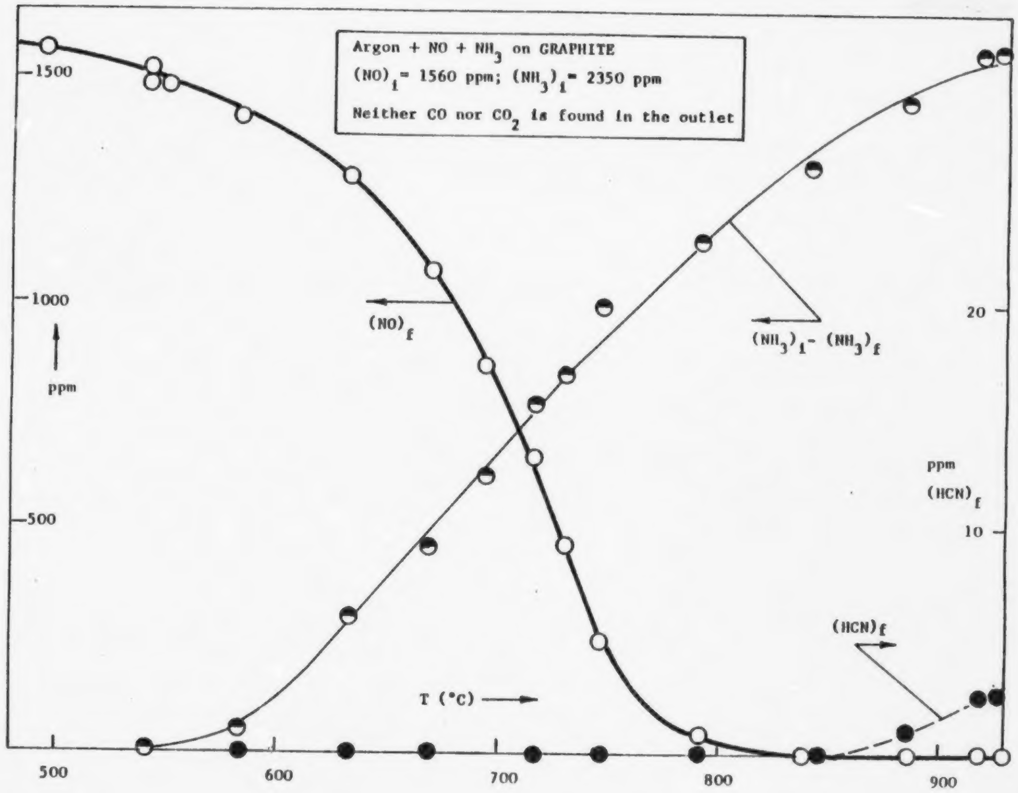

Figure 64. Argon + Ammonia + NO on Graphite: D = 14.5 cm^{3}s^{-1}; (NO)$_i$ = 1560 ppm; (NH$_3$)$_i$ = 2350 ppm.

In the temperature range where NO is decreasing, the species variation can be expressed by the following:

$$d(NO)/dt = -V_1 - V_4 - V_{11} - V_{14} = -\overline{V_{R2}} \quad (92)$$

$$d(NH_3)/dt = -n\, V_4 - V_5 - V_{13} + V_{11} \quad (93)$$

$$d(HCN)/dt = V_5 \quad (94)$$

$$d(N_2)/dt = 0.5\, V_1 + \frac{1+n}{2} V_4 + 0.5\, V_{13} + 0.5\, V_{14} \quad (95)$$

Neglecting the secondary reaction (14), the combination of eqs. (92), (93), and (94) yields:

$$-d(NO)/dt - (NH_3)/dt - d(HCN)/dt = V_1 + (1+n)\, V_4 + V_{13} \quad (96)$$

Substituting the values of V_1 and V_{13} calculated according to eq. (83) and eq. (90), respectively, into eq. (96) yields an expression for V_4. Since V_1 is negligible below 700°C (see section 3.2.2.1) and V_{11} and V_{14} are secondary reactions, it is not surprising that the rate $\overline{V_{R2}}$, calculated by eq. (92), is equal to V_4 (in the following expression the coefficient n has been set equal to one):

$$\boxed{V_4 = \overline{V_{R2}} = 1.4 \times 10^{10} \exp\left[-14600(\pm 1000)/T\right] X_{NO}\, X_{NH_3}} \quad (97)$$

3.2.2.5 Argon + NO + H_2 on Graphite (Case 0.2)

A typical run is shown on Figure 65. With H_2 present, total NO depletion is achieved at 700°C. In the absence of H_2 (see section 3.2.2.1), NO reduction was just beginning at this temperature. NH_3 is formed during NO decrease but does not account for the total decrease in NO concentration observed. Two probable reaction paths are (11) and (14). Hydrogen cyanide begins to appear only after NO has disappeared. Equations 92 and 95 again describe the global variation of nitrogen-containing species, but here V_{11} and V_{14} are primary reactions. V_1 is also a primary reaction, but may be disregarded at temperatures below 700°C. V_4, V_5, and V_{13} are secondary reactions; and in the temperature range below 700°C, V_5 is vanishingly

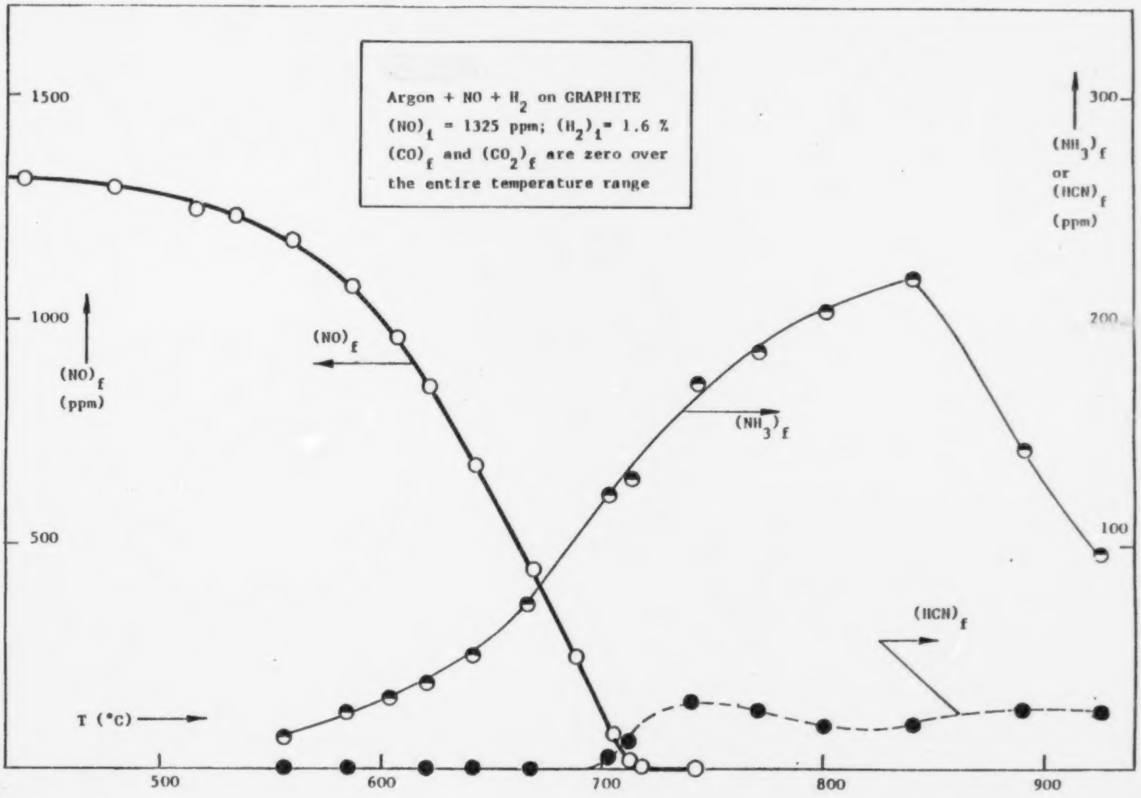

Figure 65. Argon + NO + Hydrogen on Graphite: D = 14.5 cm^3s^{-1}; $(NO)_i$ = 1325 ppm; $(H_2)_i$ = 1.60%.

small (as can be verified by the observation that no HCN is formed in this range). Combination of eqs. (92) to (94) thus yields:

$$-d(NO)/dt+d\left(NH_3\right)/dt+d(HCN)/dt = 2\ V_{11} + V_{14}\ (1-n)\ V_4-V_{13}-V_1 \tag{98}$$

$$-d(NO)/dt-d\left(NH_3\right)/dt-d(HCN)/dt = V_{14} + (1+n)\ V_4 + V_{13} + V_1 \tag{99}$$

Substituting V_4, V_{13}, and V_1, as calculated from eqs. (97), (90), and (99), yields the following expression for V_{14} (the coefficient n has been set equal to one):

$$\boxed{V_{14} = 2.3 \times 10^9 \exp\left[-14000(\pm 800)/T\right] X_{NO}\ X_{H_2}} \tag{100}$$

Similar substitution, coupled with equation (100) yields an expression for V_{11}:

$$\boxed{V_{11} = 7.1 \times 10^6 \exp\left[-13800(\pm 800)/T\right] X_{NO}^{0.5}\ \ X_{H_2}} \tag{101}$$

Finally, the overall NO disappearance rate is obtained from eq. (5):

$$\boxed{\overline{V_{02}} = 2.5 \times 10^7 \exp\left[-13100(\pm 500)/T\right] X_{NO}^{0.5}\ X_{H_2}} \tag{102}$$

3.2.3 Trials on Soot From Ethylene (Case 4)

3.2.3.1 Gas Flows Without Nitrogen-Containing Species

3.2.3.1.1 Argon on C_2H_4 Soot (Case A.4)

When heated progressively under argon flow (i.e. inert pyrolysis), the ethylene-soot begins to release CO at temperatures beyond 750°C (see Figure 66, curve A). No CO_2 is released over the whole temperature range.

3.2.3.1.2 Argon + CO on Ethylene Soot (Case B.4)

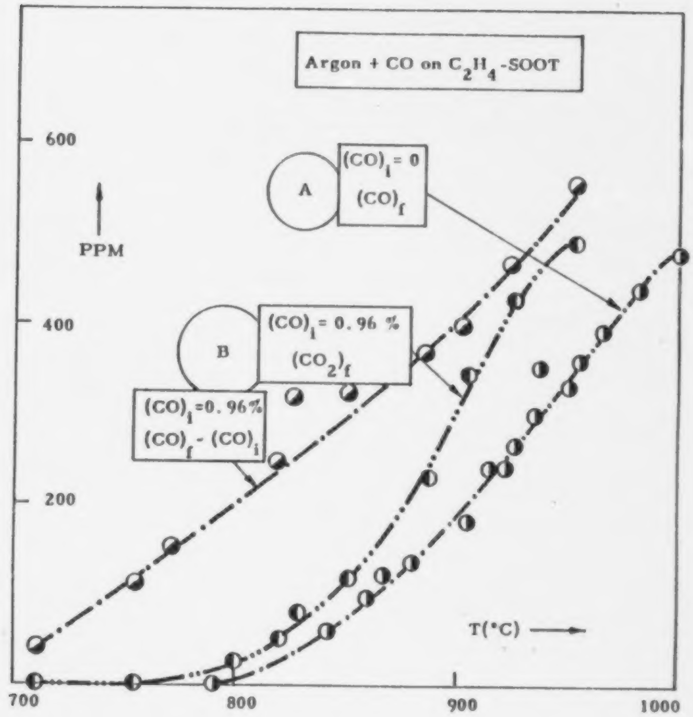

Figure 66. Argon (+CO) on Ethylene Soot: D = 14.6 cm^3s^{-1};
Curve A: $(CO)_i = 0$; Curves B: $(CO)_i = 0.96\%$.

As can be seen from Figure 66, curves B, CO addition results in the formation of CO_2 at temperatures above 750^0C. At the same time, CO concentration is observed to increase in the reactor outlet flow. This is indicated by the positive difference $(CO)_f - (CO)_i$. The concentration of $CO_{2\ f}$ measured at a given temperature when CO is present in the inlet flow, approximately equals the concentration $(CO)_f$ when no CO is present. This indicates that the bound oxygen atoms, which produced CO during thermal decomposition of the solid (Case A.4), are utilized in this case for formation of CO_2 by reaction (12).

3.2.3.1.3 Argon + O_2 on Ethylene Soot (Case E.4)

The presence of oxygen in the inlet gas flow, results in soot oxidation and generation of CO and CO_2 at much lower temperatures than for inert pyrolysis. The following reactions describe this oxidation process.

$$O_2 + (-C) \xrightarrow{24} CO,\ CO_2$$

$$O_2 + (-H) \xrightarrow{23} H_2O$$

At temperatures below 700^0C (where CO release is initiated by thermal soot decomposition trials, see section 3.2.3.1.1), the experimental oxygen balance is in total agreement with reaction path (24) (see Figure 67):

$$(O_2)_i - (O_2)_f = (CO_2)_f + 0.5\ (CO)_f + 0.5\ \frac{H}{C}\ (CO)_f + (CO_2)_f \qquad (103)$$

The oxidation rate of soot is found to have an order of 0.83 with respect to oxygen concentration and was found to be:

$$\boxed{\overline{V_{E4}} = V_{24} = -d(O_2)/dt = 4.4 \times 10^8 \exp\left[-15400(\pm 750)/T\right]\ X_{O_2}^{0.83}}$$

For the ethylene soot used in these trials, the ratio of CO_2 to CO concentration in the reaction products, is generally between 1.1 and 1.5.

3.2.3.2 Gas Flows Containing Nitrogen Species but no Oxygen

3.2.3.2.1 Argon + NH_3 on Ethylene Soot (Case D.4)

Trials of this series are shown on Figures 68 and 69. Neither nitric oxide nor carbon dioxide is found in the reactor outlet flow. The CO

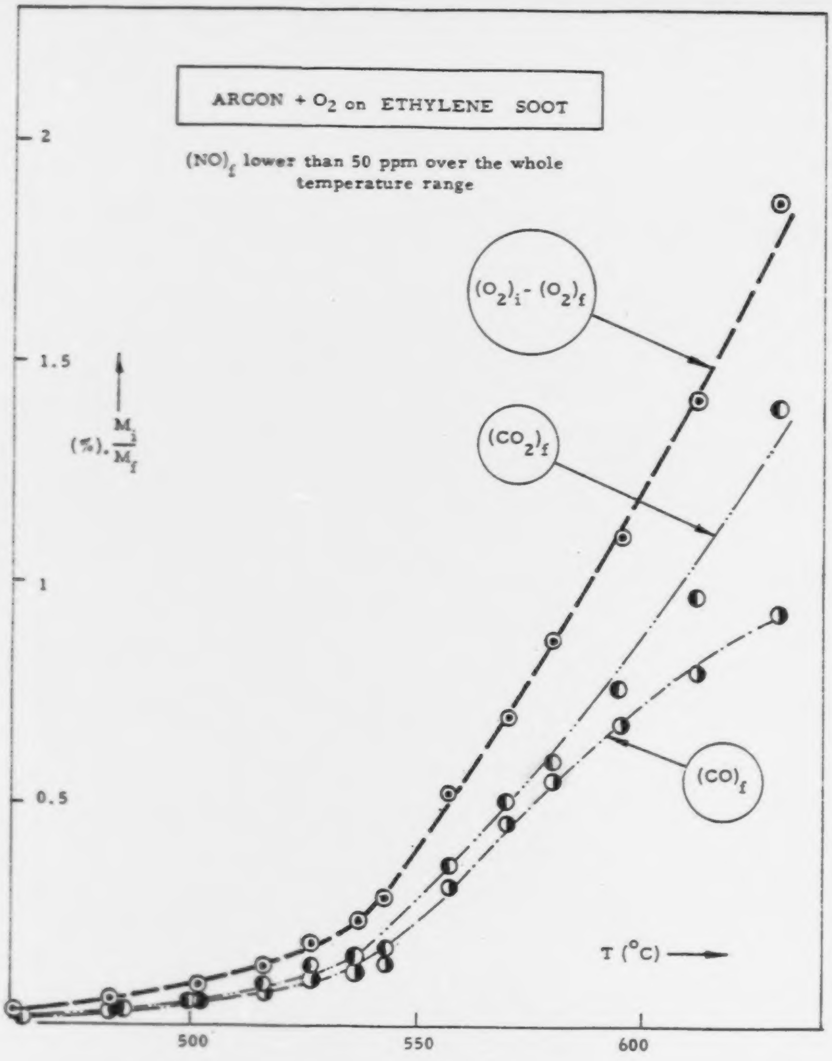

Figure 67. Argon + Oxygen on Ethylene Soot: D = 12.3 $cm^3 s^{-1}$; $(O_2)_i$ = 2.12%.

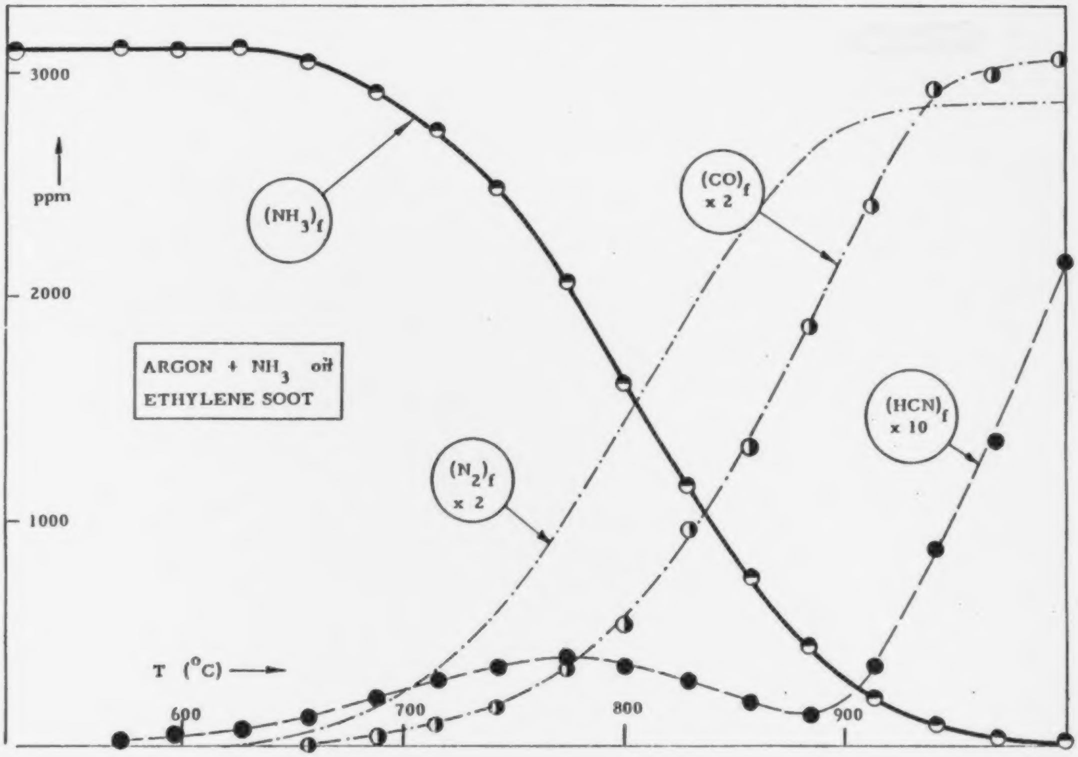

Figure 68. Argon + Ammonia on Ethylene Soot: $D = 12.4\ cm^3s^{-1}$; $(NH_3)_i = 3100$ ppm.

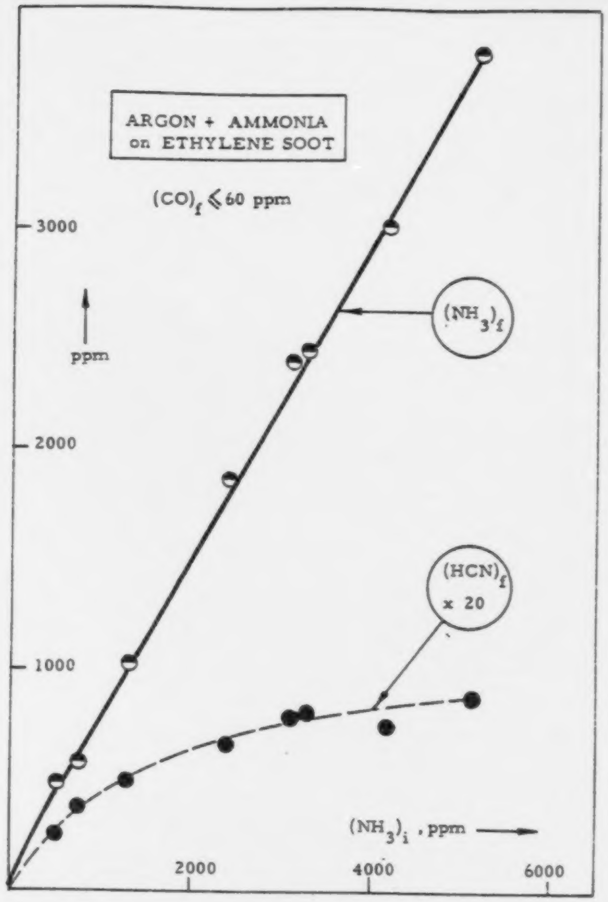

Figure 69. Argon + Ammonia on Ethylene Soot: D = 12.3 $cm^3 s^{-1}$; T = 765°C.

released is due in part to thermal decomposition of the soot (compare with Figure 66). During the decrease of the ammonia concentration, hydrogen cyanide formation is observed but never at a rate sufficient to account for the decrease of ammonia. Hydrogen cyanide formation is presumed to be a result of reaction (5) wherein NH_3 abstracts bound carbon from the solid phase. Due to the temperature range where this NH_3 decrease takes place, it is suggested that reaction (13) is the dominant reaction path. We thus have the following set of differential equations which describe the time rate of change of NH_3, HCN, and N_2. Herein, V_9, V_{10}, V_{15}, and V_{44} are secondary reactions which may be neglected to good approximation, for small advancements of NH_3 disappearance

$$d(NH_3)/dt = -V_5 - V_{10} - V_9 - V_{13} + V_{44} = -\overline{V_{D.4}} \qquad (104)$$

$$d(HCN)/dt = V_5 - V_{10} + V_9 - V_{44} - V_{15} \qquad (105)$$

$$d(N_2)/dt = +V_{10} + 0.5\ V_{13} + 0.5\ V_{15} \qquad (106)$$

Addition of eqs. (104) and (105) yields:

$$-d(NH_3)/dt - d(HCN)/dt = V_{13} + V_{15} + 2V_{10} \qquad (107)$$

Neglecting V_{15} and V_{10} as secondary reaction rates, this equation may be applied to the data in Figures 70 and 71 to yield an expression for V_{13}:

$$\boxed{V_{13} = 5.3 \times 10^8 \exp\left[-18600(\pm 1300)/T\right] X_{NH_3}} \qquad (108)$$

From eq. (105), upon neglecting the secondary reaction rates V_{10}, V_9, V_{15} and V_{44}, the reaction rate V_5 may be determined (see Figures 72 and 73):

$$\boxed{V_5 = 6 \times 10^6 \exp\left[-16600(\pm 1500)/T\right] X_{NH_3}} \qquad (109)$$

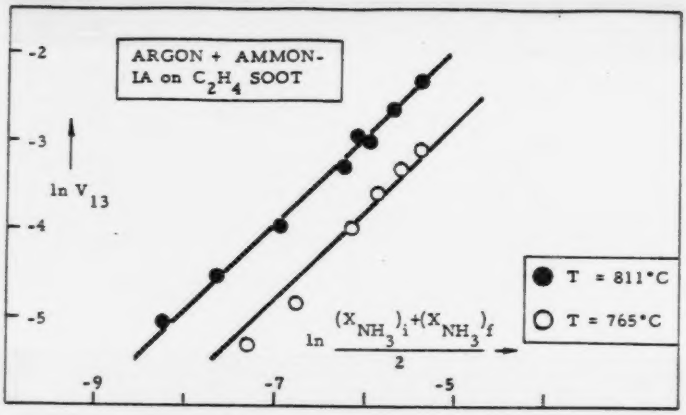

Figure 70. Argon + Ammonia on Ethylene Soot, Determination of Partial Order of V_{13} with Respect to Ammonia, According to eq. (107).

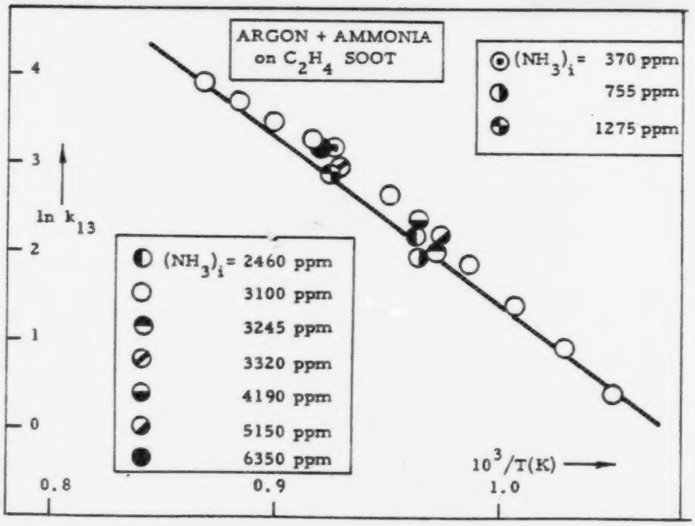

Figure 71. Argon + Ammonia on Ethylene Soot: Determination of Rate Constant k_{13} According to eq. (107), for Different Initial Ammonia Concentrations.

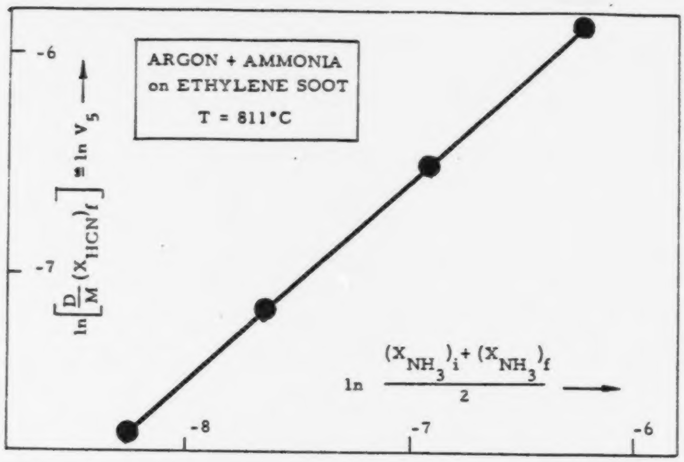

Figure 72. Argon + Ammonia on Ethylene Soot: Determination of Partial Order of V_5 with Respect to Ammonia, According to eq.(105).

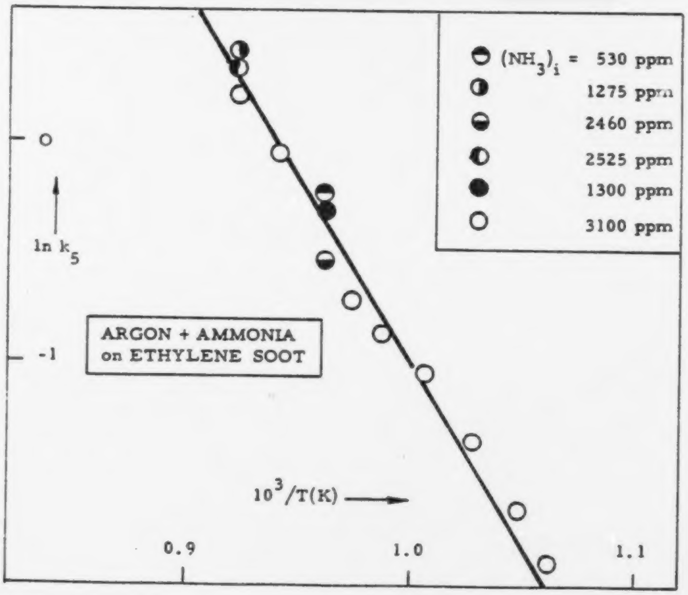

Figure 73. Argon + Ammonia on Ethylene Soot: Determination of Rate Constant k_5 According to eq.(105), for Different Initial Concentrations of Ammonia.

Finally, using equation (104), an overall disappearance rate for ammonia, may be determined and is found to have a value close to that of V_{13}:

$$\overline{V_{D4}} = -d\left(NH_3\right)/dt = 5.6 \times 10^8 \exp\left[-18600(\pm 1700)/T\right] \ X_{NH_3} \tag{110}$$

3.2.3.2.2 Argon + NO on Ethylene Soot (Case F.4)

As may be seen from Figures 74 and 75, both ammonia and hydrogen cyanide are formed during the decrease of NO. CO is also released; but, at temperatures above 750°C. As shown also by the solid mass consumption, this CO comes largely from thermal decomposition of the solid. Since ammonia is being formed, reaction path (1) is not sufficient to account for the NO disappearance. On the other hand, ammonia can only be formed using bound hydrogen and carbon atoms from the soot, together with nitrogen atoms from the nitric oxide. Thus, a reaction path of the form presented below must exist:

$$NO + a(-C) + b(-H) \xrightarrow{2} NH_3 + \left(\frac{b-5}{2} + 2a\right) CO + \left(\frac{5-b}{2} - a\right) CO_2 + \frac{b-3}{2} H_2O$$

where : $0 \leq a \leq 1$ and $5 \geq b \geq 3$. When 'a' approaches to 1, 'b' approaches to 3, CO is the only reaction product. When 'a' approaches to zero, 'b' approaches to 5, then H_2O is the only product. The following set of differential equations describes the variation of the nitrogen-containing species as a function of time:

$$d(NO)/dt = -V_1 - V_2 - V_4 - V_8 = -\overline{V_{F.4}} \tag{111}$$

$$d\ NH_3\ /dt = V_2 - nV_4 - V_5 - V_9 - V_{13} \tag{112}$$

$$d(HCN)/dt = V_5 + V_9 \tag{113}$$

$$d\ N_2\ /dt = 0.5\ V_1 + \frac{1+n}{2} V_4 + 0.5\ V_8 + 0.5\ V_{13} \tag{114}$$

In these expressions, the tertiary reaction rates V_{10}, V_{11}, V_{14}, V_{40}, and V_{44} have been deliverately neglected. Combining eqs. (111), (112), and

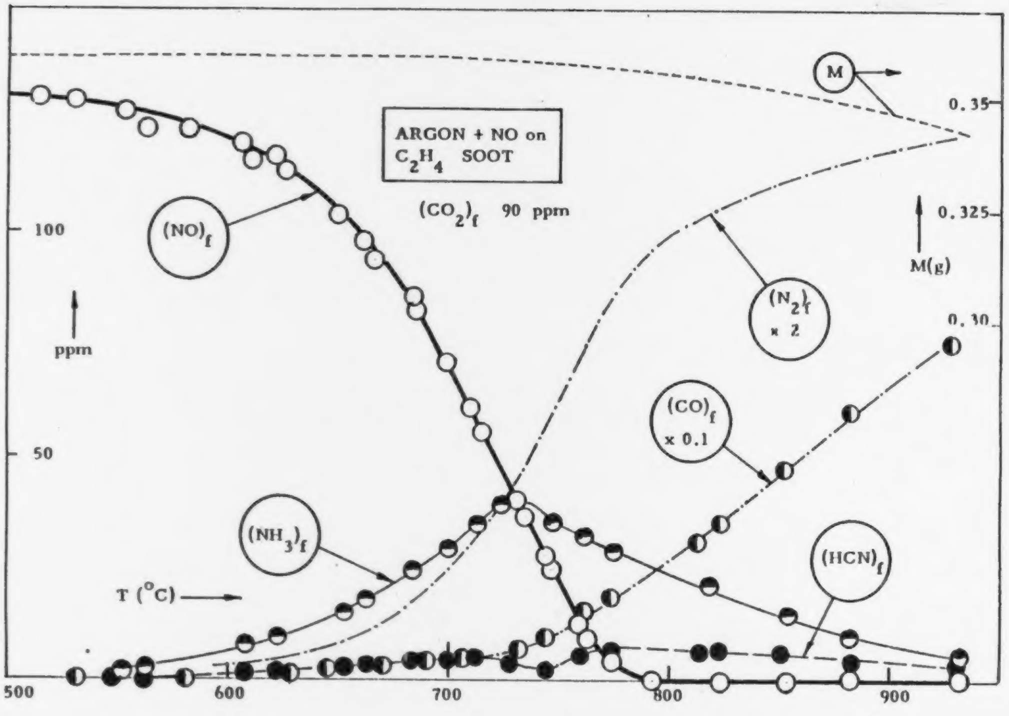

Figure 74. Argon + NO on Ethylene Soot: $D = 14.0\ cm^3 s^{-1}$; $(NO)_i = 130$ ppm.

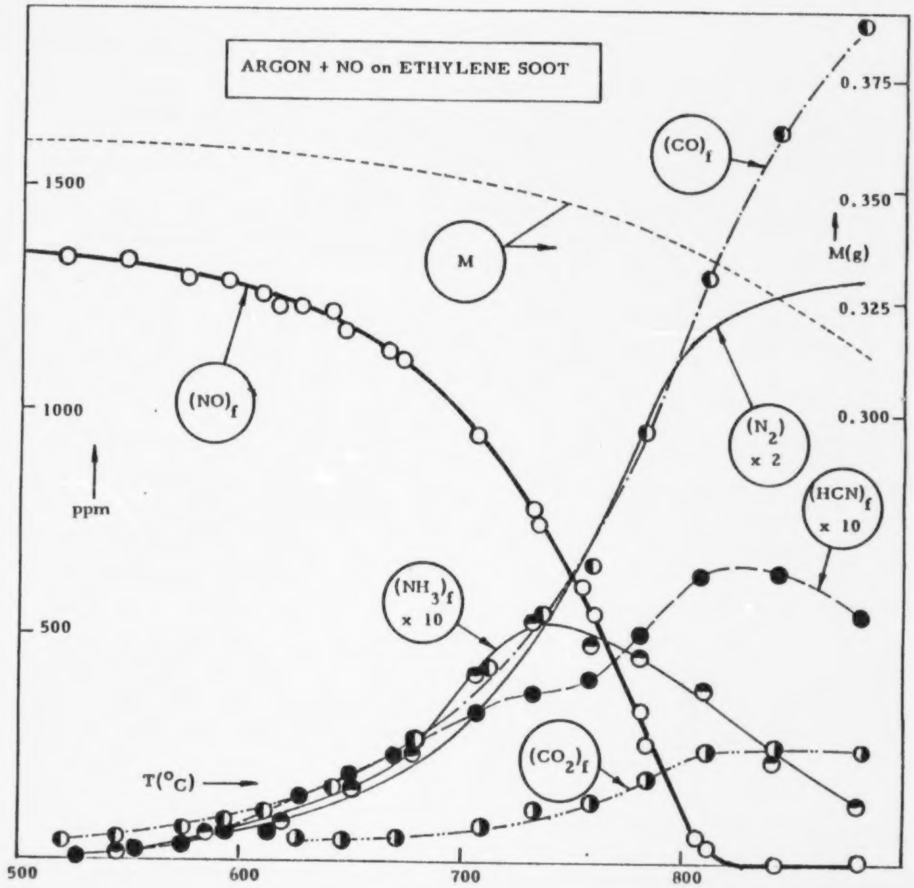

Figure 75. Argon + NO on Ethylene Soot: D = 14.0 cm^3s^{-1}; $(NO)_i$ = 1360 ppm.

(113) yields:

$$-d(NO)/dt - d\left(NH_3\right)/dt - d(HCN)/dt = V_1 + (1+n)\ V_4 + V_8 + V_{13} \tag{115}$$

$$-d(NO)/dt + d\left(NH_3\right)/dt+d(HCN)/dt = V_1 + 2V_2 + V_8 - V_{13} \tag{116}$$

(For the last expression, n has been taken equal to one). By disregarding the secondary reaction rates V_4 and V_8, and substituting a value for V_{13} obtained from eq. (108), an approximate value of V_1 may be calculated from Figure 76.

$$\boxed{V_1 = 1.3 \times 10^{10} \exp\left[-22550(\pm 2500)/T\right]\ X_{NO}^{0.75}} \tag{117}$$

Neglecting secondary reaction rate V_8, and substituting for V_1 and V_{13} as calculated according to eqs. (117) and (108), respectively, allows equation (116) to be used for the calculation of V_2. Results are shown in Figure 77, and the derived rate expression is found to be

$$\boxed{V_2 = 1.9 \times 10^{6} \exp\left[-14300(\pm 1500)/T\right]\ X_{NO}^{0.7}} \tag{118}$$

A comparison of equations (117) and (118) demonstrates that reaction 2 prevails at lower temperatures. In the temperature range where both rates have been determined, reaction (2) is seen to play the leading role. Therefore the overall NO disappearance rate, determinedfrom eq. (111), is found to be very close to V_2 (see Figure 78):

$$\boxed{\overline{V_{F.4}} = 3.4 \times 10^{7} \exp\left[-16000(\pm 1000)/T\right]\ X_{NO}^{0.75}} \tag{119}$$

3.2.3.2.3 Argon + NO + NH_3 on Ethylene Soot (Case R.4)

Examples of these trials are given in Figures 79, 80, and 81. From Figure 79, it is seen that the ratio of the reaction products $\left[(NO)_i-(NO)_f\right]/\left[\left(NH_3\right)_i-\left(NH_3\right)_f\right]$ has a value close to one for temperatures below 700°C. This is the region where reaction (13) is still negligibly small as is seen in Figure 68. Reaction (4) is dominant and its stoichiometric

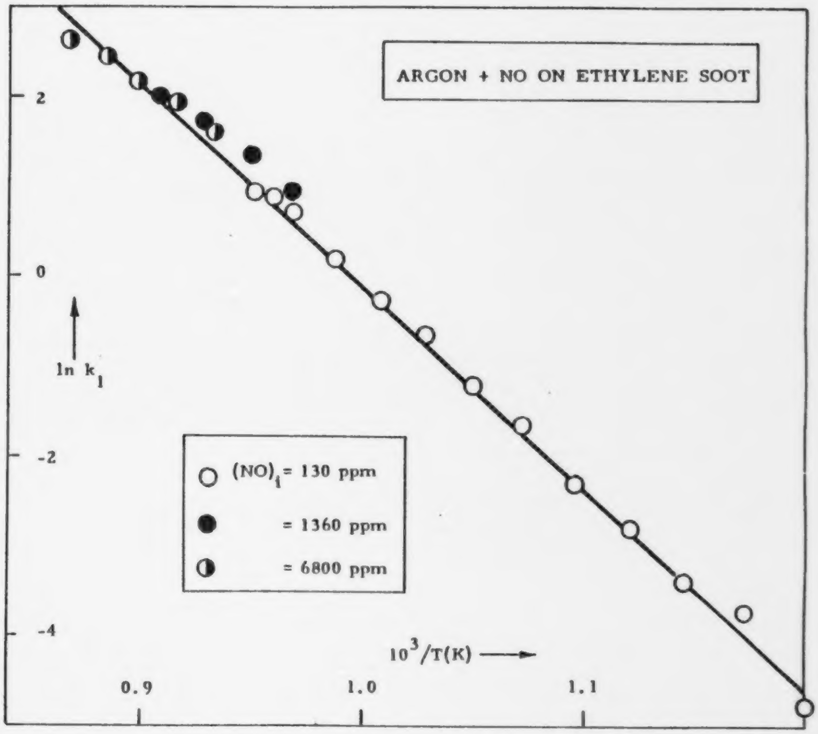

Figure 76. Argon + NO on Ethylene Soot: Determination of k_1 According to eq.(115), For Different Initial NO Concentrations.

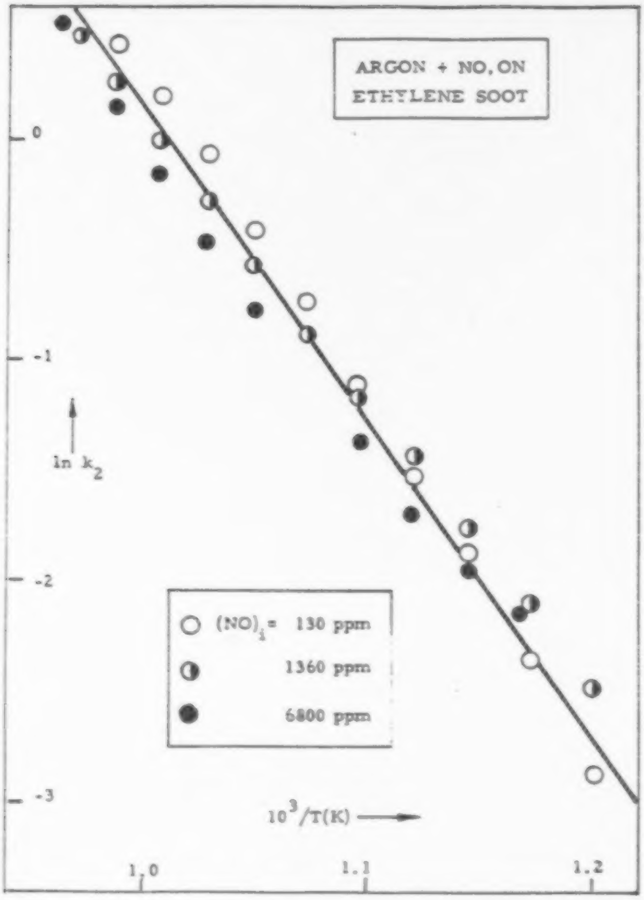

Figure 77. Argon + NO on Ethylene Soot: Determination of Rate Constant k_2 According to eq.(116), For Different Initial Concentrations of NO.

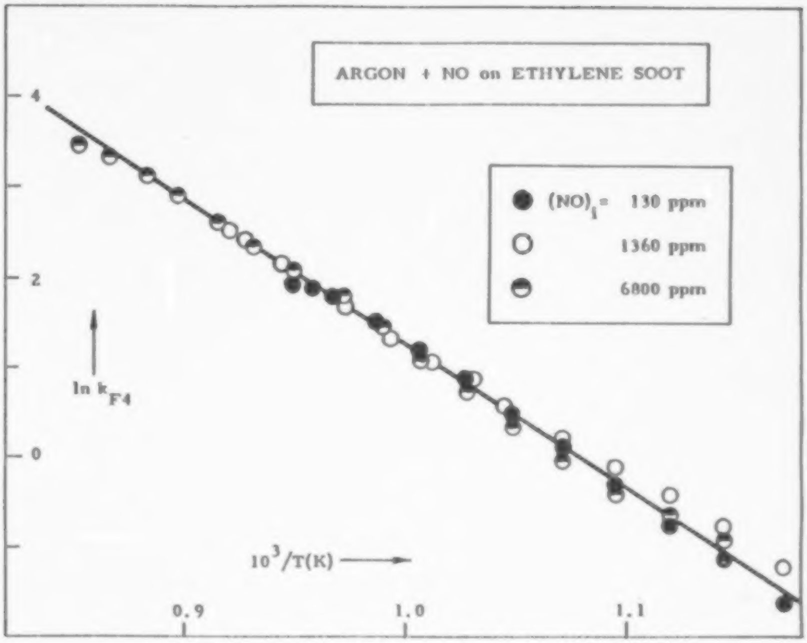

Figure 78. Argon + NO on Ethylene Soot: Determination of the Rate Constant k_{F4} According to eq.(111), For Different Initial NO Concentrations.

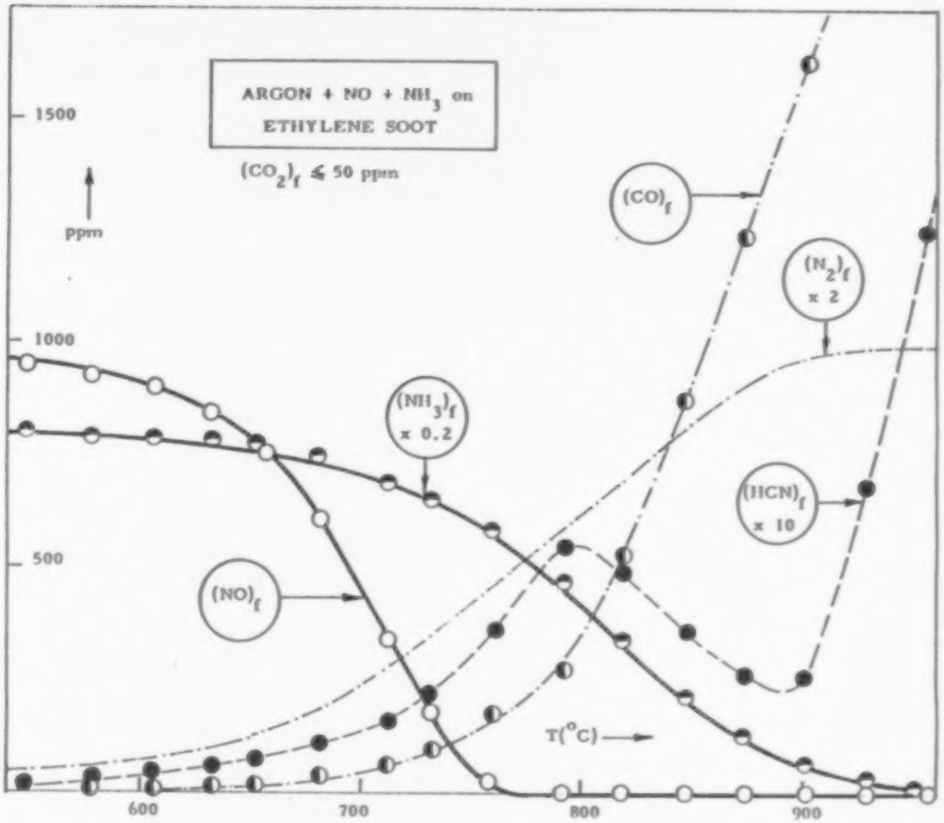

Figure 79. Argon + NO + Ammonia on Ethylene Soot: D = 12.0 cm^3s^{-1}; $(NO)_i$ = 1040 ppm; $(NH_3)_i$ = 4150 ppm.

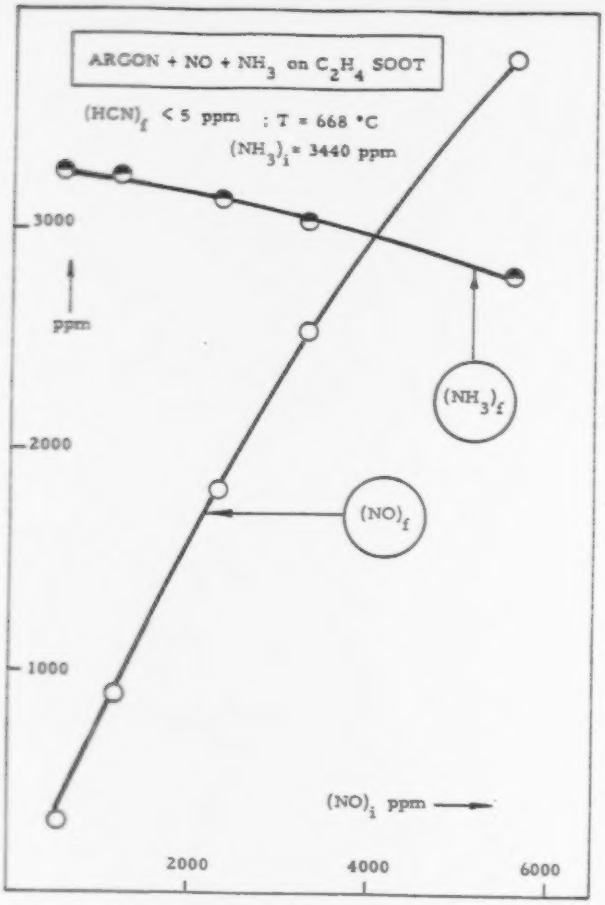

Figure 80. Argon + NO + Ammonia on Ethylene Soot: D = 13.7 $cm^3 s^{-1}$; $(NH_3)_i$ = 3440 ppm; T = 668°C.

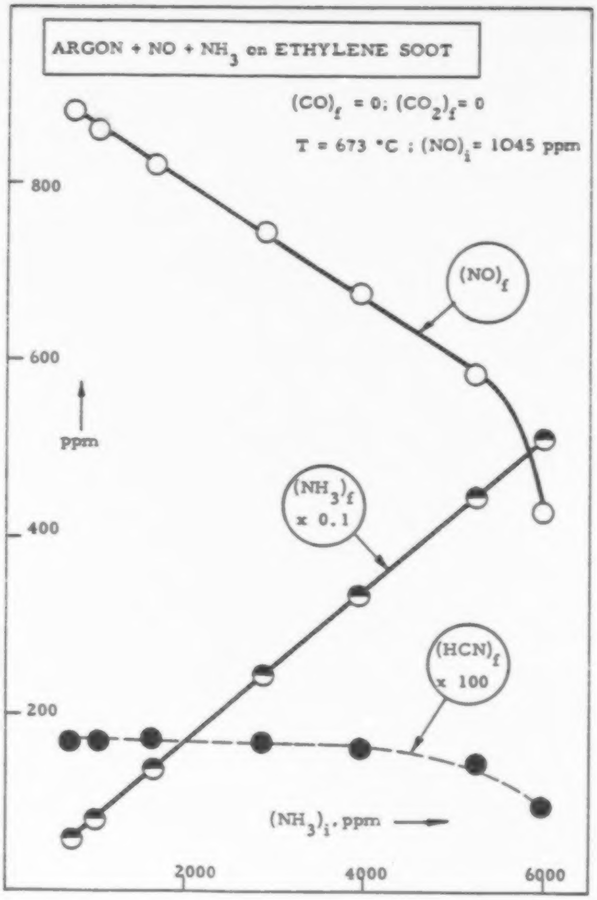

Figure 81. Argon + NO + Ammonia on Ethylene Soot: D = 12.3 cm^{3}s^{-1}; (NO)$_i$ = 1045 ppm; T = 673°C.

coefficient n is close to one.

Neglecting all secondary reactions, the variation as a function of time of the nitrogen-containing species is given by:

$$d(NO)/dt = -V_1 - V_2 - V_4 = -\overline{V_{R.4}} \qquad (120)$$

$$d\left(NH_3\right)/dt = V_2 - nV_4 - V_5 - V_{13} \qquad (121)$$

$$d(HCN)/dt = V_5 \qquad (122)$$

$$d\left(N_2\right)/dt = 0.5\ V_1 + \frac{1+n}{2}\ V_4 + 0.5\ V_{13} \qquad (123)$$

Addition of eqs. (120), (121), and (122) yields:

$$-d(NO)/dt - \left(NH_3\right)/dt = V_1 + (1+n\approx 2)V_4 + V_{13} \qquad (124)$$

Substituting values of V_1 and V_{13}, by their values calculated from equations (117) and (108) respectively, into expression (124), allows the determination of V_4. Rate values thus calculated are presented in Figures 82 through 84 and result in the following expression:

$$\boxed{V_4 = 6 \times 10^8 \exp\left[-11500(\underline{+}1500)/T\right]\ X_{NO}\ X_{NH_3}} \qquad (125)$$

The actual partial order with respect to NO is between 0.75 and 1.0. Equation (120) may now be utilized for determination of the overall nitric oxide disappearance rate $\overline{V_{R.4}}$. The precision is rather poor and the partial orders are between 0.6 and 1 for ammonia, between 0.75 and 1 for nitric oxide:

$$\boxed{\begin{aligned} \overline{V_{R.4}} &= 1.6 \times 10^8 \exp\left[-13700(\underline{+}2500)/T\right]\ X_{NO}^{0.75}\ X_{NH_3}^{0.6} && (126) \\ \overline{V_{R.4}} &= 2.1 \times 10^9 \exp\left[-12500(\underline{+}2500)/T\right]\ X_{NO}\ X_{NH_3} && (127) \end{aligned}}$$

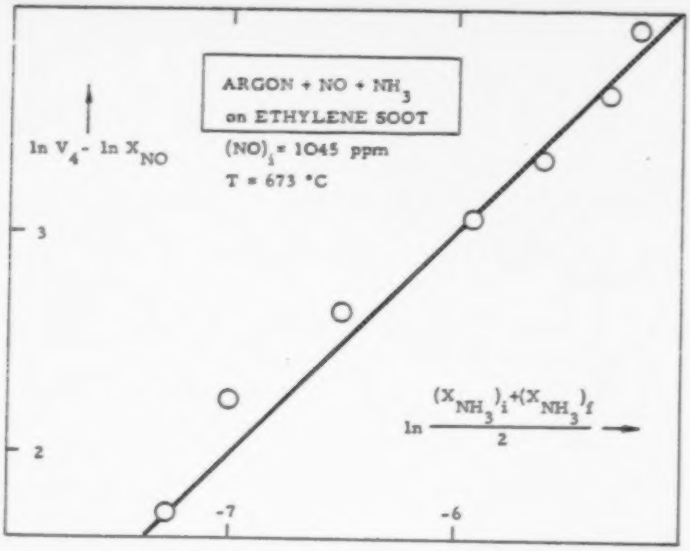

Figure 82. Argon + NO _ Ammonia on Ethylene Soot Determination of Partial Order of V_4 with Respect to Ammonia, According to eq.(124); D = 12.3 cm^3s^{-1}; $(NO)_i$ = 1045 ppm; T = 673°C.

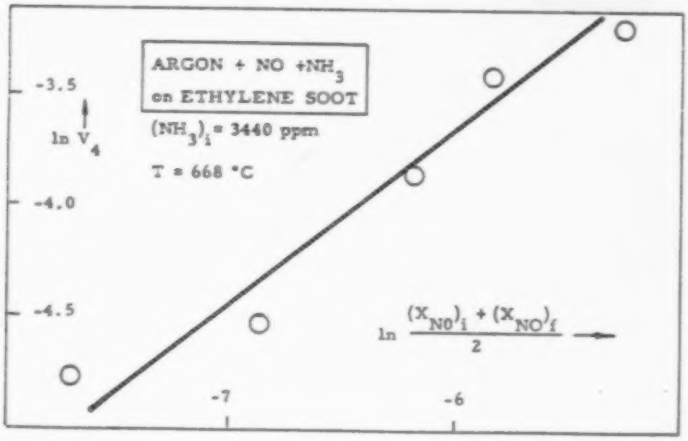

Figure 83. Argon + NO + Ammonia on Ethylene Soot: Determination of Partial Order of V_4 With Respect to Nitric Oxide, According to eq.(124); D = 13.7 cm^3s^{-1}; $(NH_3)_i$ = 3440 ppm; T = 668°C.

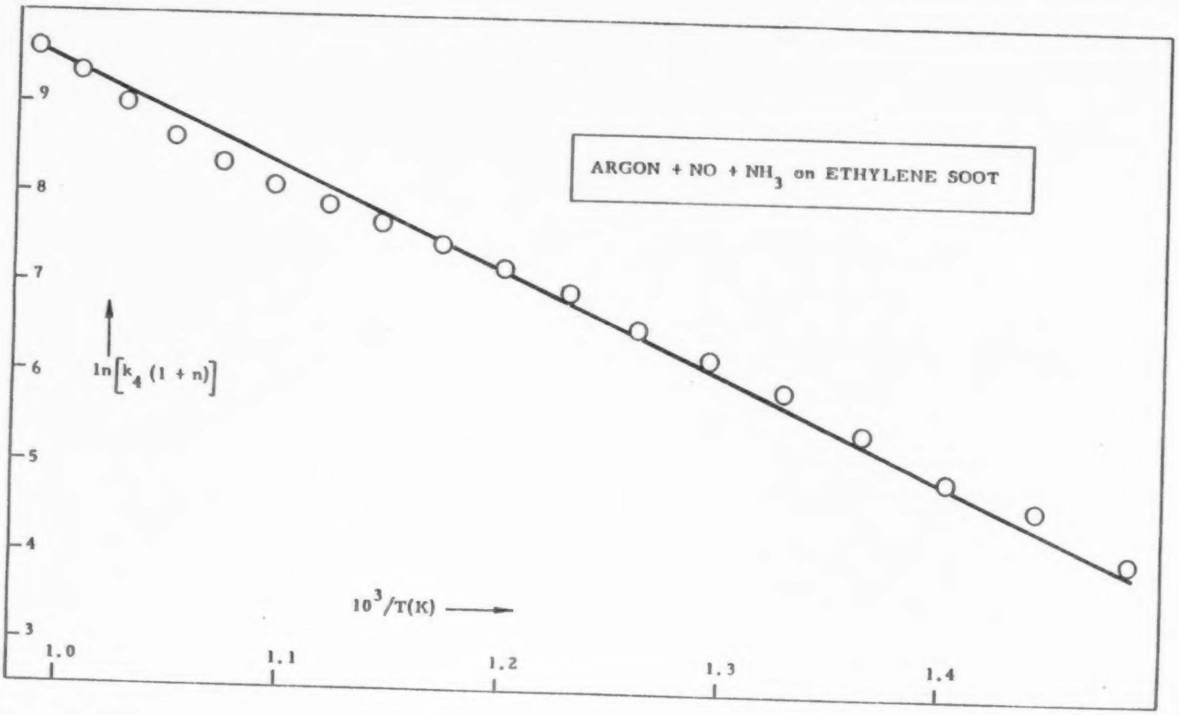

Figure 84. Argon + NO + Ammonia on Ethylene Soot: Determination of Rate Constant k_4 According to eq.(124); $(NO)_i$ = 1040 ppm; $(NH_3)_i$ = 4150 ppm; D = 12.0 cm^3s^{-1}.

3.2.3.2.4 Argon + NH_3 + CO on Ethylene Soot (Case I.4)

Typical examples from these trials are given on Figures 85 through 89. Figures 85, 86, and 87 illustrate the case where temperature is the variable parameter, whereas Figures 88 and 89, respectively, show the effect of varying initial ammonia and CO concentration.

A general feature of these trials on NH_3/CO mixtures, already mentioned in the case of alumina, is that no nitric oxide has been found in the reactor outlet gases over the entire temperature range.

When comparing with the analogous trials performed on alumina, it is observed that in the present case ammonia disappearance is shifted towards higher temperatures.

A priori, one would expect that the primary reactions (5), (9), and (13) are playing a leading role in the disappearance of ammonia. However, the contribution of reaction (9) seems to be negligible in the present case for the following reasons:

- A first indication of the negligible importance of V_9 is found in the experimental fact that the rate of ammonia decrease does not systematically increase with the initial CO concentration, as may be seen in Figure 89.
- The second indication comes from the experimental fact that there appears to be no CO decrease during the disappearance of ammonia. This, however, may be a misleading argument, since more CO is produced by thermal decomposition of the soot (see e.g. Figure 66, curves B) than would be produced by reaction (9).
- A strong confirmation is found from the numerical computation of the reaction rate V_9. The time variation of the nitrogen containing species, limited to the primary reactions, is given by:

$$d(NO)/dt = 0 \text{ (since no NO has been observed)} \qquad (128)$$

$$d\left(NH_3\right)/dt = -V_5 - V_9 - V_{13} = -\overline{V_{I.4}} \qquad (129)$$

$$d(HCN)/dt = V_5 + V_9 \qquad (130)$$

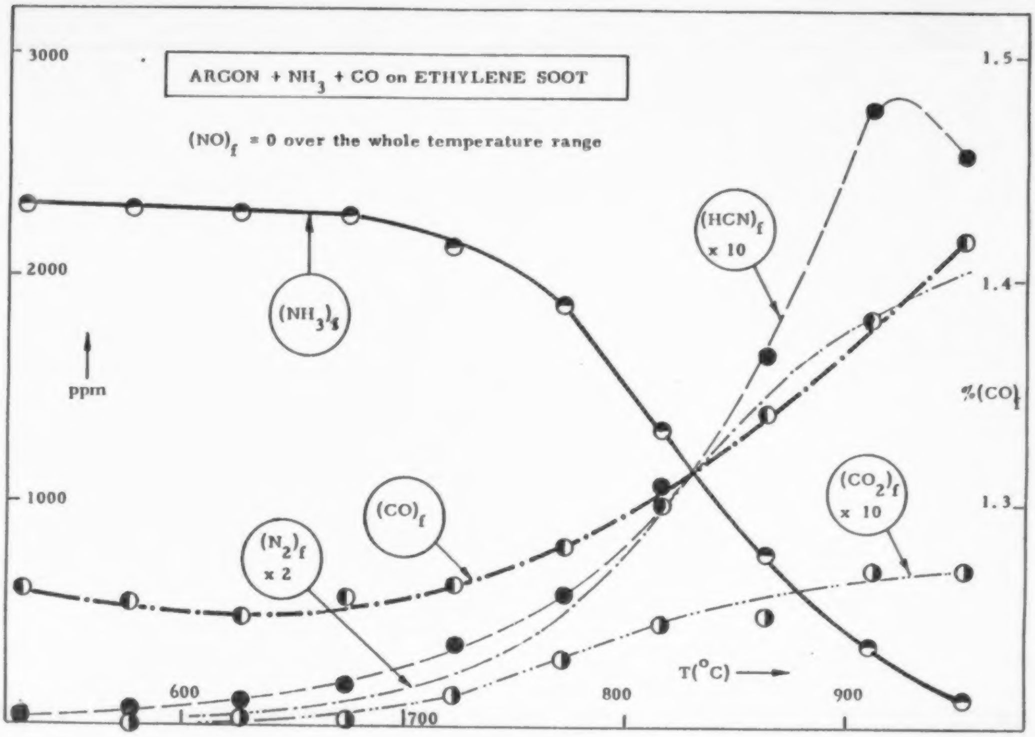

Figure 85. Argon + Ammonia + CO on Ethylene Soot: D = 12.6 cm^3s^{-1}; $(NH_3)_i$ = 2420 ppm; $(CO)_i$ = 1.26%.

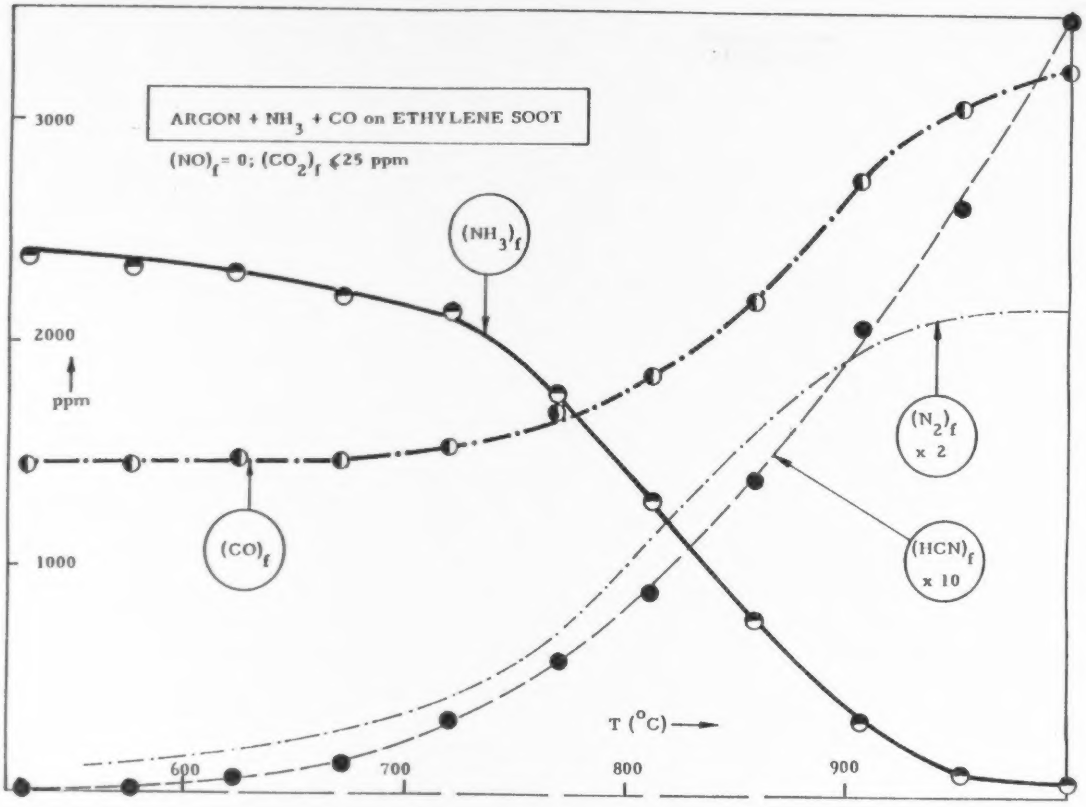

Figure 86. Argon + Ammonia + CO on Ethylene Soot: $D = 13.3\ cm^3s^{-1}$; $(NH_3)_i = 2540$ ppm; $(CO)_i = 0.15\%$.

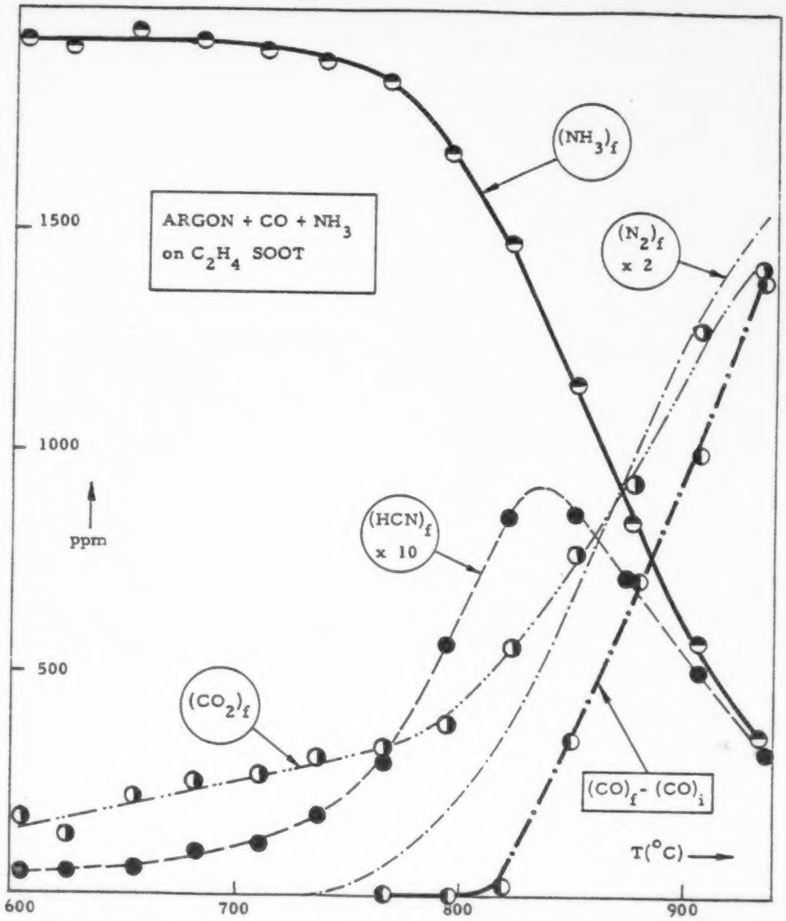

Figure 87. Argon + Ammonia + CO on Ethylene Soot: D = 13.0 cm^3s^{-1}; $(NH_3)_i$ = 1925 ppm; $(CO)_i$ = 4.15%.

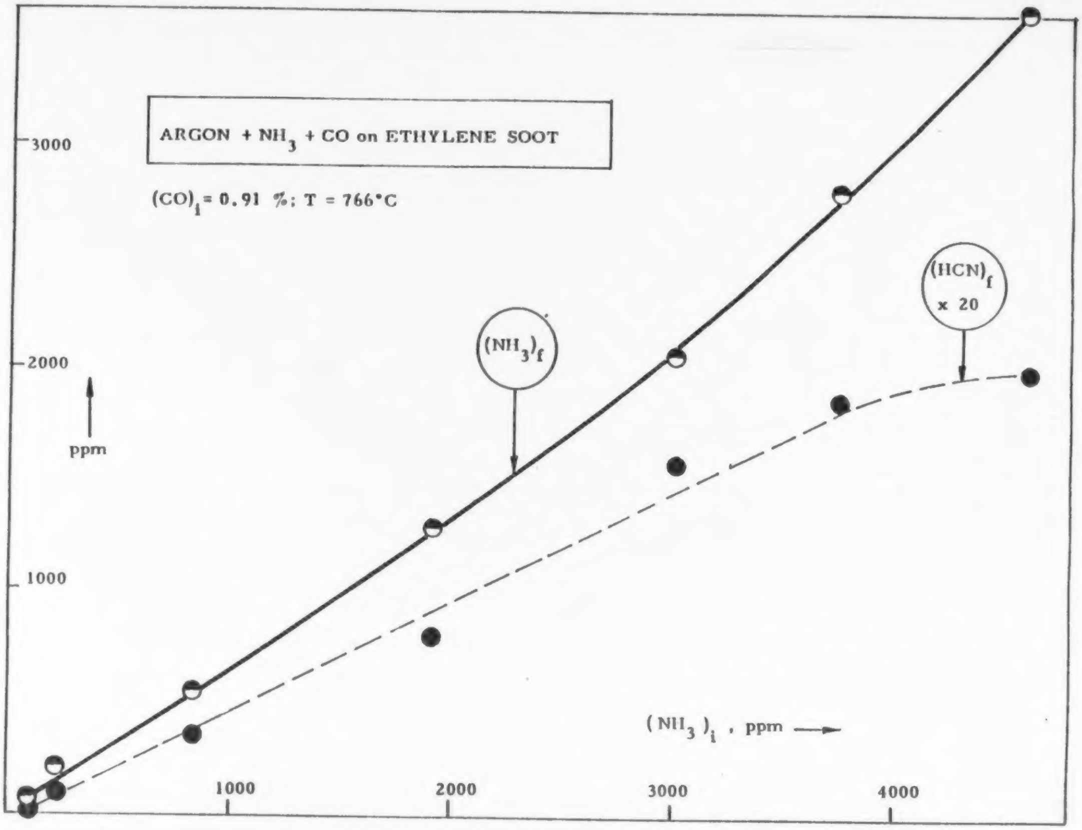

Figure 88. Argon + Ammonia + CO on Ethylene Soot: D = 11.8 cm^{3}s^{-1}; (CO)$_i$ = 0.91%; T = 766^{o}C.

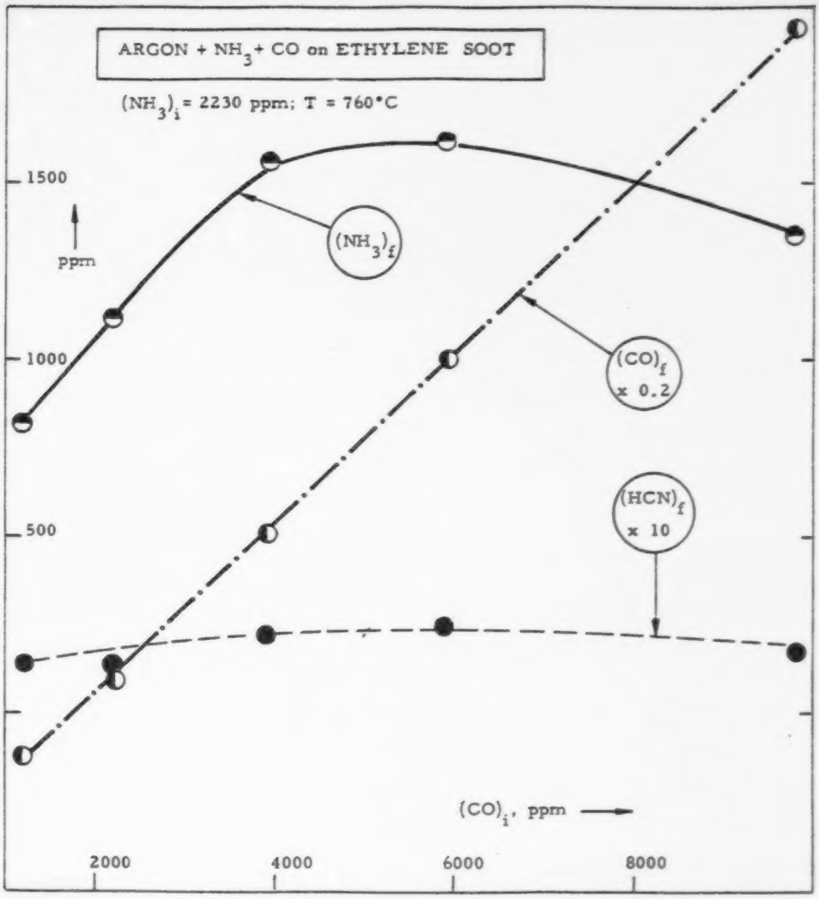

Figure 89. Argon + Ammonia + CO on Ethylene Soot: D = 13.8 $cm^3 s^{-1}$; $(NH_3)_i$ = 2230 ppm; T = 760°C.

$$d(N_2)/dt = 0.5\ V_{13} \quad (131)$$

Reaction rate V_9 may be determined from either eq. (129) or from the combination of eqs. (129) and (130):

$$d(HCN)/dt - d(NH_3)/dt = 2V_5 + 2V_9 + V_{13} \quad (132)$$

Values of V_5 and V_{13} may be obtained from equation (109) and (108), respectively.

Calculation of V_9, by either eq. (129) or eq. (132) proves that V_9 is negligible. In agreement with this, the overall ammonia disappearance rate $\overline{V_{I.4}}$, calculated from eq. (129) as the time variation of ammonia, is found to be of zero order with respect to CO, and to have a rate constant which is very close to that of reaction 13 (which prevails over reaction (5) under the present conditions):

$$\boxed{\overline{V_{I.4}} = 2.8 \text{ to } 6.5 \times 10^8 \exp\left[-18600(\pm 2000)/T\right] X_{NH_3}} \quad (133)$$

As a conclusion, the absence of reaction (9) in this soot trial may suggest that the heterogeneous transformation of ammonia into HCN by carbon monoxide is either strongly dependent on the presence of metals or metal oxides in the solid catalyst, or that the reaction is inhibited by the presence of (bound) hydrogen.

3.2.3.2.5 Argon + NO + CO on Ethylene Soot (Case K.4)

Examples of those trials are shown on Figures 90, 91, and 92. The primary reactions expected to occur here are reactions (1), (2), and (8). The decrease of the initial CO concentration, due to reaction (8), is quickly compensated by CO formation from thermal decomposition of the soot. As a result, $(CO)_f$ values are observed to increase at temperatures above 700°C (see Figure 90). When the effect of initial CO concentration (see Figure 91) at a given temperature and initial NO concentration is examined, it is observed that the ammonia concentration in the reactor outlet flow increases

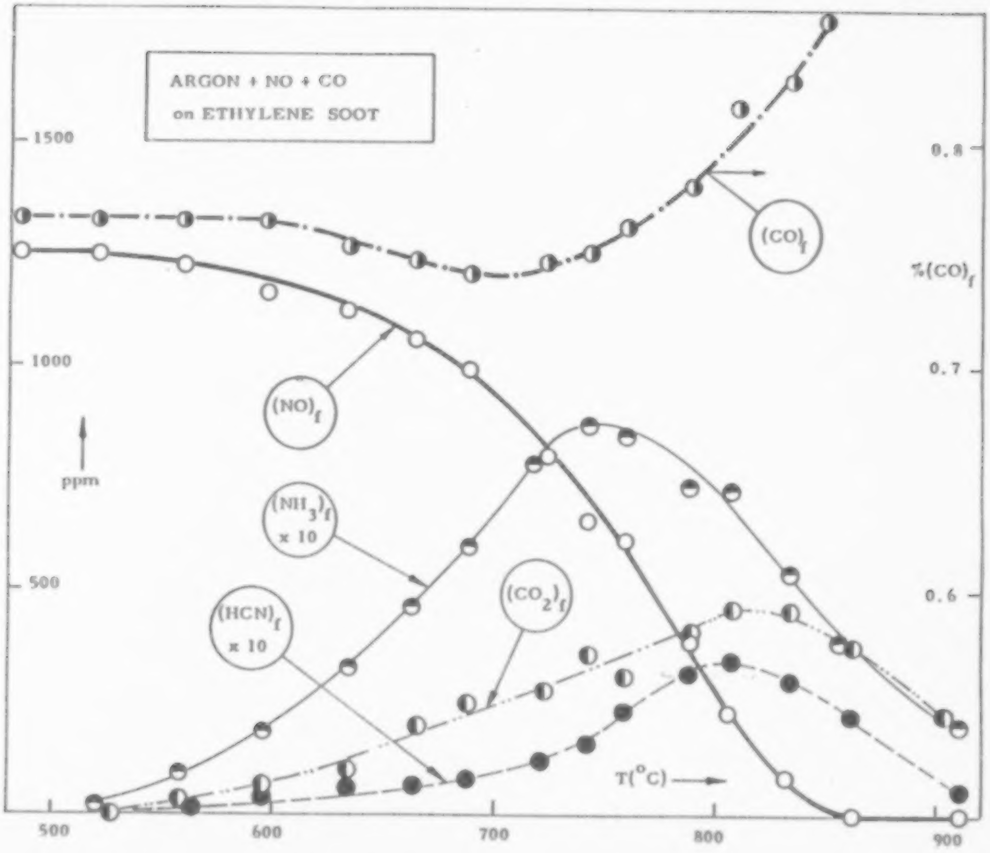

Figure 90. Argon + NO + CO on Ethylene Soot: D = 13.1 cm^{3}s^{-1}; (NO)$_i$ = 1250 ppm; (CO)$_i$ = 0.76%.

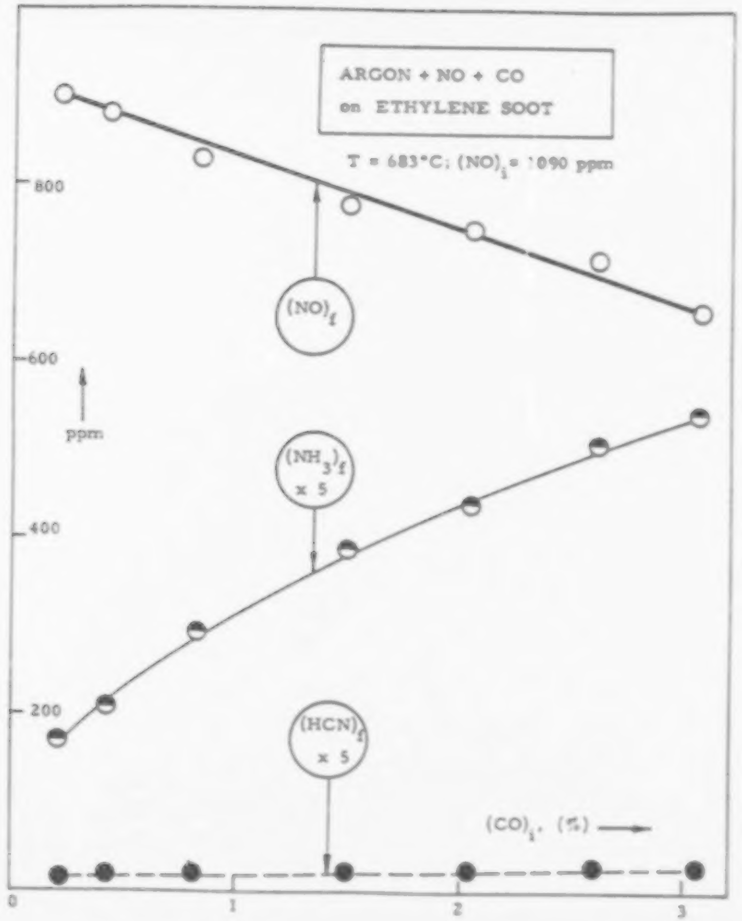

Figure 91. Argon + NO + CO on Ethylene Soot: D = 12.1 cm^{3}s^{-1}; (NO)$_i$ = 1090 ppm; T = 683°C.

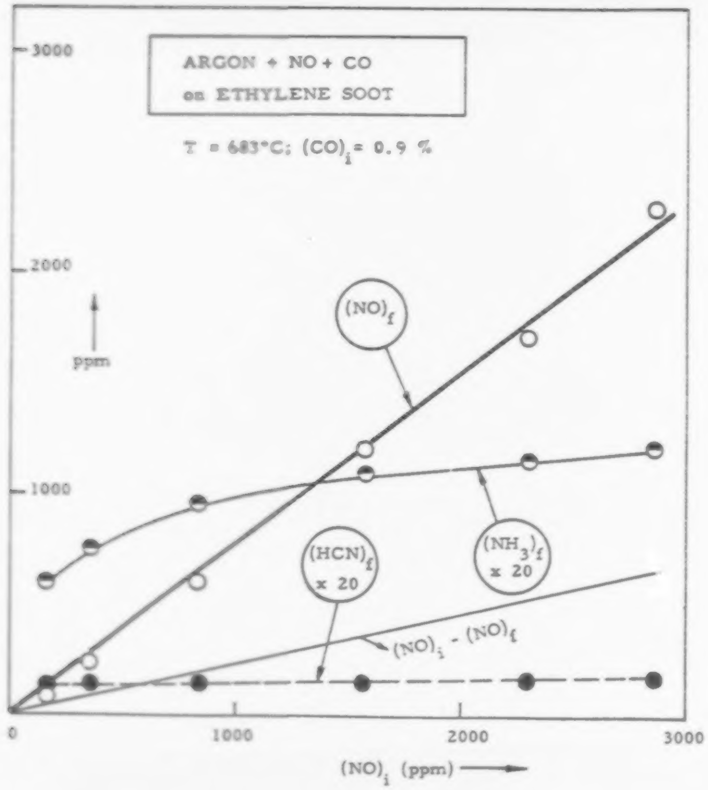

Figure 92. Argon + NO + CO on Ethylene Soot: D = 12.1 $cm^3 s^{-1}$; $(CO)_i$ = 0.90%; T = 683°C.

with increasing $(CO)_i$. Different explanations of this fact (which is also observed on heavy oil soot in the next section) can be proposed:

- According to the first hypothesis, all the ammonia is assumed to be formed by reaction (2); this reaction, however, is enhanced whenever the thermal decomposition of the soot is increased (since bound -C and -H atoms act as reactants for reaction (2). The presence of CO is expected to enhance the thermal decomposition rate of soot (see Figure 66), and therefore is expected to enhance the formation of NH_3 by reaction (2).
- Another hypothesis postulates the existence of a supplementary primary reaction, where CO serves as a reactant for NH_3 formation:

  $$NO + CO + (-H) \xrightarrow{6} NH_3 + \ldots$$

  According to the overall stoichiometry, a likely reaction product would be CO_2:

  $$NO + CO + 3(-H) \xrightarrow{6} NH_3 + CO_2$$

  This stoichiometry could not be precisely checked, due to CO_2 formation from thermal decomposition.

Regardless of which hypothesis is correct, the time derivations of the nitrogen-containing species, limited to primary reactions and previously evaluated secondary reactions are given by:

$$d(NO)/dt = -V_1 - V_2 - V_6 - V_8 - V_4 = -\overline{V_{K.4}} \qquad (134)$$

$$d(NH_3 /dt = V_2 + V_6 - nV_4 - V_5 - V_{13} \qquad (135)$$

$$d(HCN)/dt = V_5 \qquad (136)$$

$$d(N_2)/dt = 0.5\ V_1 + 0.5\ V_8 + \frac{1+n}{2}\ V_4 + 0.5\ V_{13} \qquad (137)$$

Addition of eqs. (134), (135), and (136) yields:

$$-d(NO)/dt - d(NH_3)/dt - d(HCN)/dt = V_1 + V_8 + (1+n)V_4 + V_{13} \qquad (138)$$

The value of V_8 can be determined from eq. (138) by substituting values for V_1, V_4, and V_{13} calculated from eqs. (117), (125), and (108). Applying the resultant expression to the data in Figure 92 yields the following rate for V_8.

$$\boxed{V_8 = 1.7 \times 10^8 \exp\left[-12400(\underline{+}1000)/T\right] X_{NO}\, X_{CO}} \qquad (139)$$

The value of V_6 may then be calculated either from eq. (134) or from eq. (135), using appropriate rate expression previously evaluated. Both approaches show that reaction rate V_6 is zero, at least in the present case.

The overall NO disappearance rate $\overline{V_{K.4}}$ has also been obtained from equation (134) (see Figure 93):

$$\boxed{\overline{V_{K.4}} = 3.6 \times 10^8 \exp\left[-14700(\underline{+}500)/T\right] X_{NO}\, X_{CO}^{0.45}} \qquad (140)$$

3.2.3.2.6 Argon + NO + H_2 on Ethylene Soot (Case 0.4)

These trials are illustrated in Figures 94 through 97, and include consideration of different initial concentrations of both hydrogen and nitric oxide. In the temperature range where the NO decrease occurs, the CO and CO_2 concentrations in the reactor outlet flow are small. This allows the secondary reactions, with CO as a reactant, to be disregarded.

$(NH_3)_f$ is always important and increases with both increases of $(NO)_i$ or $(H_2)_i$. At sufficiently high $(H_2)_i$ values and not too high of $(NO)_i$ values, the formation of ammonia accounts for the total decrease in nitric oxide as long as the NH_3 has not reached its maximum value. This clearly indicates the importance of reaction (11).

HCN is released in much smaller quantities than NH_3 and reaches its peak at higher temperatures than does NH_3. The principle means of HCN production probably is by reaction (5).

The following equations, limited to primary reactions and reactions previously found to be important, govern the variation of the nitrogen-containing species as a function of time:

$$d(NO)/dt = -V_1 - V_2 - V_4 - V_{11} - V_{14} = -\overline{V_{0.4}} \qquad (141)$$

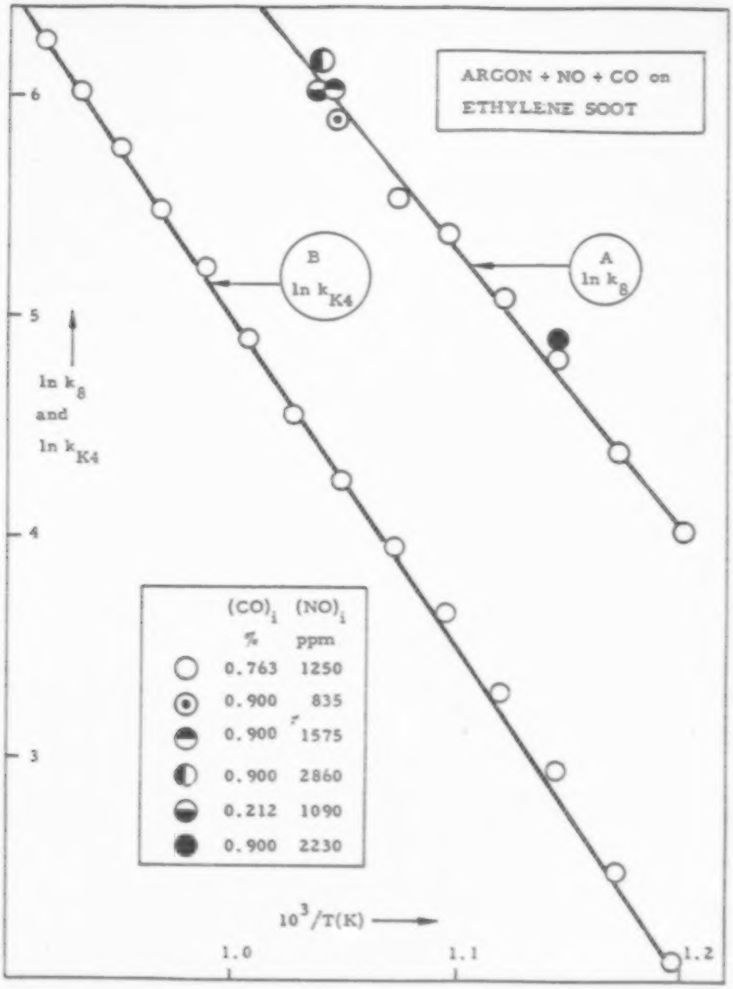

Figure 93. Argon + NO + CO on Ethylene Soot: Determination of Rate Constant k_{K4} (Curve B) According to eq.(134), and Determination of Rate Constant k_8 (Curve A) According to eq.(138), for Different Initial Concentrations of CO and NO.

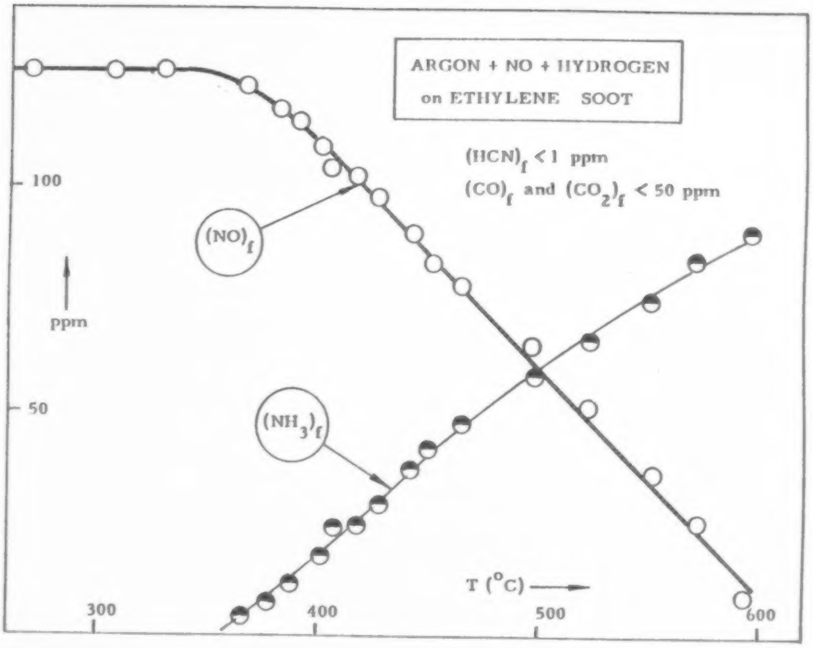

Figure 94. Argon + NO + Hydrogen on Ethylene Soot: D = 14.3 cm^3s^{-1}; $(NO)_i$ = 127 ppm; $(H_2)_i$ = 5.52%.

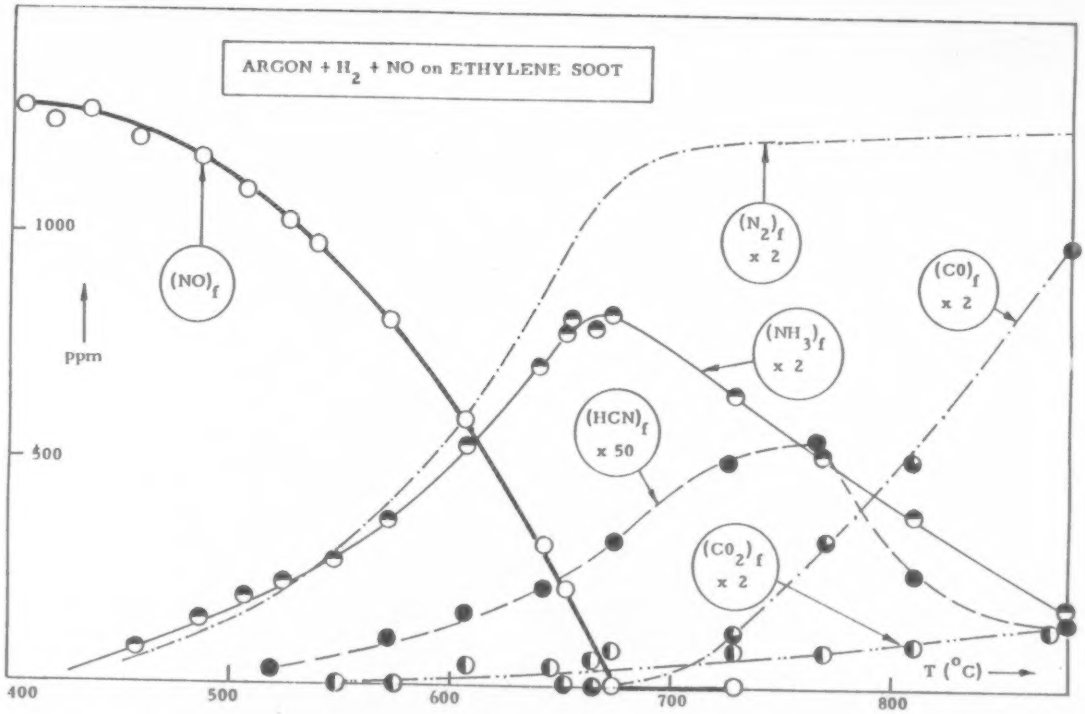

Figure 95. Argon + NO + Hydrogen on Ethylene Soot: D = 14.3 cm^3s^{-1}; $(NO)_i$ = 1280 ppm; $(H_2)_i$ = 5.52%.

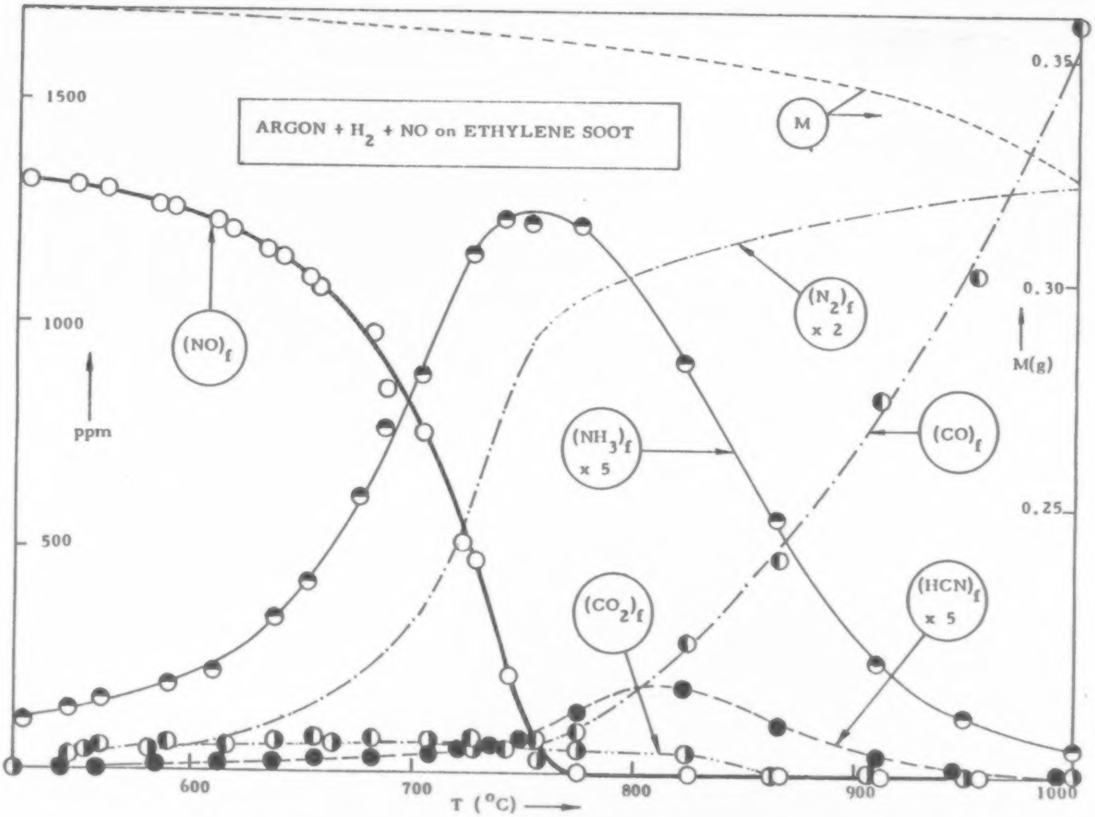

Figure 96. Argon + NO + Hydrogen on Ethylene Soot: D = 14.3 cm^3s^{-1}; $(NO)_i$ = 1330 ppm; $(H_2)_i$ = 1.63%.

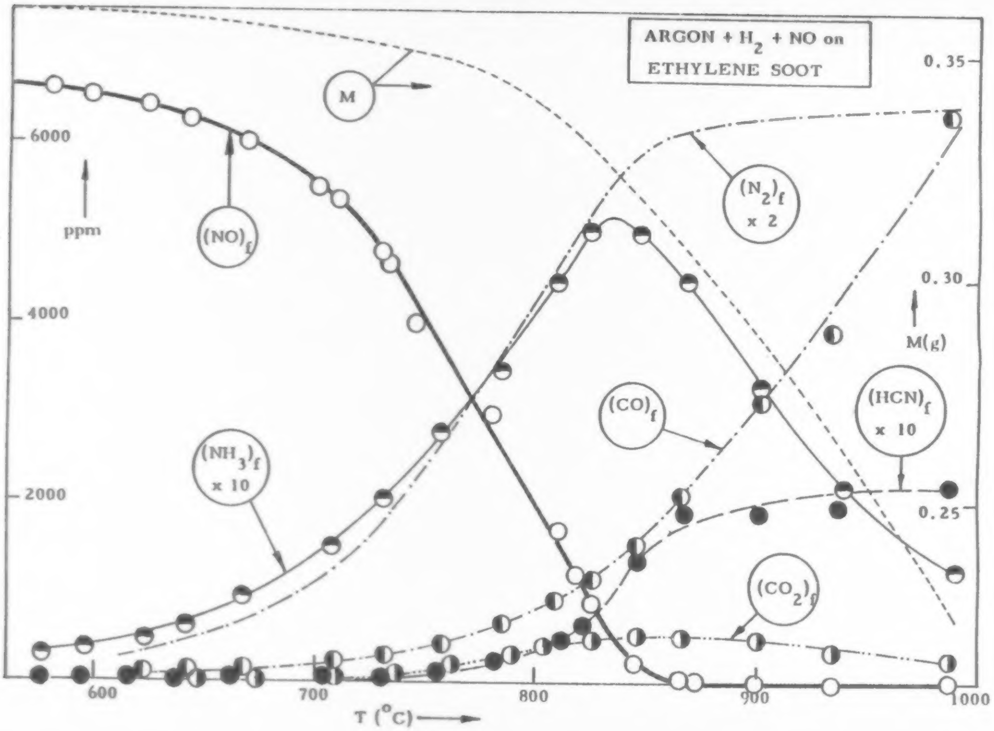

Figure 97. Argon + NO + Hydrogen on Ethylene Soot: D = 14.3 cm^3s^{-1}; $(NO)_i$ = 6800 ppm; $(H_2)_i$ = 1.63%.

$$d\left(NH_3\right)/dt = V_2 - nV_4 + V_{11} - V_{13} - V_5 \qquad (142)$$

$$d(HCN)/dt = -V_5 \qquad (143)$$

$$d\left(N_2\right)/dt = 0.5\ V_1 + \frac{1+n}{2}\ V_4 + 0.5\ V_{14} + 0.5\ V_{13} \qquad (144)$$

The sum of equations (142)and (143) yields:

$$-d(NO)/dt - d\left(NH_3\right)/dt - d(HCN)/dt = V_1 + V_{14} + (1+n)\ V_4 + V_{13} \qquad (145)$$

Upon substitution of previously determined rates for V_1, V_4, and V_{14} [equations (117), (125), and (108), respectively] into equation (145), a value of V_{14} has been obtained:

$$\boxed{V_{14} = 6.8 \times 10^8 \exp\left[-13260(\pm 1500)/T\right] X_{NO}\ X_{H_2}} \qquad (146)$$

The rate V_{11} has been obtained from eq. (142), by appropriate substitution for V_2, V_4, V_5, and V_{13} by their values calculated from eqs. (118), (125), (109), and (108), respectively. V_{11} may also be determined by combining eqs. (141), (142), and (143):

$$-d(NO)/dt + d\left(NH_3\right)/dt + d(HCN)/dt = V_1 + 2V_2 + 2V_{11} + V_{14} + V_{13} \qquad (147)$$

Both calculations produce the following expression for V_{11}:

$$\boxed{V_{11} = 1.3 \times 10^{10} \exp\left[-17100(\pm 2500)/T\right] X_{NO}^{0.5}\ X_{H_2}} \qquad (148)$$

Finally, calculation of the overall NO disappearance rate $\overline{V_{0.4}}$ has been made from eq. (141) (see Figure 98):

$$\boxed{\overline{V_{0.4}} = 1.7 \times 10^9 \exp\left[-13500(\pm 1500)/T\right] X_{NO}^{0.4}\ X_{H_2}^2} \qquad (149)$$

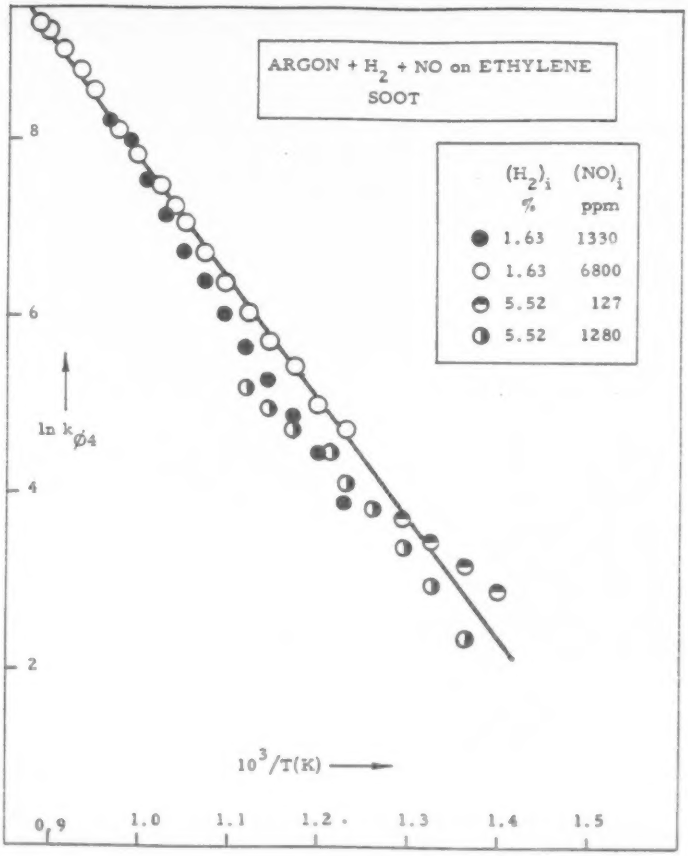

Figure 98. Argon + NO + Hydrogen on Ethylene Soot: Determination of Rate Constant k_{O4} According to eq.(141), For Different Initial Concentrations of Hydrogen and Nitric Oxide.

3.2.3.3 Effects of Molecular Oxygen on Selected Reactions

Two particular cases will be considered in the present section: the reactions of oxygen with ammonia on ethylene soot, and the interference of oxygen on the heterogeneous reduction of NO by this specific kind of soot. Effects of oxygen on NO reduction on soot in the presence of either CO or hydrogen have not been experimentally studied to date, although some information on the first of these two cases will be obtained.

3.2.3.3.1 Argon + NH_3 + O_2 on Ethylene Soot (Case Q.4)

Examples of these trials are given on Figures 99 through 103. During trials in which gases containing oxygen are fed over the soot bed, the consumption of the solid material during the trial must be considered. The evolution of total mass of solid (M) in the reactor, calculated according to the expression given at the end of section 1 of this report, are given in Figures 99 to 101. On Figures 102 and 103, however, the values plotted on the coordinate axis have been reduced to the (constant) initial value (M_i = value of M at the beginning of the trial) of the mass M, for the sake of comparison.

A concentration $(Y)_f$, reduced at M_i is obtained from the value of (Y) measured at the current value of M by the following expression:

$$(Y)_f \text{ reduced at } M_i = (Y)_i - \left[(Y)_i - (Y)_{f,M}\right] \cdot \qquad (150)$$

From both figures 100 and 101, it is clear that the presence of molecular oxygen typically has a promoting effect on the overall disappearance rate $\overline{V_{Q.4}}$ of ammonia. As may be seen from Figures 98 and 99, nitric oxide is but a secondary product formed during that decrease of ammonia, the main product being molecular nitrogen. (NO_2 was not present in the reactor outlet flow). This is due to reaction (16) prevailing over reaction path (17). The determination of these two reactions rates can be made from the following differential equations which give the time variation for nitrogen containing species concentrations:

$$d(NH_3)/dt = -nV_4 - V_5 + V_2 - V_{13} - V_{16} - V_{17} = -\overline{V_{Q.4}} \qquad (151)$$

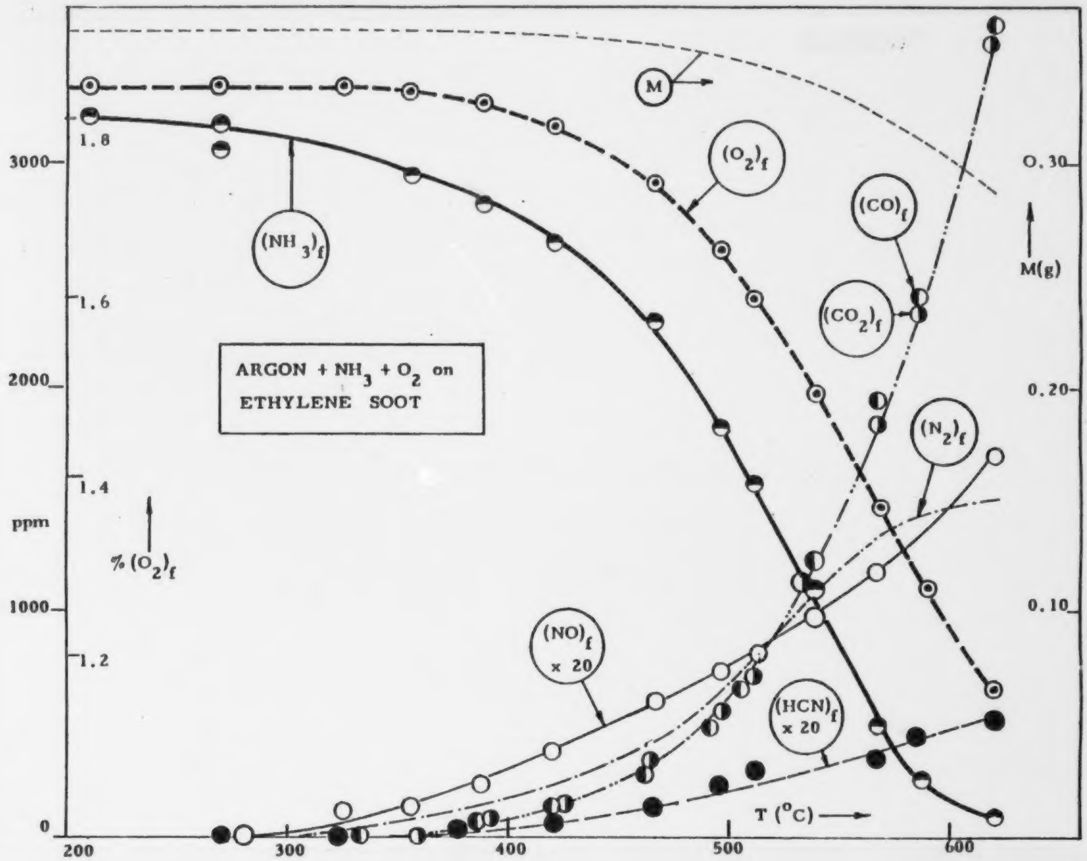

Figure 99. Argon + Ammonia + O_2 on Ethylene Soot: D = 13.4 cm^3s^{-1}; $(NH_3)_i$ = 3200 ppm; $(O_2)_i$ = 1.84%.

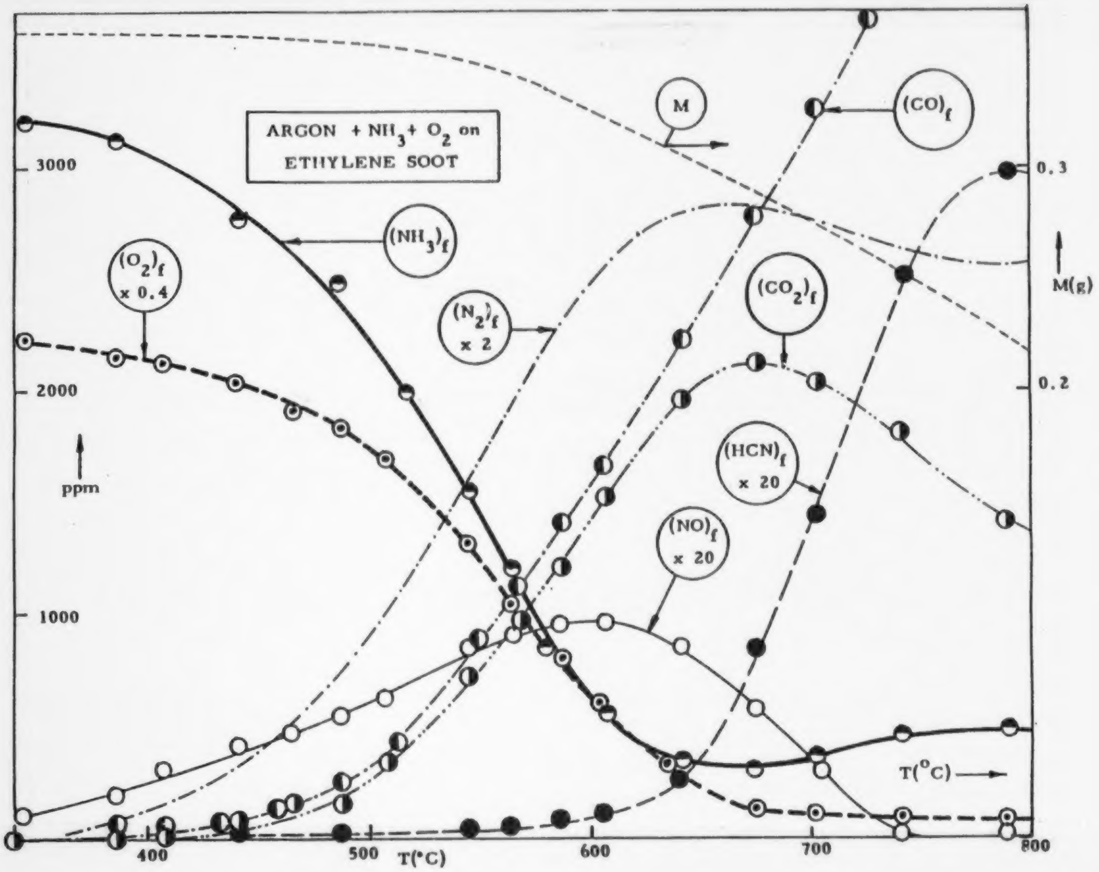

Figure 100. Argon + Ammonia + O_2 on Ethylene Soot: D = 13.4 cm^3s^{-1}; $(NH_3)_i$ = 3200 ppm; $(O_2)_i$ = 0.55%.

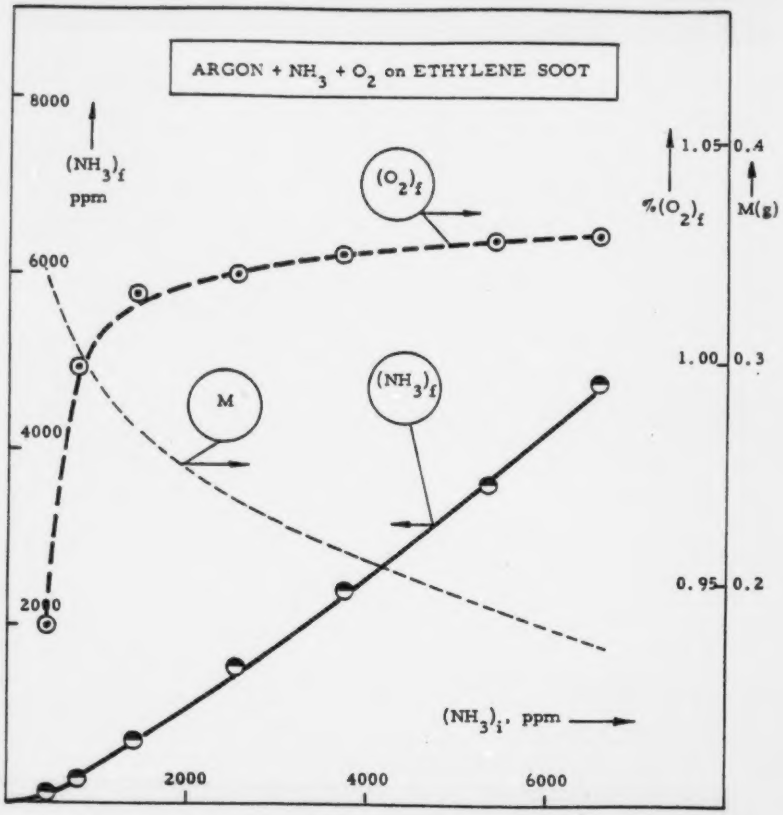

Figure 101. Argon + Ammonia + O_2 on Ethylene Soot: D = 12.3 cm^3s^{-1}; $(O_2)_i$ = 1.12%; T = 538°C.

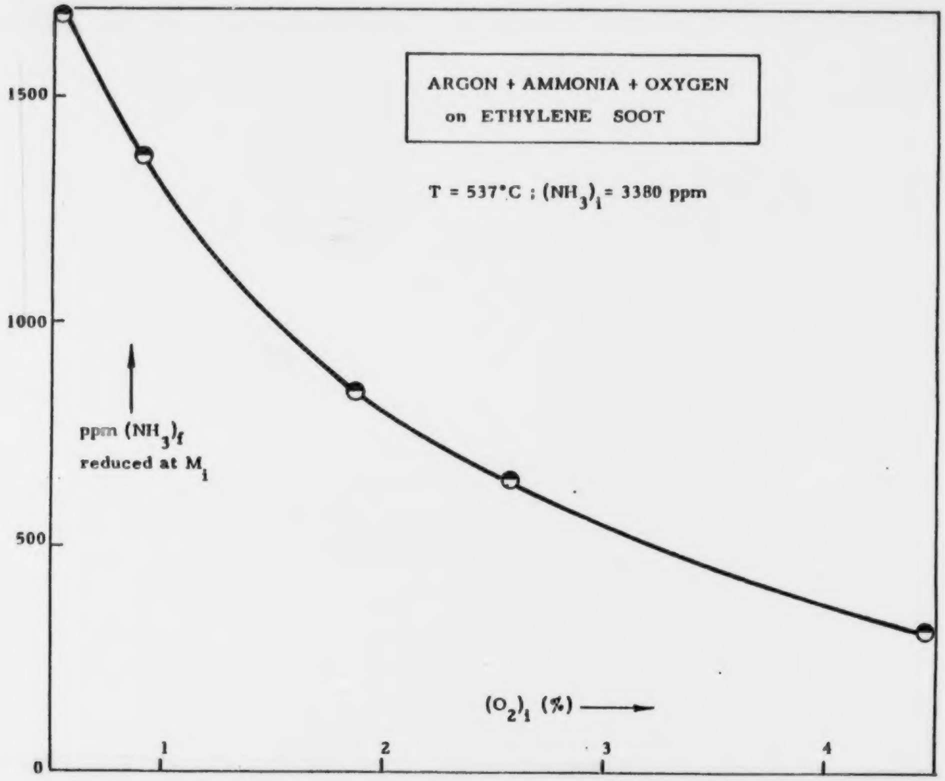

Figure 102. Argon + Ammonia + O_2 on Ethylene Soot: D = 13.4 cm^3s^{-1}; $(NH_3)_i$ = 3380 ppm; T = 537°C.

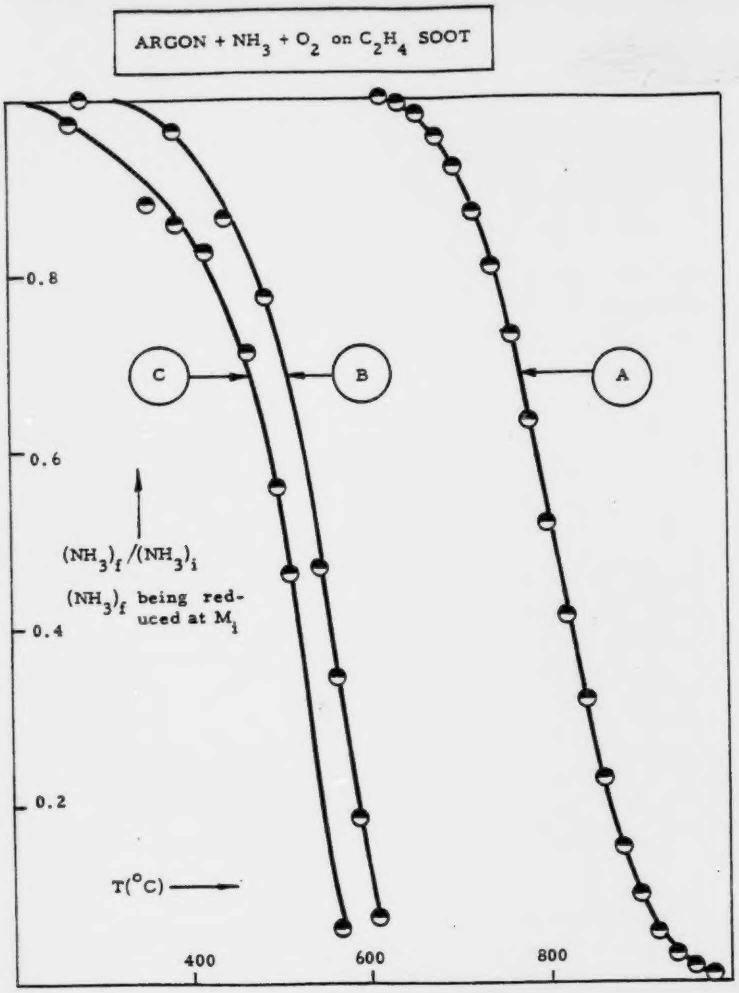

Figure 103. Argon + Ammonia + O_2 on Ethylene Soot: D = 13.4 cm^3s^{-1}; $(NH_3)_i$ = 3200 ppm; Curve A: $(O_2)_i = 0$; Curve B: $(O_2)_i$ = 0.55%; Curve C: $(O_2)_i$ = 1.84%.

$$d(HCN)/dt = +V_5 \tag{152}$$

$$d(NO)/dt = -V_4 - V_2 + V_{17} - V_1 \tag{153}$$

$$d\left(N_2\right)/dt = \frac{1+n}{2} V_4 + 0.5\ V_{13} + 0.5\ V_{16} + 0.5\ V_1 \tag{154}$$

Addition of eqs. (151), (152), and (153) yields:

$$-d\left(NH_3\right)/dt - d(HCN)/dt - d(NO)/dt = (1+n)\ V_4 + V_{13} + V_{16} + V_1 \tag{155}$$

The expression of V_{16} has been calculated from eq. (155), by substituting values for the rates of V_4, V_{13}, and V_1 calculated from eqs. (125), (108), and (117), respectively (see Figure 104):

F104

$$\boxed{V_{16} = 9.8 \times 10^6 \exp\left[-9900(\pm 800)/T\right]\ X_{NH_3}^{0.83}\ X_{O_2}^{0.33}} \tag{156}$$

Substitution of equations (117), (118), and (125) into eq. (153) allows the value of rate V_{17} to be determined (see Figure 105):

F105

$$\boxed{V_{17} = 2.7 \times 10^2 \exp\left[-6050(\pm 300)/T\right]\ X_{NH_3}^{0.5}\ X_{O_2}^{0.3}} \tag{157}$$

The overall ammonia disappearance rate $\overline{V_{Q.4}}$, calculated from equation (151), is found to be almost identical to the rate V_{16}. This fact demonstrates that N_2 formation from the reaction between ammonia and oxygen prevails over NO formation from those two reactants (see Figure 104):

$$\boxed{\overline{V_{Q.4}} = 9.8 \times 10^6 \exp\left[-9900(\pm 1000)/T\right]\ X_{NH_2}^{0.83}\ X_{O_2}^{0.33}} \tag{158}$$

3.2.3.3.2 Argon + NO + O_2 on Ethylene Soot (Case T.4)

An analogous study would have been trivial in the case of refractory oxides such as SiO_2 or Al_2O_3, since no NO reduction could be found in the presence of oxygen. In the case of soot, the effect of oxygen is a worthwhile area of study.

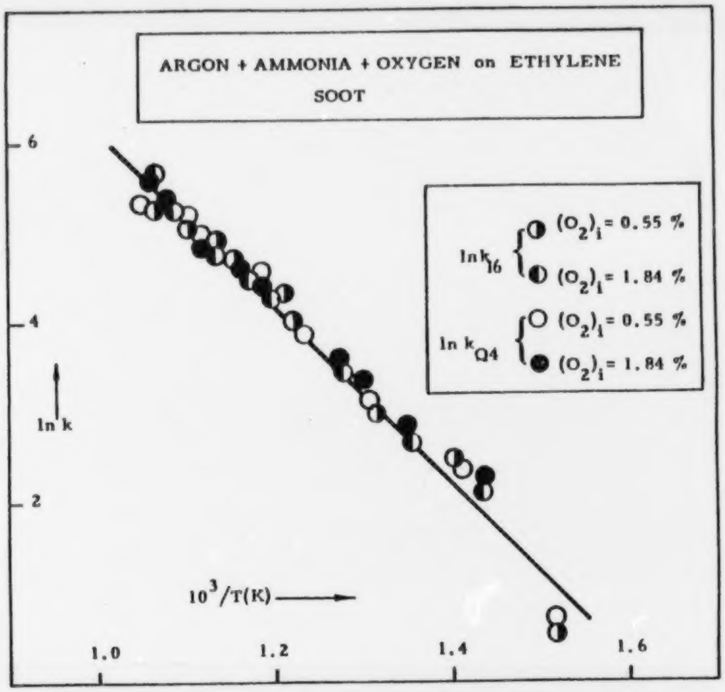

Figure 104. Argon + Ammonia + O_2 on Ethylene Soot: Determination of Rate Constant k_{Q4} According to eq.(151), and Determination of Rate Constant k_{16} According to eq.(155), for Two Different Initial Oxygen Concentrations.

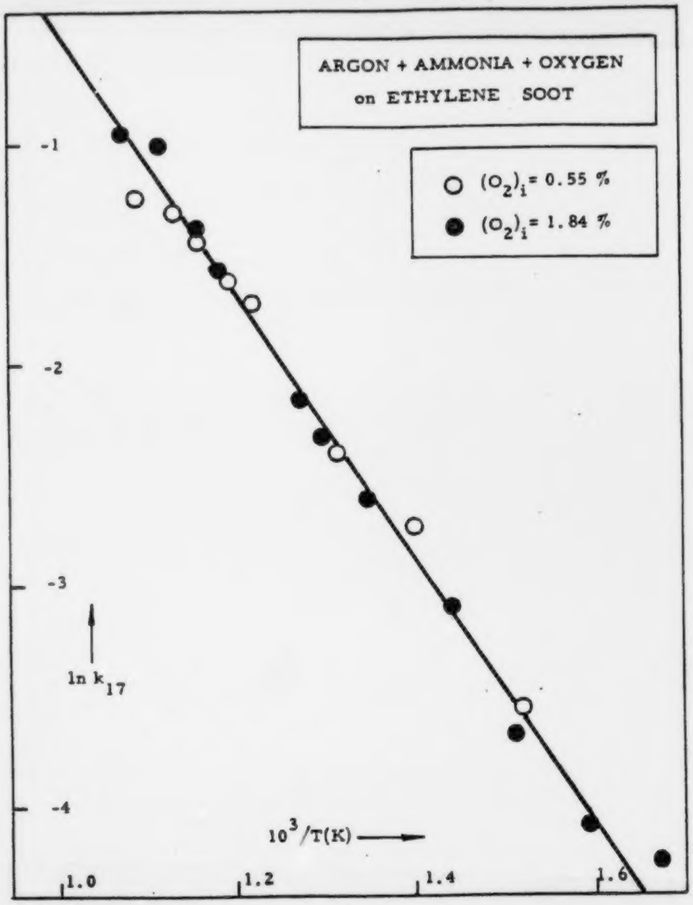

Figure 105. Argon + Ammonia + O_2 on Ethylene Soot: Determination of Rate Constant k_{17} According to eq.(153), For Two Different Initial Oxygen Concentrations.

F106

An example of these trials is given in Figure 106, where the logarithm of $\overline{V_{T.4}}$, calculated by eq. (5), is presented as a function of temperature for three different initial oxygen concentrations (zero, 1.56 percent and 2.53 percent, respectively). It is clearly seen from this figure, that the presence of oxygen enhances the overall NO disappearance rate. As in the case of argon + oxygen on ethylene soot (case E.4), CO and CO_2 formation is observed at temperatures above 500°C. Up to temperatures of about 650°, all the CO and CO_2 is formed from reactions with oxygen and NO, as evidenced by the oxygen balance:

$$2(O_2)_i + (NO)_i = 2(O_2)_f + (NO)_f + (CO)_f + 2(CO_2)_f \qquad (159)$$

Beyond that temperature, the righthand side of eq. (159) becomes larger than the lefthand side, due to supplementary CO formation from bound oxygen atoms (see section 3.2.3.1.1, and Figure 66).

The ratio $(CO)_f/(CO_2)_f$ is always relatively high. Beginning with values between 0.5 and 1.0 at temperatures below 580°C, it becomes greater than 2.0 for higher temperatures. The presence of oxygen decreases the quantities of HCN and NH_3 found in the reactor outlet gas flow which may be due to the secondary reactions (16), (17), and (38) involving ammonia, hydrogen cyanide and oxygen.

The variation in concentration of nitrogen-containing species as a function of time is given by the following set of equations. Here all secondary reactions except for V_8 should be vanishingly small since HCN and NH_3 concentrations are very small.

$$d(NO)/dt = V_1 - V_2 - V_8 \left(+V_{17} - V_4\right) = -\overline{V_{T.4}} \qquad (160)$$

$$d(NH_3)/dt = V_2 \quad \left(-V_{17} - nV_4 - V_{16} - V_5 - V_{13}\right) \qquad (161)$$

$$d(HCN)/dt = \left(V_5\right) \qquad (162)$$

$$d(N_2)/dt = 0.5\ V_1 + 0.5V_8 + \frac{1+n}{2} V_4 + 0.5\ V_{16} + 0.5\ V_{13} \qquad (163)$$

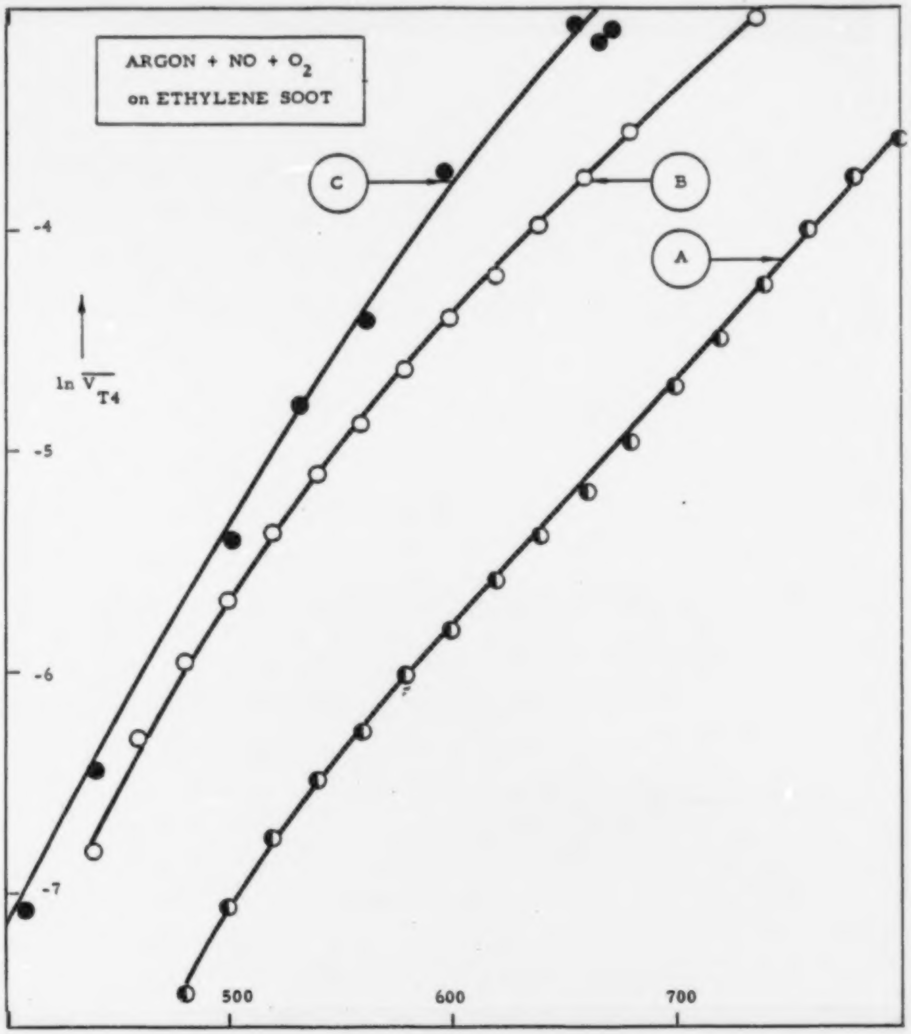

T (^oC) →

Figure 106. Argon + NO + O_2 on Ethylene Soot: D = 12.4 cm^3s^{-1}; $(NO)_i$ = 940 ppm; Curve A: $(O_2)_i$ = 0; Curve B: $(O_2)_i$ = 1.56%. Curve C: $(O_2)_i$ = 2.53%.

From the variation of nitric oxide given by eq. (160), a reasonable expression for the overall NO disappearance rate $\overline{V_{T.4}}$ is obtained. This expression shows the promoting effect of oxygen on the rate:

$$\boxed{\overline{V_{T.4}} = 3.4 \times 10^7 \exp\left[-16000(\pm 1000)/T\right] X_{NO}^{0.75} \left(1+33\ X_{O_2}^{0.25}\right)} \qquad (164)$$

By comparing equation (164) with equation (119), $\overline{V_{T.4}}$ may also be written in the following manner, which emphasizes the effect of oxygen on the overall reaction $\overline{V_{F.4}}$:

$$\boxed{\overline{V_{T.4}} = \overline{V_{F.4}} \left(1 + 33\ X_{O_2}^{0.25}\right)} \qquad (165)$$

The following suggestions can be made concerning an explanation of the promoting effect of oxygen on the overall NO disappearance rate:

- The promoting effect of oxygen on NO reduction seems to be strongly linked to the presence of carbon monoxide (CO being made in the present case from the xidation of the soot). This statement is based on the following two observations:
  - In the trials on ethylene soot, when very large amounts of oxygen are used, the $(CO)_f/(CO_2)_f$ ratio, which is normally greater than one, drops to very low values at sufficiently high temperatures, viz. where the oxidation of carbon into CO_2 is favored.
  - In the trials on Porcheville soot (from heavy oil), which will be treated in the next section, it is observed that CO_2 is the main oxidation product at all temperatures. As well, in case E.5 (argon + O_2 on Porcheville soot) and in the case T.5 (argon + NO + O_2 on Porcheville soot), the ratio $(CO)_f/(CO_2)_f$ is always very small. In these cases, it is observed that the presence of oxygen exerts an inhibiting effect on the NO reduction rate (see section 3.2.4).

- The promoting effect of oxygen (in the present ethylene soot case) is not limited, however, to the mere enhancement of reaction path (8) (reduction of NO with the CO formed by oxidation of the soot). Indeed, when calculating values of V_8 from eq. (139) utilizing the experimental values of T, X_{NO} and X_{CO}, measured in the T.4 trials, it is found that V_8 is one or two orders of magnitude smaller than the corresponding value if $\overline{V_{T.4}}$. From this it is clear that the promoting effect of oxygen cannot be restricted to the mere increase of CO concentration.

- Upon calculating the value of V_8 from differential equation (160):

  $$V_8 = -d(NO)/dt = V_1 - V_2 - V_4 + V_{17}$$

  and assuming that reaction rates V_1, V_2, and V_4 are not perturbed by the presence of oxygen (placing the whole effect of the latter on reaction rate V_8), one finds an alternative expression for V_8. The value of V_8 computed according to eq. (160) will be designated by the symbol V_8', to differentiate it from the value computed according to equation (139).

$$\boxed{V_8 = 1.5 \text{ to } 2.2 \times 10^{12} \exp\left[-12000(\pm 2500)/T\right] X_{CO} X_{NO} X_{O_2}^{(0.25 \text{ to } 1)}} \qquad (166)$$

Although the values of the activation temperature and the partial order with respect to oxygen are only approximate, it is of interest to compare this expression with eq. (139) and get an idea of the ratio V_8'/V_8:

$$V_8'/V_8 \simeq 10^4 \, X_{O_2} \simeq 3 \times 10^2 \, X_{O_2}^{0.25}$$

If this effect of oxygen on reaction path (8) is assumed (i.e. heterogeneous reduction of NO by CO), one finds a qualitative analogy with the effect of oxygen previously observed in the case JKT.1 [i.e. Ar + NO + CO + O_2 on alumina, section 3.2.1.3.1 and equation (60)].

To summarize, the following provisional conclusions may be drawn concerning the effects of oxygen on the heterogeneous reduction of NO in the absence of hydrogen:

- Under conditions of temperature, oxygen concentration and soot type leading to the preferential oxidation of soot into CO_2, oxygen exerts an inhibiting effect on the NO reduction reactions (V_1 and V_2 most probably). This will be clearly exemplified in the case of soot from heavy fuel oils.
- Under conditions of temperature, soot type, and oxygen concentrations leading to partial oxidation of soot into CO, oxygen is found to have a promoting effect, in that:
    - It is responsible for CO formation, allowing reaction path (8) to be an effective NO reducing mechanism.
    - It enhances, or seems to enhance, the very reaction rate V_8 which allows the reduction path.

3.2.4 Trials on Soot From Heavy Fuel Oil (Porcheville Soot) (Case 5)

3.2.4.1 Gas Flows Without Nitrogen-containing Species

3.2.4.1.1 Argon on Porcheville Soot (Case A.5)

As may be seen from Figure 107, during thermal treatment of this soot, CO, CO_2, and HCN are released. The quantities released as a function of the temperature of the solid are fairly reproducible. At temperatures above 500°C, some CO_2 is released, disappearing at still higher temperatures. At these higher temperatures, the presence of CO is detected while at the same time HCN is found in the reactor outlet flow. Since the amounts of CO, CO_2, and HCN do not decrease with the age of the bed (i.e. with the number of runs made on the same bed), it may be concluded that they are formed from bound carbon, oxygen, hydrogen, and nitrogen atoms. As a consequence, the quantities of HCN released in this trial, for example, should be used to correct data taken in later trials.

This thermal treatment of Porcheville soot under argon flow never yielded NO or NH_3 in the reactor outlet flow. In direct contrast to these trials on Porcheville soot, an analogous treatment of gas-phase-generated

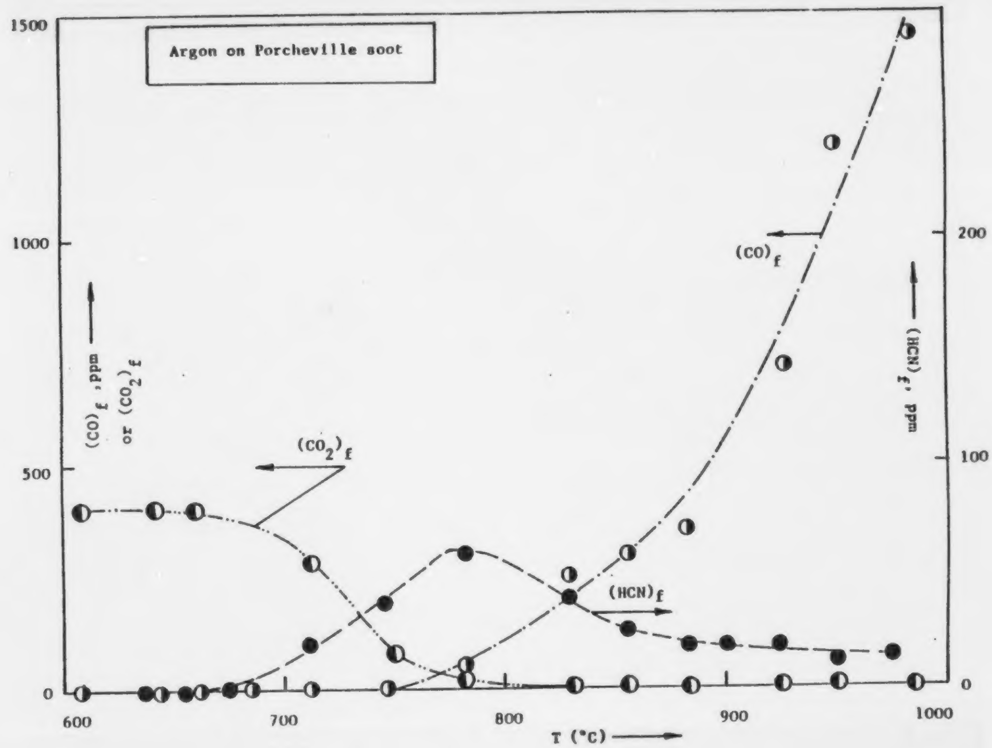

Figure 107. Argon on Porcheville Soot: D = 15.0 cm^3s^{-1}.

soot (e.g. ethylene soot, see Figure 66, curve A) never yielded CO_2.

3.2.4.1.2 Argon + CO on Porcheville Soot (Case B.5)

Case B.5 is illustrated in Figure 108 where 2.1 percent carbon monoxide has been added to the argon flow. Again the formation of CO_2 is observed at temperatures above 400°C; however, the quantities are much larger than in the pyrolysis case discussed above and are largely formed from the introduced CO gas. The source of CO_2 is indicated by the decrease of CO as seen in Figure 108. Again this is different from what was observed in the analogous runs over soot generated in an ethylene flame (compare with Figure 66, curves B). There, a decrease of (CO) was not observed in the reactor outlet flow.

3.2.4.1.3 Argon + O_2 on Porcheville Soot (Case E.5)

NO formation is accounted for by reaction (25). Since all three reactions involving oxidation of bound species, (23), (24), and (25), result in a progressive destruction of the soot lattice, their respective rates should be interconnected through the H/C and N/C ratios which characterize the soot. From this, a rough estimation of molecular nitrogen formed during soot oxidation may be obtained:

$$(N_2)_f = 0.5\left[(CO)_f + (CO_2)_f\right]\left[\frac{N}{C} - \frac{(HCN)_f + (NO)_f}{(CO)_f + (CO_2)_f}\right] \tag{168}$$

Values calculated in that way are plotted in Figure 109 and 110. The overall oxygen disappearance rate, $\overline{V_{E.5}}$, is defined as:

$$-d(O_2)/dt = \overline{V_{E.5}} = V_{23} + V_{24} + V_{25} \simeq V_{23} + V_{24} \tag{169}$$

As determined for different initial oxygen concentrations and as a function of temperature, $\overline{V_{E.5}}$ is given by the following rate expression:

$$\boxed{\overline{V_{E.5}} = 3.0 \times 10^{11} \exp\left[-16700(\pm 800)/T\right] X_{NO}} \tag{170}$$

3.2.4.1.4 Argon + H_2 on Porcheville Soot (Case C.5)

When hydrogen is added to the argon carrier gas, an increase in HCN release is observed and small amounts of NH_3 are found in the reactor

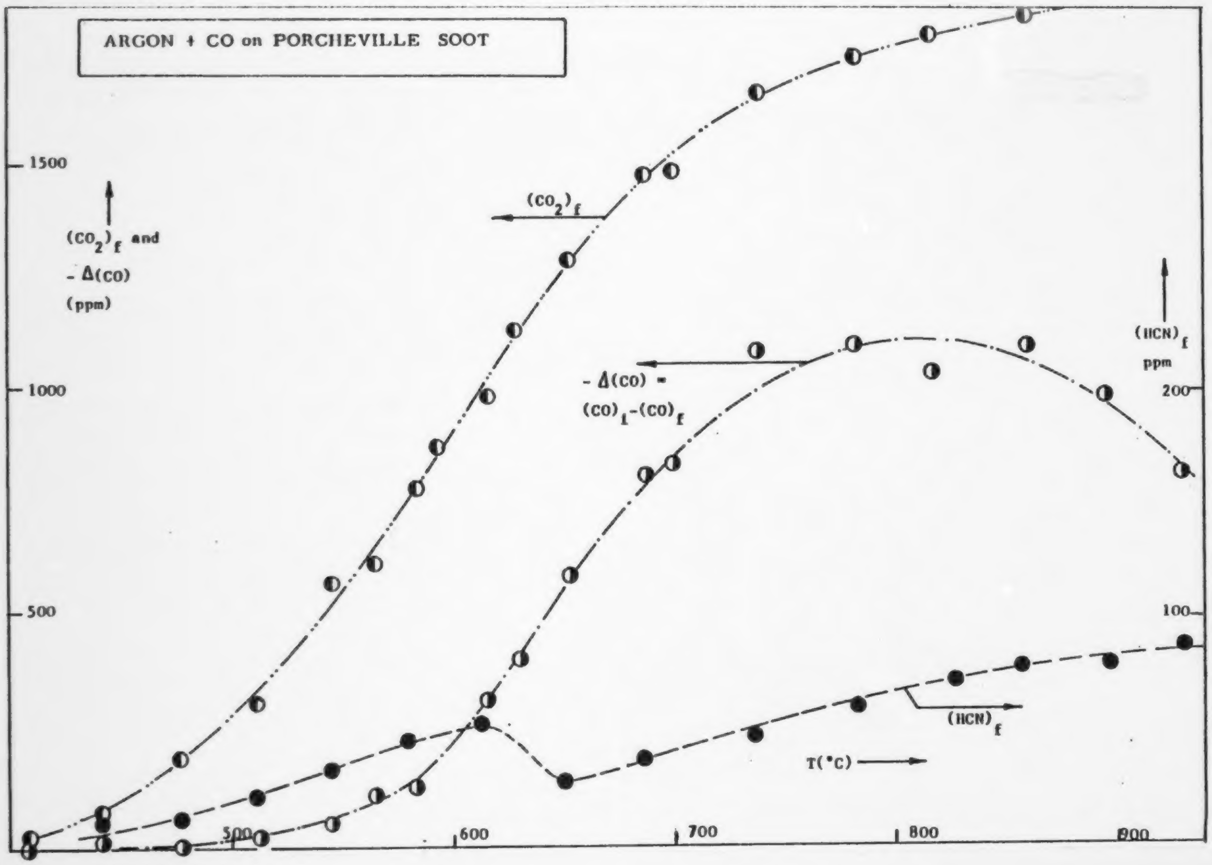

Figure 108. Argon + CO on Porcheville Soot: D = 14.5 cm^3s^{-1}; $(CO)_i$ = 2.10%.

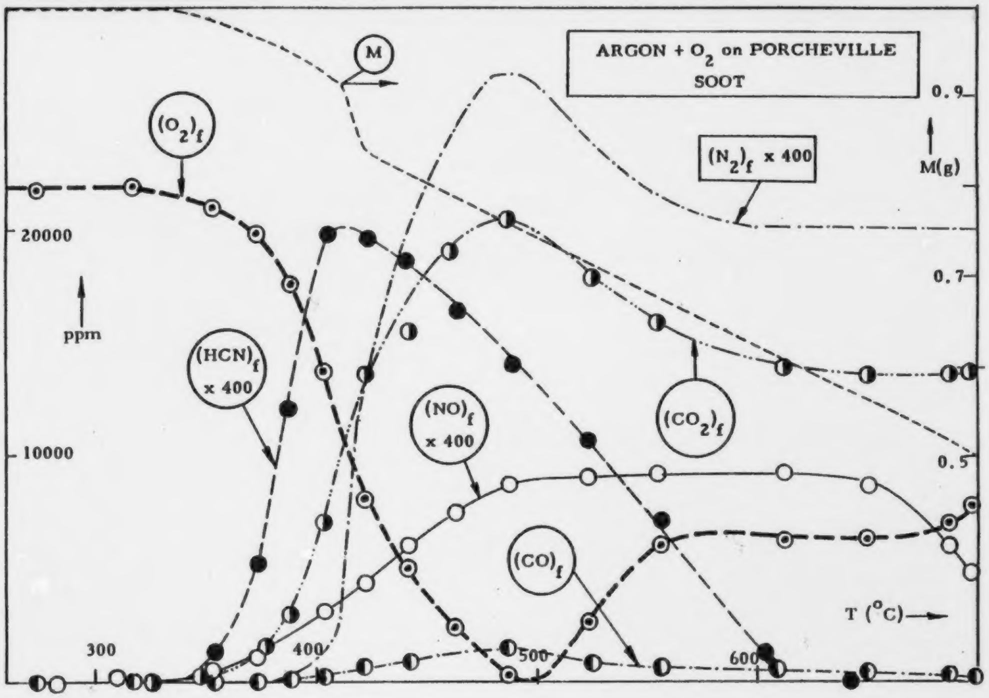

Figure 109. Argon + O_2 on Porcheville Soot: D = 13.4 $cm^3 s^{-1}$; $(O_2)_i$ = 2.19%.

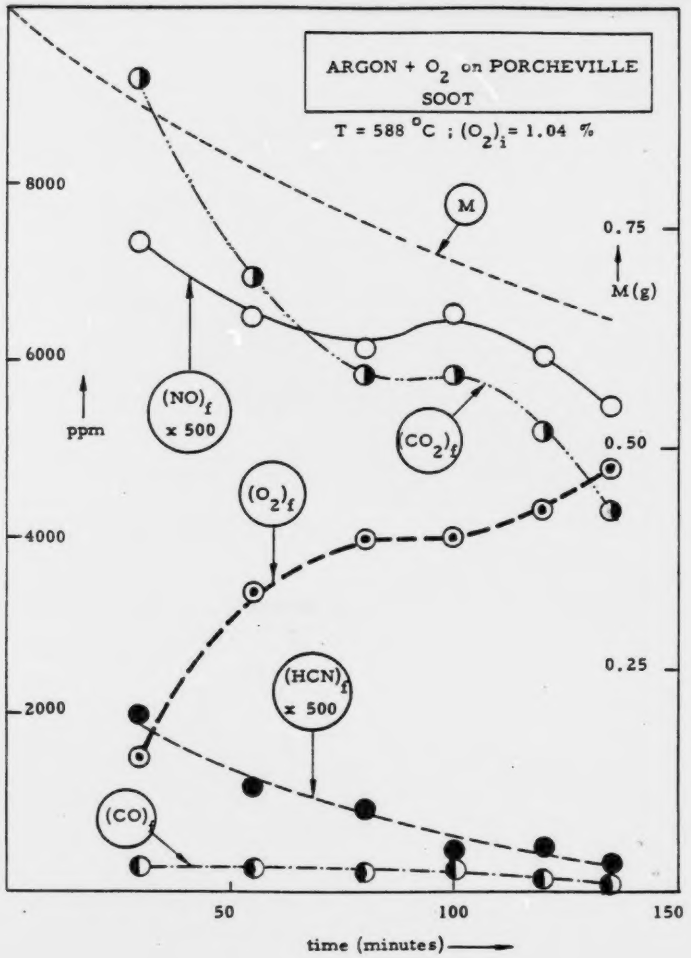

Figure 110. Argon + O_2 on Porcheville Soot: D = 13.3 cm^3s^{-1}; $(O_2)_i$ = 1.04%; M_i = 1.00 g; T = 588°C.

outlet flow (see Figure 111). This suggests the existence of reactions (21) and (22).

F111

CO and CO_2 are released in smaller quantities than in case A.5, which may be explained by the formation of water from bound oxygen (reaction 19).

3.2.4.2 Gas Flows Containing Nitrogen Species but No Oxygen

3.2.4.2.1 Argon + NH_3 on Porcheville Soot (Case D.5)

A typical run is presented in Figure 112. A decrease of ammonia begins at a temperature of 600°C. The hydrogen cyanide observed in the reactor outlet flow, is only partly accounted for by thermal decomposition of the soot. Since the HCN concentrations are substantially larger than in the pyrolysis case A.5, and since HCN is detected at lower temperatures, reaction (5) is of importance. This is a similar observation to that previously made for ethylene soot (case D.4).

F112

The relatively fast ammonia disappearance is not accounted for by the observed concentrations of HCN which suggests a strong role for reaction (13). The poor precision of N_2 determination by the chromatographic method did not allow the existence of a N_2 formation path to be directly checked. However, if reaction (26) does exist, it should be negligible compared to reaction (13). Ignoring secondary reactions one has:

$$d\left(NH_3\right)/dt = -V_5 - V_{13} = -\overline{V}_{D.5} \tag{171}$$

$$d(HCN)/dt = V_5 \tag{172}$$

$$d\left(N_2\right)/dt = 0.5\ V_{13} \tag{173}$$

Reaction rate V_{13} may be obtained from the sum of eqs. (171) and (172):

$$d\left(NH_3\right)/dt - d(HCN)/dt = V_{13} \tag{174}$$

The following expression has been obtained in that way:

$$\boxed{V_{13} = 5.3 \times 10^9 \exp\left[-19800(\pm 2000)/T\right] X_{NH_3}} \tag{175}$$

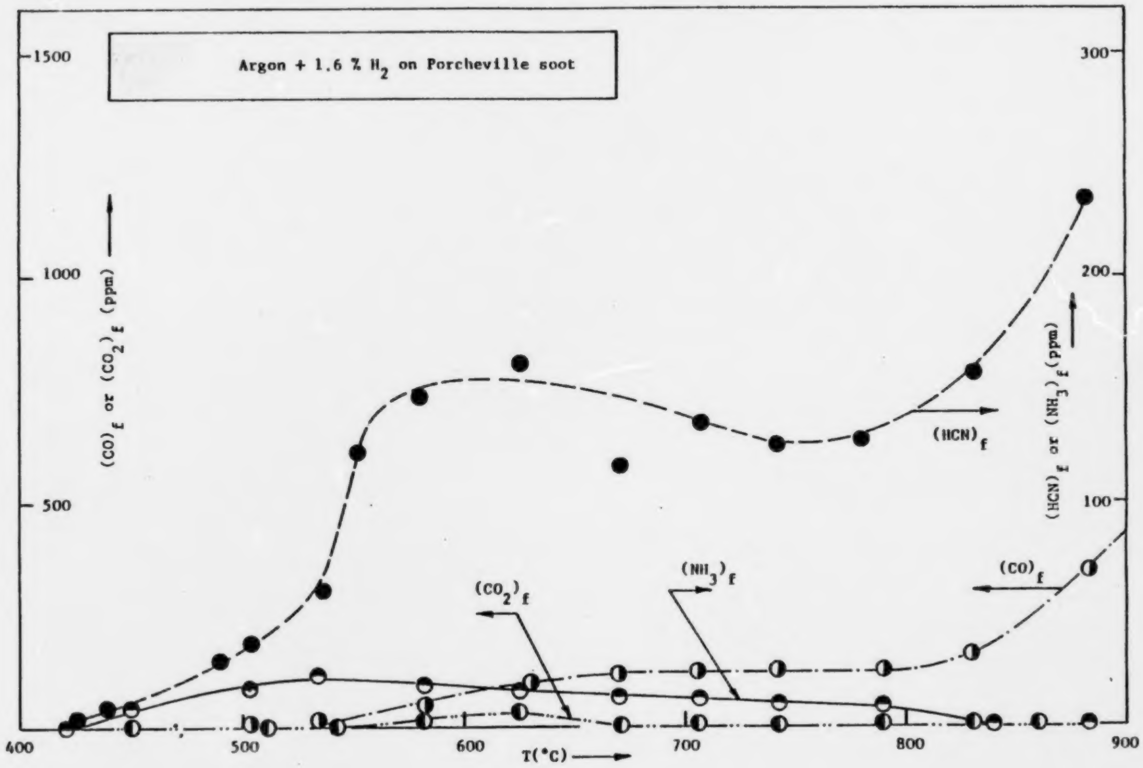

Figure 111. Argon + Hydrogen on Porcheville Soot: D = 14.5 cm^3s^{-1}; $(H_2)_i$ = 1.60%.

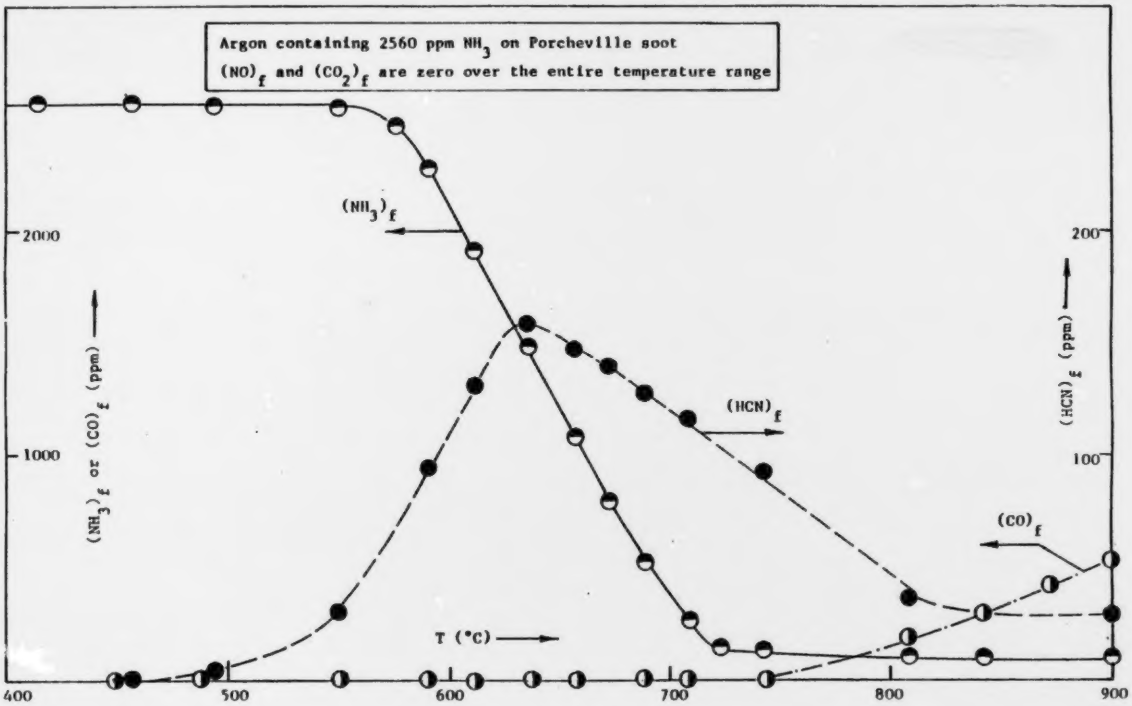

Figure 112. Argon + Ammonia on Porcheville Soot: D = 14.5 cm^3s^{-1}; $(NH_3)_i$ = 2560 ppm.

The value of V_5 may be calculated either from eq. (171) or from the difference between eq. (171) and eq. (172):

$$-d(NH_3)/dt + d(HCN)/dt = 2V_5 + V_{13} \tag{176}$$

Upon substitution for V_{13} by the value calculated according to eq. (175), the following expression is obtained:

$$\boxed{V_5 = 7.3 \times 10^7 \exp\left[-16600(\pm 2000)/T\right] X_{NH_3}} \tag{177}$$

The overall ammonia disappearance rate $\overline{V_{D.5}}$, calculated by eq. (171), yields:

$$\boxed{\overline{V_{D.5}} = 1.1 \times 10^8 \exp\left[-15600(\pm 2000)/T\right] X_{NH_3}} \tag{178}$$

3.2.4.2.2 Argon + NO on Porcheville Soot (Case F.5)

F113
114

These trials are illustrated in Figures 113 and 114, for two different initial nitric oxide concentrations. The general shape of these figures is similar to the analogous trials performed on gas-phase-generated soot (see Figure 74 and 75). An exception is the $(CO_2)_f/(CO)_f$ ratio, which is much higher in the present case, and is a general characteristic of this heavy oil soot.

The ammonia observed during the nitric oxide decrease is formed from NO via reaction (2). This is experimentally indicated by the fact that the amount of ammonia released increases with increasing initial nitric oxide concentration. During the NO disappearance, the oxygen balance is not perfectly equilibrated, due to CO_2 formation by thermal decomposition of the soot (see section 3.2.4.1.1):

$$(CO_2)_f \geq 2\left[(NO)_i - (NO)_f\right] \tag{179}$$

Hydrogen cyanide which is released at the end of the NO disappearance, is mostly formed from ammonia by reaction path (5), but is also generated by thermal decomposition.

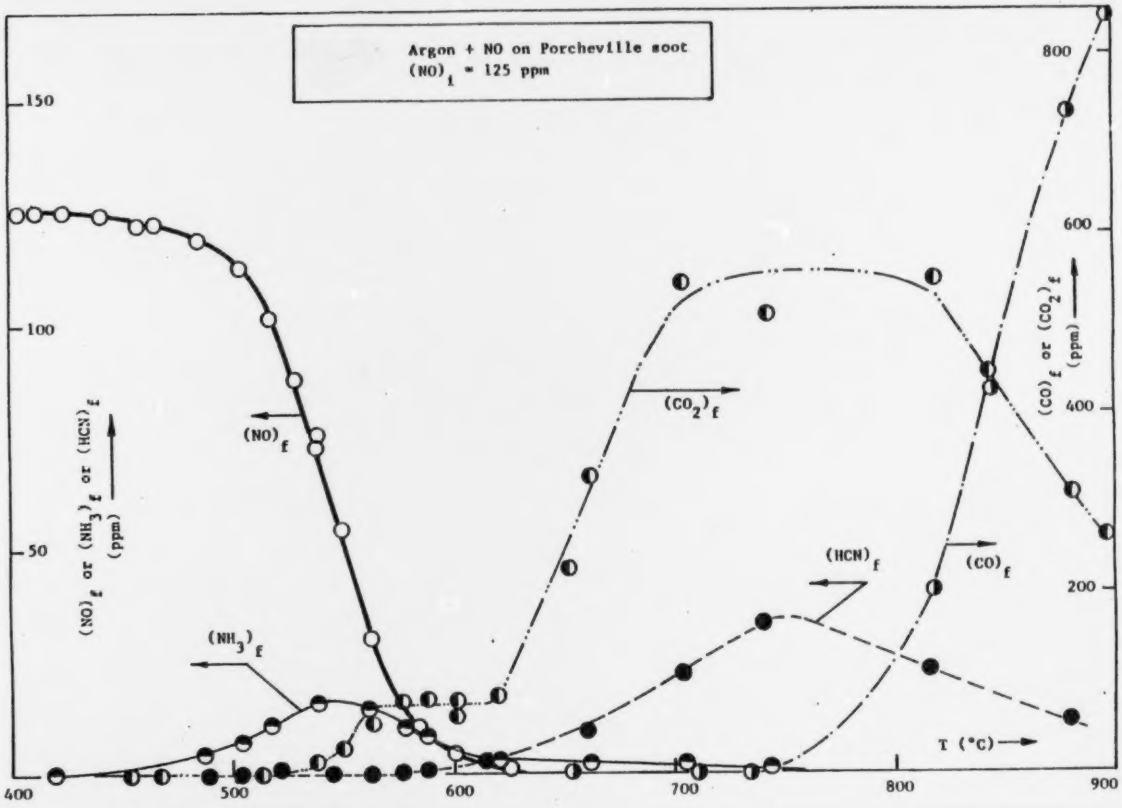

Figure 113. Argon + NO on Porcheville Soot: D = 14.5 cm^{3}s^{-1}; (NO)$_i$ = 125 ppm.

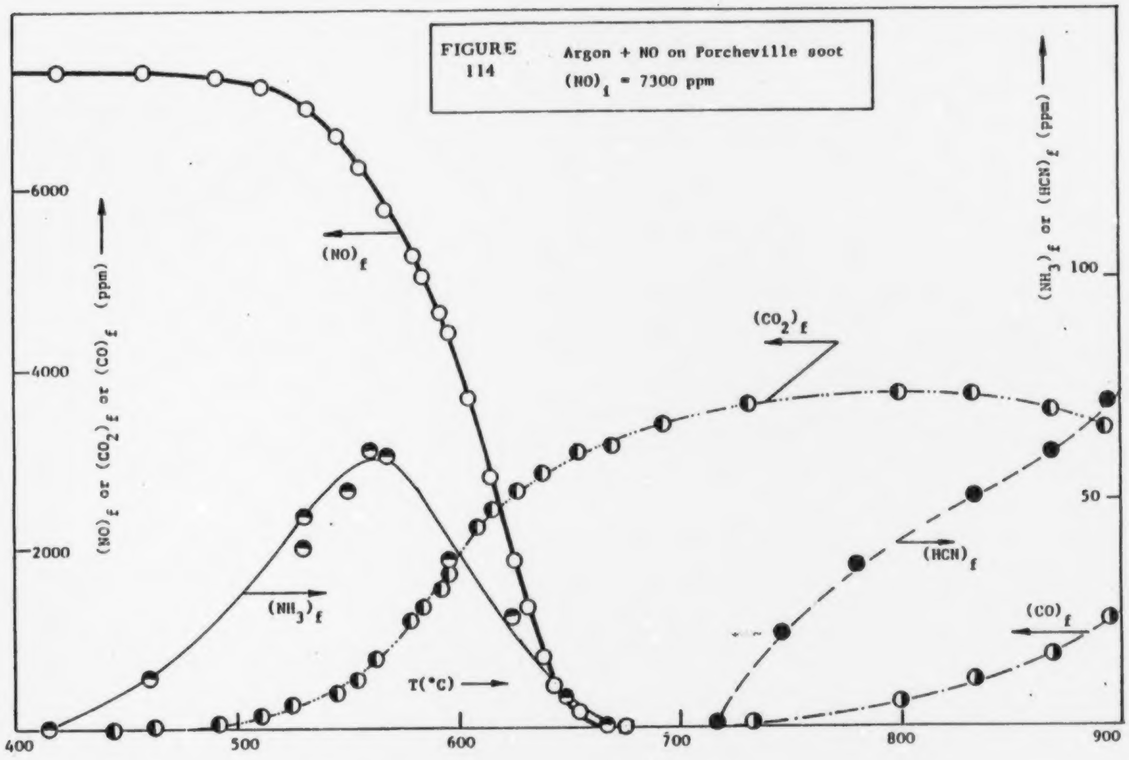

Figure 114. Argon + NO on Porcheville Soot: D = 14.5 cm^{3}s^{-1}; (NO)$_i$ = 7300 ppm.

Neglecting all but the known secondary reactions, the following equations apply during the nitric oxide decrease:

$$d(NO)/dt = -V_1 - V_2 = -\overline{V_{F.5}} \qquad (180)$$

$$d(NH_3)/dt = V_2 - V_{13} - V_5 \qquad (181)$$

$$d(N_2)/dt = 0.5\ V_1 + 0.5\ V_{13} \qquad (182)$$

$$d(HCN)/dt = V_5 \qquad (183)$$

The sum of eqs. (180, (181), and (183) yields:

$$-d(NO)/dt - d(NH_3)/dt - d(HCN)/dt = V_1 + V_{13} \qquad (184)$$

The expression of reaction rate V_2 can be calculated from eq. (181), by substituting V_{13} obtained from eq. (177):

$$\boxed{V_2 = 2.1 \times 10^6 \exp\left[-16000(\pm 2000)/T\right] X_{NO}^{0.35}} \qquad (185)$$

The rate expression V_1 has been calculated from eq. (184), by substituting V_{13} as calculated from eq. (177):

$$\boxed{V_1 = 9.8 \times 10^{16} \exp\left[-33500(\pm 2500)/T\right] X_{NO}^{0.63}} \qquad (186)$$

The overall nitric oxide disappearance rate $\overline{V_{F.5}}$ is calculated from eq. (180) (see Figure 115):

$$\boxed{\overline{V_{F.5}} = 6.6\ 10^8 \exp\left[-18600(\pm 2000)/T\right] X_{NO}^{0.5}} \qquad (187)$$

3.2.4.2.3 Argon + NO + NH_3 on Porcheville Soot (Case R.5)

An example of these runs is given in Figure 116. As in previous cases R.2 and R.4, the general decrease of nitric oxide is balanced by an equal decrease of ammonia. This indicates that the principal reaction is reaction (4) and its stoichiometric coefficient n is essentially equal to one.

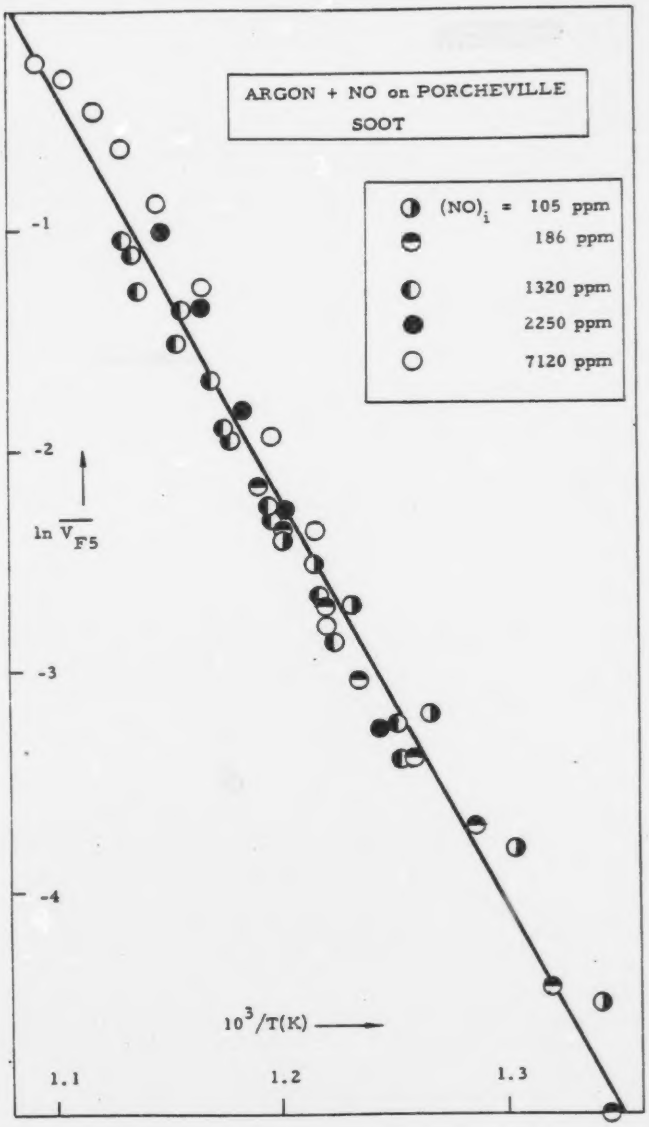

Figure 115. Argon + NO on Porcheville Soot: Determination of the Rate Constant k_{F5} of Overall NO Removal, According to eq.(180), for Different Initial Concentrations of NO.

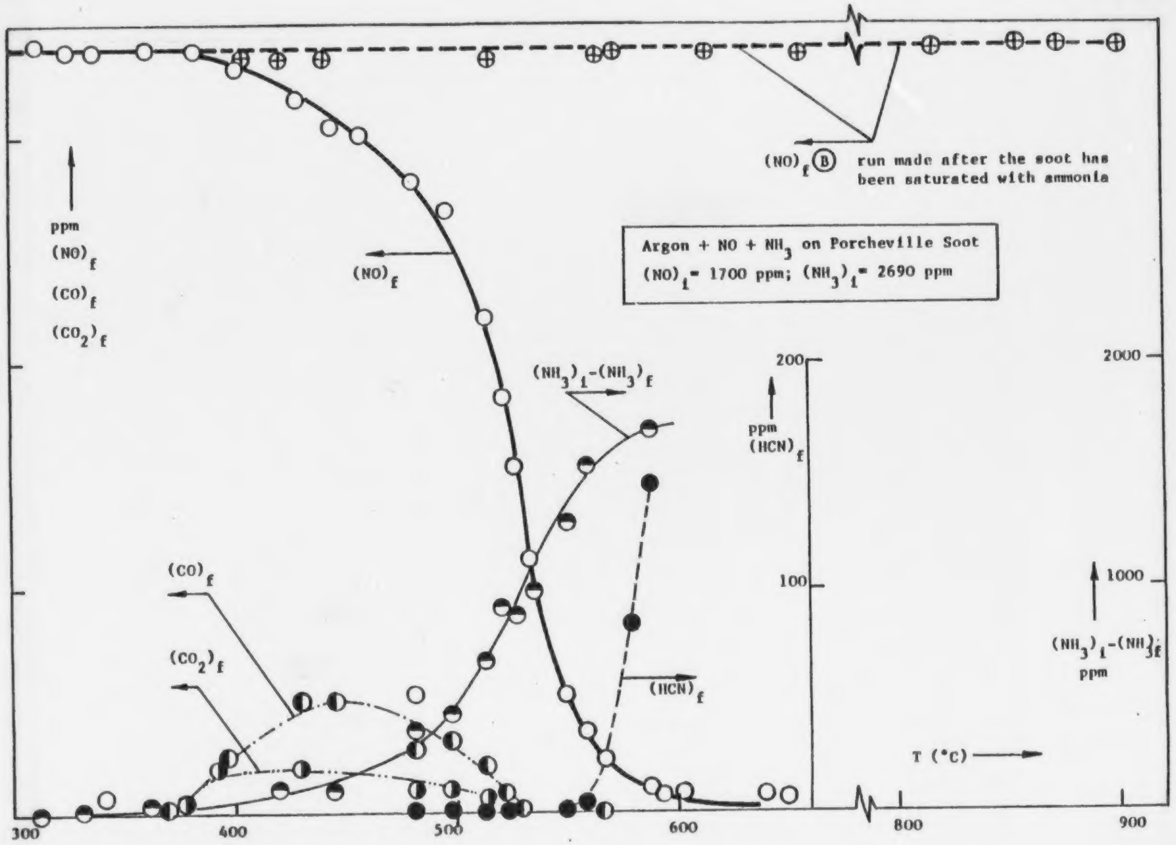

Figure 116. Argon + NO + Ammonia on Porcheville Soot: D = 14.5 cm^3s^{-1}; $(NO)_i$ = 1700 ppm; $(NH_3)_i$ = 2690 ppm.

HCN formation is initiated after NO has disappeared, and is primarily accounted for by reaction (5).

The variation of nitrogen-containing species as a function of time can be described by the same set of differential equations already utilized in case R.4 (see section 3.2.3.2.3), i.e. by eqs. (120) through (124). In exactly the same manner as described in section 3.2.3.2.3, it is found that:

$$\boxed{V_4 = 3.0 \times 10^{10} \exp\left[-15300(\underline{+}1000)/T\right] X_{NO}\, X_{NH_3}} \tag{188}$$

$$\boxed{\overline{V_{R.5}} = 3.3 \times 10^{11} \exp\left[-14600(\underline{+}1000)/T\right] X_{NO}\, X_{NH_3}} \tag{189}$$

It has been observed that, when Ar + NO + NH_3 mixtures are fed over Porcheville soot, which has been saturated with ammonia, NO does not disappear even at temperatures as high as 900^{0}C (see Figure 116, curve B). This may suggest that in order for reaction (4) to take place, the reacting nitric oxide must first be adsorbed on the solid.

3.2.4.2.4 Argon + NH_3 + CO on Porcheville Soot (Case I.5)

Case I.5 is illustrated by Figure 117. The experimental findings are generally comparable to the one observed in the analogous trials on ethylene soot (see section 3.2.3.2.4). No nitric oxide whatsoever is formed. The variation of nitrogen-containing species as a function of time is given by equations (128) through (131).

A calculation of V_9 from eq. (129) has been made by substituting V_5 and V_{13} as calculated according to eq. (177) and eq. (175), respectively. As in case I.4, it is found that V_9 is almost zero. The overall ammonia disappearance rate $\overline{V_{I.5}}$, determined as $-d\left(NH_3\right)/dt$, is found to have values close to the rate V_{13} (see Figure 118):

$$\boxed{\overline{V_{I.5}} = 1.3 \times 10^{9} \exp\left[-19500(\underline{+}1500)T\right] X_{NH_3}} \tag{190}$$

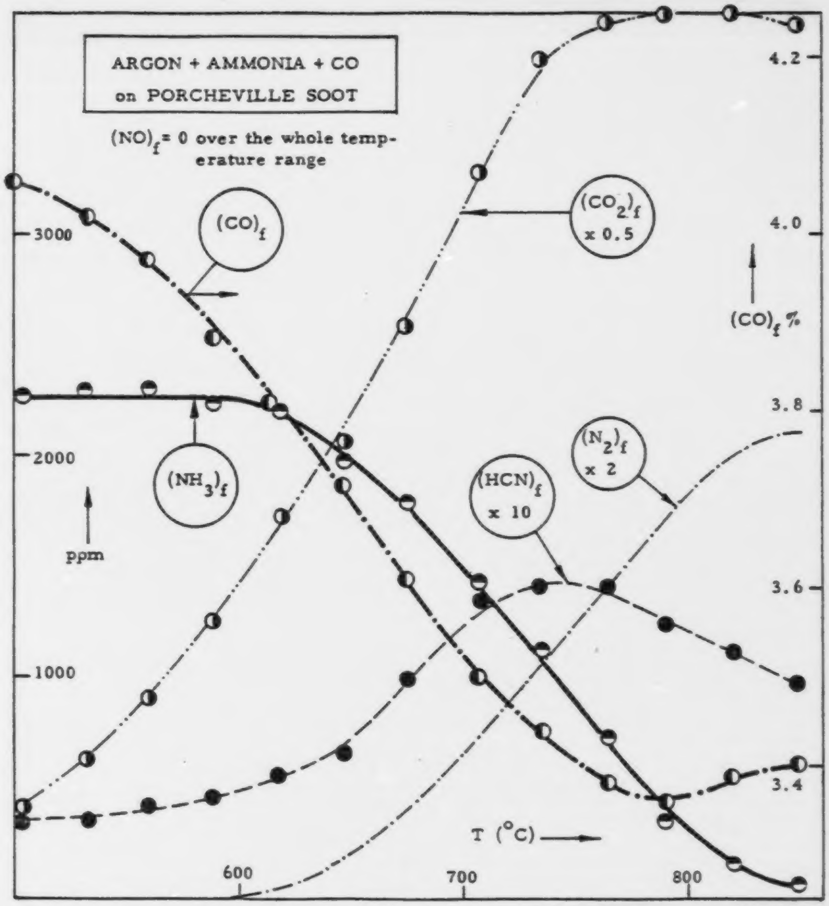

Figure 117. Argon + Ammonia + CO on Porcheville Soot; D = 12.6 cm^3s^{-1}; $(NH_3)_i$ = 2270 ppm; $(CO)_i$ = 4.15%.

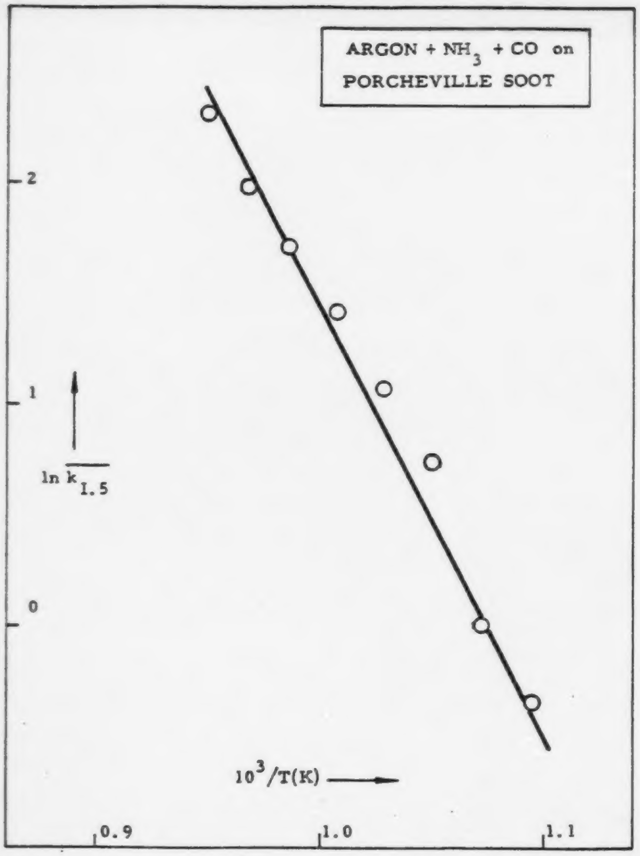

Figure 118. Argon + Ammonia + CO on Porcheville Soot: Determination of the Overall NO Removal Rate Constant $k_{I.5}$; D = 12.6 cm^3s^{-1}; $(NH_3)_i$ = 2270 ppm; $(CO)_i$ = 4.15%.

The absence of reaction path (9) seems to confirm the conclusion put forward in section 3.2.3.2.4. However, since the present heavy fuel oil soot is characterized by nonnegligible quantities of vanadium, nickel, or their oxides, the second assumption (inhibition of reaction 9 by the presence of hydrogen) is preferred. From very recent trials performed on gaseous mixtures containing HCN and water vapor, this "inhibition" seems to be the reverse reaction of (9). This reverse reaction is very sensitive to the H_2O concentration and therefore, in turn, to the presence of hydrogen. This may be either molecular hydrogen or bound hydrogen atoms (see Part III of this volume).

3.2.4.2.5 Argon + NO + CO on Porcheville Soot (Case K.5)

These trials are illustrated by the results given in Figures 119, 120, and 121 for initial $(CO)_i = 2.1$ percent, and $(NO)_i$ being equal to 110, 1325, and 7150 ppm, respectively. Figure 122 demonstrates data for which $(CO)_i = 9.8$ percent and $(NO)_i = 1350$ ppm.

Specific features of these trials are as follows:

- Nitric oxide begins to decrease at even lower temperatures than in the absence of CO (e.g. compare Figures 121 and 114, or Figures 119 and 113).
- Ammonia is observed as an intermediate species which increases when $(NO)_i$ increases (compare Figures 119, 120, and 121), and when $(CO)_i$ increases (compare figures 121 and 122).
- During the decrease of nitric oxide, the increase in CO_2 is roughly balanced by the decrease of CO and NO and the decrease of CO and NO are almost equal:

$$2\left(CO_2\right)_f = (CO)_i - (CO)_f + (NO)_i - (NO)_f \qquad (191)$$

$$(CO)_i - (CO)_f = (NO)_f - (NO)_f \qquad (192)$$

As already stated for the case K.4 (see section 3.2.3.2.5), the increase of ammonia concentration with increasing initial CO concentration may be explained in two different ways. The explanation which includes reaction

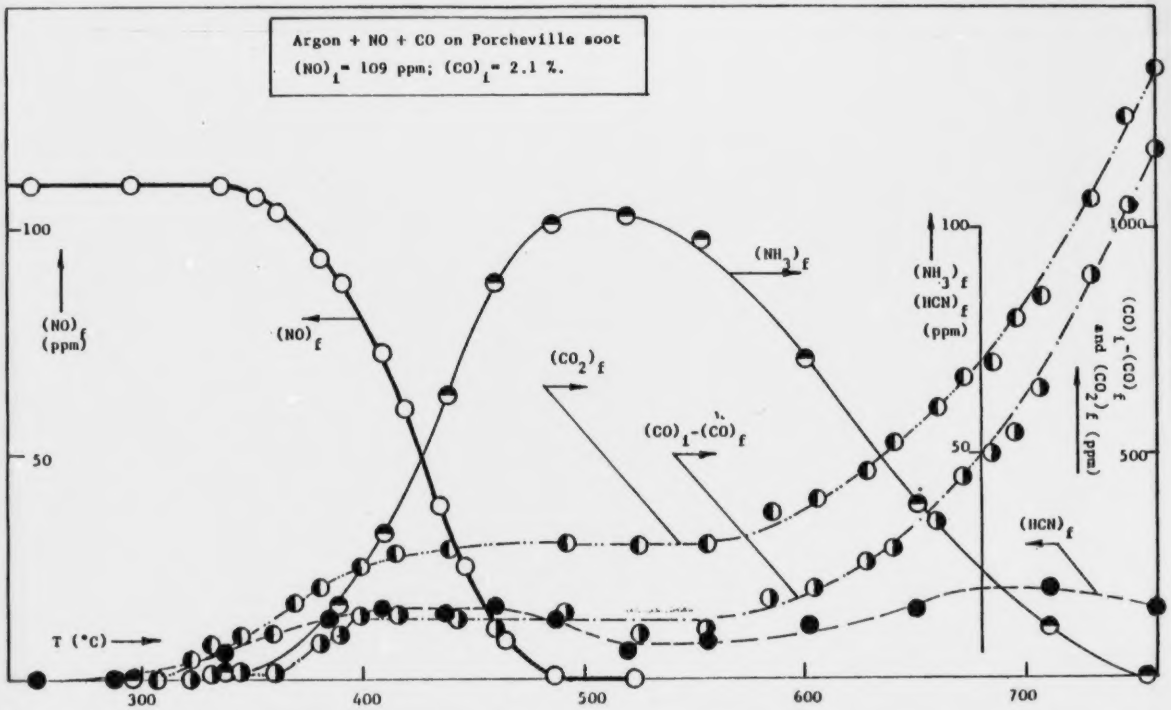

Figure 119. Argon + NO + VO on Porcheville Soot: D = 14.5 cm^3s^{-1}; $(NO)_i$ = 109 ppm; $(CO)_i$ = 2.10%.

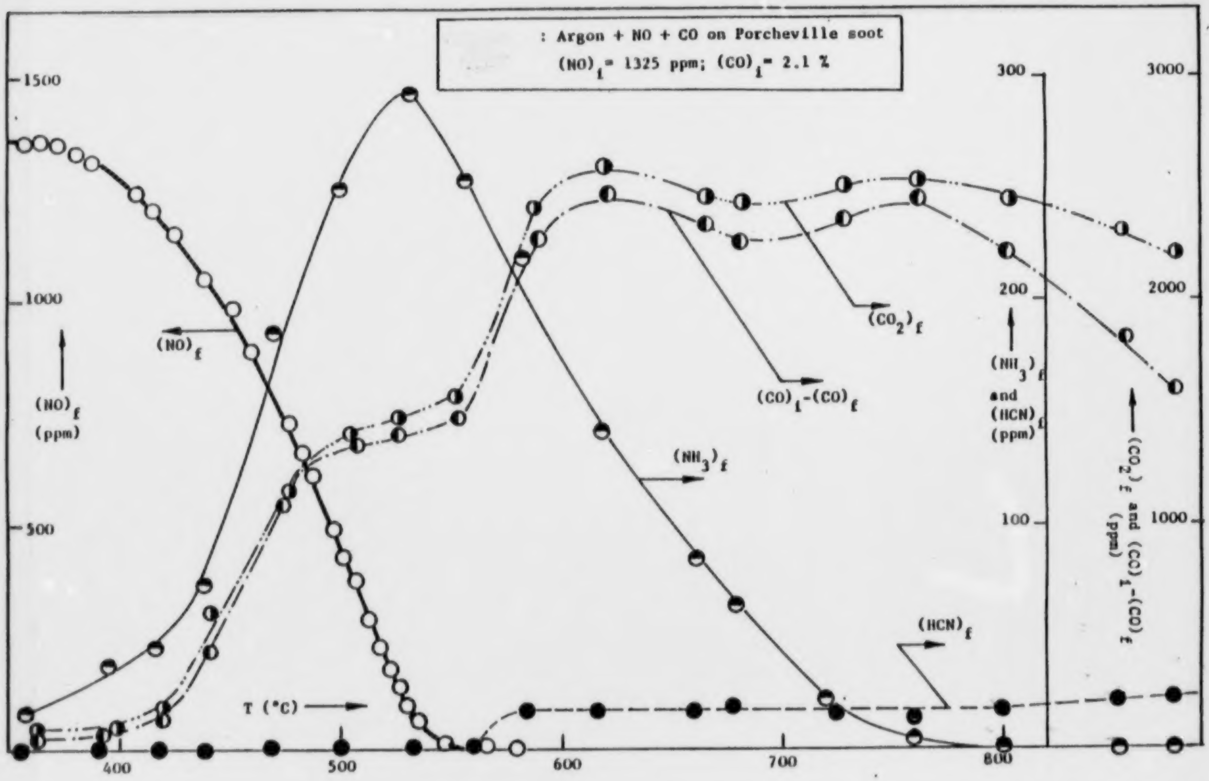

Figure 120. Argon + NO + CO on Porcheville Soot: D = 14.5 cm^3s^{-1}; $(NO)_i$ = 1325 ppm; $(CO)_i$ = 2.10%.

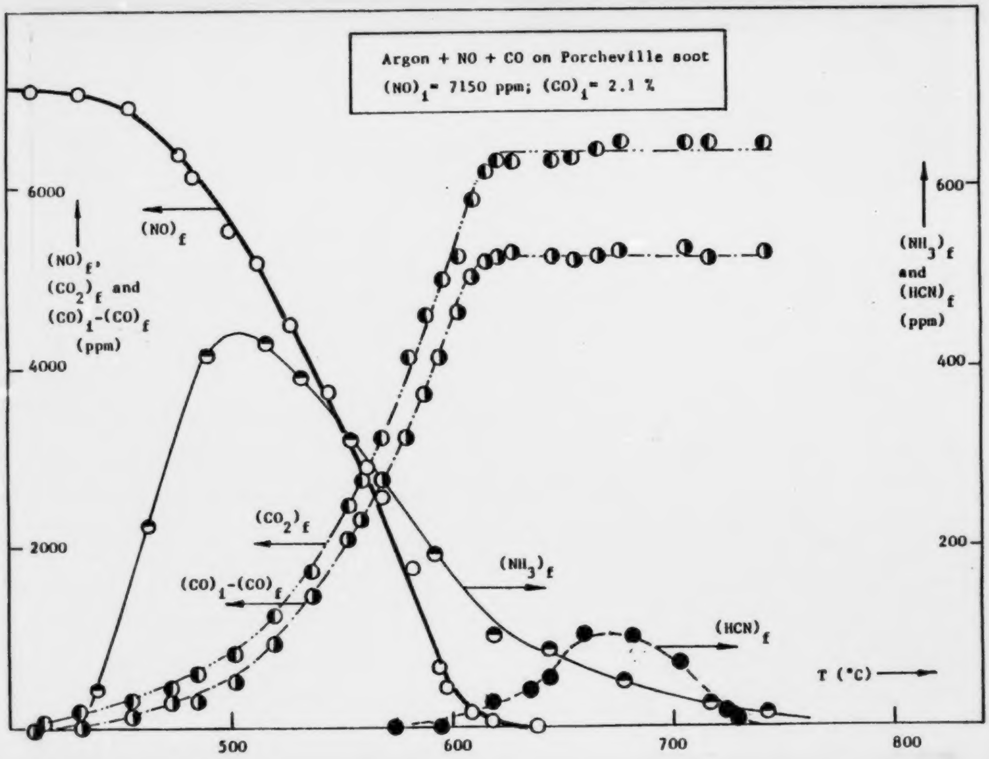

Figure 121. Argon + NO + CO on Porcheville Soot; D = 14.5 cm^3s^{-1}; $(NO)_i$ = 7150 ppm; $(CO)_i$ = 2.10%.

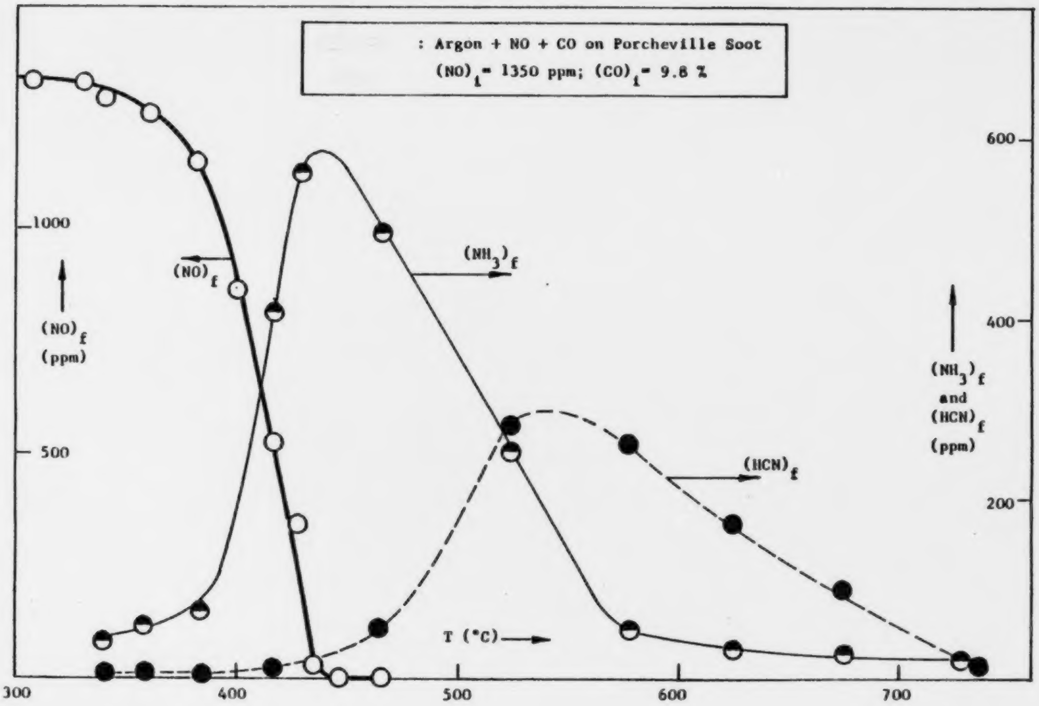

Figure 122. Argon + NO + CO on Porcheville Soot: D = 14.5 cm^3s^{-1}; $(NO)_i$ = 1350 ppm; $(CO)_i$ = 9.80%.

path (6) is supported in the present trials, since V_6 was found to have a finite value.

The variation of the nitrogen-containing species as a function of time is given by equations (134) through (138), presented previously for case K.4.

The rate V_8 has been obtained from eq. (138) by substituting for V_1, V_4, and V_{13} with values calculated from eqs. (186), (188), and (175), respectively, and by taking the stoichiometric coefficient of reaction (4) equal to one:

$$\boxed{V_8 = 2.1 \times 10^{10} \exp\left[-14800(\pm 2500)/T\right] X_{NO}\ X_{CO}^{0.7}} \qquad (193)$$

After the values of V_1, V_2, V_8, and V_4, calculated respectively from eqs. (186), (185), (193), and (188), have been substituted into eq. (134), a finite value of V_6 is obtained, the expression of which is given by:

$$\boxed{V_6 = 2.7 \times 10^{9} \exp\left[-17100(\pm 2000)/T\right] X_{NO}^{0.1}\ X_{CO}} \qquad (194)$$

The very low partial reaction order with respect to nitric oxide is surprising and somewhat suspect. Mass balances (191) and (192) suggest that CO_2 is a reaction product of reaction (6).

The overall nitric oxide disappearance rate $\overline{V_{K.5}}$ as obtained from -d(NO)/dt and is given by:

$$\boxed{\overline{V_{K.5}} = 8.4 \times 10^{6} \exp\left[-10600(\pm 800)/T\right] X_{NO}^{0.5}\ X_{CO}} \qquad (195)$$

3.2.4.2.6 Argon + NO + H_2 on Porcheville Soot (Case 0.5)

Examples of these trials are shown in Figures 123 and 124 (for which $(H_2)_i$ = 1.6 percent, $(NO)_i$ equal to 1290 and 7400 ppm, respectively) and in Figures 125 and 126 for which $(H_2)_i$ = 5.5 percent, $(NO)_i$ equal to 129 and 1290 ppm, respectively. Characteristics of these trials are as follows:

F 123
124
125
126

- The temperature ranges for NO disappearance are comparable to

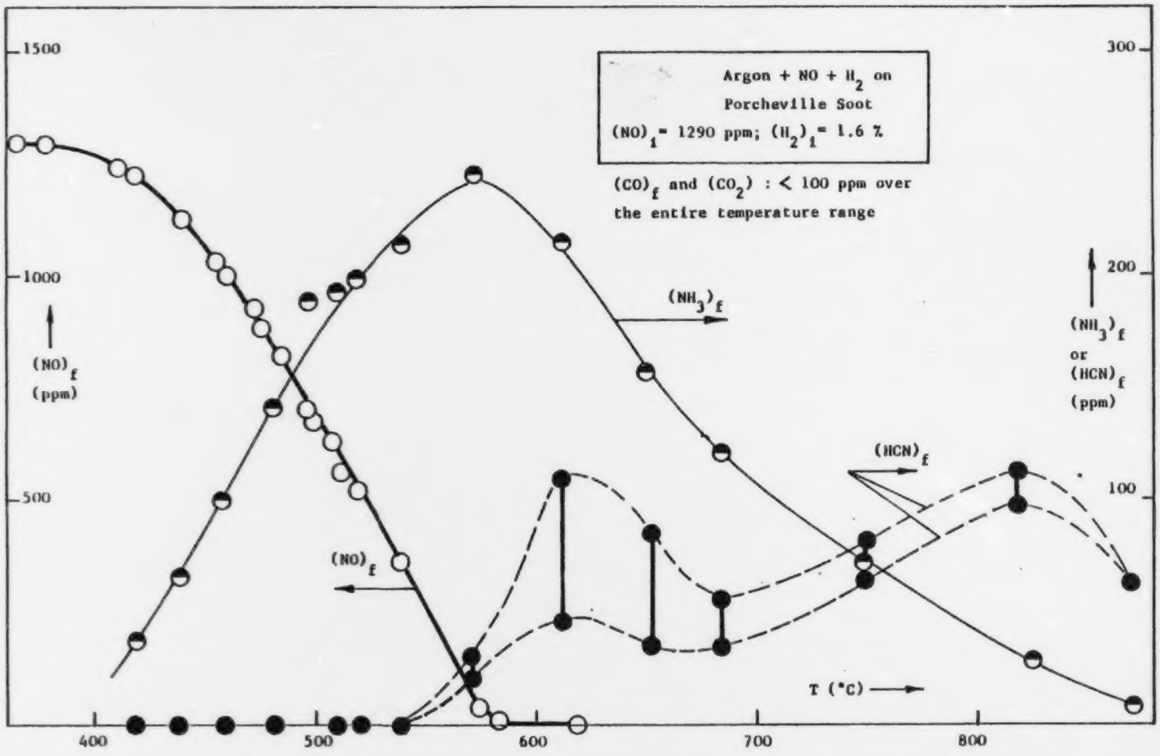

Figure 123. Argon + NO + Hydrogen on Porcheville Soot: D = 14.5 cm^{3}s^{-1}; $(NO)_i$ = 1290 ppm $(H_2)_i$ = 1.60%.

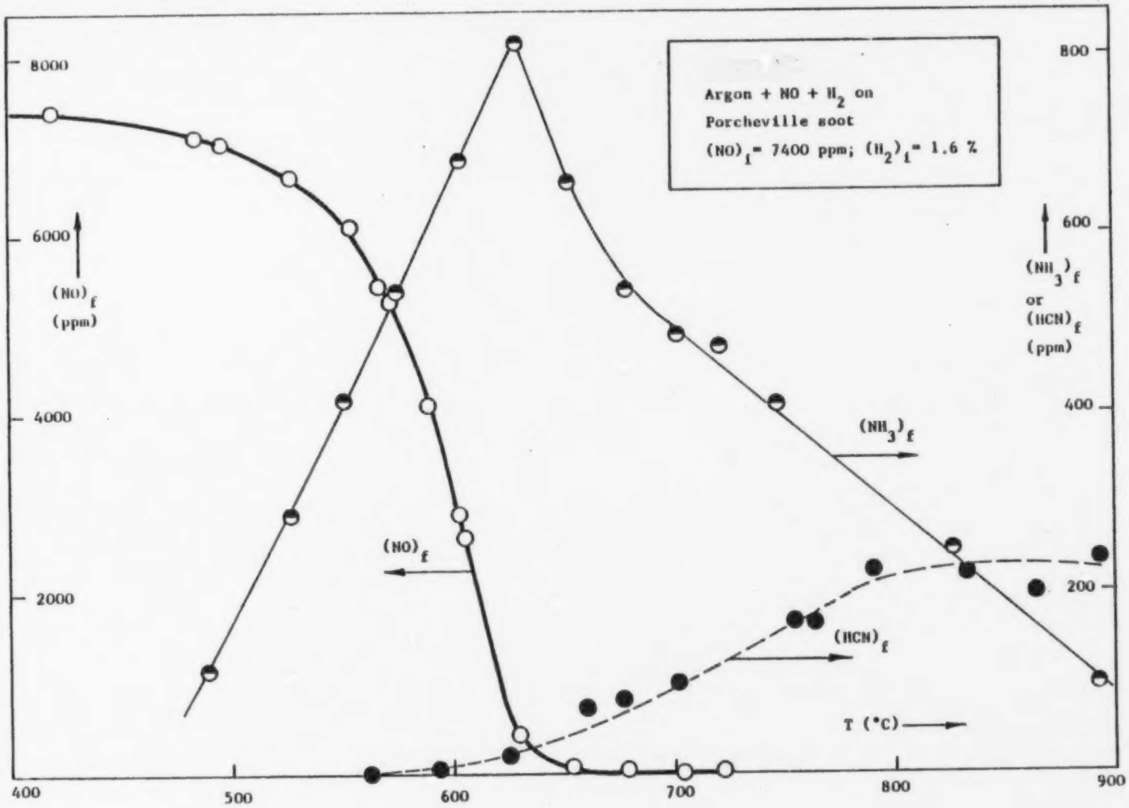

Figure 124. Argon + NO + Hydrogen on Porcheville Soot: $D = 14.5\ cm^3s^{-1}$; $(NO)_i = 7400$ ppm; $(H_2)_i = 1.60\%$.

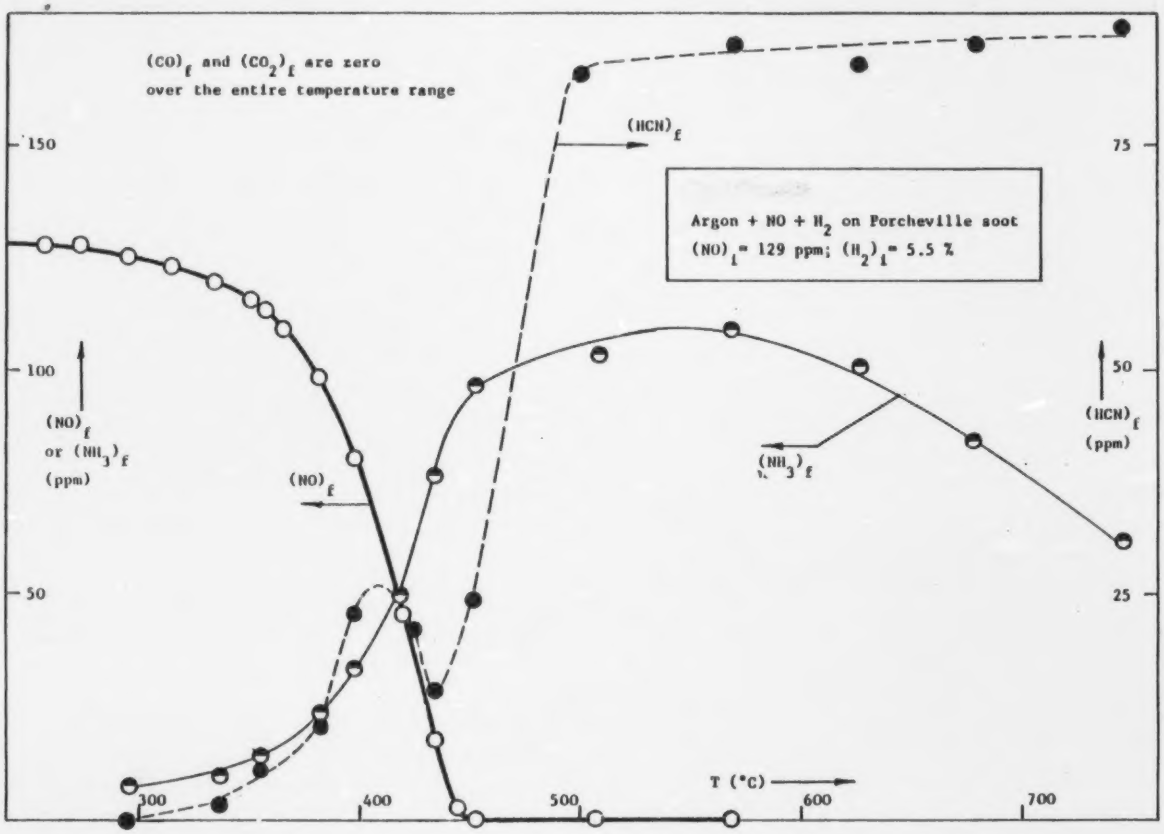

Figure 125. Argon + NO + Hydrogen on Porcheville Soot: D = 14.5 cm^3s^{-1}; $(NO)_i$ = 129 ppm; $(H_2)_i$ = 5.50%.

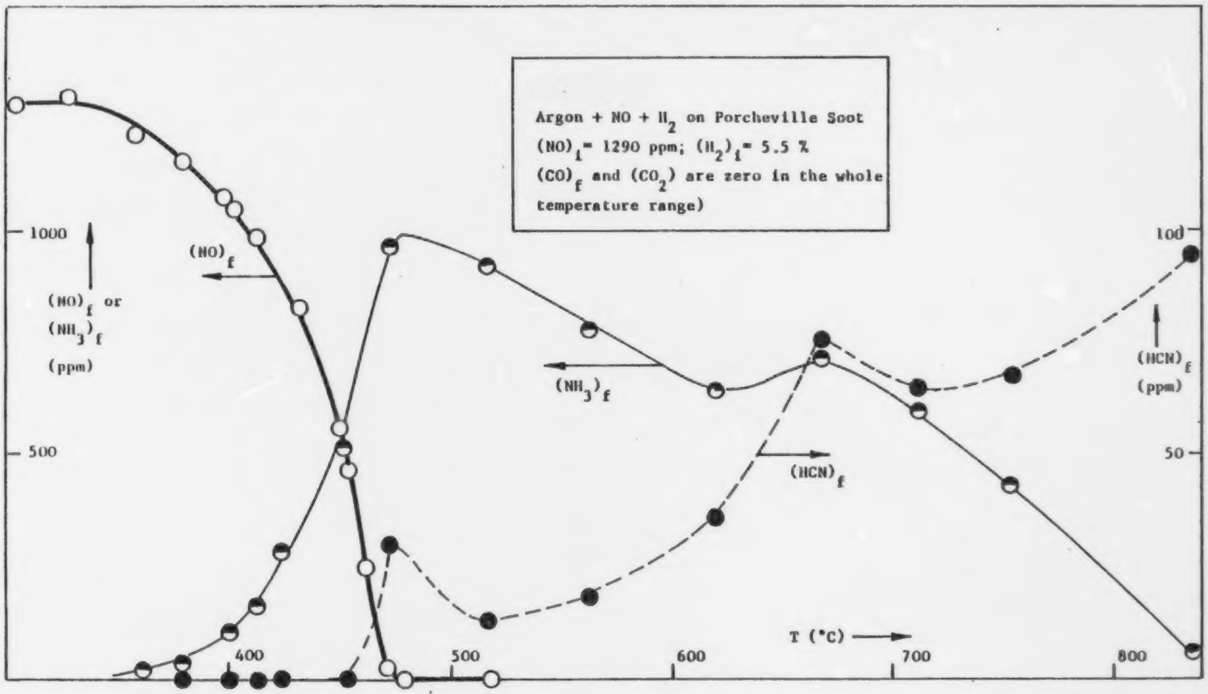

Figure 126. Argon + NO + Hydrogen on Porcheville Soot: D = 14.5 cm^3s^{-1}; $(NO)_i$ = 1290 ppm; $(H_2)_i$ = 5.50%.

those observed when CO is added to the initial gas (case K.5).

- Very high amounts of ammonia are formed during the decrease of nitric oxide. The peak values of NH_3 increase with increasing $(NO)_i$ and with increasing $(H_2)_i$. At sufficiently high initial hydrogen concentrations, these peak values are of the same order as the initial NO concentration (see e.g. Figures 125 and 126).
- Only small quantities of CO or CO_2 are released over the whole temperature range studied. Actually, these amounts are of the same order as those released during a thermal treatment of the soot in the presence of hydrogen (see section 3.2.4.1.4). From this it may be concluded that hardly any CO or CO_2 is formed during NO reduction in the presence of gaseous hydrogen.
- Hydrogen cyanide is released during the decrease of ammonia, at temperatures where NO has almost dropped to zero. HCN formation is primarily accounted for by thermal soot decomposition and by reaction (5). Reaction (9) is not operational as described in section 3.2.4.2.4 .

The foregoing observations are consistent with the existence of primary reactions V_1, V_2, and with a dominant role being played by V_{11} and V_{14}. Reactions (21) and (22) may be neglected, since ammonia and hydrogen cyanide formed by them are negligible (see e.g. Figure 111). Including known secondary reactions (4), (5), and (13), the variation of the nitrogen-containing species, as a function of time, is given by equations (141) through (144) and by equations (145) and (147).

The rate expression V_{14} has been calculated from equation (145), after the rates V_1, V_4, and V_{13} have been substituted for using eqs. (186), (188), and (175), respectively:

$$\boxed{V_{14} = 1.9 \times 10^7 \exp\left[-10800(\pm 800)/T\right] X_{NO}^{0.8} X_{H_2}^{0.7}} \qquad (196)$$

The rate expression V_{11} is obtained from equation (147) by substituting values for rates V_1, V_2, V_{13}, and V_{14} calculated from eqs. (186), (185), (175), and (196):

$$\boxed{V_{11} = 2.0 \times 10^9 \exp\left[-15300(\pm 1000)/T\right] X_{NO}^{0.5} \quad X_{H_2}^{1.5}} \qquad (197)$$

The overall nitric oxide disappearance rate $\overline{V_{0.5}}$, as obtained from the expression -d(NO)/dt (eq. 141), is given by:

$$\boxed{\overline{V_{0.5}} = 5.0 \times 10^8 \exp\left[-14300(\pm 1500)/T\right] X_{NO}^{0.5} \quad X_{H_2}} \qquad (198)$$

3.2.4.3 Effects of Molecular Oxygen on NO Reduction

In the case of Porcheville soot, the effect of molecular oxygen has been studied only in the case where neither H_2 nor CO are present in the initial gas flow. Trials are restricted to the case of argon + NO + O_2 on Porcheville soot (case T.5).

Three typical trials, corresponding to three different oxygen concentrations, are shown in Figure 127. It is clear from this figure that oxygen has a pronounced inhibiting effect on the heterogeneous reduction of nitric oxide on this soot. The effect observed is not due to the progressive consumption of soot (M) as the temperature increases. Consumption is, of course, faster when the initial oxygen concentration is increased. Indeed, the values of the overall NO disappearance rate $\overline{V_{T.5}}$, calculated from eq. (5) which take into account the instantaneous value of M, clearly decrease when the initial oxygen concentration is increased (see Figure 128).

This inhibiting effect, as covered in the discussion of the analogous trials performed on ethylene soot (see section 3.2.3.3.2), is related to the fact that the oxidation of the heavy fuel oil soot preferentially yields carbon dioxide instead of carbon monoxide, as was the case with the ethylene soot.

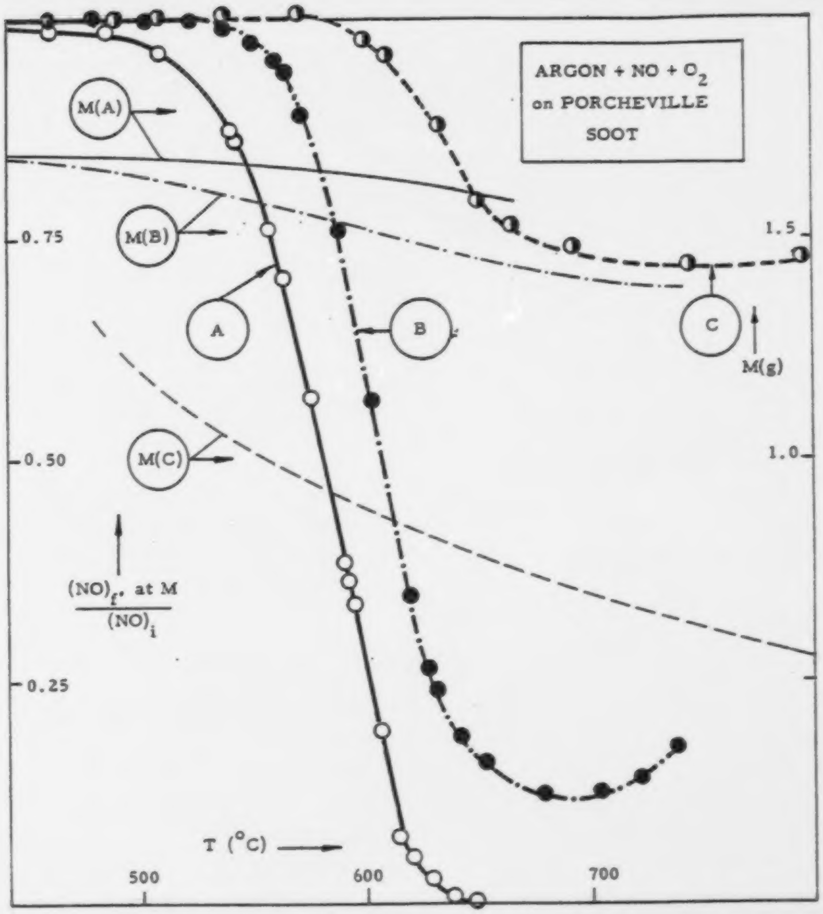

Figure 127. Argon + NO + O_2 on Porcheville Soot: D = 14.5 cm^3s^{-1}; $(NO)_i$ = 1310 ppm; Curve A: $(O_2)_i$ = 0.06%; Curve B: $(O_2)_i$ = 0.82%; Curve C: $(O_2)_i$ = 5.08%.

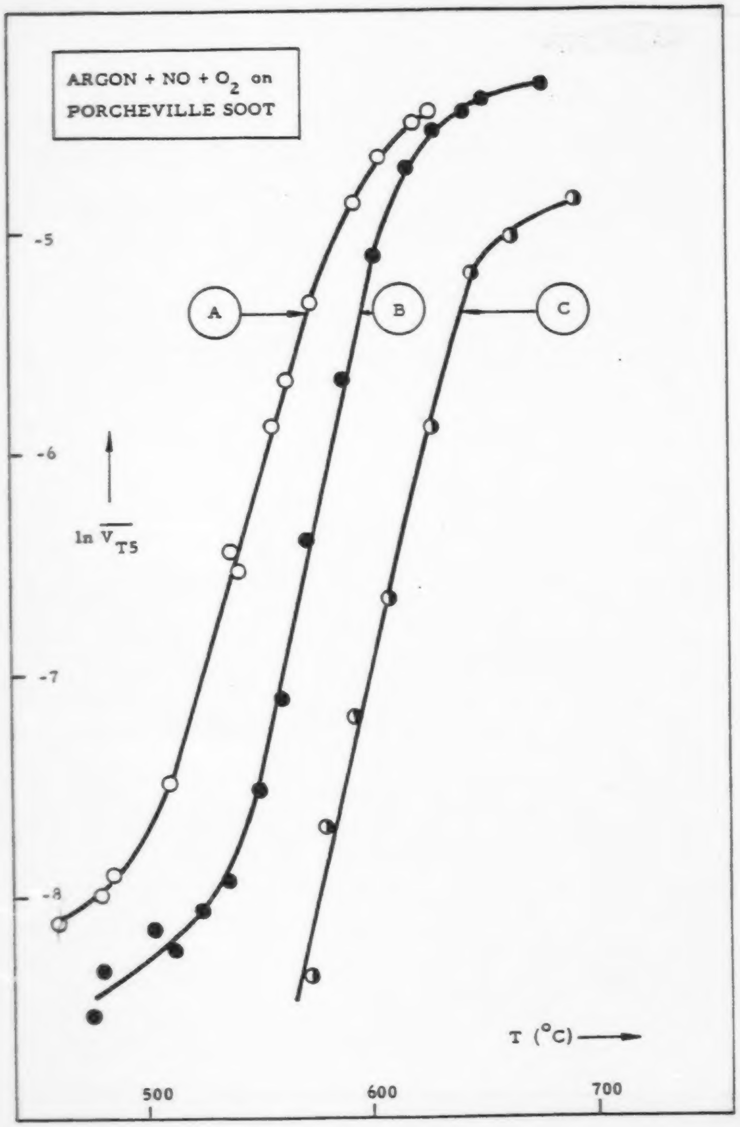

Figure 128. Argon + NO + O_2 on Porcheville Soot; Variation of the Overall NO Removal Rate V_{T5}, Calculated from eq.(5), as a Function of Temperature, for Three Different Initial Oxygen Concentrations; Curve A: $(O_2)_i$ = 0.06%; Curve B: $(O_2)_i$ = 0.82%; Curve C: $(O_2)_i$ = 5.04%. $(NO)_i$ = 1310 ppm.

The inhibiting effect of oxygen also depends on temperature, as shown in the following expression of the overall NO disappearance rate, calculated according to equation (5):

$$\boxed{\overline{V_{T.5}} = \frac{6.6 \times 10^{8} \exp\left[-18600(\pm 2500)/T\right] X_{NO}^{0.5}}{1 + 4(\pm 3)\, 10^{5} \exp\left[-10300(\pm 2000)/T\right] X_{O_2}}} \qquad (199)$$

When comparing this expression with the one derived in the absence of oxygen $\left(\text{see equation 187 giving the overall rate } \overline{V_{F.5}}\right)$, it is found that:

$$\boxed{\overline{V_{T.5}} = \overline{V_{F.5}} \,/\, \left[1 + 4(+3)\, 10^{5} \exp\left[-10300(\pm 2000)/T\right] X_{O_2}\right]} \qquad (200)$$

4.0 GENERAL CONCLUSIONS

To facilitate the presentation of these general conclusions, two summarizing tables are included at the end of the report: Table 3, giving the overall rate expressions of NO reduction determined in this report, and Table 4, giving the overall NO disappearance rates, as a function of gas composition and nature of solid particle.

4.1 Direct Reduction of NO

Except in cases where noble metals, typical metal or metal oxide catalysts are present in the solid particles, the direct transformation of NO into molecular nitrogen in the absence of any reducing agent, is a relatively slow reaction. At temperatures below one thousand degrees centigrade it was impossible to measure any reduction of nitric oxide under the experimental conditions of this study, either alumina or quartz (see section 3.2.1.2.1).

In the presence of reducing agents, the direct transformation of nitric oxide into molecular nitrogen is significantly enhanced. The following chemical species have been shown to act as a reducing agent in the direct reduction of NO into N_2:

- Solid bound carbon atoms are able to reduce NO by a solid/gas heterogeneous reaction path (reaction 1) as shown in the following trials:

  Argon + NO on graphite (see section 3.2.2.1).

  Argon + NO on gas-phase-generated soot (section 3.2.3.2.2).

  Argon + NO on liquid-phase-generated cenospheric soot (section 3.2.4.2.2).

  Reaction 1 is always characterized by a strong temperature dependence, resulting in an overall activation temperature between 22,000 and 34,000^{o}K.

- Carbon monoxide is able to reduce NO by a gas/gas heterogeneous reaction path (reaction 8) as shown in the trials:

  Argon + NO + CO on alumina (section 3.2.1.2.3).

Table 3. Overall Rates of Heterogeneous NO Reduction $\left(cm^3\ g^{-1}\ s^{-1}\right)$

GAS COMPOSITION	OVERALL REACTION	SOLID PARTICLES	
		ALUMINA (-O bound atoms)	GRAPHITE (-C bound atoms)
Ar + NO	$NO + a\ (-C) \xrightarrow{1} 0.5\ N_2 + (2a - 1)\ CO$ $+ (1 - a)\ CO_2$		$V_1 = -d\ (NO)/dt =$ $1.9\ 10^{11}\ \exp\ (-29000/T)\ X_{NO}$
	$NO + a\ (-C) + b\ (-H) \xrightarrow{2} NH_3 + \frac{b-3}{2}\ H_2O$ $+ (\frac{b-5}{2} + 2a)\ CO + (\frac{5-b}{2} - a)\ CO_2$		
Ar + NH_3	$NH_3 \xrightarrow{13} 0.5\ N_2 + 1.5\ H_2$	$V_{13} = -d\ (NH_3)/dt =$ $3\ 10^8\ \exp\ (-18600/T)\ X_{NH_3}$	$V_{13} = -d\ (NH_3)/dt =$ $1\ 10^8\ \exp\ (-\ 18800/T)\ X_{NH_3}$
	$NH_3 + (-C) \xrightarrow{5} HCN + H_2$		
Ar + NO + NH_3	$NO + nNH_3 \xrightarrow{4} \frac{1+n}{2}\ N_2 + H_2O$ $+ (\frac{3n-2}{2})\ H_2$	$V_4 = -d\ (NO)/dt =$ $5.1\ 10^9\ \exp\ (-15000/T)\ X_{NO}\ X_{NH_3}$	$V_4 = -d\ (NO)/dt =$ $1.5\ 10^{10}\ \exp\ (-14600/T)\ X_{NO}\ X_{NH_3}$
Ar + NO + CO	$NO + CO \xrightarrow{8} 0.5\ N_2 + CO_2$	$V_8 = -d\ (NO)/dt =$ $6\ 10^8\ \exp\ (-15800/T)\ X_{NO}\ X_{CO}^{0.3}$	$V_8 = -d\ (NO)/dt =$ $10^5\ \exp\ (-10100/T)\ X_{NO}\ X_{CO}$

Table 3. Overall Rates of Heterogeneous NO Reduction $\left(cm^3\ g^{-1}\ s^{-1}\right)$ (Continued)

GAS COMPOSITION	OVERALL REACTION	SOLID PARTICLES	
		SOOT from C_2H_4	SOOT from HEAVY FUEL OIL (Thermal Plant of Porcheville, France)
Ar + NO	$NO + a\ (-C) \xrightarrow{1} 0.5\ N_2 + (2a - 1)\ CO + (1 - a)\ CO_2$	$V_1 = -d\ (NO)/dt =$ $1.3\ 10^{10}\ \exp\ (-22550/T)\ X_{NO}^{0.75}$	$V_1 = -d\ (NO)/dt =$ $9.8\ 10^{16}\ \exp\ (-\ 33500/T)\ X_{NO}^{0.63}$
	$NO + a\ (-C) + b\ (-H) \xrightarrow{2} NH_3 + \frac{b-3}{2}\ H_2O + (\frac{b-5}{2} + 2a)\ CO + (\frac{5-b}{2} - a)\ CO_2$	$V_2 = -d\ (NO)/dt =$ $1.9\ 10^{6}\ \exp\ (-14300\ /T)\ X_{NO}^{0.7}$	$V_2 = -d\ (NO)/dt =$ $2.1\ 10^{6}\ \exp\ (-16000/T)\ X_{NO}^{0.35}$
Ar + NH_3	$NH_3 \xrightarrow{13} 0.5\ N_2 + 1.5\ H_2$	$V_{13} = -d\ (NH_3)/dt =$ $5.3\ 10^{8}\ \exp\ (-18600/T)\ X_{NH_3}$	$V_{13} = -d\ (NH_3)/dt =$ $5.3\ 10^{9}\ \exp\ (-19800/T)\ X_{NH_3}$
	$NH_3 + (-C) \xrightarrow{5} HCN + H_2$	$V_5 = -d\ (NH_3)/dt =$ $6\ 10^{6}\ \exp\ (-16600/T)\ X_{NH_3}$	$V_5 = -d\ (NH_3)/dt =$ $7.3\ 10^{7}\ \exp\ (-16600/T)\ X_{NH_3}$
Ar + NO + NH_3	$NO + nNH_3 \xrightarrow{4} \frac{1+n}{2}\ N_2 + H_2O + (3n - 2)\ H_2$	$V_4 = -d\ (NO)/dt =$ $6\ 10^{8}\ \exp\ (-11500/T)\ X_{NO}\ X_{NH_3}$	$V_4 = -d\ (NO)/dt =$ $3\ 10^{10}\ \exp\ (-15300/T)\ X_{NO}\ X_{NH_3}$
Ar + NO + CO	$NO + CO \xrightarrow{8} 0.5\ N_2 + CO_2$	$V_8 = -d\ (NO)/dt =$ $1.7\ 10^{8}\ \exp\ (-12400/T)\ X_{NO}\ X_{CO}$	$V_8 = -d\ (NO)/dt =$ $2.1\ 10^{10}\ \exp\ (-14800/T)\ X_{NO}\ X_{CO}^{0.7}$

Table 3. Overall Rates of Heterogeneous NO Reduction $\left(cm^3\ g^{-1}\ s^{-1}\right)$ (Continued)

GAS COMPOSITION	OVERALL REACTION	SOLID PARTICLES	
		ALUMINA (-O bound atoms)	GRAPHITE (-C bound atoms)
Ar + NO + CO	$NO + CO + 3\ (-H) \xrightarrow{6} NH_3 + CO_2$		
Ar + NH_3 + CO	$NH_3 + CO \xrightarrow{9} HCN + H_2O$	$V_9 = -d\ (NH_3)/dt =$ $1.3\ 10^7\ \exp\ (-13800/T)\ X_{NH_3}^{0.75}\ X_{CO}$	
Ar + NO + H_2	$NO + H_2 \xrightarrow{14} 0.5\ N_2 + H_2O$	$V_{14} = -d\ (NO)/dt =$ $6.4\ 10^7\ \exp\ (-13500/T)\ X_{NO}\ X_{H_2}$	$V_{14} = -d\ (NO)/dt =$ $2.3\ 10^9\ \exp\ (-14000/T)\ X_{NO}\ X_{H_2}$
	$NO + 2.5\ H_2 \xrightarrow{11} NH_3 + H_2O$	$V_{11} = -d\ (NO)/dt =$ $3.5\ 10^3\ \exp\ (-8200/T)\ X_{NO}^{0.5}\ X_{H_2}$	$V_{11} = -d\ (NO)/dt =$ $7.1\ 10^6\ \exp\ (-13800/T)\ X_{NO}^{0.5}\ X_{H_2}$
Ar + NH_3 + O_2	$NH_3 + 0.75\ O_2 \xrightarrow{16} 0.5\ N_2 + 1.5\ H_2O$	$V_{16} = -d\ (NH_3)/dt =$ $2.2\ 10^6\ \exp\ (-13000/T)\ X_{NH_3}^{0.5} X_{O_2}^{0.5}$	
	$NH_3 + 1.25\ O_2 \xrightarrow{17} NO + 1.5\ H_2O$	$V_{17} = -d\ (NH_3)/dt =$ $1\ 10^5\ \exp\ (-12200/T)\ X_{NH_3}^{0.6}\ X_{O_2}^{0.3}$	

Table 3. Overall Rates of Heterogeneous NO Reduction $\left(cm^3\ g^{-1}\ s^{-1}\right)$ (Concluded)

GAS COMPOSITION	OVERALL REACTION	SOLID PARTICLES	
		SOOT from C_2H_4	SOOT from HEAVY FUEL OIL (Thermal Plant of Porcheville, France)
Ar + NO + CO	$NO + CO + 3\,(-H) \xrightarrow{6} NH_3 + CO_2$		$V_6 = -d\,(NO)/dt =$ $2.7\ 10^9\ \exp\,(-17100/T)\ X_{NO}^{0.1}\ X_{CO}$
Ar + NH_3 + CO	$NH_3 + CO \xrightarrow{9} HCN + H_2O$		
Ar + NO + H_2	$NO + H_2 \xrightarrow{14} 0.5\ N_2 + H_2O$	$V_{14} = -d\,(NO)/dt =$ $6.8\ 10^8\ \exp\,(-13260/T)\ X_{NO}\ X_{H_2}$	$V_{14} = -d\,(NO)/dt =$ $1.9\ 10^7\ \exp\,(-10800/T)\ X_{NO}^{0.8}\ X_{H_2}^{0.7}$
	$NO + 2.5\ H_2 \xrightarrow{11} NH_3 + H_2O$	$V_{11} = -d\,(NO)/dt =$ $1.3\ 10^{10}\ \exp\,(-17100/T)\ X_{NO}^{0.5}\ X_{H_2}$	$V_{11} = -d\,(NO)/dt =$ $2\ 10^9\ \exp\,(-15300/T)\ X_{NO}^{0.5}\ X_{H_2}^{1.5}$
Ar + NH_3 + O_2	$NH_3 + 0.75\ O_2 \xrightarrow{16} 0.5\ N_2 + 1.5\ H_2O$	$V_{16} = -d\,(NH_3)/dt =$ $9.8\ 10^6\ \exp\,(-9900/T)\ X_{NH_3}^{0.83}\ X_{O_2}^{0.33}$	
	$NH_3 + 1.25\ O_2 \xrightarrow{17} NO + 1.5\ H_2O$	$V_{17} = -d\,(NH_3)/dt =$ $2.7\ 10^2\ \exp\,(-6050/T)\ X_{NH_3}^{0.5}\ X_{O_2}^{0.3}$	

Table 4. Overall NO Disappearance Rates $\left[-d\ (NO)/dt,\ cm^3\ g^{-1}\ s^{-1}\right]$ as a Function of Gas Composition and Nature of Solid Particles

GAS COMPOSITION	SOLID PARTICLES	
	ALUMINA	GRAPHITE
Ar + NO		$\overline{V_{F2}} = 1.9\ 10^{11}\ \exp\ (-29200/T)\ X_{NO}$
Ar + NO + CO	$\overline{V_{K1}} = 6.8\ 10^{8}\ \exp\ (-15750/T)\ X_{NO}\ X_{CO}^{0.3}$	$\overline{V_{K2}} = 10^{5}\ \exp\ (-10100/T)\ X_{NO}\ X_{CO}$
Ar + NO + H_2	$\overline{V_{01}} = 8.6\ 10^{5}\ \exp\ (-11900/T)\ X_{NO}^{0.5}\ X_{H_2}$	$\overline{V_{02}} = 2.5\ 10^{7}\ \exp\ (-13100/T)\ X_{NO}^{0.5}\ X_{H_2}$
Ar + NO + NH_3	$\overline{V_{R1}} = 3\ 10^{11} \exp(-18200/T)\ X_{NO} X_{NH_3}$	$\overline{V_{R2}} = 1.5\ 10^{10} \exp(-14600/T) X_{NO} X_{NH_3}$
Ar + NO + CO + O_2	$\overline{V_{JKT\ 1}} =$ $6.2\ 10^{8}\ \exp\ (-15600/T)\ X_{NO}\ X_{CO}^{0.3}$ $\times\ (1 + 43\ X_{O_2}^{0.35})$	
Ar + NO + H_2 + O_2	$\overline{V_{N0T\ 1}} =$ $\frac{8.6\ 10^{5}\ \exp\ (-11900/T)}{1+1.1\ 10^{8}\ \exp\ (-6000/T) X_{O_2}^{+2}}\ X_{H_2}\ X_{NO}^{0.5}$	

Table 4. Overall NO Disappearance Rates $\left[-d\,(NO)/dt,\ cm^3\ g^{-1}\ s^{-1}\right]$ as a Function of Gas Composition and Nature of Solid Particles (Concluded)

GAS COMPOSITION	SOLID PARTICLES	
	SOOT from C_2H_4	SOOT from HEAVY FUEL OIL (Thermal Plant of Porcheville, France)
Ar + NO	$\overline{V_{F4}} = 3.4\ 10^7\ \exp\ (-16000/T)\ X_{NO}^{0.75}$	$\overline{V_{F5}} = 6.6\ 10^8\ \exp\ (-18600/T)\ X_{NO}^{0.5}$
Ar + NO + CO	$\overline{V_{K4}} = 3.6\ 10^8\ \exp\ (-14700/T)\ X_{NO}\ X_{CO}^{0.45}$	$\overline{V_{K5}} = 8.4\ 10^6\ \exp\ (-10600/T)\ X_{NO}^{0.5}\ X_{CO}$
Ar + NO + H_2	$\overline{V_{\O 4}} = 1.7\ 10^9\ \exp\ (-13500/T)\ X_{NO}^{0.4}\ X_{H_2}^{2}$	$\overline{V_{\O 5}} = 5\ 10^8\ \exp\ (-14300/T)\ X_{NO}^{0.5}\ X_{H_2}$
Ar + NO + NH_3	$\overline{V_{R4}} = 1.6\ 10^8\ \exp\ (-13700/T)\ X_{NO}^{0.75}\ X_{NH_3}^{0.6}$	$\overline{V_{R5}} = 3.3\ 10^{11}\ \exp\ (-14600/T)\ X_{NO}\ X_{NH_3}$
Ar + NO + O_2	$\overline{V_{T4}} = 3.4\ 10^7\ \exp\ (-16000/T)\ X_{NO}^{0.75}$ $\times\ (1 + 33\ X_{O_2}^{0.25})$	$\overline{V_{T5}} = 6.6\ 10^8\ \exp\ (-18600/T)\ X_{NO}^{0.5}$ $\times \left[1 + 4\ 10^5\ \exp\ (-10300/T)\ X_{O_2}\right]^{-1}$

Argon + NO + CO on graphite (section 3.2.2.2).

Argon + NO + CO on gas-phase-generated soot (section 3.2.3.2.5).

Argon + NO + CO on liquid-phase-generated soot from heavy fuel oil (section 3.2.4.2.5).

- Molecular hydrogen is able to reduce NO directly into N_2 by a gas/gas heterogeneous reaction path (reaction 14), as shown in the trials:

  Argon + NO + H_2 on alumina (section 3.2.1.2.6).

  Argon + NO + H_2 on graphite (section 3.2.2.5).

  Argon + NO + H_2 on gas-phase-generated soot (section 3.2.3.2.6).
  Argon + NO + H_2 on liquid-phase-generated soot from heavy fuel oil (section 3.2.4.2.6).

- It was not possible to identify a direct transformation of NO into N_2 by a solid/gas reaction of the form: $NO + 2\ (-H) \dashrightarrow 0.5\,N_2 + H_2O$.

4.2 Indirect Reduction With Hydrogen

As soon as a hydrogen source becomes available, an indirect transformation of nitric oxide into molecular nitrogen, via the intermediate formation of ammonia is observed. The intermediate formation of ammonia from nitric oxide has been observed with the following hydrogen sources:

- Solid bound hydrogen atoms are able to transform NO into NH_3 by a gas/solid reaction (reaction 2), as shown in the trials:

  Argon + NO on gas-phase-generated soot (section 3.2.3.2.2).

  Argon + NO on liquid-phase-generated soot from heavy fuel oil (section 3.2.4.2.2).

- Molecular hydrogen transforms NO into NH_3 by a gas/gas heterogeneous reaction (reaction 11) as shown in the trials:

  Argon + NO + H_2 on alumina (section 3.2.1.2.6).
  Argon + NO + H_2 on graphite (section 3.2.2.5).

Argon + NO + H_2 on gas-phase-generated soot (section 3.2.3.2).

Argon + NO H_2 on liquid-phase-generated soot from heavy fuel oil (section 3.2.4.2.6).

- Hydrocarbons (see section 3.2.1.2.7: argon + NO + methane on alumina), although it is not clear whether the hydrocarbon itself or its cracking products are acting as a coreactant.

The intermediate formation of ammonia delays the final transformation of nitric oxide into molecular nitrogen due to the fact that the pathway involves a set of secondary reactions. These reactions are responsible for the ultimate transformation of ammonia into N_2. The transformation of ammonia into molecular nitrogen may be realized via one of the following reaction paths:

- Directly, by one of the following heterogeneous gas/gas reactions:
  - Ammonia + ammonia ----- N_2 (reaction 13), as shown by the following trials:

    Argon + NH_3 on alumina (section 3.2.1.2.2).

    Argon + NH_3 on graphite (section 3.2.2.3).

    Argon + NH_3 on gas-phase-generated soot (section 3.2.3.2.1).

    Argon + NH_3 on liquid-phase-generated soot from heavy fuel oil (section 3.2.3.2.1).
  - Ammonia + nitric oxide ----- N_2 (reaction 4), as shown by the following trials:

    Argon + NO + NH_3 on alumina (section 3.2.1.2.5).

    Argon + NO + NH_3 on graphite (section 3.2.2.4)

    Argon + NO + NH_3 on gas-phase-generated soot (section 3.2.3.2.3).

    Argon + NO + NH_3 on liquid-phase-generated soot from heavy fuel oil (section 3.2.4.2.3).

  - The existence of a gas/solid reaction $NH_3 + (-N) \text{---} N_2$ could not be checked.

- Indirectly, passing through the intermediate formation of hydrogen cyanide as long as a carbon source is available. The following carbon sources were able to act as a reactant for the transformation of ammonia into hydrogen cyanide:
  - In all cases, the solid bound carbon atoms, by a solid/gas reaction path (reaction 5), as has been shown in the following trials:

    Argon + NH_3 on graphite (see Figure 63; actually only very small quantities of HCN have been found in that particular case).

    Argon + NH_3 on gas-phase-generated soot (section 3.2.3.2.1).

    Argon + NH_3 on liquid-phase-generated soot from heavy fuel oil (section 3.2.4.2.1).

  - In the absence of H_2O, carbon monoxide may act as a carbon source for the transformation of ammonia into hydrogen cyanide, by a gas/gas heterogeneous reaction (reaction 9) as shown by the trials:

    Argon + CO + NH_3 on alumina (section 3.2.1.2.4).

The intermediate formation of hydrogen cyanide from ammonia delays further the ultimate transformation of nitric oxide into molecular nitrogen due to tertiary reactions. These reactions are responsible for the ultimate transformation of HCN into molecular nitrogen (reactions 10, 15, 27, and 40). These reactions are still under investigation in the present stage of this work.

It should also be kept in mind, that under certain conditions, HCN may be transformed back into ammonia, especially when reacting with either hydrogen molecules or H_2O (presently under investigation).

4.3 Enhancement of Reduction With Gaseous Reducing Species

A further conclusion concerns the question of how far the overall NO removal reaction rate is helped by the presence of gaseous reducing agents, especially hydrogen and carbon monoxide. From results presented in this report:

- As long as the solid particles do not contain bound hydrogen atoms, e.g. in the case of alumina or graphite, the presence of either carbon monoxide or molecular hydrogen causes a very strong increase in the overall NO removal rate. This effect was previously discussed in point4.1 for the case of alumina. In the case of graphite, this can be clearly seen by comparing figures 60 and 65 (concerning the effect of hydrogen addition) and Figures 61 and 62 (concerning the effect of CO addition). The enhancing effect of both hydrogen and carbon monoxide are of the same order as may be seen by comparing Figure 16 (CO addition) with Figure 30 (H_2 addition) in the case of alumina, or by comparing Figure 65 (hydrogen addition) with Figure 62 (CO addition) in the case of graphite.
- When the solid particle already contains bound hydrogen atoms, then the addition of either CO or H_2 (although the reaction mechanism is markedly changed by adding some supplementary reaction paths), does not significantly effect the overall NO removal rate. This can be seen:
    - in the case of soot from ethylene by comparing Figure 75 with Figure 90 (effect of CO addition), or by comparing Figure 75 with Figure 96 (effect of H_2 addition);
    - in the case of Porcheville soot for the effect of CO addition by comparing Figure 113 and Figure 119, or by comparing Figure 114 and Figure 121; and for the effect of H_2 addition by comparing Figure 114 and Figure 124.

4.4 Effects of Molecular Oxygen

A final conclusion concerns the effects of the presence of molecular oxygen on heterogeneous NO reduction. Strongly inhibiting as well as strongly promoting effects have been recorded:

- Inhibition of NO reduction by oxygen has been observed in the following cases:
  - In the presence of hydrogen (see section 3.2.1.3.3), the effect not being limited to the mere oxidation of the reducing agent.
  - In the case where the oxidation of soot by molecular oxygen yields CO_2 or preferentially CO_2 (see trials of Argon + NO + O_2 on Porcheville soot, section 3.2.4.3).
- A promoting effect of oxygen on the NO reduction has been observed:
  - in the presence of CO (see section 3.2.1.3.1); and
  - in relation to the foregoing point, in cases where the oxidation of soot by molecular oxygen yields preferentially CO (see trials of argon + NO + O_2 on ethylene soot, section 3.2.3.3.2).
  - A promoting effect of oxygen is also observed on the secondary reactions transforming the intermediate species, ammonia and HCN, into molecular nitrogen, due to the existence of reaction paths 16 and 38. These are in competition with the respective NO formation paths. In the particular case of ammonia, it has been shown that reaction 16 prevails over the competing reaction 17 even at high oxygen concentrations. For example, see trials:

    Argon + NH_3 + O_2 on alumina (section 3.2.1.3.2).

    Argon + NH_3 + O_2 on gas-phase-generated soot (section 3.2.3.3.1).

5.0 REFERENCES

1. Shelef, M. and Kummer, J. T. Chemical Engineering Progress. Symposium Series 67 (n°115), 1971, 74.

2. Yureva, T. M., Popovskii, V. V., and Boreskov, G. K. Kinetika i Katiliz, 6, 1965, 1041.

3. Winter, E. R. S. Journ Catal., 22, 1971, 158.

4. Shelev, M. and Gandhi, H. S. Platinum Metals Rev., 18, 1974, 2.

5. Kobylinski, T. P. and Taylor, B. W. Journ. Catal., 33, 1974, 376.

6. Klimisch, R. L. and Larson, J. G. "The Catalytic Chemistry of Nitrogen Oxides." Symposium on the Catalytic Chemistry of Nitrogen Oxides. Plenum Press: Warren, Michigan, 1974; New York, 1975.

7. Tucker, J. R. "The Reduction of Nitric Oxide on Activated Carbon at Elevated Temperatures." Ph.D. Thesis, Clemson University, South Carolina, 1972.

8. Sheppard, W. M. "A Kinetic Study of the Reaction of Nitric Oxide and Activated Carbon." Ph.D. Thesis, Clemson University, South Carolina, 1974.

9. Edwards, H. W. AIChE Symposium Series, n° 126, 68, 91, 1972.

10. Cerney, A. and Dobovisek, Z. Fourth International Clean Air Congress, 1977, Proceedings, p. 447.

11. Bedjal, G., Orbach, H. K., and Riesenfeld, F. C. Ind. Eng. Chem. 50, 1958, 1165.

12. Puri, B. R., Singh, D. D., Kumar, P., and Sharma, L. R. Chemistry and Industry, 1958, 1921.

13. Smith, R. N., Swinehart, J., and Lesnini, D. Journ. of Phys. Chem. 63, 1959, 544.

14. De Soete, G. G. Internal Report I.F.P., n° 23309, June 1975.

15. Levenspiel, O. "Chemical Reaction Engineering." New York: John Wiley and Sons Inc., 1962, Ch. 14.

16. Gupta, B. P. "Study of the Catalytic Reaction Between Nitric Oxide and Ammonia." Ph.D. Thesis, University of Cincinnati, Ohio, 1970.

17. Otto, K., Shelef, M., and Kummer, J. T. Journ. Phys. Chem., 76 ,1972, 37.

REFERENCES (Continued)

18. Katzer, J. R. Symposium on the Catalytic Chemistry of Nitrogen Oxides. New York: Plenum Press, 1975. p. 140.

19. De Soete, G. G. Fifteenth Symposium (Internat.) on Combustion. Pittsburgh: The Combustion Institute, 1974. p. 1093.

20. Markvart, M. and Pour, V. Journ. Catal., 7, 1967, 279; IIDEM, Chem. Prum., 19 (1), 1969, 8.

II. Comparative Study of Coal and Char Particles

Prepared by:

G. G. De Soete
Ch. Giorgetti
A. Querad

Institut Francais du Petrole

Prepared for:

Energy and Environmental Research Corporation

TABLE OF CONTENTS

Section Page (II-)

INTRODUCTION 1

1.0 EXPERIMENTAL METHOD 2

1.0 Experimental Apparatus 2
1.2 Treatment of the Results 2
1.3 Characteristics of Coals and Chars 4

1.3.1 Coals 4
1.3.2 Chars (see Table 2) 4

2.0 NITRIC OXIDE REDUCTION ON COALS AND CHARS IN THE ABSENCE OF OXYGEN 13

2.1Direct Experimental Results and Kinetic Implications 14

2.1.1 Trials With Pure Argon 14
2.1.1.1 Trials on Coal Particles 14
2.1.1.2 Trials on Char Particles 24
2.1.2 Trials With Argon + NO 25
2.1.2.1 Trials on Char Particles 25
2.1.2.2 Trials on Coal Particles 46
2.1.3 Trials With Argon + NO + CO 48
2.1.3.1 Trials on Char Particles 48
2.1.3.2 Trials on Coal Particles 66
2.1.4 Trials With Argon + NO + H_2 67
2.1.4.1 Trials on Char Particles 67
2.1.4.2 Trials on Coal Particles 67

2.2 Comparison of NO Removal Rates and N_2 Formation Rates for Different Coals and Chars . . 87

2.2.1 Over NU Removal Rates: Dependence on Nature of Coal or Char and on the Eventual Presence of Gaseous Reducing Agents 87
2.2.1.1 Coal/Char Comparison 87
2.2.1.2 Effects of CO or H_2 Presence 97
2.2.1.3 Effect of Coal Nature 97
2.2.2 Overall N_2 Formation Rates, Compared to Overall NO Removal Rates 98

TABLE OF CONTENTS

Section | Page (II-)

2.3 Comparison of Rate Constants of Overall Nitric Oxide Removal and N_2 Formation From Coals and Chars 104

3.0 NITRIC OXIDE REDUCTION ON COAL AND CHAR IN THE PRESENCE OF OXYGEN 115

3.1 Argon Containing O_2 Fed Over Coal and Char 115

3.1.1 Argon + O_2 on Coal 115
3.1.2 Argon + O_2 on Char 117

3.2 Argon Containing NO and O_2 Fed Over Coal and Char 122

3.2.1 Trials on Char 122
3.2.2 Trials on Coal 127

4.0 CONCLUSIONS 130

4.1 General 130
4.2 Particular Observations 130
4.3 Effects of Oxygen on Overall NO Removal Rate 131

5.0 REFERENCES 132

LIST OF FIGURES

Figure Page (II-)

1 Pocahontas Medium Volatile Coal; Particle Size Distribution 6

2 Cedar Grove High Volatile Coal; Particle Size Distribution 7

3 Pocahontas Low-Volatile, High-Ash Coal; Particle Size Distribution . 8

4 Prosper Ruhr Coal; Particle Size Distribution 9

5 Particle Size Distribution (Pennsylvania Anthracite, Beulah Lignite, and Utah Bituminous Coal) 10

6 Argon Pure on Pocahontas Medium Volatile (Coal and Char): Coal Trial, $M_0 = 1.49$ g, $D =-12.2$ cm^{3}s^{-1}; Char Trial, $M_0 = 1.32$ g, $D = 12.2$ cm^{3}s^{-1} 16

7 Argon Pure on Cedar Grove (Coal and Char): Coal Trial, $M_0 = 1.48$ g, $D = 12.2$ cm^{3}s^{-1}; Char Trial, $M_0 = 1.6$ g, $D = 12.2$ cm^{3}s^{-1} 17

8 Argon Pure on Pocahontas Low-Volatile, High-Ash (Coal and Char): Coal Trial, $M_0 = 1.55$ g, $D = 12.2$cm^{3}s^{-1}; Char Trial, $M_0 = 1.6$ g, $D = 12.2$ cm^{3}s^{-1}. 18

9 Argon Pure on South African "Rietspruit" (Coal and Char): Particle size, 50 to 100 microns; Coal Trial, $M_0 = 1.45$ g, $D = 12.2$ cm^{3}s^{-1}; Char Trial, $M_0 = 1$ g, Do = 9.4 cm^{3}s^{-1} 19

10 Argon Pure on "Prosper" Ruhr (Coal and Char): Coal Trial, $M_0 = 1$ g, $D = 10.9$ cm^{3}s^{-1}; Char Trial, $M_0 = 1$ g, $D = 0.6$ cm^{3}s^{-1} 20

11 Argon Pure on Pennsylvania Anthracite (Coal and Char): Coal Trial, $M_0 = 1.92$ g, $D = 9.7$ cm^{3}s^{-1}; Char Trial, $M_0 = 1.7$ g; $D = 9.3$ cm^{3}s^{-1} 21

12 Argon Pure on "Beulah" Lignite (Coal and Char): Coal Trial, $M =$ 1.47 g, $D = 9.7$ cm^{3}s^{-1}; Char Trial, $M_0 = 0.8$ g, $D = 9.7$ cm^{3}s^{-1} . . . 22

13 Argon Pure on Utah Bituminous (Coal and Char): $D = 9.7$ cm^{3}s^{-1}; Coal Trial, $M_0 = 1.97$ g; Char Trial, $M_0 = 1.08$ g 23

LIST OF FIGURES (Continued)

Figure — Page (II-)

14 Argon + NO on Pocahontas Medium Volatile Coal: M_o = 1.49 g; D = 12.1 cm^3s^{-1}; $(NO)_i$ = 1590 ppm 26

15 Argon + NO (1580 ppm) on Pocahontas Medium Volatile (Char): M_o = 1.28 g; D = 12.1 cm^3s^{-1} 27

16 Argon + NO on Pocahontas Medium Volatile (Char); M_o = 1.28 g; D = 12.1 cm^3s^{-1}; T = 764°C 28

17 Argon + NO (1740 ppm) on Cedar Grove High Volatile (Coal); M_o = 1.48 g; D = 12.0 cm^3s^{-1} 29

18 Argon + NO (1700 ppm) on Cedar Grove High Volatile (Char); M_o = 1.6 g; D = 12.0 cm^3s^{-1} 30

19 Argon + NO on Cedar Grove High Volatile (Char); D = 12.1 cm^3s^{-1}; M_o = 1.59 g; Effect of Initial NO Concentration 31

20 Argon + NO (1620 ppm) on Pocahontas Low Volatile, High Ash (Coal); M_o = 1.55 g; D = 12.0 cm^3s^{-1} 32

21 Argon + NO (1690 ppm) on Pocahontas Low Volatile, High Ash (Char); M_o = 1.6 g; D = 12.0 cm^3s^{-1} 33

22 Argon + NO on Pocahontas Low Volatile, High Ash (Char); Effect of Initial NO Concentration; M_o = 1.54 g; D = 12.1 cm^3s^{-1} 34

23 Argon + NO (1740 ppm) on South African "Rietspruit" (Coal); M_o 1.45 g; D = 12.0 cm^3s^{-1}; (50 to 100 microns) 35

24 Argon + NO (1770 ppm) on South African "Rietspruit" (Char); N_o = 1.6 g; D = 11.5 cm^3s^{-1}; (50 to 100 microns) 36

25 Argon + NO (1770 ppm) on Ruhr Coal "Prosper" (Coal); M_o = 1 g; D = 12.0 cm^3s^{-1} 37

26 Argon + NO (1800 ppm) on "Prosper" Ruhr (Char); M_o = 1.6 g; D = 11.5 cm^3s^{-1} 38

27 Argon + NO (1810 ppm) on Pennsylvania Anthracite (Coal); M_o = 1.92 g; D = 11.5 cm^3s^{-1} 39

LIST OF FIGURES (Continued)

Figure Page(II-)

28 Argon + NO (1800 ppm) on Pennsylvania Anthracite (Char); M_o 1.7 g; D = 11.5 cm^3s^{-1} 40

29 Argon + NO (1810) on "Beulah" Lignite (Coal); M_o = 1.47 g; D = 11.7 cm^3s^{-1} 41

30 Argon + NO (1790 ppm) on "Beulah" Lignite (Char); M_o = 1.8 g; D = 11.7 cm^3s^{-1} 42

31 Argon + NO (1820 ppm) on Utah Bituminous (Coal); M_o = 1.97 g; D = 11.3 cm^3s^{-1} 43

32 Argon + NO (1830 ppm) on Utah Bituminous (Char); M_o = 1.08 g; D = 11.3 cm^3s^{-1} 44

33 Argon + NO (3000 ppm) + CO (0.32%) on Pocahontas Medium Volatile (Coal); M_o = 1.49 g; D = 10.8 cm^3s^{-1} . . . 49

34 Argon + NO (2880 ppm) + CO (0.32%) on Pocahontas Medium Volatile (Char); M_o = 1.6 g; D = 10.8 cm^3s^{-1} . . . 50

35 Argon + NO (3000 ppm) + CO (0.80%) on Pocahontas Medium Volatile (Char); M_o = 1.6 g; D = 10.4 cm^3s^{-1} . . . 51

36 Argon + NO (3150 ppm) + CO (1.45%) on Pocahontas Medium Volatile (Char); M_o = 1.6 g; D = 10.4 cm^3s^{-1} . . . 52

37 Argon + NO (6700 ppm) + CO (0.75%) on Pocahontas Medium Volatile (Char); M_o = 1.6 g; D = 10.5 cm^3s^{-1} . . . 53

38 Argon + NO + CO (0.8%) on Pocahontas Medium Volatile (Char): Effect of Initial NO Concentration; M_o = 1.6 g; D = 10.4 cm^3s^{-1} 54

39 Argon + NO (3000 ppm) + CO on Pocahontas Medium Volatile (Char): Effect of Initial CO Concentration . . . 54

40 Argon + NO + CO on Pocahontas Medium Volatile (Char); Relative Importance of (V_8) and V_1 + V_2) in the Heterogeneous Reduction of NO, as a Function of the Initial (CO)/(NO) Ratio; M_o = 1.6 g; D = 10.4 cm^3s^{-1}; T = 700^oC . . 55

41 Argon + NO (3180 ppm) + CO (0.83%) on South African "Rietspruit" (Coal); M_o = 1.45 g; D = 9.7 cm^3s^{-1}; (50/100 μ) 56

LIST OF FIGURES (Continued)

Figure Page (II-)

42 Argon + NO (3200 ppm) + CO (0.83%) on South African "Rietspruit" (Char); M_o = 1.6 g; D = 10.4 cm^3s^{-1} (50/100 μ) 57

43 Argon + NO (3200 ppm) + CO (0.83%) on Ruhr Coal "Prosper" (Coal); M_o = 1 g; D = 9.8 cm^3s^{-1} 58

44 Argon + NO (3200 ppm) + CO (0.83%) on "Prosper" Ruhr (Char); M_o = 1 g; D = 9.8 cm^3s^{-1} 59

45 Argon + NO (3080 ppm) + CO (0.82%) on Pennsylvania Anthracite (Coal); M_o = 1.92 g; D = 9.9 cm^3s^{-1} 60

46 Argon + NO (3200 ppm) + CO (0.84%) on Pennsylvania Anthracite (Char): M_o = 1.7 g; D = 9.9 cm^3s^{-1} 61

47 Argon + NO (3180 ppm) + CO (0.84%) on "Beulah" Lignite (Coal): M_o = 1.47 g; D = 9.8 cm^3s^{-1} 62

48 Argon + NO (3200 ppm) + CO (0.83%) on "Beulah" Lignite (Char): M_o = 0.8 g; D = 9.8 cm^3s^{-1} 63

49 Argon + NO (3200 ppm) + CO (0.83%) on Utah Bituminous (Coal): M_o = 1.97 g; D = 9.8 cm^3s^{-1} 64

50 Argon + NO (3200 ppm) + CO (0.84%) on Utah Bituminous (Char): M_o = 1.08 g; D = 9.8 cm^3s^{-1} 65

51 Argon + NO (2900 ppm) + H_2 (1.52%) on Pocahontas Medium Volatile (Coal): M_o = 1.49 g; D = 11.8 cm^3s^{-1} 68

52 Argon + NO (2950 ppm) + H_2 (1.52%) on Pocahontas Medium Volatile (Char): M_o = 1.1 g; D = 11.8 cm^3s^{-1} 69

53 Argon + NO (2900 ppm) + H_2 on Pocahontas Medium Volatile (Char): Effect of Initial Hydrogen Concentration; M_o = 1.5 g; D = 11.8 cm^3s^{-1} 70

54 Argon + NO + H_2 (1.5%) on Pocahontas Medium Volatile (Char): Effect of Initial NO Concentration; M_o = 1.5 g; D = 11.8 cm^3s^{-1} 70

55 Argon + NO (2900 ppm) + H_2 (1.52%) on Cedar Grove High Volatile (Coal): M_o = 1.48 g; D = 11.8 cm^3s^{-1} 71

56 Argon + NO (2980 ppm) + H_2 (1.52%) on Cedar Grove High Volatile (Char): M_o = 1.6 g; D = 11.8 cm^3s^{-1} 72

LIST OF FIGURES (Continued)

Figure . . . Page (II-)

57 Argon + NO + H_2 (1.5%) on Cedar Grove High Volatile (Char): Effect of Initial NO Concentration; M_o = 1.6 g; D = 11.8 cm^3s^{-1} 73

58 Argon + NO (3100 ppm) + H_2 on Cedar Grove High Volatile (Char): Effect of Initial Hydrogen Concentration; M_o = 1.55 g; D = 11.8 cm^3s^{-1} 74

59 Argon + NO (3150 ppm) + H_2 (1.5%) on Pocahontas Low Volatile, High Ash (Coal): M_o = 1.55 g; D = 11.8 cm^3s^{-1} 75

60 Argon + NO (3050 ppm) + H_2 (1.5%) on Pocahontas Low Volatile, High Ash (Char): M_o = 1.6 g; D = 11.8 cm^3s^{-1} 76

61 Argon + NO (3000 ppm) + H_2 (1.5%) on South African "Rietspruit" (Coal): Particle Size--50 to 100 microns; M_o = 1.45 g; D = 10.6 cm^3s^{-1} 77

62 Argon + NO (2800 ppm) + H_2 (1.5%) on South African "Rietspruit" (Char): Particle size--50 to 100 microns; M_o = 1.6 g; D = 10.3 cm^3s^{-1} 78

63 Argon + NO (2900 ppm) + H_2 (1.5%) on "Prosper" Ruhr (Coal): M_o = 1 g; D = 10.1 cm^3s^{-1} 79

64 Argon + NO (2900 ppm) + H_2 (1.5%) on "Prosper" Ruhr (Char): M_o = 1.6 g; D = 10.8 cm^3s^{-1} 80

65 Argon + NO (2900 ppm) + H_2 (1.5%) on Pennsylvania Anthracite (Coal): M_o = 1.92 g; D = 9.8 cm^3s^{-1} 81

66 Argon + NO (3180 ppm) + H_2 (1.5%) on Pennsylvania Anthracite (Char): M_o = 1.7 g; D = 9.8 cm^3s^{-1} 82

67 Argon + NO (3200 ppm) + H_2 (1.4%) on "Beulah" Lignite (Coal): M_o = 1.47 g; D = 9.6 cm^3s^{-1} 83

68 Argon + NO (3200 ppm) + H_2 (1.5%) on "Beulah" Lignite (Char): M_o = 0.8 g; D = 9.6 cm^3s^{-1} 84

69 Argon + NO (3300 ppm) + H_2 (1.5%) on Utah Bituminous (Coal): M_o = 1.97 g; D = 9.5 cm^3s^{-1} 85

70 Argon + NO (3200 ppm) + H_2 (1.5%) on Utah Bituminous (Char): M_o 1.08 g; D = 9.5 cm^3s^{-1} 86

LIST OF FIGURES (Continued)

Figure Page (II-)

71 Overall NO Removal Rates Measured on Pocahontas Medium Volatile Coal and Char 88

72 Overall NO Removal Rates Measured on Cedar Grove High Volatile Coal and Char 89

73 Overall NO Removal Rates Measured on Pocahontas Low Volatile Coal and Char 90

74 Overall NO Removal Rates Measured on South African "Rietspruit" Coal and Char 91

75 Overall NO Removal Rates Measured on Ruhr Coal "Prosper," Coal and Char 92

76 Overall NO Removal Rates Measured on Pennsylvania Anthracite, Coal, and Char 93

77 Overall NO Removal Rates Measured on "Beulah" North Dakota Lignite, Coal, and Char 94

78 Overall NO Removal Rates Measured on Utah Bituminous Coal and Char 95

79 Comparison of Overall N_2 Formation Rates and Overall NO Removal Rates, Measured on South African "Rietspruit" Coal and Char 99

80 Comparison of Overall N_2 Formation Rates and Overall NO Removal Rates, Measured on Ruhr Coal, "Prosper" Coal, and Char 100

81 Comparison of Overall N_2 Formation Rates and Overall NO Removal Rates, Measured on Pennsylvania Anthracite Coal and Char 101

82 Comparison of Overall N_2 Formation Rates and Overall NO Removal Rates, Measured on "Beulah" North Dakota Lignite, Coal and Char 102

83 Comparison of Overall N_2 Formation Rates and Overall NO Removal Rates, Measured on Utah Bituminous Coal and Char 103

84 Argon + O_2 on Pocahontas Medium Volatile Coal: $M_0 = 1.49$ g; (A) $D = 13.1\ cm^3s^{-1}$, $(O_2)_i = 0.76\%$; (B) $D = 10.6\ cm^3s^{-1}$, $(O_2)_i = 1.64\%$ 116

LIST OF FIGURES (CONCLUDED)

Figure Page (II-)

85 Argon + O_2 on Pocahontas Medium Volatile Char: (A) $M_0 = 1.52$ g, $D = 13.1$ cm^3s^{-1}, $(O_2)_i = 0.78\%$; (B) $M_0 = 2$ g, $D = 10.6$ cm^3s^{-1}, $(O_2)_i = 1.63\%$ 118

86 Argon + O_2 on Pocahontas Medium Volatile Char: Effect of Initial Oxygen Concentration on NO Formed During Oxidation 119

87 Argon + O_2 on Pocahontas Medium Volatile Char: Effect of Initial Oxygen Concentration on NH_3 and HCN Formed During Char Oxidation 120

88 Argon + O_2 on Pocahontas Medium Volatile Char: Effect of Oxygen Concentration and Temperature on the Ratio $(CO_2)_f/(CO)_f$ 121

89 Argon + NO + O_2 on Pocahontas Medium Volatile Char: $M_0 = 2$ g (M as a Function of Time--as Indicated); $D = 10.5$ cm^3s^{-1}; $(NO)_i = 2880$ ppm 123

90 Same Experimental Conditions as for Figure 89: Ammonia and Hydrocyanic Acid Released as a Function of Temperature and Initial Oxygen Concentration. Numbers on Curves: See Key Given in Figure 89 124

91 Same Experimental Conditions as for Figure 89: Ratio $(CO_2)_f/(CO)_f$ as a Function of Temperature and Initial Oxygen Concentration. Numbers on Curves: See Key Given in Figure 89 125

92 Argon + NO (2880 ppm) + O_2 on Pocahontas Medium Volatile Char: Variation of Overall NO Removal Rate $(\overline{V})$ as a Function of Temperature and Initial Oxygen Concentration . . . 126

93 Argon + NO + O_2 on Pocahontas Medium Volatile Coal: (A) $M_0 = 1.86$ g, $D = 10.4$ cm^3s^{-1}, $(NO)_i = 2800$ ppm, $(O_2)_i = 1.36\%$; (B) $M = 1.86$ g, $D = 10.6$ cm^3s^{-1}, $(NO)_i = 2700$ ppm, $(O_2)_i = 2.88\%$ 128

94 Argon + NO + O_2 on Pocahontas Medium Volatile Coal: Variation of NO Removal Rate With Initial Oxygen Concentration 129

LIST OF TABLES

Table Page (II-)

1 Chemical and Physical Characteristics of Utilized Coals 5

2 Chemical and Physical Characteristics of Chars From the Following Coals 11

3 Figures Related to Different Coal/Char Trials in the Absence of Oxygen 15

4 Overall NO Removal Rates and N_2 Formation Rates 105

INTRODUCTION

The previous work performed on heterogeneous NO reduction was an analytical study of the general reaction paths on which the mechanism depends.* In the present part of this final report, results are discussed on a comparative study made for coals and chars of different nature. The principal comparison investigated is their efficiency for heterogeneous NO reduction in the absence of other gaseous reductants, as well as in the presence of carbon monoxide, hydrogen, or oxygen. The scope is twofold: (a) find out if there exist any important effect of the coal structure on the overall NO reducing kinetics, and (b) see if the general experimental observations made for coal and char particles support the kinetic mechanism previously determined for less complex particles.

The overall NO removal rates and N_2 formation rates have been determined in a systematic way for coals and char particles of different origin by the packed bed method. The gas flow utilized is an argon carrier gas containing either NO, NO and CO, NO and H_2, or NO and oxygen. Proper interpretation of the results in terms of overall reaction rates also required the performance of runs in which pure argon or oxygen containing argon was fed over the solid. This allowed the contribution of coal pyrolysis and coal or char oxidation to the products released during NO reduction to be evaluated.

The following coals and chars have been studied systematically to date: (1) "Pocahontas" medium-volatile coal (West Virginia, U.S.A.), (2) "Pocahontas" low-volatile, high-ash coal (West Virginia, U.S.A.), (4) "Prosper" coal (Ruhr, Germany), (5) Coal from the "Rietspruit" region (South Africa), (6) Anthracite (Pennsylvania, U.S.A.), (7) "Beulah" lignite (North Dakota, U.S.A.) and (8) Utah bituminous coal (Utah, U.S.A.). The first three coals were obtained by courtesy of Dr. Damian de Soete, Coal Arbed International Trade Company, 1300 South Eisenhower drive, Beckley, WV. The next two coals were donated by the I.F.R.F. Research Station, IJmuiden, The Netherlands (courtesy of Dr. Roy Payne). The last three coals were obtained by courtesy of Dr. Michael Heap, E.E.R.C., Irvine, CA.

---

*See Part I of this report.

1.0 EXPERIMENTAL METHOD

1.1 Experimental Apparatus

The apparatus has been described in Part I of this final report. The only adaptation made for the present part of the study consists of the addition of a gas/liquid-phase separator at the outlet of the packed bed reactor. This, together with a filter located on the gas flow line leading to the analyzers, prevents the introduction of tar into the analyzers.

During the present trials, molecular nitrogen in the outlet gas flow was systematically determined by chromatographic analysis. The experimentally measured concentrations of N_2 are in good agreement with the concentrations obtained by the difference of the nitrogen-containing species; that is to say, the relationship

$$\left(N_2\right)_f = 0.5\left[(NO)_i - (NO)_f - \left(NH_3\right)_f - (HCN)_f\right] \tag{1}$$

holds true for N_2 concentrations larger than 200 ppm as long as the ammonia and hydrogen cyanide concentrations in the reactor outlet flow are corrected for ammonia and hydrogen cyanide released by coal pyrolysis. In order for this to be done, separate trials were made in which pure argon was fed over the coal particles.

The coal charges have been dried prior to each run by passing argon over them at a temperature of about 150°C (pyrolytic coal devolatilization does not occur at temperatures this low).

1.2 Treatment of the Results

Overall NO removal rates ($\overline{V}$) and overall N_2 formation rates $\left(\overline{V_n}\right)$ have been systematically determined from the experimental results. Using the following expressions:

$$\overline{V} = \frac{D}{M}\left[\left(X_{NO}\right)_f - \left(X_{NO}\right)_i\right] \qquad \left(cm^3 s^{-1} g^{-1}\right) \tag{2}$$

$$\overline{V}_n = \frac{D}{M}\left(X_{N_2}\right)_f \qquad \left(cm^3 s^{-1} g^{-1}\right) \tag{3}$$

The subscript "i" indicates the reactor inlet flow and the subscript "f" the reactor outlet flow. D is the total flow rate under standard conditions and M the instantaneous value of the mass of the packed bed. For trials on chars, M is almost a constant and equal to the initial mass of char, as long as there is no oxygen present in the inlet gas flow. In the case of trials on coal, the precise value of M is unknown during the devolatilization of the coal. In these cases, it is assumed that M varies linearly as a function of residence time between its initial value (raw coal) and the value it assumes when the coal is totally devolatilized. Due to the very slow temperature/time increase, 90 percent of the total devolatilization measured, occurs at a temperature of 700 to 800°C even for high volatile bituminous coals. This observation is based upon measurements of light volatiles (e.g. methane).

Whenever oxygen is present in the inlet gas flow, the instantaneous value of the mass M is obtained by calculating the mass losses (ΔM) due to oxidation of the solid charge. The change in mass is given by:

$$\Delta M = \left[(CO)_f + (CO_2)_f\right]\left(M_C + qM_H\right) \frac{D}{v_M} \Delta t \qquad (4)$$

where M_C and M_H are the atomic mass of carbon and hydrogen, respectively, q is the characteristic atomic ratio H/C for the solid, Δt is the time interval during which CO and CO_2 concentrations in the reactor outlet flow are constant and v_M is the molar volume at standard conditions. Equation (4) yields good estimation of the mass losses when the volatile content is very small (as in the cases of chars or anthracite coals). In the case of bituminous coals, however, it only yields a rough approximation, since (a) some volatile matter is driven off without being oxidized, and (b) the ratio "q" of the oxidized matter varies with time and temperature due to volatile oxidation. Throughout this report, the initial mass of the dry solid charge in the reactor will be designated by the symbol M_0.

Simple rate expressions are utilized to describe overall NO removal and overall N_2 formation. For example,

$$\overline{V} \left(\text{or } \overline{V}_n\right) = k\, X_{NO}^{a}\, X_{Y}^{b} \qquad (5)$$

where Y is coreactant e.g. CO or H_2 for NO reduction, present in the initial gas flow. Determination of these rates according to eq. (5) is made by the differential reactor method. The technique utilized in the determination of the rate constant k and of the partial orders a and b has already been explained in Part I of this final report

1.3 Characteristics of Coals and Chars

1.3.1 Coals

Some physical and chemical characteristics of the coals utilized are listed in Table 1. Unfortunately it was not possible to obtain samples of coals covering the entire ASTM coal classification. In the first row of Table 1 an approximate ASTM rank is assigned to each coal, according to the normalized ASTM classification (Ref. 1,2). Only coals numbered 14, 16, 18, and 20 have size distributions which correspond to the size range commonly used in pulverized-coal combustion. The three West Virginia coals (6, 8, and 10) are coarsely crushed with about 70 percent of the mass being between 0.1 and 1 mm, as shown by Figures 1 to 3. In the case of the South African coal (12), two well-defined size fractions have been utilized, 0.5 to 0.10 and 0.5 to 1.0 mm, in order to study the effect of particle size on NO reduction. Size distribution of coal samples numbered 16, 18, and 20 are shown in Figure 5.

1.3.2 Chars (see Table 2)

It should be stressed that the name "char," utilized throughout this report, is in most cases not appropriate. The name "char" should only be used for "residual solid matter following fast pyrolysis" (2). Only for char 15 does this designation fully apply. Char numbers 7, 9, 11, and 13 have been obtained by a slow pyrolysis process in which the crushed coal was treated at high temperature (1000^{o}C) with argon flow for about two hours. Char numbers 17, 19, and 21 are the solid residue which remained after the analogous run on pulverized coal. Since these runs were conducted at 1000^{o}C and were characterized by relatively slow heating rates (0.03 to 0.04 degree/s), the char "left" after a coal run is very comparable to the coke obtained by treating the coal under argon flow at 1000^{o}C. Chars 7, 9, and 11 have a coarse size distribution (see Figure 1 to 3) comparable to that of the parent coal. Char 15 has a size distribution similar to typical coal dust flames (see Figure 4). The size

Table 1. Chemical and Physical Characteristics of Utilized Coals

Reference number	6	8	10	12	14	16	18	20
Designation	Pocahontas medium volatile	Cedar Grove high volatile	Pocahontas low volatile high ash	Rietspruit St. Af.	Prosper Ruhr	Pennsylvania anthracite	Beulah lignite	Utah bituminous
Approximate ASTM rank	med. vol. bituminous	high vol. bitum. A	low volatile bituminous	low to med. vol. bitum.	low volatile bituminous	anthracite	lignite A	high volatile bitumin. B
Density (picnometer) ($g.cm^{-3}$)	1.261	1.275	1.414	(a) 1.405 (b) 1.421	1.135	1.386	1.214	1.215
Apparent density ($g.cm^{-3}$)	0.70	0.63	0.96	(a) 0.54 (b) 0.73	0.63	0.83	0.68	0.73
Specific Surface Area (BET method) ($m^2.g^{-1}$)	0.5	0.35	1.1	(a) 4.5 (b) 2.0	4.3			
Size distribution (mm)	(see fig. 1)	(see fig. 2)	(see fig. 3)	(a) 0.05 to 0.10 (b) 0.5 to 1.0	(see fig. 4)	(see fig. 5)	(see fig. 5)	(see fig. 5)
Proximate analysis (dry basis, mass %):								
volatiles:	20.53	35.01	17.43	24.13	22.0	4.63	41.33	41.54
fixed carbon:	74.29	58.56	44.52	59.02	72.0	89.32	51.06	50.55
ash:	5.18	6.43	38.05	16.85	6.0	6.05	7.60	7.91
Ultimate (elemental) analysis (mass %):								
C :	84.2	81.7	55.8	63.22	81.5	88.45	66.15	73.17
H :	4.4	5.8	3.4	2.97	4.5	2.14	4.20	5.55
O :	4.0	3.8	1.0	7.73	4.5	2.10	20.72	11.18
N :	1.4	1.7	1.0	1.38	1.5	0.79	0.96	1.54
S :	0.8	0.67	0.85	0.39	1.0	0.47	0.37	0.66

32.

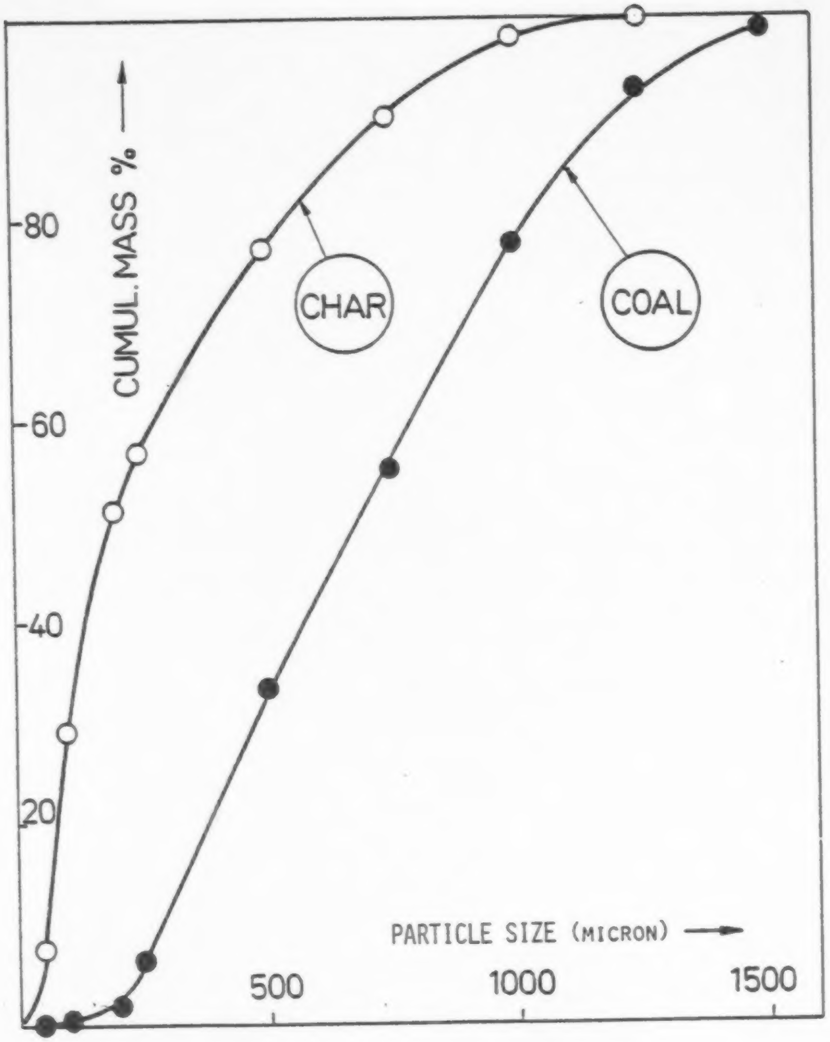

Figure 1. Pocahontas Medium Volatile Coal; Particle Size Distribution.

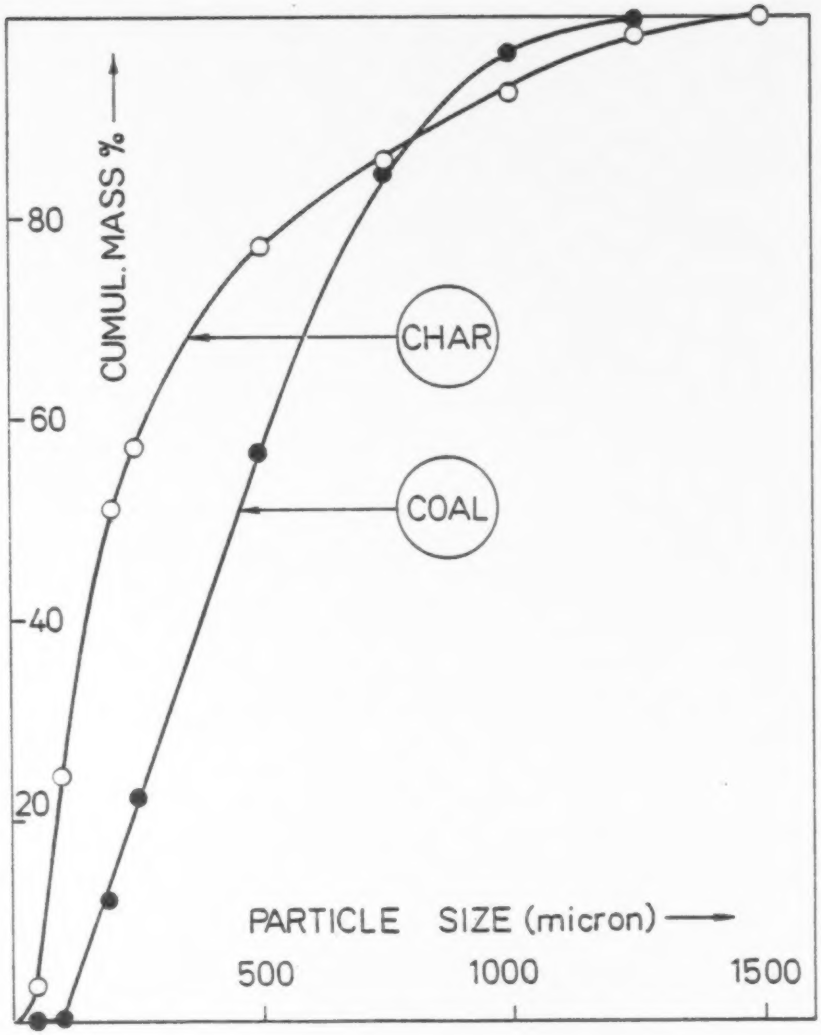

Figure 2. Cedar Grove High Volatile Coal; Particle Size Distribution.

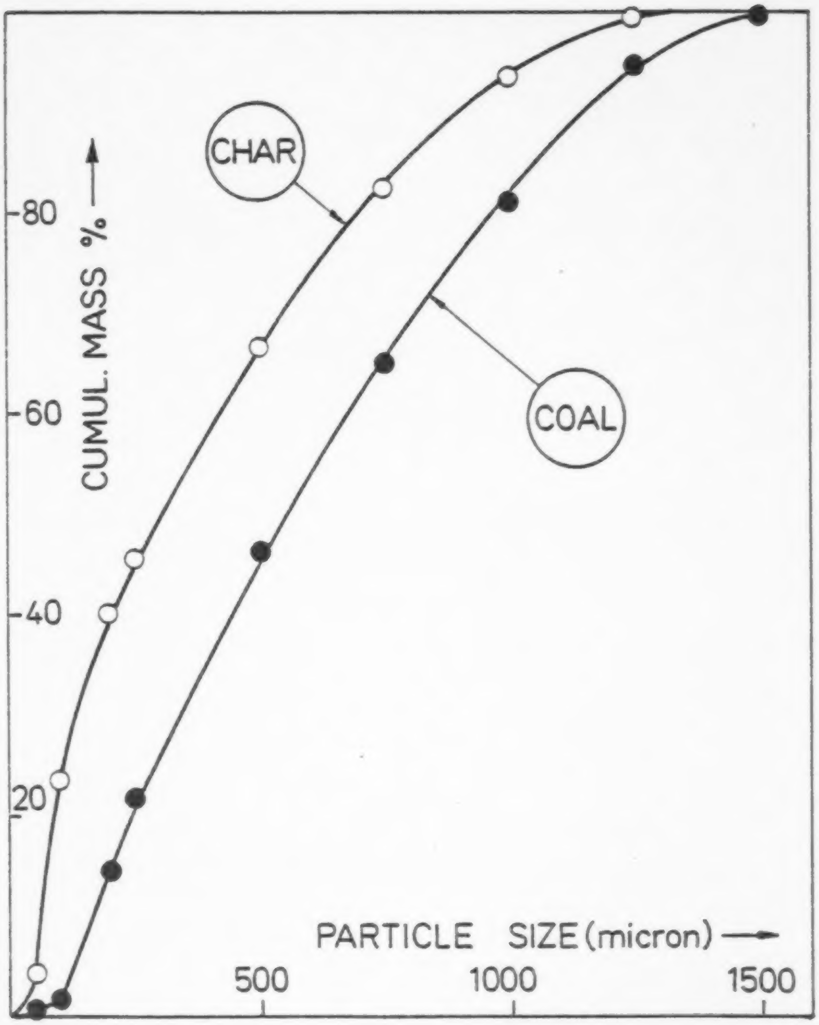

Figure 3. Pocahontas Low-Volatile, High-Ash Coal; Particle Size Distribution.

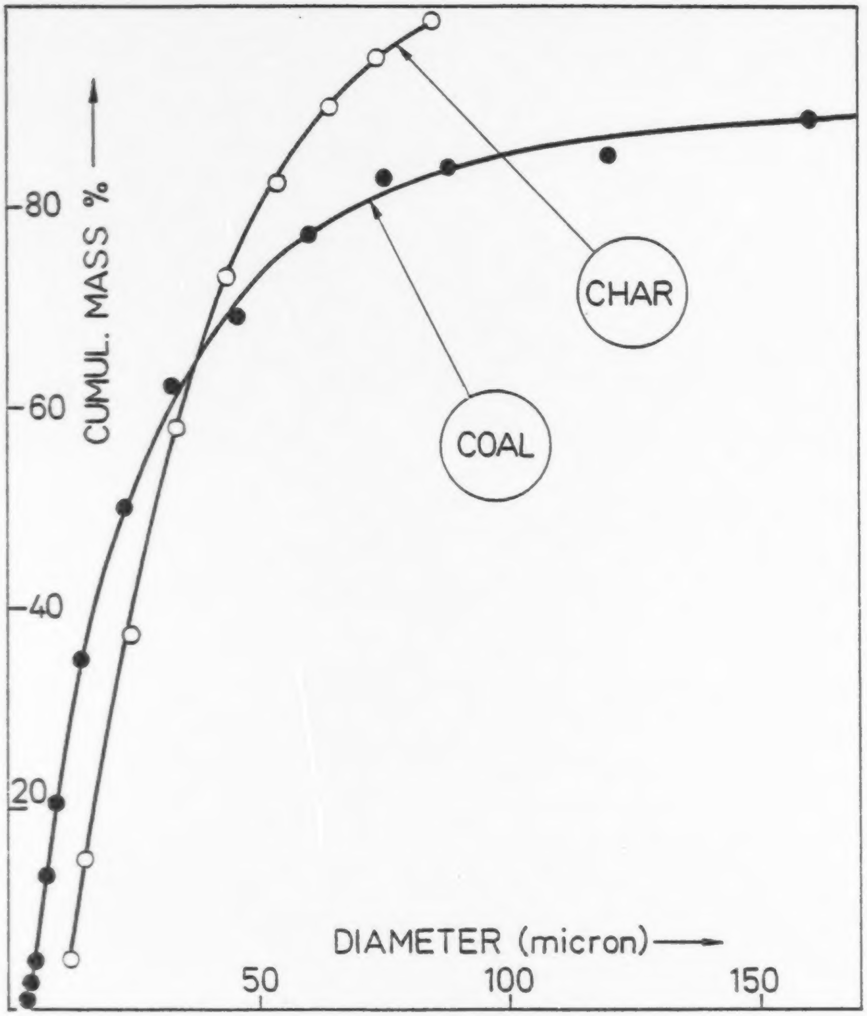

Figure 4. Prosper Ruhr Coal; Particle Size Distribution.

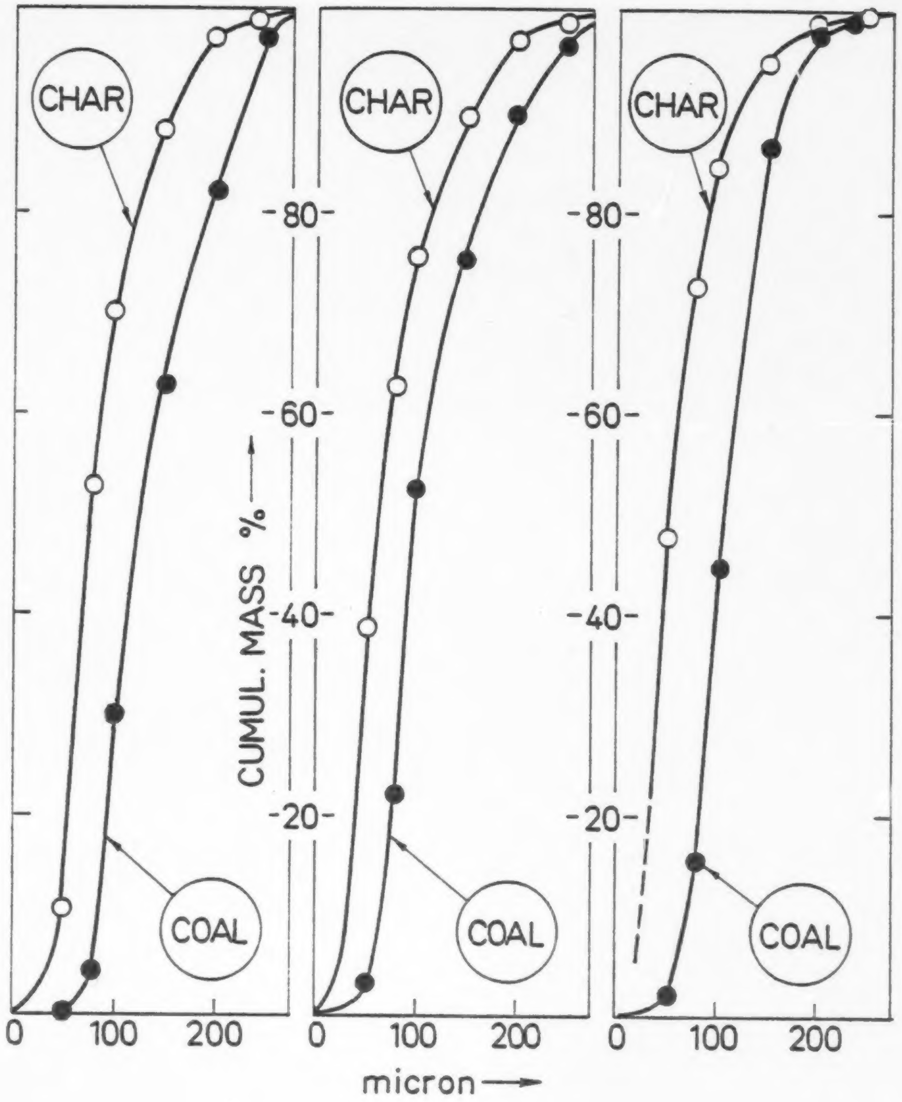

Figure 5. Particle Size Distribution (Pennsylvania Anthracite, Beulah Lignite and Utah Bituminous Coal).

Table 2. Chemical and Physical Characteristics of Chars from Following Coals

Reference number	7	9	11	13	15	17	19	21
Designation	**Pocahontas medium volatile**	**Cedar Grove high volatile**	**Pocahontas low volatile high ash**	**Rietspruit St. Af.**	**Prosper Ruhr**	**Pennsylvania anthracite**	**Beulah lignite**	**Utah bituminous**
Approximate ASTM rank of corresponding coal	**med. vol. bituminous**	**high vol. bitum. A**	**low volatile bituminous**	**low to med. vol. bitum.**	**low volatile bituminous**	**anthracite**	lignite A	**high volatile bitumin. B**
Density (picnometer) ($g.cm^{-3}$)	1.537	1.610	1.902	1.683	1.355	1.466	1.705	1.566
Apparent density ($g.cm^{-3}$)	0.66	0.74	0.95	0.85	0.53	1.04	0.83	0.90
Specific Surface Area (BET method) ($m^2.g^{-1}$)	1.75	0.55	1.3		80 to 88			
Size distribution (mm)	(see fig. 1)	(see fig. 2)	(see fig. 3)	0.05 to 0.10	(see fig. 4)	(see fig. 5)	(see fig. 5)	(see fig. 5)
Elemental analysis (mass %)								
C :	90.8	88.6	63.7	75.87	82.85	87.2	76.4	79.8
H :	0.60	0.51	0.32	0.39	0.7	0.61	0.66	0.42
O :					0.5			
N :	1.28	1.49	0.89	1.02	1.2	1.26	1.70	1.91
S :					0.75			
					volatiles: 1.8 % ash: 14.0 %			

distributions of chars 17, 19, and 21 are given in Figure 5, and may be compared to the size distribution of the corresponding coals.

2.0 NITRIC OXIDE REDUCTION ON COALS AND CHARS IN THE ABSENCE OF OXYGEN

During the pyrolysis of coals and even for most chars (which normally still contain some volatiles), nitrogen-containing species are released. These species may interfere with the nitrogenous compounds formed during heterogeneous NO reduction. Therefore, for each type of coal or char particles studied, a preliminary trial has been made, in which pure argon was fed over the particles (coal or char) under exactly the same experimental conditions (mass of solid charge, flow rate (D) and especially temperature/ time history). The results obtained in these runs are then used to correct the runs in which NO is present in the reactor inlet gas flow.

In the first paragraph of this section the results of the pure argon trials are presented. In the successive paragraphs the results obtained with gas flows containing (a) argon and NO; (b) argon, NO, and CO; and (c) argon, NO, and hydrogen are discussed. The kinetic implications of these results will be discussed in a qualitative manner by referring to the heterogeneous NO reduction mechanism which has been studied using a parametric investigation (Part I). In the second part of this section, attention will be devoted to the reaction rates for overall NO removal and overall N_2 formation as obtained for these coal and char particles. Hence, the plan of the present section is as follows:

2.1 Direct Experimental Measurements and Kinetic Implications
2.1.1 Trials With Pure Argon
2.1.1.1 Trials on Coal Particles
2.1.1.2 Trials on Char Particles
2.1.2 Trials With Argon + NO
2.1.2.1 Trials on Char Particles
2.1.2.2 Trials on Coal Particles
2.1.3 Trials With Argon + NO + CO
2.1.3.1 Trials on Char Particles
2.1.3.2 Trials on Coal Particles
2.1.4 Trials With Argon + NO + H_2

2.1.4.1 Trials on Char particles

2.1.4.2 Trials on Coal Particles

2.2 Comparison of NO Removal Rates and N_2 Formation Rates on Different Coals and Chars

2.3 Comparison of Rate Constants

Since a great number of figures are given in this section, it is of some utility to present an overview of the figure numbers related to the different coal and char particles. This is done in Table 3.

2.1 Direct Experimental Results and Kinetic Implications

2.1.1 Trials With Pure Argon

Results are shown in Figures 6 through 13, for coals and corresponding chars.

2.1.1.1 Trials on Coal Particles

As may be seen from the lower part of Figures 6 through 13, both HCN and NH_3 are released from coals during (slow) devolatilization. The hydrogen cyanide typically peaks at a temperature between 450 and 550°C, whereas the peak value of released ammonia occurs at somewhat higher temperature (575 to 675°C). In some cases, a second maximum of $(HCN)_f$ is observed at higher temperatures (e.g. Figure 13). Except for coal numbers 18 (Beulah lignite), 20 (Utah bituminous coal) and 8 (Cedar Grove), which are all high-volatile coals, the amount of HCN and NH_3 released during devolatilization is roughly proportional to $M_C(H)/(C)$, where M_C is the total mass of carbon in the bed and (H)/(C) the atomic hydrogen/carbon ratio.

During coal pyrolysis, carbon monoxide is released in nonnegligible quantities. The $(CO)_f$ versus temperature curve normally have a maximum in the temperature range where devolatilization is very intense (400 to 700°C). At temperatures above 700°C, the CO release rate again increases in a relatively fast manner. Comparison of this coal data with the CO released during thermal treatment of chars under argon flow (see paragraph 2.1.1.2), suggests that the low temperature peak of CO is a "volatiles-CO," since it is not found for chars. The steep increase of $(CO)_f$ at temperatures

Table 3. Figures Related to Different Coal/Char Trials in the Absence of Oxygen.

Solid particles		Ar (pure)	Ar + NO	Ar + NO + CO	Ar + NO + H_2
POCAHONTAS MEDIUM VOLATILE	COAL	6	14 71	33 71	51 71
	CHAR	6	15 16 71	34 35 36 37 38 39 40 71	52 53 54 71
CEDAR GROVE HIGH VOLATILE	COAL	7	17 72		55 72
	CHAR	7	18 19 72		56 57 58 72
POCAHONTAS LOW VOLATILE HIGH ASH	COAL	8	20 73		59 73
	CHAR	8	21 22 73		60 73
"RIETSPRUIT" SOUTH AFRICAN	COAL	9	23 74 79	41 74 79	61 74 79
	CHAR	9	24 74 79	42 74 79	62 74 79
"PROSPER" RUHR COAL	COAL	10	25 75 80	43 75 80	63 75 80
	CHAR	10	26 75 80	44 75 80	64 75 80
PENNSYLVANIA ANTHRACITE	COAL	11	27 76 81	45 76 81	65 76 81
	CHAR	11	28 76 81	46 76 81	66 76 81
"BEULAH" LIGNITE	COAL	12	29 77 82	47 77 82	67 77 82
	CHAR	12	30 77 82	48 77 82	68 77 82
UTAH BITUMINOUS	COAL	13	31 78 83	49 78 83	69 78 83
	CHAR	13	32 78 83	50 78 83	70 78 83

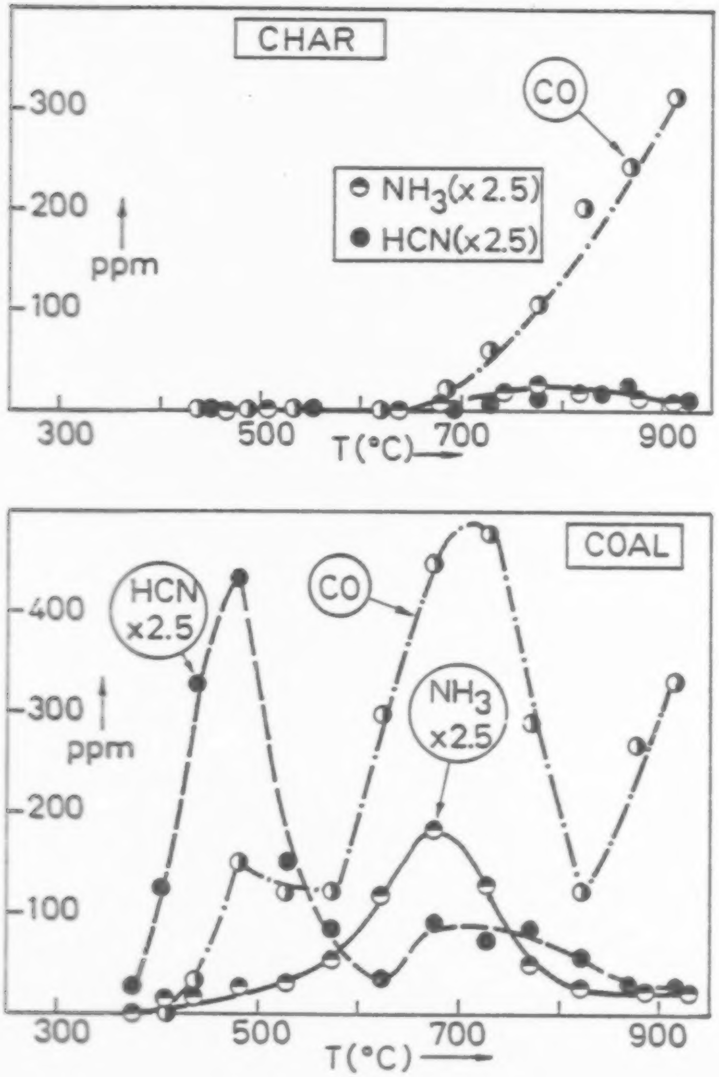

Figure 6. Argon Pure on Pocahontas Medium Volatile (Coal and Char): Coal Trial, M_o = 1.49 g, D = 12.2 cm^{3}s^{-1}; Char Trial, M_o = 1.32 g, D = 12.2 cm^{3}s^{-1}.

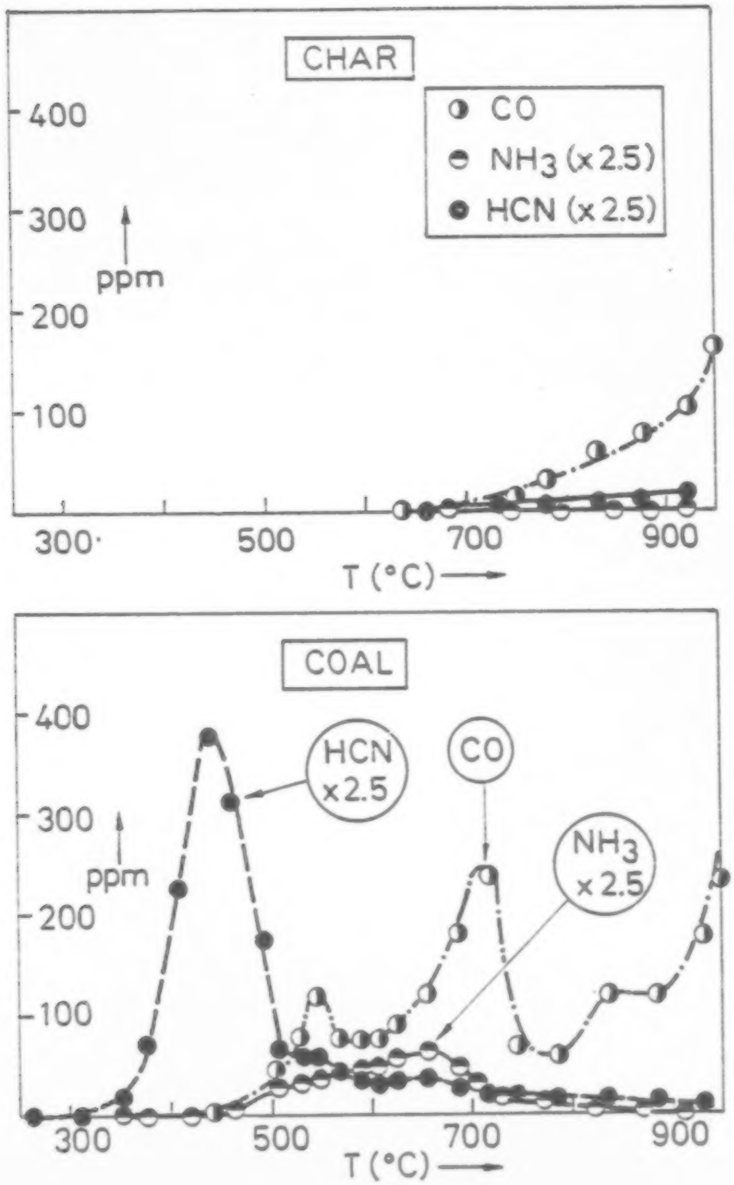

Figure 7. Argon Pure on Cedar Grove (Coal and Char): Coal Trial, M_0 = 1.48 g, D = 12.2 cm^3s^{-1}; Char Trial, M_0 = 1.6 g, D = 12.2 cm^3s^{-1}.

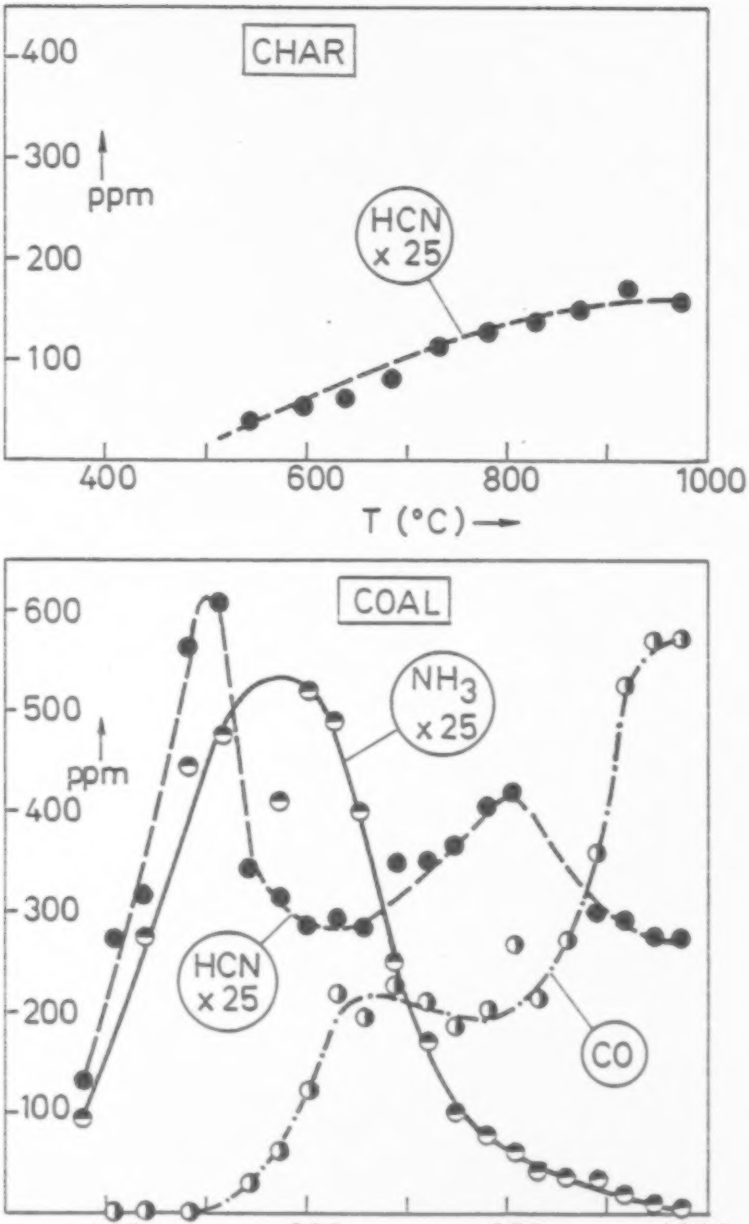

Figure 8. Argon Pure on Pocahontas Low Volatile, High Ash (Coal and Char): Coal Trial, M_0 = 1.55 g, D = 12.2 cm^{3}s^{-1}; Char Trial, M_0 = 1.6 g, D = 12.2 cm^{3}s^{-1}.

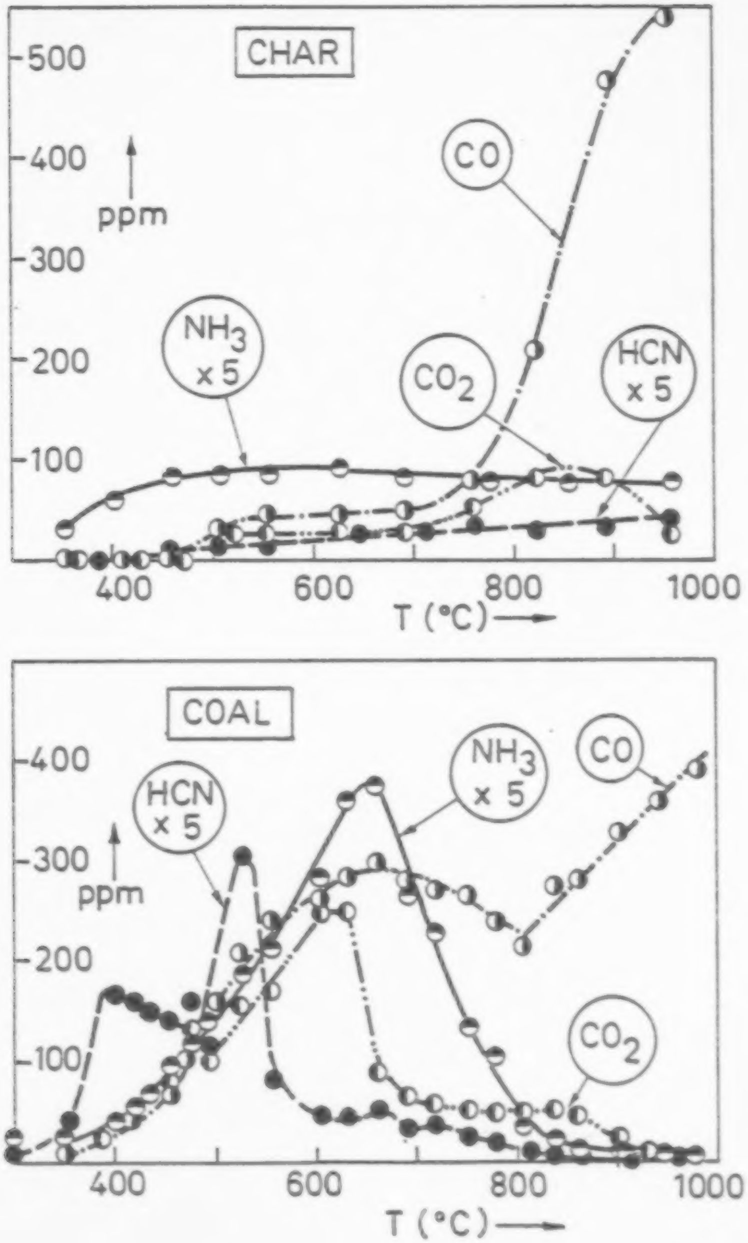

Figure 9. Argon Pure on South African "Rietspruit" (Coal and Char): Particle size, 50 to 100 microns; Coal Trial, M_0 = 1.45 g, D = 12.2 cm^3s^{-1}; Char Trial, M_0 = 1 g, D^o = 9.4 cm^3s^{-1}.

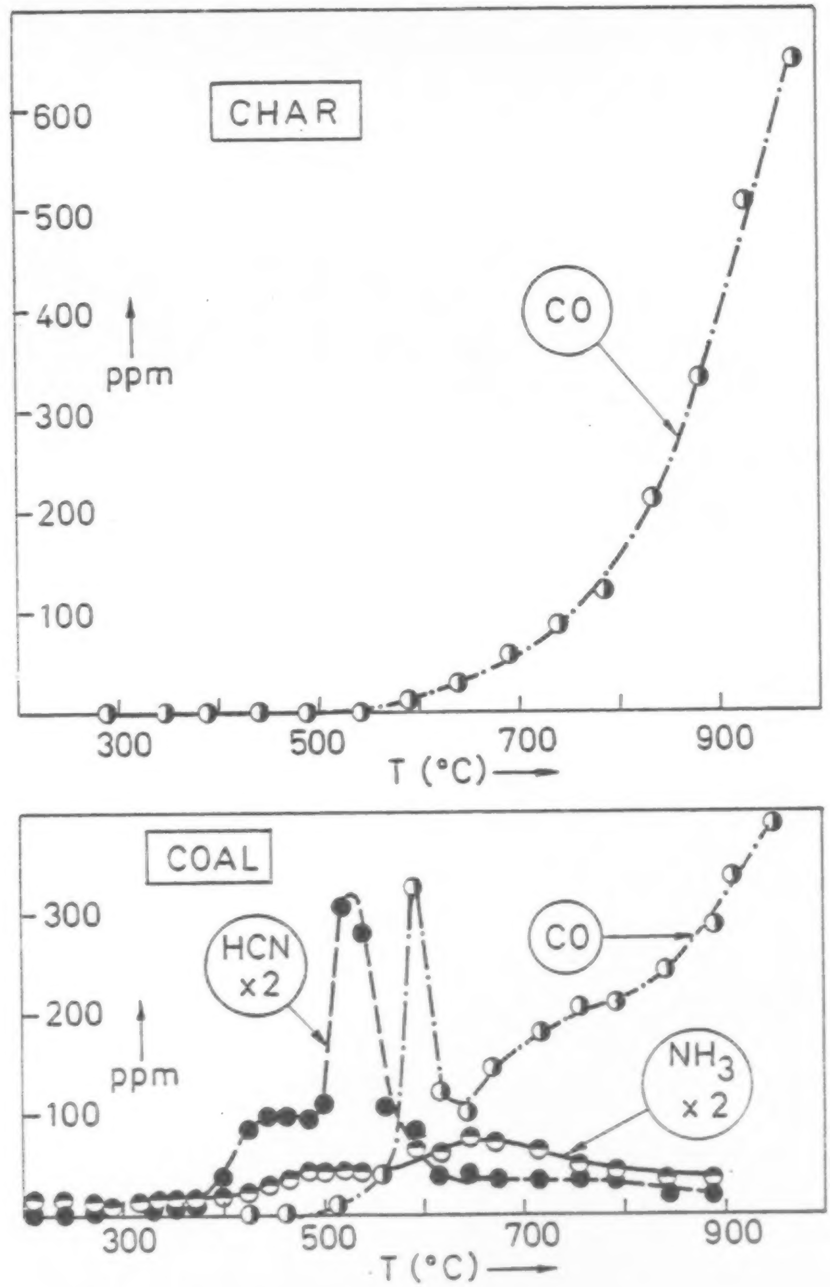

Figure 10. Argon Pure on "Prosper" Ruhr (Coal and Char): Coal Trial, M - 1 g, D = 10.9 cm^{3}s^{-1}; Char Trial, M_0 = 1g, D = 0.6 cm^{3}s^{-1}.

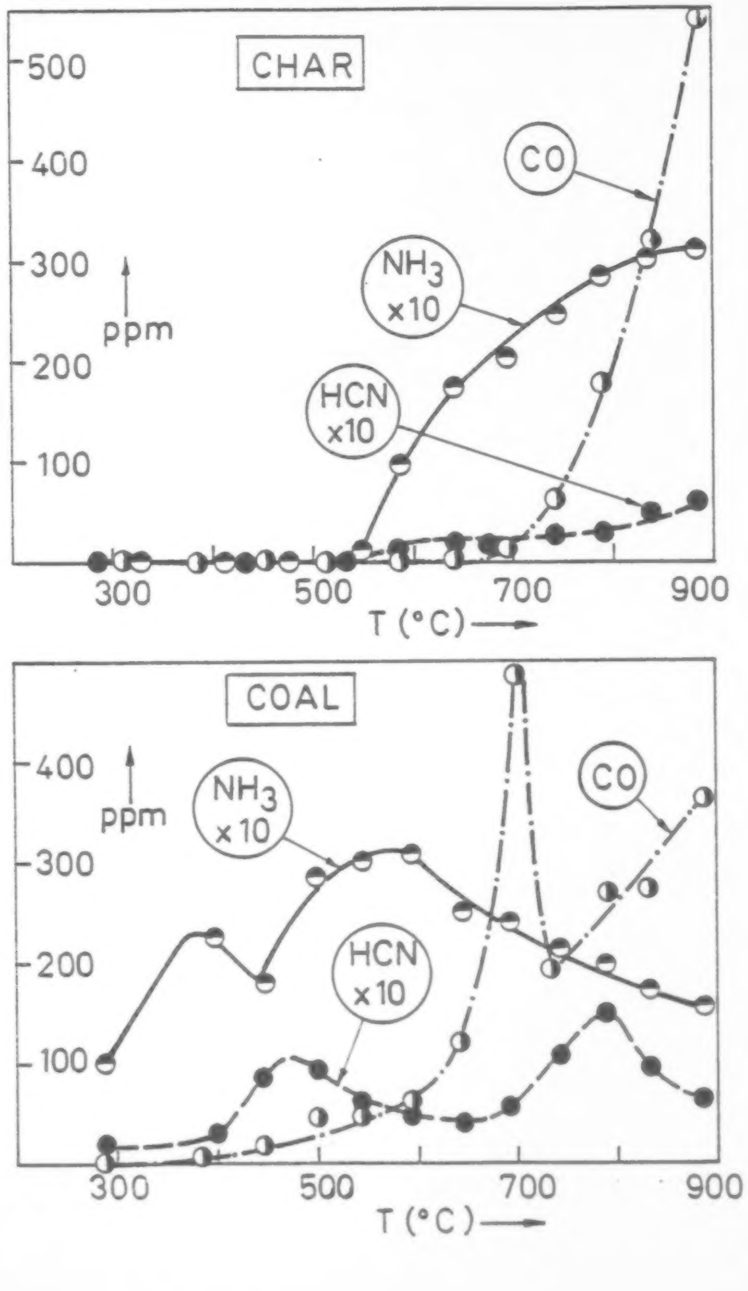

Figure 11. Argon Pure on Pennsylvania Anthracite (Coal and Char): Coal Trial, $M = 1.92$ g, $D = 9.7\ cm^3s^{-1}$; Char Trial, $M_o = 1.7$ g; $D = 9.3\ cm^3s^{-1}$.

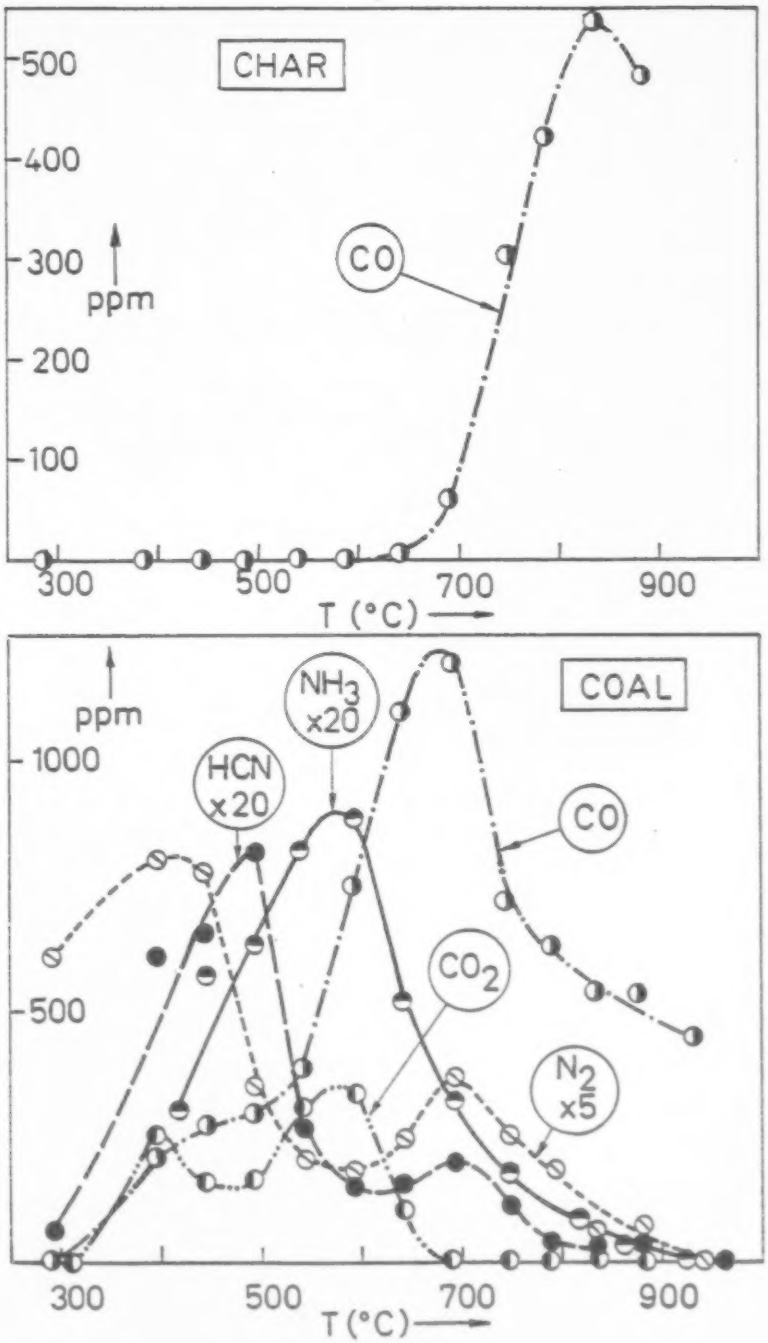

Figure 12. Argon Pure on "Beulah" Lignite (Coal and Char): Coal Trial, M = 1.47 g; D - 9.7 cm^3s^{-1}; Char Trial, M_o = 0.8 g, D = 9.7 cm^3s^{-1}.

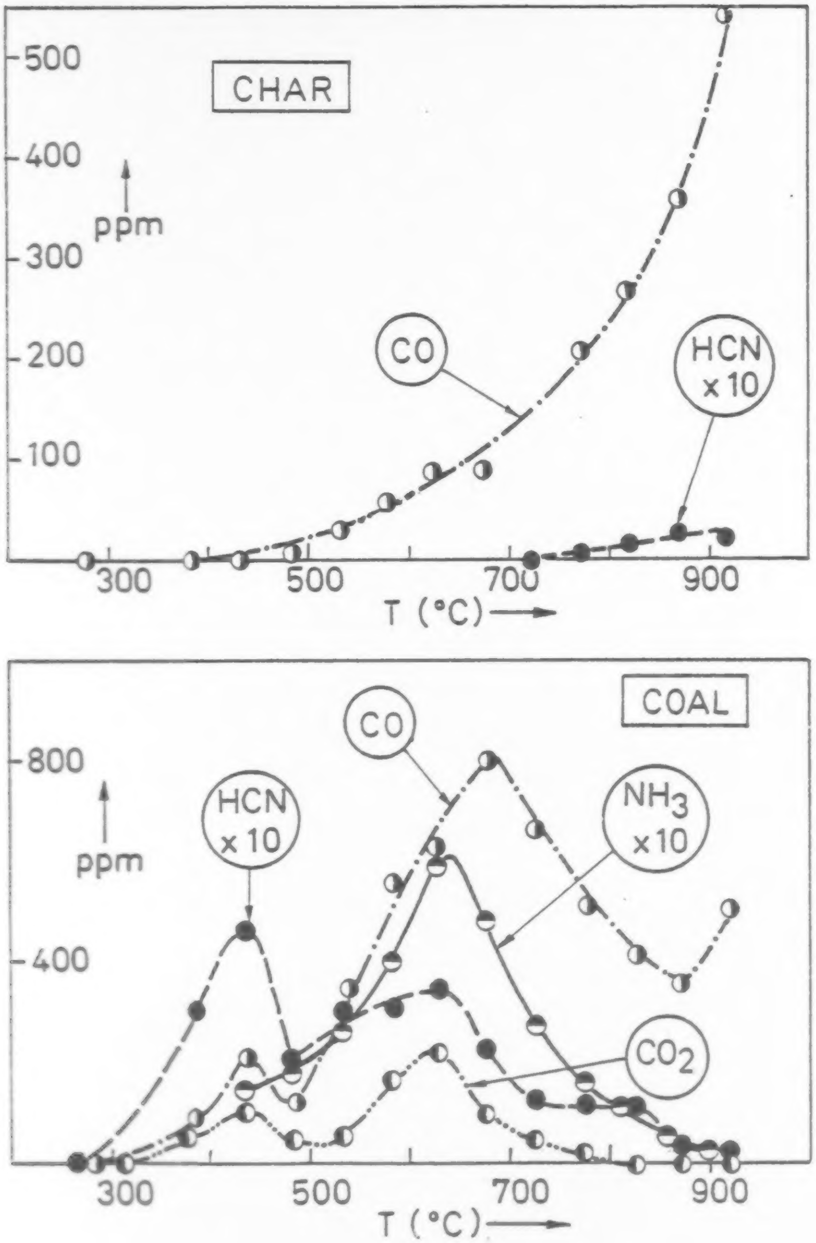

Figure 13. Argon Pure on Utah Bituminous (Coal and Char): $D = 9.7\ cm^3s^{-1}$; Coal Trial, $M_0 = 1.97$ g; Char Trial, $M_0 = 1.08$ g.

above 700^{o}C is primarily due to thermal decomposition of the almost completely devolatilized) char, and is also present, therefore, in the reactor outlet flow during thermal treatment of chars.

Some CO_2 is also released during coal devolatilization (see Figures 9, 12, and 13). Since $CO_{2\ f}$ peaks at temperatures below 700^{o}C, and since little CO_2 is released during thermal treatment of chars (see below), it may be concluded that this is a "volatiles-CO_2."

Hydrocarbons released during devolatilization of coal have not been monitored in these trials. Evidence of methane release during devolatilization of coal was obtained in later trials (see trials with argon + NO, Figures 29 and 31). In no case was nitric oxide found in the outlet gas flow during coal devolatilization runs.

2.1.1.2 Trials on Char Particles

The upper part of Figures 6 through 13 presents the results obtained during the thermal treatment of char particles with argon flow. The main species found in the reactor outlet flow is carbon monoxide. $(CO)_f$ steeply increases at temperatures above 700^{o}C and therefore should be considered as formed from bound carbon and oxygen atoms of the char. We shall refer to this CO as "char-CO."

Small quantities of ammonia and hydrogen cyanide are also observed during thermal treatment of char. At lower temperatures these species are probably formed from volatile bound nitrogen atoms, since some volatiles are still present in the initial char; however, the fact that $(HCN)_f$ and $(NH_3)_f$ may persist and even increase at temperatures above 900^{o}C, independent of the length of the run, seems to indicate that these nitrogen species are partially formed from bound nitrogen atoms. As a matter of fact, the distinction between "volatile" bound nitrogen atoms and "char" bound nitrogen atoms is quite misleading, since all species driven out during thermal treatment of coal and char should logically be considered as pyrolysis products, i.e. as volatiles. The only reality corresponding to this hazardous distinction, is that there exist different steps in the devolatilization process according to different time/temperature conditions.

2.1.2 Trials With Argon + NO

When dealing with NO reduction trials, runs on char particles will be treated first, before the runs on coal particles. This is done for two reasons:

1. The almost total absence of devolatilization during trials on chars, results in a much more simple NO reduction behavior than is the case for coal trials.
2. During the trials on coal particles, the coal is progressively "charified," and a proper understanding of the NO reduction on char may be of great utility to explain the results obtained with coal particles.

2.1.2.1 Trials on Char Particles

Results obtained when feeding NO containing argon carrier gas are shown in Figures 15, 16, 18, 19, 21, 22, 24, 26, 28, 30, and 32, for chars of different origin. Generally speaking, the following observations can be made:

- The main nitrogen-containing species formed during NO removal is molecular nitrogen see Figures 18, 21, 24, 26, 28, 30, and 32, where the experimentally measured concentrations of N_2 are in good agreement with the ones calculated from eq. (1) .
- Some ammonia and hydrogen cyanide is released during NO reduction. If these results are compared with char pyrolysis trials performed under argon flow on the same char particles (see paragraph 2.1.1), it is seen that a large part of the released NH_3 is not accounted for by thermal decomposition of the char. Therefore, it can be concluded that the NO reduction into N_2 partially goes through the intermediate formation of ammonia. Moreover, the NH_3 versus temperature curve has the typical maximum-shaped form of an intermediate product.

  At temperatures below 700 to 800°C, the HCN observed is primarily released by thermal decomposition of the char. Only at higher temperatures is the HCN formed from NO. This probably

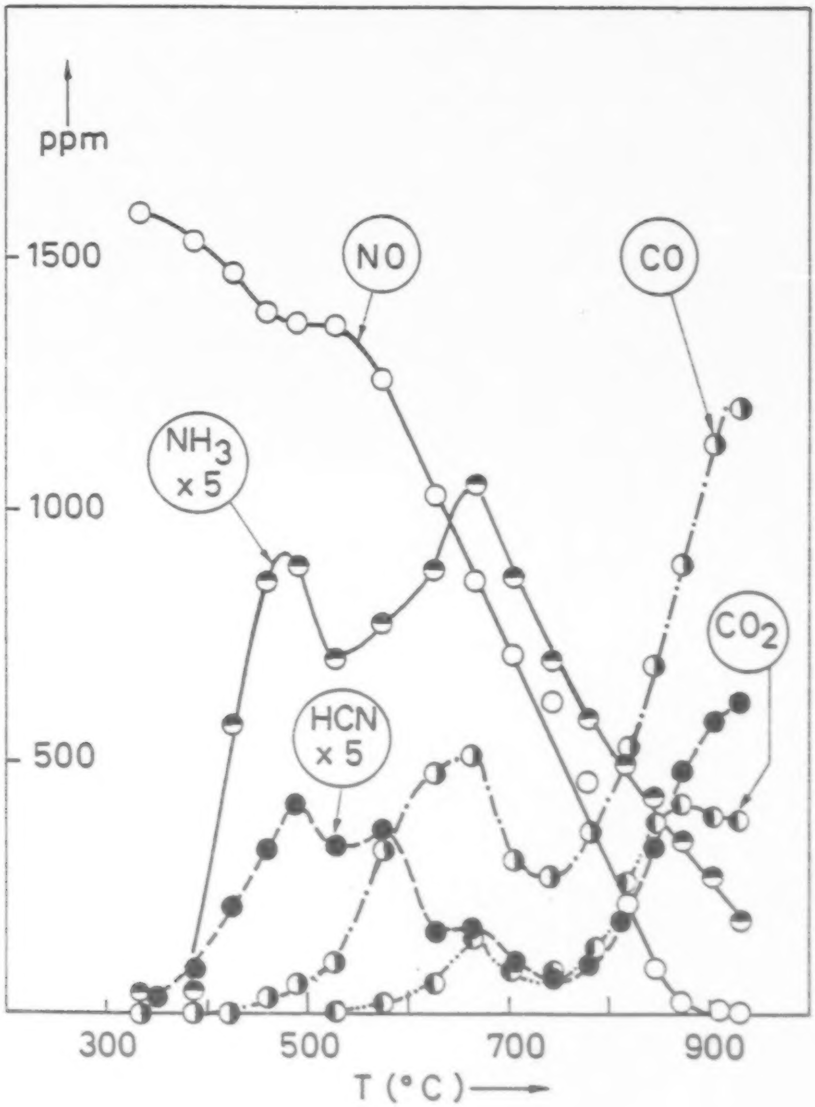

Figure 14. Argon + NO on Pocahontas Medium Volatile Coal: M_o = 1.49 g; D = 12.1 cm^3s^{-1}; $(NO)_i$ = 1590 ppm.

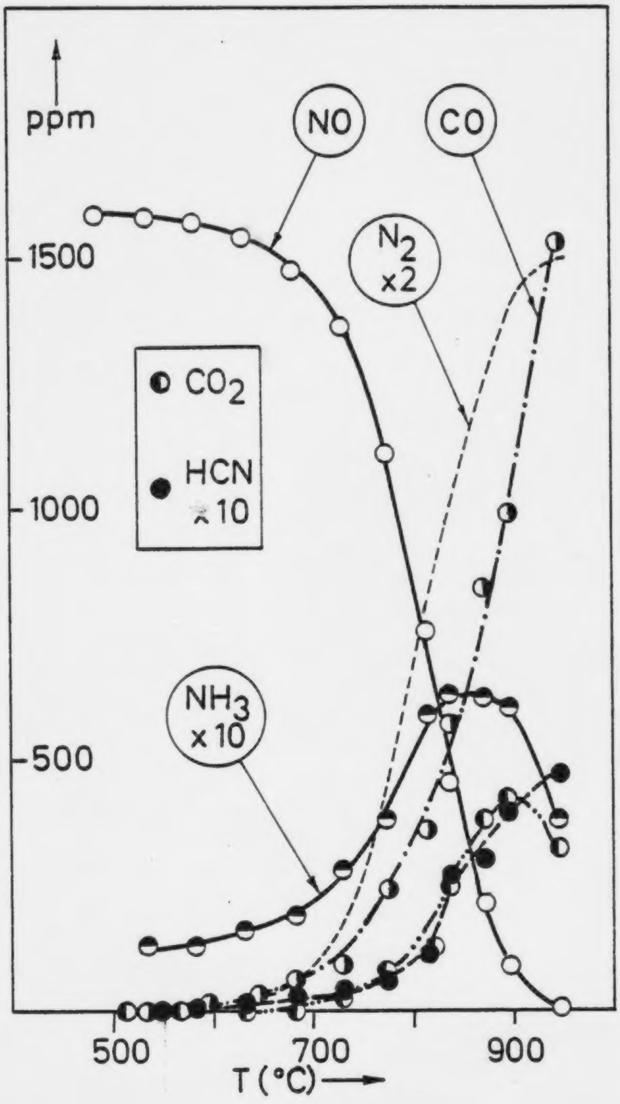

Figure 15. Argon + NO (1580 ppm) on Pocahontas Medium Volatile (Char): M_o = 1.28 g; D = 12.1 cm^3s^{-1}.

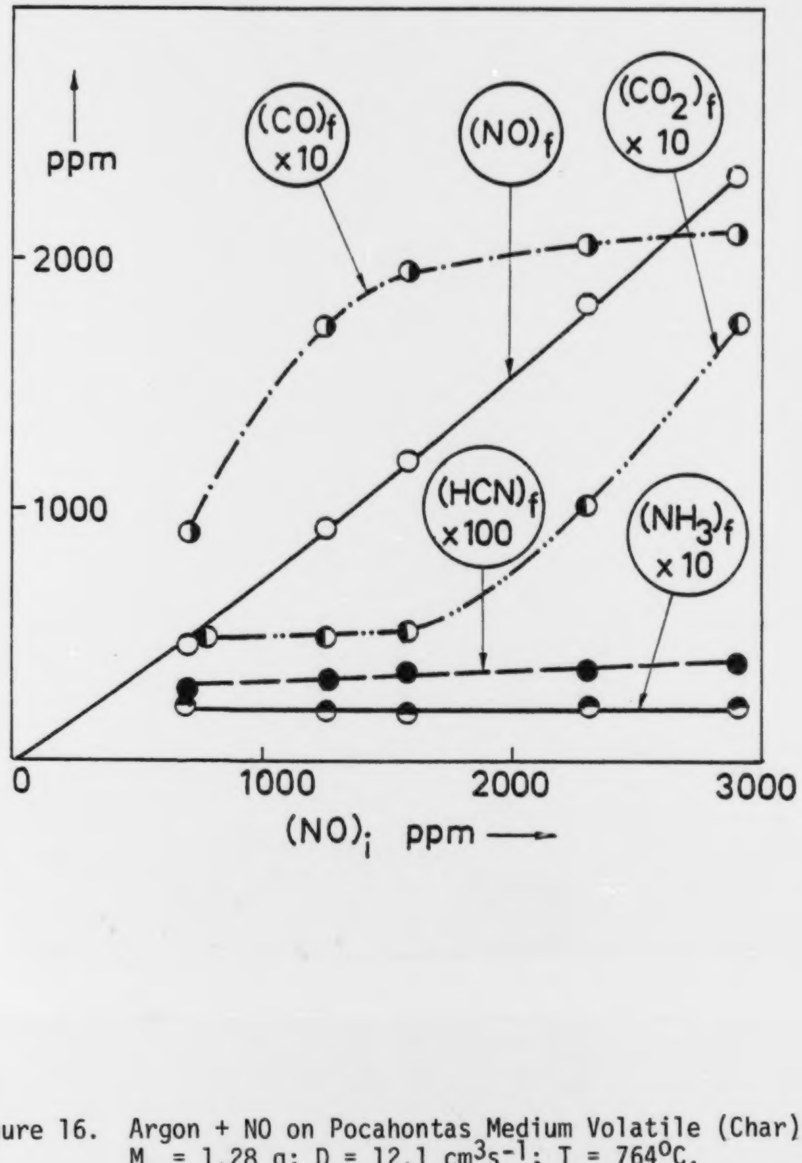

Figure 16. Argon + NO on Pocahontas Medium Volatile (Char); M_o = 1.28 g; D = 12.1 cm^3s^{-1}; T = 764°C.

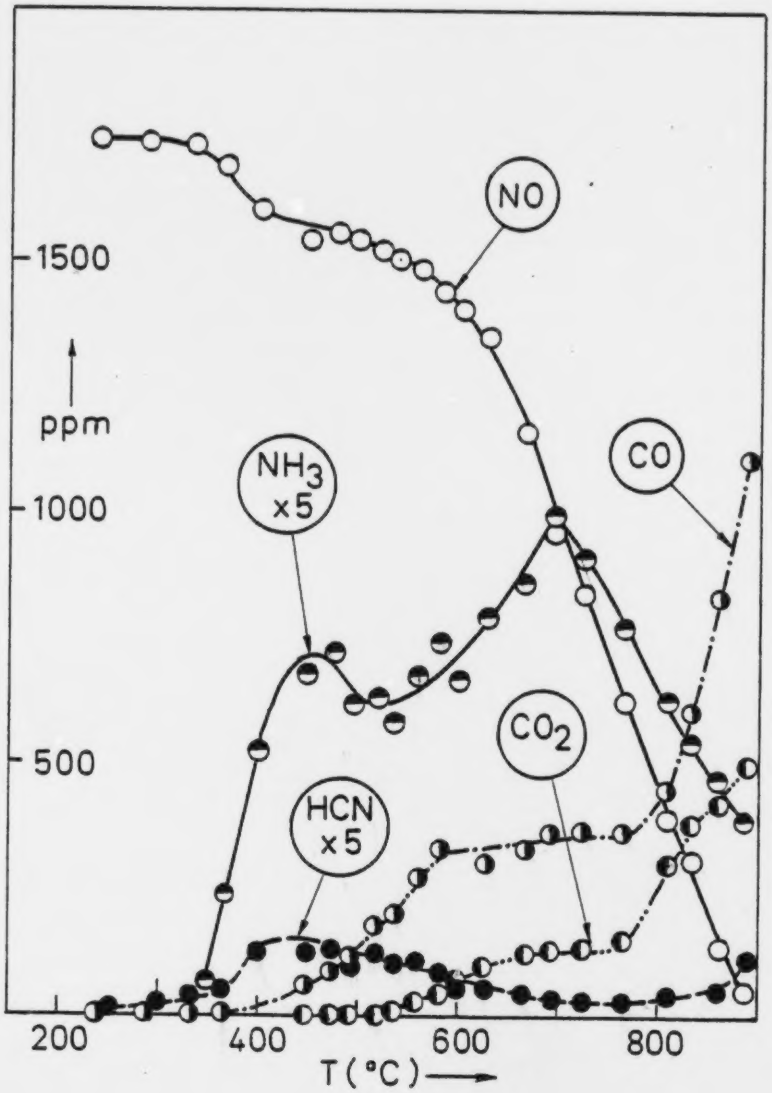

Figure 17. Argon + NO (1740 ppm) on Cedar Grove High Volatile (Coal); M_o = 1.48 g; D = 12.0 cm^{3}s^{-1}.

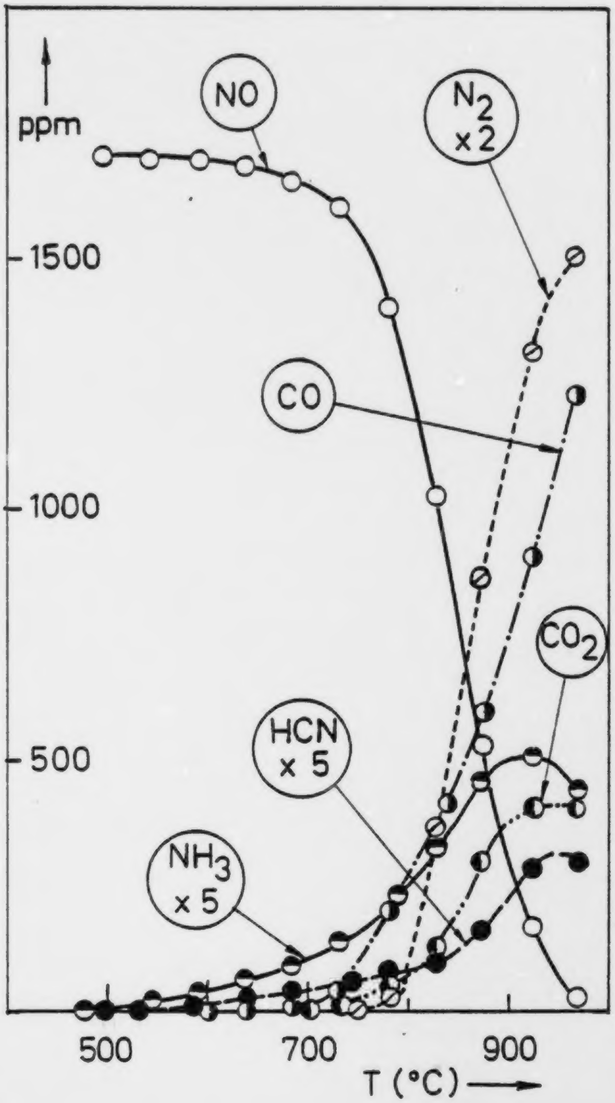

Figure 18. Argon + NO (1700 ppm) on Cedar Grove High Volatile (Char); M_o = 1.6 g; D = 12.0 cm^3s^{-1}.

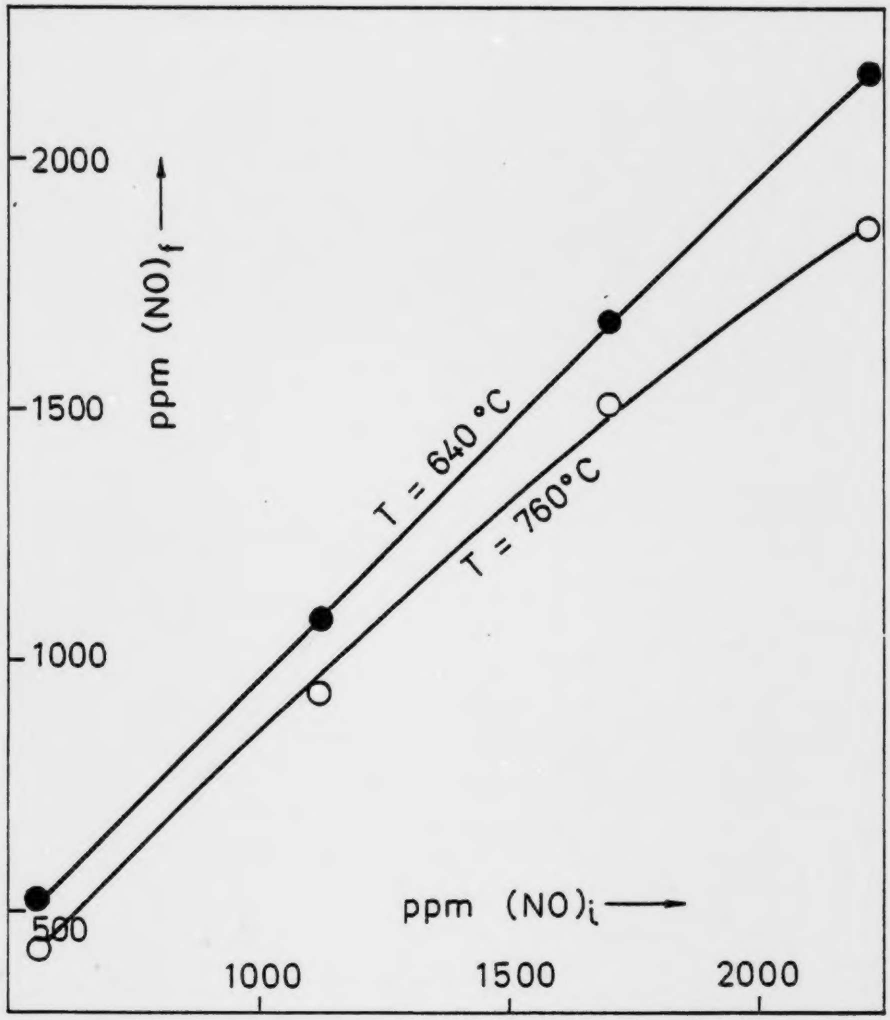

Figure 19. Argon + NO on Cedar Grove High Volatile (Char); $D = 12.1\ \text{cm}^3\text{s}^{-1}$; $M_0 = 1.59$ g; Effect of Initial NO Concentration.

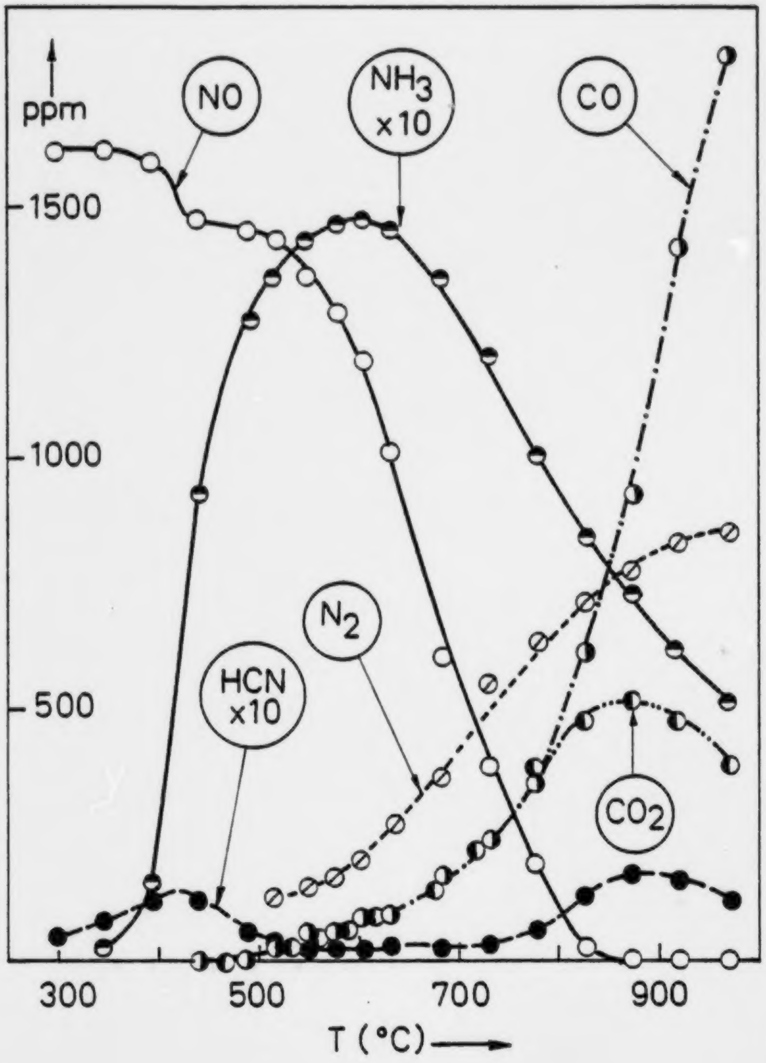

Figure 20. Argon + NO (1620 ppm) on Pocahontas Low Volatile, High Ash (Coal); M_0 = 1.55 g; D = 12.0 cm^3s^{-1}.

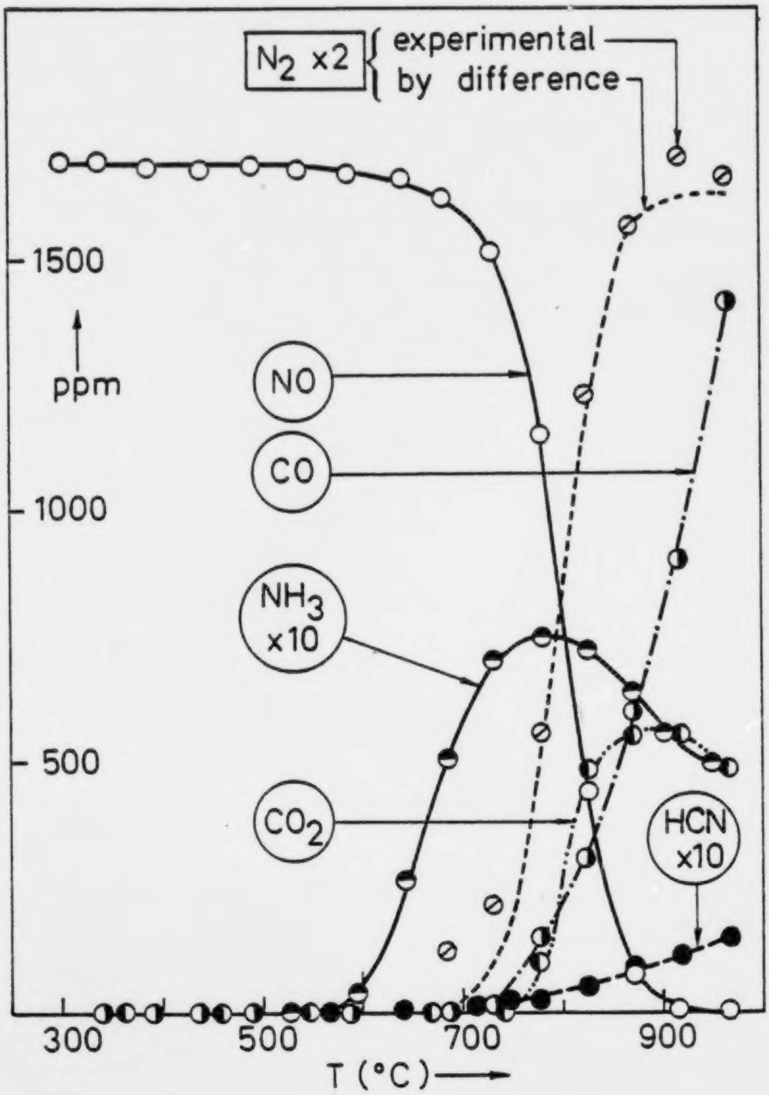

Figure 21. Argon + NO (1690 ppm) on Pocahontas Low Volatile, High Ash (Char); M_o = 1.6 g; D = 12.0 cm^3s^{-1}.

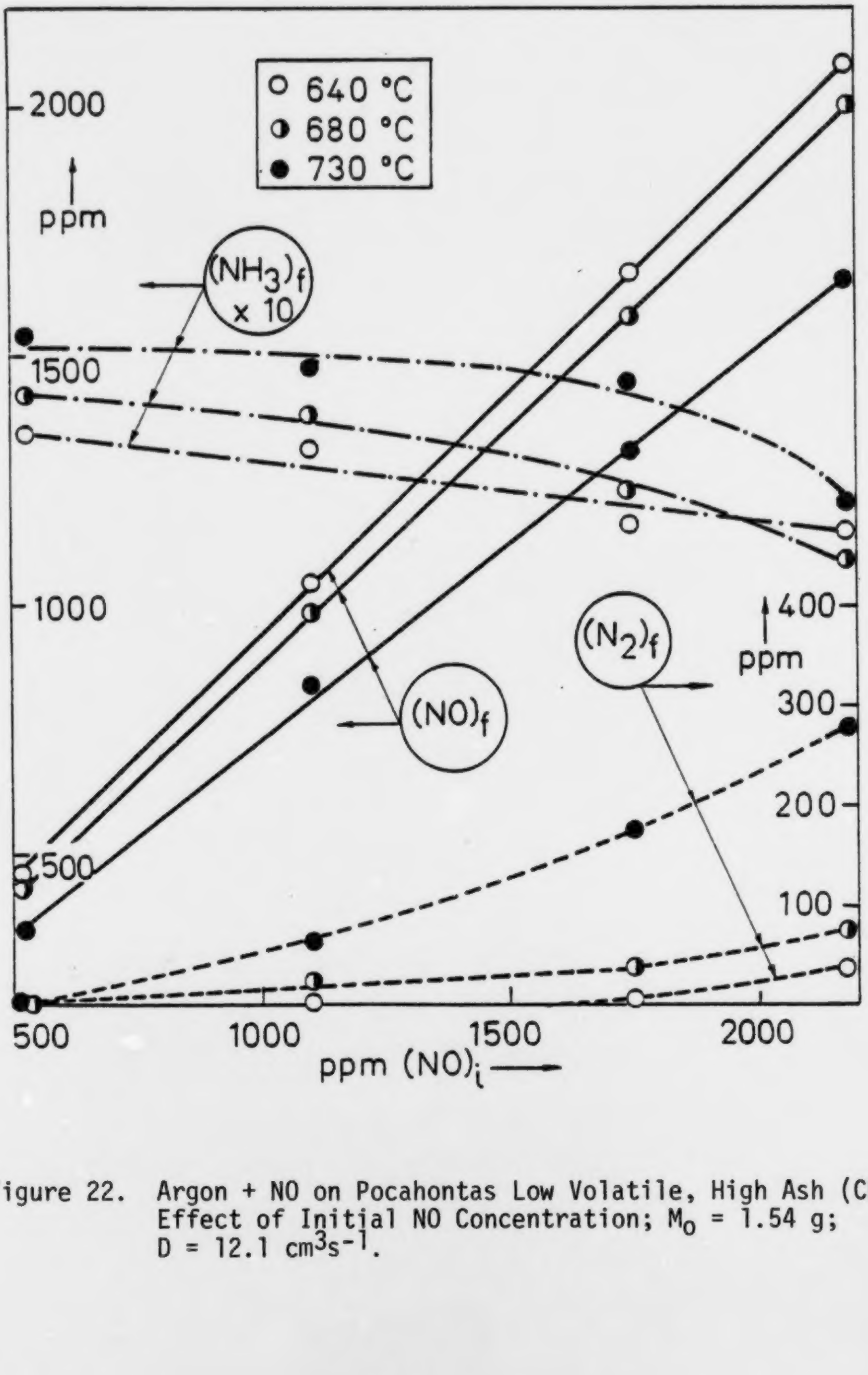

Figure 22. Argon + NO on Pocahontas Low Volatile, High Ash (Char); Effect of Initial NO Concentration; $M_0 = 1.54$ g; $D = 12.1\ cm^3s^{-1}$.

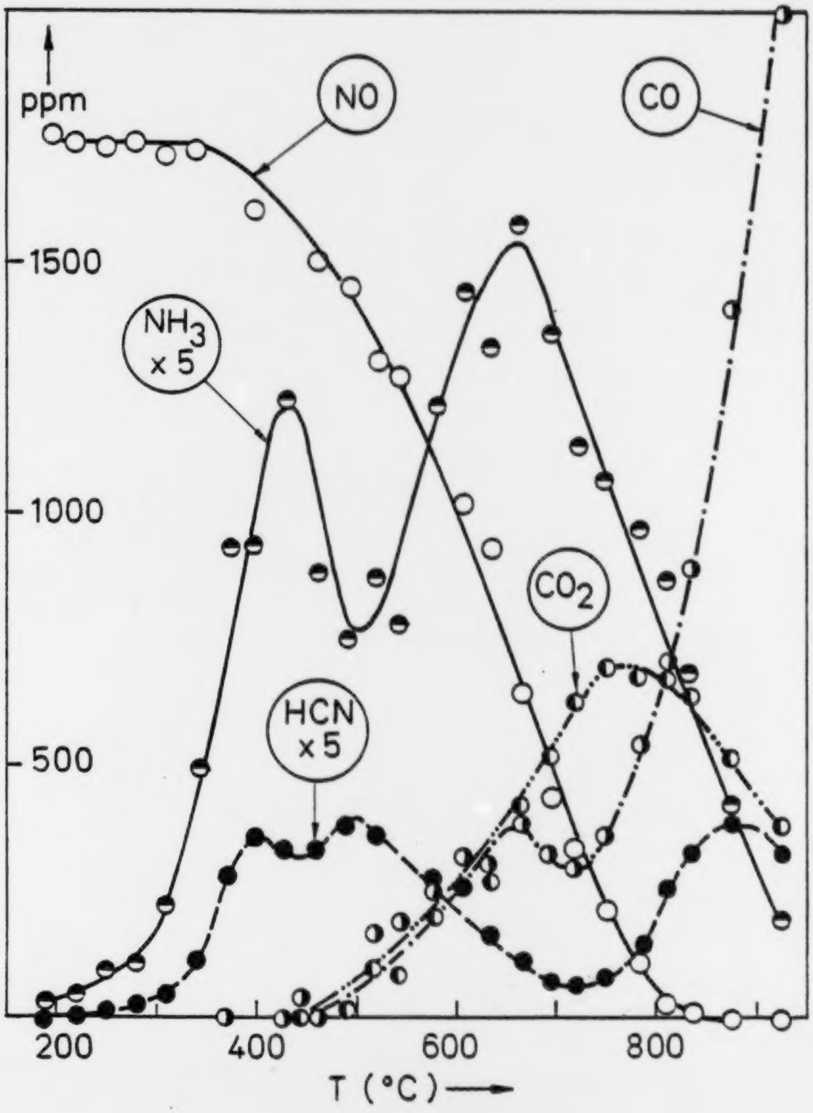

Figure 23. Argon + NO (1740 ppm) on South African "Rietspruit" (Coal); M_0 = 1.45 g; D = 12.0 cm^3s^{-1}; (50 to 100 microns).

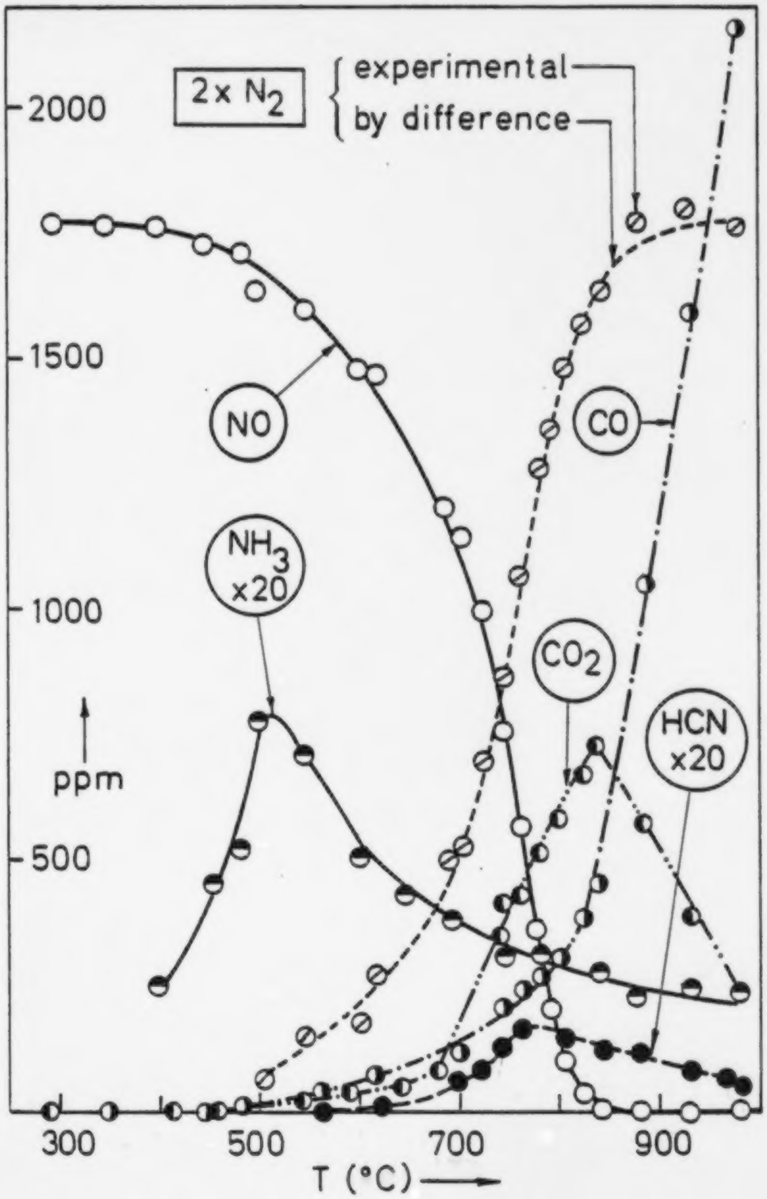

Figure 24. Argon + NO (1770 ppm) on South African "Rietspruit" (Char); M_0 = 1.6 g; D = 11.5 cm^3s^{-1}; (50 to 100 microns).

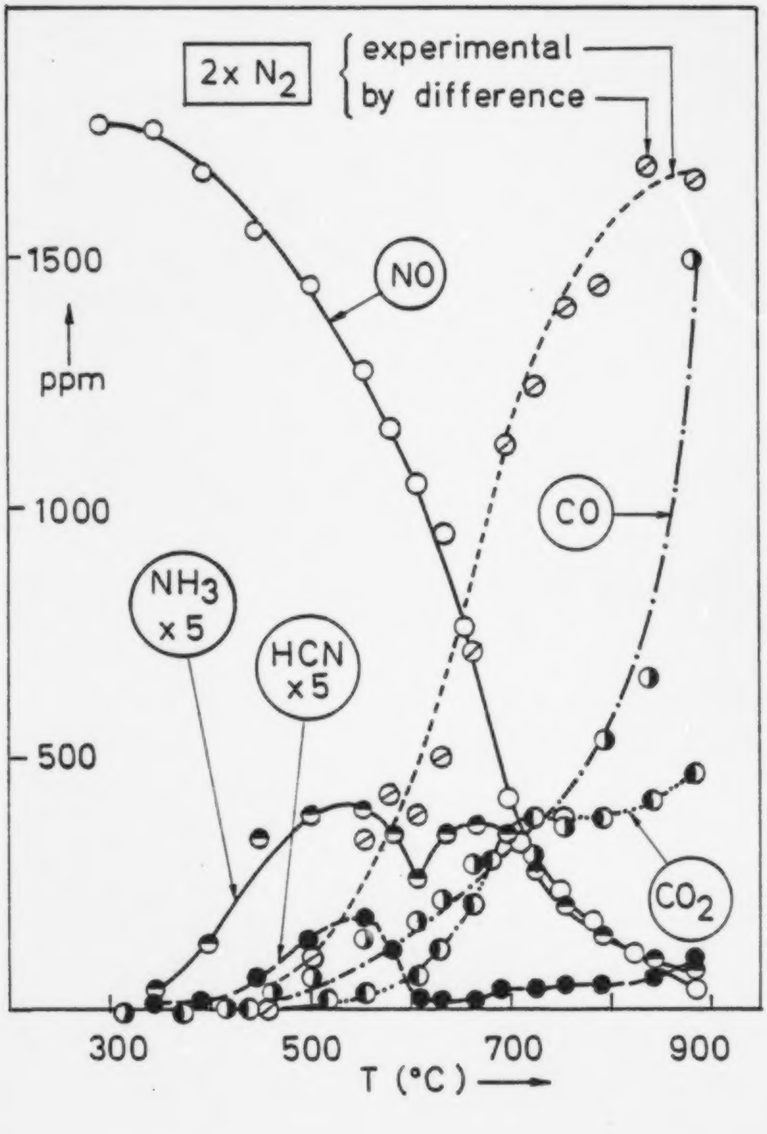

Figure 25. Argon + NO (1770 ppm) on Ruhr Coal "Prosper" (Coal); M_0 = 1 g; D = 12.0 cm^3s^{-1}.

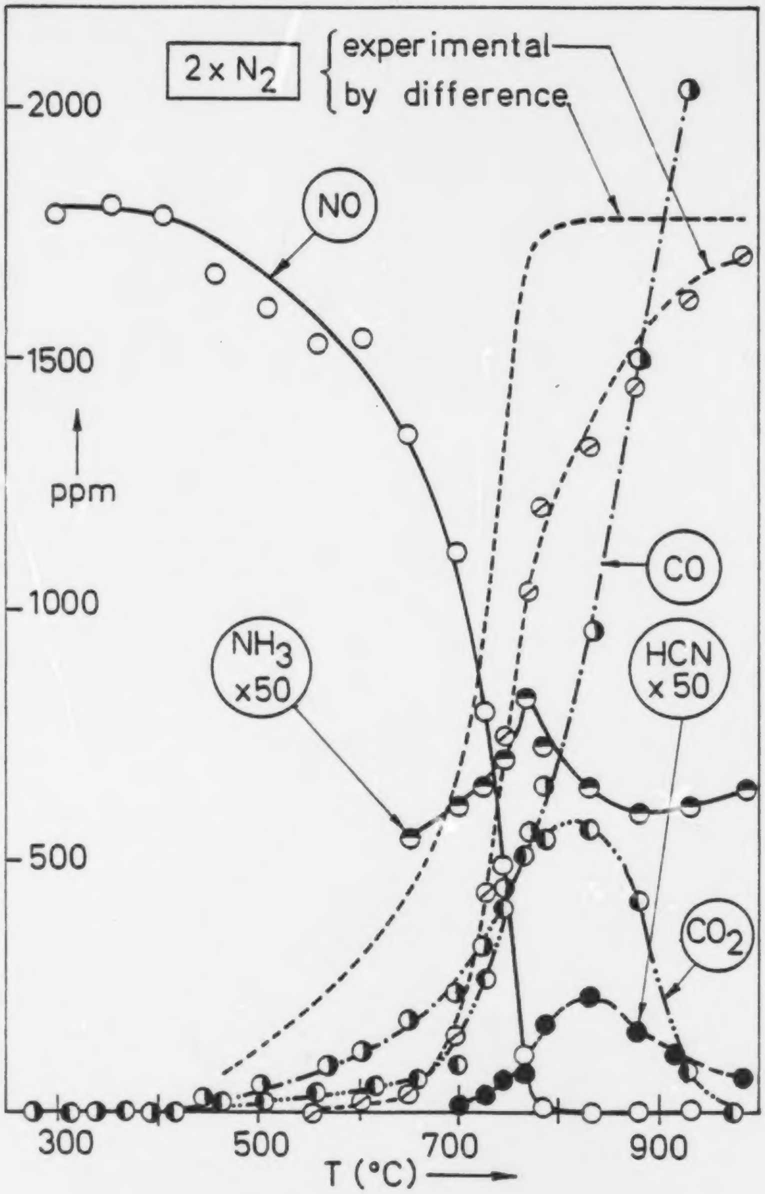

Figure 26. Argon + NO (1800 ppm) on "Prosper" Ruhr (Char); M_o = 1.6 g; D = 11.5 cm^3s^{-1}.

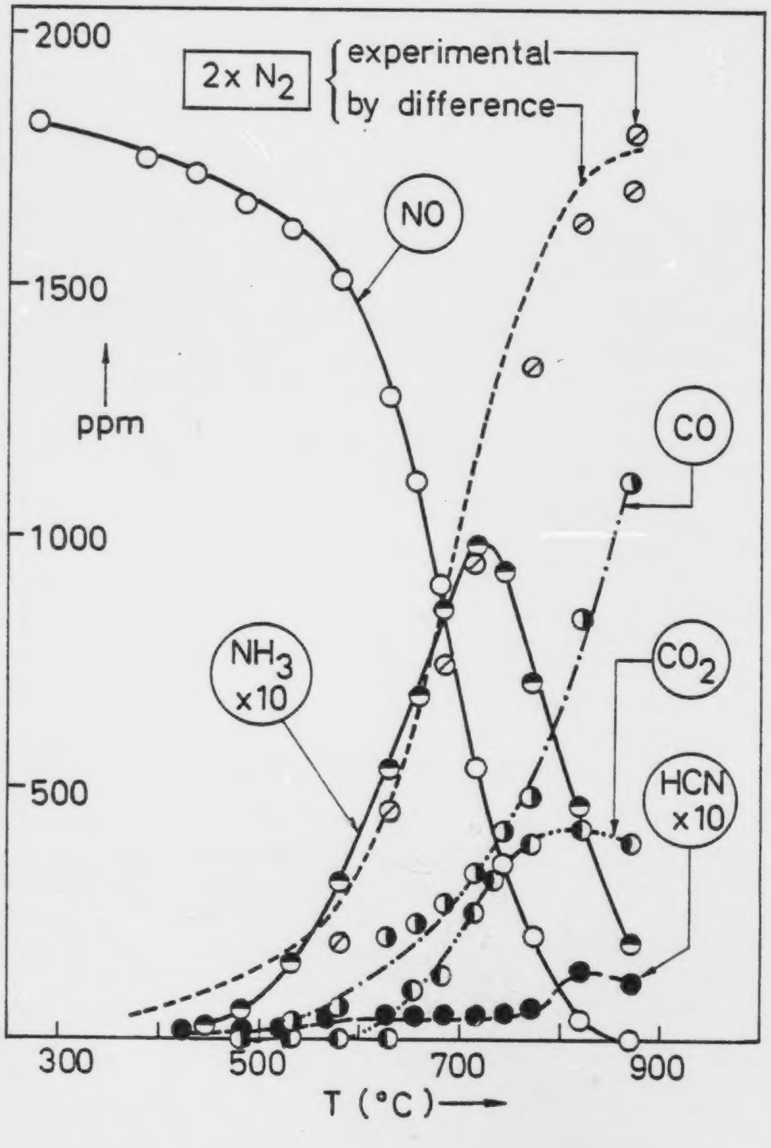

Figure 27. Argon + NO (1810 ppm) on Pennsylvania Anthracite (Coal); M_0 = 1.92 g; D = 11.5 cm^3s^{-1}.

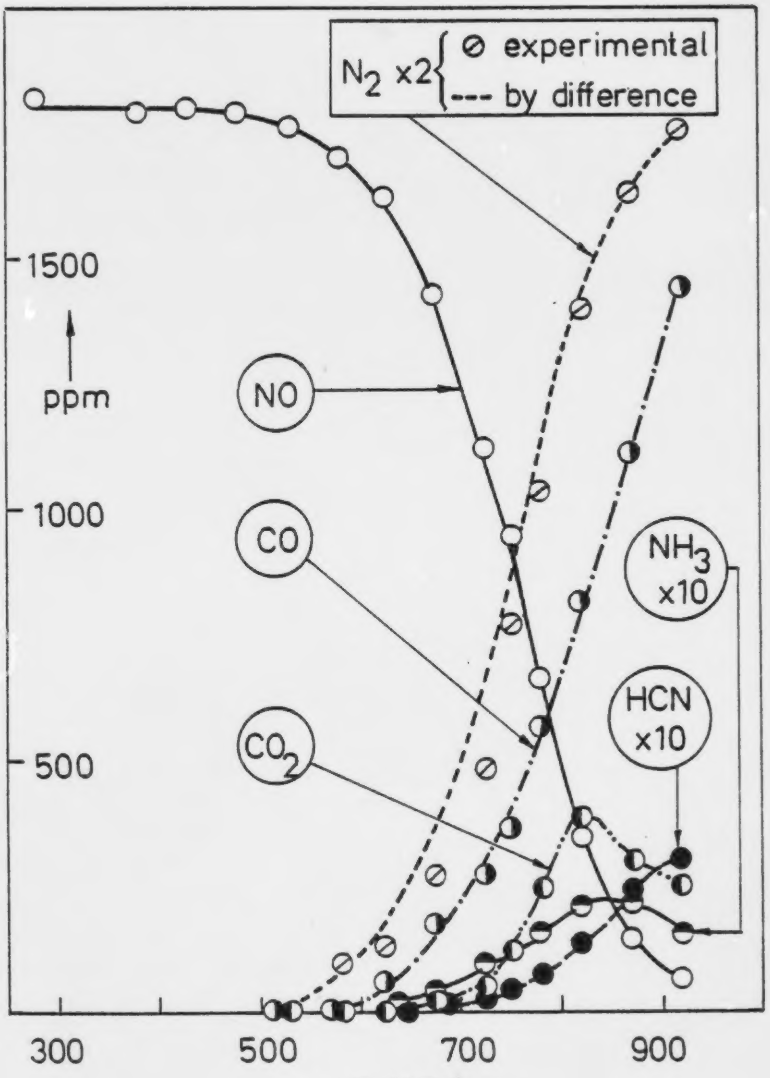

Figure 28. Argon + NO (1800 ppm) on Pennsylvania Anthracite (Char); M_0 1.7 g; D = 11.5 $cm^3 s^{-1}$.

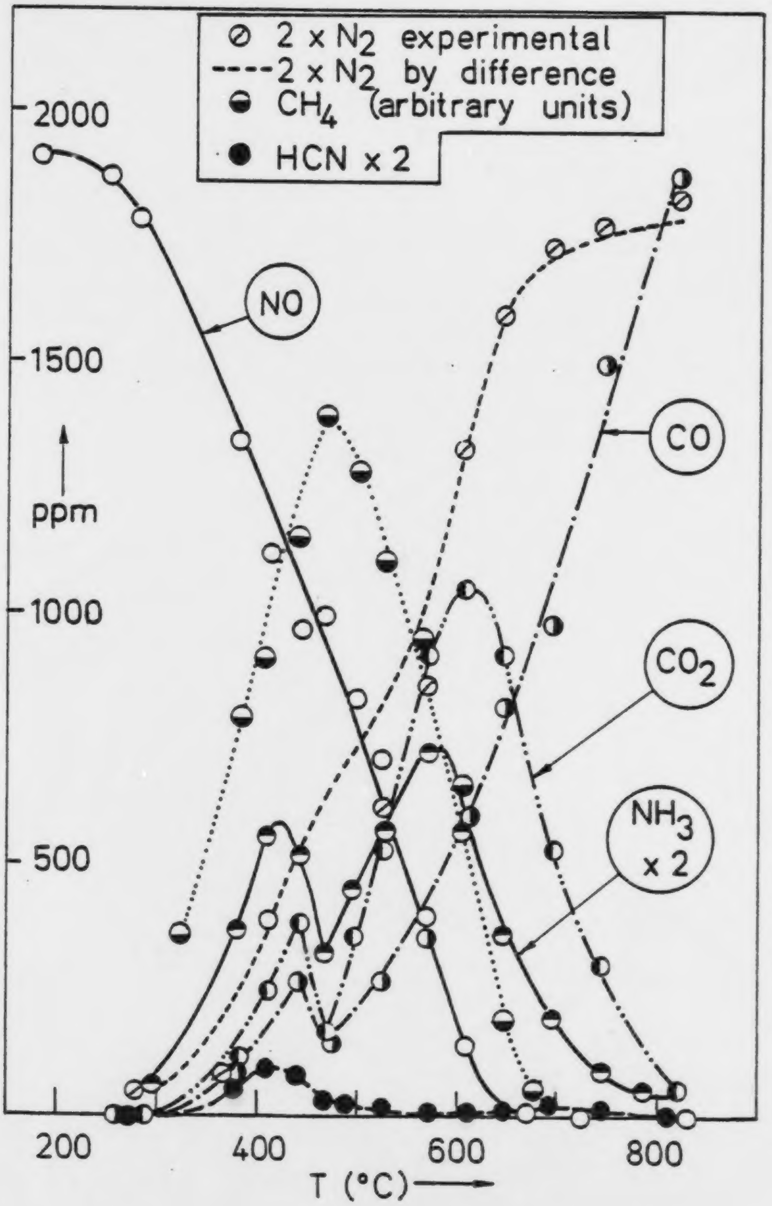

Figure 29. Argon + NO (1810 ppm) on "Beulah" Lignite (Coal); M_0 = 1.47 g; D = 11.7 cm^3s^{-1}.

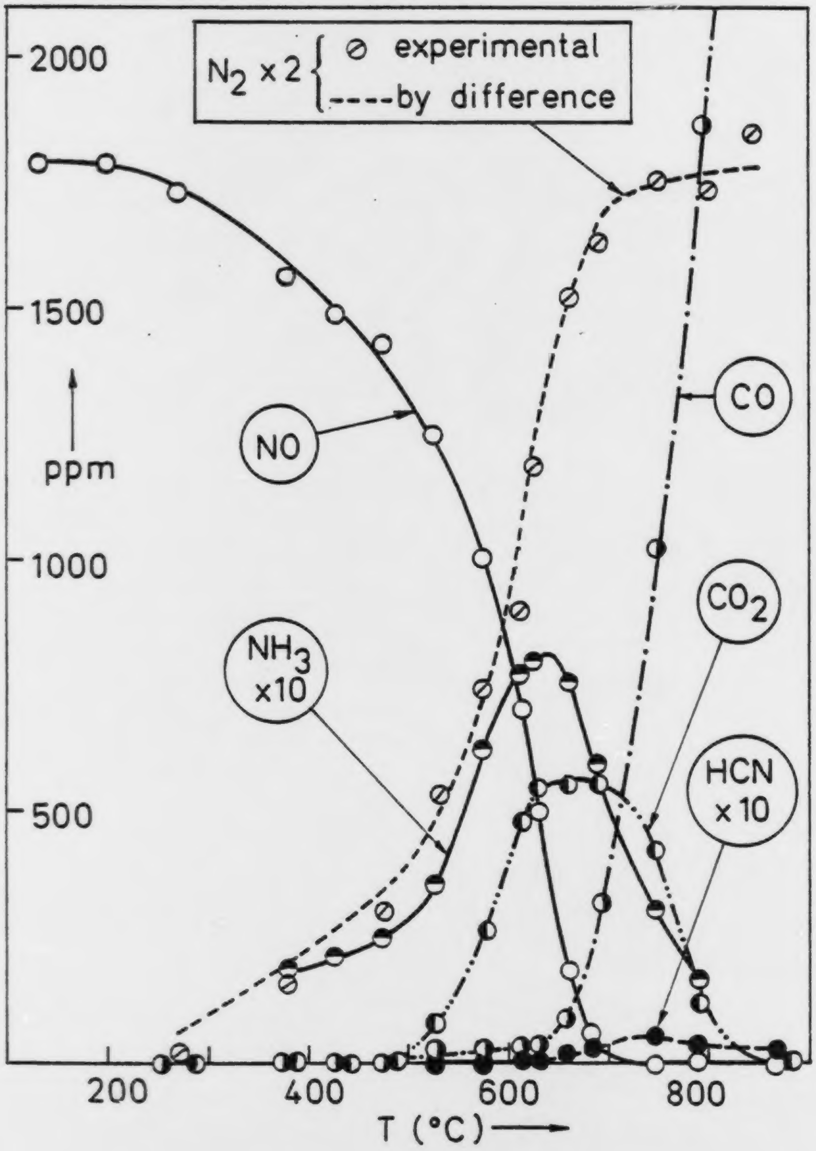

Figure 30. Argon + NO (1790 ppm) on "Beulah" Lignite (Char); M_0 = 1.8 g; D = 11.7 cm^3s^{-1}.

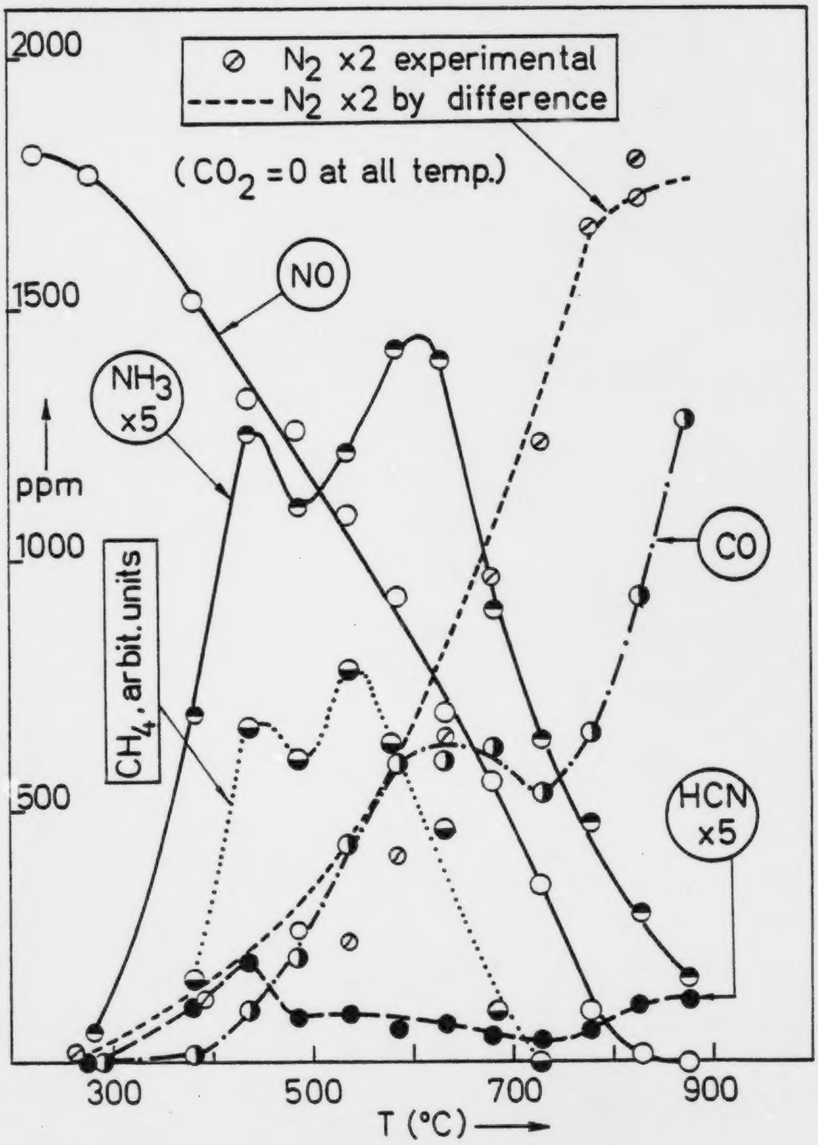

Figure 31. Argon + NO (1820 ppm) on Utah Bituminous (Coal); M_0 = 1.97 g; D = 11.3 cm^3s^{-1}.

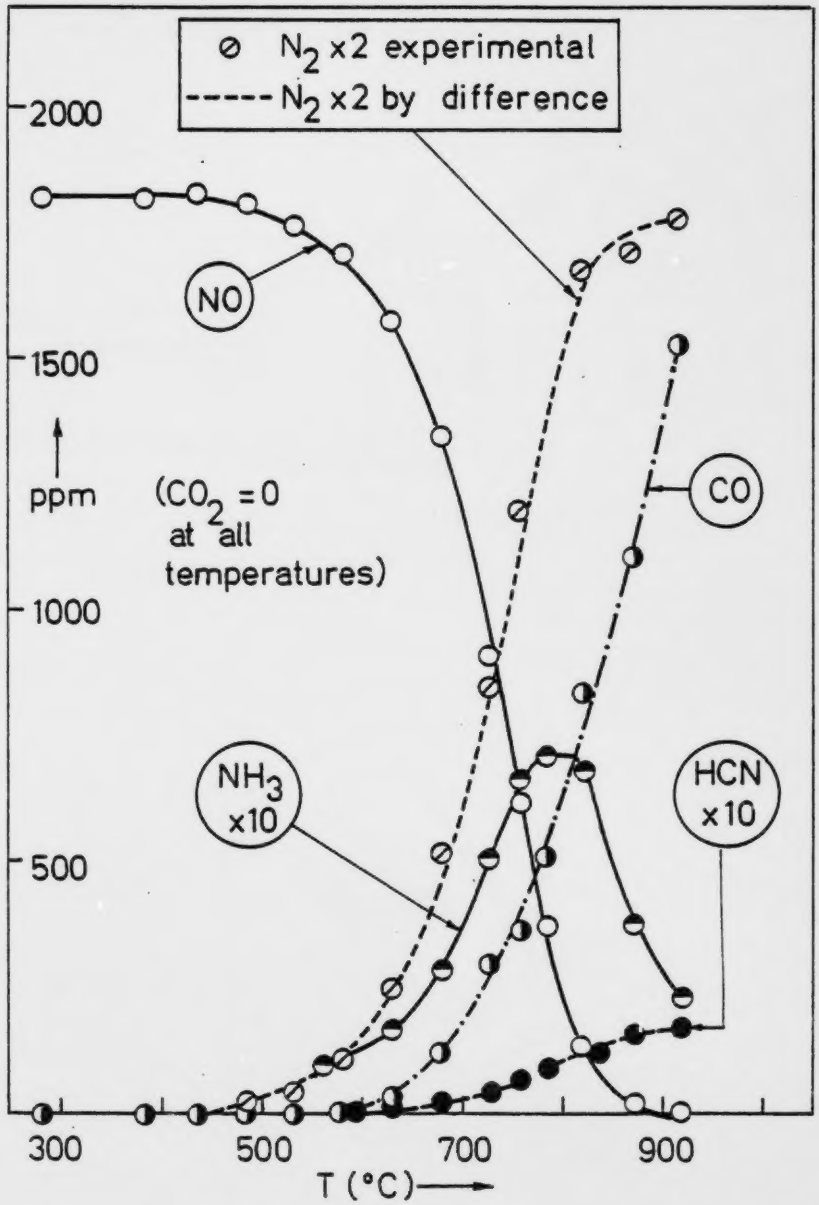

Figure 32. Argon + NO (1830 ppm) on Utah Bituminous (Char); M_0 = 1.08 g; D = 11.3 cm^3s^{-1}.

occurs by an indirect path from the ammonia intermediate, as suggested by the fact that the maximum of the HCN vs. T curve is shifted towards higher temperatures than is the case for the NH_3 maximum.

- During NO disappearance, substantial amounts of CO and nonnegligible quantities of CO_2 are formed. The CO released in these trials is much larger than the carbon monoxide released during pyrolysis runs on the same char, and therefore is probably formed partly from NO. The same applies for the CO_2 formed (normally no CO_2 at all was found in the pyrolysis products of the chars). CO and CO_2 are thus suggested to be products of the NO reduction reactions.

The above observations are consistent with the general heterogeneous NO reduction mechanism derived previously (Part I) and are in qualitative agreement with the existence of the following overall reducing reactions*:

$$NO + (-C) \xrightarrow{1} N_2 + CO + CO_2$$

$$NO + (-C) + (-H) \xrightarrow{2} NH_3 + CO + CO_2 + H_2O$$

The formation of CO (by reactions 1 and 2, as well as by char pyrolysis) also brings the following reaction into the mechanism:

$$NO + CO \xrightarrow{8} N_2 + CO_2$$

The NH_3 formed by reaction 2 can be transformed into N_2, either directly by decomposition or by reacting NH_3 with NO:

$$NH_3 \xrightarrow{13} N_2 + H_2$$

$$NH_3 + NO \xrightarrow{4} N_2 + H_2O + H_2$$

or indirectly, via the intermediate formation of HCN:

---

*Throughout this report, the specific overall reactions occurring in the NO reduction mechanism, are numbered as in the previous part of this final report. For convenience, however, the stoichiometric coefficients are not given in the present part.

$$NH_3 + (-C) \xrightarrow{5} HCN + H_2 .$$

HCN is, in turn, transformed into N_2 either by decomposition*

$$HCN \xrightarrow{15} N_2 + H_2 + C$$

or by reacting with NO:

$$HCN + NO \xrightarrow{40} N_2 + CO_2 + H_2 .$$

HCN may also be retransformed into NH_3 by the equilibrated reaction

$$HCN + H_2O \underset{9}{\overset{44}{\rightleftharpoons}} CO + NH_3$$

or by reacting with hydrogen:

$$HCN + H_2 \xrightarrow{45} NH_3 + C$$

2.1.2.2 Trials on Coal Particles

Results of these trials are illustrated in Figures 14, 17, 20, 23, 25, 27, 29, and 31. By comparing these coal results with the corresponding char trials, the following observations can be readily made:

- In all cases, the overall NO disappearance occurs at somewhat lower temperatures.
- Although the main reduction product still is molecular nitrogen (see Figures 20, 25, 27, 29, and 31 for comparison between experimental N_2 concentrations and values computed from eq. 1), the concentrations of intermediate nitrogen species are larger in the case of coal trials. This is especially the case for NH_3. This observation held true even after correction of these concentrations for HCN and NH_3 released by coal devolatilization.
- At temperatures between 400 and 600°C the first NO decrease is observed for some trials (see e.g. Figures 14, 17, and 20; it should be noted that in all these cases the coal particles are

---

*Identification and reaction rates of reactions including HCN as a reactant, will be discussed in Part III of this report.

relatively large). This early partial NO decrease seems to be related to the devolatilization process, which is most important in this temperature range, as is exemplified by the methane released (see Figures 29 and 31).

- In this same temperature range, NH_3 and HCN primarily go through a first maximum (except in the case of anthracite coal, where the volatiles content is too small, see Figure 27). This first maximum of HCN in the coal devolatilization phase, is almost entirely accounted for by the HCN released during devolatilization, as may be seen by comparing with pyrolysis trials under pure argon flow (see paragraph 2.1.1.1). On the other hand, the first NH_3 peak observed during the intense devolatilization phase is much higher than the NH_3 peak observed with pure argon flow.

Two main conclusions are suggested from the observations made above:

- In the temperature range (400 to 600°C approximately) where coal devolatilization is relatively intense, there seems to exist a fast, although limited, NO reduction (as shown by the (NO)/T profiles and the enhanced NH_3 formation). It is not clear whether this reduction is of a homogeneous or a heterogeneous character, although it is obvious that the released volatiles (H_2, CO, hydrocarbons) play a role as coreactants. There are indications that particle size plays a role in the existence or extent of this low temperature reduction.

- At higher temperatures, where devolatilization rates become less important, the NO decrease nevertheless is much faster than for the corresponding char. This probably is due to the fact that, since devolatilization is more incomplete in the coal runs than in the char runs (at a given temperature), and the bound hydrogen content is larger than in the char runs, reaction 2 is enhanced. This explanation is in agreement with the higher $\left(NH_3\right)_f$ concentrations observed in the coal runs as compared to the char runs.

2.1.3 Trials With Argon + NO + CO

2.1.3.1 Trials on Char Particles

Typical results of these runs are presented in Figures 34 to 39 and in Figures 42, 44, 46, 48, and 50. The following experimental observations can be made for these trials:

- An examination of the CO/T profiles reveals much concerning the reaction mechanism. In the temperature range where NO begins to disappear, the CO concentration decreases and CO_2 appears. These facts indicate that reaction 8 is at least partially responsible for NO reduction, and is even more important than reactions 1 and 2, which yield CO as a product. The relative importance of reactions 1, 2, and 8 will be discussed later.

  At higher temperatures (especially above $700^{o}C$) substantial amounts of CO are released by char pyrolysis (see Figures related to argon on char). This CO release starts to compensate for the CO removal by reaction 8 and, at still higher temperatures, the net effect of these two contrary factors results in an overall increase of $(CO)_f$.

- During NO disappearance, the HCN release can be entirely accounted for by char pyrolysis, and is independent of the initial NO and CO concentrations. The ammonia released during NO decrease does not depend directly on the initial CO concentration, nor does it increase with the initial NO concentration (see Figure 38). The latter point may be surprising, since NH_3 should be formed primarily by reaction 2. This discrepancy, however, may be explained by the fact that, when $(NO)_i$ is increased, the rate of reaction 4 also increases, which in turn reduces NH_3 into N_2. The NH_3 levels are slightly higher than for trials in which CO is absent (see paragraph 2.1.2.1). This may be considered to be an indication of the existence of an ammonia formation reaction in which CO is a reactant:

$$CO + NO + (-H) \xrightarrow{6} NH_3 + CO_2$$

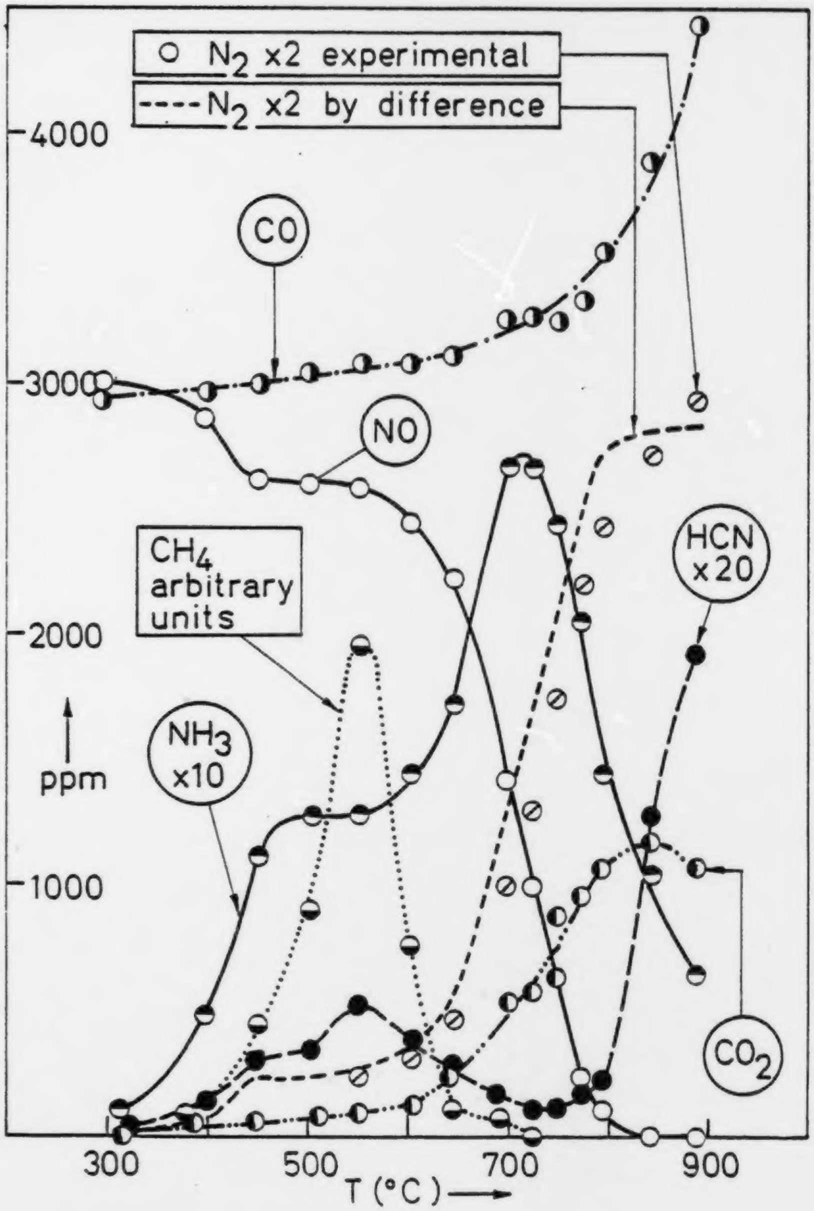

Figure 33. Argon + NO (3000 ppm) + CO (0.32%) on Pocahontas Medium Volatile (Coal); M_o = 1.49 g; D = 10.8 cm^3s^{-1}.

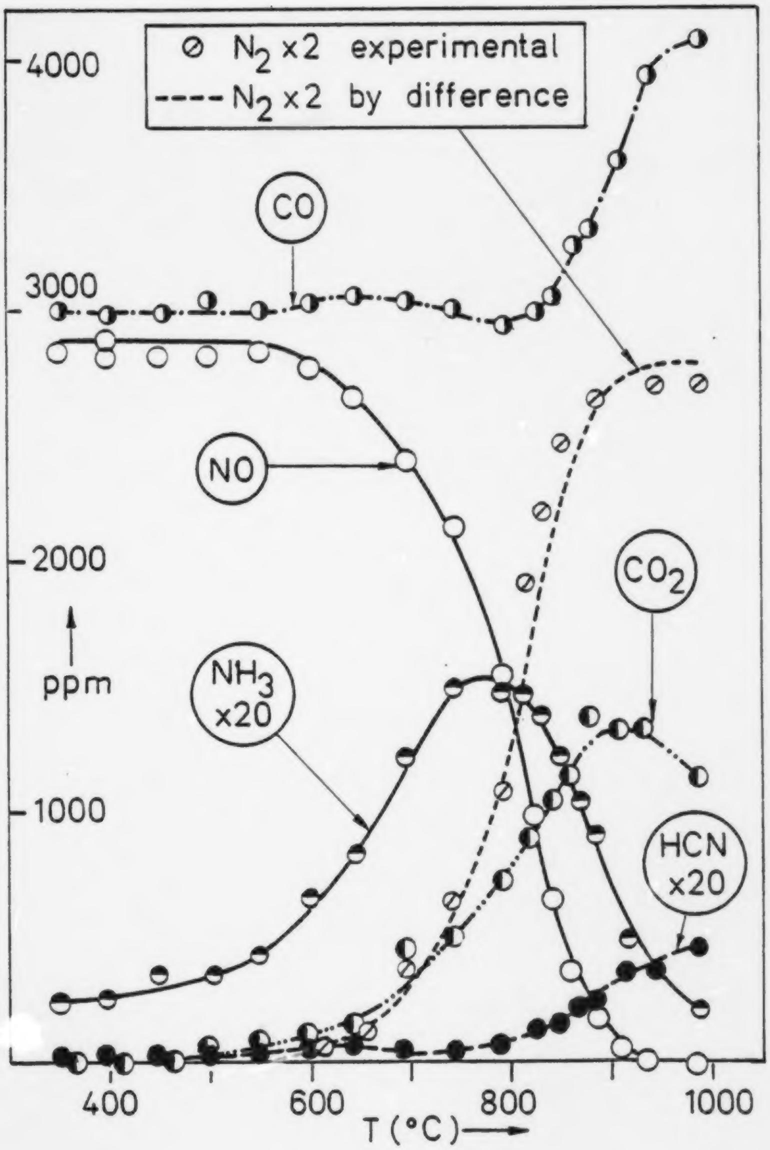

Figure 34. Argon + NO (2880 ppm) + CO (0.32%) on Pocahontas Medium Volatile (Char); M_0 = 1.6 g; D = 10.8 cm^3s^{-1}.

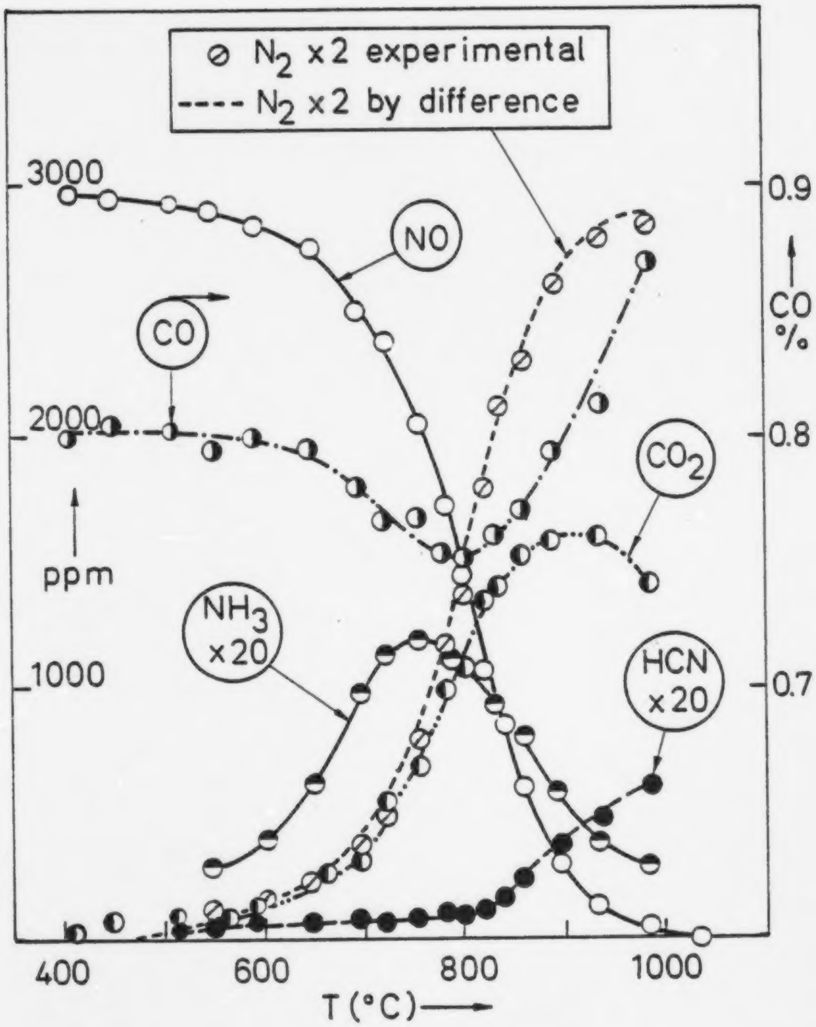

Figure 35. Argon + NO (3000 ppm) + CO (0.80%) on Pocahontas Medium Volatile (Char); M_0 = 1.6 g; D = 10.4 cm^3s^{-1}.

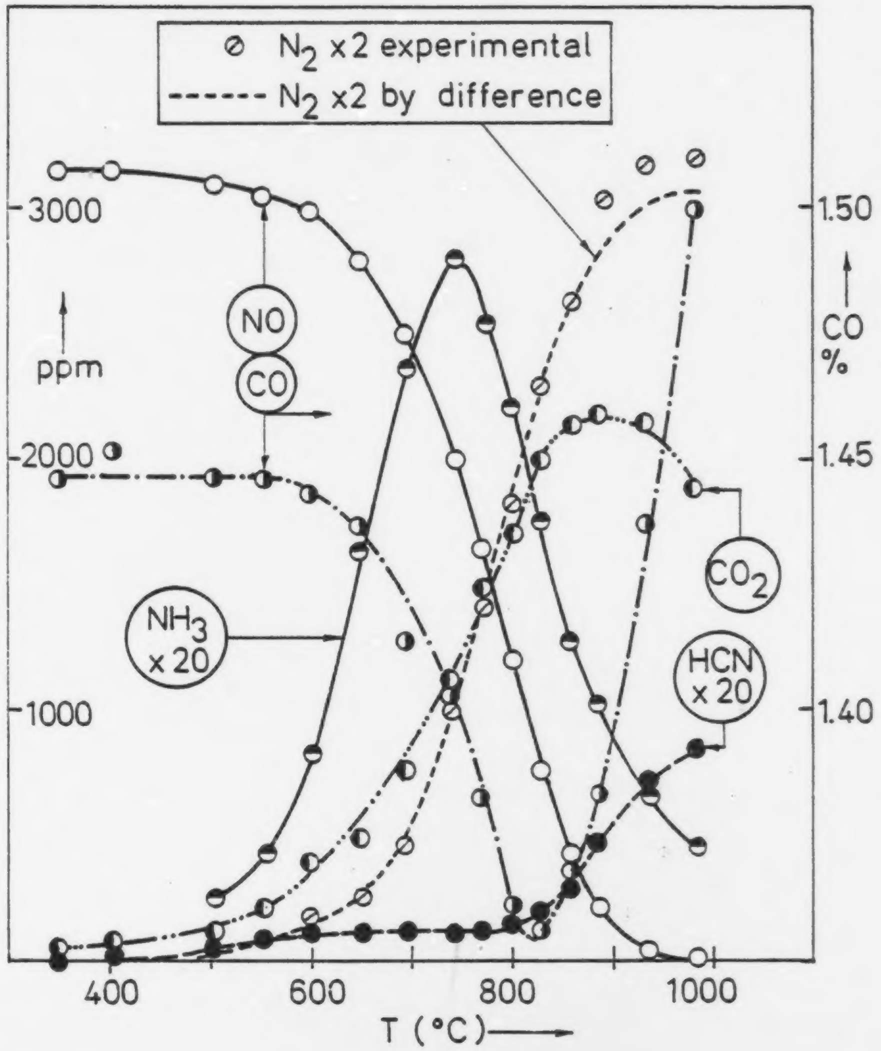

Figure 36. Argon + NO (3150 ppm) + CO (1.45%) on Pocahontas Medium Volatile (Char); M_0 = 1.6 g; D = 10.4 cm^3s^{-1}.

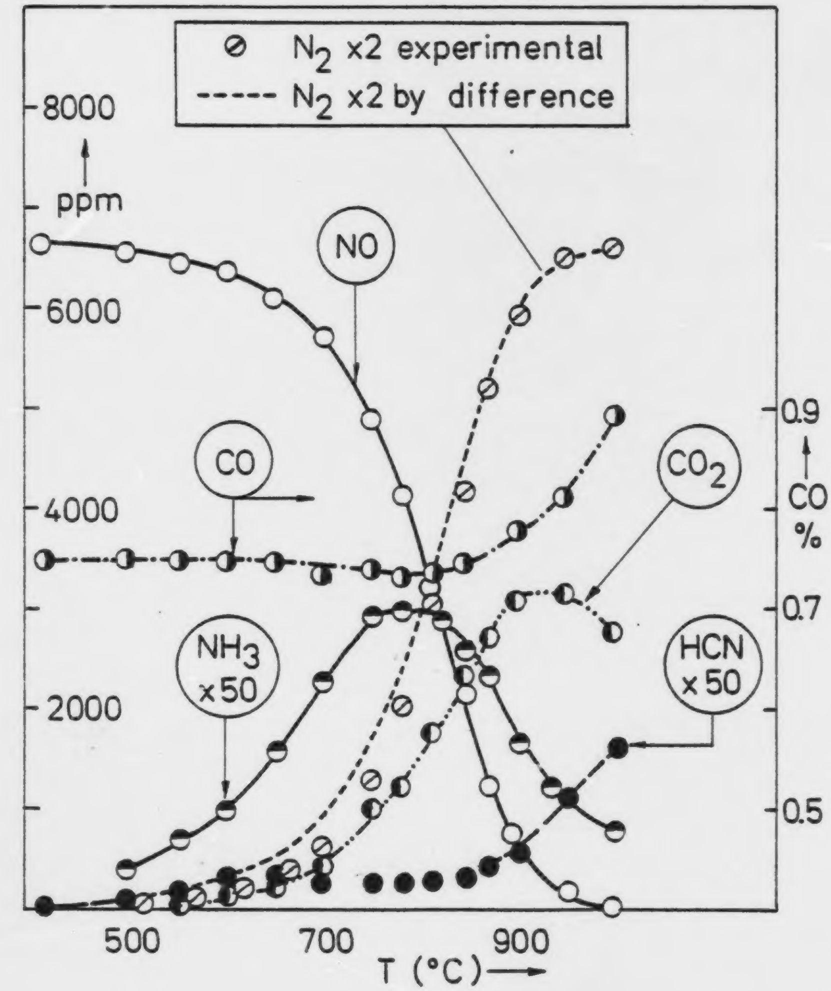

Figure 37. Argon + NO (6700 ppm) + CO (0.75%) on Pocahontas Medium Volatile (Char); M_0 = 1.6 g; D = 10.5 cm^3s^{-1}.

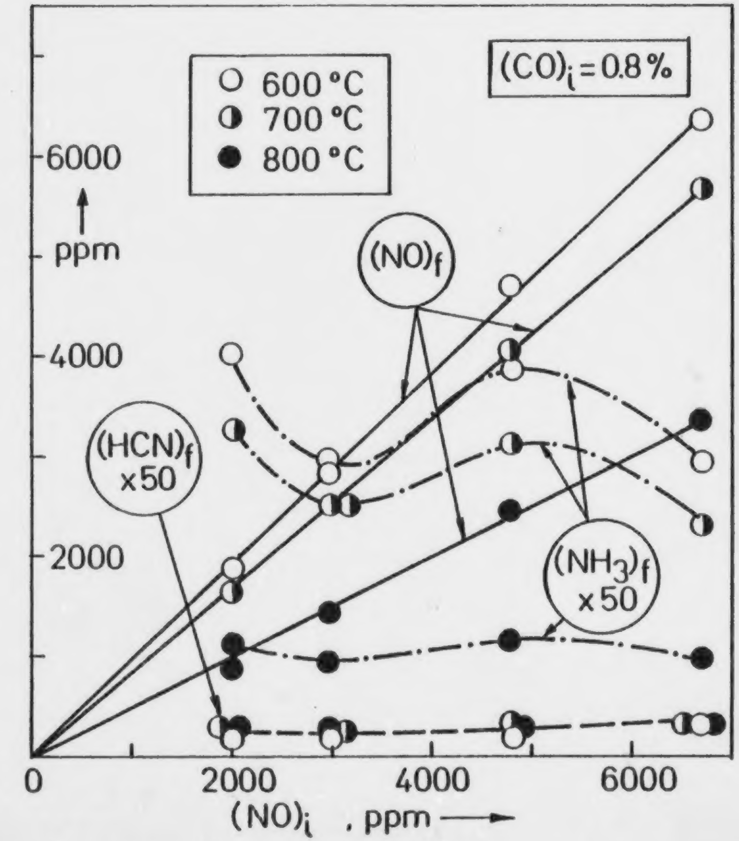

Figure 38.

Argon + NO + CO (0.8%) on Pocahontas Medium-Volatile (Char): Effect of Initial NO Concentration; $M_0 = 1.6$g; $D = 10.4$ cm^{3}s^{-1}.

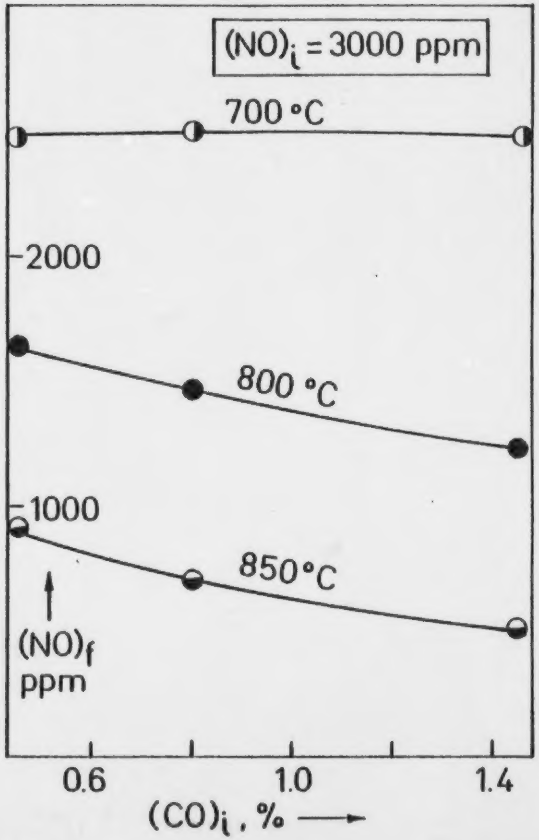

Figure 39.

Argon + NO (3000 ppm) + CO on Pocahontas Medium-Volatile (Char): Effect of Initial CO Concentration.

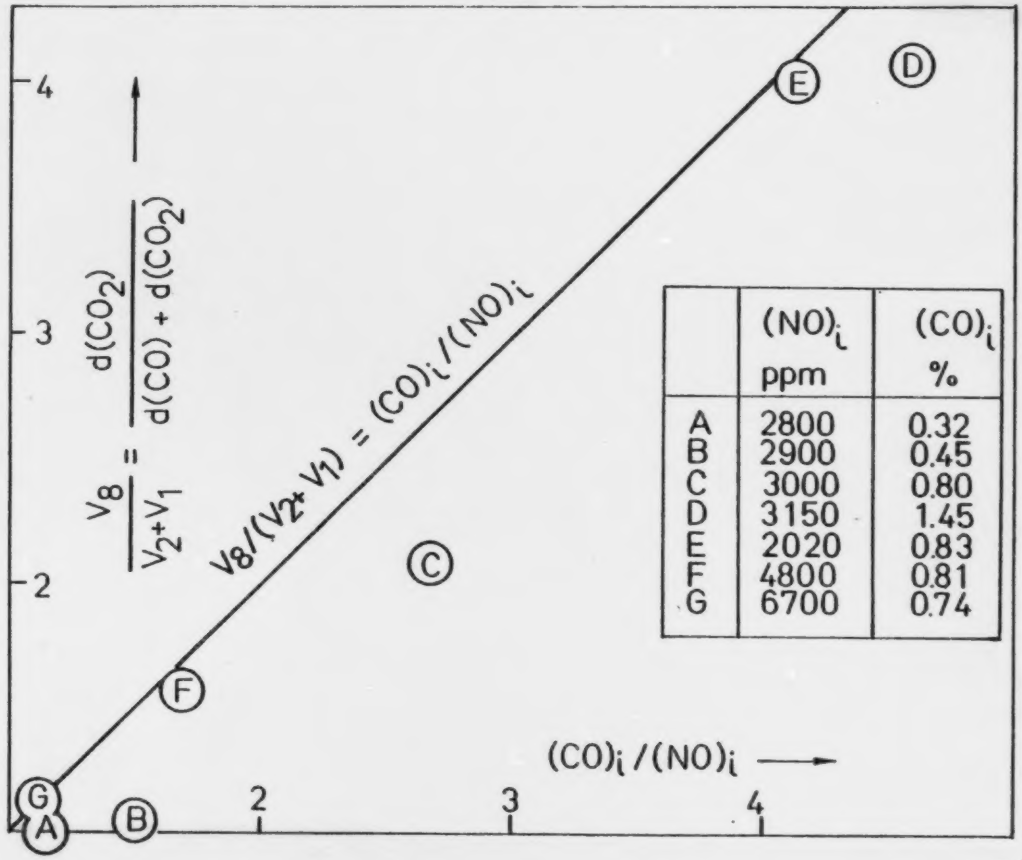

	$(NO)_i$ ppm	$(CO)_i$ %
A	2800	0.32
B	2900	0.45
C	3000	0.80
D	3150	1.45
E	2020	0.83
F	4800	0.81
G	6700	0.74

Figure 40. Argon + NO + CO on Pocahontas Medium Volatile (Char); Relative Importance of (V_8) and $V_1 + V_2$) in the Heterogeneous Reduction of NO, as a Function of the Initial (CO)/(NO) Ratio; M_0 = 1.6 g; D = 10.4 cm^3s^{-1}; T = 700°C.

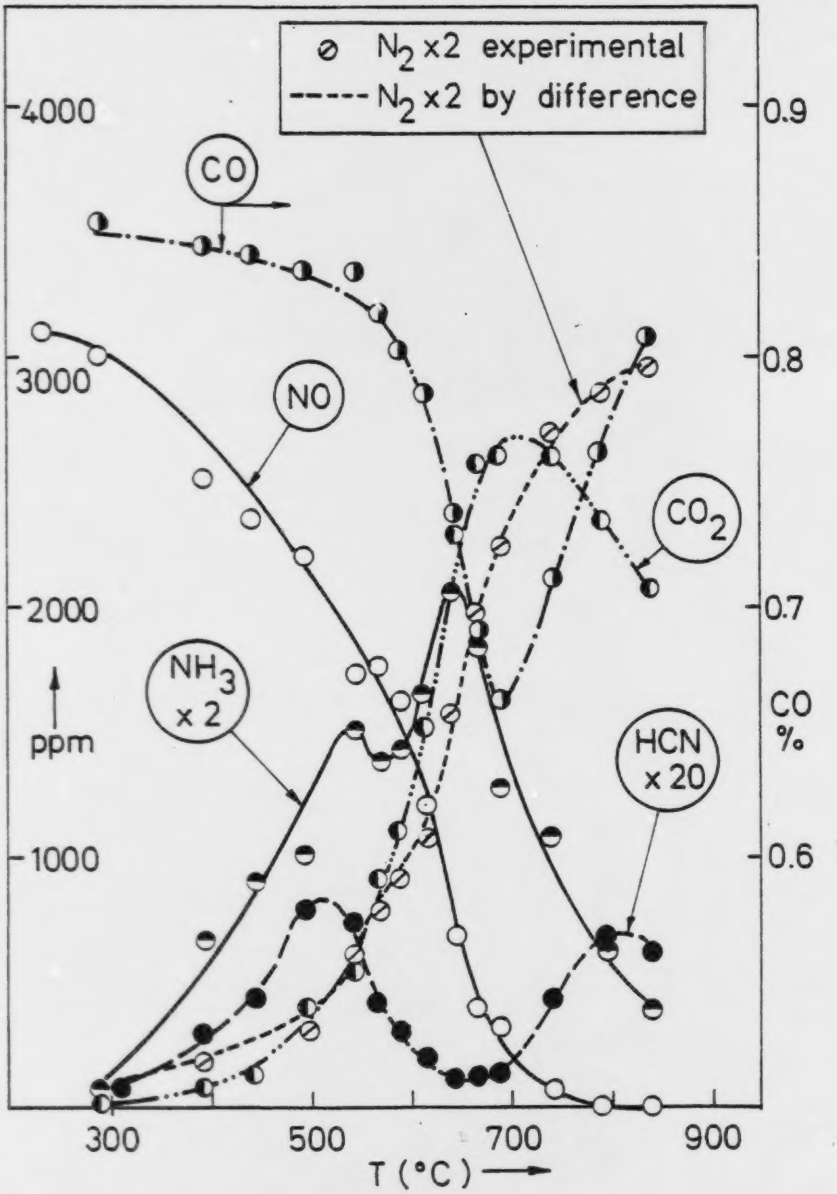

Figure 41. Argon + NO (3180 ppm) + CO (0.83%) on South African "Rietspruit" (Coal); M_0 = 1.45 g; D = 9.7 cm^3s^{-1}; (50/100 μ).

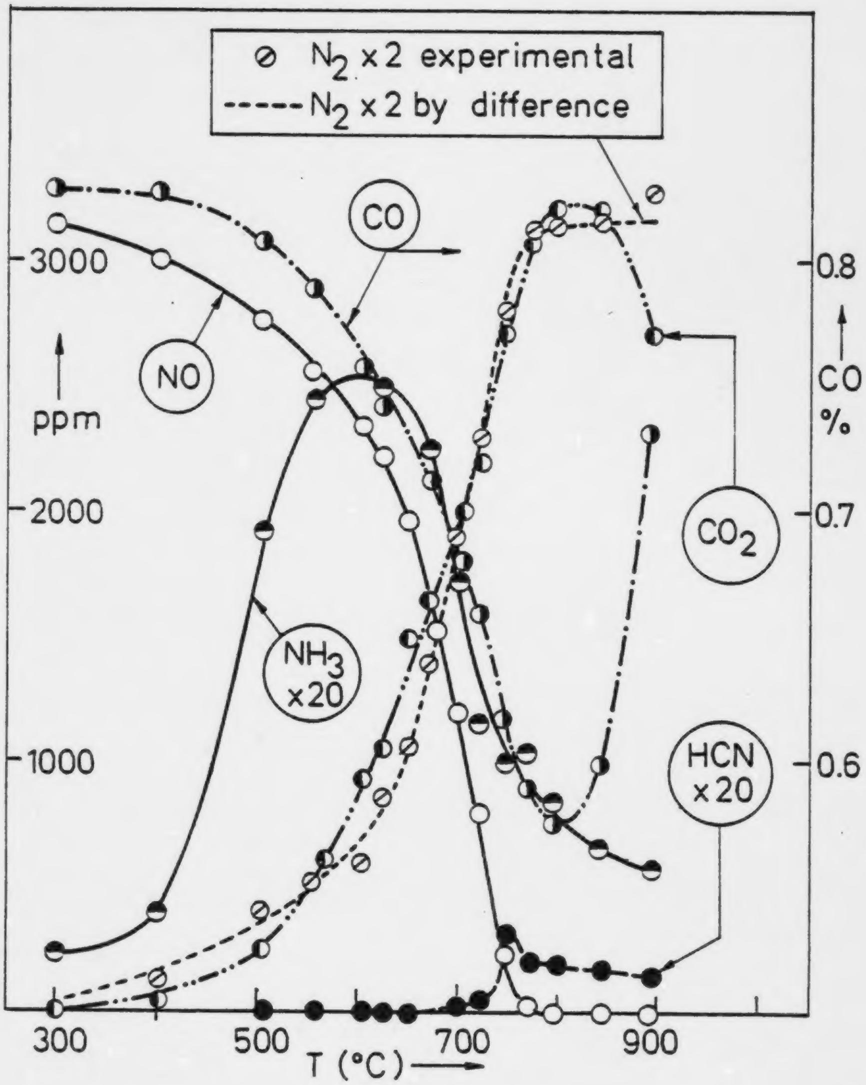

Figure 42. Argon + NO (3200 ppm) + CO (0.83%) on South African "Rietspruit" (Char); M_0 = 1.6 g; D = 10.4 cm^3s^{-1}. (50/100 μ).

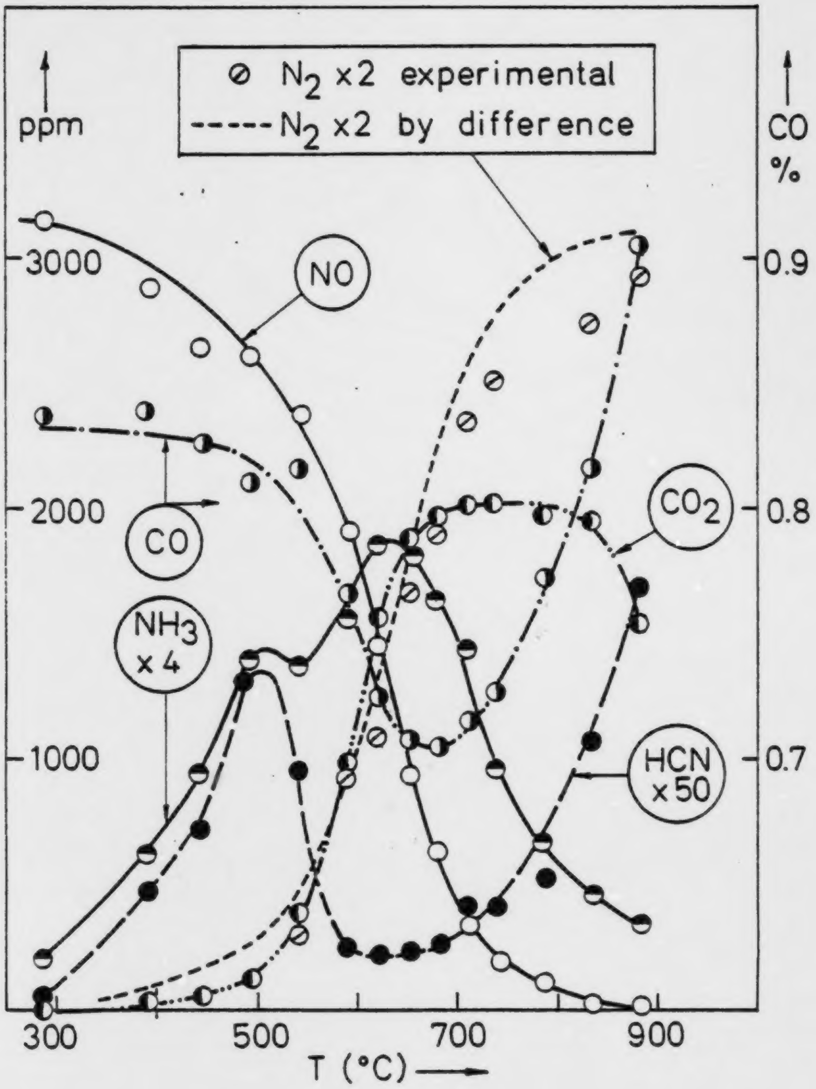

Figue 43. Argon + NO (3200 ppm) + CO (0.83%) on Ruhr Coal "Prosper" (Coal); M_0 = 1 g; D = 9.8 cm^3s^{-1}.

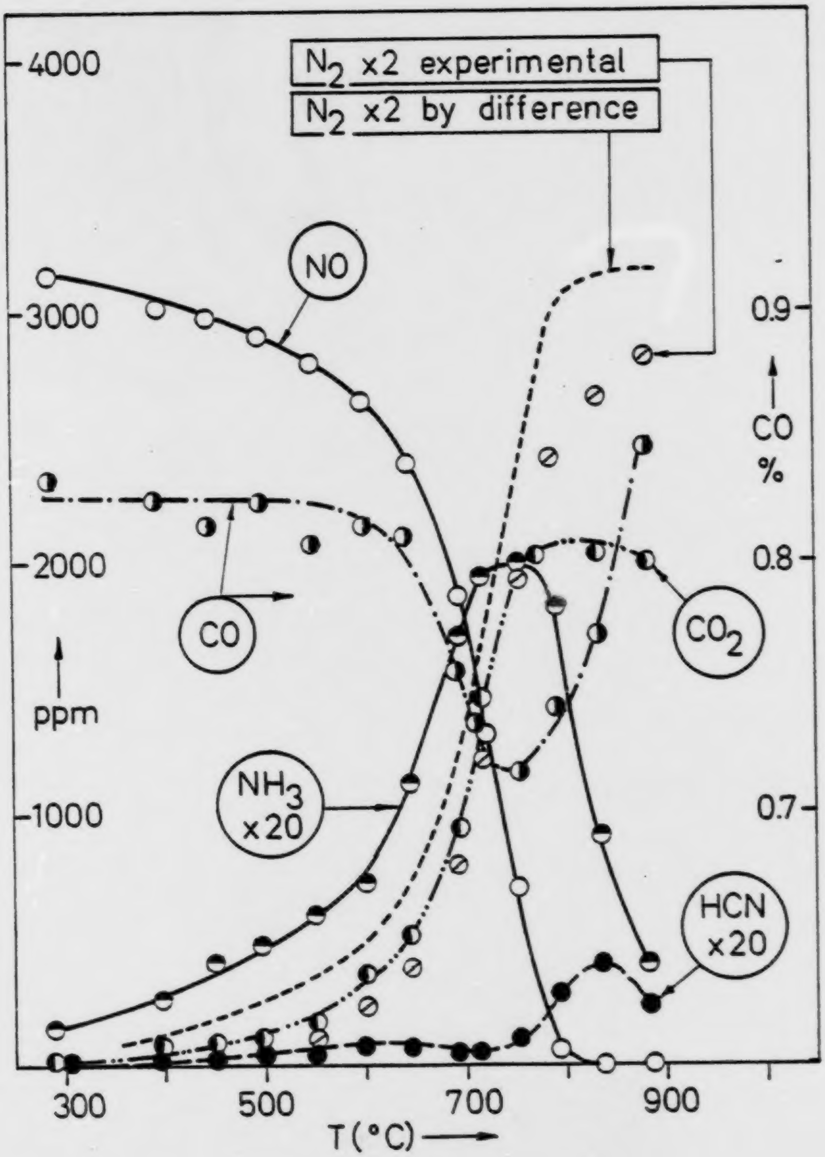

Figure 44. Argon + NO (3200 ppm) + CO (0.83%) on "Prosper" Rhur (Char); M_0 = 1 g; D = 9.8 cm^3s^{-1}.

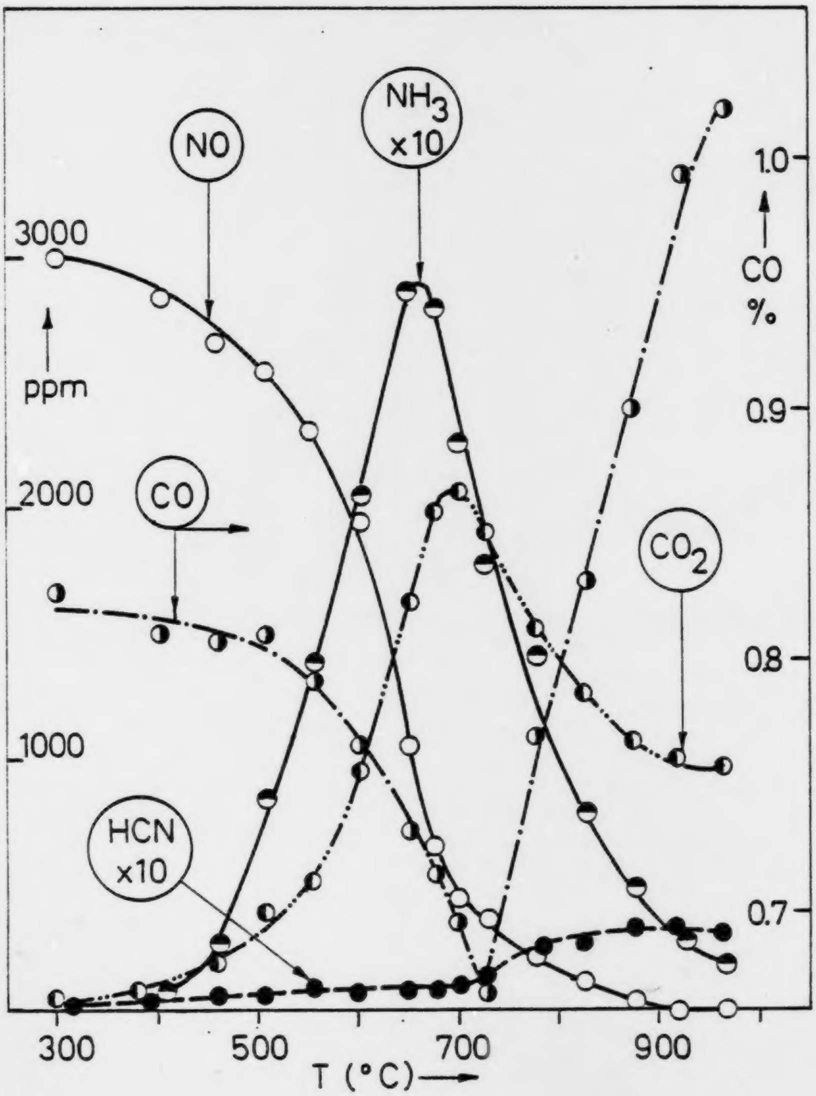

Figure 45. Argon + NO (3080 ppm) + CO (0.82%) on Pennsylvania Anthracite (Coal); M_o = 1.92 g; D = 9.9 cm^3s^{-1}.

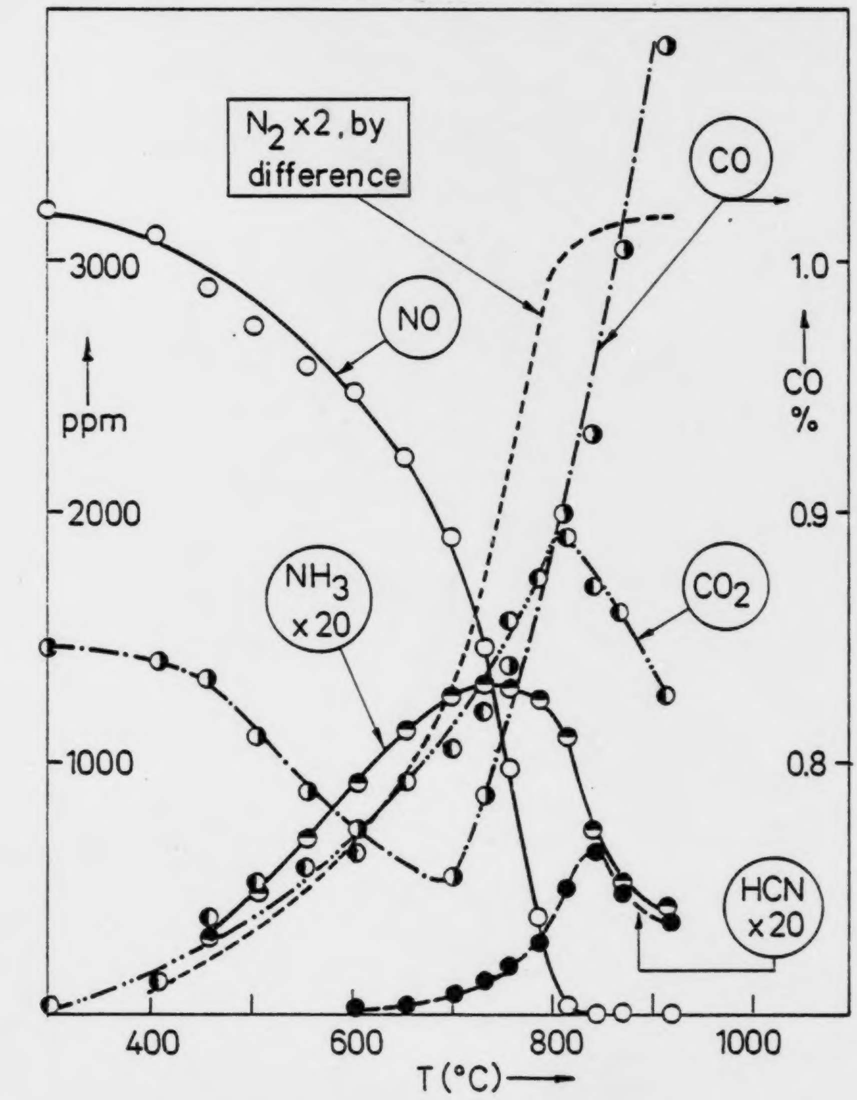

Figure 46. Argon + NO (3200 ppm) + CO (0.84%) on Pennsylvania Anthracite (Char): M_0 = 1.7 g; D = 9.9 cm^3s^{-1}.

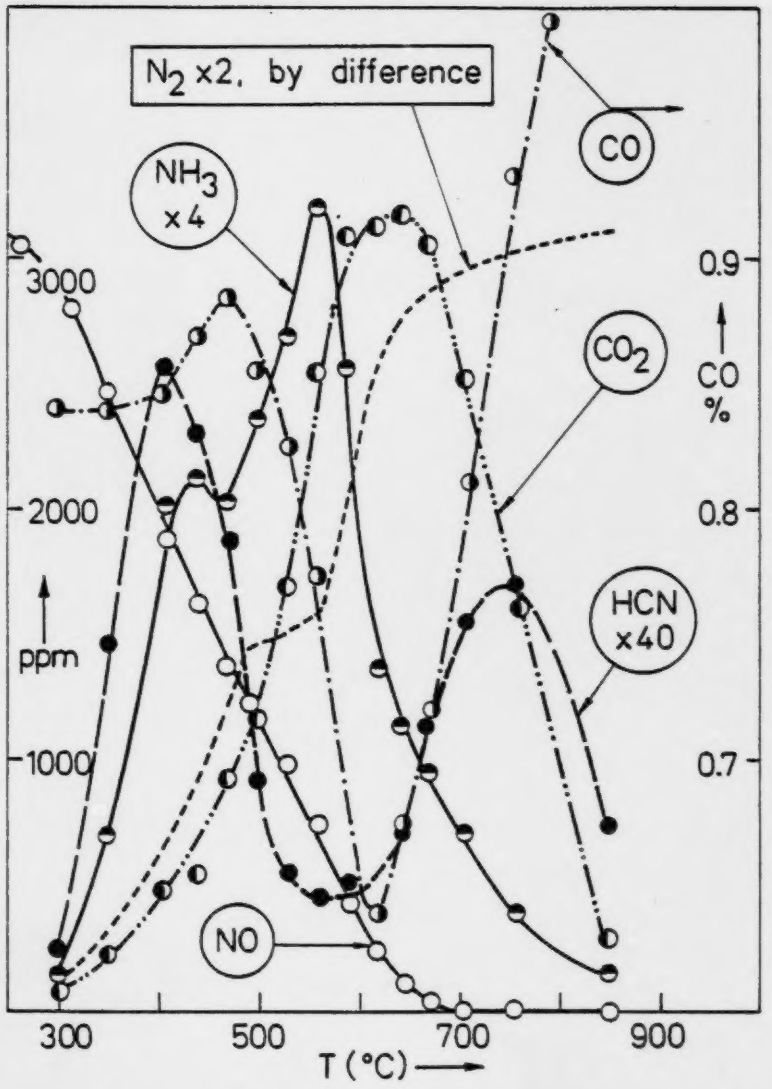

Figure 47. Argon + NO (3180 ppm) + CO (0.84%) on "Beulah" Lignite (Coal): M_0 = 1.47 g; D = 9.8 cm^{3}s^{-1}.

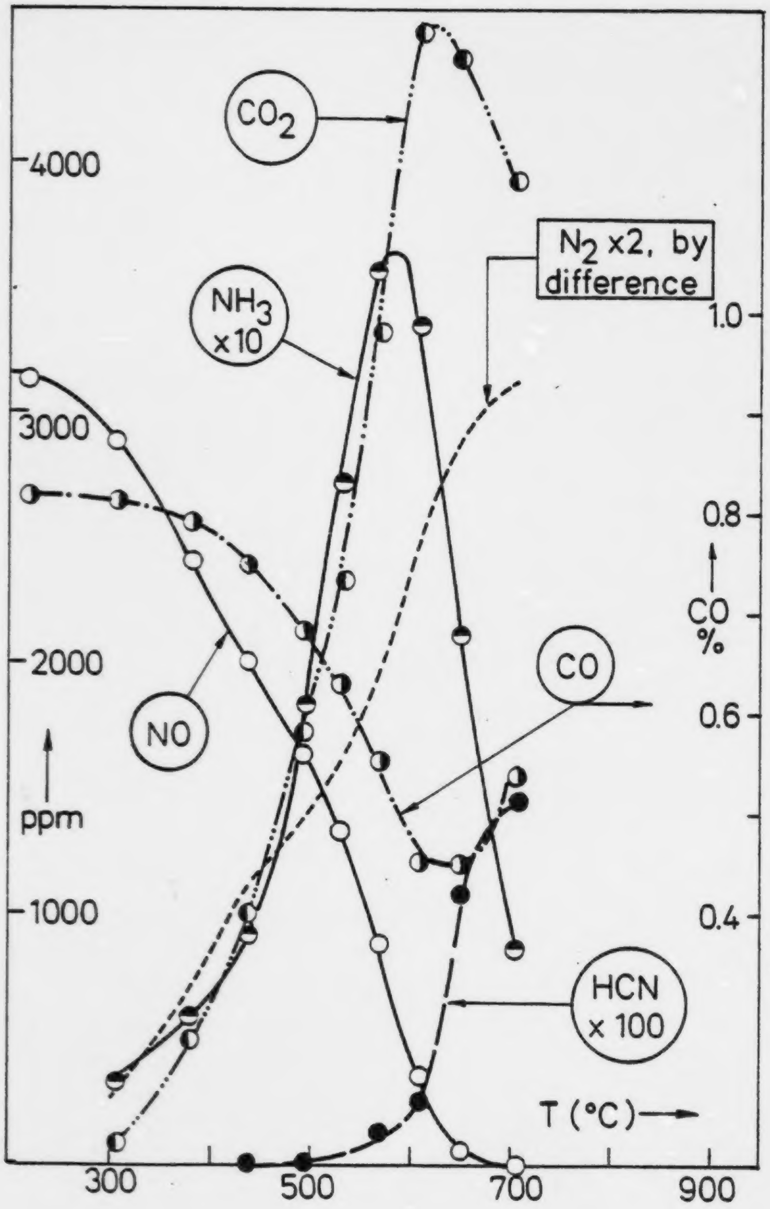

Figure 48. Argon + NO (3200 ppm) + CO (0.83%) on "Beulah" Lignite (Char): M_o = 0.8 g; D = 9.8 cm^3s^{-1}.

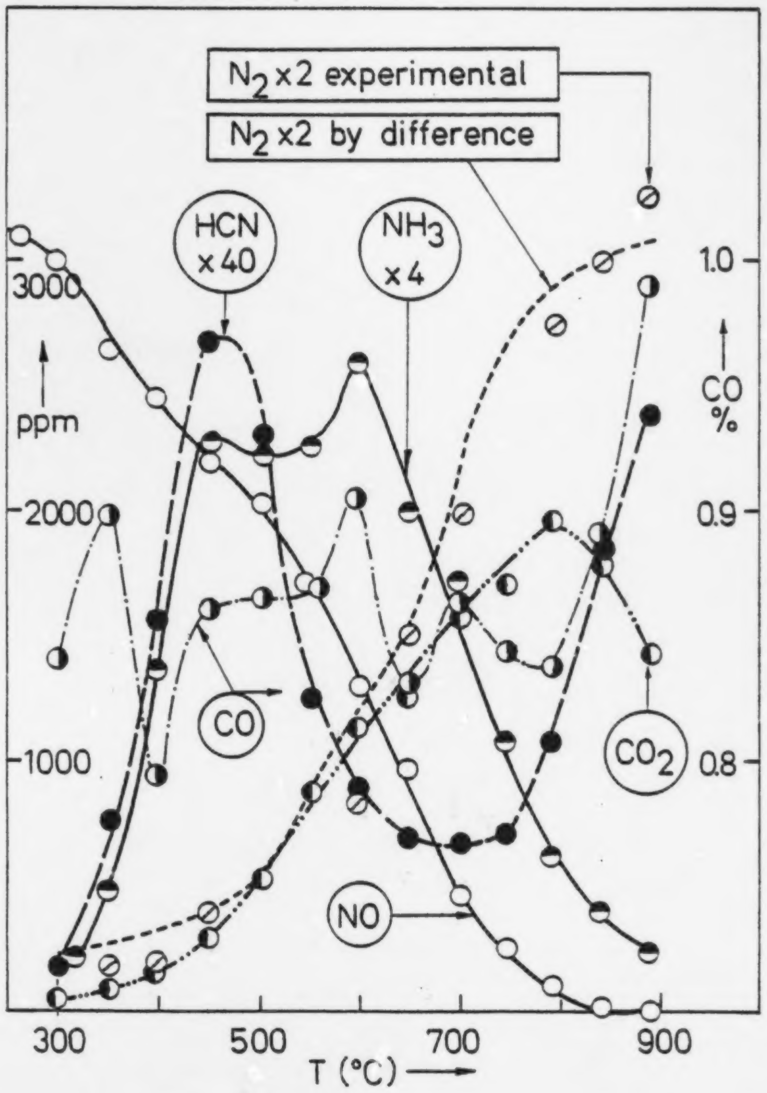

Figure 49. Argon + NO (3200 ppm) + CO (0.83%) on Utah Bituminous (Coal): M_0 = 1.97 g; D = 9.8 cm^3s^{-1}.

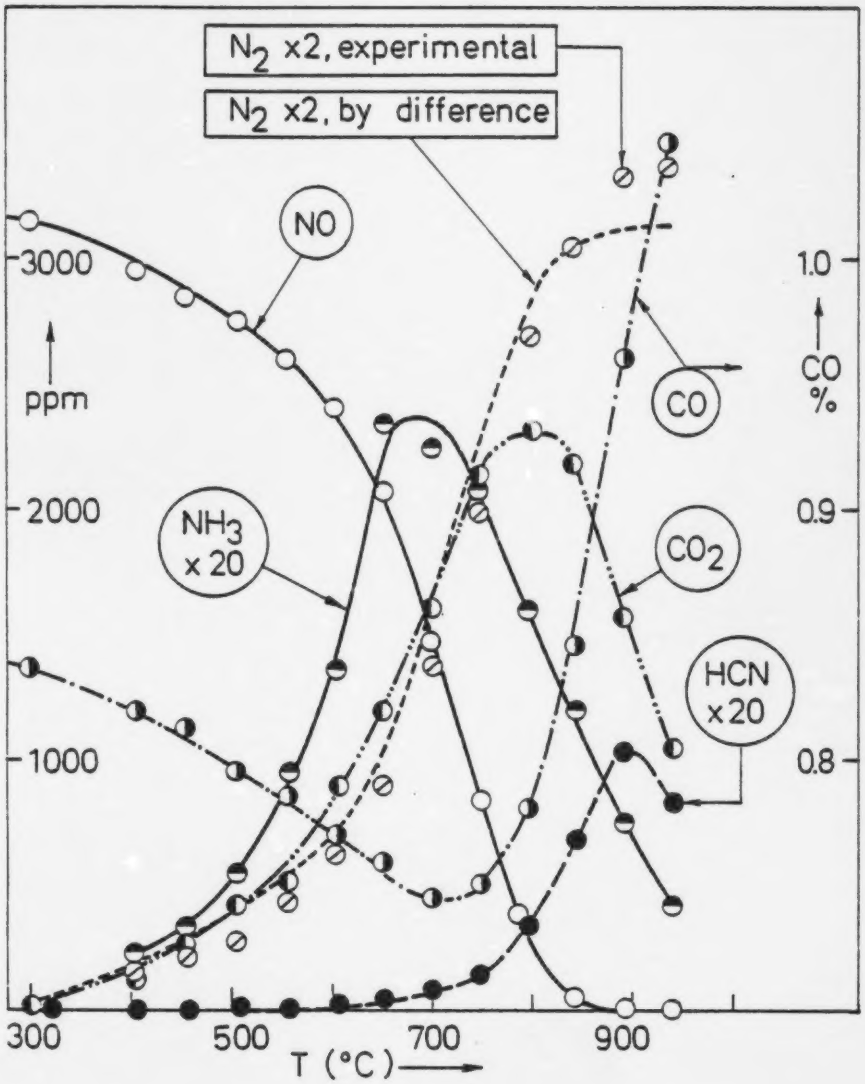

Figure 50. Argon + NO (3200 ppm) + CO (0.84%) on Utah Bituminous (Char): M_0 = 1.08 g; D = 9.8 cm^3s^{-1}.

Nonetheless, such a reaction path, if existent at all, should be negligible compared to reaction 2.

- Although there is a positive effect of CO on the overall NO removal rate, the partial order of that rate with respect to CO is very small, as suggested from Figure 39.

An approximate indication of the relative importance of the reaction paths (V_1 and V_2) and (V_8) during NO reduction on chars in the presence of carbon monoxide, may be obtained from the experimental results. At temperatures where the CO released from char pyrolysis may be neglected (i.e. at T below 750°C) and limiting the NO reduction mechanism to the primary reactions V_1, V_2, and V_8 (V_6 being neglected), the important equations are:

$$d(NO)/dt = -V_1 - V_2 - V_8 \tag{6}$$

$$d(CO)/dt = V_1 + V_2 - V_8 \tag{7}$$

$$d(CO_2)/dt = V_8 \tag{8}$$

Equations (7) and (8) implicitly contain the simplifying approximation, according to which CO_2 may be neglected as a product of reactions 1 and 2 with respect to CO.

Addition of equations (7) and (8) yields:

$$V_1 + V_2 = d(CO)/dt + d(CO_2)/dt \tag{9}$$

The following is obtained by dividing equation (8) by equation (9):

$$V_8/(V_1 + V_2) = d(CO_2)/ \left[d(CO) + d(CO_2) \right] \tag{10}$$

Experimentally one finds that this ratio of reaction rate V_8 and the reaction rates ($V_1 + V_2$) is roughly equal to the ratio of the initial CO and NO concentrations, as shown in Figure 40.

2.1.3.2 Trials on Coal Particles

Results of these trials are shown on Figures 33, 41, 43, 45, 47, and 49. As for the case discussed in paragraph 2.1.2.2, in which CO is present, coal demonstrates a NO decrease shifted to somewhat lower temperatures than for the corresponding char. The other remarks discussed in paragraph 2.1.2.2 also generally apply for the case of when CO is present for coals.

2.1.4 Trials With Argon + NO + H_2

2.1.4.1 Trials on Char Particles

These trials are illustrated in Figures 52 to 54, 56 to 58, 60, 62, 64, 66, 68, and 70. The main feature of these trials performed in the presence of hydrogen molecules, consists in the very large amounts of intermediate ammonia formed during the NO reduction. For this reason, at temperatures below 1000°C, the formation of N_2 substantially lags the removal of NO. This is obviously due to the existence of reaction 11

F51-70

$$NO + H_2 \xrightarrow{11} NH_3 + H_2O$$

which, together with reaction 14

$$NO + H_2 \xrightarrow{14} N_2 + H_2O$$

plays a substantial role in the NO reduction.

In a qualitative way this is clearly suggested by the enhancement of the NO decrease along with the enhancement of NH_3 release when the initial hydrogen concentration is increased (see Figures 53 and 58). In many cases (see for example Figures 52 and 56) ammonia is the only nitrogen species formed during NO reduction at lower temperatures (below 600 to 700°C).

In these types of trials, wall reactions begin to seriously interfere with reactions on the char particles, as may be seen for example in Figure 52.

2.1.4.2 Trials on Coal Particles

Examples of these trials are given in Figures 51, 55, 59, 61, 63, 65, 67, and 69. An important ammonia release is again noted which appears to be due to the existence of reactions 11 and 14.

For this reason, exactly as it was for the case of char trials, the N_2 formation lags appreciably behind the NO disappearance. In some cases, the same "irregularity" in the NO/T profiles are found at lower temperatures

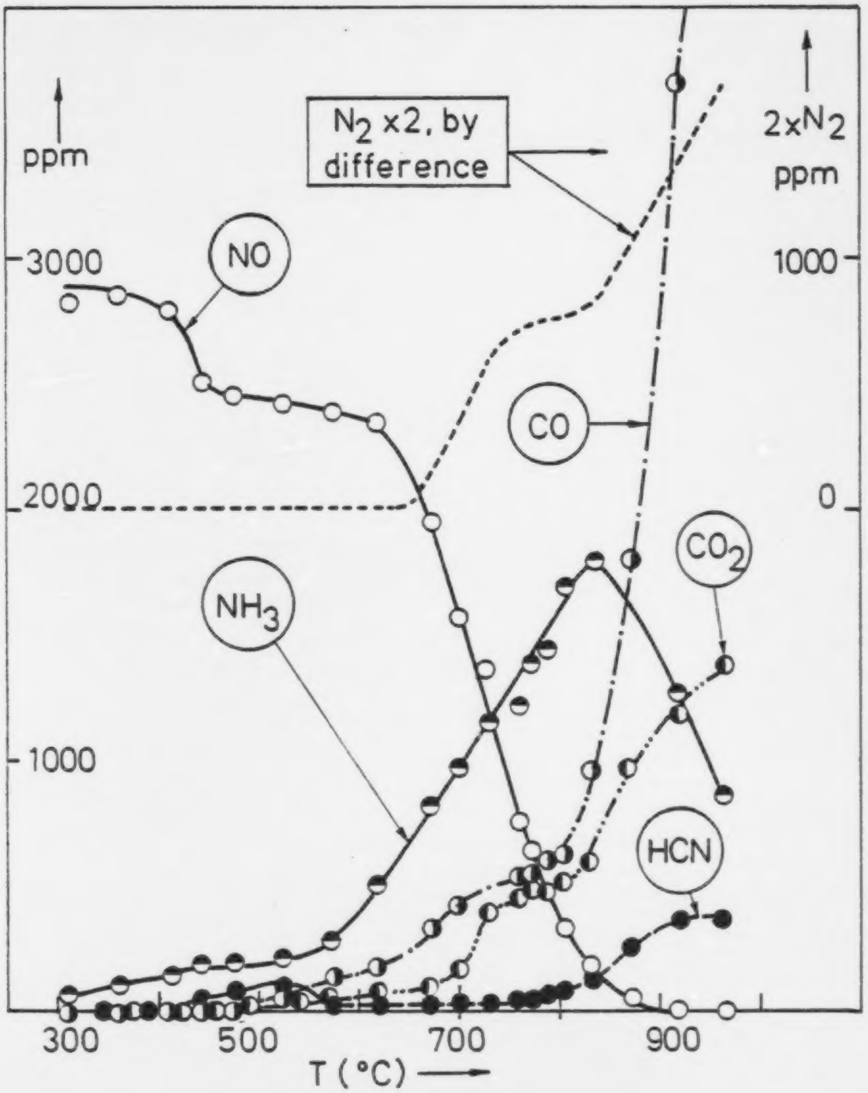

Figure 51. Argon + NO (2900 ppm) + H_2 (1.52%) on Pocahontas Medium Volatile (Coal): M_0 = 1.49 g; D = 11.8 cm^3s^{-1}.

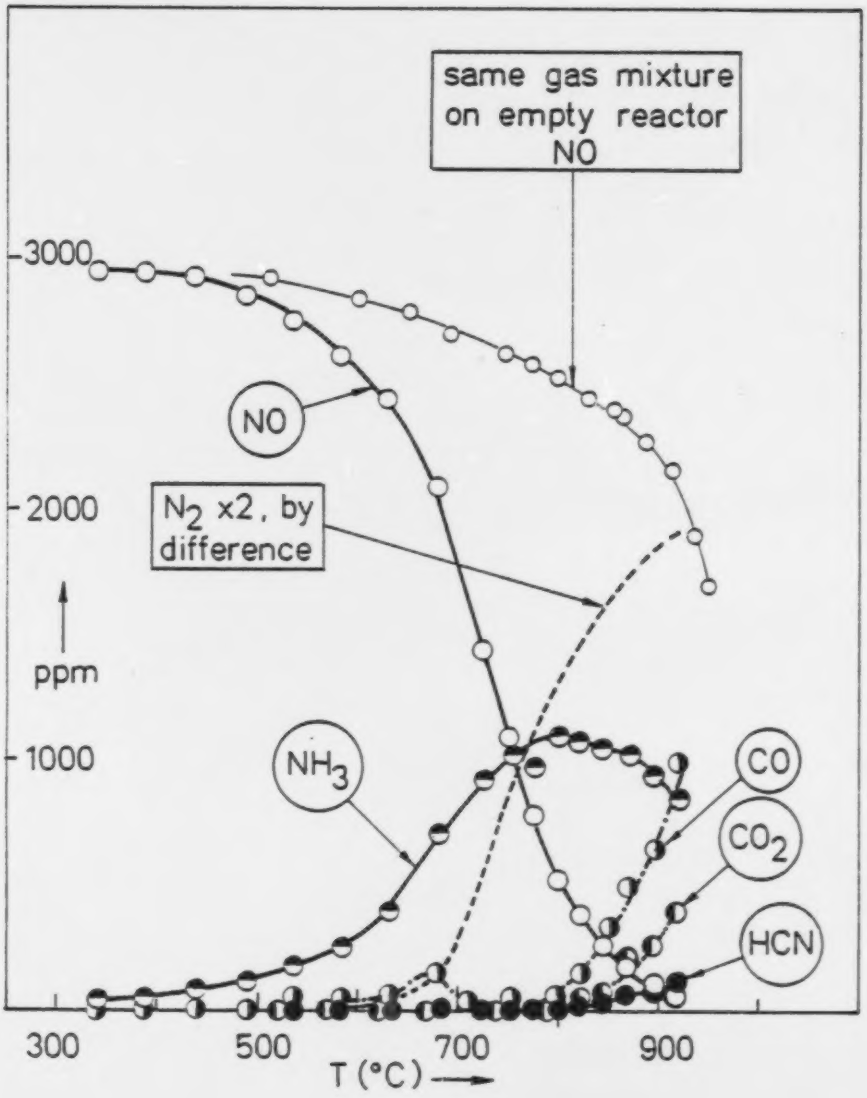

Figure 52. Argon + NO (2950 ppm) + H_2 (1.52%) on Pocahontas Medium Volatile (Char): M_o = 1.1 g; D = 11.8 cm^3s^{-1}.

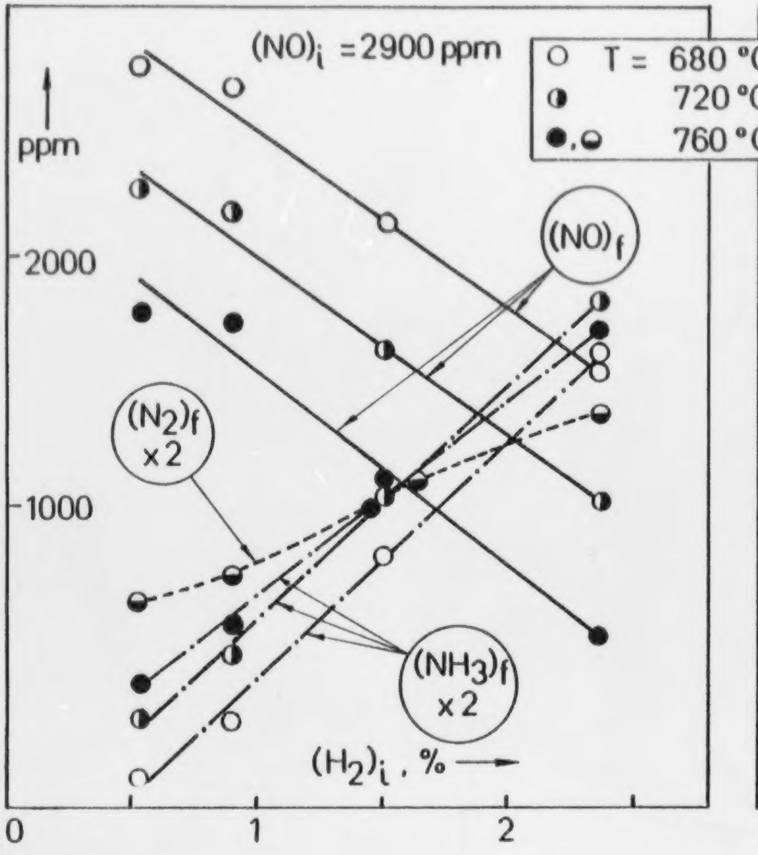

Figure 53.

Argon + NO (2900 ppm) + H_2 on Pocahontas Medium-Volatile (Char): Effect of Initial Hydrogen Concentration; $M_o = 1.5g$; $D = 11.8$ cm^3s^{-1}.

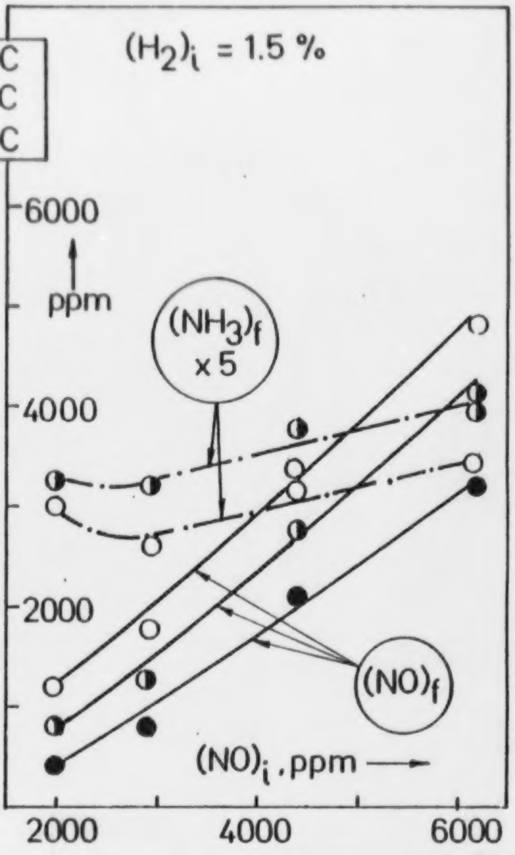

Figure 54.

Argon + NO + H_2 (1.5%) on Pocahontas Medium-Volatile (Char): Effect of Initial NO Concentration; $M_o = 1.5g$; $D = 11.8\ cm^3s^{-1}$.

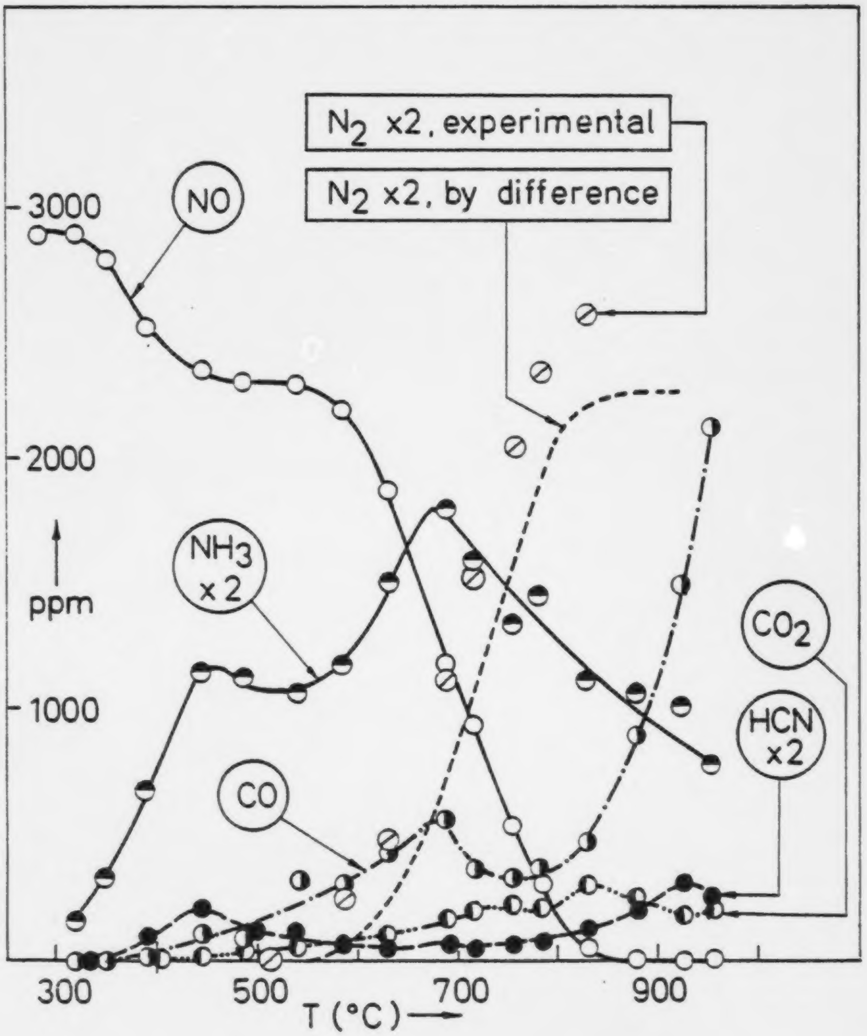

Figure 55. Argon + NO (2900 ppm) + H_2 (1.52%) on Cedar Grove High Volatile (Coal): M_o = 1.48 g; D = 11.8 cm^3s^{-1}.

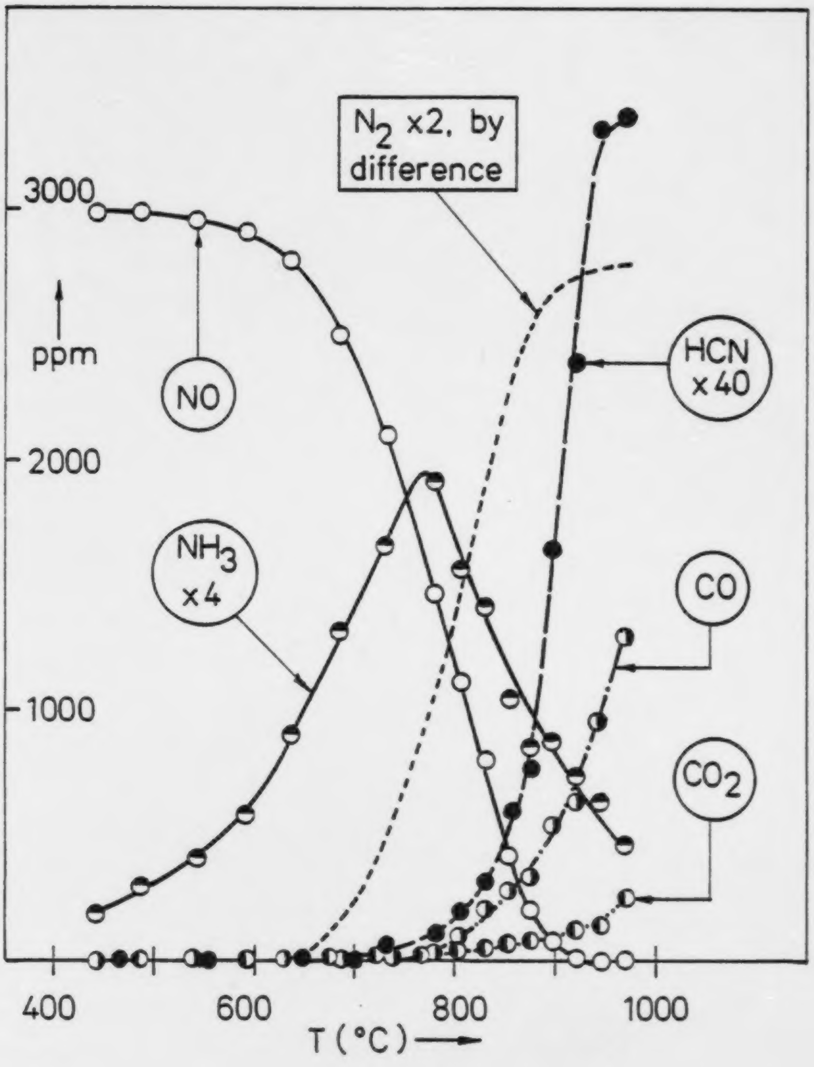

Figure 56. Argon + NO (2980 ppm) + H_2 (1.52%) on Cedar Grove High Volatile (Char): M_o = 1.6 g; D = 11.8 cm^3s^{-1}.

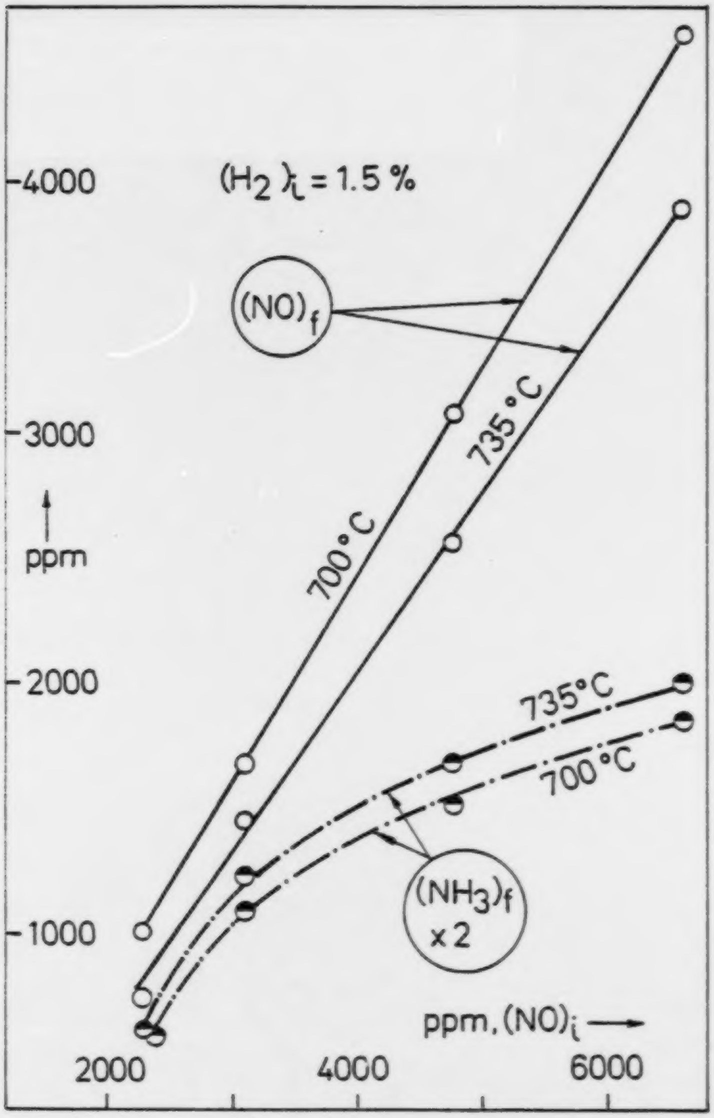

Figure 57. Argon + NO + H_2 (1.5%) on Cedar Grove High Volatile (Char): Effect of Initial NO Concentration; M_0 = 1.6 g; D = 11.8 cm^3s^{-1}.

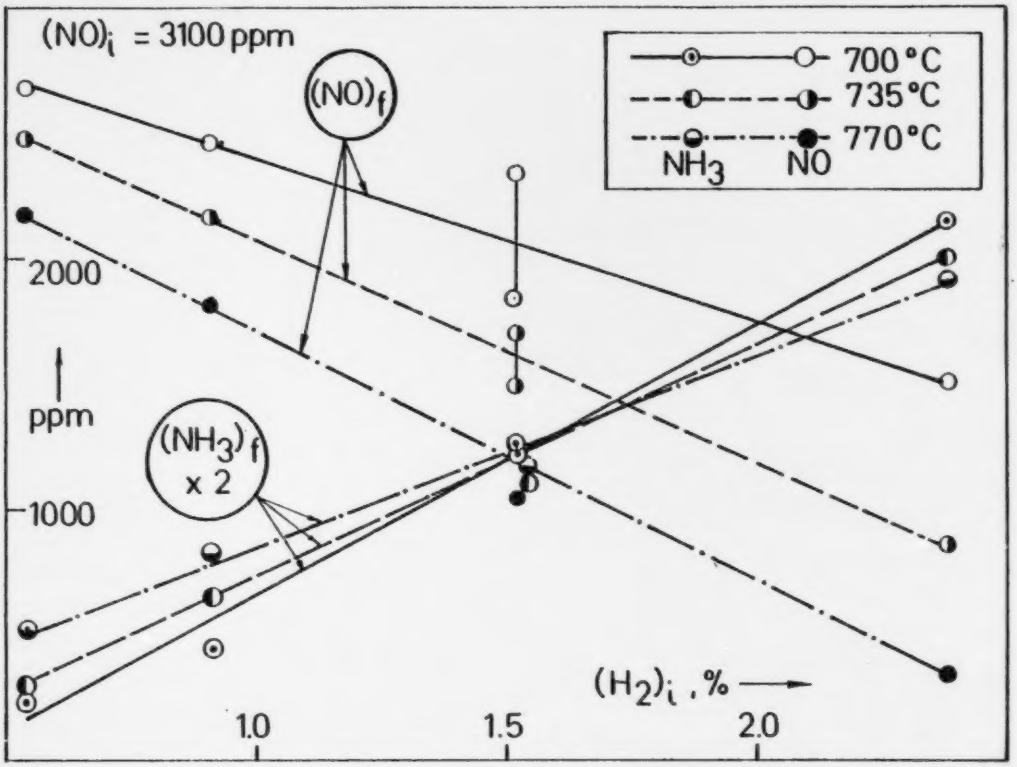

Figure 58. Argon + NO (3100 ppm) + H_2 on Cedar Grove High Volatile (Char): Effect of Initial Hydrogen Concentration; M_0 = 1.55 g; D = 11.8 cm^3s^{-1}.

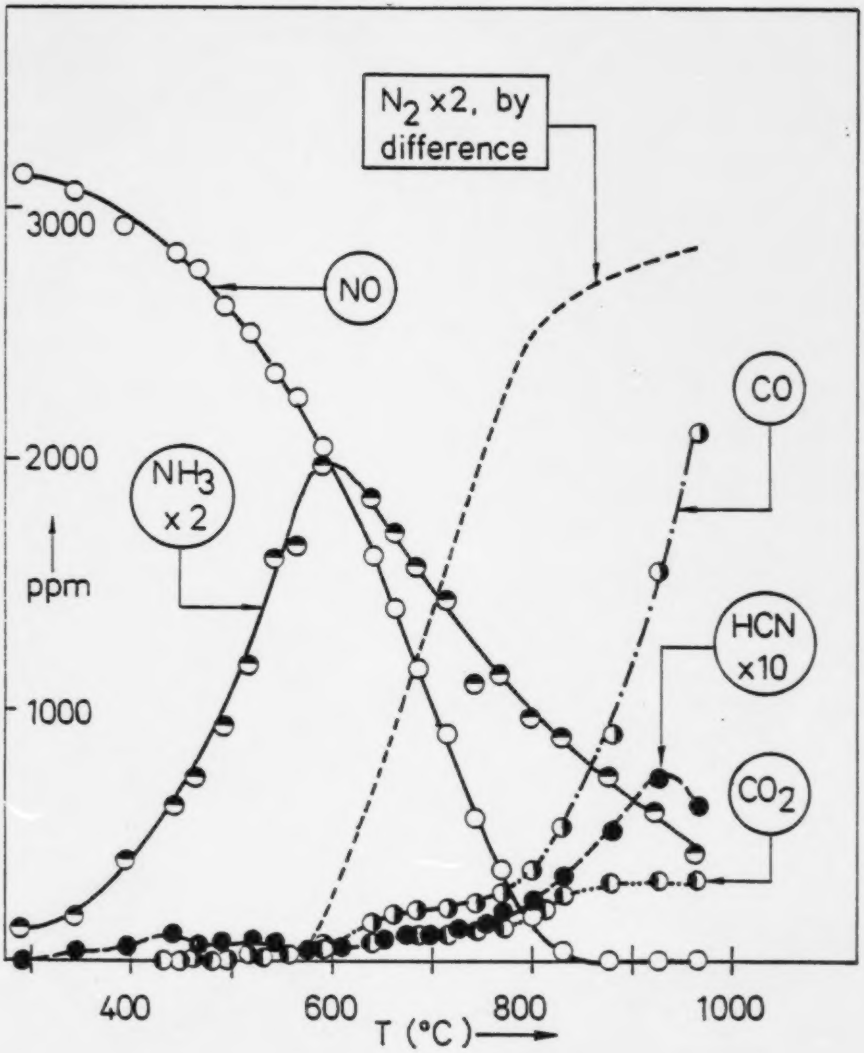

Figure 59. Argon + NO (3150 ppm) + H_2 (1.5%) on Pocahontas Low Volatile, High Ash (Coal): M_0 = 1.55 g; D = 11.8 $cm^3 s^{-1}$.

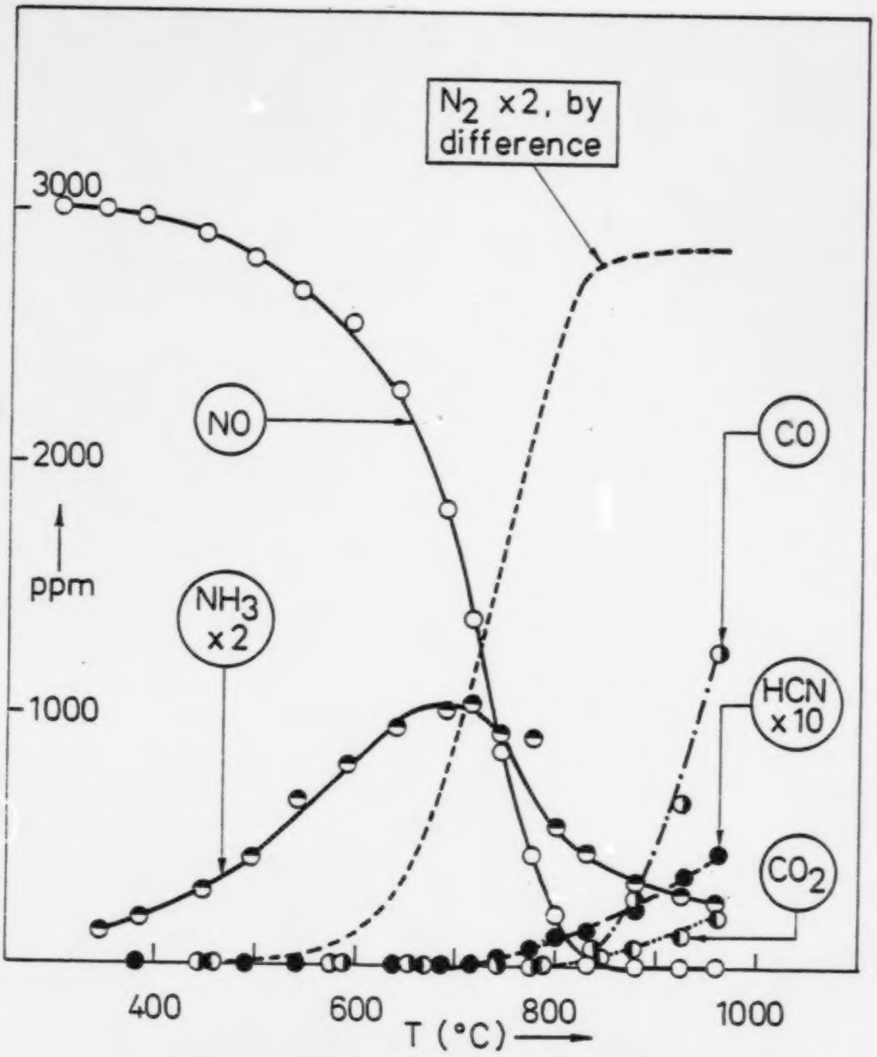

Figure 60. Argon + NO (3050 ppm) + H_2 (1.5%) on Pocahontas Low Volatile, High Ash (Char): M_0 = 1.6 g; D = 11.8 cm^3s^{-1}.

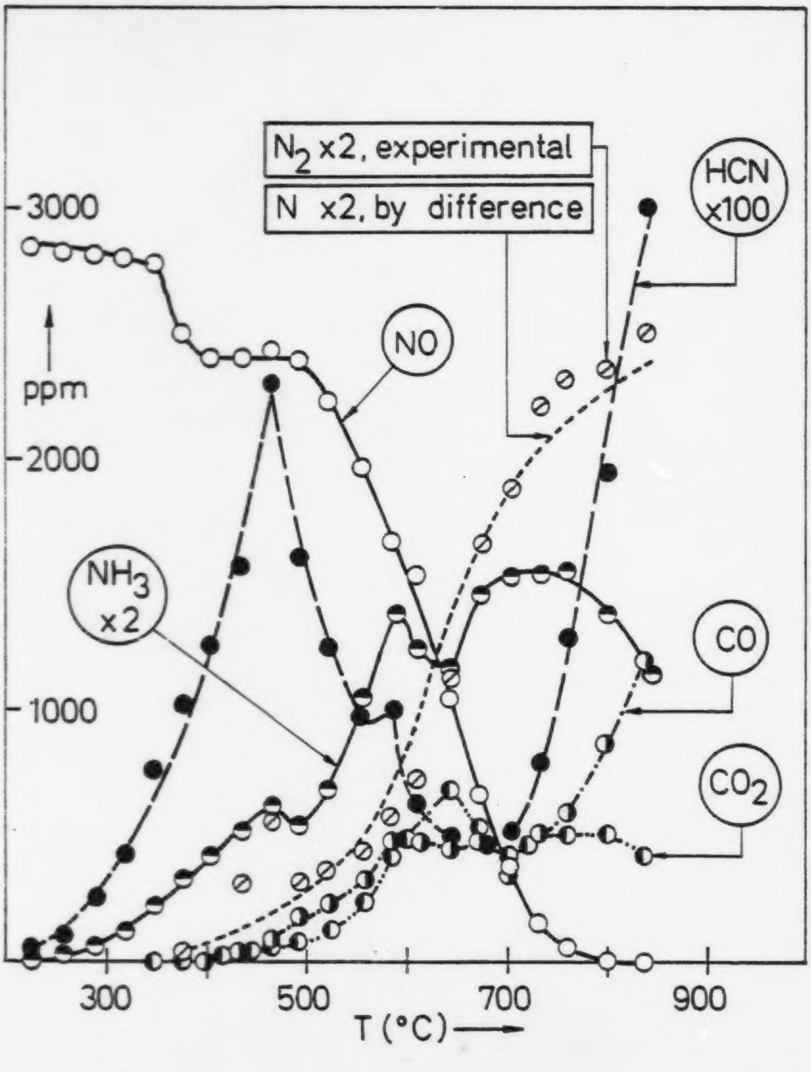

Figure 61. Argon + NO (3000 ppm) + H_2 (1.5%) on South African "Rietspruit" (Coal): Particle size--50 to 100 microns. M_o = 1.45 g; D = 10.6 cm^3s^{-1}.

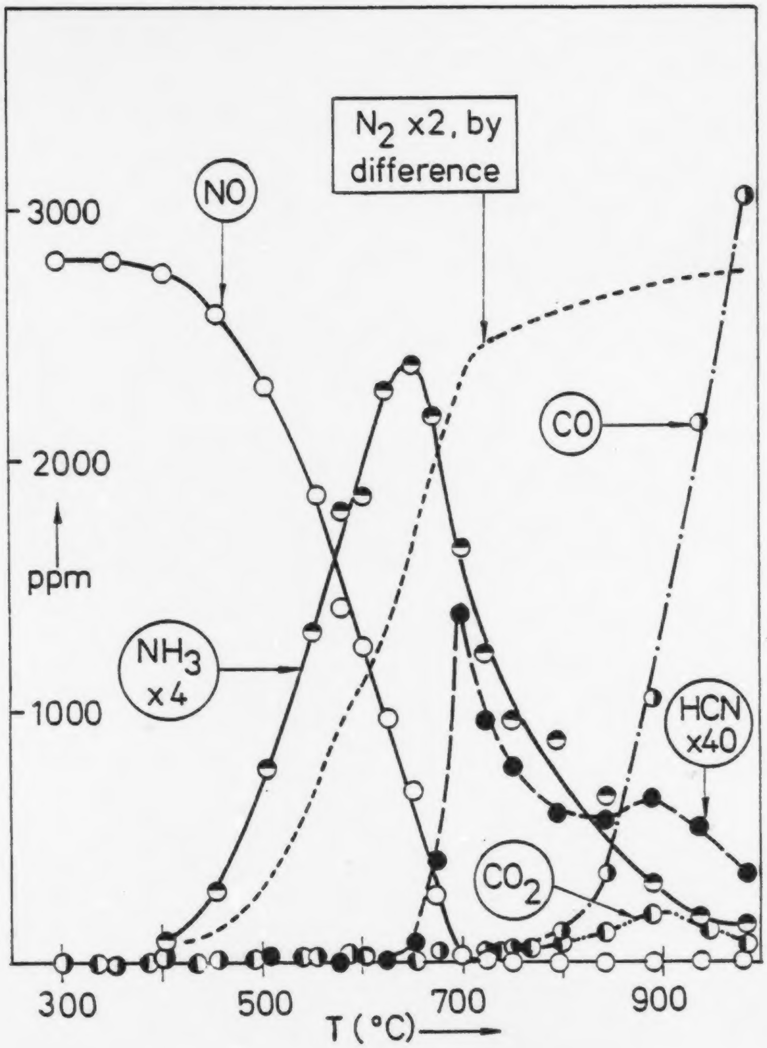

Figure 62. Argon + NO (2800 ppm) + H_2 (1.5%) on South African "Rietspruit" (Char): Particle size--50 to 100 microns; M_0 = 1.6 g; D = 10.3 cm^3s^{-1}.

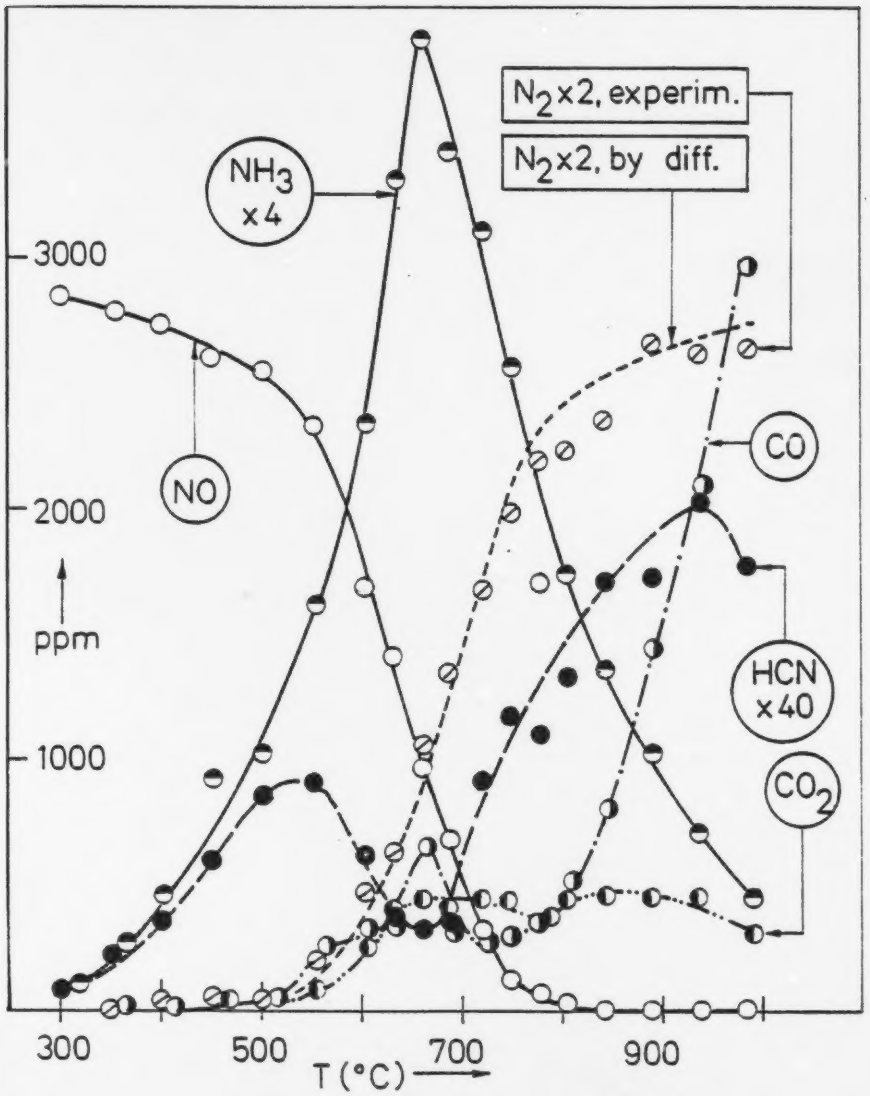

Figure 63. Argon + NO (2900 ppm) + H_2 (1.5%) on "Prosper" Ruhr (Coal): M_0 = 1 g; D = 10.1 cm^3s^{-1}.

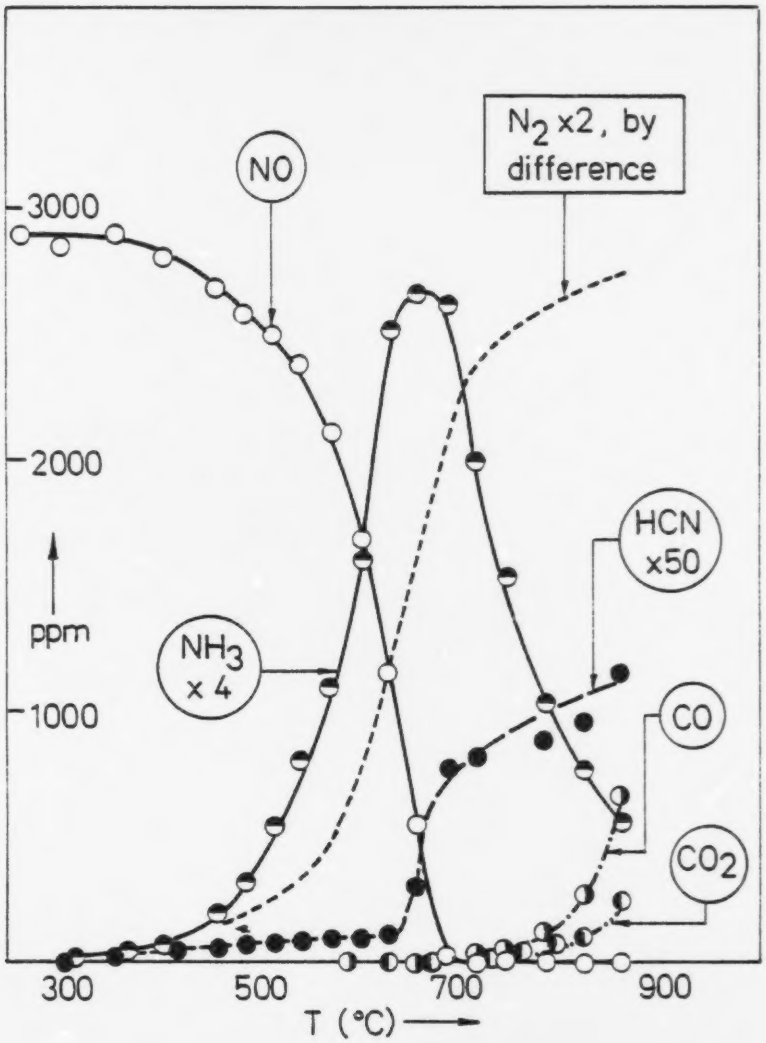

Figure 64. Argon + NO (2900 ppm) + H_2 (1.5%) on "Prosper" Ruhr (Char): M_0 = 1.6 g; D = 10.8 cm^3s^{-1}.

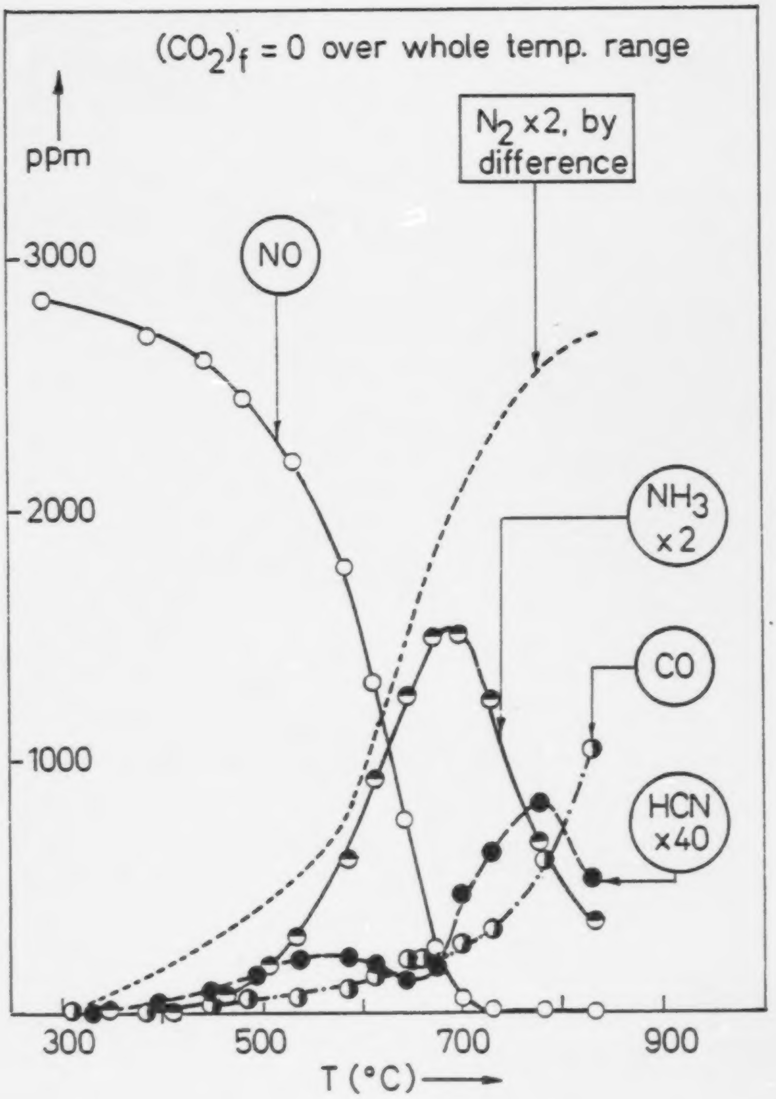

Figure 65. Argon + NO (2900 ppm) + H_2 (1.5%) on Pennsylvania Anthracite (Coal): M_0 = 1.92 g; D = 9.8 cm^3s^{-1}.

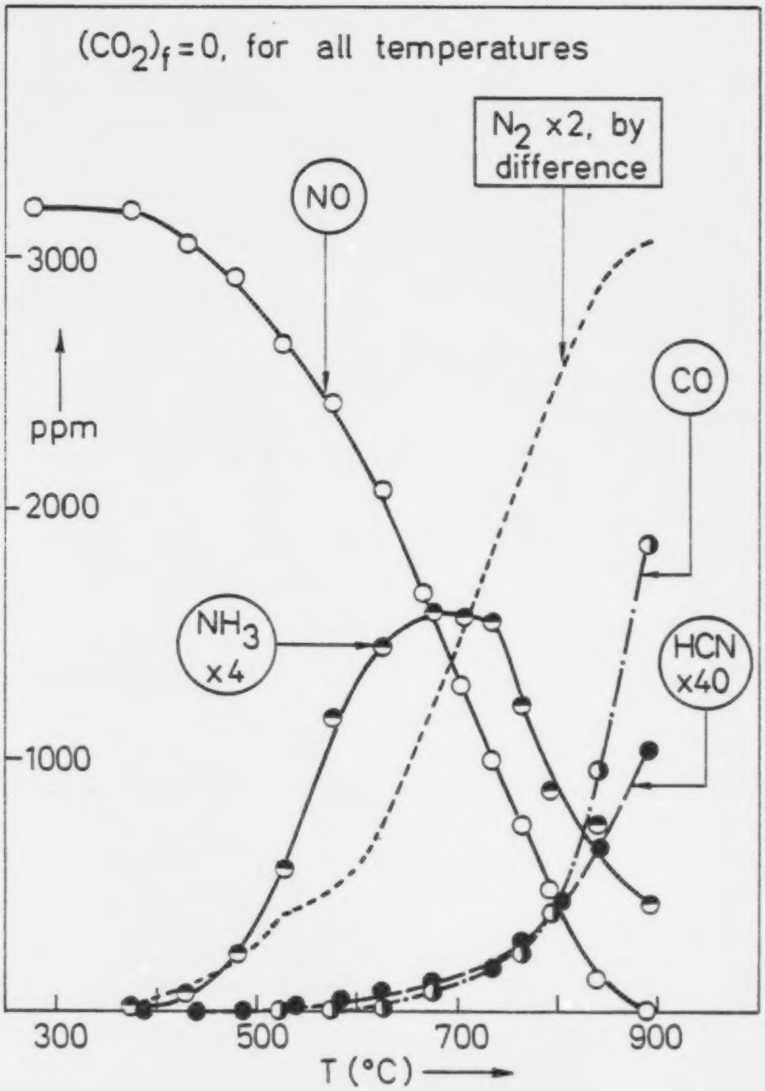

Figure 66. Argon + NO (3180 ppm) + H_2 (1.5%) on Pennsylvania Anthracite (Char): M_0 = 1.7 g; D = 9.8 cm^3s^{-1}.

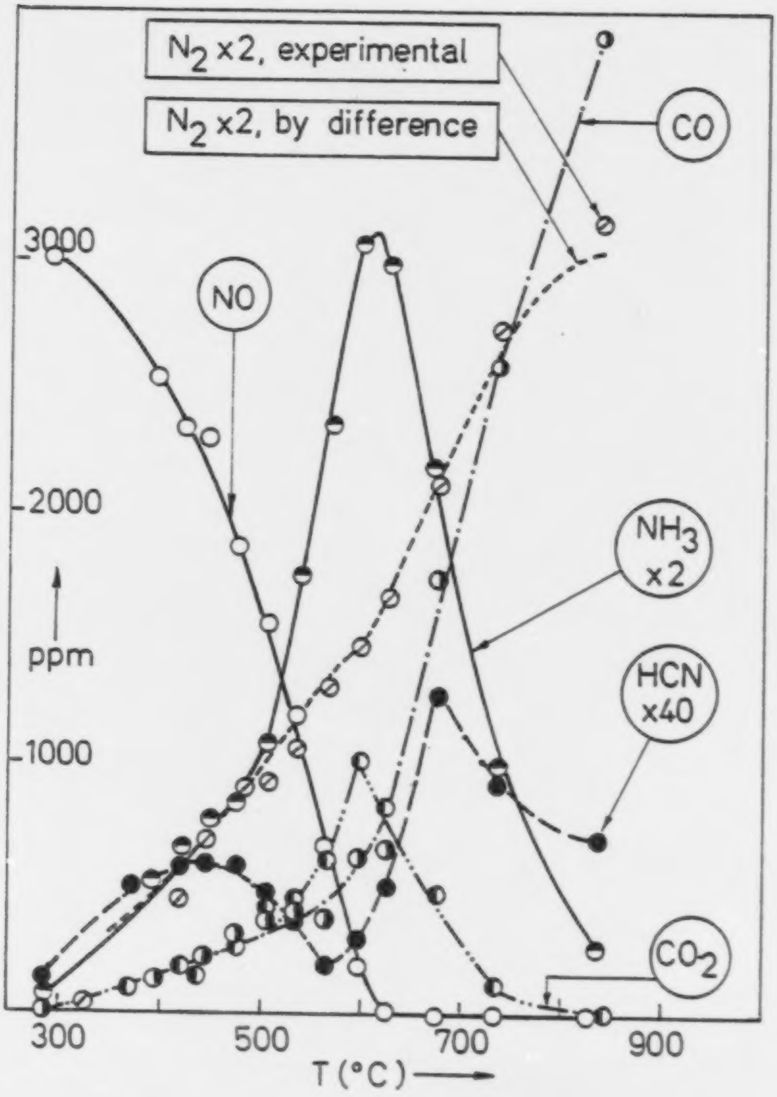

Figure 67. Argon + NO (3200 ppm) + H_2 (1.5%) on "Beulah" Lignite (Coal): M_0 = 1.47 g; D = 9.6 cm^3s^{-1}.

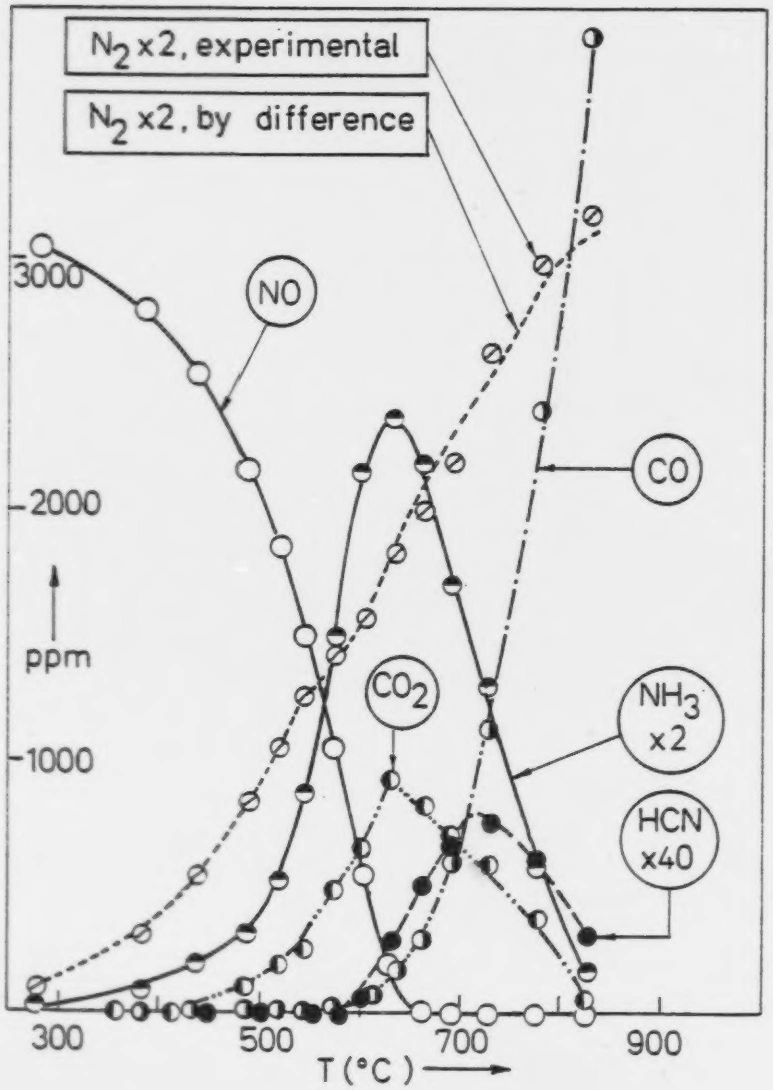

Figure 68. Argon + NO (3200 ppm) + H_2 (1.5%) on "Beulah" Lignite (Char): M_0 = 0.8 g; D = 9.6 cm^3s^{-1}.

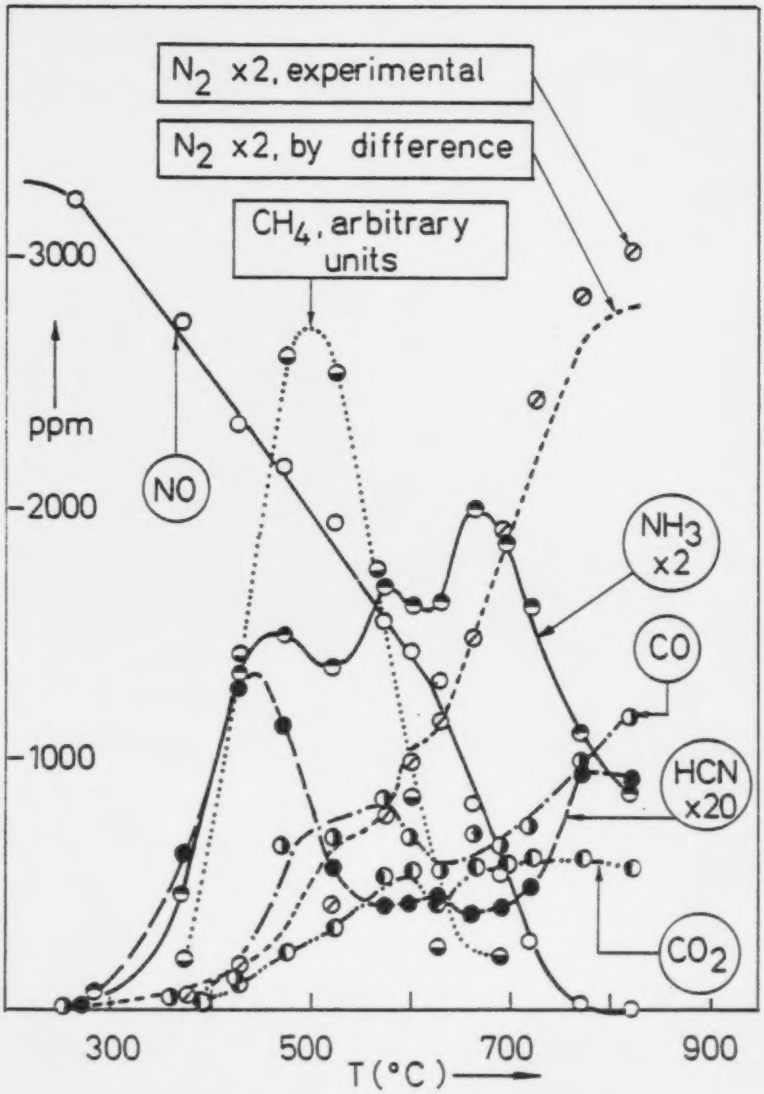

Figure 69. Argon + NO (3300 ppm) + H_2 (1.5%) on Utah Bituminous (Coal): M_o = 1.97 g; D = 9.5 cm^3s^{-1}.

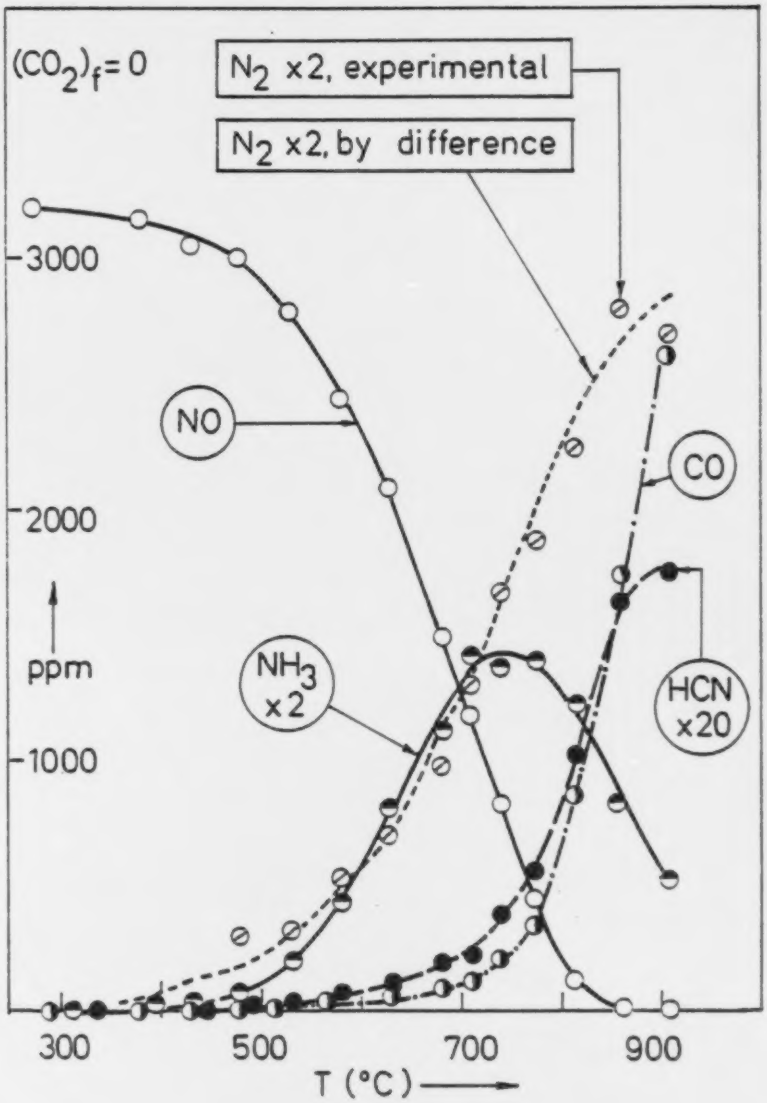

Figure 70. Argon + NO (3200 ppm) + H_2 (1.5%) on Utah Bituminous (Char): M_0 = 1.08 g; D = 9.5 cm^3s^{-1}.

(i.e. during the devolatilization process) as has been discussed in paragraph 2.1.2.2). An example of this phenomenon in Figures 51, 55, and 61.

2.2 Comparison of NO Removal Rates and N_2 Formation Rates for Different Coals and Chars

In this section we intend to make the comparison of overall NO removal rates ($\overline{V}$) and overall N_2 formation rates ($\overline{V}_n$) given by eqs. (2) and (3), respectively, for different experimental conditions. A fourfold comparison will be made:

- Comparison of reaction rates determined on coal and on its char (coal/char comparison).
- Comparison of reaction rates determined in the absence or in the presence of gaseous reducing agents such as hydrogen or carbon monoxide (effect of H_2 and CO presence).
- Comparison of reaction rates obtained with coals (and chars) of different nature and rank (effect of coal nature).
- Comparison between NO removal rate and N_2 formation rate determined on a given type of particle and under identical experimental conditions.

In the first three, comparisons are made in the first subsection, which will be limited to comparisons of the overall NO removal rate. The combination of these comparisons with the fourth one, made in the second subsection, will automatically enable the three first comparisons to be made with respect to the N_2 formation rates.

2.2.1 Overall NO Removal Rates: Dependence on Nature of Coal or Char and on the Eventual Presence of Gaseous Reducing Agents

2.2.1.1 Coal/Char Comparison

Experimental values of the overall NO removal rate $\overline{V}$, obtained according to eq. (2), are shown in Figures 71 through 78, for different coals and chars as well as for different gas compositions. On the ordinate axis of these graphs, the overall rate $\overline{V}$ has been divided by the initial NO concentration in order to allow a convenient comparison between materials. For Ar + NO gas streams, $(NO)_i$ is 1700 ± 100 ppm; for all Ar + NO + CO and

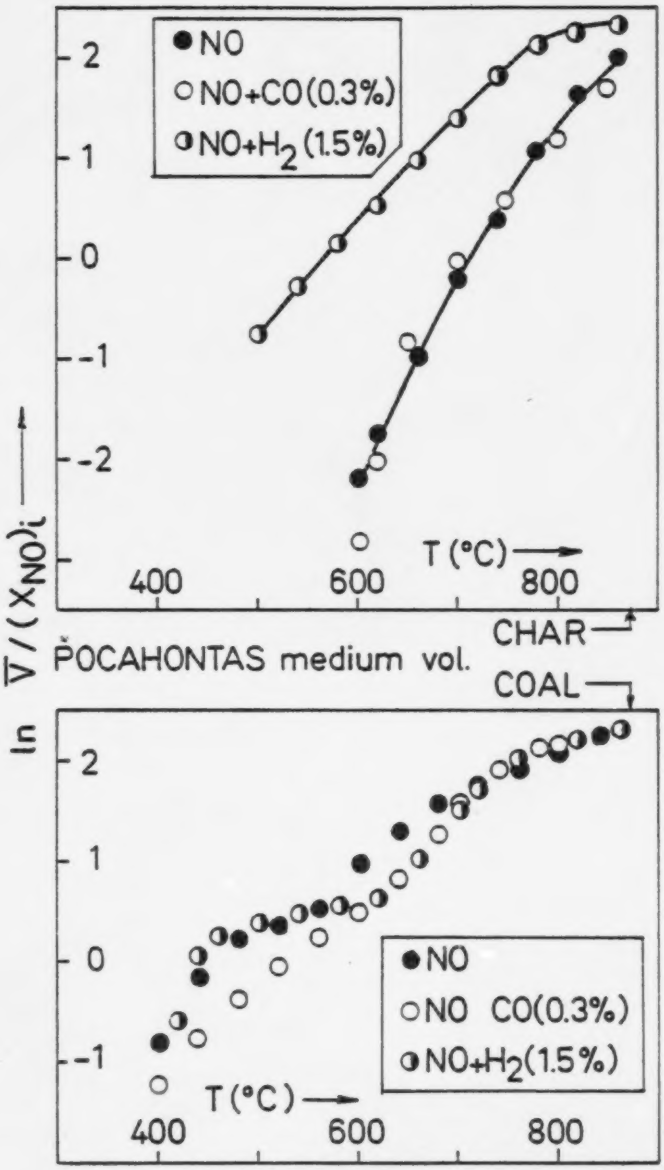

Figure 71. Overall NO Removal Rates Measured on Pocahontas Medium Volatile Coal and Char.

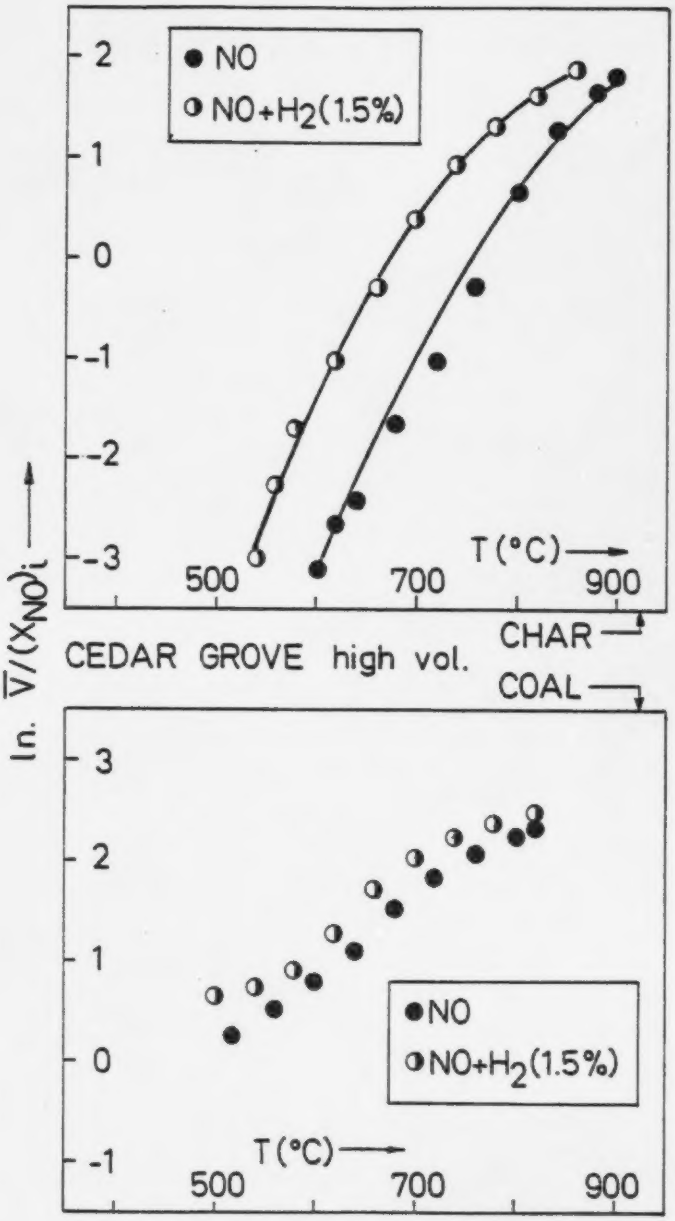

Figure 72. Overall NO Removal Rates Measured on Cedar Grove High Volatile Coal and Char.

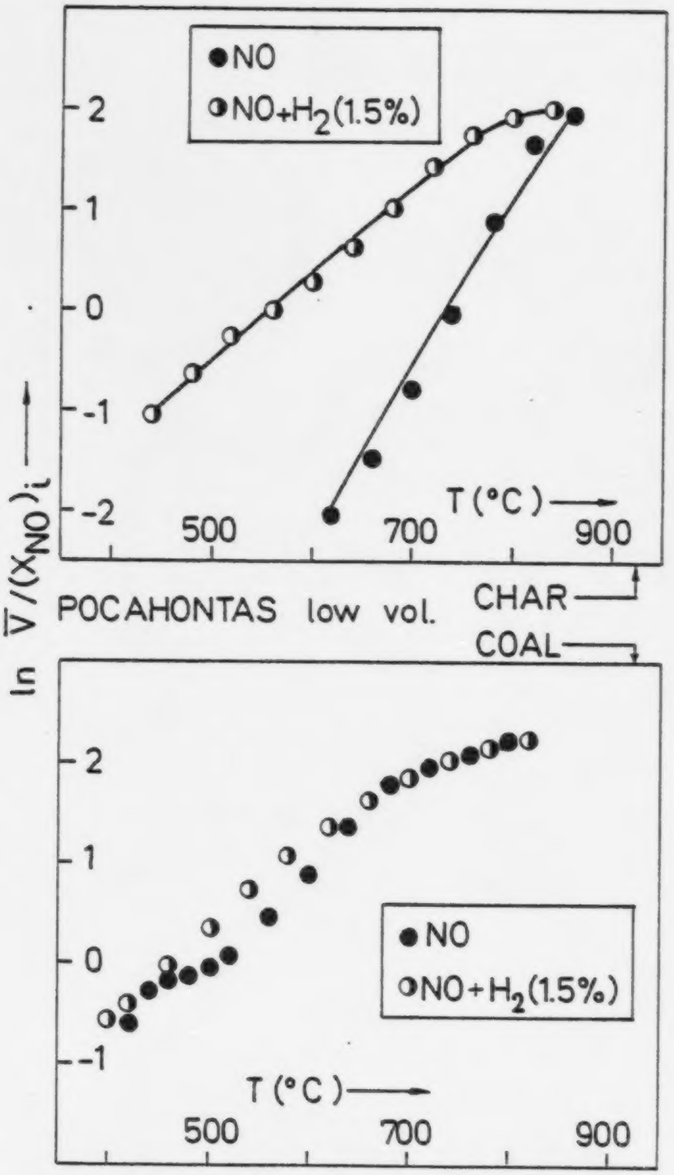

Figure 73. Overall NO Removal Rates Measured on Pocahontas Low Volatile Coal and Char.

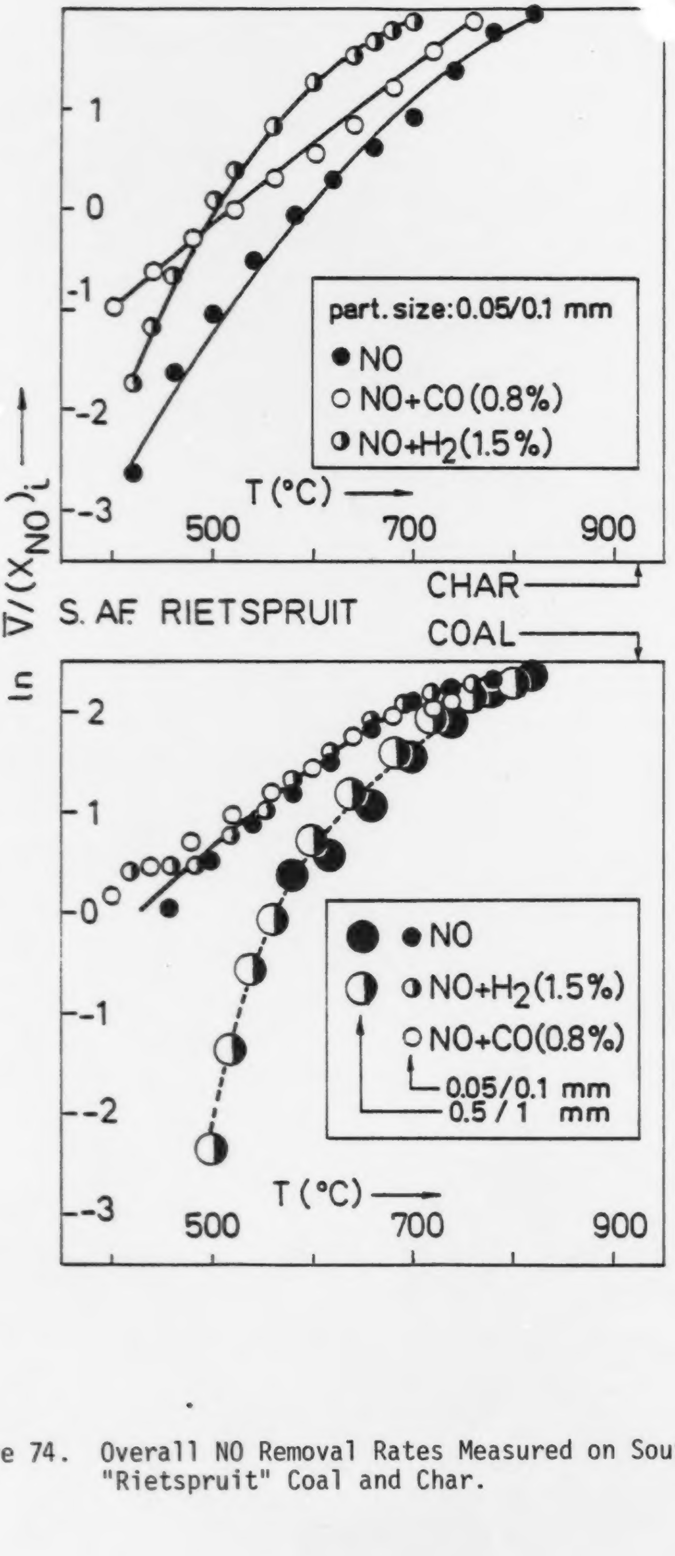

Figure 74. Overall NO Removal Rates Measured on South African "Rietspruit" Coal and Char.

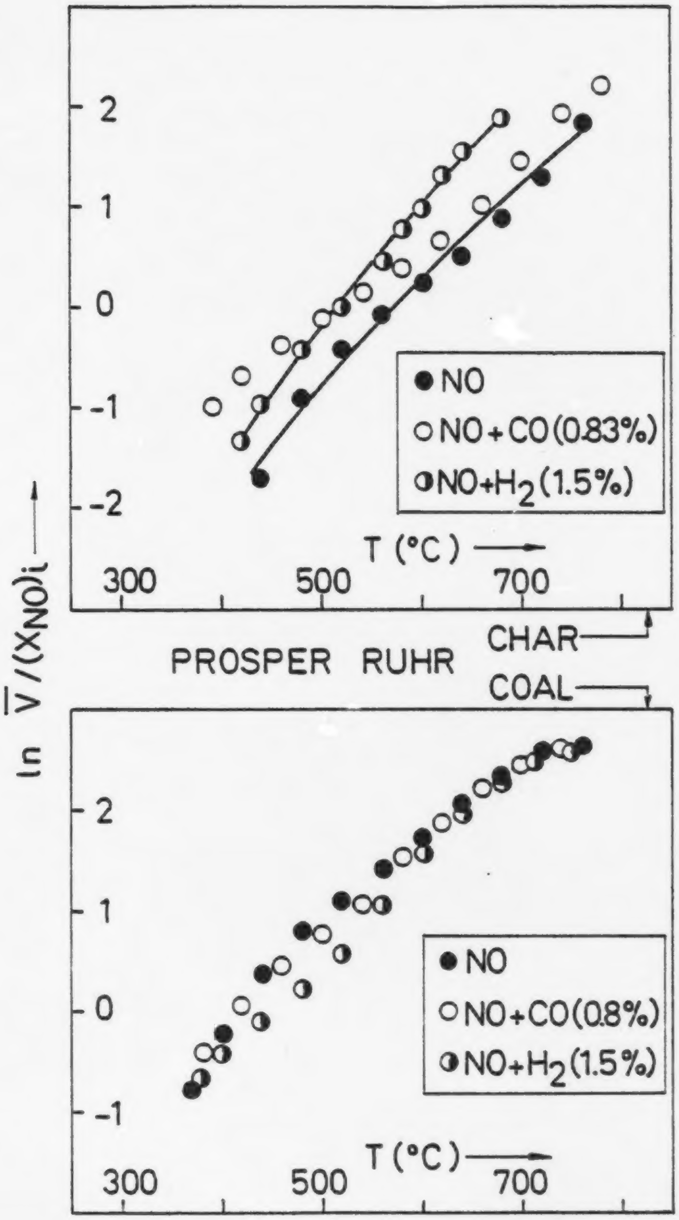

Figure 75. Overall NO Removal Rates Measured on Ruhr Coal "Prosper," Coal and Char.

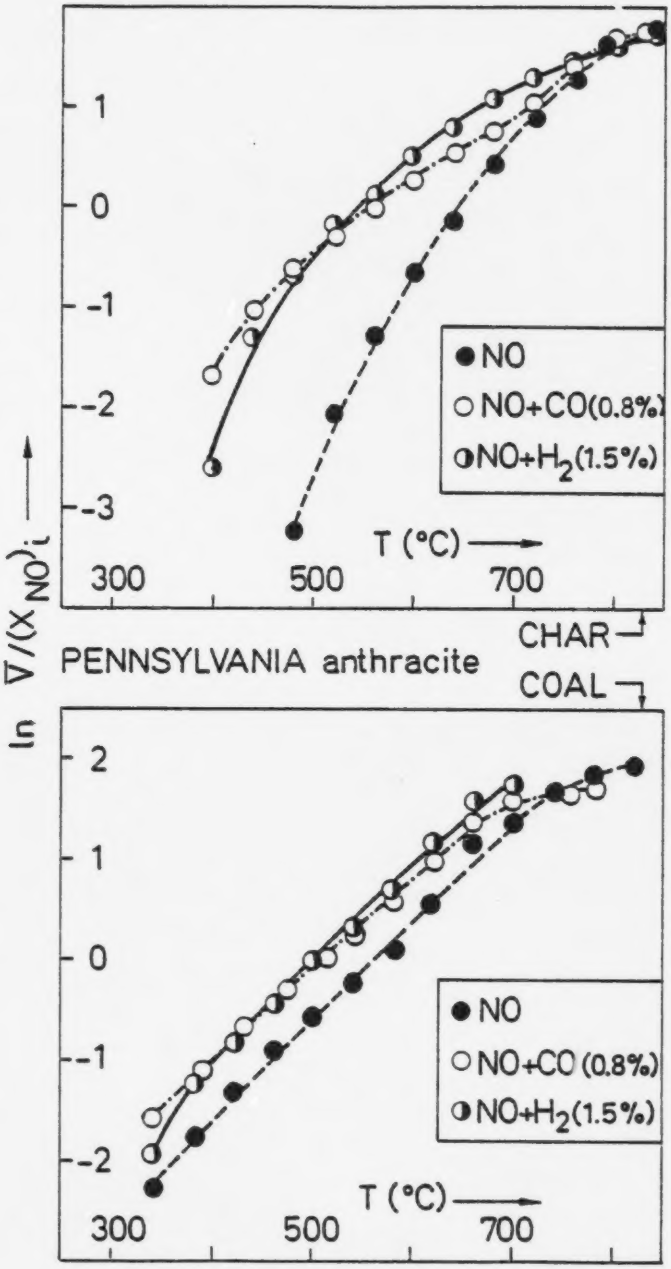

Figure 76. Overall NO Removal Rates Measured on Pennsylvania Anthracite, Coal and Char.

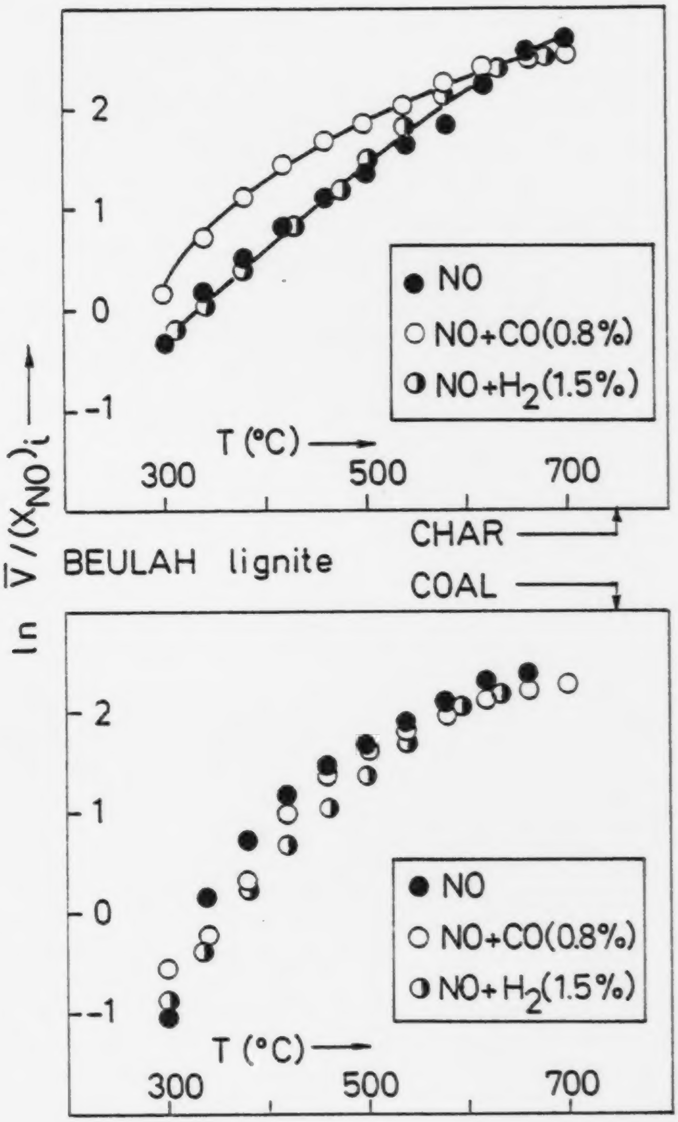

Figure 77. Overall NO Removal Rates Measured on "Beulah" North Dakota Lignite, Coal and Char.

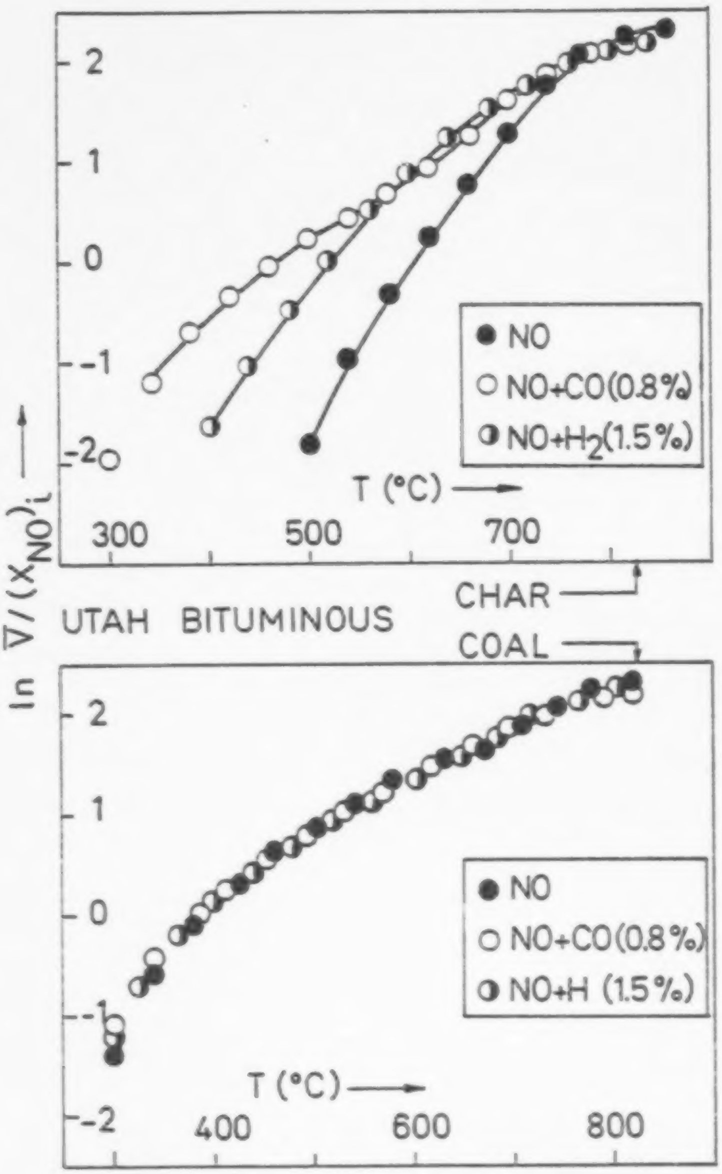

Figure 78. Overall NO Removal Rates Measured on Utah Bituminous Coal and Char.

ar + NO + H_2 trials, $(NO)_i$ is 3000 ± 150 ppm. This approach assumes a partial reaction order with respect to NO equal to one, which is experimentally found to be valid in practically all cases (see section 2.3). From these figures the following observations may be made:

- Both in the absence and in the presence of gaseous reducing agents (H_2 or CO), the overall NO removal rate is always larger for coals than for the corresponding chars, despite the fact that the specific surface area of the chars is typically higher than that of the coal (see Table 1 and 2).
- The difference between $\overline{V}$ measured on a coal and on the corresponding char is largest when H_2 is absent, i.e. for Ar + NO gas streams. This, together with the fact that NH_3 release is more important for coal than for char (see paragraph 2.1.2.2), emphasizes the role played by indirect NO reduction with ammonia as an intermediate product. In the case of Ar + NO mixtures, the hydrogen source required for this ammonia formation can only be solid bound hydrogen atoms. Since the (-H) content of chars is substantially smaller than for coals, the reducing reaction path going through ammonia is more important in the latter case. Whenever H_2 is present in the gas stream, it substantially takes over the role of a hydrogen donor to the intermediate ammonia formation; and, as a consequence, the difference of $\overline{V}$ for coals and corresponding chars tends to disappear.
- The succession of reactions 2, 13, and 4 (which constitute the principal sequence by which NO is indirectly reduced through NH_3 into N_2) is less temperature dependent than the direct reduction of NO into N_2 by reaction 1 (see Reference 1, Table 3). Thus, it is not surprising to find that, when Ar + NO mixtures are fed over coals and chars in the absence of CO and H_2, the increase of the overall NO removal rate with temperature (i.e. $d\overline{V}/dT$) is usually larger for the char than for the corresponding coal (see Figures 71, 72, 73, 76, and 78). This can be seen in a more quantitative way from the overall activation energies of these reactions (see Table 4). On the other hand, when hydrogen

is added to the gas flow, it takes over the role of the hydrogen donor for ammonia formation, and consequently $(d\overline{V}/dT)$ becomes almost identical for coals and corresponding chars (see Figures 71 and 73 through 78).

2.2.1.2 Effects of CO or H_2 Presence

- As a general rule, it is observed that, for a given bituminous coal, the addition of either CO or H_2 does not enhance in a measurable manner the overall NO removal rate (see lower parts of Figures 71 to 75 and Figures 77 and 78).
- On the other hand, the addition of CO or H_2 does enhance the overall NO removal rate in the case of anthracite (see Figure 76, lower part); and, especially in the case of chars (see upper part of Figures 71 through 78). It is worthwhile to compare this with the results obtained on char in drop-tube reactors, where, at much higher temperatures, only a very small enhancement of the NO removal rate has been found (Ref. 3). As may be seen from the figures presented in this report, the effect of H_2 and CO addition tend to decrease with temperature and to vanish at temperatures above 900 to 1000°C.

The bound hydrogen content is much smaller in chars than in coals, and is smaller in anthracite than in bituminous coals; thus, these observations are in full agreement with (1) what has been mentioned earlier (paragraph 2.2.1.1) and (2) the results obtained in the earlier parametric investigation of the heterogeneous NO reduction mechanism (see Part I), according to which the overall NO removal rate $\overline{V}$ is not enhanced by CO or H_2 addition as soon as there exists sufficient bound hydrogen atoms in the solid lattice.

2.2.1.3 Effect of Coal Nature

- Since for coals the overall NO removal rate does not depend, to a first approximation, on the CO or H_2 content of the gas phase (see paragraph 2.2.2), no distinction between gas streams with and without those gaseous reductants should be made for coals. A proper comparison of the overall rate $\overline{V}$ for different coals should account for differences in specific surface area (SSA). The effect of SSA on $\overline{V}$ is clearly shown in Figure 74. The overall NO removal rates are found to be proportional to the SSA for a given coal; however, values of the ratio $\overline{V}/(X_{NO})_i$ or of $\overline{V}/(X_{NO})_i/SSA$, determined on different coals, do not systematically vary with coal rank. For all the coals studied, the extreme (maximum and minimum) values of these two ratios, measured at $650^{o}C$, differ by a factor 7.4 and 12.3, respectively.

- Chars

  For all chars studied, the extreme values of the ratios $\overline{V}/(X_{NO})_i$ and $\overline{V}/(X_{NO})_i/SSA$, measured at $650^{o}C$, may differ by a factor F_1, and F_2, respectively, as indicated below:

	Coals	Chars ($650^{o}C$)		
	$650^{o}C$	NO	NO+CO	NO+H_2
$F_1 = \frac{\left[\overline{V}/(X_{NO})_i\right]_{max}}{\left[\overline{V}/(X_{NO})_i\right]_{min}}$	7.4	28.8	17.3	10.5
$F_2 = \frac{\left[\overline{V}/(X_{NO})_i\right]^{SA}_{max}}{\left[\overline{V}/(X_{NO})_i\right]^{SA}_{min}}$	12.3	12.2	12.4	34.1

2.2.2 Overall N_2 Formation Rates, Compared to Overall NO Removal Rates

Figures 79 through 83 show the ratio of the N_2 formation rate and the overall NO removal rate, determined according to eqs. (2) and (3), for different coals and their chars. As a general rule, the N_2 formation lags behind the NO removal, due primarily to the intermediate formation of ammonia. Consequently, it is found that the ratio $2\overline{V}_n/\overline{V}$ decreases when $(NH_3)_f$ increases, i.e.:

- At lower temperatures, where the NH_3 formation rates are larger than the rates of transformation of ammonia into N_2.
- At a given temperature the ratio $2\overline{V}_n/\overline{V}$ is generally smaller for the coal than for the corresponding char.

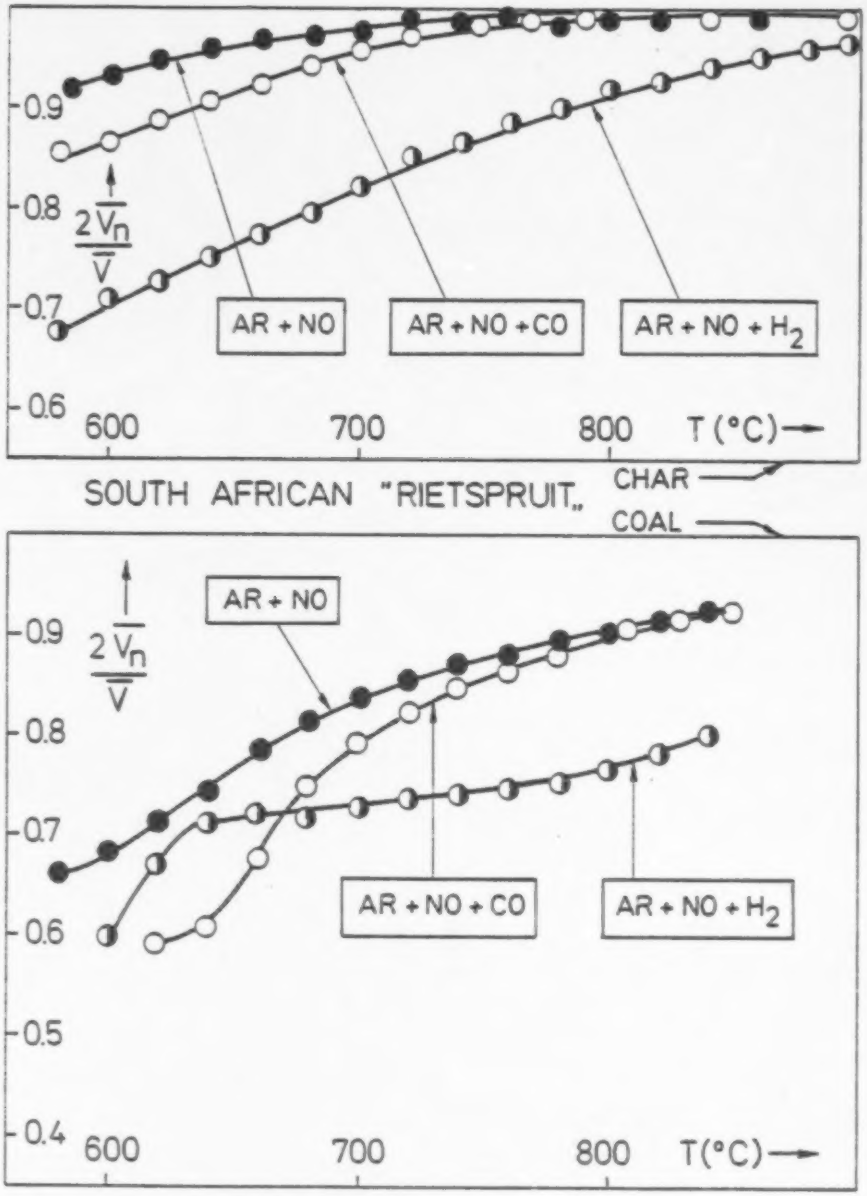

Figure 79. Comparison of Overall N_2 Formation Rates and Overall NO Removal Rates, Measured on South African "Rietspruit" Coal and Char.

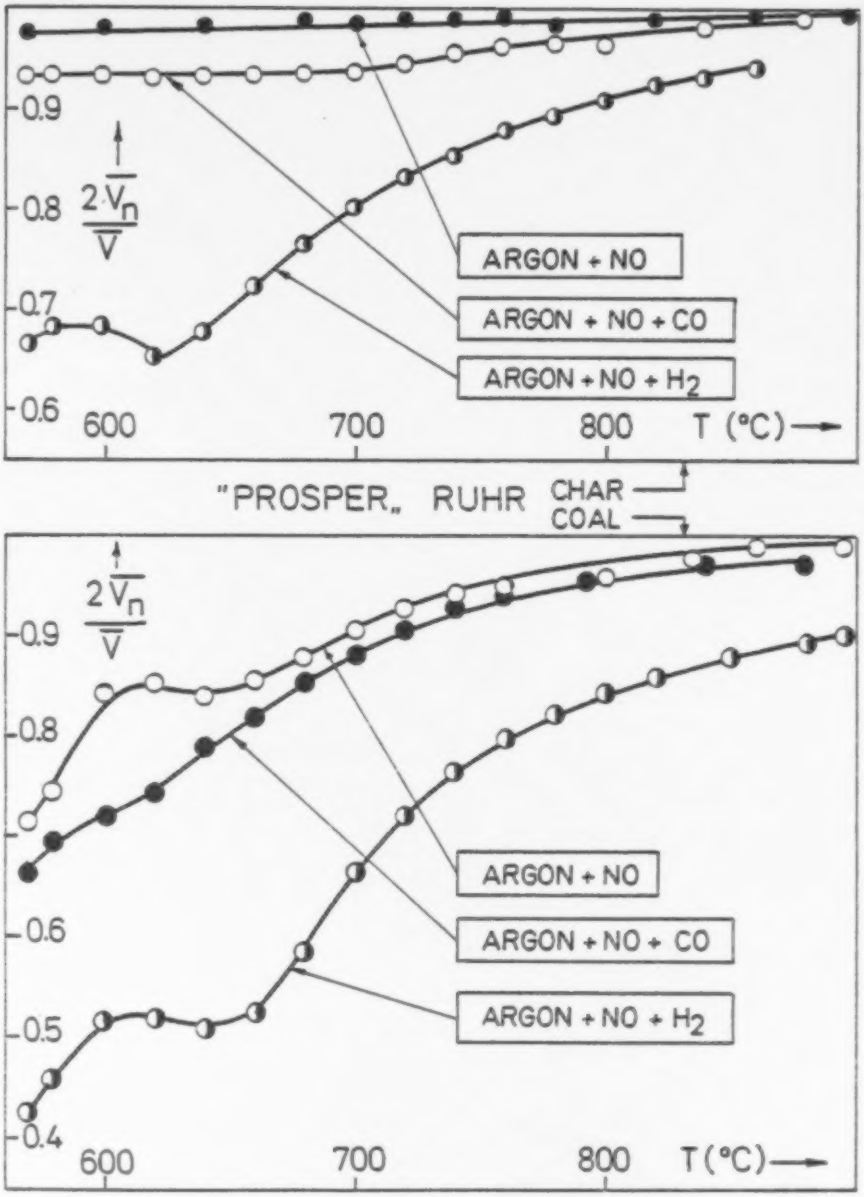

Figure 80. Comparison of Overall N_2 Formation Rates and Overall NO Removal Rates, Measured on Ruhr Coal "Prosper," Coal and Char.

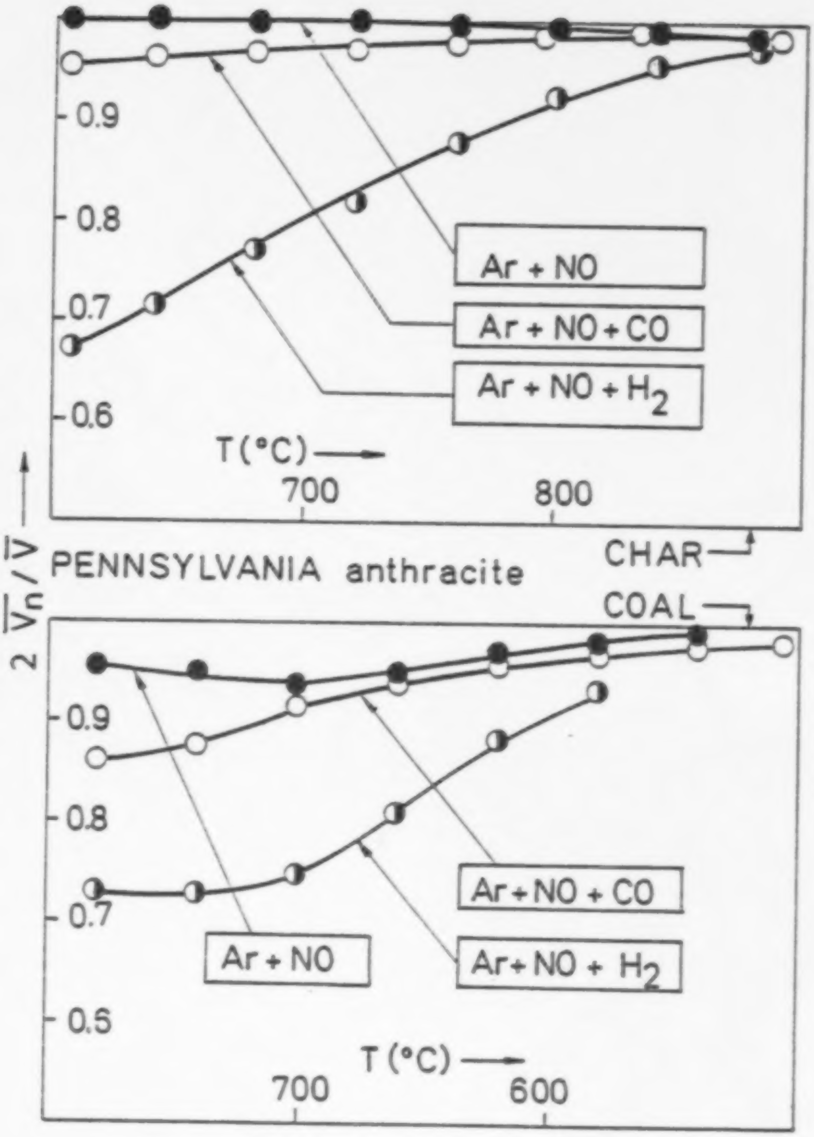

Figure 81. Comparison of Overall N_2 Formation Rates and Overall NO Removal Rates, Measured on Pennsylvania Anthracite, Coal and Char.

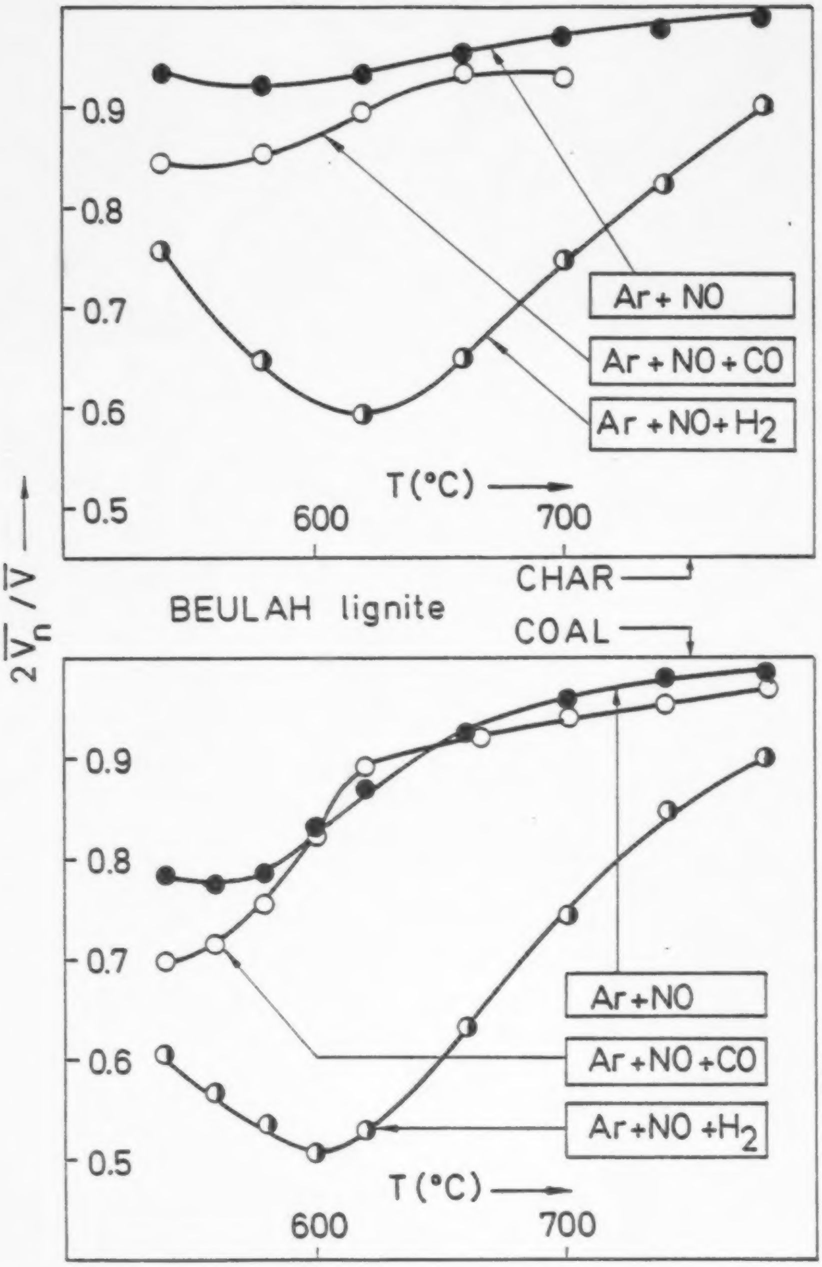

Figure 82. Comparison of Overall N_2 Formation Rates and Overall NO Removal Rates, Measured on "Beulah" North Dakota Lignite, Coal and Char.

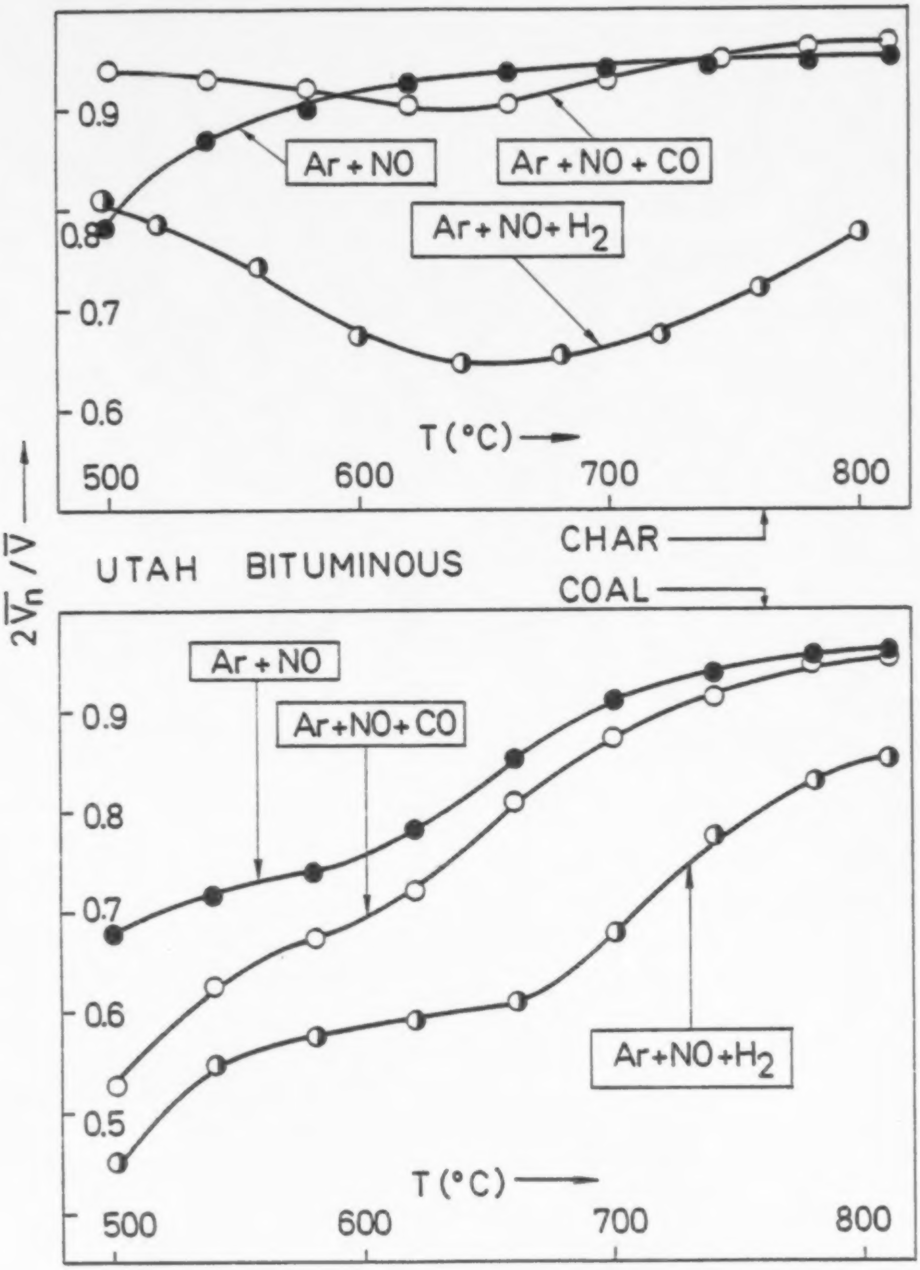

Figure 83. Comparison of Overall N_2 Formation Rates and Overall NO Removal Rates, Measured on Utah Bituminous Coal and Char.

- Addition of CO and especially H_2 to the gas stream substantially decreases the ratio $2\overline{V}_n/\overline{V}$.

2.3 Comparison of Rate Constants of Overall Nitric Oxide Removal and N_2 Formation From Coals and Chars

Simple rate expressions determined for the different coals and chars are presented in Table 4. Partial reaction orders with respect to NO, CO, and H_2 have been determined for the chars exclusively but also utilized in the rate expressions for the corresponding coals.

The observations made in section 2.2 concerning the comparison of rates obtained from coals/chars, concerning the effect of the nature of the coals, concerning the effect of addition of gaseous reducing agents (CO or H_2) and concerning the comparison of $\overline{V}_n$ and $\overline{V}$, generally are confirmed by the rate constants listed in Table 4. These data also provide some further informations:

- In the absence of any added gaseous reducing agent, the overall N_2 formation rate (x 2) is, in many cases, almost identical to the overall NO removal rate for chars (see Table 4, d, e, f, g, and h) and anthracite coal (see Table 4, f). This is due, of course, to the relatively small quantities of ammonia formed in these conditions (reaction 1 being much more important than reaction 2).

  However, for bituminous coals, even in the absence of CO or H_2, the N_2 formation rate has a temperature dependence (θ = activation temperature) which is slightly higher than that of the overall NO removal rate.

- In the presence of gaseous reducing agents, especially hydrogen molecules, the activation temperature, θ, for N_2 formation is normally higher than that of the overall NO removal, both for chars and for coals. (Caution: These findings should not be extrapolated beyond the temperature range for which these constants have been determined.)

- The above information generally applies at temperatures above 600^oC (and below 1000^oC). In some cases, especially in cases

Table 4a. Overall NO Removal Rates and N_2 Formation Rates

GAS COMPOSITION	TEMPERATURE RANGE(°C)	POCAHONTAS medium volatile (BECKLEY, WEST VIRGINIA)			
		$-d(NO)/dt\ (cm^3 g^{-1} s^{-1})$		$2\ d(N_2)/dt\ (cm^3 g^{-1} s^{-1})$	
		COAL	CHAR	COAL	CHAR
NO	$T < 450$	$3.32\ 10^4 \exp(-9090/T)\ X_{NO}^{0.66}$	$2.4\ 10^4 \exp(-11600/T)\ X_{NO}^{0.66}$	$4.4\ 10^2 \exp(-6230/T)\ X_{NO}^{0.66}$	$3.27\ 10^7 \exp(-19360/T)\ X_{NO}^{0.66}$
	$450 < T < 560$	$2.95\ \exp(-2290/T)\ X_{NO}^{0.66}$		$8.8\ 10^{-2}\ X_{NO}^{0.66}$	
	$T > 560$	$5.21\ 10^3 \exp(-8500/T)\ X_{NO}^{0.66}$		$2.06\ 10^5 \exp(-12120/T)\ X_{NO}^{0.66}$	
$NO+H_2$	$T < 450$	$6.48\ 10^{14} \exp(-21200/T)\ X_{NO} X_{H_2}$	$8.9\ 10^6 \exp(-10200/T)\ X_{NO} X_{H_2}$	$4\ 10^{12} \exp(-18700/T)\ X_{NO} X_{H_2}$	$2.65\ 10^8 \exp(-14180/T)\ X_{NO} X_{H_2}$
	$450 < T < 600$	$7.46\ 10^2 \exp(-1530/T)\ X_{NO} X_{H_2}$		15 to $40\ X_{NO} X_{H_2}$	
	$T > 600$	$9.4\ 10^7 \exp(-12120/T)\ X_{NO} X_{H_2}$		$2.1\ 10^{10} \exp(-18700/T)\ X_{NO} X_{H_2}$	
$NO+CO$	$T < 640$	$6.58\ 10^3 \exp(-5500/T)\ X_{NO} X_{CO}^{0.33}$	$2\ 10^6 \exp(-12200/T)\ X_{NO} X_{CO}^{0.33}$	$3.2\ 10^4 \exp(-6450/T)\ X_{NO} X_{CO}^{0.33}$	$4.4\ 10^6 \exp(-13100/T)\ X_{NO} X_{CO}^{0.33}$
	$T > 640$	$8.54\ 10^7 \exp(-14200/T)\ X_{NO} X_{CO}^{0.33}$		$1.45\ 10^8 \exp(-14200/T)\ X_{NO} X_{CO}^{0.33}$	

Table 4b. Overall NO Removal and N_2 Formation Rates

GAS COMPOSITION	TEMPERATURE RANGE(°C)	CEDAR GROVE high volatile (BECKLEY, WEST VIRGINIA)			
		$-d(NO)/dt \quad (cm^{3} g^{-1} s^{-1})$		$2\ d(N_2)/dt \quad (cm^{3} g^{-1} s^{-1})$	
		COAL	CHAR	COAL	CHAR
NO	T < 610	$7.0\ 10^{2} \exp(-5000/T)$ X_{NO}	$2.9\ 10^{8} \exp(-19800/T)$ X_{NO}	$1.65\ 10^{3} \exp(-6100/T)$ X_{NO}	$9.2\ 10^{9} \exp(-24000/T)$ X_{NO}
	T > 610	$6.6\ 10^{4} \exp(-8970/T)$ X_{NO}		$2.9\ 10^{5} \exp(-10660/T)$ X_{NO}	
NO + H_2	T < 560	$1.9\ 10^{2} \exp(-1000/T)$ $X_{NO}^{0.9} X_{H_2}^{0.9}$	$7.8\ 10^{8} \exp(-16000/T)$ $X_{NO}^{0.9}\ X_{H_2}^{0.9}$	$3.2\ 10^{1} \exp(-2640/T)$ $X_{NO}^{0.8} X_{H_2}^{0.7}$	$4.8\ 10^{8} \exp(-17700/T)$ $X_{NO}^{0.8}\ X_{H_2}^{0.7}$
	T > 560	$7.2\ 10^{6} \exp(-9960/T)$ $X_{NO}^{0.9} X_{H_2}^{0.9}$		$6.1\ 10^{8} \exp(-16530/T)$ $X_{NO}^{0.8}\ X_{H_2}^{0.7}$	

Table 4c. Overall NO Removal and N_2 Formation Rates

GAS COMPOS-ITION	TEMPER-ATURE RANGE(°C)	POCAHONTAS low volatile, high ash (= Pocah. med.vol. $^{as}_{mined}$) (BERKLEY, WEST VIRGINIA)			
		$-d(NO)/dt$ $(cm^3 g^{-1} s^{-1})$		$2\ d(N_2)/dt$ $(cm^3 g^{-1} s^{-1})$	
		COAL	CHAR	COAL	CHAR
NO	T < 540	$1.25\ 10^1 \exp(-2000/T)\ X_{NO}$	$1.2\ 10^9 \exp(-20480/T)\ X_{NO}$	$5\ 10^1 \exp(-3600/T)\ X_{NO}$	$6.8\ 10^{10} \exp(-25100/T)\ X_{NO}$
	T > 540	$2.63\ 10^5 \exp(-10000/T)\ X_{NO}$		$5.5\ 10^6 \exp(-12900/T)\ X_{NO}$	
NO + H_2	ALL TEM-PERATURES	$5.4\ 10^4 \exp(-6300/T)\ X_{NO}^{0.68} X_{H_2}$	$4.7\ 10^6 \exp(-10900/T)\ X_{NO}^{0.68} X_{H_2}$	$7.1\ 10^4 \exp(-10100/T)\ X_{NO}^{0.5} X_{H_2}^{0.5}$	$1.7\ 10^7 \exp(-15700/T)\ X_{NO}^{0.5} X_{H_2}^{0.5}$

Table 4d. Overall NO Removal and N_2 Formation Rates

GAS COMPOSITION	TEMPERATURE RANGE(°C)	SOUTH AFRICAN low-to-medium volatile bituminous			
		$-d(NO)/dt \quad (cm^3 g^{-1} s^{-1})$		$2\ d(N_2)/dt \quad (cm^3 g^{-1} s^{-1})$	
		COAL	CHAR	COAL	CHAR
NO	T > 560	0.05 to 0.10 mm size: $2.67\ 10^5 \exp(-9600/T) X_{NO}$	$3.7\ 10^4 \exp(-8900/T)\ X_{NO}$	$5.9\ 10^5 \exp(-10400/T) X_{NO}$	$3.6\ 10^4 \exp(-8900/T)\ X_{NO}$
		0.5 to 1 mm size: $1.08\ 10^5 \exp(-9600/T) X_{NO}$		$1.82\ 10^5 \exp(-10400/T) X_{NO}$	
$NO + H_2$	T > 500	0.05 to 0.10 mm size: $2.27\ 10^6 \exp(-7600/T)\ X_{NO} X_{H_2}$	$1.56\ 10^7 \exp(-9500/T)\ X_{NO} X_{H_2}$	$3.15\ 10^6 \exp(-8200/T)\ X_{NO} X_{H_2}$	$1.07\ 10^7 \exp(-9500/T)\ X_{NO} X_{H_2}$
		0.5 to 1 mm size: $7.71\ 10^7 \exp(-11500/T)\ X_{NO} X_{H_2}$		$1.04\ 10^8 \exp(-12200/T)\ X_{NO} X_{H_2}$	
NO + CO	T < 570	$3.13\ 10^3 \exp(-4200/T)\ X_{NO} X_{CO}^{0.33}$	$2.00\ 10^3 \exp(-4690/T)\ X_{NO} X_{CO}^{0.33}$	$6.93\ 10^2 \exp(-3670/T)\ X_{NO} X_{CO}^{0.33}$	$1.72\ 10^3 \exp(-4680/T)\ X_{NO} X_{CO}^{0.33}$
	T > 570	$2.10\ 10^6 \exp(-9830/T)\ X_{NO} X_{CO}^{0.33}$	$4.87\ 10^6 \exp(-11700/T)\ X_{NO} X_{CO}^{0.33}$	$4.69\ 10^6 \exp(-11020/T)\ X_{NO} X_{CO}^{0.33}$	$4.87\ 10^6 \exp(-11700/T)\ X_{NO} X_{CO}^{0.33}$

Table 4e. Overall NO Removal and N_2 Formation Rates

GAS COMPOS-ITION	TEMPER-ATURE RANGE(°C)	RUHRKOHL "PROSPER" , low volatile bituminous (West GERMANY)			
		$-d(NO)/dt \quad (cm^3 g^{-1} s^{-1})$		$2\ d(N_2)/dt \quad (cm^3 g^{-1} s^{-1})$	
		COAL	CHAR	COAL	CHAR
NO	T < 600	$6.13\ 10^3 \exp(-5930/T)\ X_{NO}$	$1.03\ 10^5 \exp(-9700/T)\ X_{NO}$	$4.20\ 10^5 \exp(-9170/T)\ X_{NO}$	$10^5 \exp(-9700/T)\ X_{NO}$
	T > 600	$4.1\ 10^5 \exp(-9660/T)\ X_{NO}$		$1.22\ 10^6 \exp(-10180/T) X_{NO}$	
$NO + H_2$	T < 540	$4.83\ 10^4 \exp(-4750/T)\ X_{NO} X_{H_2}$	$6.39\ 10^8 \exp(-12900/T)\ X_{NO} X_{H_2}$	$1.59\ 10^4 \exp(-4650/T)\ X_{NO} X_{H_2}$	$4.95\ 10^8 \exp(-13050/T)\ X_{NO} X_{H_2}$
	T > 540	$1.28\ 10^8 \exp(-11100/T)\ X_{NO} X_{H_2}$		$6.23\ 10^8 \exp(-13160/T)\ X_{NO} X_{H_2}$	
NO + CO	T < 600	$1.09\ 10^4 \exp(-5290/T)\ X_{NO} X_{CO}^{0.33}$	$9.2\ 10^2 \exp(-4080/T)\ X_{NO} X_{CO}^{0.33}$	$1.23\ 10^4 \exp(-5970/T)\ X_{NO} X_{CO}^{0.33}$	$8.28\ 10^2 \exp(-4080/T)\ X_{NO} X_{CO}^{0.33}$
	T > 600	$3.03\ 10^6 \exp(-9970/T)\ X_{NO} X_{CO}^{0.33}$	$4.58\ 10^7 \exp(-13890/T)\ X_{NO} X_{CO}^{0.33}$	$8.31\ 10^6 \exp(-11110/T)\ X_{NO} X_{CO}^{0.33}$	$5.01\ 10^7 \exp(-14090/T)\ X_{NO} X_{CO}^{0.33}$

Table 4f. Overall NO Removal and N_2 Formation Rates

GAS COMPOS-ITION	TEMPER-ATURE RANGE(°C)	PENNSYLVANIA ANTHRACITE			
		$-d(NO)/dt \quad (cm^3 g^{-1} s^{-1})$		$2\ d(N_2)/dt \quad (cm^3 g^{-1} s^{-1})$	
		COAL	CHAR	COAL	CHAR
NO	$T > 440$	$1.5\ 10^4 \exp(-7700/T)\ X_{NO}$	$6.1\ 10^5 \exp(-12200/T) X_{NO}$	$1.5\ 10^4 \exp(-7700/T) X_{NO}$	$6.1\ 10^5 \exp(-12200/T) X_{NO}$
$NO + H_2$	$T > 440$	$8.7\ 10^5 \exp(-7100/T)$ $X_{NO} X_{H_2}$	$5.2\ 10^5 \exp(-7200/T)$ $X_{NO} X_{H_2}$	$7.5\ 10^5 \exp(-7200/T)$ $X_{NO} X_{H_2}$	$5.8\ 10^5 \exp(-7500/T)$ $X_{NO} X_{H_2}$
$NO + CO$	$T < 600$	$1.9\ 10^3 \exp(-4600/T)$ $X_{NO} X_{CO}^{0.33}$	$4.86\ 10^3 \exp(-5640/T)$ $X_{NO} X_{CO}^{0.33}$	$1.9\ 10^3 \exp(-4600/T)$ $X_{NO} X_{CO}^{0.33}$	$5.58\ 10^3 \exp(-5830/T)$ $X_{NO} X_{CO}^{0.33}$
	$T > 600$	$8.6\ 10^5 \exp(-9700/T)$ $X_{NO} X_{CO}^{0.33}$	$2.64\ 10^6 \exp(-11730/T)$ $X_{NO} X_{CO}^{0.33}$	$7.8\ 10^5 \exp(-9700/T)$ $X_{NO} X_{CO}^{0.33}$	$2.64\ 10^6 \exp(-11730/T)$ $X_{NO} X_{CO}^{0.33}$

Table 4g. Overall NO Removal and N_2 Formation Rates

GAS COMPOS-ITION	TEMPER-ATURE RANGE	NORTH DAKOTA "BEULAH" LIGNITE			
		$-\ d(NO)/dt \quad (cm^3 g^{-1} s^{-1})$		$2\ d(N_2)/dt \quad (cm^3 g^{-1} s^{-1})$	
		COAL	CHAR	COAL	CHAR
NO	$T \gtrsim 340$	$6.0\ 10^3 \exp(-5200/T)\ X_{NO}$	$4.5\ 10^3 \exp(-5200/T)\ X_{NO}$	$1.2\ 10^4\ \exp(-5900/T)\ X_{NO}$	$4.5\ 10^3 \exp(-5200/T)\ X_{NO}$
$NO + H_2$	$T \gtrsim 440$	$8.7\ 10^5 \exp(-7100/T)$ $X_{NO}\ X_{H_2}$	$5.2\ 10^5 \exp(-7200/T)$ $X_{NO}\ X_{H_2}$	$7.5\ 10^5 \exp(-7200/T)$ $X_{NO}\ X_{H_2}$	$5.8\ 10^5 \exp(-7500/T)$ $X_{NO}\ X_{H_2}$
NO + CO	$T \gtrsim 300$	$1.6\ 10^4\ \exp(-4800/T)$ $X_{NO}\ X_{CO}^{0.33}$	$2.0\ 10^4\ \exp(-4700/T)$ $X_{NO}\ X_{CO}^{0.33}$	$2.1\ 10^4\ \exp(-5200/T)$ $X_{NO}\ X_{CO}^{0.33}$	$1.8\ 10^4\ \exp(-4730/T)$ $X_{NO}\ X_{CO}^{0.33}$

Table 4h. Overall NO Removal and N_2 Formation Rates

GAS COMPOSITION	TEMPERATURE RANGE	UTAH BITUMINOUS			
		$-\,d(NO)/dt$ $(cm^3 g^{-1} s^{-1})$		$2\,d(N_2)/dt$ $(cm^3 g^{-1} s^{-1})$	
		COAL	CHAR	COAL	CHAR
NO	$T > 440$	$2.3\ 10^3\ \exp(-5200/T) X_{NO}$	$1.2\ 10^6 \exp(-12200/T) X_{NO}$	$4.8\ 10^3 \exp(-6100/T)\ X_{NO}$	$1.7\ 10^6 \exp(-12600/T) X_{NO}$
$NO + H_2$	$T > 400$	$1.0\ 10^5\ \exp(-4800/T)\ X_{NO}\ X_{H_2}$	$1.5\ 10^6\ \exp(-7800/T)\ X_{NO}\ X_{H_2}$	$5.1\ 10^5\ \exp(-6650/T)\ X_{NO}\ X_{H_2}$	$1.1\ 10^6\ \exp(-7800/T)\ X_{NO}\ X_{H_2}$
$NO + CO$	$T > 460$	$8.1\ 10^3\ \exp(-4900/T)\ X_{NO}\ X_{CO}^{0.33}$	$3.6\ 10^4 \exp(-6700/T)\ X_{NO}\ X_{CO}^{0.33}$	$2.6\ 10^4\ \exp(-6300/T)\ X_{NO}\ X_{CO}^{0.33}$	$3.3\ 10^4\ \exp(-6700/T)\ X_{NO}\ X_{CO}^{0.33}$

where the solid particles are of relatively large sizes (see Table 4, a, b, and c) a quite different rate expression may be found for coals at lower temperatures, i.e. during the coal devolatilization. In these cases. the two different temperature regimes may be separated by a small temperature range where the temperature dependence θ for $\overline{V}$ and $\overline{V}_n$ becomes very small (see for example Table 4a).

- Normally, the temperature dependence of $\overline{V}$ and of $\overline{V}_n$, both for coals and chars, increases with the addition of CO or H_2 in the temperature range between 600 and 1000^{0}C. Two coals and chars were found to be different such that the temperature dependence decreased with the addition of CO or H_2 (see Pocahontas low-volatile, Table 4c and Utah bituminous, Table 4h).
- Both in the absence and the presence of CO or H_2, at temperatures above 600^{0}C, the temperature dependence (θ) of $\overline{V}$ and $\overline{V}_n$ is higher for chars than for the corresponding coals. However, there are a few exceptions: NO + CO and NO + H_2 on Pocahontas medium volatile (Table 4a); NO on South African Rietspruit (Table 4d) or on Ruhrcoal Prosper (Table 4e); NO or NO + CO or NO + H_2 on North Dakota Beulah lignite (Table 4g).
- No systematic variation of the activation temperature (θ) of $\overline{V}$ and $\overline{V}_n$ could be found with respect to the coal rank, either with or without CO or H_2. The lowest values of θ have been found for Beulah lignite and Utah bituminous coal, but also the Pennsylvania anthracite is characterized by a fairly low activation temperature.
- The overall reaction order with respect to nitric oxide (determined on chars exclusively) is usually found to be equal to one. The only exceptions which have been observed are with chars of relatively large particle sizes: 0.66 in the case of NO fed on Pocahontas medium volatile (Table 4a) and 0.5 to 0.68 in the case of NO + H_2 fed over Pocahontas low-volatile (Table 4c).

Even in the presence of CO or H_2, the order with respect to NO is generally very close or equal to one.

- The partial order with respect to hydrogen is close to one, except for one char (Pocahontas low-volatile).
- The partial order with respect to CO is relatively low and close to one-third. This suggests that CO may be chemisorbed on the active sites, which in turn means that the coreactant CO is self-inhibiting in reaction 8. An analogous conclusion has been previously obtained on other solid particles, during the parametric investigation of the heterogeneous NO reduction mechanism (Part I).
- The experimental uncertainty of the activation temperatures defined in this study is relatively important. The maximum dispersion is ± 600 K for the rate $\overline{V}$ as determined on char, ± 800 K for $\overline{V}$ as determined on coal, and ± 900 K for the rate $\overline{V}_n$ as determined on chars and coals.

3.0 NITRIC OXIDE REDUCTION ON COAL AND CHAR IN THE PRESENCE OF OXYGEN

In Part I, the previous parametric study on the mechanism of heterogeneous NO reduction on solid particles, it has been found that O_2 may present both inhibiting effects and promoting effects on NO reduction at the surface of solids. In particular a promoting effect has been found in the presence of CO. Since coal and char pyrolysis and oxidation processes yield nonnegligible quantities of carbon monoxide, the effect of oxygen on NO reduction was expected to be worthwhile investigating. This supplementary part of the study has not been conducted in a systematical gas fed over one type of coal and its char. For proper comparison with cases conducted in the absence of O_2, a preliminary study of the oxidation of coal and char had to be made in the same reactor.

3.1 Argon Containing O_2 Fed Over Coal and Char

3.1.1 Argon + O_2 on Coal

Results are shown in Figure 84 for two different initial oxygen concentrations fed over the Pocahontas medium-volatile coal. The following observations are of interest with respect to NO reduction:

- For the given experimental conditions (i.e. the initial oxygen concentrations not larger than 4 percent), the oxidation products are both CO and CO_2 in comparable quantities. Only at temperatures above 500°C is the CO_2 concentration larger than the CO concentration.
- Not only NO but HCN and NH_3 are released during coal oxidation. Hydrogen cyanide is released at lower temperatures than is ammonia, as was previously observed during coal pyrolysis with pure argon flow (compare with lower part of Figure 6). At still higher temperatures, NO levels become significant (unlike in the case of pyrolysis trials).

At temperatures for which there still exists oxygen in the reactor outlet stream, the disappearance rate of oxygen and the formation rates of CO and CO_2 can be determined. For Pocahontas medium-volatile coal the following

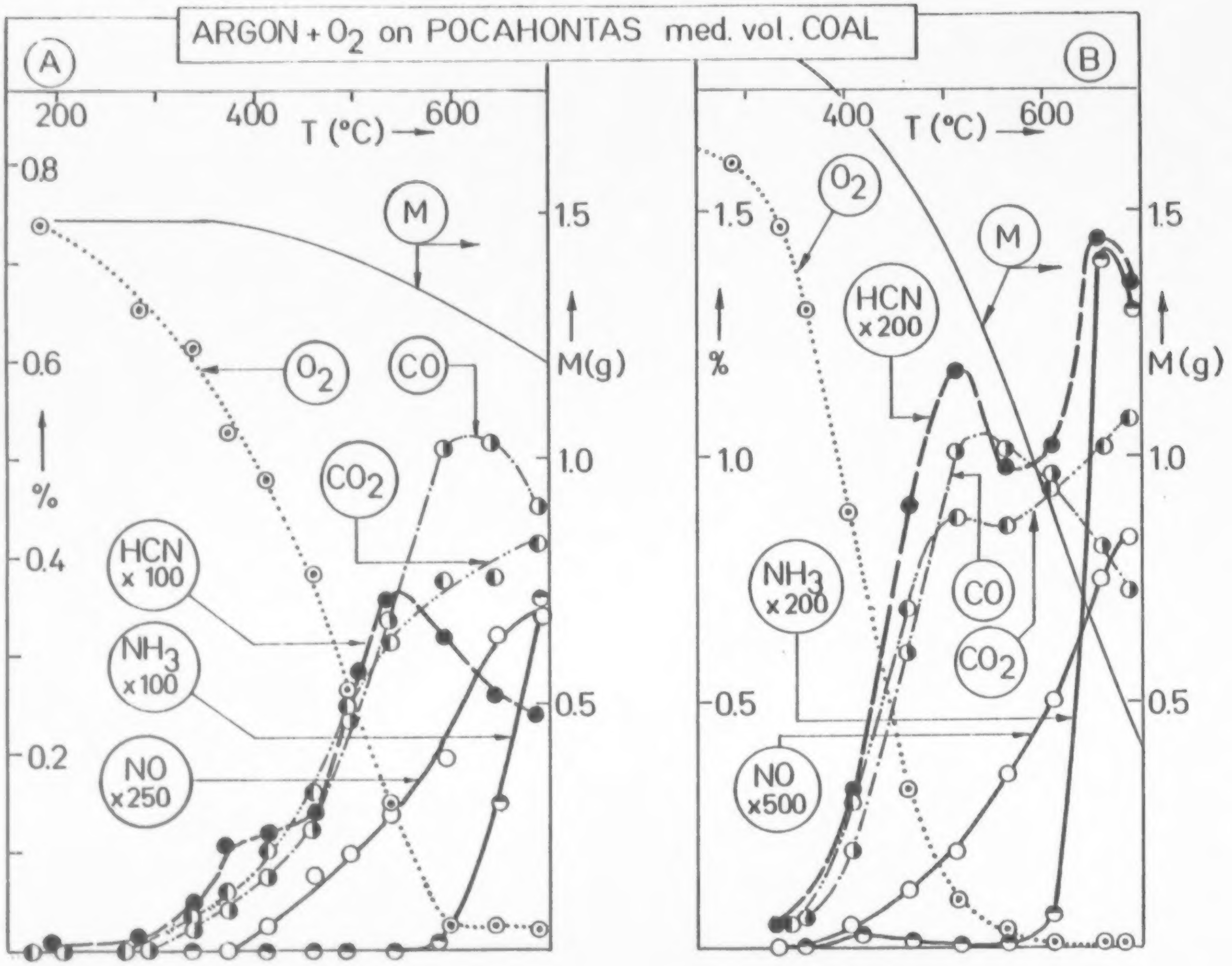

Figure 84. Argon + O_2 on Pocahontas Medium-Volatile Coal: $M_0 = 1.49$g; (A) D = 13.1 cm^3s^{-1}, $(O_2)_i = 0.76\%$; (B) D = 10.6 cm^3s^{-1}, $(O_2)_i = 1.64\%$.

(rather rough) espressions are obtained, assuming the partial order with respect to oxygen is equal to one:

$$d(CO)/dt = 6.1 \times 10^5 \exp\left[-8800(\pm 800)/T\right] X_{O_2} \quad \left(cm^3g^{-1}s^{-1}\right) \qquad (11)$$

$$d\left(CO_2\right)/dt = 1.6 \times 10^4 \exp\left[-6400(\pm 800)/T\right] X_{O_2} \quad \left(cm^3g^{-1}s^{-1}\right) \qquad (12)$$

A comparison of the solid mass decrease (-dM/dt) measured was made with the one calculated from the variation of the oxidation products (eq. 4). This indicates that at temperatures below 600°C, this oxidation accounts both for partial volatiles combustion and for partial char combustion.

3.1.2 Argon + O_2 on Char

An analogous study has been made on char of Pocahontas medium volatile. Results are shown in Figures 85 through 88. The following is observed:

- CO and CO_2 are formed as combustion products. For all temperatures the ratio $(CO_2)_f/(CO)_f$ is larger than one, this ratio increasing steeply at temperatures above 700°C for initial oxygen concentrations larger than 2 percent (see Figure 88).

  The following CO and CO_2 formation rates apply at temperatures below 600°C (at higher temperatures the oxygen has been consumed before the end of the bed):

  $$d(CO)/dt = 5.5 \times 10^7 \exp\left(-13900 \pm 700/T\right) X_{O_2} \quad \left(cm^3g^{-1}s^{-1}\right) \quad (13)$$

  $$d\left(CO_2\right)/dt = 7.1 \times 10^8 \exp\left(-15700 \pm 700/T\right) X_{O_2} \quad \left(cm^3g^{-1}s^{-1}\right) \quad (14)$$

  The partial order with respect to oxygen is found to be equal to one.

- During char oxidation, the nitrogen-containing species released are ammonia, hydrogen cyanide and nitric oxide (see Figure 85). Roughly speaking, the NO release rate is first order with respect to oxygen and is described by the following rate expression:

  $$d(NO)/dt = 1.0 \times 10^8 \exp\left(-19300 \pm 1500/T\right) X_{O_2} \left(cm^3g^{-1}s^{-1}\right) \quad (15)$$

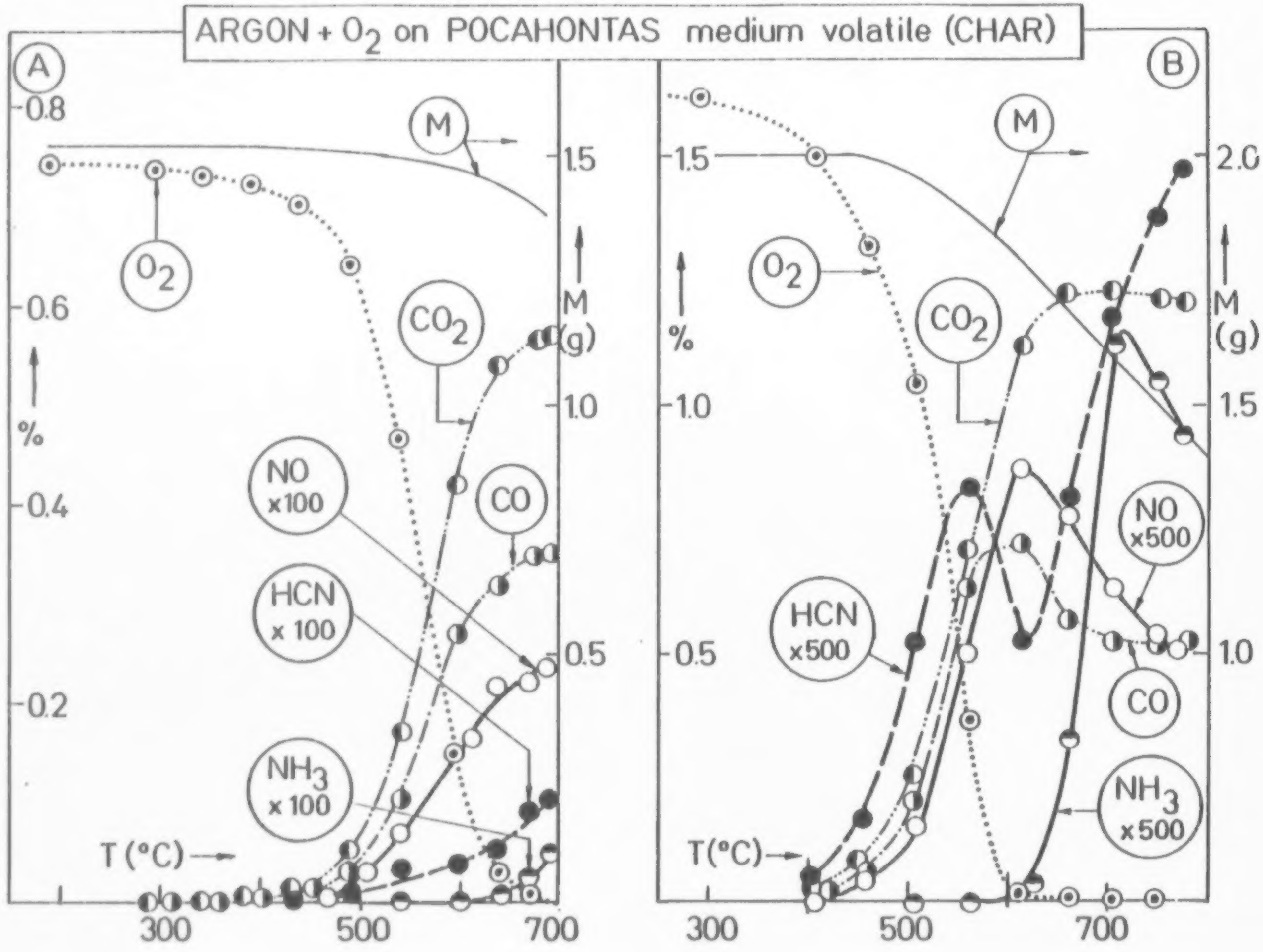

Figure 85. Argon + O_2 on Pocahontas Medium-Volatile Char: (A) $M_o = 1.52g$, $D = 13.1\ cm^3s^{-1}$, $(O_2)_i = 0.78\%$; (B) $M_o = 2g$, $D = 10.6\ cm^3s^{-1}$, $(O_2)_i = 1.63\%$.

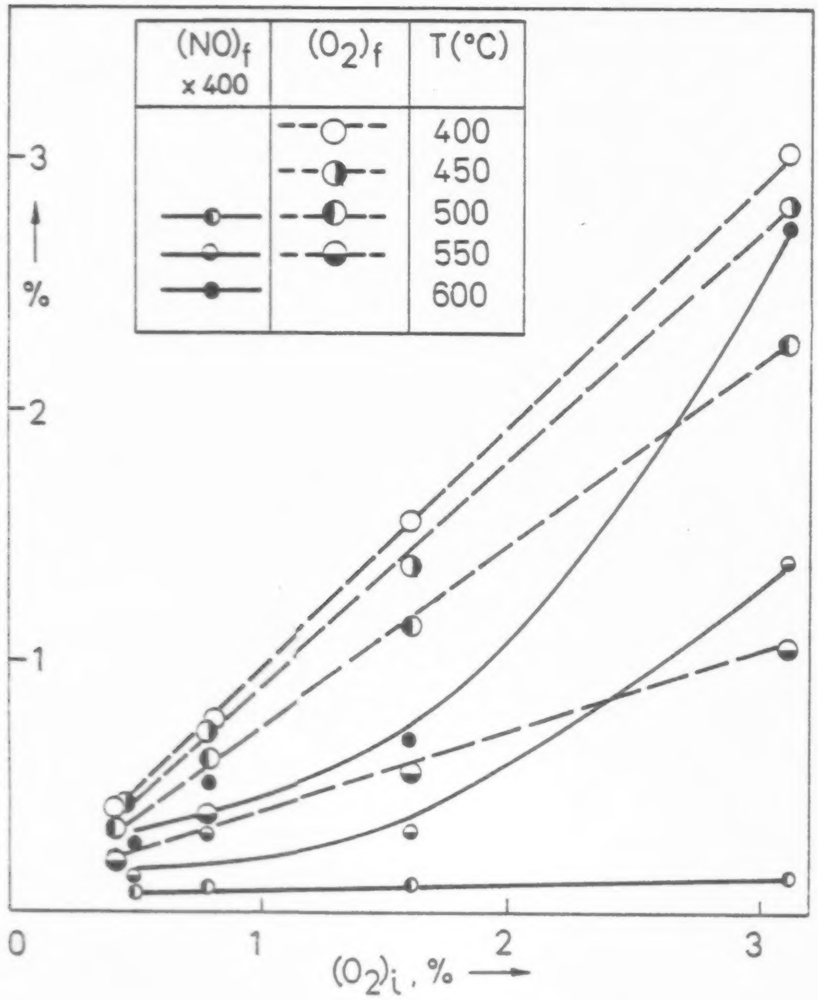

Figure 86. Argon + O$_2$ on Pocahontas Medium Volatile Char: Effect of Initial Oxygen Concentration on NO Formed During Oxidation.

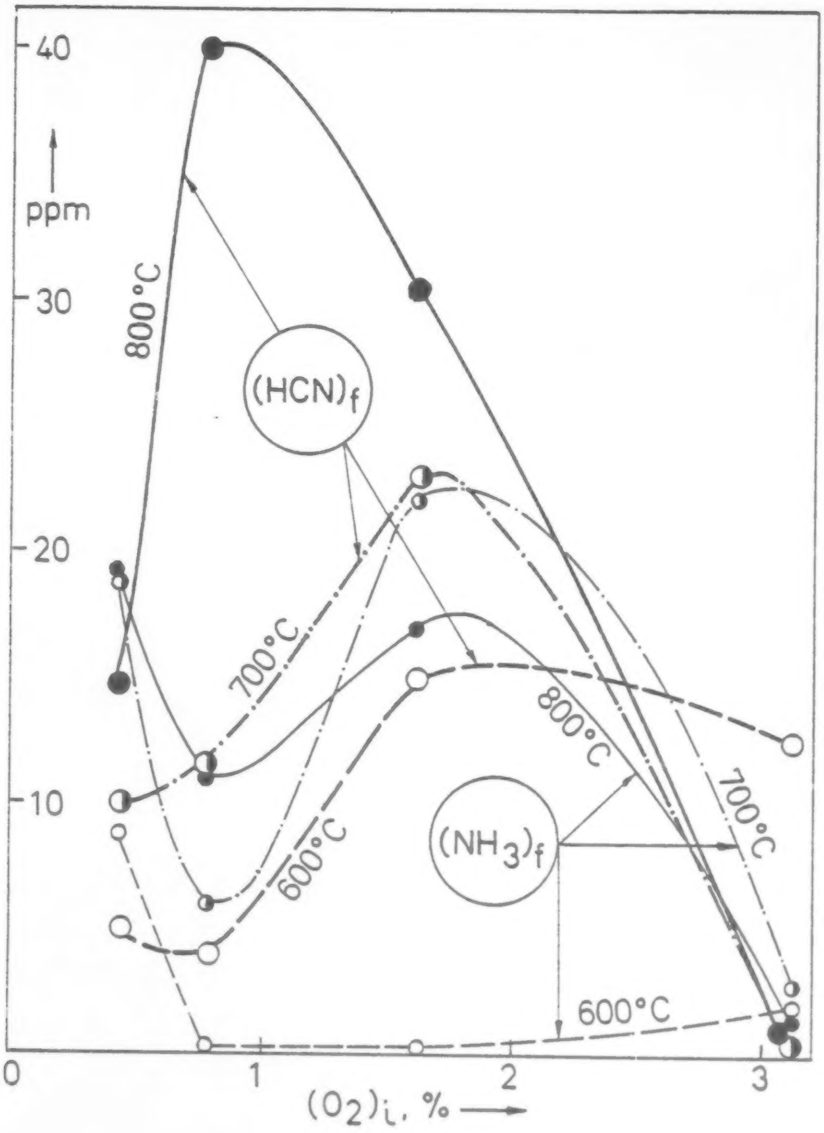

Figure 87. Argon + O_2 on Pocahontas Medium Volatile Char: Effect of Initial Oxygen Concentration on NH_3 and HCN Formed During Char Oxidation.

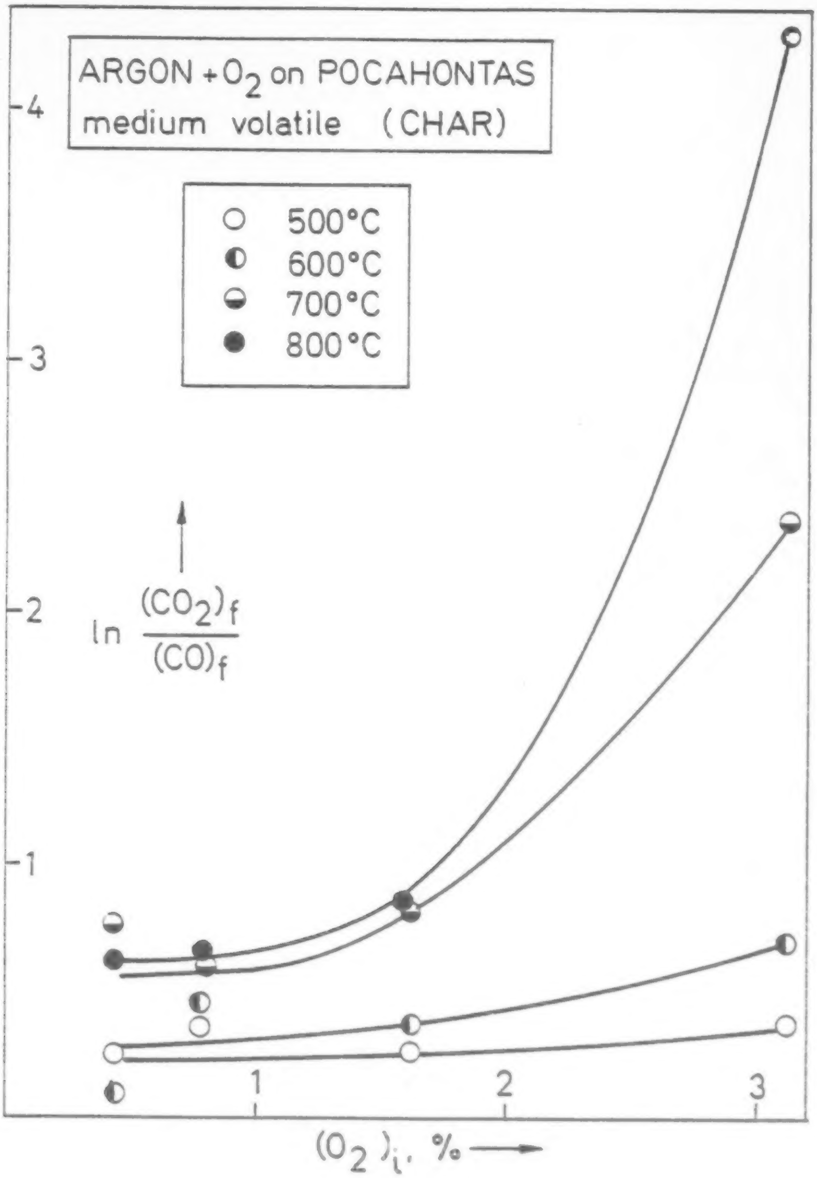

Figure 88. Argon + O_2 on Pocahontas Medium Volatile Char: Effect of Oxygen Concentration and Temperature on the Ratio $(CO_2)_f/(CO)_f$.

It is important to note that the ammonia and the hydrogen cyanide are released in amounts comparable to that of NO (see Figure 85). For temperatures above 600^{o}C both NH_3 and HCN seem to pass through a maximum with respect to $(O_2)_i$ (see Figure 87). The NH_3 and HCN concentrations in the outlet stream are much enhanced by the presence of oxygen (compare Figure 85 with Figure 6, upper part), NH_3 appearing at somewhat higher temperatures than does HCN and NO. From these observations, one conclusion that could be made is that NH_3 is primarily a reduction product of NO (e.g. via heterogeneous reaction 8), whereas NO and HCN are directly released during the oxidation of the char lattice.

3.2 Argon Containing NO and O_2 Fed Over Coal and Char

3.2.1 Trials on Char

Trials made on Pocahontas medium-volatile char are illustrated on Figures 89 through 92, for different initial oxygen concentrations. From Figure 89 it is found that the overall NO removal is enhanced when the initial oxygen concentration increases, at least up to a certain critical value. For $(O_2)_i$ = 4.95 percent, the NO removal enhancement stops and, at higher temperatures (above 760^{o}C), NO is less and less reduced. As may be seen from Figure 91, which gives the $(CO_2)_f/(CO)_f$ ratio as a function of temperature and initial oxygen concentration, this coincides with a steep increase of the $(CO_2)_f/(CO)_f$ ratio. From the previous study of heterogeneous NO reduction in the presence of oxygen (see Part I, paragraphs 3.2.1.3.1, 3.2.3.3.2, and 3.2.4.3), this may be explained by a scavenging effect of oxygen resulting in the removal of chemisorbed CO from the active sites, counteracting the self-inhibiting effect of CO in reaction 8 (NO + CO ----- CO_2 + 0.4 N_2). As also explained in this previous part, this promoting effect of oxygen on NO reduction is only observed as long as the ratio $(CO_2)/(CO)$ is sufficiently small (see Part I, compare trials Ar + NO + O_2 on Ethylene soot with trials Ar + NO + O_2 on cenospherical soot). In Figure 92, showing the overall NO removal rate $\overline{V}$ as a function of oxygen concentration at different temperatures, one may see this double effect of oxygen most clearly: (a) for initial oxygen

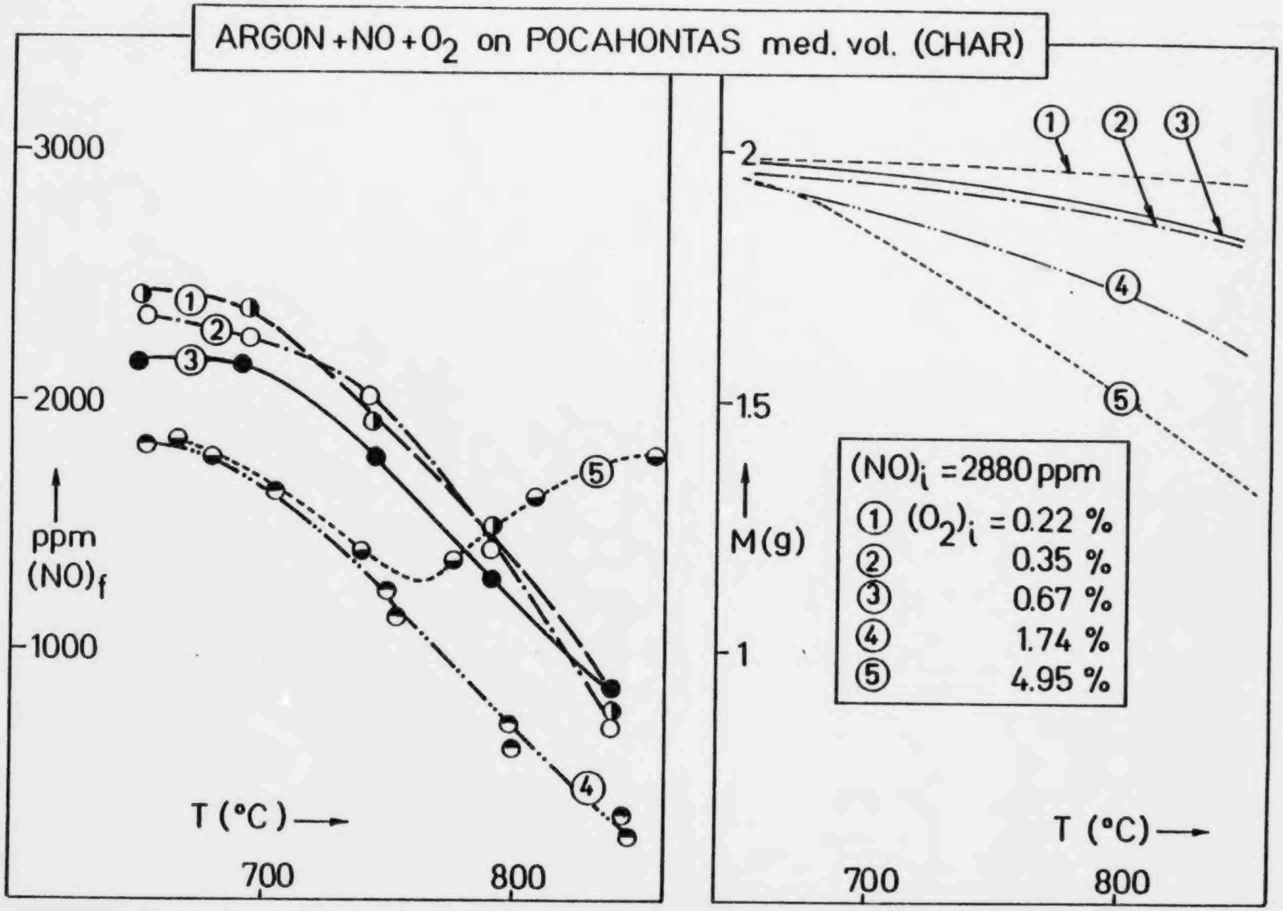

Figure 89. Argon + NO + O_2 on Pocahontas Medium-Volatile Char: M_o = 2g (M as a Function of Time--as Indicated); D = 10.5 $cm^3 s^{-1}$; $(NO)_i$ = 2880 ppm.

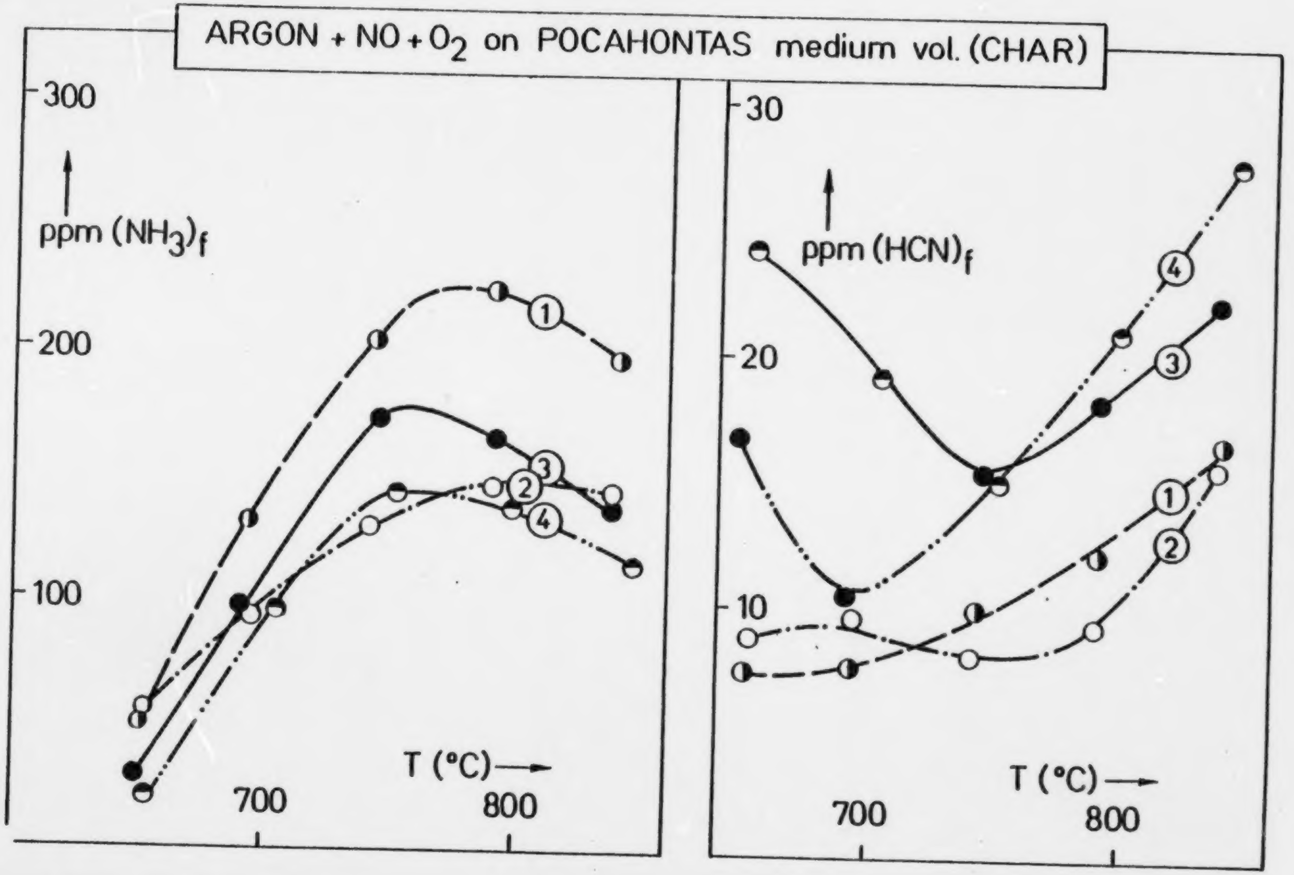

Figure 90. Same Experimental Conditions as for Figure 89: Ammonia and Hydrocyanic Acid Released as a Function of Temperature and Initial Oxygen Concentration. Numbers on Curves: See Key Given in Figure 89.

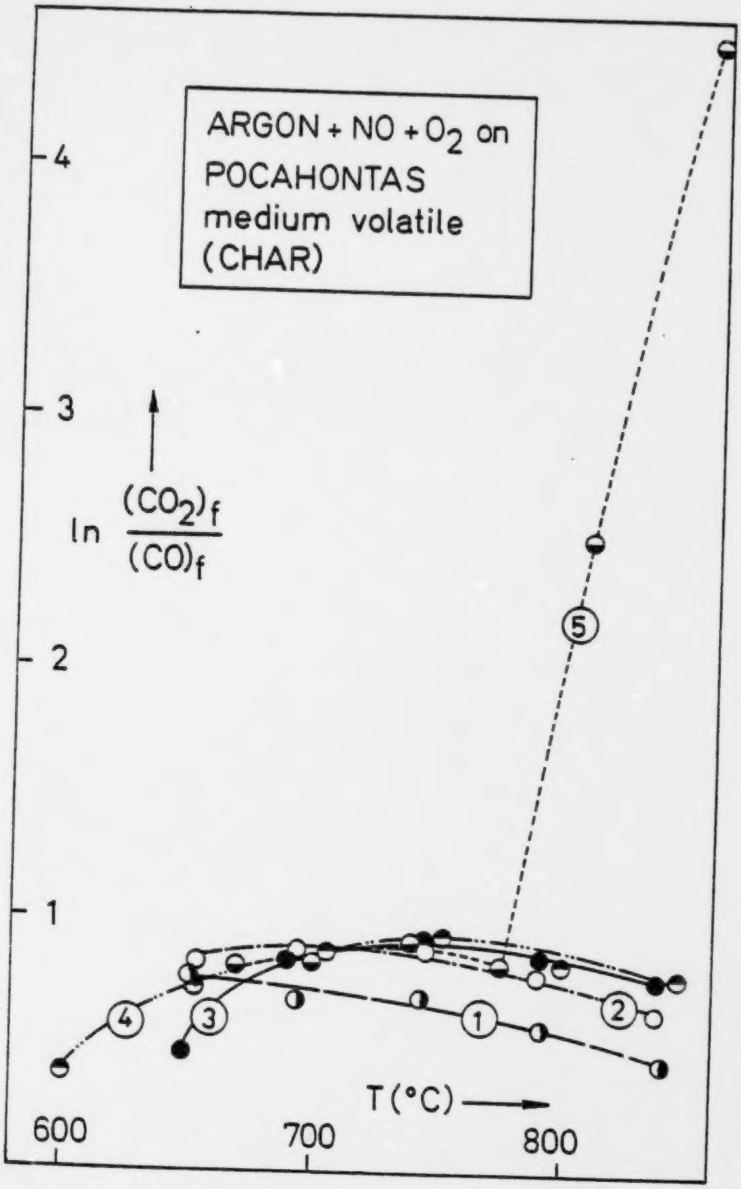

Figure 91. Same Experimental Conditions as For Figure 89: Ratio $(CO_2)_f/(CO)_f$ as a Function of Temperature and Initial Oxygen Concentration. Numbers on Curves: See Key Given on Figure 89.

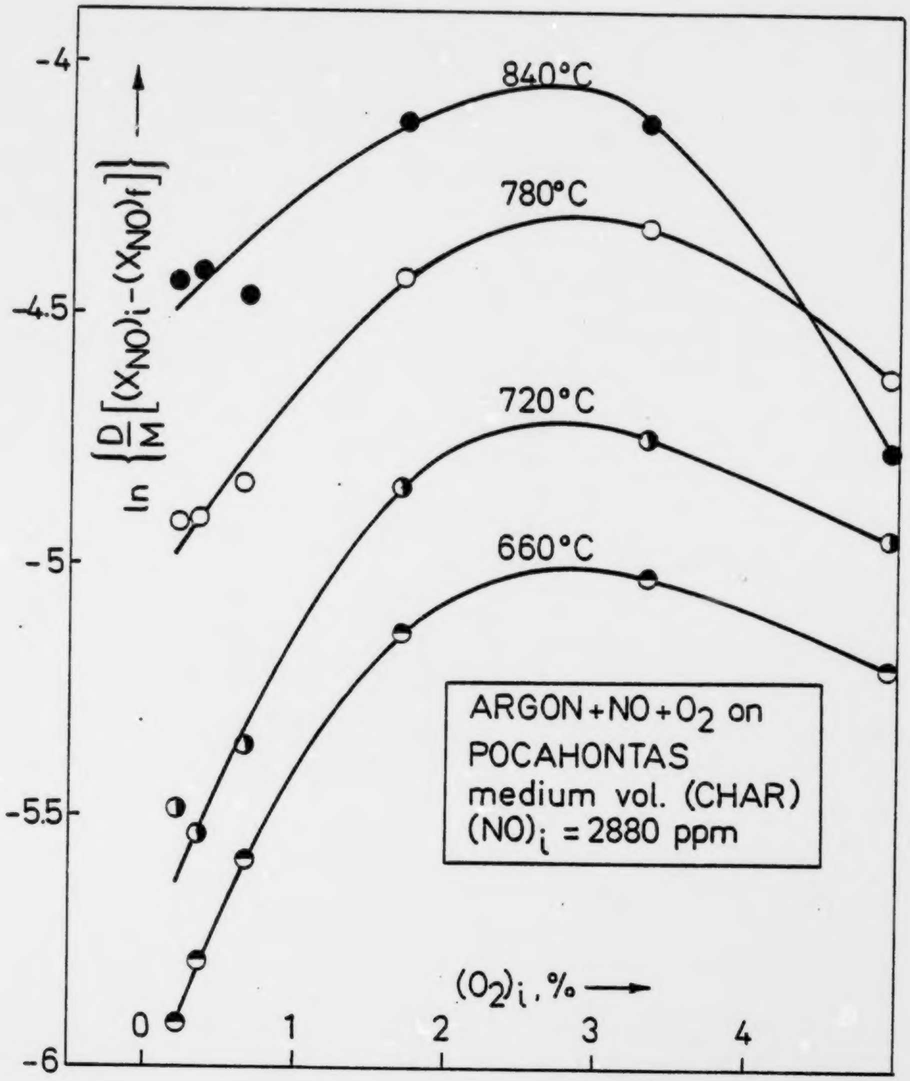

Figure 92. Argon + NO (2880 ppm) + O_2 on Pocahontas Medium Volatile Char: Variation of Overall NO Removal Rate ($\overline{V}$) as a Function of Temperature and Initial Oxygen Concentration.

concentrations lower than 2 percent, a promoting effect of O_2 on NO reduction is found, whereas (b) for oxygen concentrations beyond 3 percent there is a pronounced inhibiting effect. For high concentrations, the $(CO_2)f/(CO)_f$ ratio has become large enough to minimize the contribution of reaction 8 to the NO reduction and the chemisorption of oxygen (inhibiting the other NO reducing reactions, e.g. reactions 1 and 2) begins to prevail over the (reaction 8 promoting) scavenging effect.

In a more quantitative way, the promoting effect of small quantities of oxygen on overall NO removal for this given char can be expressed by the following rate:

$$-d(NO)/dt = 2.4 \times 10^4 \exp(-11600 \pm 1000/T)\, X_{NO}^{0.66} \tag{16}$$

$$\times \left[1 + 1.8\ 10^6 \exp(+7200 \pm 600/T)\, X_{O_2}^{1.9}\right] \left(cm^3 g^{-1} s^{-1}\right)$$

3.2.2 Trials on Coal

Results obtained upon feeding argon + NO + O_2 on Pocahontas medium-volatile coal are illustrated in Figures 93 and 94. The same discussion applies in this case as for the case of char. For initial oxygen concentrations below 3 percent the effect of oxygen on overall NO removal rate is a promoting one (see Figure 94). The rate expression obtained for overall NO removal is given by:

$$-d(NO)/dt = 5.2 \times 10^3 \exp(-8500/T)\, X_{NO}^{0.66} \tag{17}$$

$$\times \left[1 + 7.7\ 10^5 \exp(+3500 \pm 500/T)\, X_{O_2}^{2}\right] \left(cm^3 g^{-1} s^{-1}\right)$$

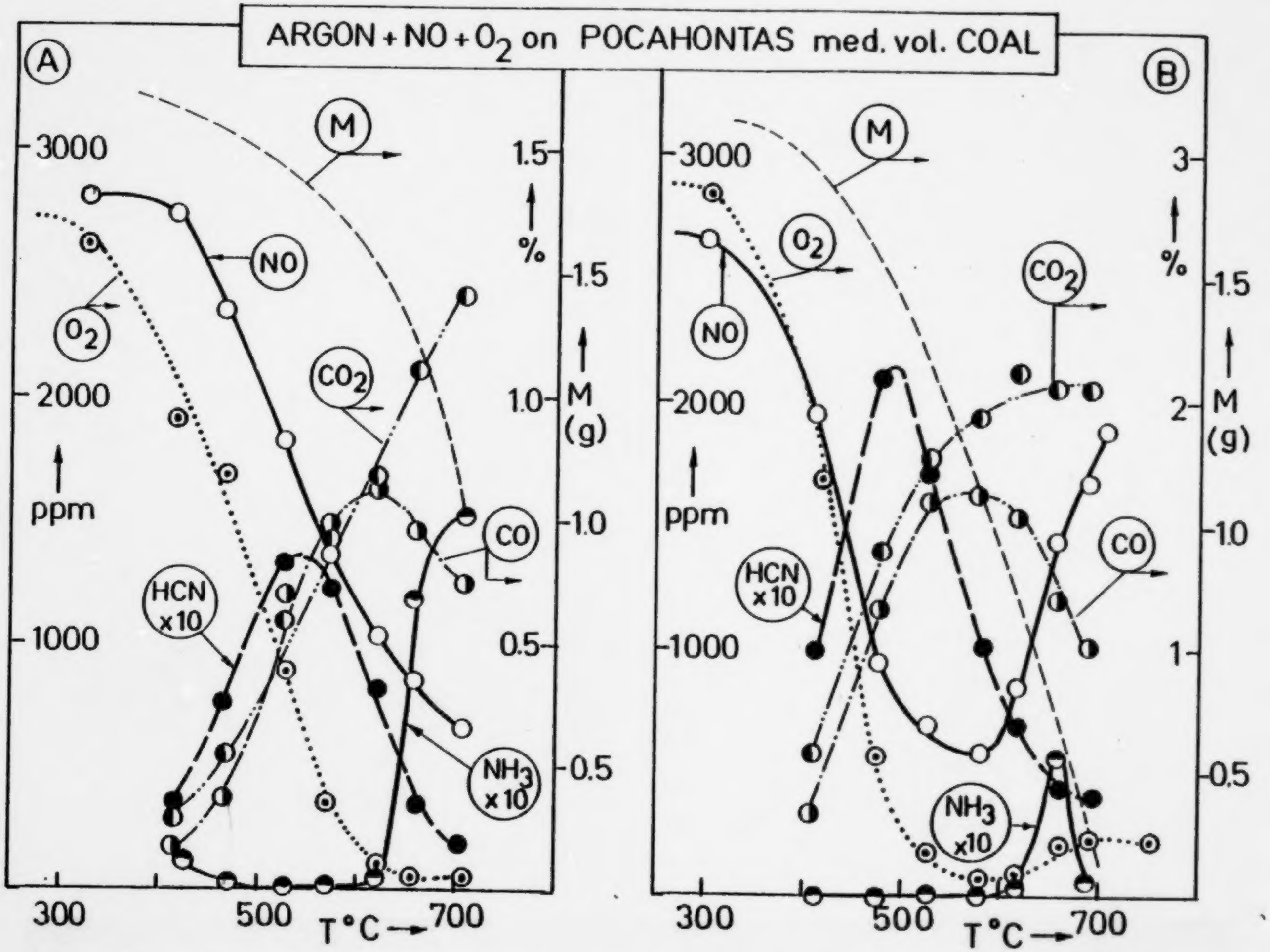

Figure 93. Argon + NO + O_2 on Pocahontas Medium-Volatile Coal: (A) M_o = 1.86g, D = 10.4 cm^3s^{-1}, $(NO)_i$ = 2800 ppm, $(O_2)_i$ = 1.36%; (B) M = 1.86g, D = 10.6 cm^3s^{-1}, $(NO)_i$ = 2700 ppm, $(O_2)_i$ = 2.88%.

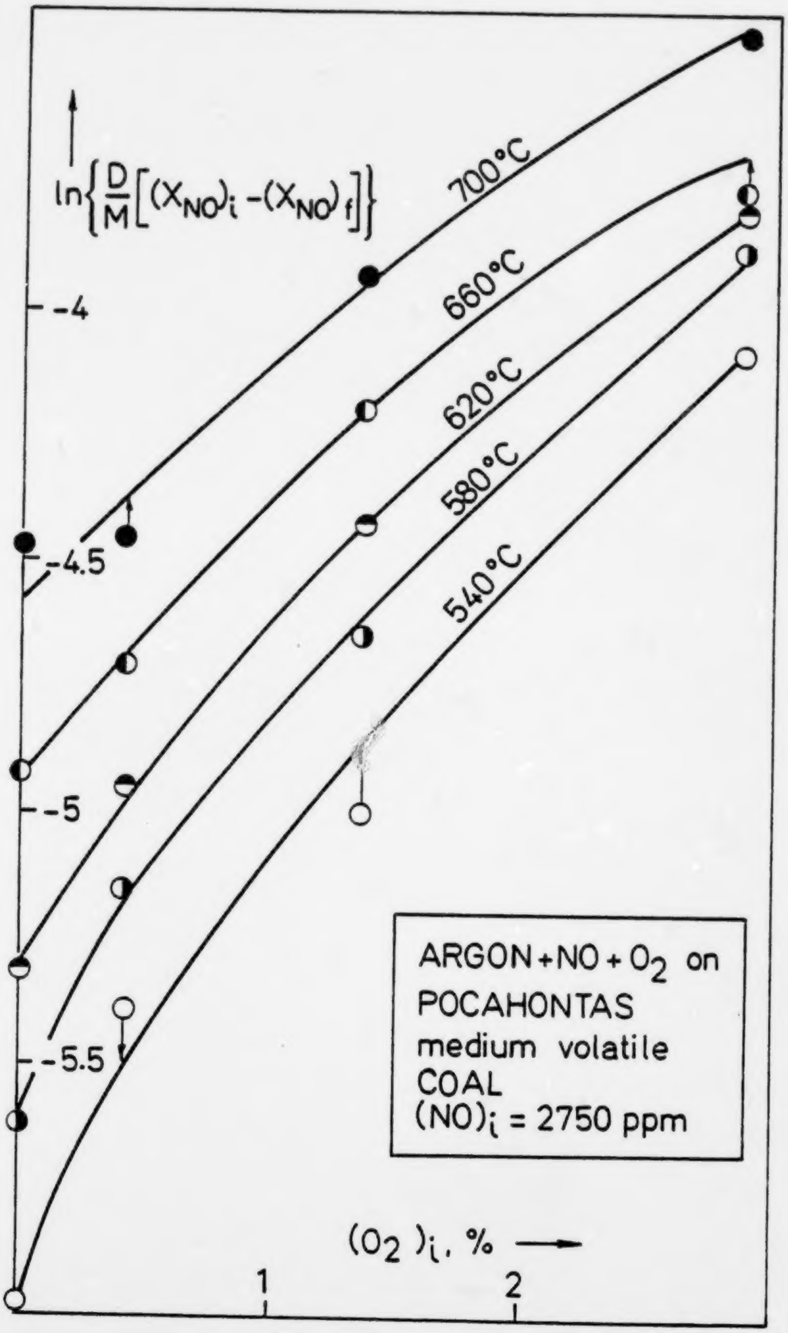

Figure 94. Argon + NO + O_2 on Pocahontas Medium Volatile Coal: Variation of NO Removal Rate with Initial Oxygen Concentration.

357

4.0 CONCLUSIONS

4.1 General

As a first general conclusion, it is found that the characteristics of NO reduction on coal and chars of different rank are in good agreement with the general reaction mechanism of heterogeneous NO reduction derived earlier in a parametric study (see Part I).

4.2 Particular Observations

In particular, it is found that:

- Due to the presence of bound hydrogen atoms, there exists also an indirect reduction path, passing through the intermediate formation of ammonia. As a consequence, the overall NO removal rate is faster on bituminous coals than on anthracite or on chars.
- The addition of a supplementary hydrogen source (especially hydrogen molecules) enhances this indirect NO reduction with respect to the direct one, as shown by the increased intermediate ammonia formation. As a consequence, the lag of overall N_2 formation rate behind overall NO removal rate may be important in these cases, at least at lower temperatures.
- For solid particles where the solid bound hydrogen atom concentration is relatively low (anthracite coal and especially chars) the addition of H_2 (or CO) enhances the overall NO removal rate, which is not the case when already large amounts of bound hydrogen are present (like in the case of bituminous coals).
- In the absence of gaseous reducing agents, the NO removal rate measured on chars is generally lower and more temperature-dependent than for the corresponding coals (despite the normally larger specific surface areas of the chars). This in turn is due to the fact that indirect NO reduction (by the succession of reactions 2, 13, and 4), plays a more important role on coals than on chars, and is less temperature-dependent than the direct NO reduction (by reaction 1). This difference of overall NO removal rate between coals and corresponding chars tends to

vanish upon addition of H_2 since the latter then takes over the role of hydrogen source for the indirect NO reduction over ammonia.

- Overall NO removal rates determined on coals of different rank (as well in the presence as in the absence of hydrogen or carbon monoxide) only differ by a factor of the order of ten, which is only slightly higher than the precision of these rate determinations. On the other hand, no systematic variation of the overall NO removal rate could be detected as a function of coal rank. Therefore, in a very first and rough approximation, one might consider a unique mean value for the sake of modeling heterogeneous NO reduction on coal or partly devolatilized coal particles. For chars of different nature, the overall NO removal rates may be more different (a factor of 30 has been found in extreme cases).
- With a few exceptions, the temperature dependence of the overall NO removal rate increases when CO or H_2 are added, both for coals and for chars.
- Partial orders of NO removal rates and N_2 formation rates, as defined on chars, are in general:
  - Primarily close to one with respect to NO.
  - Equal to one with respect to hydrogen molecules.
  - Close to one-third with respect to carbon monoxide; this value suggests the existence of chemisorbed CO resulting in an auto-inhibition of CO in reaction 8.

4.3 Effects of Oxygen on Overall NO Removal Rate

The effects of oxygen on the overall NO removal rate, observed on coals and chars, are either promoting (for CO_2/CO ratios not much larger than one, i.e. for initial oxygen concentrations below 2 to 3 percent) or inhibiting (for large CO_2/CO ratios, occurring at higher temperatures and larger oxygen concentrations). These findings may also be explained by results obtained during the previous parametric investigation of the heterogeneous NO reducing mechanism.

5.0 REFERENCES

1. Hendrickson, T. A. (editor). "Synthetic Fuels Data Handbook." Cameron Engineers Inc., Denver, 1975.

2. Smoot, L. D. and Pratt, D. T. (editors). "Pulverized-Coal Combustion and Gasification." New York and London: Plenum Press, 1979.

3. Levy, J. M.; Chan, L. K.; Sarofim, A. F.; and Beer, J. M. NO-Char reactions at pulverized coal flame conditions. Eighteenth Symposium (International) on Combustion. Waterloo, Canada, 1980.

III. Trials on Fly Ashes and Study of Reactions Involving Hydrogen Cyanide

Prepared by:

G. G. De Soete

Institute Francais du Petrole

Prepared for:

Energy and Environmental Research Corporation

TABLE OF CONTENTS

Section Page (III-)

INTRODUCTION 1

1.0 TRIALS ON FLY ASHES 2

1.2 Argon + Ammonia on Rietspruit Fly Ashes (Case D) 3
1.3 Argon + NO + CO on Fly Ashes (Case K) 3
1.4 Argon + NO + H_2 on Fly Ashes (Case O) 8
1.5 Conclusions 13

2.0 REACTIONS INVOLVING HCN AS A REACTANT 18

2.1 Argon + HCN Mixtures (Case G) 19

2.1.1 Argon + HCN on Graphite 19
2.1.2 Argon + HCN on Refractory Oxides (Alumina and Fly Ashes) 22
2.1.2.1 Experimental Observations 22
2.1.2.2 Overall Mechanism 22
2.1.2.3 Reaction Rate Determination 26
2.1.2.4 Wall Effects 27
2.1.3 Argon + HCN on Carbonaceous Materials (Soot, Char) 27

2.2 Argon + HCN + NH_3 Mixtures (Case S) 31
2.3 Argon + HCN + H_2O (Vapor) on Alumina 33

2.3.1 Experimental Method 33
2.3.2 Observations 34
2.3.3 Determination of Rate V_{44} 34

2.4 Argon + HCN + H_2 on Alumina (Case P.1) and Graphite (Case P.2) 37

2.4.1 Experimental Observations 37

2.5 Argon + HCN + NO (Case V) 41

2.5.1 Argon + HCN + NO on Alumina (Case V.1) . 41
2.5.1.1 Experimental Observations 41
2.5.1.2 Determination of Reactions Rates and Stoichiometric Coefficients "a" and "c" 44
2.5.2 Argon + HCN + NO on Rietspruit Fly Ash . 46

TABLE OF CONTENTS (CONCLUDED)

Section

Page (III-)

2.5.3 Argon + HCN + NO on Carbonaceous Materials 46
2.5.3.1 Cenospherical Soot 52
2.5.3.2 Ethylene Soot 52
2.5.3.3 Rietspruit Char 53

2.6 Argon + HCN + O_2 Mixtures (Case U) 53

2.6.1 Experimental Observations 53
2.6.2 Determination of the Rate V_{38} 57

2.7 Conclusions 58

LIST OF FIGURES

Figure Page(III-)

1 Ammonia (in Argon) on "Rietspruit" Fly Ash: Flow Rate D = 9.8 cm^3s^{-1}; M = 2.0g; Different Initial NH_3 Concentrations 4

2 Argon + NO + CO on "Rietspruit" Fly Ash: D = 10.0 cm^3s^{-1}; M = 2.0g $(CO)_i$ = 1.2%; $(NO)_i$ = 3400 ppm 5

3 Argon + NO + CO on "Rietspruit" Fly Ash: Effect of Initial NO Concentration; $(CO)_i$ = 5250 ppm 6

4 Argon + NO + CO on "Rietspruit" Fly Ash: Effect of Carbon Monoxide Concentration; $(NO)_i$ = 3400 ppm 7

5 Argon + NO H_2 on "Rietspruit" Fly Ash: D = 10.2 cm^3s^{-1}; M = 2g $(H_2)_i$ = 2.38%; $(NO)_i$ = 3400 ppm 9

6 Argon + NO + H_2 on "Rietspruit" Fly Ash: Effect of Initial NO Concentration; $(H_2)_i$ = 1.52% 10

7 Argon + NO + H_2 on "Rietspruit" Fly Ash: Effect of Hydrogen Concentration; $(NO)_i$ = 3000 ppm 11

8 Values of V_{11}, V_{14}, and $\overline{V_\phi}$ as a Function of Temperature; Comparison between Alumina and "Rietspruit" Fly Ash. Gas Composition: Argon + NO (0.001 atm) + H_2 (0.01 atm) . . . 14

9 Ratio of Reaction Rates on Fly Ash (Rietspruit) and on Alumina as a Function of Temperature. Gas Composition: Argon + NO (0.001 atm) + NH_3 (0.001 atm) + CO (0.01 atm) + H_2 (0.01 atm) 16

10 Ratio of Reaction Rates on "Rietspruit" Char and "Rietspruit" Fly Ash, as a Function of Temperature. Gas Composition: Argon + NO (0.001 atm) + CO (0.01 atm) + H_2 (0.01 atm) 17

11 Argon + HCN on Graphite: D = 9.9 cm^3s^{-1}; M = 0.59g; $(HCN)_i$ = 995 ppm 20

12 Argon + HCN on Alumina: D = 12.3 cm^3s^{-1}; M = 6g; $(HCN)_i$ = 1100 ppm 23

13 Argon + HCN on Alumina: Effect of Initial HCN Concentration 24

14 Argon + HCN on "Rietspruit" Fly Ash: D = 10.3 cm^3s^{-1}; M = 2g; $(HCN)_i$ = 700 ppm 25

LIST OF FIGURES (Continued)

Figure Page (III-)

15 Argon + HCN on Ethylene Soot: D = 10.4 cm^3s^{-1}; M = 0.36g; $(HCN)_i$ = 510 ppm 28

16 Argon + HCN on Cenospheric Soot: D = 10.4 cm^3s^{-1}; M = 1.3g; $(HCN)_i$ = 840 ppm 29

17 Argon + HCN on "Rietspruit" Char: D = 10.4 cm^3s^{-1}; M = 1.6g; $(HCN)_i$ = 690 ppm 30

18 Argon + HCN + NH_3 on Alumina: D = 11.5 cm^3s^{-1}; M = 6g; $(HCN)_i$ = 1600 ppm; $(NH_3)_i$ 2880 ppm 32

19 Argon + HCN + H_2O on Alumina: D = 12.9 cm^3s^{-1}; $(HCN)_i$ = 500 ppm; $(H_2O)_i$ = 2860 ppm; M = 6g 35

20 Argon + HCN + H_2O on Alumina: Effect of Initial Concentrations of HCN and H_2O 36

21 Argon + HCN + H_2 on Alumina: D = 11.6 cm^3s^{-1}; M = 6g; $(HCN)_i$ = 930 ppm; $(H_2)_i$ = 5.55% 38

22 Argon + HCN + H_2 on Alumina: Effect of Hydrogen Concentration 39

23 Argon + HCN + H_2 on Graphite: D = 10 cm^3s^{-1}; M = 0.59g; $(HCN)_i$ = 1050 ppm; Percent $H_{2\ i}$ = 0 (Curve A); 0.58 (Curve B); 1.08 (Curve C); 3.32 (Curve D) and 6.82 (Curve E) 40

24 Argon + HCN + NO on Alumina: D = 11.4 cm^3s^{-1}; M = 6g; $(HCN)_i$ = 800 ppm; $(NO)_i$ = 3000 ppm 42

25 Argon + HCN + NO on Alumina: Effect of Initial HCN Concentration 43

26 Argon + HCN + NO on Alumina: Effect of Initial NO Concentration 43

27 Argon + HCN_3 + NO on "Rietspruit" Fly Ash: D = 10.4 cm^3s^{-1}; M = 2g; $(HCN)_i$ = 285 ppm; $(NO)_i$ = 1110 ppm 47

28 Argon + HCN + NO on "Rietspruit" Fly Ash: D = 10.4 cm^3s^{-1}; M = 2g; $(HCN)_i$ = 610 ppm; $(NO)_i$ = 3450 ppm 48

LIST OF FIGURES (Concluded)

Figure		Page (III-)
29	Argon + HCN + NO on Cenospheric Soot: D = 10.3 cm^3s^{-1}; M = 1.3g; $(HCN)_i$ = 480 ppm; $(NO)_i$ = 1000 ppm	49
30	Argon + HCN + NO on Ethylene Soot; D = 10.4 cm^3s^{-1}; m = 0.36g; $(HCN)_i$ = 900 ppm $(NO)_i$ = 890 ppm	50
31	Argon + HCN + NO on "Rietspruit" Char: D = 10.4 cm^3s^{-1}; M = 1.6g; $(HCN)_i$ = 730 ppm; $(NO)_i$ = 1080 ppm	50
32	Argon + HCN + O_2 on Alumina: D = 13.1 cm^3s^{-1}; M = 6g; $(HCN)_i$ = 340 ppm; $(O_2)_i$ = 0.69%	54
33	Argon + HCN + O_2 on Alumina: Effect of Initial HCN Concentration	55
34	Argon + HCN + O_2 on Alumina: Effect of Initial Oxygen Concentration	56
35	Comparison of the Intrinsic Rate Constants (k in moles.s^{-1}.m^{-2}.atmos.$^{-0.38}$) Measured on Different Solids. Dashed Curves = k_{15}; Continuous Curves = k_{HCN} (Overall HCN Removal Rate Constant, Measured in Argon + HCN Mixtures)	59
36	Comparison of Intrinsic Rate Constants (Moles.s^{-1}.m^{-2}.P^{-n}; n = Sum of Partial Reaction Orders) k_{40} and k_{HCN} (Rate Constant of Overall HCN Removal Rate as Measured in Argon + HCN + NO Mixtures). Dashed Curves = k_{40}; Continuous Curves = k_{HCN}	60
37	Comparison of Some Specific Reactor Rates $(moles \cdot s^{-1} m^{-2})$ on Alumina for Different Gas Compositions	61

LIST OF TABLES

Table		Page (III-)
1	HCN Destruction Rates: -d(HCN)/dt (moles/s/m^2)	62

INTRODUCTION

The present report is devoted to the discussion of results obtained from (a) trials performed on coal fly ashes and (b) trials aiming at the study of heterogeneous reactions involving hydrogen cyanide as a reactant. Both subjects will be treated successively and constitute the natural continuation of the previous work performed on alumina, graphite, soots, coals and chars which was discussed in Parts I and II of this report. It will often be necessary to refer to those two previous parts, which will be accomplished by utilizing their part number. Specific reactions used in the present report will be numbered as indicated in Part I, Tables I and II*.

The three parts are complementary. Together they constitute the final Reporting on the total work performed under Contract EER-8318-6 during the period between October 1, 1978 and September 30, 1980.

---

*It should be noted that reaction ($HCN + H_2 \rightarrow NH_3 + \ldots$) has received two different numbers (36 and 45) on Table II of Part I; we here designate it as Number 45.

1.0 TRIALS ON FLY ASHES

The first portion of this report is related to the study of heterogeneous NO reduction on a typical fly ash. However, reactions involving hydrogen cyanide on that fly ash will be deferred to the second portion of this report, which is specially devoted to reactions of HCN.

The results discussed in this first part of the report have been obtained on fly ashes from a medium volatile South African coal (Rietspruit-region). The chemical and physical characteristics of the parent coal and char are given in Tables I and II of Part II. The fly ashes have been prepared by oxidation of the 50 to 100 micron size char (using an Argon + oxygen flow). The characteristics of these fly ashes are given on the table below.

Physical Characteristics of Rietspruit Fly Ash

Bulk density (picnometer): 2.60 g/cm^3

Specific surface area (N_2-BET Method): 5.2 m^2/g

Size distribution:

microns	cumul. mass percent under the given size
50	9.08
80	27.22
100	48.01
200	81.82
250	93.51
500	99.48

The experimental apparatus and method are essentially identical to those described in Part I.

It is assumed that these fly ashes are mainly composed of refractory oxides; therefore, it may be of interest to compare the results obtained with those previously measured for alumina.

1.1 Argon + NO on Rietspruit Fly Ash (Case F)*

As in the case where alumina was used as the solid, no measureable nitric oxide reduction could be observed when + NO mixtures were fed over fly ashes, up to a temperature of 1100°C.

---

*The capital letters refer to the different rows of Table I of Part I.

1.2 Argon + Ammonia on Rietspruit Fly Ashes (Case D)

An example of these trials is illustrated in Figure 1. As previously indicated in the case of alumina, the only specific reaction which can occur under these conditions is reaction (13) (see Part I); therefore the rate of change NH_3 can be written as:

$$-d(NH_3)/dt = 2\ d(N_2)/dt = \overline{V}_D = V_{13} = k_o \exp(-\theta/T)\ X^a_{NH_3} \quad (1)$$

where $\overline{V}_D$ is the overall ammonia removal rate and V_{13} the rate of the specific reaction:

$$NH_3 \xrightarrow{13} 0.5\ N_2 + 1.5\ H_2$$

Experimentally it is found that the partial order "a" is between 0.9 and 1.25. When "a" is set equal to 1, the following rate can be determined (for $740\ K < T < 1180\ K$):

$$\boxed{V_{13} = \overline{V}_D = 6.1 \times 10^5 \exp(-13250 \pm 1000/T)\ X_{NH_3}} \quad (cm^3 s^{-1} g^{-1}) \quad (2)$$

This rate expression may be compared to the one obtained in the case of alumina (see Part I):

$$V_{D.1} = V_{13} = 4.8 \text{ to } 9 \times 10^6 \exp(-16700/T)\ X_{NH_3} \quad (cm^3 s^{-1} g^{-1})$$

When the intrinsic rate constants ($k_{13} = k_o \exp(-\theta/T)$, expressed in units of $moles/s/m^2/atm$) are compared, it is found that fly ash has a much greater rate than does alumina. The ratio $k_{13(fly\ ash)}/k_{13(alumina)}$ is equal to 240 at 770 K and to 51 at 1176 K.

1.3 Argon + NO + CO on Fly Ashes (Case K)

Experimental data for these trials are illustrates by Figures 2 through 4. As in the case of alumina the following material balance is experimentally observed:

$$(NO)_i - (NO)_f = (CO)_i - (CO)_f = (CO_2)_f \quad (3)$$

Therefore (see Part I):

$$-\ d(NO)/dt = V_8 = \overline{V}_K = 2\ d(N_2)/dt \quad (4)$$

where V_8 is the rate of reaction:

$$CO + NO \xrightarrow{8} 0.5\ N_2 + CO_2$$

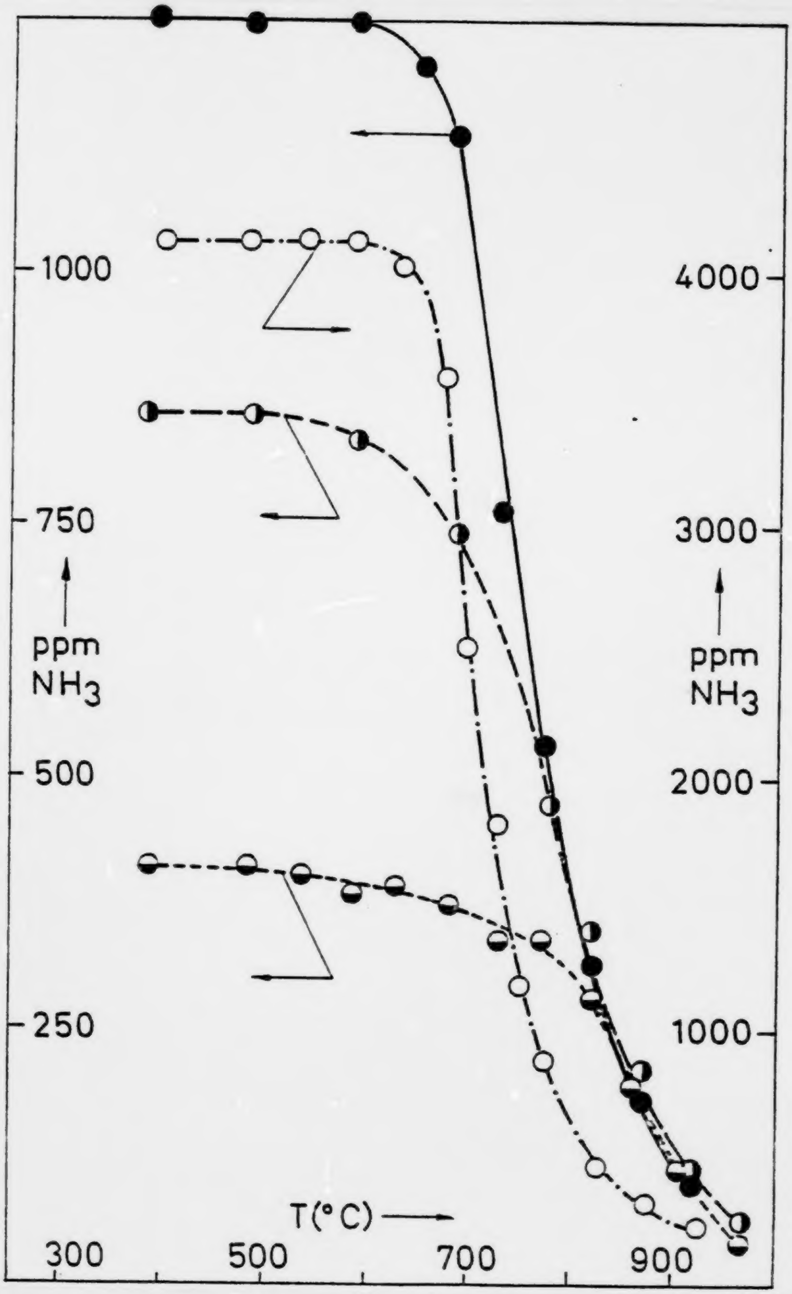

Figure 1. Ammonia (in Argon) on "Rietspruit" Fly Ash: Flow Rate D = 9.8 cm^{3}s^{-1}; M = 2.0g; Different Initial NH$_3$ Concentrations.

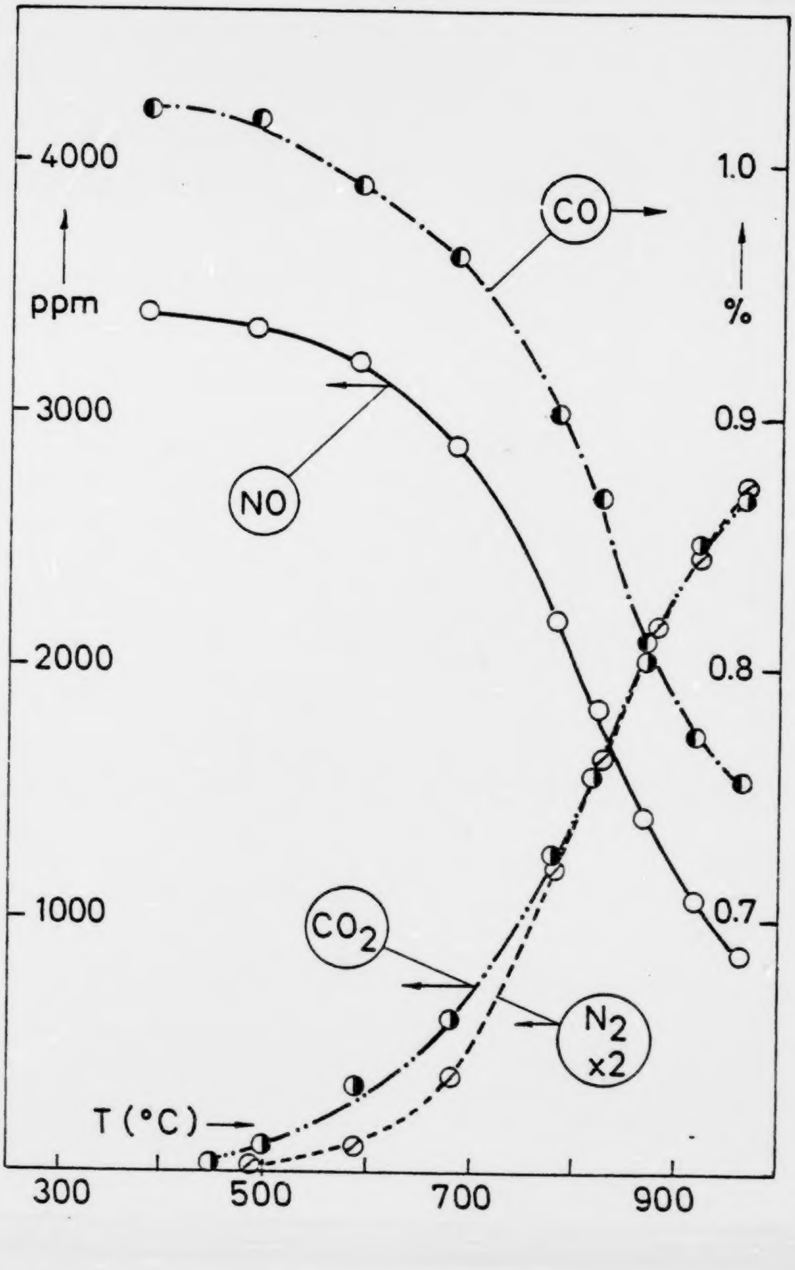

Figure 2. Argon + NO + CO on "Rietspruit" Fly Ash: $D = 10.0\ cm^3s^{-1}$; M = 2.0g $(CO)_i = 1.2\%$; $(NO)_i = 3400$ ppm.

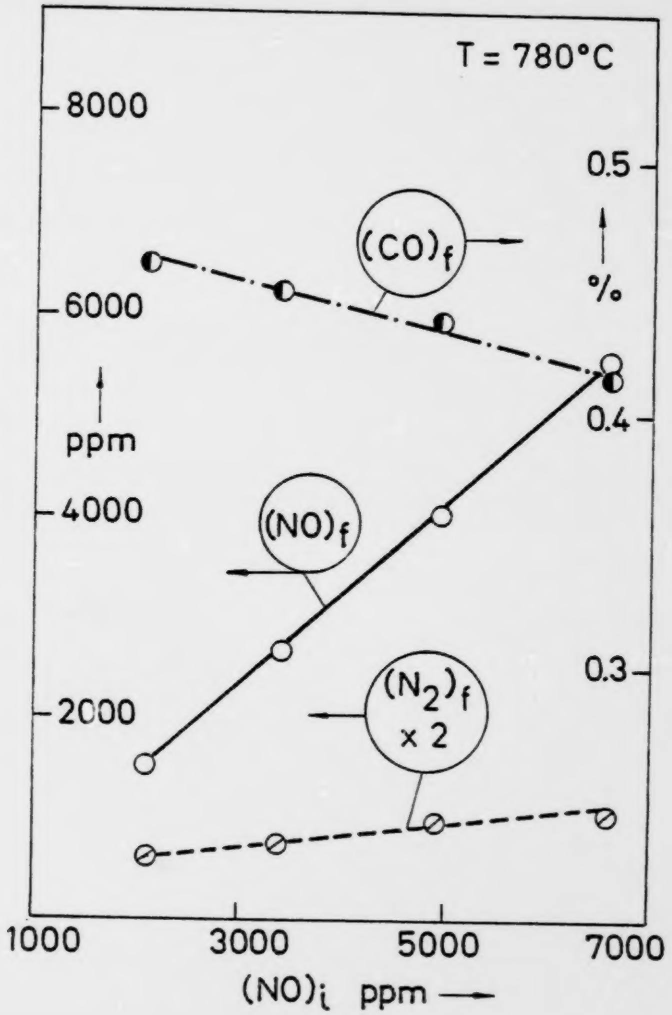

Figure 3. Argon + NO + CO on "Rietspruit" Fly Ash: Effect of Initial NO Concentration; $(CO)_i$ = 5250 ppm.

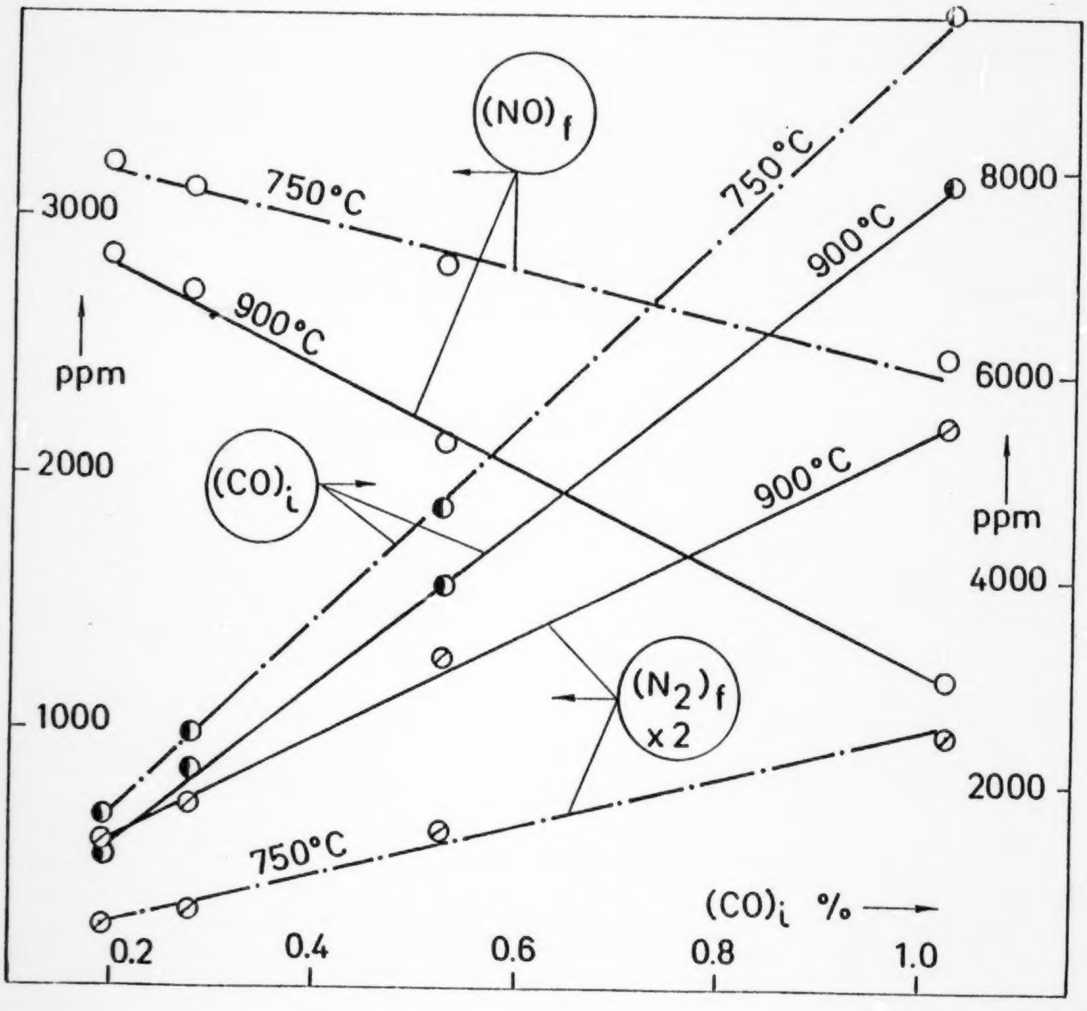

Figure 4. Argon + NO + CO on "Rietspruit" Fly Ash: Effect of Carbon Monoxide Concentration; $(NO)_i$ = 3400 ppm.

Experimentally it was found that for fly ashes:

$$V_8 = \overline{V}_K = 5.3 \times 10^3 \ \exp(-6000 \pm 1000/T)\ X_{NO}^{0.5}\ X_{CO} \quad (cm^3 s^{-1} g^{-1}) \qquad (5)$$

The partial reaction order with respect to NO is between 0.45 and 0.55, while the partial order with respect to CO is between 0.9 and 1.0. Again, there is a substantial difference in the derived rate expressions between fly ash and alumina; both the temperature dependence as well as the partial reaction orders are different. When comparing intrinsic values of V_{13} for alumina and fly ashes, e.g. at $X_{CO} = 0.01$ and $X_{NO} = 0.001$, the ratio $V_{13(fly\ ash)}/V_{13(alumina)}$ is found to be about 90 at 770 K while at 1190 K this ratio approaches one.

1.4 Argon + NO + H_2 on Fly Ashes (Case 0)

Examples of data from these trials are illustrated in Figures 5 through 7. Figure 5 shows the decrease of NO as a function of temperature; Figure 6 demonstrates the effect of increasing initial nitric oxide concentration, whereas Figure 7 illustrates the influence of increasing initial hydrogen concentration. Both N_2 and ammonia are reaction products indicating a competition between reactions (11) and (14):

$$NO + 2.5\ H_2 \xrightarrow{11} NH_3 + H_2O$$

$$NO + H_2 \xrightarrow{14} 0.5\ N_2 + H_2O$$

It may be seen from Figure 6 that NO itself inhibits the formation of ammonia, whereas its effect on N_2 formation is positive but rather small. Therefore, a negative partial order with respect to nitric oxide concentration is expected for reaction (11) while a partial order not very different of zero is expected for reaction (14).

The ammonia concentration in the reaction products passes through a maximum at temperature above 800°C. This can be attributed to reaction (13), the rate of which becomes measurable on alumina above 700°C (see e.g. Figure 13 of Part I):

$$NH_3 \xrightarrow{13} 0.5\ N_2 + 1.5\ H_2$$

The time variation of the nitrogen containing species are therefore described by the following set of differential equations:

$$d(NO)/dt = -V_{11} - V_{14} = -\overline{V}_0 \qquad (6)$$

$$d(NH_3)/dt = V_{11} - V_{13} \qquad (7)$$

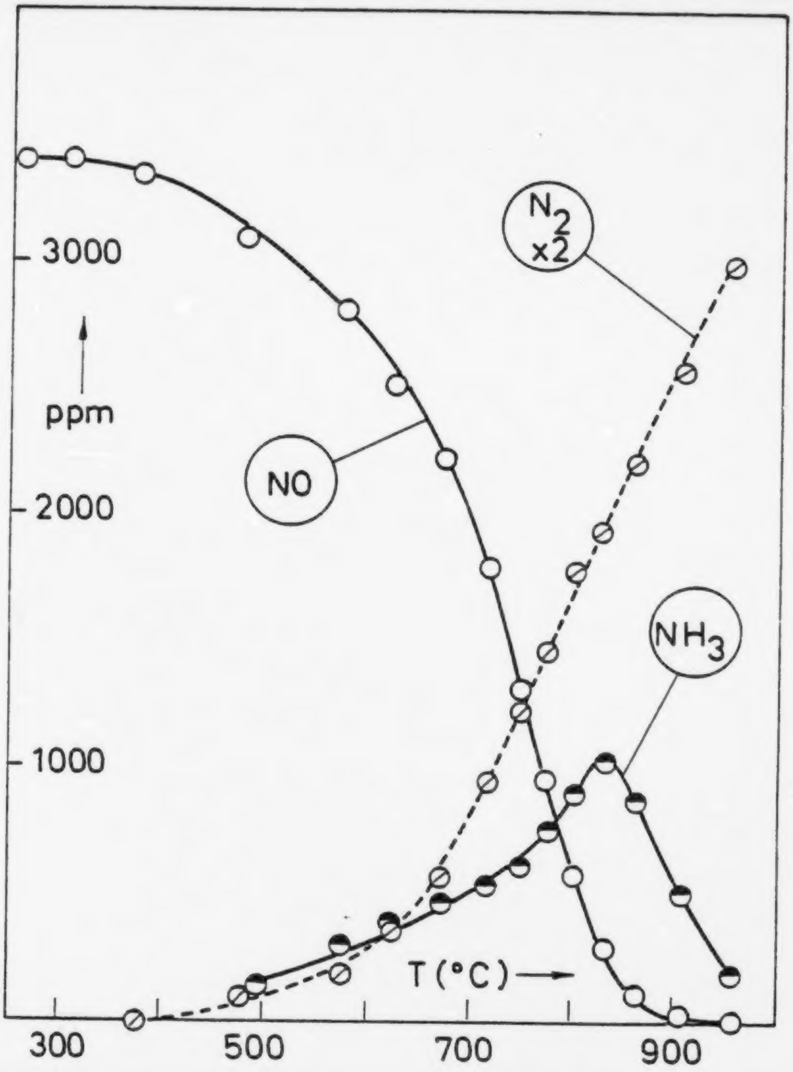

Figure 5. Argon + NO H_2 on "Rietspruit" Fly Ash: $D = 10.2\ cm^3 s^{-1}$; $M = 2g$ $(H_2)_i = 2.38\%$; $(NO)_i = 3400$ ppm.

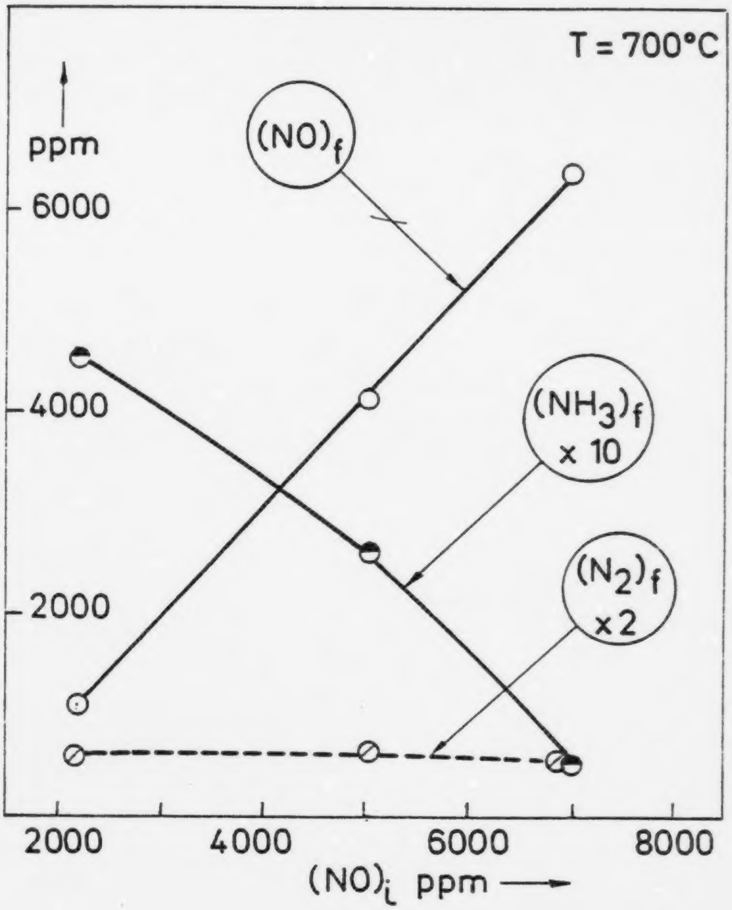

Figure 6. Argon + NO + H_2 on "Rietspruit" Fly Ash: Effect of Initial NO Concentration; $(H_2)_i$ = 1.52%.

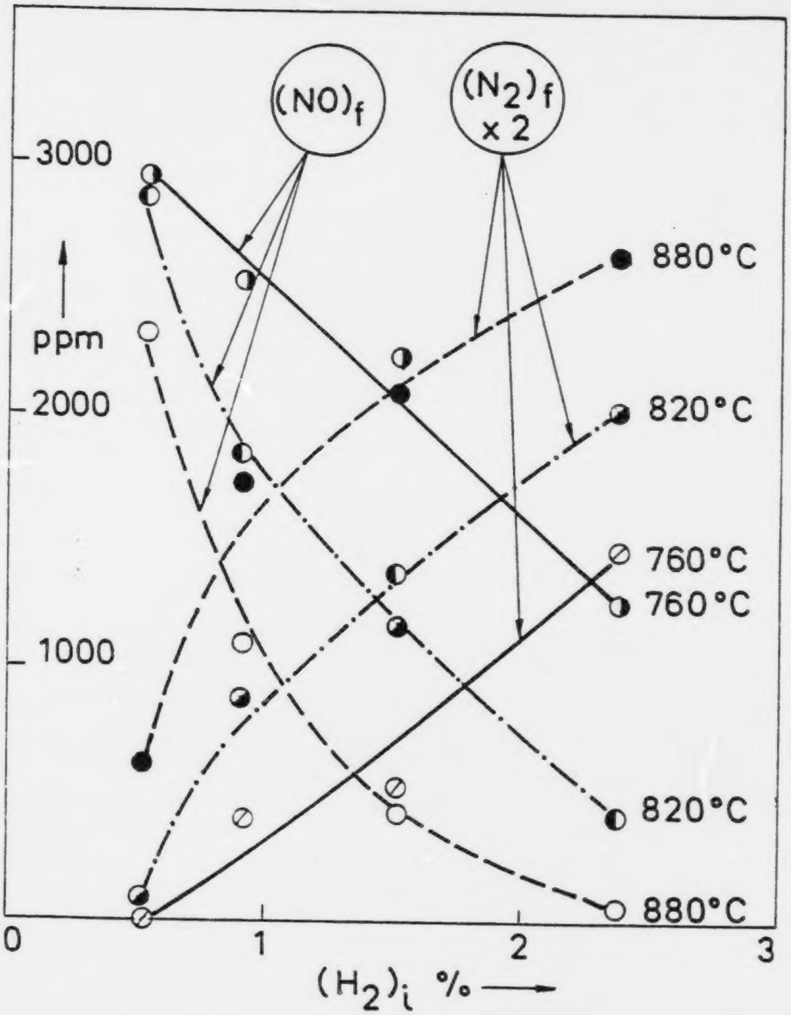

Figure 7. Argon + NO + H_2 on "Rietspruit" Fly Ash: Effect of Hydrogen Concentration; $(NO)_i$ = 3000 ppm.

$$d(N_2)/dt = 0.5\ V_{14} + 0.5\ V_{13} = \overline{V}_n \qquad (8)$$

Combining of equations (6) and)7) yields:

$$-d(NO)/dt - d(NH_3)/dt = V_{14} + V_{13} \qquad (9)$$

A. Calculation of the overall nitric oxide removal rate $\overline{V}_0$ from equation (6): The partial order of $\overline{V}_0$ with respect to NO is found to be equal to -0.32. The partial order with respect to hydrogen is found to depend on temperature, for example:

at 760°C, order with respect to H_2 = 1.58
at 820°C, order with respect to H_2 = 1.08
at 880°C, order with respect to H_2 = 0.58

Using a partial order with respect ot hydrogen equal to one, the following rate expression is determined:

$$\boxed{\begin{array}{c}\overline{V}_0 = -d(NO)/dt = 2.8 \times 10^1 \exp(-5350 \pm 700/T)\ X_{NO}^{-0.32} X_{H_2} \\ (cm^3 s^{-1} g^{-1})\end{array}} \qquad (10)$$

One may compare this expression with the rate determined for alumina (see Part I, equations (56) or (57)).

B. An overall N_2 formation rate may be determined from equation (8). It is found that the reaction order with respect to both NO and to H_2 depend on temperature, as shown below:

Temperature (°C)	Order with Respect to NO	Order with Respect to H_2
660	0.17	
740	-0.09	
780		1.80
840		0.60

Utilizing values of zero and +1 for the partial orders with respect to NO and hydrogen respectively, the following rate expression is determined:

$$\boxed{\overline{V}_n = d(N_2)/dt = 1.4 \times 10^2\ \exp(-7000 \pm 1000/T)\ X_{H_2}\ (cm^3 s^{-1} g^{-1})} \qquad (11)$$

C. The rate expression of V_{14} may be determined by substituting the rate V_{13} as calculated according to equation (2), into equation (9). Again the partial reaction orders with respect to NO and H_2 are found to depend on temperature, e.g.:

Temperature (^oC)	Order with Respect to NO	Order with Respect to H_2
700	0.08	2.00
800	0.34	1.00
940	0.46	0.22

With partial orders of 1 (for hydrogen) and 0.3 (for NO), the following rate expression is obtained:

$$\boxed{V_{14} = 5.0 \times 10^3 \ \exp(-8160 \pm 700/T)\ X_{NO}^{0.3}\ X_{H_2}\ (cm^3 s^{-1} g^{-1})} \qquad (12)$$

D. Finally, V_{11} may be determined by substituting the previously determined value of V_{14} in equation (6). The partial reaction order of V_{11} with respect to NO is found to be equal to -1, whereas the order with respect to H_2 is between 2 and 2.2. The approximate value of V_{11} determined from equation (6) is:

$$\boxed{V_{11} = 2.1 \exp(-4570 \pm 1000/T)\ X_{NO}^{-1}\ X_{H_2}^{2} \qquad (cm^3 s^{-1} g^{-1})} \qquad (13)$$

Since the overall reaction order with respect to NO is smaller than one (for reaction 14) or even negative (for reaction 11), a rather strong chemisorption of the nitric oxide on the solid is suggested.

Reaction rates V_{11}, V_{14} and $\overline{V}_0$ are found to be much larger for the fly ashes than for alumina. This is evidenced by intrinsic rate values as seen in Figure 8. Also, these reaction rates are all characterized by a greater temperature dependence for alumina than for fly ashes.

1.5 Conclusions

As a conclusion, it is instructive to compare the rates of some overall reactions as well as some specific reactions playing a role in heterogeneous nitric oxide reduction on (1) fly ashes compared to alumina and (2) fly ashes compared to char of the same coal. The comparison utilizes intrinsic rate expressions (in moles/s/m^2) calculated according to the following equations:

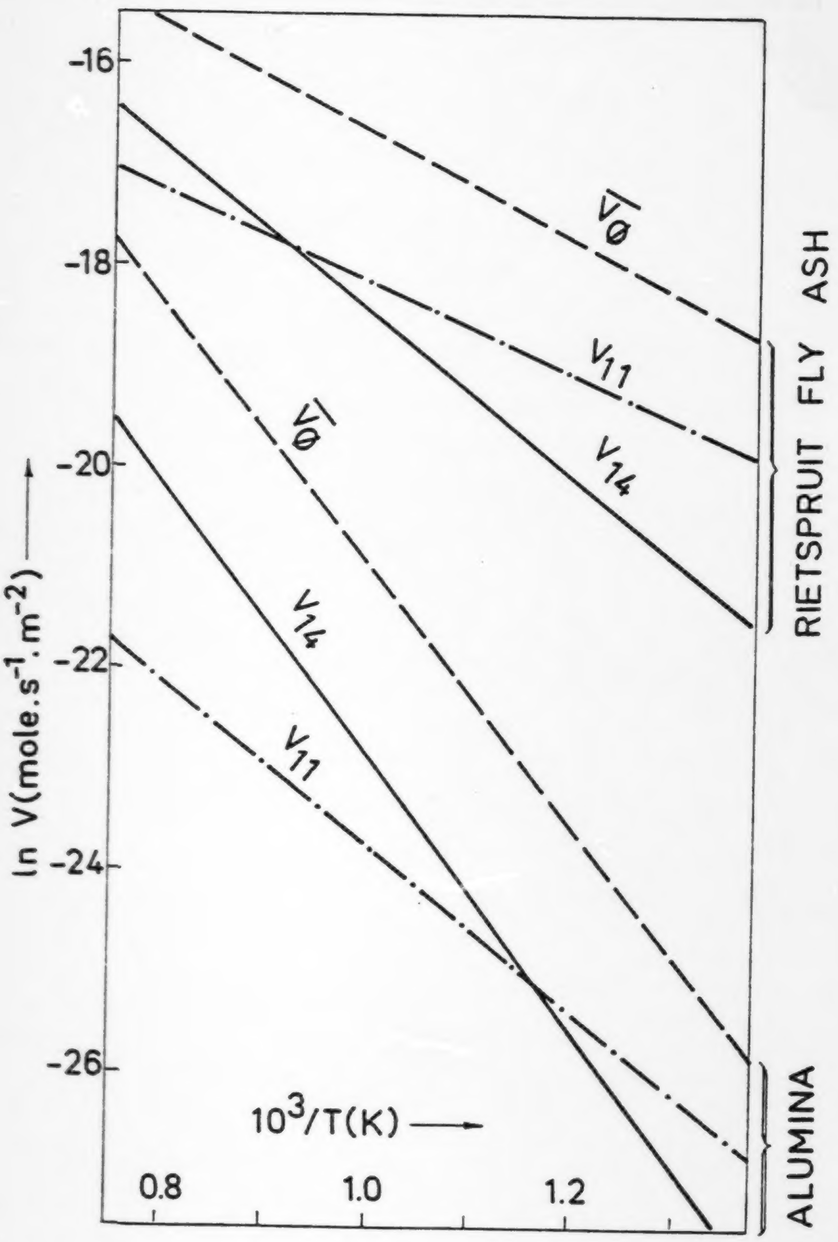

Figure 8. Values of V_{11}, V_{14}, and $\overline{V\phi}$ as a Function of Temperature; Comparison between Alumina and "Rietspruit" Fly Ash. Gas Composition: Argon + NO (0.001 atm) + H_2 (0.01 atm).

Rate	Utilized Equation		
	Alumina	Rietspruit char (0.05/0.1 mm)	Rietspruit Fly Ashes
V_8	Part I, eq.25		Part III, eq.5
$\overline{V}_K$	Part I, eq.25	Part II, Table IVa	Part III, eq.5
V_{11}	Part I, eq.59		Part III, eq.13
V_{14}	Part I, eq.58		Part III, eq.12
V_0	Part I, eq.57	Part II, Table IVa	Part III, eq.10
$V_{13}=V_D$	Part I, eq.19		Part III, eq.2

The calculations have been made for an atmospheric gas mixture with a composition as follows: argon containing 1000 ppm NO, + 1 percent CO, + 1 percent H_2, + 1000 ppm NH_3.

The ratio $V_{\text{fly ashes}}/V_{\text{alumina}}$ for different specific and overall reactions is shown in Figure 9. At temperatures below about 1200 K, all these reactions are seen to be much faster for fly ash than for alumina. As previously stated, the temperature dependence is much greater for alumina than for Rietspruit fly ashes.

Figure 10 illustrates the comparison of overall NO removal reactions in the presence of hydrogen or carbon monoxide, between Rietspruit char and Rietspruit fly ashes. The upper part of the figure shows the intrinsic reaction rates $\overline{V}_K$ (NO + CO) and $\overline{V}_0$ (NO + H_2) for both solids. For the char, these two overall NO removal reactions are more temperature dependent than for fly ash. Therefore, the ratio $V_{\text{char}}/V_{\text{fly ash}}$ is greater than unity at temperatures above about 700 K.

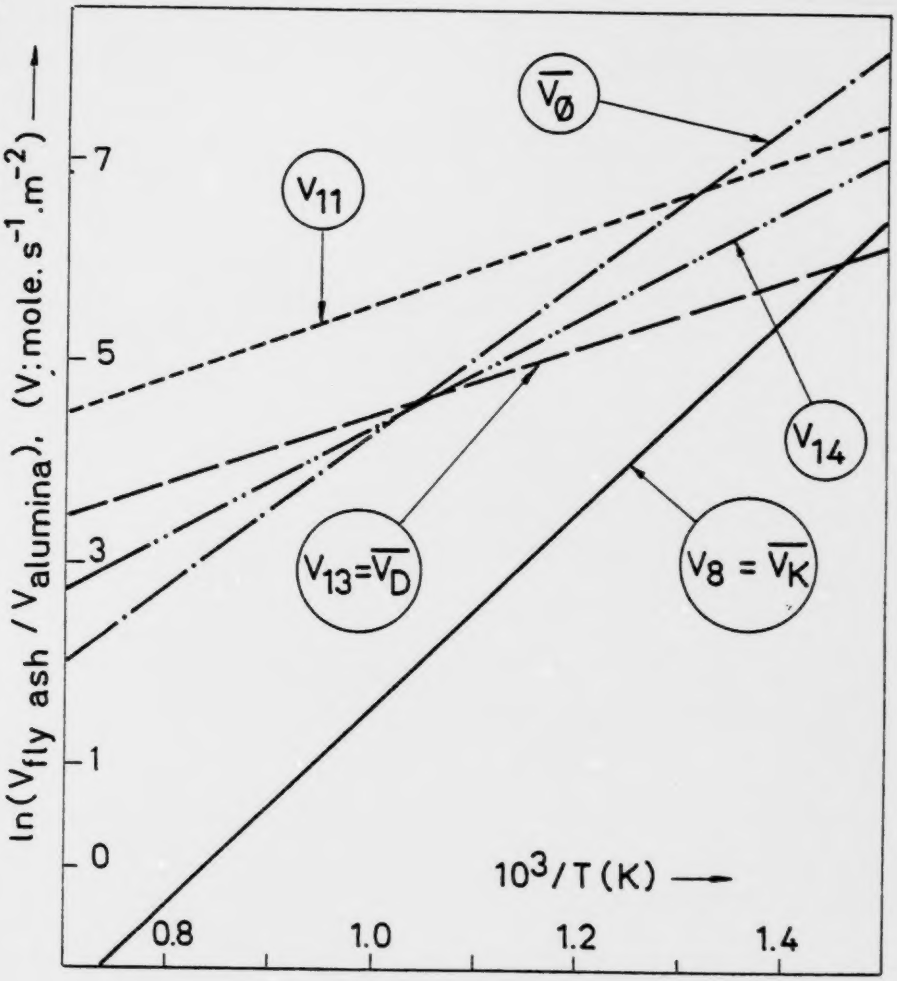

Figure 9. Ratio of Reaction Rates on Fly Ash (Rietspruit) and on Alumina as a Function of Temperature. Gas Composition: Argon + NO (0.001 atm) + NH_3(0.001 atm) + CO (0.01 atm) + H_2 (0.01 atm).

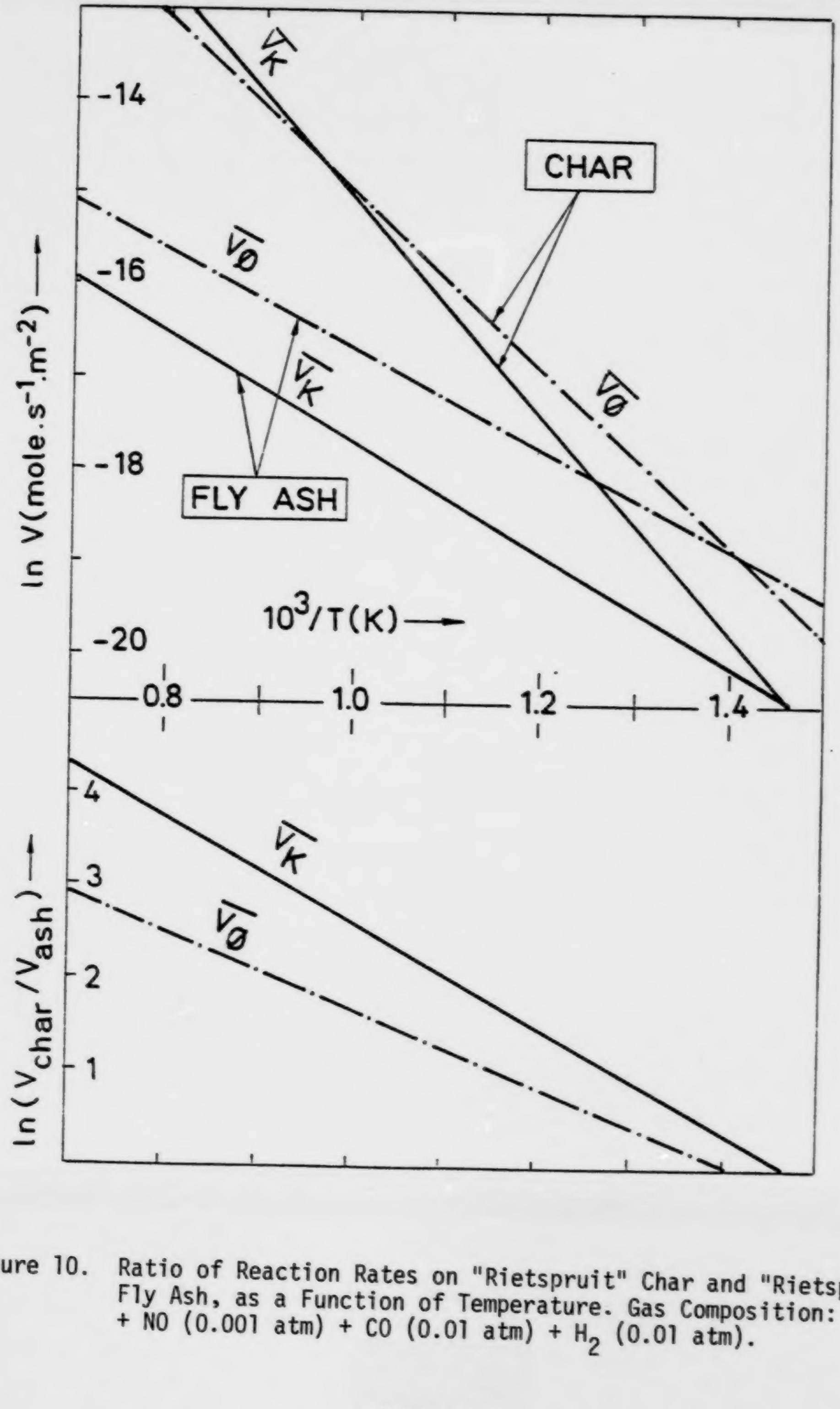

Figure 10. Ratio of Reaction Rates on "Rietspruit" Char and "Rietspruit" Fly Ash, as a Function of Temperature. Gas Composition: Argon + NO (0.001 atm) + CO (0.01 atm) + H_2 (0.01 atm).

2.0 REACTIONS INVOLVING HCN AS A REACTANT

The work discussed in Part I clearly points out that the final transformation of ammonia (itself being formed from NO and a hydrogen source) into molecular nitrogen, may occur either directly or indirectly through the intermediate formation of hydrogen cyanide. The following specific reactions have been identified for HCN formation from ammonia:

$$NH_3 + (-C) \xrightarrow{5} HCN + H_2$$

$$NH_3 + CO \xrightarrow{9} HCN + H_2O$$

To this list should be added the possibility of HCN formation from bound carbon and nitrogen atoms (which has not been identified):

$$H_2 + (-N) + (-C) \xrightarrow{22} HCN + \ldots$$

Finally, HCN has also been observed as a product of coal devolatilization (see Part II, Figures 6 through 13).

The subject of the second part of the present report is the identification of the reaction paths by which HCN may be transformed into molecular nitrogen, as well as the determination of the reaction rates of these transformations. To accomplish this goal, argon containing HCN (and other coreactants) has been fed over different types of solids. The approach to be followed uses the previously described method of progressively increasing the complexity of both gas and solid phase composition (Part I).

The experimental procedure is essentially identical to that described in previous parts. The main difference involves the special care that was taken to thoroughly dry the hydrogen cyanide containing gas mixture. The reason for that will be evident from the study of the reaction between HCN and water vapor, which was found to be very fast. Therefore, that part of the argon flow which contains the hydrogen cyanide was dried over either P_2O_5 or anhydrous magnesiumperchlorate, prior to being mixed with other input constiuents. In earlier trials, performed in 1979, the required hydrogen cyanide was obtained by reacting sulfuric acid with kaliumcyanide. During this preparation, non-negligible amounts of CO were sometimes formed, due to insufficient cooling of the reacting medium. However, in the majority of trials in this part of the program, argon/HCN mixtures of high purity (although containing up to 50 ppm water vapor) have been utilized.

The following solids and gas compositions have been used in this study:

- Solids
  - Alumina (characteristics given in Part I);
  - Rietspruit Fly Ashes (characteristics given in this report);
  - Gas phase generated soot from C_2H_4 flames (characteristics given in Part I);
  - Cenospherical soot from heavy fuel oil, Procheville Plant (characteristics given in Part I);
  - Rietspruit char, size: 50 to 100 microns (characteristics given in Part II, Table II);
  - Graphite (characteristics given in Part I).
- Gas mixtures
  - Argon + HCN (Row G, Table I, Part I);
  - Argon + HCN + NH_3 (Ros S, Table I, Part I);
  - Argon + HCN + H_2O (Not mentioned in Table I, Part I);
  - Argon + HCN + H_2 (Row P, Table I, Part I);
  - Argon + HCN + NO (Row V, Table I, Part I);
  - Argon + HCN + O_2 (Row U, Table I, Part I).

2.1 Argon + HCN Mixtures (Case G)

The transformation of hydrogen cyanide into N_2 in the absence of other co-reactants has been studied on alumina, Rietspruit fly ashes, C_2H_4 soot, cenospherical soot, graphite and Rietspruit char.

2.1.1 Argon + HCN on Graphite

An example of these trials is shown on Figure 11. Reaction products are NH_3 and N_2, both appearing during the first stages of HCN removal. Ammonia goes through a maximum, due to the existence of the secondary reactions (13) and (10), although the latter may be very small.

The primary reaction should thus account for both NH_3 and N_2 formation:

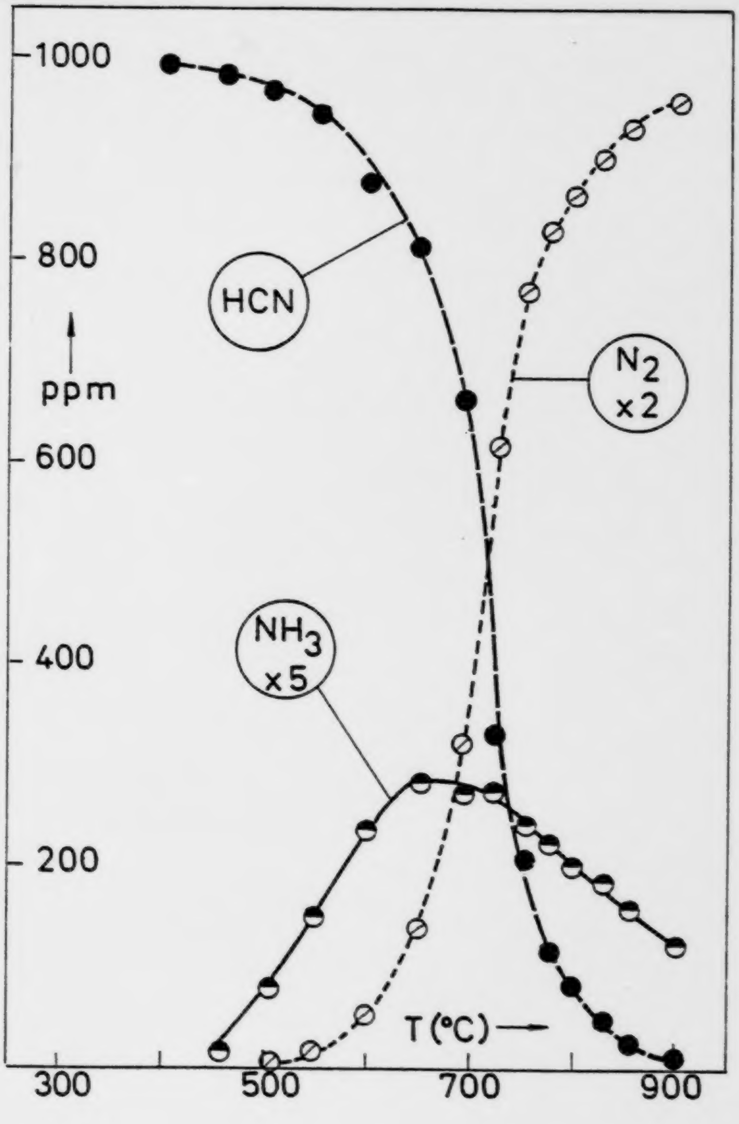

Figure 11. Argon + HCN on Graphite: D = 9.9 cm^3s^{-1}; M = 0.59g; $(HCN)_i$ = 995 ppm.

$$HCN \xrightarrow{15} a\ NH_3 + \frac{1-a}{2} N_2 + \frac{1-3a}{2} H_2 + C$$

where a ≤ 1/3.

The two secondary reactions which are likely to play a role include:

$$NH_3 \xrightarrow{13} 0.5\ N_2 + 1.5\ H_2$$

$$HCN + NH_3 \xrightarrow{10} N_2 + 2\ H_2 + C$$

as well as the tertiary reaction (which becomes a secondary reaction if H_2 is formed by reaction (15)):

$$HCN + H_2 \xrightarrow{45} NH_3 + C$$

We therefore have the following set of differential equations:

$$d(HCN)/dt = -V_{15} - V_{45} - V_{10} = -\overline{V_{HCN}} \qquad (14)$$

$$d(NH_3)/dt = a\ V_{15} + V_{45} - V_{10} - V_{13} \qquad (15)$$

$$d(N_2)/dt = \frac{1-a}{2} V_{15} + \tfrac{1}{2}V_{13} + V_{10} \qquad (16)$$

From equations (14) and (15) it follows that:

$$-d(HCN)/dt\ \ -d(NH_3)/dt = (1-a)V_{15} + V_{13} + 2V_{10} \qquad (17)$$

Principly $\overline{V_{HCN}}$, V_{15} and the stoichiometric coefficient "a" can be determined as follows: neglecting V_{10}, which is always very small (see Part I), as confirmed by the findings of the present report, (see below), $(1-a)V_{15}$ may be determined from equation (17) by substituting the value of V_{13}, calculated according to equation (90) of Part I. In a second step, V_{15} is determined from equation (14), again neglecting the secondary reaction V_{10} and the tertiary (or secondary) reaction V_{45}. Comparison of values obtained for $(1-a)V_{15}$ and V_{15} then allows the determination of the stoichiometric coefficient "a".

Due to the imprecision in the expression for V_{13} there is substantial scatter in the derived value of "a" which is seen to be between 0.1 and 0.6. Since the coefficient "a" cannot be larger than 1/3, this value can be accepted with some confidence. The following stoichiometry for reaction (15) is thus probable:

$$HCN \xrightarrow{15} 1/3\ NH_3 + 1/3\ N_2 + C$$

The reaction order of V_{15} ($\cong \overline{V_{HCN}}$) is experimentally found to be between 0.3

and 0.7. Assuming a value of 0.5 for that reaction order, the following expression is obtained for V_{15}:

$$\boxed{V_{15}(\cong \overline{V_{HCN}}) = 7.8 \times 10^4 \ \exp(-12500 \pm 700/T) \ X_{HCN}^{0.5} \ (cm^3 s^{-1} g^{-1})} \quad (18)$$

2.1.2 Argon + HCN on Refractory Oxides (Alumina and Fly Ashes)

Typical results of these trials are illustrated in Figures 12 through 14. Figures 12 and 13 are related to alumina, whereas Figure 14 is related to Rietspruit fly ash.

2.1.2.1 Experimental Observations

1. To a good approximation, the following carbon balance seems to hold (see Figure 12 through 14):

$$(HCN)_i - (HCN)_f = (CO)_f \quad (18)$$

2. N_2 and NH_3 appear as nitrogen containing reaction products during the HCN disappearance. The ammonia concentration passes through a maximum.

2.1.2.2 Overall Mechanism

The following sequence of primary and secondary reactions may account for the experimental observations:

Primary reaction:

$$HCN \xrightarrow{15} a\ NH_3 + \frac{1-a}{2} N_2 + \frac{1-3a}{2} H_2 + C$$

Secondary reactions:

$$C + (-O) \xrightarrow{47} CO$$ (this reaction accounting for CO formation)

If H_2 is formed from reaction (15), which has not been checked, then the following secondary and tertiary reactions may occur:

$$H_2 + (-O) \xrightarrow{19} H_2O$$

$$H_2O + HCN \xrightarrow{44} NH_3 + CO$$ (tertiary reaction)

The sum of reactions (15), (19), (44) and (47) yields the following overall balance, which is in accord with the carbon balance (18) and with the previously determined stoichiometric coefficient "a" of reaction (15):

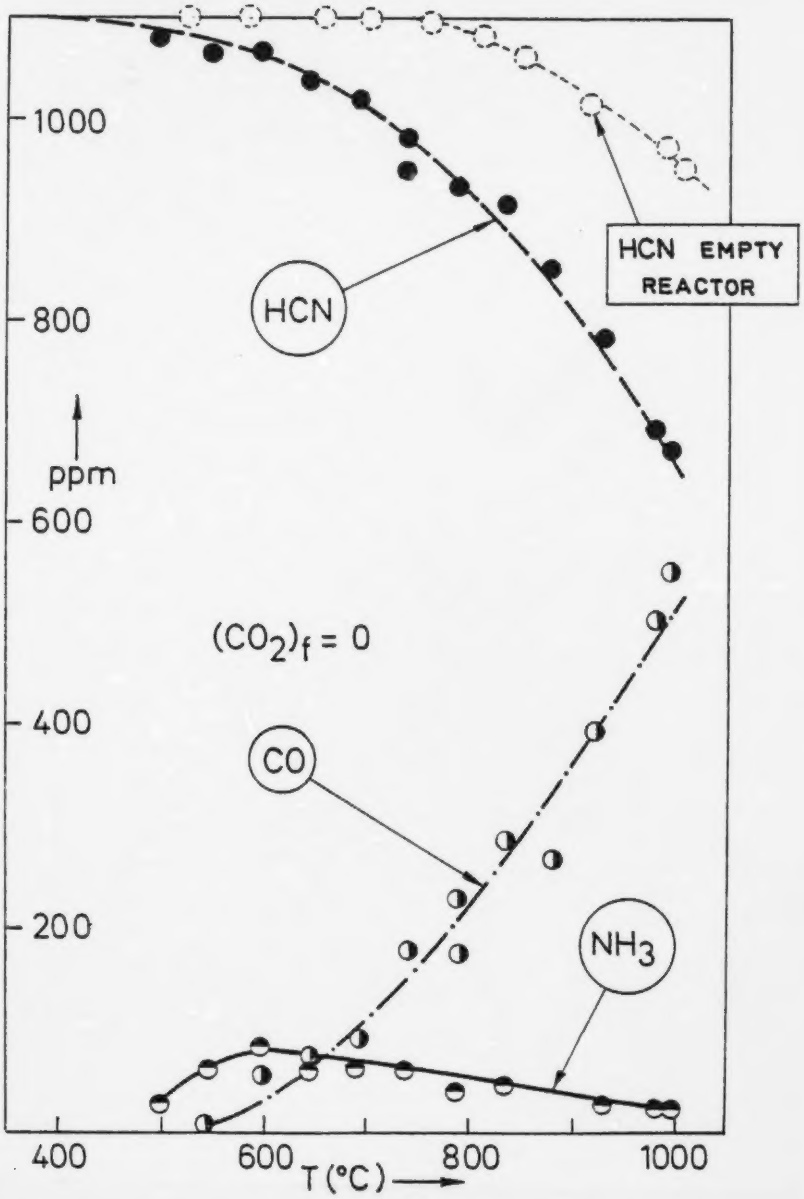

Figure 12. Argon + HCN on Alumina: $D = 12.3\ cm^3s^{-1}$; $M = 6g$; $(HCN)_i = 1100$ ppm.

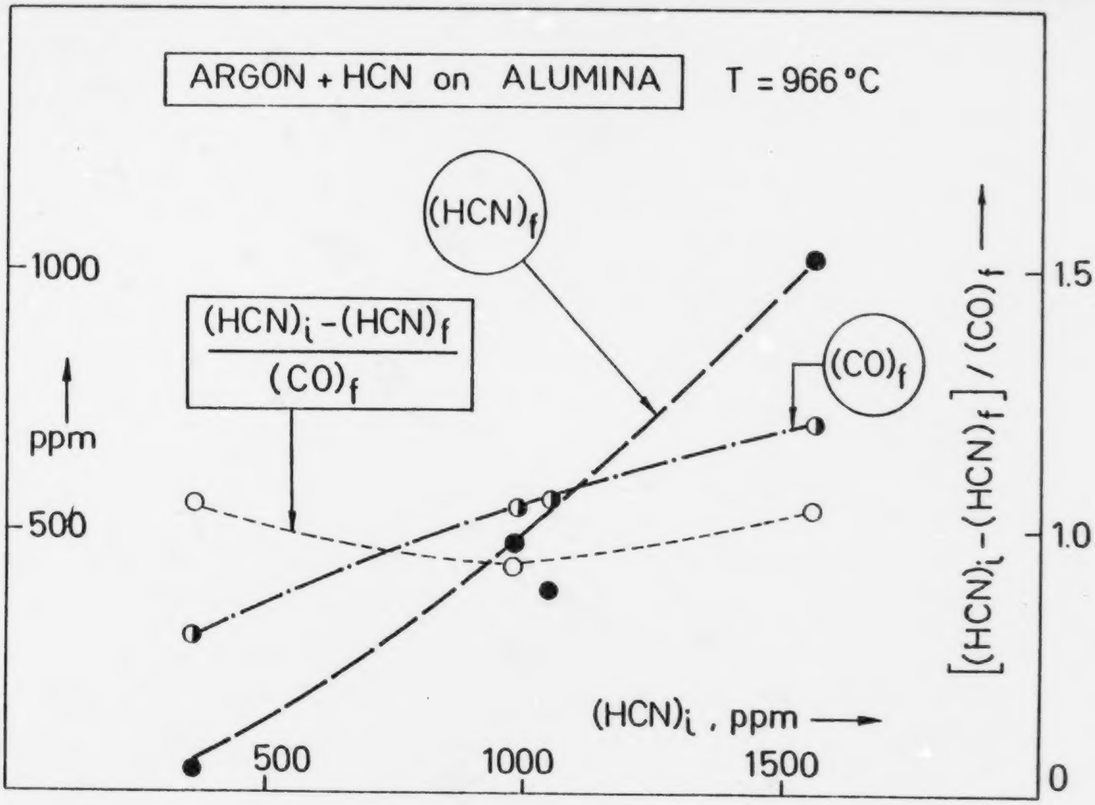

Figure 13. Argon + HCN on Alumina: Effect of Initial HCN Concentration.

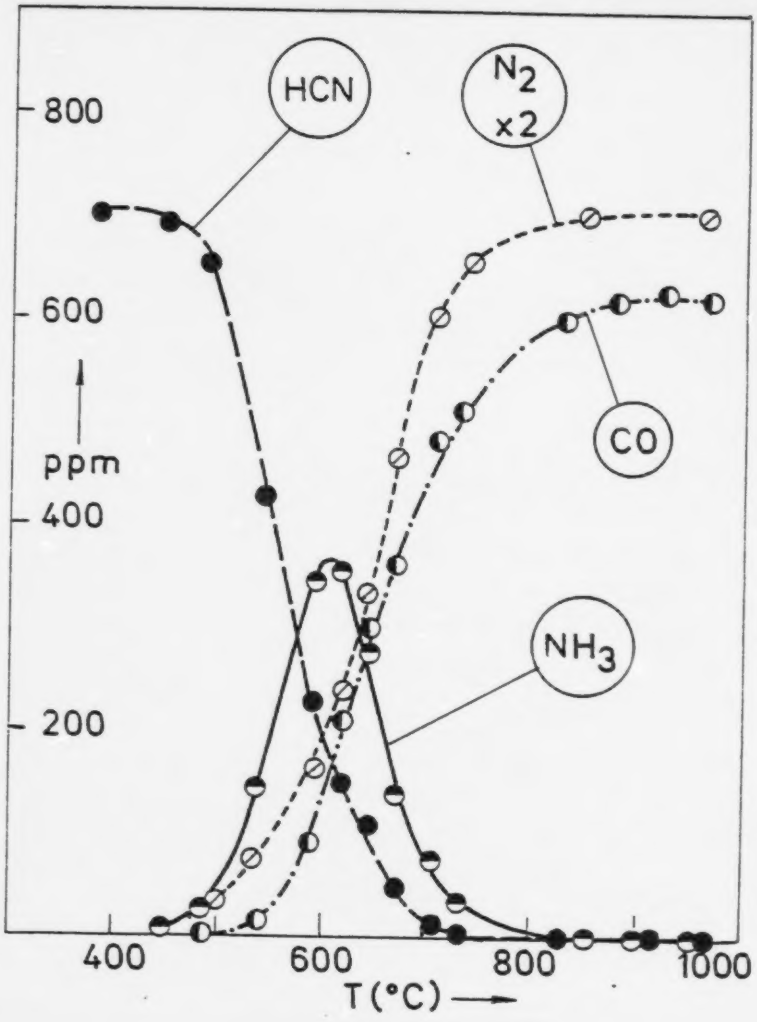

Figure 14. Argon + HCN on "Rietspruit" Fly Ash: $D = 10.3\ cm^3 s^{-1}$; $M = 2g$; $(HCN)_i = 700$ ppm.

$$HCN + (-O) \longrightarrow 1/3\ NH_3 + 1/3\ N_2 + CO$$

This overall balance, however, is also obtained when no H_2 is formed by reaction (15), and thus the value of the coefficient "a" must be rechecked.

Other secondary and tertiary reactions may also occur:

$NH_3 \xrightarrow{13} 0.5\ N_2 + 1.5\ H_2$ (switching H_2 into the pool of reactants also)

$NH_3 + CO \xrightarrow{9} HCN + NO$

$HCN + H_2 \xrightarrow{45} NH_3 + \ldots$ (see below, Section 2.4)

The following set of differential equations thus describes the time variation of the nitrogen containing products (secondary and tertiary reactions are placed between brackets):

$$d(HCN)/dt = -V_{15}\ (+V_9 - V_{44} - V_{45}) = -\overline{V_{HCN}} \tag{19}$$

$$d(NH_3)/dt = a\ V_{15}\ (-V_9 + V_{44} + V_{45} - V_{13}) \tag{20}$$

$$d(N_2)/dt = \frac{1-a}{2}\ V_{15}\ (+\tfrac{1}{2}V_{13}) \tag{21}$$

Addition of equations (19) and (20) yields:

$$-d(HCN)/dt - d(NH_3)/dt = (1-a)V_{15} + V_{13} \tag{22}$$

2.1.2.3 Reaction Rate Determination

2.1.2.3.1 For Alumina

- From equation (22), the value $(1-a)V_{15}$ is determined by substituting the value of V_{13} calculated according to equation (17) of Part I;
- From equation (19), neglecting all secondary reactions but V_9 (the latter calculated according to equation (40) of Part I), V_{15} is determined;
- The stoichiometric coefficient "a" of reaction (15) is then obtained from the ratio $(1-a)V_{15}/V_{15}$. For the case of alumina it is found that $0.2 < a < 0.32$. Considering the poor precision of the calculation, the result is in basic agreement with the previous assumption that $a = 1/3$;
- Partial reaction order of V_{15} is determined and found to be equal to 0.38 ± 0.15;

- The rate constant is then found to be:

$$\boxed{V_{15} = 5.8 \ \exp(-7780 \pm 600/T) \ X_{HCN}^{0.38} \quad (cm^3 s^{-1} g^{-1})} \tag{23}$$

- The overall HCN removal reaction rate ($\overline{V_{HCN}}$) is determined directly from equation (19). Since in that equation and for the experimental conditions prevailing in the trials, the term V_9 is more than two orders of magnitude smaller than V_{15}. Thus, the value of $\overline{V_{HCN}}$ is found to be essentially equal to that of V_{15}.

2.1.2.3.2 For Rietspruit Fly Ashes

- Applying equation (19) to results from Reitspruit ash the following value is obtained for the overall HCN removal rate:

$$\boxed{\overline{V_{HCN}} = 1.6 \times 10^4 \ \exp(-11100 \pm 1000/T) \ X_{HCN}^{0.38} \ (cm^3 s^{-1} g^{-1})} \tag{24}$$

- By similarly substituting for V_{13} in equation (22), a value of $(1-a)V_{15}$ is found. Further, assuming that a = 1/3 yields:

$$\boxed{V_{15} = 6.2 \times 10^4 \ \exp(-12900 \pm 1000/T) \ X_{HCN}^{0.38} \quad (cm^3 s^{-1} g^{-1})} \tag{25}$$

2.1.2.4 Wall Effects

Reactions (15) and (47) also occur on the quartz reactor walls, although to a smaller extent than on the refractory oxide particles. A curve of HCN removal measured in the empty reactor is shown in Figure 12.

2.1.3 Argon + HCN on Carbonaceous Materials (Soot, Char)

Trials on solids containing both bound C and H atoms are illustrated on Figure 15 (C_2H_4 soot), Figure 16 (cenospherical soot) and Figure 17 (Rietspruit char).

Experimental observation are substantially the same as in the case of oxides, except that ammonia formation exceeds N_2 formation at lower temperatures (see, for example, Figures 15 and 16). In addition to reaction (15), another primary reaction might explain ammonia formation from hydrogen cyanide and bound hydrogen:

$$HCN + 2(-H) \xrightarrow{46} NH_3 + C$$

Neglecting all secondary reactions except reaction (13), one has:

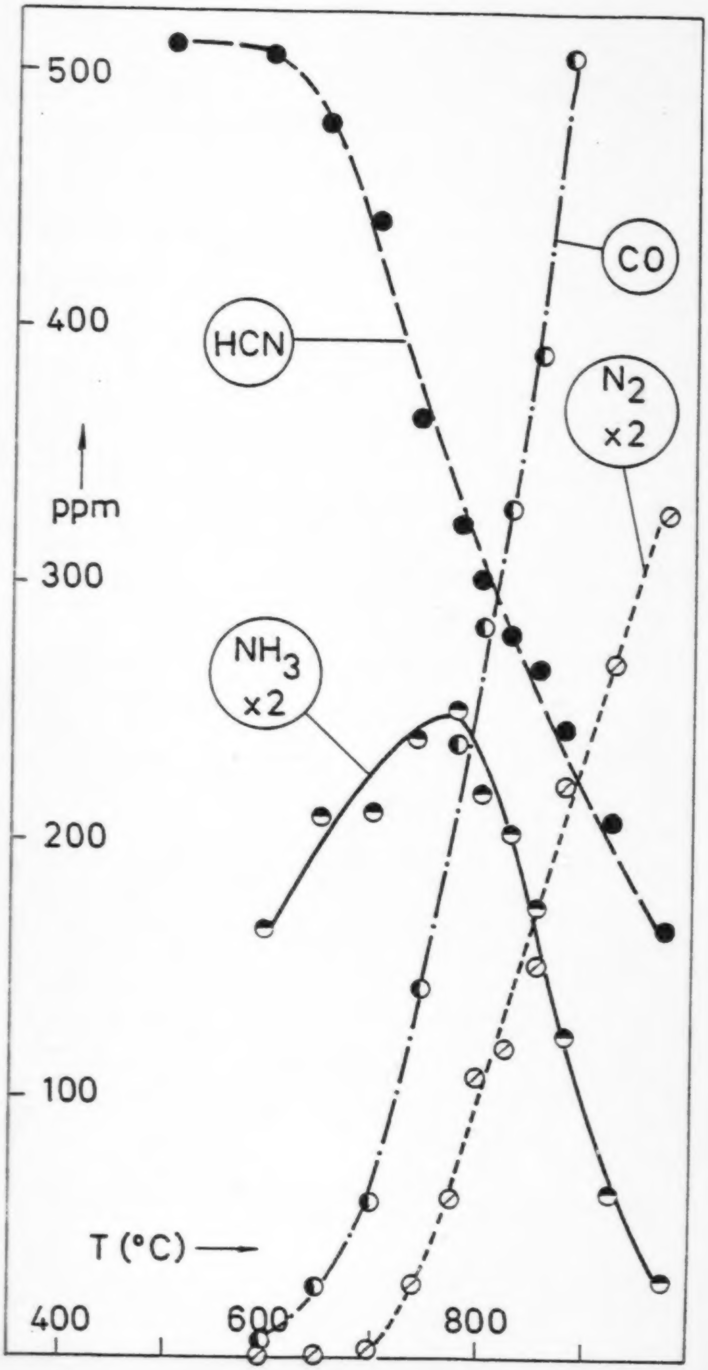

Figure 15. Argon + HCN on Ethylene Soot: D = 10.4 $cm^3 s^{-1}$; M = 0.36g; $(HCN)_i$ = 510 ppm.

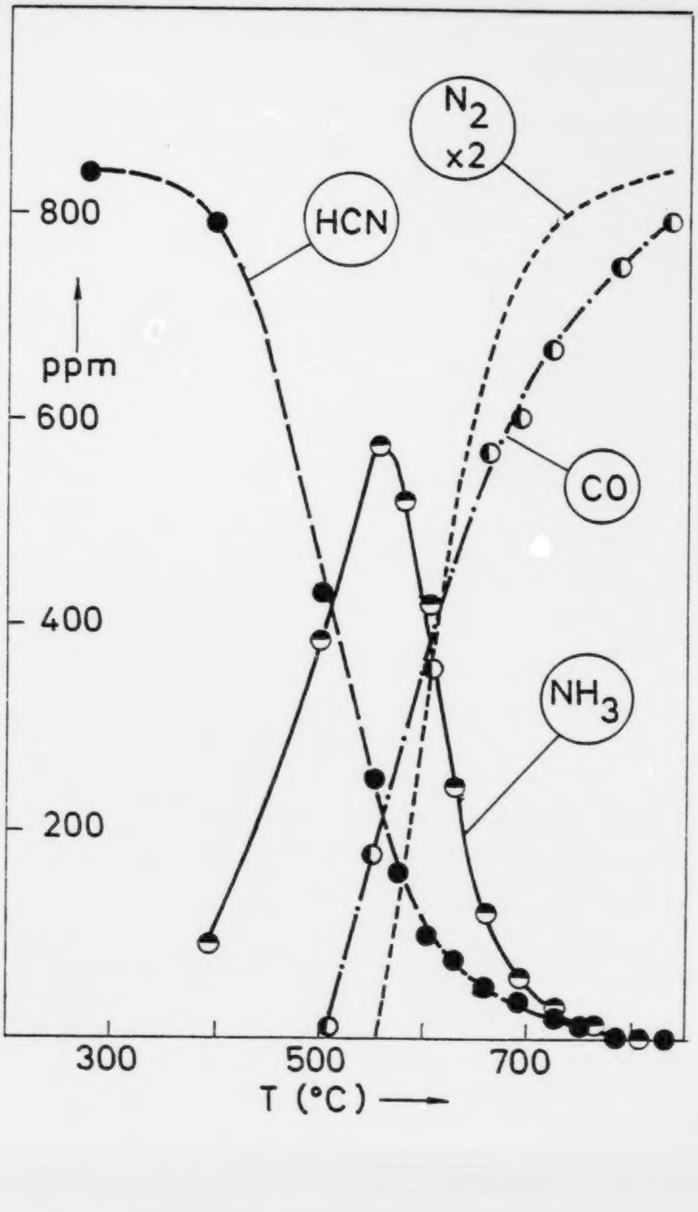

Figure 16. Argon + HCN on Cenospheric Soot: D = 10.4 cm^3s^{-1}; M = 1.3g; $(HCN)_i$ = 840 ppm.

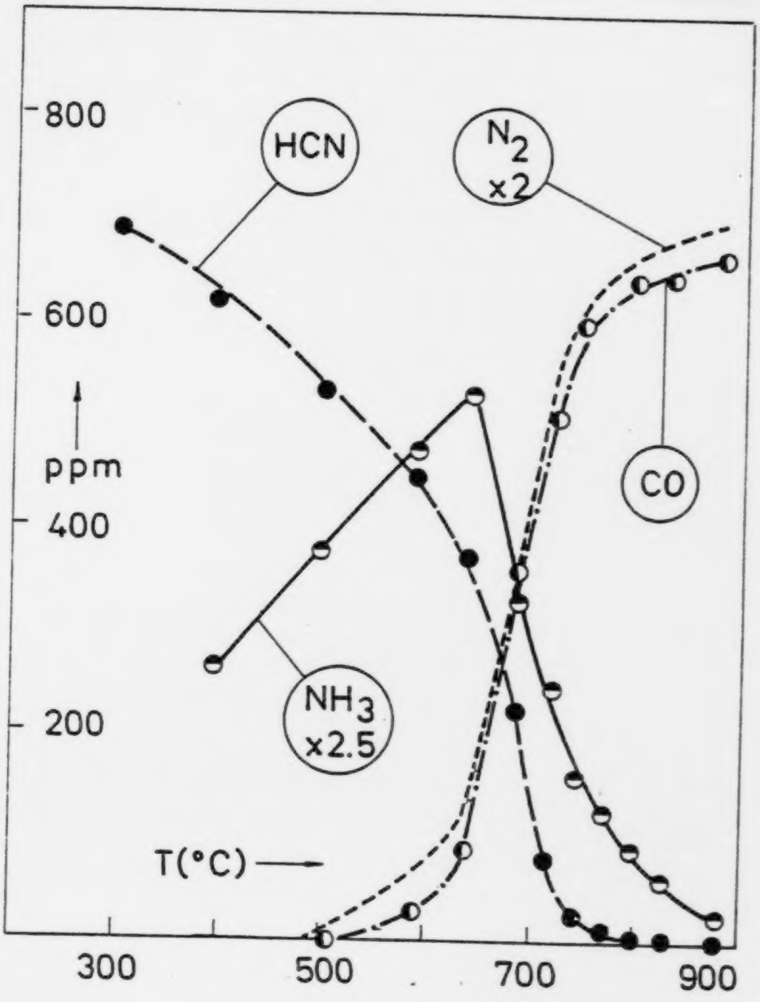

Figure 17. Argon + HCN on "Rietspruit" Char: D = 10.4 $cm^3 s^{-1}$; M = 1.6g; $(HCN)_i$ = 690 ppm.

$$d(HCN)/dt = -V_{15} - V_{46} = -\overline{V_{HCN}} \tag{26}$$

$$d(NH_3)/dt = aV_{15} + V_{46} - V_{13} \tag{27}$$

from which it follows that:

$$-d(HCN)/dt - d(NH_3)/dt = (1-a)V_{15} + V_{13} \tag{28}$$

The overall HCN removal rate, $\overline{V_{HCN}}$, is determined from equation (26). For ethylene soot and cenospherical soot, equation (28) may be used to obtain V_{15}, if "a" is assumed equal to 1/3 and by appropriate substitution for V_{13}. Numerical value of V_{13} may be calculated from equation (108) (for ethylene soot), and from equation (175) (for cenospherical soot) of Part I. For the solids discussed here, the partial reaction order with respect to HCN has not been experimentally determined but, in analogy to the other solids, has been set equal to 0.38. It should be noted that the uncertainty associated with this order is at least ±0.15. Application of this procedure yields the following rates:

A. Ethylene Soot

$$\boxed{V_{HCN} = 8.0 \exp(-4580 \pm 800/T)\ X_{HCN}^{0.38}\ (cm^3 s^{-1} g^{-1})} \tag{29}$$

$$\boxed{V_{15} = 6.3 \times 10^5 \exp(-17860 \pm 1000/T)\ X_{HCN}^{0.38}\ (cm^3 s^{-1} g^{-1})} \tag{30}$$

B. Cenospherical Soot

$$\boxed{\overline{V_{HCN}} = 3.8 \times 10^1 \exp(-5440 \pm 1000/T)\ X_{HCN}^{0.38}\ (cm^3 s^{-1} g^{-1})} \tag{31}$$

$$\boxed{V_{15} = 2.3 \times 10^5 \exp(-13700 \pm 1500/T)\ X_{HCN}^{0.38}\ (cm^3 s^{-1} g^{-1})} \tag{32}$$

C. Rietspruit Char

$$\boxed{\overline{V_{HCN}} = 1.9 \times 10^1 \exp(-5880 \pm 800/T)\ X_{HCN}^{0.38}\ (cm^3 s^{-1} g^{-1})} \tag{33}$$

2.2 Argon + HCN + NH_3 Mixtures (Case S)

These type of trials were previously performed (in 1979) on alumina, using "self-made" HCN (containing CO and some water vapor). An example is shown in Figure 18.

In these early trials, the gas mixture was insufficiently dried prior to being fed into the reactor. The transient decrease of HCN between 250 and

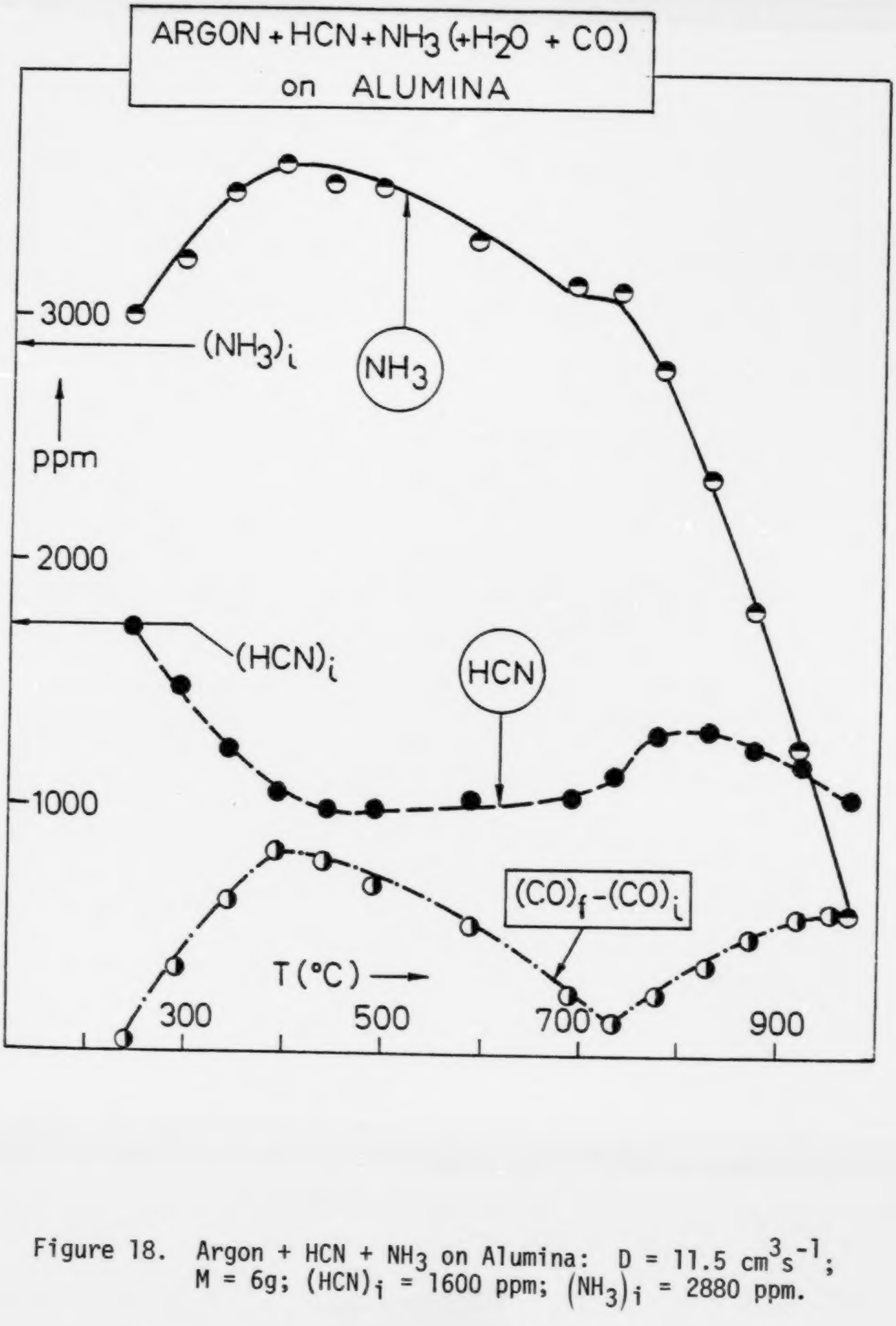

Figure 18. Argon + HCN + NH$_3$ on Alumina: D = 11.5 cm^{3}s^{-1}; M = 6g; (HCN)$_i$ = 1600 ppm; (NH$_3$)$_i$ = 2880 ppm.

700^{0}C (associated with a transient formation of NH_3 and CO, as may be seen from Figure 18) is explained by the reaction between HCN and water vapor (see Section 2.3):

$$HCN + H_2O \xrightarrow{44} NH_3 + CO$$

Between 400 and 700^{0}C there is net formation of NH_3 and CO probably due to the reverse of reaction (9). Above 700^{0}C ammonia is destroyed relatively rapidly and HCN again starts to disappear, due to reaction (15) and to a hypothetical reaction between ammonia and hydrogen cyanide:

$$HCN + NH_3 \xrightarrow{10} N_2 + 2\ H_2 + C$$

Taking into account the presence of some water vapor and CO in these trials, the following primary reactions describe the time variation of the nitrogen containing species:

$$d(HCN)/dt = -V_{10} - V_{15} + V_9 - V_{44} = -\overline{V_{HCN}} \qquad (34)$$

$$d(NH_3)/dt = -V_{10} + aV_{15} - V_9 + V_{44} - V_{13} \qquad (35)$$

$$d(N_2)/dt = V_{10} + \frac{1-a}{2} V_{15} + \tfrac{1}{2}V_{13} \qquad (36)$$

The sum of equations (34) and (35) yields:

$$-d(HCN)/dt - d(NH_3)/dt = 2V_{10} + (1-a)\ V_{15} + V_{13} \qquad (37)$$

By substituting V_{15} and V_{13}, calculated according to equation (23) of this report, and equation (17) of Part I, respectively, the values of V_{10} may be determined from equation (37). This calculation demonstrates that V_{10} is negligibly small (at least three orders of magnitude smaller than $V_{15} + V_{13}$) under the given experimental conditions of concentrations and temperature. This conclusion is in full agreement with the estimation of V_{10} from trials where CO and NH_3 were fed over alumina (Case I.1, see Part I).

2.3 Argon + HCN + H_2O (Vapor) on Alumina

2.3.1 Experimental Method

In these trials a known amount of water vapor is added to a dried argon + HCN mixture. The experimental procedure employed is as follows: part of the argon is passed through a duplex scrubber device, where it is saturated with water vapor at a well-defined, constant temperature. The temperature of the water in each of the two scrubbers is kept constant within 0.1°C. The first scrubber has a slightly higher temperature than the second. In the first scrubber, the argon gas is nearly saturated with water vapor. When passed through the second scrubber a small amount of the water recondenses at the lower temperature of the second scrubber. The temperature of the second scrubber together with the flow rate of the argon gas fractions thus determines the total water content of the mixture.

2.3.2 Observations

Figures 19 and 20 illustrate the results obtained in these trials:

- HCN is very rapidly destroyed at very low temperatures (between 100 and 300°C;

- The reaction products in that temperature range are CO and ammonia, in equimolar quantities:

  $$(HCN)_i - (HCN)_f = (CO)_f = (NH_3)_f \tag{38}$$

  This balance suggests the following overall reaction:

  $$HCN + H_2O \xrightarrow{44} NH_3 + CO$$

  Eventually, at temperatures higher than 500°C, some HCN is transiently formed by the inverse reaction (9). This is also accompanied by a transient decrease of ammonia (see Figure 19):

  $$NH_3 + CO \xrightarrow{9} HCN + H_2O$$

  This inverse reaction occurs at much higher temperatures than the direct path as was previously discovered (see Part I);

- At these more elevated temperatures reaction (13) is primarily responsible for the final decrease of ammonia. Reaction (15) removes the quantities of HCN which have been formed transiently by reaction (9). The competition between V_{15} and V_{13} results in a transient increase of ammonia (see Figure 19, second peak of ammonia at 770°C).

2.3.3 Determination of Rate V_{44}

Since reaction (44) occurs at very low temperatures, its rate may be determined without taking into account the interference of other reactions, which are negligibly slow in this temperature range. Thus, for $T < 300°C$:

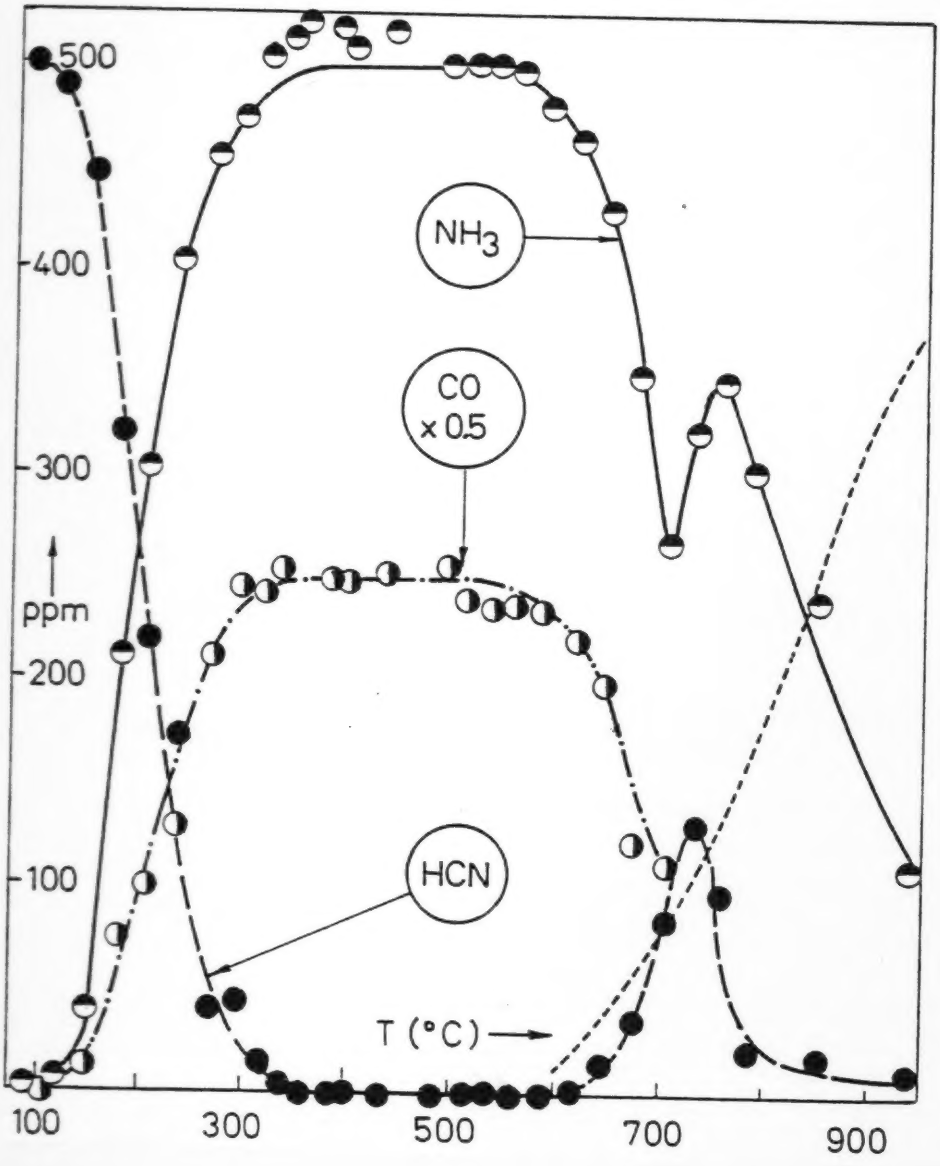

Figure 19. Argon + HCN + H_2O on Alumina: $D = 12.9\ cm^3s^{-1}$; $(HCN)_i$ = 500 ppm; $(H_2O)_i$ = 2860 ppm; M = 6g.

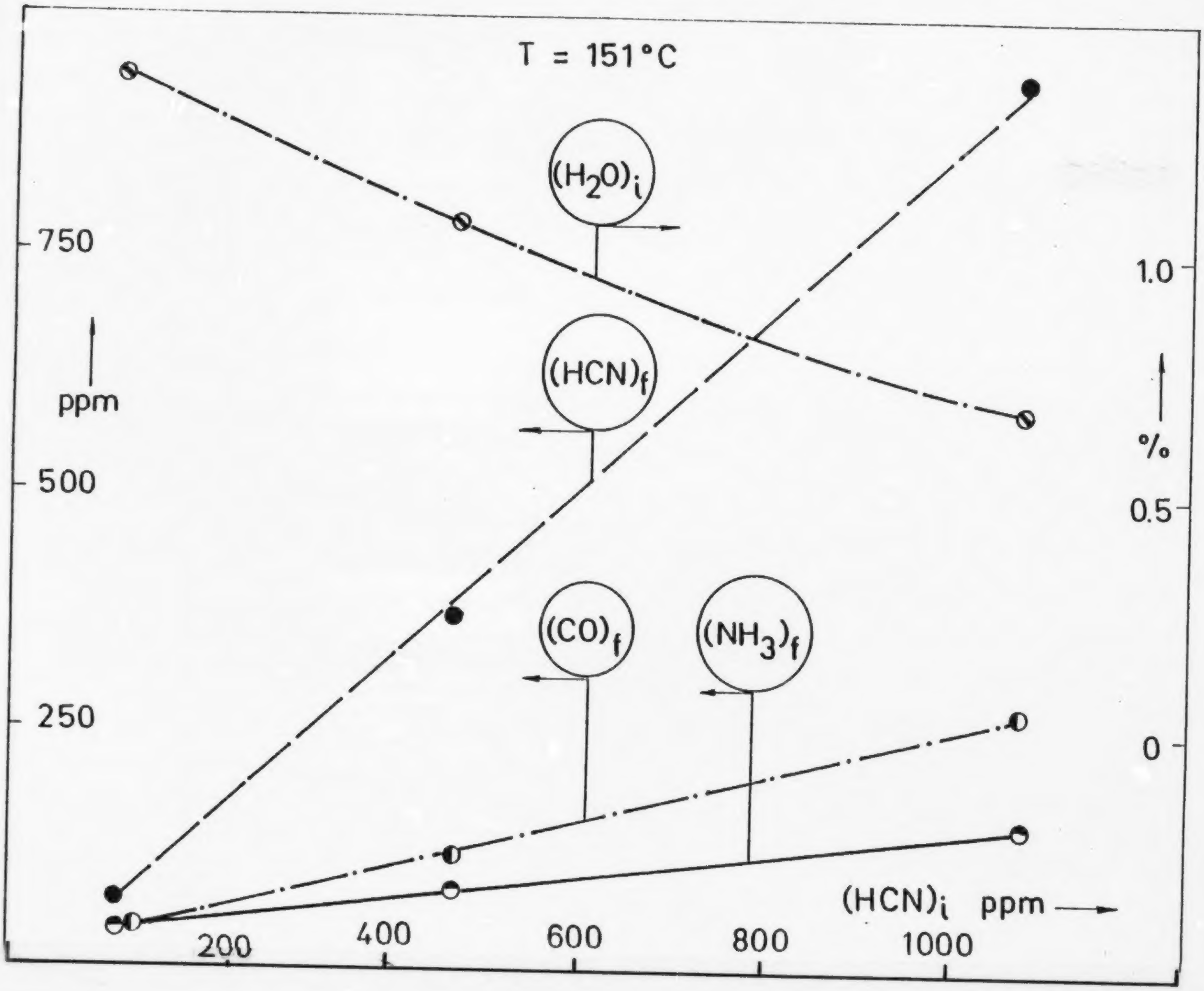

Figure 20. Argon + HCN + H_2O on Alumina: Effect of Initial Concentrations of HCN and H_2O.

$$V_{44} = -d(HCN)/dt = \overline{V_{HCN}} \tag{39}$$

from which the following rate expression has been determined:

$$\boxed{V_{44} = \overline{V_{HCN}} = 3.7 \times 10^{9} \exp(-7550 \pm 500/T)\ X_{HCN}\ X_{H_2O}\ (cm^3 s^{-1} g^{-1})} \tag{40}$$

The validity of the empirical rate expressions obtained for V_{44} (equation (40)) and V_9 (equation (40)) of Part I may be checked by comparing them to the equilibrium constant K_{theor} of reactions (44) and (9), which should also apply for heterogeneous reactions. From published thermochemical data the equilibrium constant is found to be:

$$K_{theor} = X_{NH_3}\ X_{CO}/X_{HCN}\ X_{H_2O} = 0.62 \exp(6150/T) \tag{41}$$

Using empirical values of the rate constants for V_{44} and V_9 and assuming a unit reaction order for V_9 with respect to ammonia, which results in a value of the pre-expotential part of the rate constant of 1.3×10^8, the empirical equilibrium constant is:

$$K_{exp} = k_{44}/k_9 = 28 \exp(6250/T) \tag{42}$$

Considering the expreimental imprecisions, the agreement between the theoretical and the experimental values of this equilibrium constant is acceptable and the temperature dependence agreement is surprisingly good.

2.4 Argon + HCN + H_2 on Alumina (Case P.1) and Graphite (Case P.2)

This trial series is illustrated by Figures 21 and 22 (relative to alumina) and by Figure 23 (relative to graphite).

F 21
22

2.4.1 Experimental Observations

As a general rule, the overall removal rate of hydrogen cyanide ($\overline{V_{HCN}}$) decreases progressively when hydrogen is added to the argon + HCN mixture in increasing amounts. This is clearly suggested from Figure 22 in the case of alumina, and shown directly in Figure 23 for graphite. In the case of graphite, the ratio of the overall HCN removal rate with and without hydrogen present is given by the following empirical expression:

F23

$$\boxed{\frac{\overline{V_{P.2}}}{\overline{V_{G.2}}} = \frac{\overline{V_{HCN}}(\text{with } H_2)}{\overline{V_{HCN}}(\text{without } H_2)} = \frac{1}{1 + 5.5 \times 10^{6} \exp(+9670 \pm 1000/T)\ X^{1.75}}} \tag{43}$$

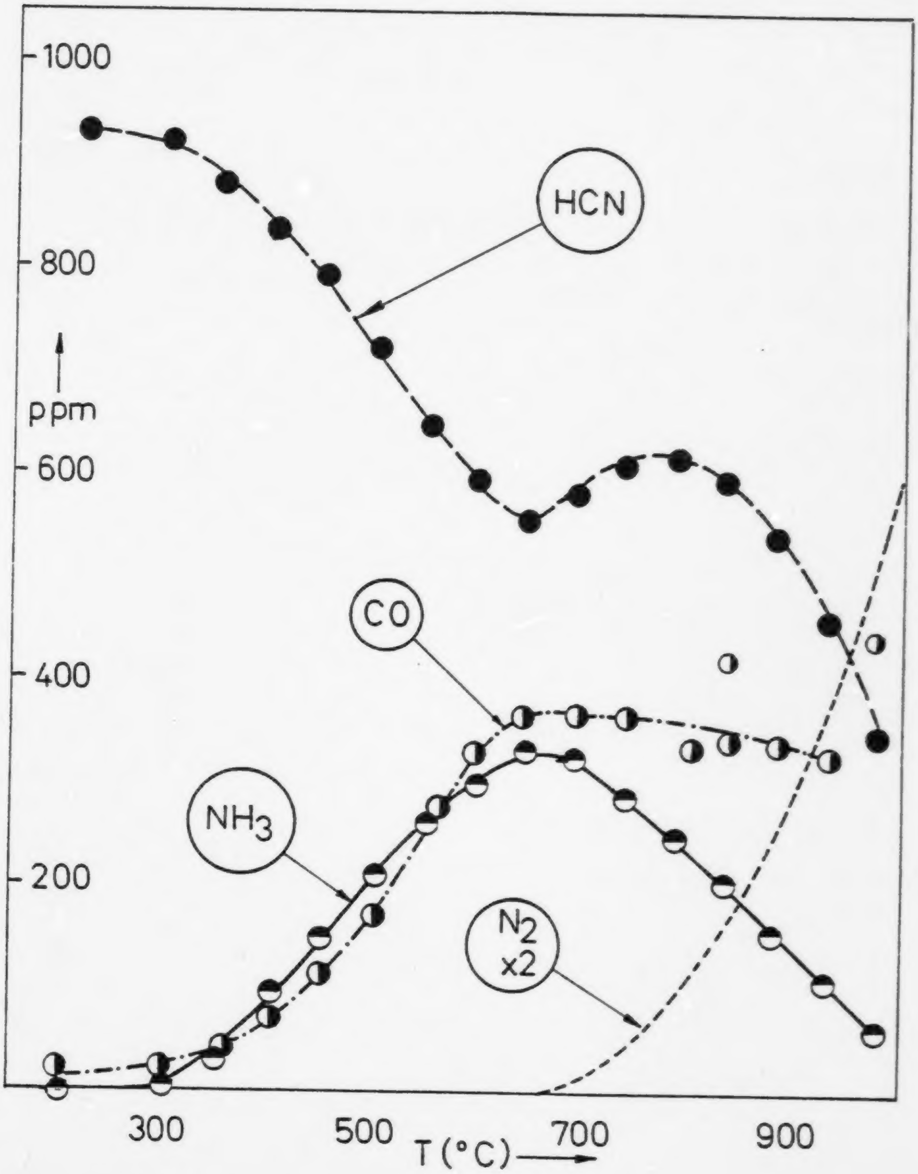

Figure 21. Argon + HCN + H_2 on Alumina: D = 11.6 $cm^3 s^{-1}$; M = 6g; $(HCN)_i$ = 930 ppm; $(H_2)_i$ = 5.55%.

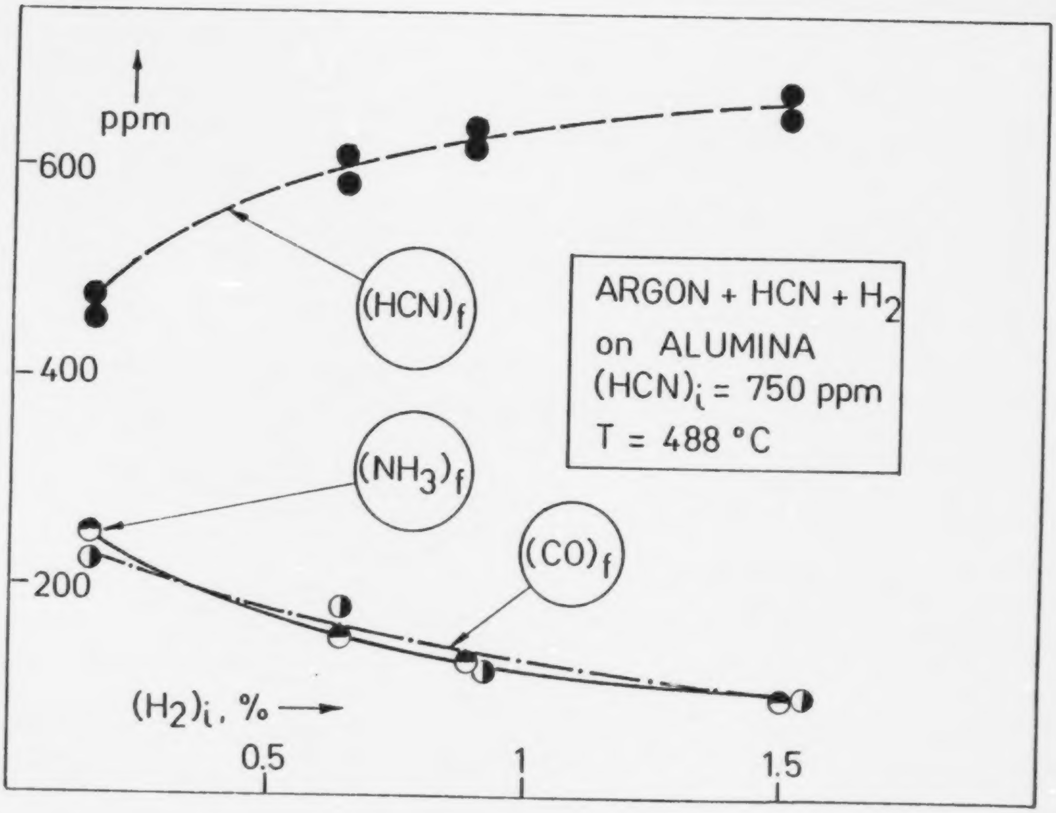

Figure 22. Argon + HCN + H_2 on Alumina: Effect of Hydrogen Concentration.

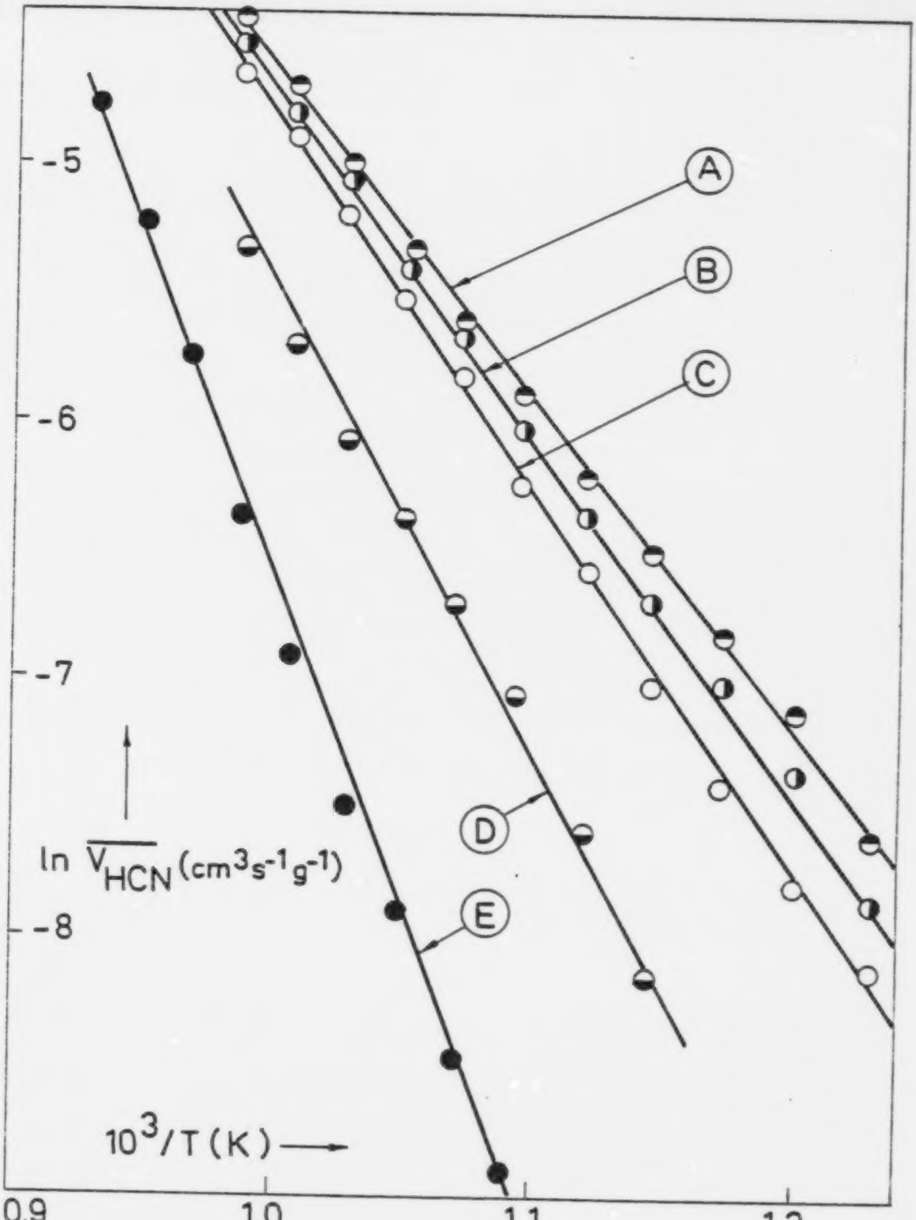

Figure 23. Argon + HCN + H_2 on Graphite: D = 10 cm^{3}s^{-1}; M = 0.59 g; $(HCN)_i$ = 1050 ppm; Percent $(H_2)_i$ = 0 (Curve A); 0.58 (Curve B); 1.08 (Curve C); 3.32 (Curve D) and 6.82 (Curve E).

Since hydrogen inhibits $\overline{V_{HCN}}$, it may be concluded that there does not seem to exist a specific reaction between H_2 and HCN. Thus the reaction:

$$H_2 + HCN \xrightarrow{45} NH_3 + C$$

does not appear to take place. It is more likely that the HCN removal is due to reaction (15) and (44), after H_2O has been formed by reaction (19). Both reactions (15) and (44) may be inhibited by the presence of adsorbed hydrogen. Formtion of CO as observed in Figures 21 and 22, is due to reaction (47).

2.5 Argon + HCN + NO (Case V)

2.5.1 Argon + HCN + NO on Alumina (Case V.1)

Figures 24, 25 and 26 provide examples of these trials.

2.5.1.1 Experimental Observations

1. The value of the ratio

$$r = [(HCN)_i - (HCN)_f] / [(NO)_i - (NO)_f]$$

observed during the decrease of hydrogen cyanide depends on the initial ratio

$$r_i = (HCN)_i/(NO)_i$$

as illustrated in the following table:

r_i	r	Figure
0.18	0.26 to 0.40	28
0.27	0.44 to 0.50	24
0.74	0.70 to 2.00	27

The ratio r decreases with the ratio r_i, indicating that the hydrogen cyanide removed by reaction of HCN and NO (reaction (40)) prevails over the HCN removal by reaction (15). Thus, there must exist a reaction between HCN and NO:

$$HCN + NO \xrightarrow{40} \dots$$

2. The ammonia observed in these trials as a product may be formed either by reaction (40) or (15), or even by the secondary reaction (44) if H_2O is also a product of reaction (40).

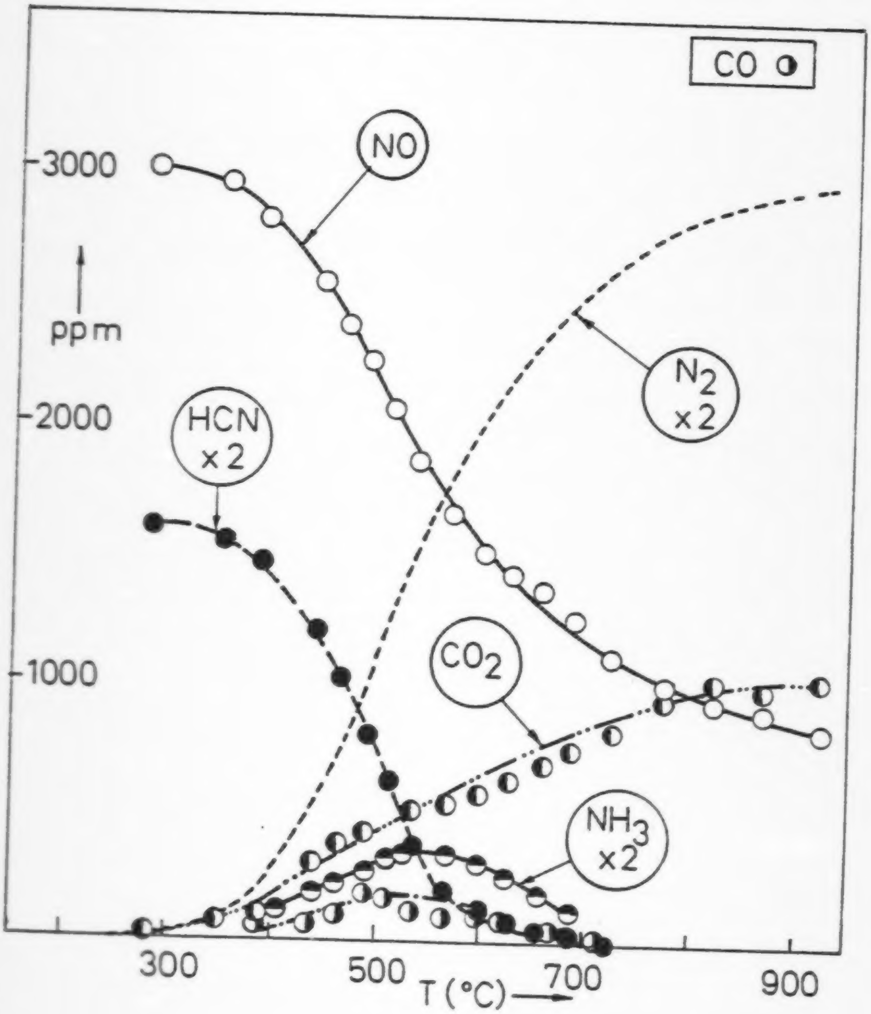

Figure 24. Argon + HCN + NO on Alumina: D = 11.4 cm^3s^{-1}; M = 6g; $(HCN)_i$ = 800 ppm; $(NO)_i$ = 3000 ppm.

Figure 25. Argon + HCN + NO on Alumina: Effect of Initial HCN Concentration.

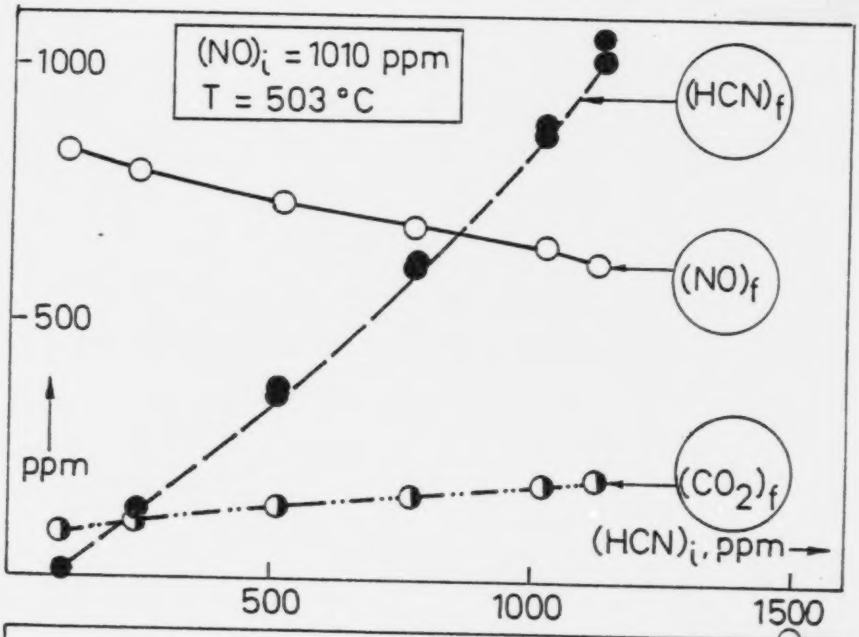

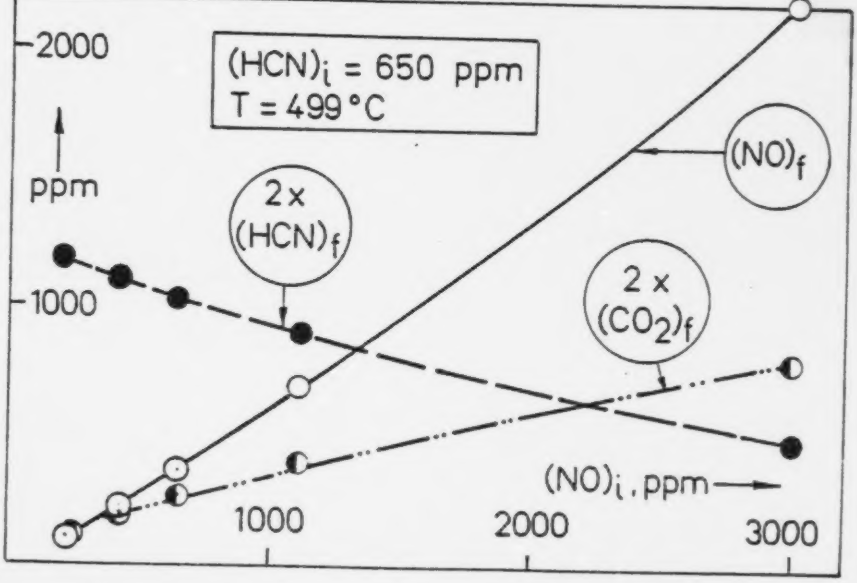

Figure 26. Argon + HCN + NO on Alumina: Effect of Initial NO Concentration.

3. N_2 appears as a product during the first stages of HCN and NO removal. It is a product of reaction (15) and reaction (40) and is also created in the secondary reaction (13).

4. Other reaction products are CO and CO_2, which may be formed by reaction (47) (C + (-O) -- CO) and (12) (CO + (-O) -- CO_2), as well as by the sequence of the two secondary reactions (9) and (44) if H_2 is a product of reaction (40). The fact that CO and CO_2 formation starts just as NO begins to decrease (see Figures 24 and 28), and the fact that their concentration in the reaction products increases with $(NO)_i$ (see Figure 26) suggests that CO and CO_2 are also products of reaction (40).

From these observations it follows that reaction (40) should satisfy the following formal balance:

$$\mathrm{HCN} + a\ \mathrm{NO} \xrightarrow{40} b\ \mathrm{H_2O} + \frac{1-2b-3c}{2}\mathrm{H_2} + d\ \mathrm{CO} + (1-d)\ \mathrm{CO_2} + c\ \mathrm{NH_3} + \frac{1+a-c}{2}\mathrm{N_2} \qquad (44)$$

with: $b \leq 0.5$; $c \leq 1/3$; $d \leq 1$; $a - b = 2 - d$

We thus have the following set of differential equations (secondary reactions are between brackets):

$$d(NO)/dt = -a\ V_{40}\ (-V_8 - V_4) = -\overline{V_{NO}} \qquad (45)$$

$$d(HCN)/dt = -V_{40} - V_{15}\ (-V_{44} - V_{45} + V_9) = -\overline{V_{HCN}} \qquad (46)$$

$$d(NH_3)/dt = c\ V_{40} + 1/3V_{15}\ (+V_{44} + V_{45} - V_9 - V_{13}) \qquad (47)$$

$$d(N_2)/dt = \frac{1+a-c}{2}V_{40} + 1/3V_{15}\ (+\tfrac{1}{2}V_8 + \frac{1+n}{2}V_4 + \tfrac{1}{2}V_{13}) \qquad (48)$$

from equations (46) and (47) it is found that:

$$-d(HCN)/dt - d(NH_3)/dt - 2/3V_{15} - V_{13} = (1-c)V_{40} \qquad (49)$$

2.5.1.2 Determination of Reactions Rates and Stoichiometric Coefficients "a" and "c"

1. From equation (45) the overall NO removal rate $\overline{V_{NO}}$ may be determined. From the same equation the value of (a V_{40}) can be determined by substituting the values of V_8 and V_4 calculated according to equation

(25) of Part I and equation (53) of the same report, respectively. Based upon the results discussed in Part I, the value of n has been taken equal to 0.5, since the ratio NO/NH_3 is always large.

In this manner, the following rate expressions are obtained:

$$\boxed{\overline{V_{NO}} = 2.6 \times 10^4 \exp(-7820 \pm 300/T)\ X_{HCN}^{0.3}\ X_{NO}^{0.7}\ (cm^3 s^{-1} g^{-1})} \qquad (50)$$

$$\boxed{a\ V_{40} = 2.3 \times 10^4 \exp(-7820 \pm 300/T)\ X_{HCN}^{0.3}\ X_{NO}^{0.7}\ (cm^3 s^{-1} g^{-1})} \qquad (51)$$

This calculation demonstrates that the overall NO removal is almost entirely governed by reaction V_{40} and that V_{40} and $\overline{V_{NO}}$ have the same temperature dependence and the same partial reaction orders with respect to HCN and NO for the experimental conditions in these trials.

2. Neglecting the secondary reactions V_{44} and V_9, the value of V_{40} may be determined from equation (46), by substituting for the primary reaction V_{15} as calculated according to equation (23) of the present report:

$$\boxed{V_{40} = 1.3 \times 10^4 \exp(-7820 \pm 300/T)\ X_{HCN}^{0.3}\ X_{NO}^{0.7}\ (cm^3 s^{-1} g^{-1})} \qquad (52)$$

3. The ratio of equation (51) to equation (52) gives the value of the coefficient "a":

$$a = 1.8 \pm 0.4 \cong 2. \qquad (53)$$

In the following sections, we shall assume the value of "a" to be equal to 2.

4. The overall HCN removal rate ($\overline{V_{HCN}}$) may also be determined from equation (46) and is found to be given by the following expression:

$$\boxed{\overline{V_{HCN}} = 6.4 \times 10^4 \exp(-9560 \pm 500/T)\ X_{HCN}^{0.5}\ X_{NO}^{0.34}\ (cm^3 s^{-1} g^{-1})} \qquad (54)$$

5. From equation (49) the value of $(1-c)V_{40}$ can be determined by substitution of the rates V_{15} and V_{13} by their values calculated according to equation (23) of the present report, and equation (17) of Part I:

$$(1-c)V_{40} = 5.14 \text{ to } 5.77 \times 10^3 \exp(-7820 \pm 800/T)\ X_{HCN}^{0.3}\ \ X_{NO}^{0.7} \qquad (55)$$
$$(cm^3 s^{-1} g^{-1})$$

6. Comparison of equations (55) and (52) yields an approximate value of the coefficient "c", which is found to be between 0.37 and 0.44. Actually, the maximum allowable value of c is 1/3, so that the experimental values indicate that maximum value.

   Since the formal balance coefficients given in equation (44) are $b = 0$ and $(1 - 2b - 3c) = 0$, there is neither H_2O nor H_2 formed by reaction (40). Further, since $a - b = 2 - d$ (equation (44)), and since $a = 2$ (equation (53)), d is also equal to zero (i.e. no CO is formed under these conditions).

Based upon these observations, the stoichiometric balance of reaction (40) can now be written, at least in the case of alumina, as follows:

$$HCN + 2\ NO \xrightarrow{40} 1/3\ NH_3 + 4/3\ N_2 + CO_2$$

2.5.2 Argon + HCN + NO on Rietspruit Fly Ash

These trials are illustrated by Figures 27 and 28 for two values of the ratio $(HCN)_i/(NO)_i$. The same reactions occuring for the case of alumina occur in this case. Partial orders have not been directly determined for this case, but are assumed to be the same as in the case of alumina. Using this assumption, the following rates may be determined:

From equation (45) and equation (46) respectively, the overall NO and HCN removal rates are found (in $cm^3s^{-1}g^{-1}$) to be:

$$\boxed{\overline{V_{NO}} = 0.9 \text{ to } 1.3 \times 10^{10} \exp(-18100 \pm 1500/T)\ X_{HCN}^{0.3}\ X_{NO}^{0.7}} \qquad (56)$$

$$\boxed{\overline{V_{HCN}} = 1.3 \text{ to } 2.0 \times 10^{8} \exp(-15600 \pm 1500/T)\ X_{HCN}^{0.5}\ X_{NO}^{0.34}} \qquad (57)$$

From equation (46), neglecting the secondary reactions, V_{40} is determined by substituting the rate V_{15} as calculated according to equation (25) of this report:

$$\boxed{V_{40} = 2.5 \text{ to } 5.5 \times 10^{7} \exp(-13700 \pm 1000/T)\ X_{HCN}X_{NO}\ (cm^3s^{-1}g^{-1})} \qquad (58)$$

2.5.3 Argon + HCN + NO on Carbonaceous Materials

Figures 29 through 31 show results obtained in the cases of cenospherical soot, ethylene soot and Rietspruit char, respectively. In these trials, two

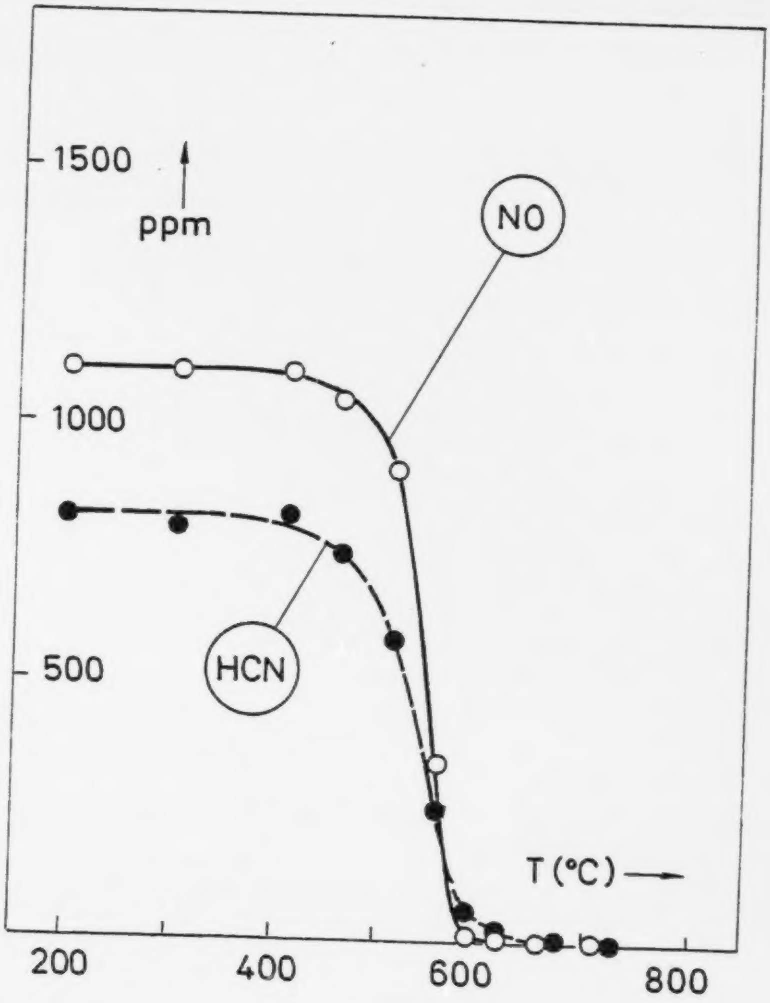

Figure 27. Argon + HCN + NO on "Rietspruit" Fly Ash: $D = 10.4\ cm^3s^{-1}$; M = 2g; $(HCN)_i$ = 285 ppm; $(NO)_i$ = 1110 ppm.

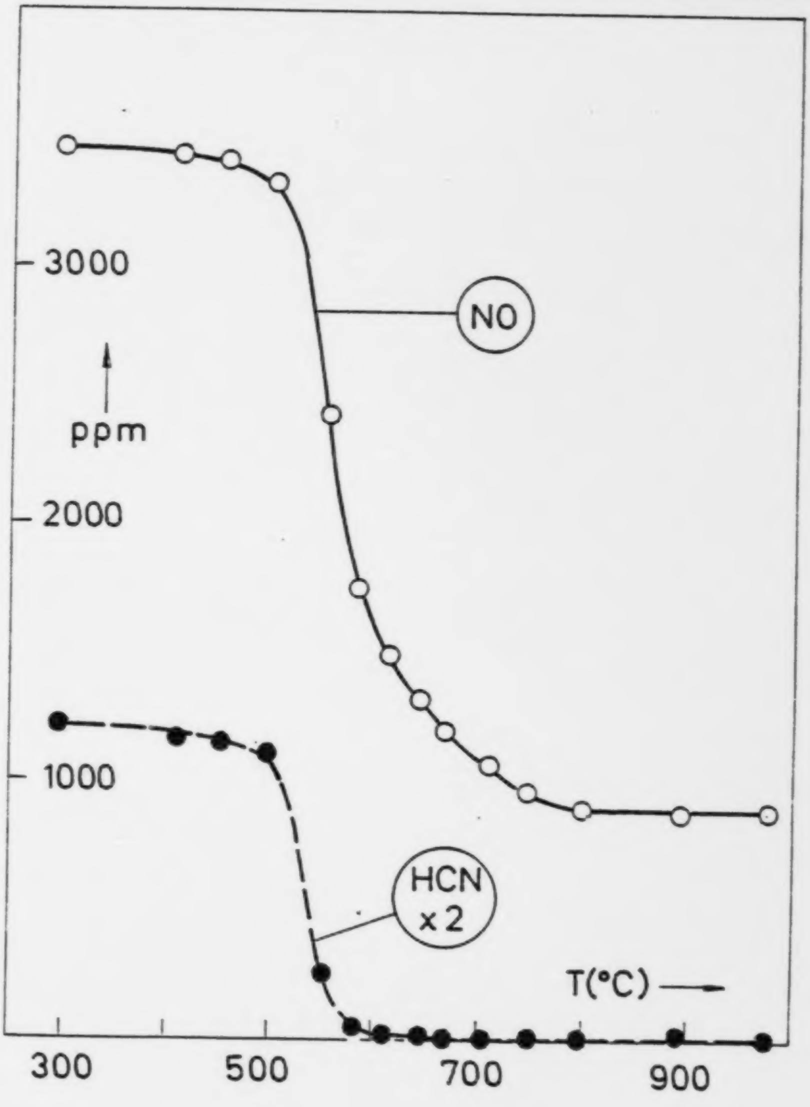

Figure 28. Argon + HCN + NO on "Rietspruit" Fly Ash: D = 10.4 cm^3s^{-1}; M = 2 g; $(HCN)_i$ = 610 ppm; $(NO)_i$ = 3450 ppm.

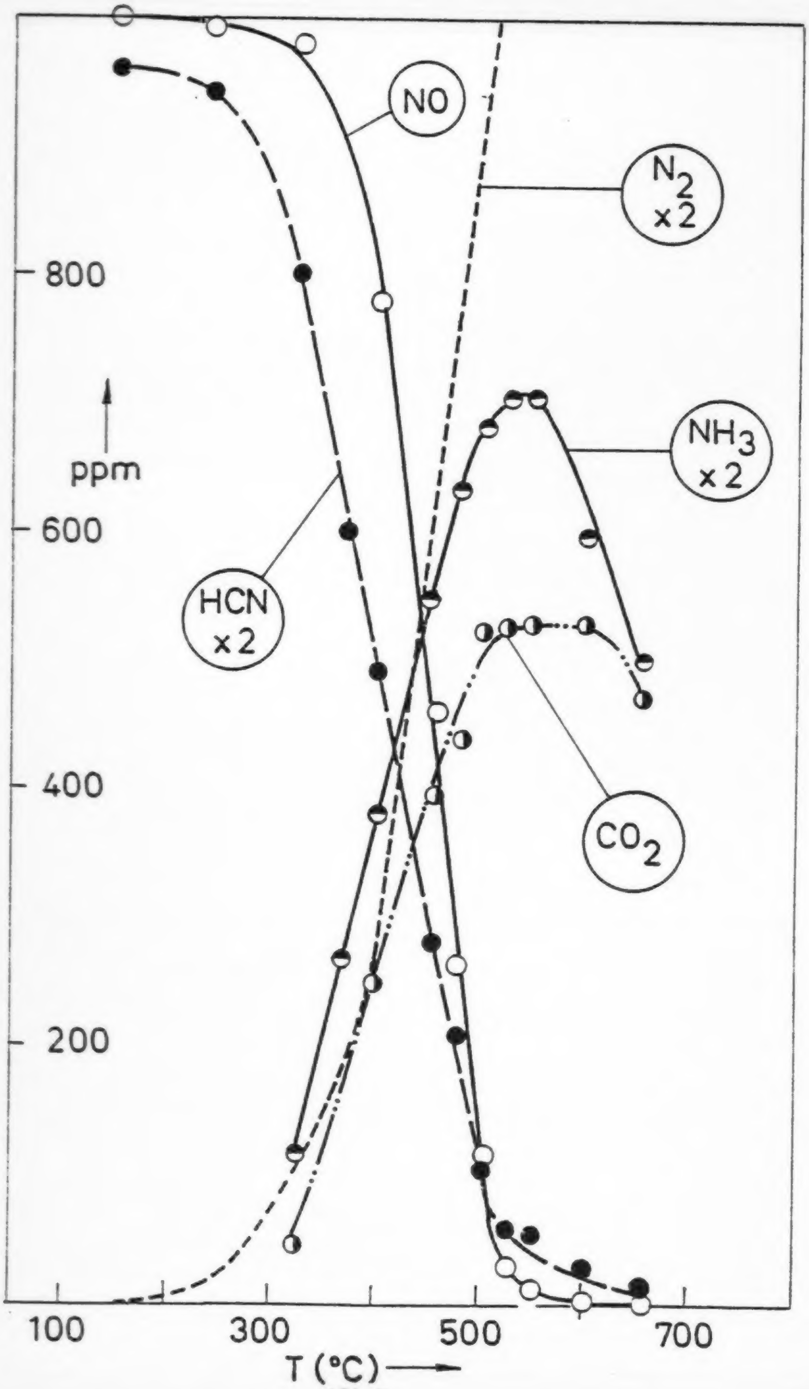

Figure 29. Argon + HCN + NO on Cenospheric Soot: D = 10.3 cm^3s^{-1}; M = 1.3 g; $(HCN)_i$ = 480 ppm; $(NO)_i$ = 1000 ppm.

Figure 30. Argon + HCN + NO on Ethylene Soot; D = 10.4 cm^3s^{-1}; M = 0.36 g; $(HCN)_i$ = 900 ppm; $(NO)_i$ = 890 ppm.

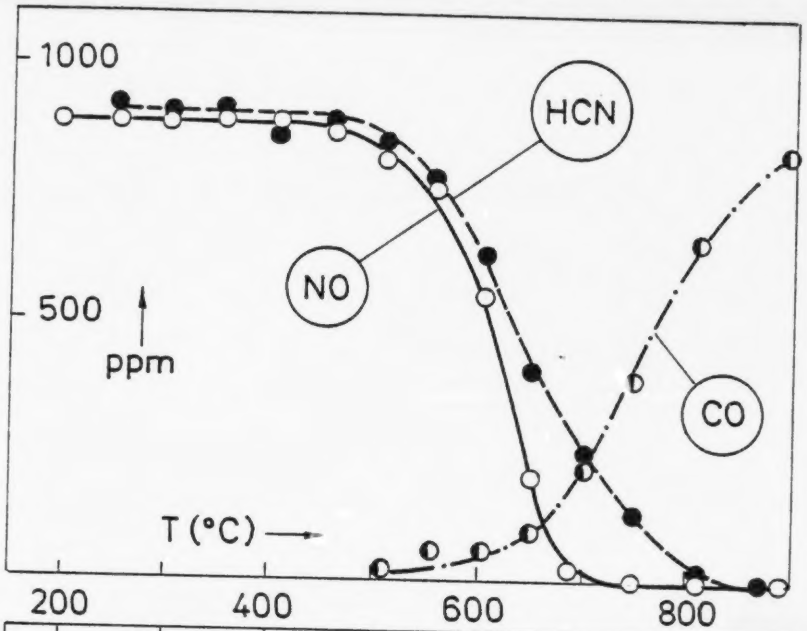

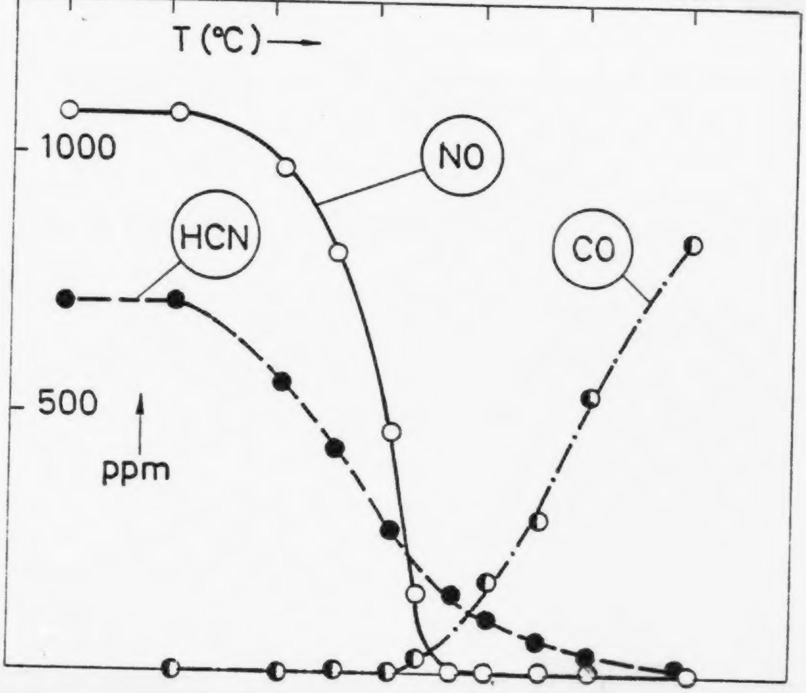

Figure 31. Argon + HCN + NO on "Rietspruit" Char: D = 10.4 cm^3s^{-1}; M = 1.6 g; $(HCN)_i$ = 730 ppm; $(NO)_i$ = 1080 ppm.

supplementary primary reactions by which NO can be reduced, must be considered:

$$NO + a(-C) \xrightarrow{1} 0.5\ N_2 + (2a - 1)\ CO + (1 - a)\ CO_2$$

$$NO + a(-C) + b(-H) \xrightarrow{2} NH_3 + (\frac{b-5}{2} + 2a)CO + (\frac{5-b}{2} - a)CO_2 + (\frac{b-3}{2})H_2O$$

These have already been discussed in Part I.

In addition to these two supplementary reactions (1 and 2) the ammonia and N_2 formation from these reactions must be considered. The destruction of ammonia also admits a supplementary secondary reaction:

$$NH_3 + (-C) \xrightarrow{5} HCN + H_2$$

Therefore, tertiary reactions involving H_2 (e.g. V_{11}, V_{14}, V_{21}) may also occur, but will be disregarded in that which follows.

Finally, HCN may additionally disappear by the previously discussed reaction:

$$HCN + 2(-H) \xrightarrow{46} NH_3 + C$$

If we disregard secondary reactions occurring in the mechanism, the following set of equations approximately describes the variation of the nitrogen containing species:

$$d(NO)/dt = -a\ V_{40} - V_1 - V_2 = -\overline{V_{NO}} \tag{59}$$

$$d(HCN)/dt = -V_{40} - V_{15} - V_{46} = -\overline{V_{HCN}} \tag{60}$$

$$d(NH_3)/dt = c\ V_{40} + 1/3V_{15} + V_2 + V_{46} \tag{61}$$

$$d(N_2)/dt = \frac{1+a-c}{2}\ V_{40} + 1/3V_{15} + \tfrac{1}{2}V_1 \tag{62}$$

The overall NO and HCN removal rates, $\overline{V_{NO}}$ and $\overline{V_{HCN}}$, are directly obatined from equation (59) and equation (60), respectively. From equation (59) the rate V_{40} may also be determined by substituting V_1 and V_2 as calculated according to the following equations of Part I: equations (186) and (185) for cenospherical soot; equations (117) and (118) for ethylene soot. In this calculation for V_{40}, the coefficient "a" has been set equal to 2 (see Section 2.5.1).

Finally, the rate V_{46} can be obtained from equation (60) by substituting the value of V_{40} calculated previously and of V_{15} as calculated according to equations (32) for cenospherical soot or (30) for ethylene soot.

2.5.3.1 Cenospherical Soot

For this soot, the ratio $(CO_2)/(CO)$ in the reaction products is relatively high, as has been observed with other gas mixtures studied earlier (see Part I).

The following rates have been determined, as previously explained:

$$\boxed{\overline{V_{HCN}} = 1.45 \times 10^3 \exp(-4900 \pm 500/T)\ X_{HCN}^{0.5}\ X_{NO}^{0.34}\ (cm^3 s^{-1} g^{-1})} \qquad (63)$$

When calculating the overall NO removal rate from equation (59), the rates V_1 and V_2, for the given experimental conditions, were found to be very small compared to V_{NO}. Therefore aV_{40} is almost equal to $\overline{V_{NO}}$ and should be characterized by the same partial reaction orders with respect to HCN and NO as is V_{40}:

$$\boxed{\overline{V_{NO}} = aV_{40} = 1.3 \times 10^7 \exp(-10500 + 1000/T)\ X_{NO}^{0.7}\ X_{HCN}^{0.3}\ (cm^3 s^{-1} g^{-1})} \qquad (64)$$

From equation (60) the following value of V_{46} is obtained:

$$\boxed{V_{46} = 1.8 \times 10^2 \exp(-2840 \pm 300/T)\ X_{HCN}\ \ (cm^3 s^{-1} g^{-1})} \qquad (65)$$

2.5.3.2 Ethylene Soot

In the case of ethylene soot, CO is the main carbon-containing product in the outlet flow of the reactor. As previously discussed the ratio of $(CO)/(CO_2)$ in the reaction products is always large for this solid material (see Part I). The same holds true for the trials on Rietspruit char (see Figure 31).

From equation (60) one finds:

$$\boxed{\overline{V_{HCN}} = 3.5 \times 10^7 \exp(-14200 \pm 800/T)\ X_{HCN}^{0.5}\ X_{NO}^{0.34}\ (cm^3 s^{-1} g^{-1})} \qquad (66)$$

The overall NO removal rate is determined from equation (59). $\overline{V_{NO}}$ is found to be always much larger than the rates V_1 and V_2, at least for the actual experimental conditions studied here. Therefore the value of aV_{40} should be very close to that of $\overline{V_{NO}}$:

$$\boxed{\overline{V_{NO}} = aV_{40} = 5.3 \times 10^8 \exp(-15050\ \pm 800/T0\ X_{NO}^{0.7}\ X_{HCN}^{0.3}\ (cm^3 s^{-1} g^{-1})} \qquad (67)$$

For V_{46}, the following expression is determined from equation (60):

$$\boxed{V_{46} = 4.0 \times 10^7 \exp(-14200 \pm 600/T)\ X_{HCN}\ (cm^3 s^{-1} g^{-1})} \qquad (68)$$

2.5.3.2 Rietspruit Char

Since neither V_1, V_2, nor V_{15} have been determined for chars, only the overall HCN and NO removal rates can be determined here. They are found from equations (60) and (59). Reaction orders with respect to HCN and NO have been taken arbitrarily equal to one for $\overline{V_{NO}}$.

$$\boxed{\overline{V_{HCN}} = 3.8 \times 10^3 \exp(-6200 \pm 400/T)\ X_{NO}^{0.34}\ X_{HCN}^{0.5}\ (cm^3 s^{-1} g^{-1})} \qquad (69)$$

$$\boxed{\overline{V_{NO}} = 3.6 \times 10^{10} \exp(-12000 \pm 800/T) X_{NO}\ X_{HCN}\ (cm^3 s^{-1} g^{-1})} \qquad (70)$$

2.6 Argon + HCN + O_2 Mixtures (Case U)

An analogous reaction between hydrogen cyanide and oxygen might be expected, as has been previously found between ammonia and oxygen (see Part I). HCN + oxygen mixtures have been studied exclusively on alumina. Examples are given in Figures 32 through 34.

2.6.1 Experimental Observations

1. In the presence of oxygen, HCN disappears at lower temperatures than in the absence of it (compare for example Figure 32 with Figure 12). Thus there must exist a supplementary primary reaction involving oxygen as a reactant in addition to reaction (15).
2. The following species appear as reaction products:
    - Nitrogen Containing Species. N_2, NH_3, and NO. Of these three only NO is not formed as soon as HCN begins to disappear. NO appears only when NH_3 begins to decrease. Therefore NO formation must be due to the secondary reaction (17):

      $$NH_3 + 1.25\ O_2 \xrightarrow{38} NO + 1.5\ H_2O$$

    - Carbon Monoxide and Dioxide. Carbon dioxide increases progressively during the HCN decrease. Almost no CO is formed over the entire temperature range (at least 75 percent of the $(CO)_f$ concentration shown in Figure 32 comes from the 60 ppm CO concentration present in the inlet flow).
3. To an acceptable approximation, the following carbon and oxygen balances hold for the temperature range where HCN disappears (i.e. in

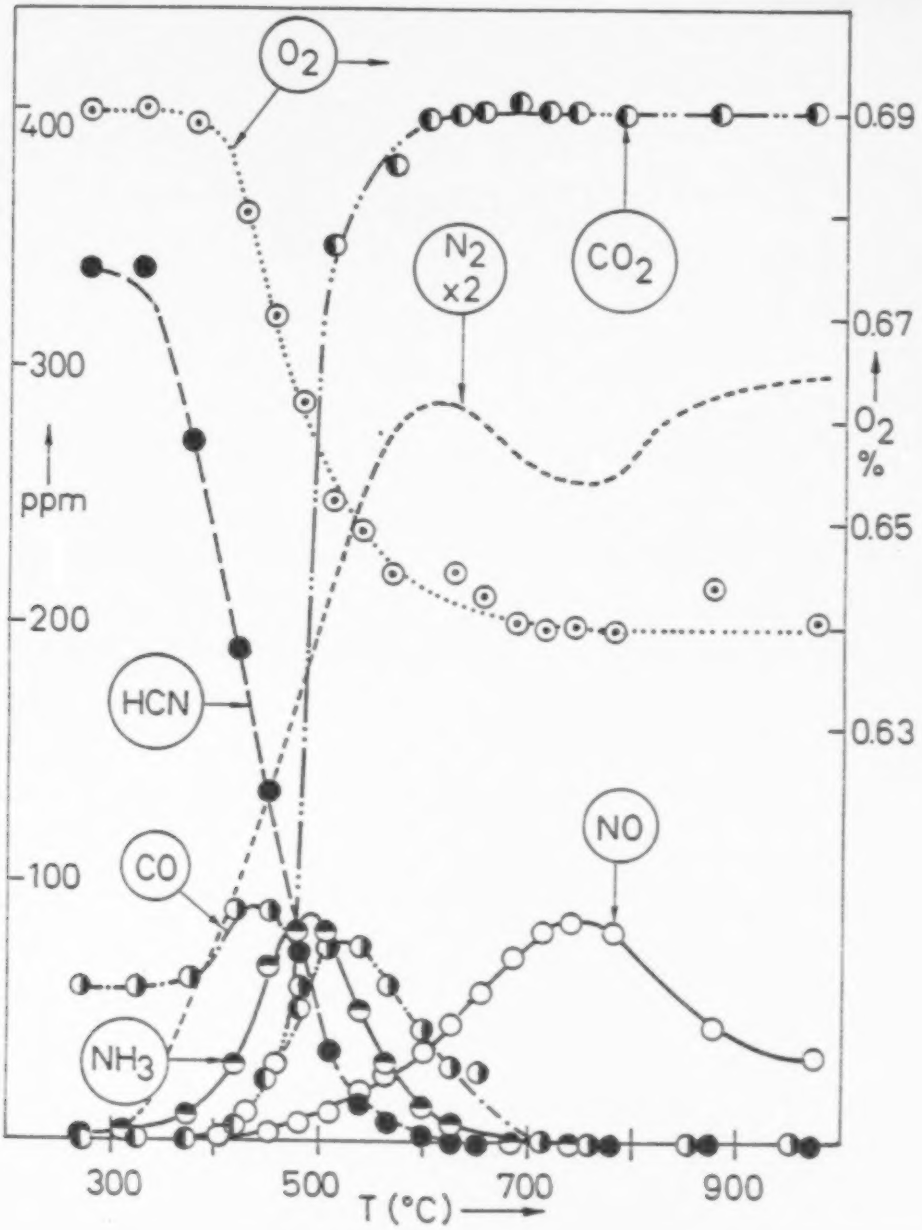

Figure 32. Argon + HCN + O_2 on Alumina: D = 13.1 cm^3s^{-1}; M = 6 g; $(HCN)_i$ = 340 ppm; $(O_2)_i$ = 0.69%.

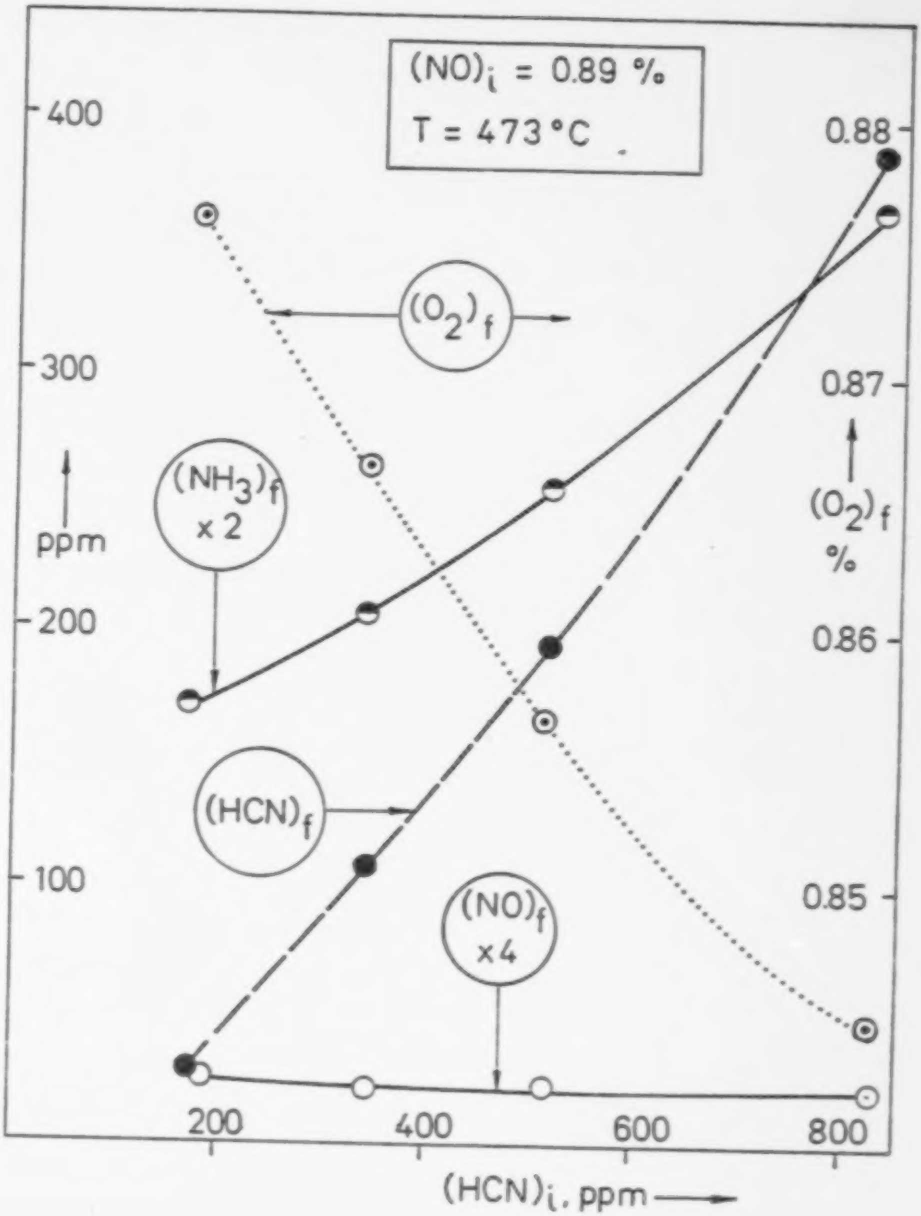

Figure 33. Argon + HCN + O_2 on Alumina: Effect of Initial HCN Concentration.

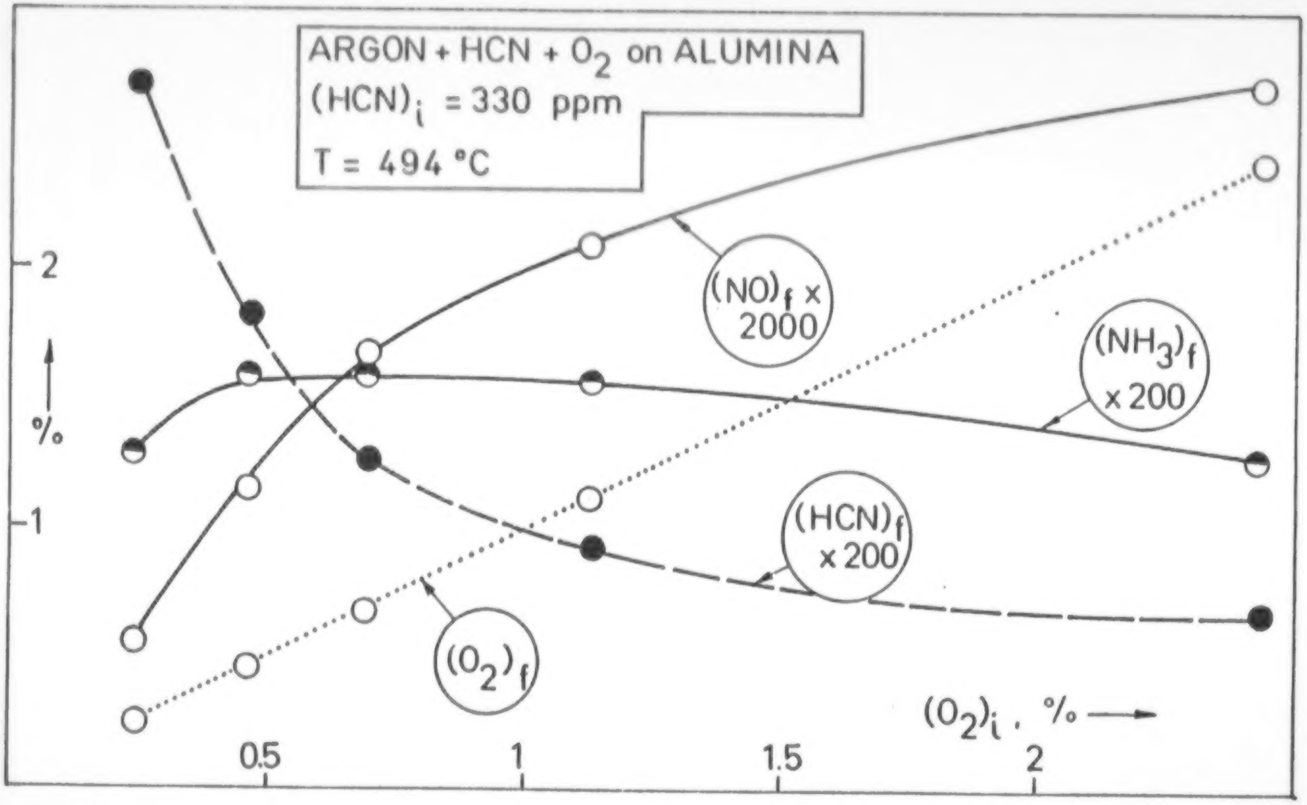

Figure 34. Argon + HCN + O_2 on Alumina: Effect of Initial Oxygen Concentration.

the temperature range where reaction (15) is vanishingly small:

$$(HCN)_i - (HCN)_f = (CO_2)_f \tag{71}$$

The following oxygen balance is observed as long as $(NH_3)_f$ is sufficiently small (i.e. as long as reaction (17) is negligible):

$$2[(O_2)_i - (O_2)_f] = 2\ (CO_2)_f + (NO)_f \cong 2\ (CO_2)_f \tag{72}$$

In the temperature ranges where reaction (13) and (17) are negligible (i.e. below about 500 to 550°C) the following nitrogen balance is observed:

$$[(HCN)_i - (HCN)_f]/2 = (NH_3)_f + (N_2)_f \tag{73}$$

From these observations, the following stoichiometry is suggested for reaction (38):

$$HCN + O_2 \xrightarrow{38} 1/3N_2 + 1/3\ NH_3 + CO_2$$

The following differential equation thus describe the variation of the nitrogen-containing species (secondary reactions being written between brackets):

$$d(NO)/dt = (-2V_{40} + V_{17} - V_8) \tag{74}$$

$$d(HCN)/dt = -V_{38} - V_{15}\ (+V_9 - V_{44} - V_{40}) = -\overline{V_{HCN}} \tag{75}$$

$$d(NH_3)/dt = 1/3V_{38}\ (-V_9 + V_{44} + 1/3V_{40} - V_{17} - V_{13} - V_{16}) \tag{76}$$

$$d(N_2)/dt = 1/3V_{13} = 1/3V_{15}\ (+\ 4/3V_{40} + \tfrac{1}{2}V_{13} + \tfrac{1}{2}V_{16}) \tag{77}$$

From equations (74), (75) and (76) it follows that:

$$\begin{aligned} -d(NO)/dt - d(HCN)/dt - d(NH_3)/dt = {} & 2/3V_{38} + V_{15} + 8/3V_{40} + V_8 \\ & + V_{16} + V_{13} \end{aligned} \tag{78}$$

2.6.2 Determination of the Rate V_{38}

All reaction rates in the right hand side of equation (78), except V_{38}, have previously been evaluated. Thus V_{38} may be determined by substituting for V_3, V_{13}, V_{15}, V_{16} and V_{40} as calculated respectively according to equation (25) of Part I, equation (17) of Part I, equation (23) of the present report, equation (70) of Part I and equation (52) of the present report, respectively. In this manner one finds that:

$$\boxed{V_{38} = 1.7 \times 10^5 \exp(-9700 \pm 700/T) X_{HCN}^{0.5}\ X_{O_2}^{0.27} \quad (cm^3 s^{-1} g^{-1})} \tag{79}$$

This calculation demonstrates that, in the temperature range where HCN disappearance occurs, and under the condition that the oxygen concentration is not too small, the rates V_8, V_{13}, V_{15}, V_{16} and V_{40} are all small compared to the rate V_{38}. Therefore, the overall HCN removal rate, $\overline{V_{HCN}}$ is governed by V_{38} and equal to it as a first approximation.

2.7 Conclusions

As a conclusion, some specific reactions involving hydrogen cyanide as a reactant will be compared for solid particles having different chemical nature. In order for this to be done, the reaction rates have been listed in Table I as intrinsic rate constants. These are expressed in moles/s/m/atm^n, where "n" is the sum of all the partial reaction orders and the concentrations of reactants appearing in the rate expression are expressed in atmospheres.

A. Graphical comparison of the intrinsic rate constants k_{15} and k_{HCN} (rate constant of overall HCN removal rate = -d(HCN)/dt), determined with argon + HCN mixtures on different solid particles, is presented in Figure 35.

   For solids having no bound hydrogen atoms (refractory oxides, graphite) both constants k_{HCN} and k_{15} are almost identical. However, for solids containing bound hydrogen atoms(soots, chars), k_{HCN} is larger than k_{15} (in the temperature range considered in this study) due to the existence of the competing reaction (46).

B. For the same solids, a comparison of the intrinsic rates k_{40} and k_{HCN} in the presence of NO (i.e. with argon + HCN + NO mixtures) is shown in Figure 36. One finds that the temperature dependence of k_{40} is larger than that of k_{HCN}, i.e. $\theta_{40} > \theta_{HCN}$. The fact that $k_{40} > k_{HCN}$ is due to the difference in partial reaction orders with respect to NO and HCN for these two reaction rates. In actuality, V_{HCN} is always larger than or at least as large as V_{40}.

C. Comparison of V_{15}, V_{40}, V_{38} and V_{44} is made for alumina in Figure 37, for selected mixture compositions. This figure clearly illustrates the effects of H_2O, NO and O_2 on the destruction of hydrogen cyanide.

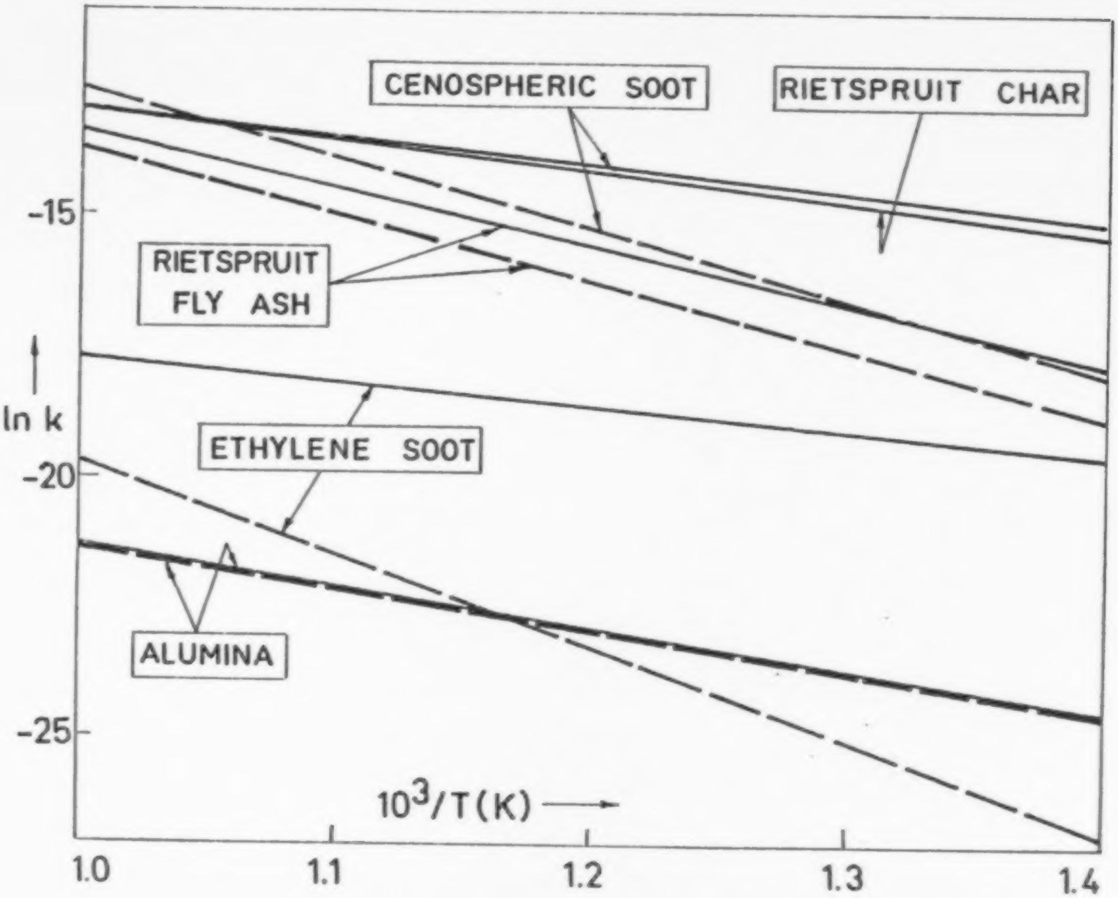

Figure 35. Comparison of the Intrinsic Rate Constants (k in moles.s^{-1}.m^{-2} .atmos.$^{-0.38}$) Measured on Different Solids. Dashed Curves = k_{15}; Continuous Curves = k_{HCN} (Overall HCN Removal Rate Constant, Measured in Argon + HCN Mixtures).

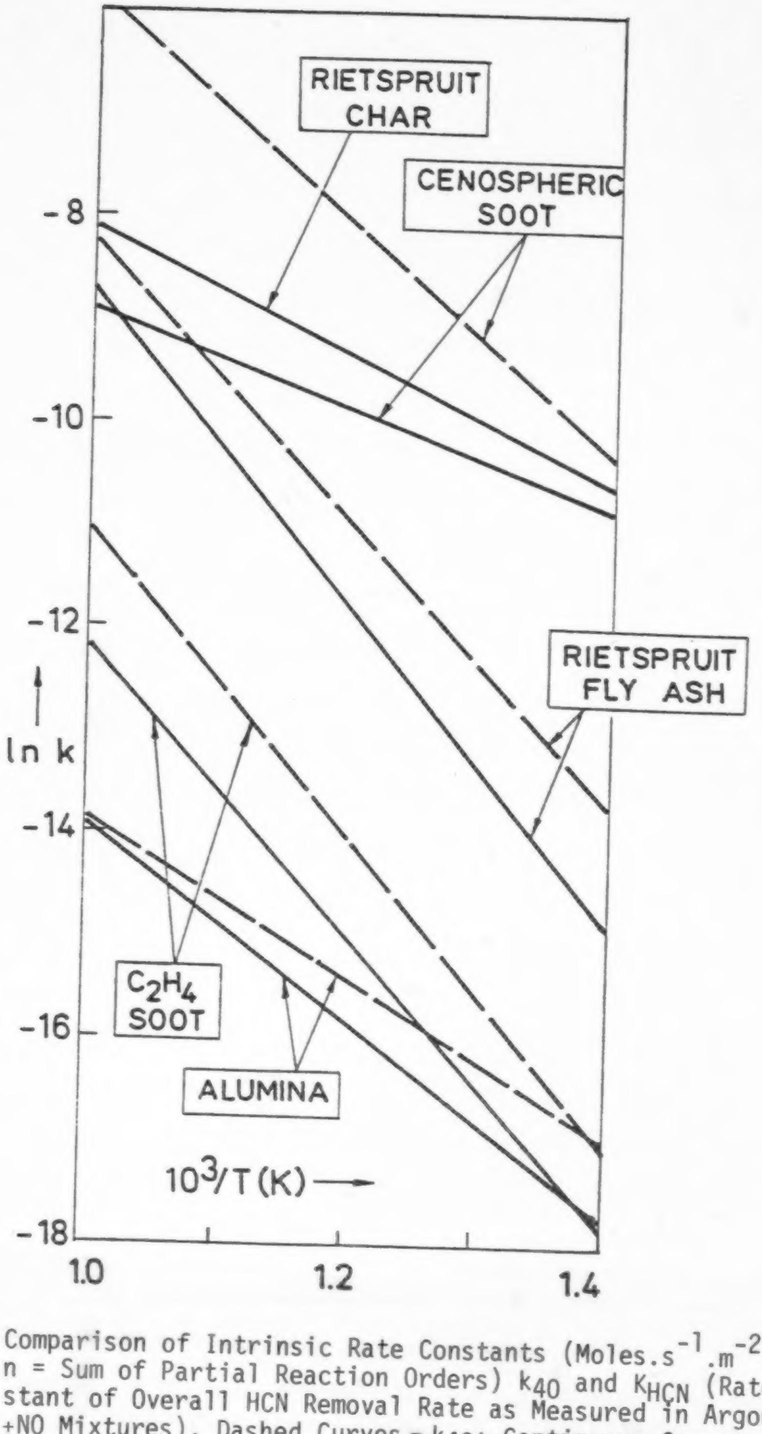

Figure 36. Comparison of Intrinsic Rate Constants (Moles.s^{-1}.m^{-2}.p^{-n}; n = Sum of Partial Reaction Orders) k_{40} and K_{HCN} (Rate Constant of Overall HCN Removal Rate as Measured in Argon + HCN +NO Mixtures). Dashed Curves = k_{40}; Continuous Curves = k_{HCN}.

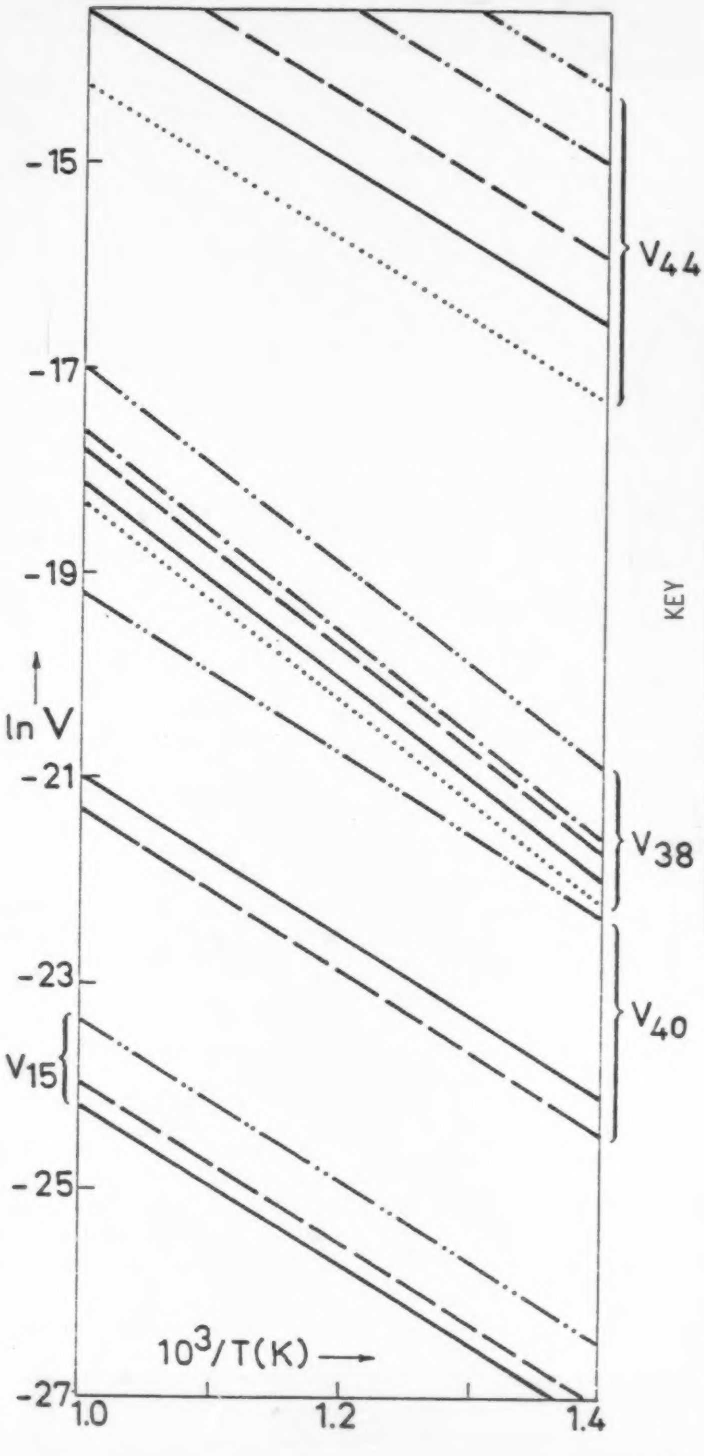

KEY

Curves:	P_{HCN} (bar)	P_{NO} (bar)	P_{H_2O} (bar)	P_{O_2} (bar)
Dash/Double Dotted	0.005	0.005	0.01	0.01
Dash/Dotted	0.0005	0.001	0.05	0.05
Dashed	0.001	0.0005	0.01	0.01
Continuous	0.0005	0.001	0.01	0.01
Dotted	0.0005	0.001	0.005	0.005

Figure 37. Comparison of Some Specific Reactor Rates $\left(\text{moles}\cdot s^{-1} m^{-2}\right)$ on Alumina for Different Gas Compositions.

Table 1. HCN Destruction Rates: $-d(HCN)/dt$ (moles/s/m^2)

Gas Composition	Alumina	Fly Ash (Rietspruit)	Graphite
	Overall HCN Removal Rates $\overline{V_{HCN}}$		
Argon + HCN	$1.3 \times 10^6 \exp(-7780/T)\ P_{HCN}^{0.38}$	$1.1 \times 10^{-1} \exp(-11100/T)\ P_{HCN}^{0.38}$	$1.6 \exp(-12500/T)\ P_{HCN}^{0.5}$
Argon + HCN + H_2)	$5.0 \times 10^2 \exp(-7550/T)\ P_{HCN} P_{H_2O}$		
Argon + HCN + NO	$1.3 \times 10^{-2} \exp(-9560/T) P_{HCN}^{0.5}\ P_{NO}^{0.34}$	$1.0 \times 10^3 \exp(-15600/T) P_{HCN}^{0.5}\ P_{NO}^{0.34}$	
Argon + HCN + O_2	$3.4 \times 10^{-2} \exp(-9700/T)\ P_{HCN}^{0.5}\ P_{O_2}^{0.27}$		
Reaction	Specific HCN Destructive Reactions		
V_{15}	$1.3 \times 10^{-6} \exp(-7780/T)\ P_{HCN}^{0.38}$	$4.4 \times 10^{-1} \exp(-12900/T)\ P_{HCN}^{0.38}$	$1.6 \exp(-12500/T)\ P_{HCN}^{0.5}$
V_{44}	$5 \times 10^2 \exp(-7550/T)\ P_{HCN} P_{H_2O}$		
V_{40}	$2.4 \times 10^{-3} \exp(-7820/T)\ P_{HCN}^{0.3}\ P_{NO}^{0.7}$	$2.3 \times 10^2 \exp(-13700/T)\ P_{HCN}^{0.3}\ P_{NO}^{0.7}$	
V_{38}	$3.4 \times 10^{-2} \exp(-9700/T)\ P_{HCN}^{0.5}\ P_{O_2}^{0.27}$		
V_{46}	0	0	0
Gas Composition	Ethylene Soot	Cenospheric Soot	Char (Rietspruit)
	Overall HCN Removal Rates ($\overline{V_{HCN}}$)		
Argon + HCN	$2.0 \times 10^{-6} \exp(-4580/T)\ P_{HCN}^{0.38}$	$5.6 \times 10^{-4} \exp(-5440/T)\ P_{HCN}^{0.38}$	$8.2 \times 10^{-4} \exp(-5880/T)\ P_{HCN}^{0.38}$
Argon + HCN + NO	$7.6 \exp(-14200/T)\ P_{HCN}^{0.5}\ P_{NO}^{0.34}$	$1.8 \times 10^{-2} \exp(-4900/T)\ P_{HCN}^{0.5}\ P_{NO}^{0.34}$	$1.4 \times 10^{-2} \exp(-6190/T)\ P_{HCN}^{0.5}\ P_{NO}^{0.34}$
Reaction	Specific HCN Destructive Reaction		
V_{15}	$1.6 \times 10^{-1} \exp(-17860/T)\ P_{HCN}^{0.38}$	$3.3 \exp(-13700/T)\ P_{NO}^{0.38}$	
V_{40}	$5.4 \times 10^1 \exp(-15050/T)\ P_{HCN}^{0.3}\ P_{NO}^{0.7}$	$7.8 \times 10^1\ \mathrm{esp}(-10500/T)\ P_{HCN}^{0.3}\ P_{NO}^{0.7}$	
V_{46}	$8.2 \exp(-14200/T)\ P_{HCN}$	$2.2 \times 10^{-3} \exp(-2840/T)\ P_{HCN}$	